Nonlinear singular switched systems in discrete-time

Sutrisno, Sutrisno; Yin, Hao; Trenn, Stephan; Jayawardhana, Bayu

42nd Benelux Meeting on Systems and Control

March 21 – 23, 2023

Elspeet, The Netherlands

Book of Abstracts

The 42nd Benelux Meeting on Systems and Control is sponsored by

Raffaella Carloni, Javier Alonso-Mora, Bayu Jayawardhana, and Erjen Lefeber (Eds.)
Book of Abstracts - 42nd Benelux Meeting on Systems and Control

University of Groningen
PO Box 72
9700 AB Groningen
The Netherlands

ISBN (e-book): 978-94-034-3010-2

Part 1

Programmatic Table of Contents

Tuesday, March 21, 2023

Plenary: P0 **De Grote Zaal**
Welcome and Opening
Chair: Raffaella Carloni **11.25–11.30**

Plenary: P1 **De Grote Zaal**
Saturated linear feedback design
Luca Zaccarian
Chair: Bayu Jayawardhana **11.30–12.30**

Plenary: P2 **De Grote Zaal**
Quadratically stabilizing saturated feedback
Luca Zaccarian
Chair: Javier Alonso-Mora **13.40–14.40**

TuA01 **Groenendaal**
Games and Agent-Based Models
Chair: Nima Monshizadeh **15.00-17.20**

TuA02 **Solse Gat**
Distributed Control and Estimation 1
Chair: Bart Besselink **15.00-17.20**

Part 2

Contributed Lectures

A game-theoretic market mechanism for procuring flexibility services in distribution networks under limited information sharing

Xiupeng Chen, Koorosh Shomalzadeh, Jacquelien M. A. Scherpen, Nima Monshizadeh
Jan C. Willems Center for Systems and Control, University of Groningen, Groningen, the Netherlands
Email: {xiupeng.chen,k.shomalzadeh,j.m.a.scherpen,n.monshizadeh}@rug.nl

1 Introduction

The high penetration of variable and uncertain renewable energy brings an unprecedented challenge for system operators to ensure the instantaneous stability of power systems in a cost effective manner [1]. This challenge could be handled by providing flexibility services from the energy consumption side through utilizing various distributed energy resource. We propose a game-theoretic market mechanism for energy balancing in a real-time market and formulate the competition among energy consumers as a Generalized Nash Game (GNG). In this framework, the supply function based bidding method is adopted to mitigate the market power of active energy consumers. Moreover, the physical constraints are incorporated to guarantee the secure operation of the distribution network. To steer consumers to the Generalized Nash Equilibrium (GNE) of this game, we design a preconditioned forward-backward based algorithm with provable convergence, by which a market participant only needs to share limited non-private information with others.

2 Problem Formulation

We use $X \in \mathbb{R}^+$ to denote the mismatch between supply and demand in real-time energy market. The Balance Responsible Party (BRP) is responsible for cancelling out this mismatch. Each active energy consumer n is required to submit its supply function $x_n = \alpha\lambda + \beta_n$ as a bid. Upon gathering of the bids of all active consumers, the BRP determines the market clearing price λ as $\lambda = (X - \mathbf{1}^\top\beta)/(\alpha N_a)$ and the allocated flexibility of consumer n as $x_n = (X - \mathbf{1}^\top\beta)/N_a + \beta_n$. Then the consumer n's goal is to maximize its net profit as

$$\min_{\beta_n} \; J_n(\beta_n, \beta_{-n}) = C_n\big((X - \mathbf{1}^\top\beta)/N_a + \beta_n\big) - (X - \mathbf{1}^\top\beta + N_a\beta_n)(X - \mathbf{1}^\top\beta)/(\alpha N_a^2)$$

We write the noncooperative game among consumers in a compact form as the triple

$$\mathscr{G} = \{\mathscr{N}_a, K, \mathrm{col}(J_n(\beta_n, \beta_{-n}))_{n\in\mathscr{N}_a}\},$$

where $\mathscr{N}_a$ is the set of the active energy consumers as before, $\beta_{-n} = col(\beta_m)_{m\in\mathscr{N}_a/\{n\}}$ denotes the strategy profile of all consumers excluding consumer n, and $K := \prod_{n\in\mathscr{N}_a}\Omega_n \cap \Lambda \cap \Psi$ is the set of possible strategies of the consumers. Here the local feasible set $\Omega_n = \mathbb{R}$, and we write the coupling sets separately as Λ and Ψ, since the former contains the local technical characteristics of energy consumers and will be handled by the consumers themselves in our algorithm while the latter involves the distribution network configurations and will be handled by the Distributuin System Operator (DSO). The algorithm for seeking the GNE of this game is provided below.

3 Algorithm Design

Algorithm 1 v-GNE Seeking Algorithm

Initialization: Each active energy consumer $n \in \mathscr{N}_a$, sets $\beta_n(0) \in \mathbb{R}$ and $\gamma_n(0) \in \mathbb{R}^+$.

Preparation: BRP collects $\gamma_n(0)$ and $\beta_n(0)$, and broadcasts the price $\lambda(0)$ and the summation of $\gamma_n(0)$s, i.e., $\mathbf{1}^\top\gamma(0)$ to all the consumers.

Iterate until convergence:

1. Energy consumer $n \in \mathscr{N}_a$ updates its primary bid as

$$\beta_n'(k) = \beta_n(k) - \rho_n\Big(C_n'(\alpha\lambda(k) + \beta_n(k))\frac{N_a - 1}{N_a} + \frac{\alpha\lambda(k)(2 - N_a) + \beta_n(k)}{\alpha N_a} - \frac{1}{N_a}\mathbf{1}^\top\gamma(k) + \gamma_n(k)\Big)$$

and communicates $\beta_n'(k)$ to BRP.

2. DSO collects $\beta_n'(k)$ from BRP and checks the feasibility of the bids by solving the following optimization problem,

$$\beta(k+1) = argmin_{z\in\Psi}||z - \beta'(k)||$$

and sends $\beta(k+1)$ back to BRP.

3. BRP updates $\lambda(k+1)$ and broadcasts $\lambda(k+1)$ and $\beta_n(k+1)$ to consumer n.

4. Energy consumer $n \in \mathscr{N}_a$ updates its dual variable γ_n as

$$\gamma_n(k+1) = \mathrm{Proj}_{\mathbb{R}^+}(\gamma_n(k) + v(2x_n(k+1) - x_n(k) - \hat{x}_n))$$

and communicates $\gamma_n(k+1)$ to BRP.

5. BRP broadcasts $\mathbf{1}^\top\gamma(k+1)$ to all energy consumers.

References

[1] Simon R Sinsel, Rhea L Riemke, and Volker H Hoffmann. Challenges and solution technologies for the integration of variable renewable energy sources—a review. renewable energy, 145:2271–2285, 2020.

Simulation-based Optimization of Electric Truck Freight Logistics for The Netherlands

Juan Pablo Bertucci, Mauro Salazar, Theo Hofman
Eindhoven University of Technology
{j.p.bertucci, m.r.u.salazar, t.hofman}@tue.nl

1 Introduction

Freight transport electrification is mandatory for reducing greenhouse gas emissions, improving air quality, and reducing dependence on fossil fuels. The Netherlands has put forward an ambitious plan to foment the electrification of freight transport with the placement of Zero Emission Zones (ZEZs) in major cities of the country, where only zero-emission commercial vehicles will be permitted to operate [3]. Providing explainable and robust models to logistic distribution operators would be an important step to help transition faster to electric truck usage. We focus on dimensioning the infrastructure and vehicle specifications that would help implement a smooth and robust transition from an existing ICE vehicle operation to electric-powered freight.

2 Methods

The approach taken in this research is two-pronged: given an initial itinerary (VRP solution) of an existing logistic operator we first solve for the optimal number of chargers at each distribution center (DC) and charging schedule (CS) of each vehicle. Secondly, the different components of the system are modeled as individual objects in an agent-based model (ABM) to test the robustness of the solution and identify bottlenecks in specific situations [1].

2.1 Preliminary Optimization

This paper deals with a special instance of a facility location problem. We are provided with an itinerary for each truck k of pickup and deliveries that must be completed with an electric truck fleet. The daily itinerary of a truck k is given by the set $\mathscr{L}^k$ composed of individual trip legs l between origins i and destinations j. By discretizing our problem time into steps of size T, we can have a binary decision variable $Y_{l,k}^{t,r}$ that identifies whether a truck k charges at a certain trip leg l at a charger of type r at time interval t. Thus, we guarantee that state of charge $E_j^{k,l}$ at the destination j is sufficient to perform the trips from i to j:

$$E_j^{k,l} \geq E_i^{k,l} + d_{ij} \cdot c_{\text{cons}}^k + T \cdot \sum_{t,r} Y_{t,r}^{k,l} \cdot P_{\text{ch}}^r \quad \forall l \in \mathscr{L}^k, \forall r \in \mathscr{R}, \forall k \in \mathscr{K}. \quad (1)$$

To fulfill this charging schedule, the optimal locations i, quantity X, and types r of chargers are denoted by the integer decision variable X_i^r. The number of chargers must be enough to satisfy the energy needs of the fleet (i.e, satisfy the constraints given by equation (1)) whilst minimizing the delays produced by vehicle queuing (in case of having to wait for a charge) and total cost of infrastructure.

$$X_i^r \geq \sum_{k,l} Y_{l,k}^{t,r} \quad \forall t \in \mathscr{T}, \forall r \in \mathscr{R}, \forall l \in \mathscr{L}^k. \quad (2)$$

2.2 Agent Based Simulation

To test for the robustness of the solution an ABM is developed, where the trucks, distribution centres and chargers are modeled as objects that interact according to an existing fleet plan. Three types of trucks endowed with respective physics-based power consumption model [2] and internal decision logic. The distribution centers considered have fast chargers fast chargers compliant with Megawatt Charging Systems (MCS) of level 1 and 2. Monte Carlo simulations are leveraged to obtain critical metrics of logistic performance and power requirements with probabilistic bounds.

3 Findings

A tradeoff between the number of vehicles, chargers and flexibility of the schedules becomes patent in terms of waiting times and peak energy requirements. Increased charger power rates provide more time flexibility for charging, but create considerable stress on local power grids. The complementary nature of ABM with global optimization is highlighted in this context of varying operational conditions coupled with infrastructure decision-making.

References

[1] M. Barbati, G. Bruno, and A. Genovese. Applications of agent-based models for optimization problems: A literature review. 39(5):6020–6028. DOI: 10.1007/978-3-642-35913-2.

[2] Lino Guzzella and Antonio Sciarretta. *Vehicle Propulsion Systems*. Springer Berlin Heidelberg, Berlin, Heidelberg, 2013. DOI: 10.1007/978-3-642-35913-2.

[3] Rijksoverheid. Nieuwe afspraken om steden te bevoorraden zonder co2-uitstoot, 2021. [Online; accessed 2022-08-09].

Urgency-aware Optimal Routing in Repeated Games through Artificial Currencies

Leonardo Pedroso[1], Dario Paccagnan[2], Andrea Agazzi[3], W.P.M.H. (Maurice) Heemels[1], Mauro Salazar[1]

[1] Eindhoven University of Technology, Eindhoven, The Netherlands

[2] Computational Optimization group, Department of Computing, Imperial College London, United Kingdom

[3] Department of Mathematics, Duke University, NC, United States

1 Abstract

When people choose routes minimizing their individual delay, the aggregate congestion can be much higher compared to that experienced by a centrally-imposed routing. Yet centralized routing is incompatible with the presence of self-interested users. How can we reconcile the two? In this paper we address this question within a *repeated game* framework and propose a fair incentive mechanism based on artificial currencies that routes selfish users in a system-optimal fashion, while accounting for their temporal preferences. We instantiate the framework in a parallel-network whereby users commute repeatedly (e.g., daily) from a common start node to the end node. Thereafter, we focus on the specific two-arcs case whereby, based on an artificial currency, the users are charged when traveling on the first, fast arc, whilst they are rewarded when traveling on the second, slower arc. We assume the users to be rational and model their choices through a game where each user aims at minimizing a combination of today's discomfort, weighted by their urgency, and the average discomfort encountered for the rest of the period (e.g., a week). We show that, if prices of artificial currencies are judiciously chosen, the routing pattern converges to a system-optimal solution, while accommodating the users' urgency. Numerical simulations in [1] show that it is possible to achieve a system-optimal solution whilst significantly reducing the users' perceived discomfort when compared to a centralized optimal but urgency-unaware policy.

2 Problem formulation

Our framework combines three ingredients: i) a transportation network represented by a digraph, ii) cost functions representing the societal and personal costs (a measure of discomfort such as travel time) resulting from the aggregate route choices of the users, and iii) a pricing policy based on the artificial currency Karma. Consider a parallel road-network, consisting of a single origin and destination node but connected by $n \in \{1, 2, \dots\}$ directed arcs, e.g., the example in Fig. 1, whereby $n = 2$.

We assume the presence of a central operator (e.g., a municipal authority) who needs to design incentives so that the aggregate flows converge to the minimizer of the total societal cost. In order to steer users' behavior towards a social optimum $x^\star$, the central operator endows each user with the artificial currency Karma and sets a price $p_j \in \mathbb{R}$ to cross each arc j. Users are not permitted to buy or exchange Karma, and they can only select the arcs keeping their Karma-level non-negative. Crucially, some of the arcs have negative prices, so that users will be rewarded when crossing them.

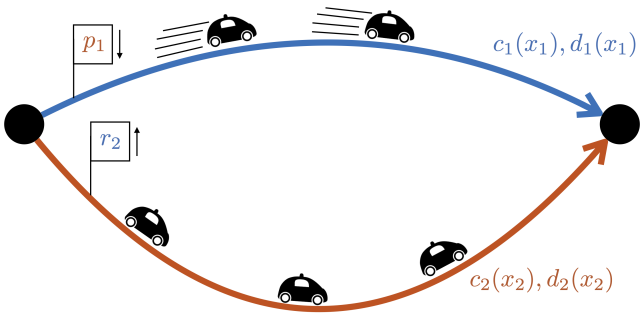

Figure 1: Network with one origin and one destination node connected by two arcs. Each arc j is traversed by x_j users per unit time, resulting in a societal cost and a discomfort cost perceived by the users.

On the microscopic level, we assume individual users to make choices in order to minimize their traveling discomfort without reaching a negative level of Karma. In contrast to conventional monetary tolling schemes, the individual user's problem cannot be captured in a static setting: In our framework, the users are playing against their future selves, and must account for their future preferences to decide when to use Karma and when to gain it.

Taking a static planning perspective, at each time-step t, we model the aggregate choices of the population with the Wardrop Equilibrium (WE) $x^{\mathrm{WE}}(t)$. The central operator's problem then is to choose the prices so that the daily WE $x^{\mathrm{WE}}(t)$ will converge to the system optimum $x^\star$.

References

[1] M. Salazar, D. Paccagnan, A. Agazzi, and W. P. M. H. Heemels, "Urgency-aware optimal routing in repeated games through artificial currencies," *European Journal of Control*, vol. 62, no. 2021 European Control Conference Special Issue, pp. 22–32, 2021.

The Co-evolution of Population Behavior and Climate Impact

Kathinka Frieswijk[1], Ming Cao[4]
Discrete Technology & Production Automation,
Engineering and Technology institute Groningen,
University of Groningen, Groningen, The Netherlands
Email: {k.frieswijk,m.cao}@rug.nl

Lorenzo Zino[2]
Department of Electronics
and Telecommunications
Politecnico di Torino, Torino, Italy,
Email: lorenzo.zino@polito.it

A. Stephen Morse[3]
Department of Electrical Engineering,
Yale University, New Haven, USA,
Email: as.morse@yale.edu

1 Introduction

Motivated by the current climate crisis, we propose and investigate a novel theoretical framework for the evolution of anthropogenic climate impact in which the evolution of human environmental behavior and environmental impact are intertwined.

2 Model

We consider a population of n individuals, where each individual is symbolized by a vertex in a directed network $\mathscr{G} := (\mathscr{V}, \mathscr{E})$, with $\mathscr{V} := \{1, \ldots, n\}$. Here, $(i, j) \in \mathscr{E}$ if and only if individual j exerts social influence on the behavior of individual i. The environmental behavior of an individual $i \in \mathscr{V}$ at a given time $t \in \mathbb{R}_{\geq 0}$ is quantified by $x_i(t) \in \{0, 1\}$, which indicates whether the individual is exhibiting environmentally responsible behavior ($x_i(t) = 1$) or environmentally irresponsible behavior ($x_i(t) = 0$).

Over the past half-century, there has been a significant and exponential rise in anthropogenic carbon dioxide concentrations in the atmosphere. In light of this trend, we model the evolution of anthropogenic environmental impact $\varepsilon(t) \in \mathbb{R}_{\geq 0}$ as $\frac{d\varepsilon}{dt} = r(t)\varepsilon(t)$, where the rate of growth or decay at time t is defined as $r(t) := \gamma \bar{x}_0(t) - \tau$. Here, we model the effect of environmentally irresponsible behavior by $\gamma \bar{x}_0(t)$, where $\gamma \in \mathbb{R}_{>0}$ and $\bar{x}_0(t) := \frac{1}{n}|i \in \mathscr{V} \,:\, x_i(t) = 0|$. The parameter $\tau \in \mathbb{R}_{>0}$ represents efforts to mitigate the environmental impact through, e.g., negative emissions technologies or large-scale tree planting initiatives. Our framework includes a human decision-making process that captures: i) social influence; ii) the cost of environmentally-friendly behavior $\kappa \in \mathbb{R}_{>0}$; iii) government subsidies, modeled by reducing the cost for responsible behavior κ by $\sigma \in [0, \kappa]$; iv) awareness campaigns $\alpha \in \mathbb{R}_{\geq 0}$, which increase the motivation to exhibit responsible environmental behavior; and v) the population response to the environmental impact $\varepsilon(t)$, which is modeled by $\mu\varepsilon(t)$ with $\mu \in \mathbb{R}_{>0}$.

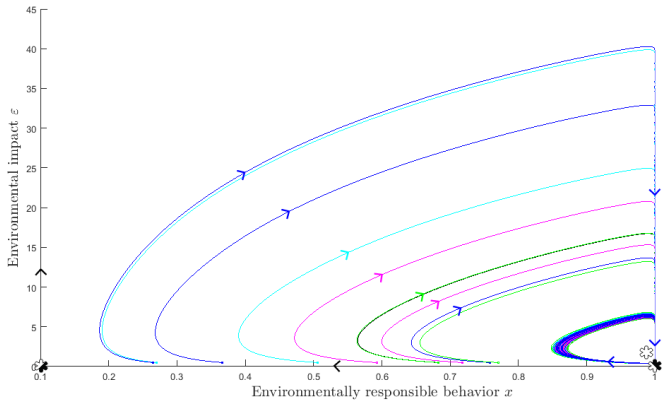

Figure 1: Simulated trajectories of the system in (1). Saddle points and unstable equilibria are marked with black-white and white asterisks, respectively.

3 Results

Utilizing a mean-field approximation in the limit of large populations, we find that the population behavior follows

$$\begin{aligned} \dot{x} &= x(1-x)(2x + \mu\varepsilon + \alpha + \sigma - \kappa - 1)\,, \\ \dot{\varepsilon} &= (\gamma(1-x) - \tau)\varepsilon\,, \end{aligned} \tag{1}$$

where x defines the average probability for a randomly selected individual to act responsibly at time t. The system in (1) has three equilibria: i) $(x, \varepsilon) = (0, 0)$, which is a saddle point; ii) $(x, \varepsilon) = (1, 0)$, which is a saddle point; and iii) $(x, \varepsilon) = (1 - \frac{\tau}{\gamma}, \frac{1}{\mu}[\frac{2\tau}{\gamma} + \kappa - \sigma - \alpha - 1])$, which is an unstable spiral. Subsequently, we show that if the initial condition is in the interior of the domain $[0, 1] \times \mathbb{R}_{\geq 0}$, then the system in (1) converges to a limit cycle, as illustrated in Fig. 1. All additional details of the model and the analytical derivations can be accessed in the preprint on arXiv [1].

References

[1] K. Frieswijk, L. Zino, A. S. Morse, and M. Cao, "Modeling the Co-evolution of Climate Impact and Population Behavior: A Mean-Field Analysis," *arXiv preprint*, arXiv:2211.11075, 2022.

Dynamic Coordinated Maintenance of Wind-Farms with Risk-Averse Agents under CVaR criterion

Stefanny Ramirez
ENTEG, University of Groningen, Nijenborgh 4, 9747 AG Groningen, Netherlands
s.g.ramirez.juarez@rug.nl

Dario Bauso
ENTEG, University of Groningen, Nijenborgh 4, 9747 AG Groningen, Netherlands.
Dipartimento di Ingegneria, Università di Palermo, 90128 Palermo, Italy
d.bauso@rug.nl

1 Abstract

We study a coordinated maintenance problem for multi-turbine offshore wind-farms. The deterioration of the turbines follows a Poisson process and the optimal order quantity for a single wind-farm, as well as for a coalition of wind-farms, is obtained based on the risk-averse newsvendor model considering the *conditional value at risk* (CVaR) criterion. We apply the theory of robust dynamic coalitional games to design a stable allocation mechanism that distributes the cost of the coalition among their participants in a fair and stable way.

2 Introduction

In this research we focus on the study of the maintenance of multi-turbine offshore wind-farms. We design a coordinated maintenance model of wind-farms assuming a Poisson deterioration of the turbines. The deterioration level determines the demand in terms of working shifts. We then use the newsvendor model as a paradigm to obtain the optimal number of working shifts. The classical newsvendor model does not consider the risk that the cost is higher than a certain accepted level. In this research we consider the risk-averse newsvendor model under the CVaR criterion [3, 5, 6], and we adapt it to determine the optimal number of maintenance working shifts. We analyse the coordinated maintenance problem from the perspective of dynamic coalitional games [1, 2, 4, 7–9]. Finaly, we design a stable allocation mechanism that consists of a feedforward part and a feedback part to distribute the cost of the coalition among their members in a fair and stable way.

3 Main contributions

- We obtain an explicit expression for the optimal order quantity under the CVaR criterion.
- We prove that the costs of the coalitions are bounded and the bounds are obtained when the demand is equal respectively to its lower and upper bound.
- We prove that the coalitional game is balanced.
- We design a robust allocation mechanism where the average allocation converges to an element of the Core of the average game.

References

[1] D. Bauso & J. Timmer (2009). Robust dynamic cooperative games. *Int. J. Game Theory*, 38, 23–36.

[2] D. Bauso, & J. Timmer (2012). On robustness and dynamics in (un)balanced coalitional game. *Automatica*, 48(10), 2592–2596.

[3] Y. Chen, M. Xu, & Z.G. Zhang (2009). A Risk-Averse Newsvendor Model Under the CVaR Criterion. *Oper. Res.*, 57(4), 1040–1044.

[4] F. Fele, J.M. Maestre, & E.F. Camacho (2017). Coalitional Control: Cooperative Game Theory and Control. *IEEE Cont. Syst.*, 37, 53–69.

[5] J. Gotoh, & Y. Takano (2007). Newsvendor solutions via conditional value-at-risk minimization. *Eur. J. Oper. Res.*, 179, 80–96.

[6] M.A.M Abdel-Aal, & S.Z. Selim (2017). Risk-averse multi-product selective newsvendor problem with different market entry scenarios under CVaR criterion. *Comput. Ind. Eng.*, 103, 250–261.

[7] A. Nedić, & D. Bauso (2012). Dynamic coalitional TU games: Distributed bargaining among Players' Neighbors. *IEEE Trans. Automat. Contr.*, 58(6), 1363–1376.

[8] M. Smyrnakis, D. Bauso, & H. Tembine (2019). Game-theoretic learning and allocations in robust dynamic coalitional games. *SIAM J. Control. Optim*, 57(4), 2902–2923.

[9] T. Wada, & Y. Fujisaki (2017). A stochastic approximation for finding an element of the core of uncertain cooperative games. *11th ASCC*, 2071–2076.

Riemannian polarization of multi-agent gradient flows

La Mi, Jorge Gonçalves, and Johan Markdahl
Luxembourg Centre for Systems Biomedicine, University of Luxembourg
6, Avenue du Swing, L-4367, Belvaux, Luxembourg
{la.mi, jorge.goncalves}@uni.lu, markdahl@kth.se

1 Introduction

Stable polarization of multi-agent systems has been shown to exist over $\mathbb{R}^n$ and highly symmetric nonlinear spaces [1, 2], especially the n-sphere $\mathscr{S}^n$. Toward a more generalized setting without assuming linearity or symmetry, our previous work [3] established the same type of emergent behavior over general hypersurfaces, subsuming the n-sphere case. In this note, we discuss our ongoing work of extending our previous hypersurface results to study the stability of polarized equilibria of multi-agent gradient flows evolving on general Riemannian manifolds. The aim is to provide sufficient conditions in terms of the manifold geometry.

2 Setup

2.1 Embedded submanifolds

As a first step, we consider Riemannian manifolds with an embedding in the Euclidean space. This is motivated by the fact that implementation of multi-agent communication protocol is considerably simpler when the relative difference between agents are measured in terms of chordal (Euclidean) rather than geodesic distances.

A key difference compared to the hypersurface $\mathscr{H}^n = \{y \in \mathbb{R}^{n+1} \,|\, c(y) = 0\}$ for some smooth function c is that the normal space of a general Riemannian manifold $\mathscr{M}$ has dimension greater 1. While defining the geometric characteristics on $\mathscr{H}^n$ relies on a unique normal vector, and consequently the conditions there hinge on a pair of aligned normals that point toward or away from each other, we extend these concepts to a general $\mathscr{M}$ by choosing a normal vector in the normal space when defining the geometric characteristics.

2.2 Multi-agent gradient flows

Evolving on the manifold is a multi-agent system with N identical agents $(x_i)_{i=1}^N$, associated with an undirected, connected, and weighted graph structure $\mathscr{G} = (\mathscr{V}, \mathscr{E}, A)$. The adjacency matrix $A = [a_{ij}]$ is symmetrical and has nonnegative entries. The vertices $\mathscr{V}$ are divided into two groups $\mathscr{V}_\mathrm{u}$ and $\mathscr{V}_\mathrm{l}$, inducing a partition of the edge set $\mathscr{E}$ into intra-group and intergroup sets $\mathscr{E}_+$ and $\mathscr{E}_-$. Such a partition is introduced to enforce different coupling rules over edges in $\mathscr{E}_+$ and $\mathscr{E}_-$. The couplings are positive over all edges in $\mathscr{E}_+$, whereas those over $\mathscr{E}_-$ can be either all positive or all negative. Accordingly, there are two potential functions with the disagreement terms expressed in chordal distances

$$V_+ = \frac{1}{2} \sum_{\{i,j\} \in \mathscr{E}} a_{ij} \|x_j - x_i\|^2$$

$$V_- = \frac{1}{2} \sum_{\{i,j\} \in \mathscr{E}_+} a_{ij} \|x_j - x_i\|^2 - \frac{1}{2} \sum_{\{i,j\} \in \mathscr{E}_-} a_{ij} \|x_j - x_i\|^2.$$

The gradient flow on a Riemannian manifold $\mathscr{M}$ embedded in the ambient space dictates the dynamics of each agent as follows

$$\dot{x}_i = -\Pi_i \left(\nabla_i V \right),$$

where Π_i is the orthogonal projection on the tangent space of $\mathscr{M}$ and ∇_i is the extrinsic gradient in the ambient space.

3 Extended results on Riemannnian manifolds

The signs of inter-agent couplings emboddied by V_+ and V_- in §2.2 together with the geometric characteristics §2.1 give rise to stable polarization under various sufficient conditions. The essential piece in the proofs is a local stability result for general Riemannian manifolds, not necessarily embedded submanifolds, which conditions Lyapunov and local asymptotic stability of the equilibrium set on its being a strict local minimizer of V and being isolated.

We additionally pay attention to special homogeneous manifolds and discuss how they are covered under our conditions for general Riemannian manifolds. For example, the polarizing dynamics on the Grassmannians $\mathrm{Gr}(n,p)$ is

$$\dot{P}_i = \sum_{j \in \mathscr{V}_\mathrm{u}} a_{ij} (P_i P_j P_i^\perp + P_i^\perp P_j P_i) - \sum_{j \in \mathscr{V}_\mathrm{l}} a_{ij} (P_i P_j P_i^\perp + P_i^\perp P_j P_i)$$

for $i \in \mathscr{V}_\mathrm{u}$ (similar for $i \in \mathscr{V}_\mathrm{l}$), where $P^\perp = I - P$ and P_i's are $n \times n$ rank p projection matrices.

References

[1] C. Altafini, "Consensus problems on networks with antagonistic interactions," *IEEE Transactions on Automatic Control*, vol. 58, no. 4, pp. 935–946, 2012.

[2] S.-Y. Ha, D. Kim, J. Lee, and S. E. Noh, "Emergence of bicluster aggregation for the swarm sphere model with attractive-repulsive couplings," *SIAM Journal on Applied Dynamical Systems*, vol. 19, no. 2, pp. 1225–1270, 2020.

[3] L. Mi, J. Gonçalves, and J. Markdahl, "Asymptotically stable polarization of multi-agent gradient flows over manifolds," *arXiv:2301.04877*, 2023.

On Lyapunov functions for open Hegselmann-Krause dynamics

Renato Vizuete[1] Paolo Frasca[2] Elena Panteley[3]

[1]ICTEAM, UCLouvain, 1348 Louvain-la-Neuve, Belgium: renato.vizueteharo@uclouvain.be
[2]GIPSA-lab, France: paolo.frasca@gipsa-lab.fr
[3]L2S CentraleSupélec, France: elena.panteley@l2s.centralesupelec.fr

1 Introduction and problem formulation

Hegselmann-Krause (HK) model is one of the most important opinion dynamics characterized by bounded confidence interactions [1]:

$$\dot{x}_i(t) = \sum_{j:|x_i(t)-x_j(t)|<1} (x_j(t)-x_i(t)), \text{ for all } i \in \mathscr{I} = \{1,\dots,n\},$$

where x_i is the opinion of agent i. In many social interactions, the group of individuals does not remain constant since new agents may join the system and others leave, generating an open HK dynamics. In the open system, the dynamics in continuous time of the agents is characterized by (1), and the additional changes are due to *arrivals* and *departures*, that generate a time-varying set of agents $\mathscr{I}(t)$.

Definition 1 (Departure) *We say that an agent $j \in \mathscr{I}(t^-)$ leaves the system at time t if $\mathscr{I}(t^+) = \mathscr{I}(t^-) \setminus \{j\}$.*

Definition 2 (Arrival) *We say that an agent j joins the system at time t if $\mathscr{I}(t^+) = \mathscr{I}(t^-) \cup \{j\}$.*

Assumption 1 (Departure process) *The departure instant of an agent j is determined by a homogeneous Poisson process $N_t^{(j)}$ with rate $\lambda_d > 0$ associated with the agent.*

Assumption 2 (Arrival process) *The arrival instants are determined by a homogeneous Poisson process $N_t^{(A)}$ with rate $\lambda_A > 0$.*

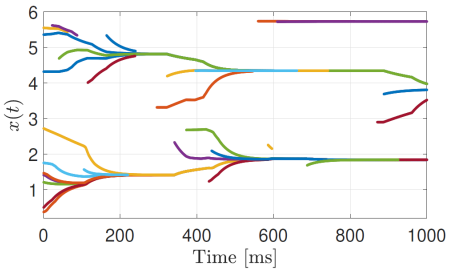

Figure 1: Evolution of the opinions for an open HK dynamics.

2 Lyapunov functions in open HK dynamics

The common Lyapunov functions used for the analysis of the HK dynamics are based on global disagreement. One of their main drawbacks is that their asymptotic values are not zero when the system presents several clusters. In the context of the open HK dynamics we would like to have functions converging to zero at least for a closed dynamics, such that any deviation from the zero value is due only to the impact of arrivals and departures. For this reason, we propose potential Lyapunov functions based on local disagreement.

Function $U(x)$: we measure the disagreement with respect to the average in each cluster:

$$U(x) := \frac{1}{n}\sum_{i=1}^{n}(x_i - \bar{x}_i)^2, \tag{1}$$

where $\bar{x}_i$ is the average of the states of the agents corresponding to the cluster to which x_i belongs.

Function $V(x)$: we restrict the disagreement to the set $D = \{i,j : |x_i(t) - x_j(t)| < 1\}$ by defining:

$$V(x) := \frac{1}{n^2}\sum_{i,j:|x_i-x_j|<1}(x_i - x_j)^2. \tag{2}$$

In Fig. 2 we can observe that the Lyapunov functions based on local disagreement have a non-zero asymptotic value only in the open scenario.

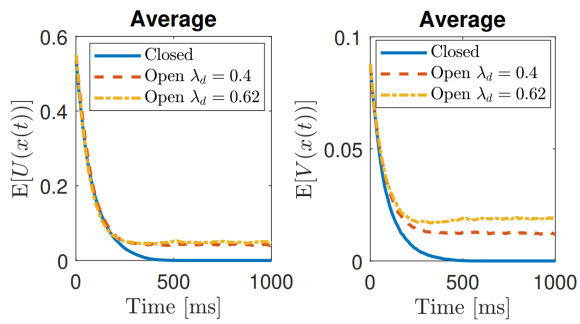

Figure 2: Evolution of the Lyapunov functions for closed and open HK dynamics with $\lambda_A = 5$.

3 Acknowledgements

This work was supported by F.R.S.-FNRS via the *KORNET* project and via the Incentive Grant for Scientific Research (MIS) *Learning from Pairwise Comparisons*, and by the *RevealFlight* Concerted Research Action (ARC) of the Fédération Wallonie-Bruxelles.

References

[1] R. Hegselmann, U. Krause, *et al.*, "Opinion dynamics and bounded confidence models, analysis, and simulation," *Journal of artificial societies and social simulation*, vol. 5, no. 3, 2002.

Contract Theory for Continuous Dynamical Systems using Simulation

Marieke Heidema
RUG, Groningen, Netherlands, FSE
h.m.heidema@rug.nl

Bart Besselink
RUG, Groningen, Netherlands, FSE
b.besselink@rug.nl

1 Introduction

Nowadays, the engineering systems that are being designed and manufactured are more and more complex. These systems often consist of many components, possibly designed by distinct teams. In order for the integrated system to have the desired dynamic behavior, however, all individual components must not only do their job properly, but also must work together nicely with the other components. This is where the notion of *contracts* comes in [1].

2 Contracts

Contracts are mathematical specifications on the behavior of a dynamical system of the form

$$\Sigma: \quad \dot{x} = Ax + Bu + Fd, \quad y = Cx,$$

with state x, input u, output y and disturbance d. Now, for this type of dynamics for the components, a contract basically specifies the inputs that are allowed to be fed to our system Σ and the corresponding outputs that we then expect. In particular, we define contracts on the basis of: (1) *assumptions* given by

$$A: \quad \dot{x}_A = A_A x_A + F_A d_A, \quad u_A = C_A x_A,$$

which specify what inputs u_A are allowed to be fed to our system Σ; (2) *guarantees* given by

$$G: \quad \dot{x}_G = A_G x_G + F_G d_G, \quad \begin{bmatrix} u_G \\ y_G \end{bmatrix} = C_G x_G,$$

which specify what input-output trajectories (u_G, y_G) we expect to get when feeding inputs u_A to our system Σ. With this, a *contract* $\mathscr{C}$ is defined as a pair $\mathscr{C} = (A, G)$.

Having defined contracts, we, of course, need to formulate what it means for a system Σ to satisfy a specific contract or not. In particular, we refer to this as *implementation* and say that a system Σ implements a contract $\mathscr{C} = (A, G)$ if the interconnected system $A \times \Sigma$ can be mimicked by G in such a way that the input-output data from the first (u_A, y) is indistinguishable from that of the latter (u_G, y_G). In other words, the behavior of the interconnection is captured in the behavior of the guarantees. A depiction of this can be found in the figure below.

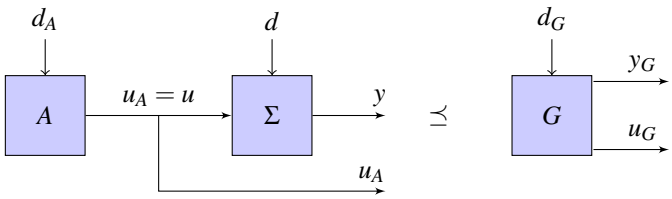

3 Results

In this context, we develop mathematical tools for the following properties:

1. **implementation**: a way of analyzing whether or not individual components meet the requirements as stated in their associated contracts.
2. **refinement**: a way to compare contracts.
3. **composition**: a way of defining a contract on the interconnection of a finite number of components on the basis of component contracts.

4 Discussion

Here, we would like to emphasize the importance of contracts, namely that, using contracts, complex multi-component engineering systems can be analyzed by analyzing each of its components with respect to their associated contract only. In particular, refinement allows us to compare the contract of one component to that of a possibly improved version of that component, which may allow for substitution of the former component by the latter. Furthermore, composition allows us to investigate what the overall contract of a multi-component system looks like. Thus, the analysis done to develop the mathematical tools (which is mainly based on [2]) allows for contracts to be used for modular design and easier analysis of large, interconnected systems.

References

[1] A. Benveniste et al. Contracts for system design. *Foundations and Trends in Electronic Design Automation*, 12(2-3):12-400, 2018.

[2] Shali, B. M., Heidema, H. M., van der Schaft, A. J., & Besselink, B. (2022). Series composition of simulation-based assume-guarantee contracts for linear dynamical systems. *arXiv preprint arXiv:2209.01844*.

Distributed formation control of networked mechanical systems

N. Javanmardi[1], P. Borja[2], M. J. Yazdanpanah[3], and J. M. A. Scherpen[1]

[1]Jan C. Wilems Center for Systems and Control, ENTEG, Faculty of Science and Engineering, University of Groningen, Groningen, The Netherlands (e-mail: n.javanmardi, j.m.a.scherpen @rug.nl)

[2]School of Engineering, Computing and Mathematics, University of Plymouth, Plymouth, UK (e-mail: pablo.borjarosales@plymouth.ac.uk)

[3]Control and Intelligent Processing Center of Excellence, School of Electrical and Computer Engineering, University of Tehran, Tehran, Iran (e-mail: yazdan@ut.ac.ir)

1 Introduction

Distributed formation controllers for networked mechanical systems have proven successful in reducing heavy computational burden, communication range, and unreliability in large-scale networked systems by using only local information of the neighboring agents. However, unstable behaviors and error amplification in large-scale networked systems may occur as the number of agents increases. This study investigates a distributed formation tracking control law for large-scale networks of mechanical systems. In particular, we adopt a distributed parameter approach to prove the Scalable Exponential Stability (SES) of the network formation, i.e., the scalability with respect to the network size and the specific formation preservation.

2 Problem Statement and Network control

Consider a large-scale networked system composed of $N \in \mathbb{N}$ agents. Each agent i is modeled as a port-Hamiltonian mechanical system, i.e.,

$$\begin{bmatrix} \dot{q}_i \\ \dot{p}_i \end{bmatrix} = \begin{bmatrix} 0_n & I_n \\ -I_n & -\mathscr{R}_i \end{bmatrix} \begin{bmatrix} \nabla_{q_i} H_i(q_i,p_i) \\ \nabla_{p_i} H_i(q_i,p_i) \end{bmatrix} + \begin{bmatrix} 0 \\ I_n \end{bmatrix} u_i, \qquad (1)$$

$$H_i(q_i,p_i) = \tfrac{1}{2} p_i^\top M_0^{-1} p_i + \mathscr{U}_i(q_i).$$

where $q_i, p_i, u_i \in \mathbb{R}^n$ are the position, the momenta, and the input of each agent i, respectively. Moreover, $M_0 \in \mathbb{R}^{n\times n}$ is the mass matrix, $\mathscr{R}_i \in \mathbb{R}^{n\times n}$ is the *positive semi-definite* damping matrix and $\mathscr{U}_i : \mathbb{R}^n \to \mathbb{R}$ denotes the potential energy of the agent i. Hence, the control objectives are

$$\begin{aligned} \lim_{t\to\infty} \|q_i(t) - q_j(t) - \Delta_{i,j}\| &= 0, \quad \forall i,j \in \mathscr{B}_L \cup \mathscr{B}_F \,|\, i \sim j \\ \lim_{t\to\infty} \|q_i(t) - q_{r,i}(t)\| &= 0, \quad \forall i \in \mathscr{B}_L \\ \lim_{t\to\infty} \|p_j(t) - p_{r,i}(t)\| &= 0, \quad \forall j \in \mathscr{B}_L \cup \mathscr{B}_F,\ \exists i \in \mathscr{B}_L \end{aligned} \qquad (2)$$

where $\mathscr{B}_L$ and $\mathscr{B}_F$ denote the non-empty sets of leaders and followers, respectively. Besides, $q_{r,i}(t)$ and $p_{r,i}(t) \triangleq M_0 \dot{q}_{r,i}(t)$ are the reference trajectory position and momenta, respectively. And $\Delta_{i,j}$ indicates the desired formation geometry between the pair of agents (i,j). In addition, we require the network to exhibit the SES property.

Definition 1 *A networked system with $N \in \mathbb{N}$ agents is said to be SES if there exist constants $c \geq 0$ and $\alpha, \lambda > 0$, such that, for any initial condition $x_i(t_0)$, $i \in \mathscr{N} := \{1,2,\ldots,N\}$, satisfying $\max_{i\in\mathscr{N}} \|x_i(t_0)\| < \alpha$, the solution $x_i(t)$, $i \in \mathscr{N}$, exists for all $t \geqslant t_0$ and satisfies*

$$\max_{i\in\mathscr{N}} \|x_i(t)\| \leq c e^{-\lambda t} \cdot \max_{i\in\mathscr{N}} \|x_i(t_0)\|, \quad \forall N \in \mathbb{N}. \qquad (3)$$

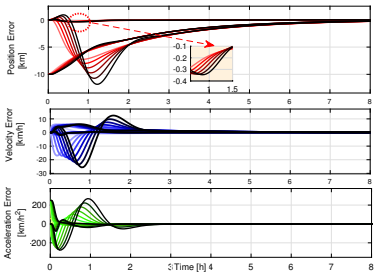

Figure 1: Unscalable stable behavior of a networked system.

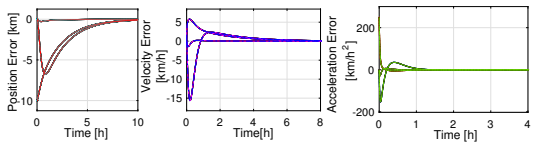

Figure 2: Scalable behavior of a SES networked system.

According to the notion of SES, the state trajectories of the networked system remain bounded for any $N \in \mathbb{N}$, i.e., boundedness is independent of the size of the network. Hence, the performance of the networked system is scalable. Consequently, the stability of the networked system is not jeopardized by adding or removing agents.

3 Main Results

We propose a distributed control protocol based on the tracking *interconnected and damping assignment passivity-based control* method (see [1]). Then, we derive a partial differential equation (PDE) approximate model of the closed-loop system that gives a 2-dimensional perspective of the networked system. Therefore, the following results are proved:

- The closed-loop system is realized as a spatial discretization of the PDE model.
- The closed-loop networked system is SES and the formation control objectives (2) are achieved.

Figure 1 illustrates an unscalable behavior, while Figure 2 shows the results of our controller, where the error responses are not amplified when increasing the number of agents in the network.

References

[1] N. Javanmardi, P. Borja, M.J. Yazdanpanah, J.M.A. Scherpen, Distributed formation control of networked mechanical systems, IFAC-PapersOnLine, Volume 55, Issue 13, 2022

Stability of switched systems with multiple equilibria: a mixed stable-unstable subsystem case

Hao Yin, Bayu Jayawardhana, and Stephan Trenn
Jan C. Willems Center for Systems and Control, University of Groningen, 9747 AG Groningen, The Netherlands.
hao.yin@rug.nl, b.jayawardhana@rug.nl and s.trenn@rug.nl

1 Introduction

This paper studies stability of switched systems that are composed of a mixture of stable and unstable modes with multiple equilibria. The main results of this paper include some sufficient conditions concerning set convergence of switched nonlinear systems. We show that under suitable dwell-time and leave-time switching laws, trajectories converge to an initial set and then stay in a convergent set. Based on these conditions, LMI conditions are derived that allow for numerical validation of practical stability of switched affine systems, which include those with all unstable modes. Two examples are provided to verify the theoretical results.

2 Problem formulation

Consider switched systems in the form of

$$\dot{x}(t) = f_{\sigma(t)}(x(t),t), \quad x(t_0) = x_0, \tag{1}$$

where $x(t) \in \mathscr{X} \subseteq \mathbb{R}^n$ is the state vector, $t_0 \in \mathbb{R}$ is the initial time and $x_0 \in \mathscr{X}$ is the initial value. The main objective of this paper is to propose a sufficient condition that guarantees the switched system (1) is set convergent with respect to switching law $\sigma(t)$, which include the case when not all modes of (1) are stable and when none of the modes is stable.

3 Main Result

We define $N(k)$, $N^{\alpha}(k)$, $L(k)$, which are a subset of $\mathscr{X}$ and parametrized by positive constant $k > 0$. These sets will be used in our main result to define the attractive invariant set of the switched systems. An illustration of these sets for two modes can be seen in Fig.1.

Theorem 1 *Suppose that for every $q \in \mathscr{Q}$ there exists $V_q : \mathscr{X} \times [0, \tau_{q,\max}) \to \mathbb{R}_+$ satisfying $\dot{V}_q(\xi,\tau) \le \eta_q V_q(\xi,\tau)$, and $V_p(\xi,0) \le \mu_q V_q(\xi,\tau)$, for all $\xi \in \mathscr{X} \setminus N(k)$, $p,q \in \mathscr{Q}$, and $\tau \in [\tau_{q,\min}, \tau_{q,\max})$, with a given η_q, μ_q and $k > 0$. Then for every switching signal $\sigma : \mathbb{R}_+ \to \mathscr{Q}$ satisfying the following dwell and leave time condition*

$$\left.\begin{array}{ll} \tau_q > \max\left\{-\frac{\ln \mu_q}{\eta_q}, \tau_{q,\min}\right\} & \forall q \in \mathscr{S}, \text{ and} \\ \tau_q < \min\left\{-\frac{\ln \mu_q}{\eta_q}, \tau_{q,\max}\right\}, & \forall q \in \mathscr{U}. \end{array}\right\} \tag{2}$$

the following properties hold for the state trajectory of the switched system (1):

(i) *there exists $T = T(x_0) > 0$ such that $x(T) \in N(k)$;*

(ii) *for any time $t \in [T, +\infty)$, the trajectory will stay in $L(k)$, i.e. $x(t) \in L(k)$;*

(iii) *for all starting points $x_0 \in N^{\alpha}(k)$, the trajectory of switched system (1) remains in the set $L(k)$, i.e. $x(t) \in L(k)$.*

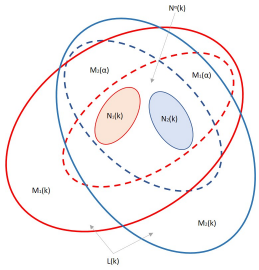

Figure 1: An illustration of the set constructions for two modes.

4 Simulation Results

Example: Let us consider the switched system composed of both unstable and stable subsystems, Figure 2 shows that when the trajectory starts on the boundary of $N(\alpha)$, the trajectory stays in $L(k)$ for all time.

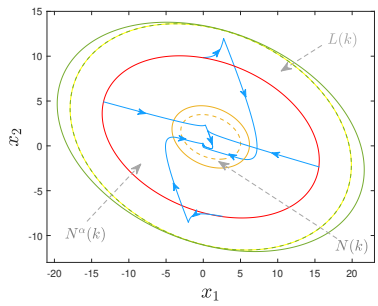

Figure 2: The plot of trajectories of switched system in Example, the green solid line is $L(k)$, the red solid line is $N^{\alpha}(k)$, the orange line is $N(k)$.

Leader-follower formation control utilizing a virtual tensegrity framework without leader motion direction information

Zhiyuan Liu
Discrete Technology & Production Automation
University of Groningen
The Netherlands
Email: z.liu@rug.nl

Ming Cao
Discrete Technology & Production Automation
University of Groningen
The Netherlands
Email: m.cao@rug.nl

1 Introduction

This paper investigates the leader-follower formation control task for a team of mobile agents. A new control method that requires no information about the leader's motion direction is proposed. Taking advantage of a virtual tensegrity framework, each follower agent measures the relative positions of its neighbors in its local coordinate system; the motion of each follower is governed by the stresses of the connections of the underlying virtual tensegrity framework, and these stresses become constant in their steady states. The advantage of not requiring the knowledge of the leader's motion direction is not requiring the alignment of the follower agents' coordinate systems. Local stability is proved for the target formation movement of our proposed method, and simulation results further provide verification.

2 Main result

Consider a group of n agents including one leader agent, moving in a 2-dimensional plane. The configuration of the formation is denoted by $p \in \mathbb{R}^{2n}$, which can be obtained by stacking the x and y coordinates of agents as follows:

$$p = \left[\, p_x^\top \, p_y^\top \,\right]^\top = [p_{1x}, p_{2x}, \ldots, p_{nx}, p_{1y}, p_{2y}, \ldots, p_{ny}]^\top. \quad (1)$$

Each agent's state $p_i = \left[\, p_{ix} \;\; p_{iy} \,\right]^\top$, $i \in \{1, 2, \ldots, n\}$ is governed by the single-integrator model. The leader agent's state $p_l = \left[\, p_{lx} \;\; p_{ly} \,\right]^\top$ is guided under direct velocity input, where l denotes the leader agent's label; the follower agents are controlled by the virtual force $F = -\left(I_2 \otimes \Omega(p)\right) p$ from the underlying virtual tensegrity framework, where $\Omega \in \mathbb{R}^{n \times n}$ is the stress matrix [1]. For a follower agent j, the virtual force on agent j is given by $f_j = \left[\, F_j \;\; F_{j+n} \,\right]^\top$, and the control law u_j is given by

$$u_j = f_j = -\sum\nolimits_{k \in \mathcal{N}_j} \Omega_{jk} \left(p_k - p_j\right), \quad (2)$$

where $\mathcal{N}_j$ denotes the set of labels of agent j's neighbors.

Now, given a configuration $p^* = \left[\, p_x^{*\top} \;\; p_y^{*\top} \,\right]^\top$ of the desired formation in an arbitrary coordinate system, and suppose the leader agent is moving at a constant velocity, of which the speed s_l is known by the follower agents, we use a two-step method for the controller design of the followers.

Note that this method deals with the formation control problem where the leader is moving, with its desired relative position not coinciding with the formation's center.

Step 1: Label the leader agent as agent 1, and the follower agents from 2 to n. Calculate the stress matrix at the desired configuration p^*, i.e. $\Omega(p^*) \in \mathbb{R}^{n \times n}$. One solution of $\Omega(p^*)$ is given by $\Omega(p^*) = DD^\top$, where D is a vector in the form of $D = kd = k\left[\, -(n-1) \;\; 1 \;\; \ldots \;\; 1 \,\right]^\top$, and k can be solved from

$$k = \pm \sqrt[4]{\frac{{s_l}^2}{\left(dp_x^*\right)^2 + \left(dp_y^*\right)^2}}. \quad (3)$$

Step 2: Allocate cables and struts among agents according to $\Omega(p^*)$, and design the member function for each allocated member. Finally, from $\Omega(p^*)$, p^*, and each member function, calculate the stress matrix $\Omega(p)$ at any configuration p and derive the control law of each follower from the virtual force F.

Remark : Proof of the existence of $\Omega(p^*)$, interpretations of Step 1, design of the member functions, and derivation of $\Omega(p)$ are omitted in this abstract due to limitations in space.

3 Simulation results

In a four-agent case, we assign the desired formation as a unit square. The simulation results are shown below:

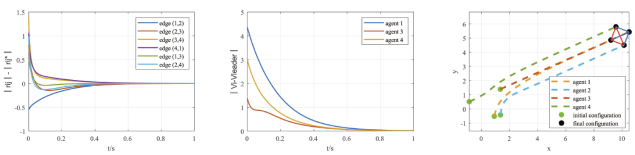

Figure 1: Member length errors and follower velocity errors converge to zero; the trajectories of the overall formation.

References

[1] Connelly, Robert, and Steven J. Gortler. "Iterative universal rigidity." Discrete Computational Geometry 53.4 (2015): 847-877.

Constrained consensus of hierarchical multi-agent systems with a time-varying set of active agents

Victor Daniel Reyes Dreke[1], Mircea Lazar[1]
[1] Control Systems Group, Eindhoven University of Technology, 5600 MB Eindhoven, The Netherlands
Email: v.d.reyes.dreke@tue.nl

1 Introduction

Hierarchical multi-agent systems (H-MAS) are important in many applications, such as modular multilevel converters (MMCs), microgrids, and water pumping systems [1]. In the examples above, a leader like the grid operator coordinates the control actions of the rest of the system's agents (followers) to reach a common goal (a consensus value), like a certain amount of power demand. Calculating and coordinating control actions is a challenge that grows in complexity depending on the common goal and system characteristics. This task is even harder if the H-MAS has a topology that changes over time or if it is limited in some way, like by having a limited number of active agents.

2 Motivation

In this paper, we refer to H-MASs with changing topologies as time-varying hierarchical multi-agent systems (TH-MAS) as it is the case with, e.g., MMCs and water pumping systems. In these situations, limiting the number of active agents can make them last longer or help reach a common goal. Therefore, it is of interest to investigate if consensus can be reached in a H-MAS with a leader-follower architecture and with a time-varying set of active agents. Figure 1 depicts a general representation of these systems.

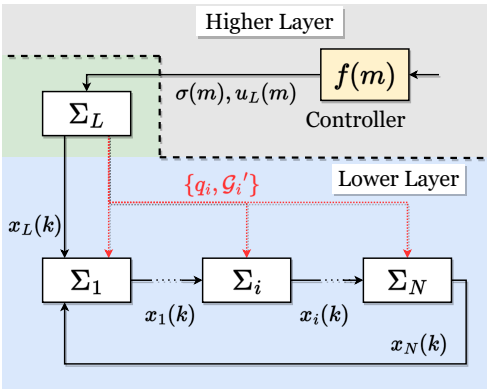

Figure 1: TH-MAS illustration.

For the studied TH-MAS, the agents dynamics is considered as

$$\Sigma_i: \; x_i(k+1) = A_i x_i(k) + q_i(k) B_i u_i(k), \tag{1}$$

where $w \in \mathbb{R}$, x_i and $u_i \in \mathbb{R}$ are the ith agent state and control input, respectively and $q_i \in \{0,1\}$ is a selection variable determining which agents are controlled at each time instant k. The control objective is to achieve consensus among the agents, such that

$$x_1(k) = \ldots = x_i(k) = \ldots = x_N(k) = x_L(k) \tag{2}$$

subject to

$$\sum_{i=1}^{N} q_i(k) = \sigma(m), \quad \forall k = mM, \tag{3}$$

where $\sigma(m) \in \{1, \ldots, N\}$ is a signal coming from a higher control layer to determine the active agents.

3 Approach

For reaching consensus in a TH-MAS, we propose a switching algorithm that will coordinate the control actions by determining which followers should be active at any discrete time instant. Moreover, based on fundamental results from [2] and [3], we prove that under the newly developed switching algorithm, the states of all follower agents reach consensus. For evaluating the results of the proposed method, we tested the proposed control algorithm in two simulation examples describing a MMC and a water pumping system. Partial results are shown in Figure 2.

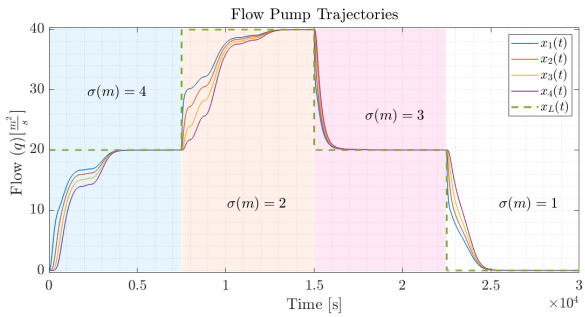

Figure 2: Pump flows using the proposed switching algorithm.

References

[1] V. D. Reyes Dreke and M. Lazar, "Consensus of hierarchical multi-agent systems with a time-varying set of active agents," *arXiv:2212.00455*, 2022.

[2] J. Lunze, *Networked Control of Multi-Agent Systems*, vol. 1. Bookmundo, 1 ed., 2019.

[3] W. Ren and R. W. Beard, "Consensus seeking in multiagent systems under dynamically changing interaction topologies," *IEEE Transactions on Automatic Control*, vol. 50, pp. 655–661, 5 2005.

Gaussian process regression with correlated noisy inputs

Thomas Edridge
Delft Center for Systems and Control, TU Delft,
Mekelweg 2, 2628 CD Delft
t.i.edridge@tudelft.nl

Manon Kok
Delft Center for Systems and Control, TU Delft,
Mekelweg 2, 2628 CD Delft
m.kok-1@tudelft.nl

1 Introduction

A Gaussian Process (GP) learns functions from noisy data [1], which can be collected from the environment using sensors. Considering an array of sensors, we explore how including this *physical knowledge* can be used to learn a function. Our goal is to use an array of magnetometers to learn the ambient magnetic field which is useful in magnetic field simultaneous localisation and mapping (SLAM) [2]. In SLAM, sensor locations are the inputs and the measured magnetic field is the output to the GP. Normally, GP regression assumes deterministic inputs but in SLAM, input locations are stochastic. One way of to handle noisy inputs is noisy input GP (NIGP) [3]. We extend on this method, by including the *physical knowledge* that sensors are placed on an array, such that the inputs become fully correlated.

2 Previous work

In GP regression, data y is collected from sensor measurements at locations x and is used to learn a function $f(x)$. The posterior is normally distributed with predictive mean μ_* and covariance Σ_{**} as

$$\begin{aligned} f(x_*) &\sim \mathcal{N}(\mu_*, \Sigma_{**}), \\ \mu_* &= \mathrm{K}(x_*,x)(\mathrm{K}(x,x)+\Sigma_y)^{-1}y, \\ \Sigma_{**} &= \mathrm{K}(x_*,x_*) - \mathrm{K}(x_*,x)(\mathrm{K}(x,x)+\Sigma_y)^{-1}\mathrm{K}(x,x_*). \end{aligned} \tag{1}$$

Here, Σ_y is sensor noise covariance and $\mathrm{K}(x,x)$ is a kernel function. The * denotes a prediction location. Here, we assume deterministic inputs, where we have stochastic inputs.

3 Our method

In NIGP, every input location is considered independent. We place multiple sensors on an array, introducing rigid-body constraints, which we include in the matrix H. This creates correlations between input locations, which allows us to take more information from the posterior gradient. The resulting predictive posterior for our method is:

$$\begin{aligned} \widetilde{f}(x_*) &\sim \mathcal{N}(\widetilde{\mu}_*, \widetilde{\Sigma}_{**}), \\ \widetilde{\mu}_* &= \mathrm{K}(x_*,x)(\mathrm{K}(x,x)+\Sigma_y+\widetilde{\Sigma}_x(x))^{-1}y, \\ \widetilde{\Sigma}_{**} &= \mathrm{K}(x_*,x_*) - \mathrm{K}(x_*,x)(\mathrm{K}(x,x)+\Sigma_y+\widetilde{\Sigma}_x(x))^{-1}\mathrm{K}(x,x_*), \\ \widetilde{\Sigma}_x(x) &= \nabla^T f(x) H \Sigma_x H^T \nabla f(x), \end{aligned} \tag{2}$$

where Σ_x is the input covariance and $\nabla f(x)$ is the gradient.

4 Results

We compare our method against NIGP and GP in with an array of 3 sensors. The results are shown in Figure 1. GP overfits and has a large RMSE of 0.334, as it neglects input uncertainty. NIGP has a smaller RMSE of 0.193 than GP, but has a larger variance. In our method we provide more information in the form of correlations, which reduces the variance and results in an RMSE of 0.133.

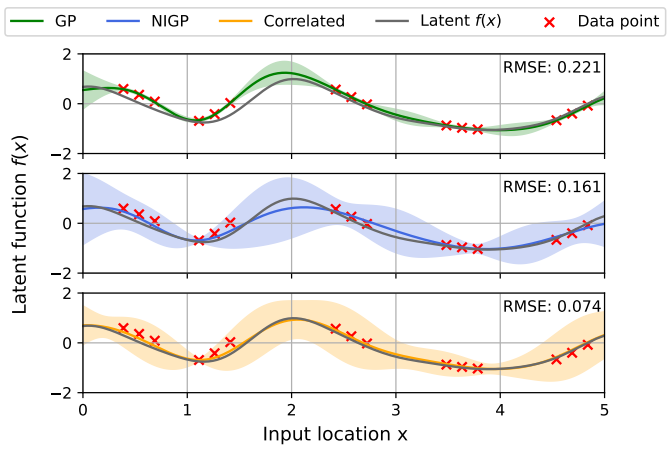

Figure 1: Regression with GP (green), NIGP (blue) and our method (orange), all with mean and a confidence interval of 95%. Data are in red and the latent function $f(x)$ is in grey.

References

[1] C.K.I. Williams and C.E. Rasmussen. *Gaussian processes for machine learning*, volume 2. MIT press Cambridge, MA, 2006.

[2] M. Kok and A. Solin. Scalable magnetic field slam in 3D using Gaussian process maps. In *Proceedings of the 21st international conference on information fusion (FUSION)*, pages 1353–1360. IEEE, 2018.

[3] A. McHutchon and C.E. Rasmussen. Gaussian process training with input noise. *Advances in Neural Information Processing Systems*, 24, 2011.

Enabling Distributed Computation in Multiagent Systems via k-dimensional Agreement

Gianluca Bianchin
ICTEAM & Dept of Mathematical Engineering
Université Chatolique de Louvain
gianluca.bianchin@uclouvain.be

Emiliano Dall'Anese
Department of Electrical Engineering
University of Colorado Boulder
emiliano.dallanese@colorado.edu

Jorge Cortés
Dept of Mechanical Engineering
University of California San Diego
cortes@ucsd.edu

Miguel Vaquero
School of Science and Technology
IE University
mvaquero@faculty.ie.edu

In this work, we study k-dimensional agreement problems, whereby a group of agents seeks to compute k linearly independent weighted means of a vector of initial estimates whose entries are known only locally. This problem is especially relevant in distributed computing and sensing applications, where a group of agents is interested in evaluating several independent functions at a common point by running a single distributed algorithm. We propose the use of continuous-time linear protocols for this task, and we show that linear dynamics can agree on quantities that are oblique projections of the vector of initial estimates. We provide necessary and sufficient conditions characterizing all protocols that can achieve an agreement, and we propose a design procedure for constructing such protocols. Overall, our results suggest that agreement requires the use of communication graphs with higher connectivity as compared to consensus algorithms; more precisely, we relate the existence of Hamiltonian decompositions in a graph with the capability of that graph to sustain an agreement protocol.

Synchronization algorithms and consensus protocols are central to many network coordination problems, including rendezvous, distributed convex optimization, and distributed computation and sensing. Although an extensive literature has been developed on consensus-based processes – whereby the states of the network nodes asymptotically reach a *common* value that is a weighted mean of the agents' initial estimates [1, 2] – in many applications it is instead of interest to assign, asymptotically, $k \geq 1$ *independent* weighted means (i.e. whose vectors of weights are linearly independent) of the initial estimates. Relevant examples of this problem include distributed computation [3], where the weighting accounts for different desired outcomes, task allocation algorithms [4], where weights account for heterogeneous computational capabilities, distributed sensing [5, 6] where the weighting is proportional to the accuracy of each sensing device, and robotic formation [7] where one agent achieves a certain configuration relative to another agent.

Given a vector $x(0)$, describing the initial estimates of the agents and an arbitrary matrix W of rank k describing desired mean weights, we say that the group reaches a k-dimensional agreement if, asymptotically, the agents' states converge to $Wx(0)$. As is commonly done, we model the flow of information between agents using a directed graph; our goal is to identify what classes of graphs are sufficiently rich to enable k-dimensional agreement and to determine, when possible, a distributed agreement protocol compatible with such graph.

References

[1] V. D. Blondel, J. M. Hendrickx, A. Olshevsky, and J. N. Tsitsiklis, "Convergence in multiagent coordination, consensus, and flocking," in *IEEE Conf. on Decision and Control*, 2005, pp. 2996–3000.

[2] R. Olfati-Saber and R. M. Murray, "Consensus problems in networks of agents with switching topology and time-delays," *IEEE Transactions on Automatic Control*, vol. 49, no. 9, pp. 1520–1533, 2004.

[3] G. Malewicz, M. H. Austern, A. J.-C. Bik, J. C. Dehnert, I. Horn, N. Leiser, and G. Czajkowski, "Pregel: a system for large-scale graph processing," in *International Conference on Management of data*, 2010, pp. 135–146.

[4] H.-L. Choi, L. Brunet, and J. P. How, "Consensus-based decentralized auctions for robust task allocation," *IEEE Transactions on Robotics*, vol. 25, no. 4, pp. 912–926, 2009.

[5] L. Zhao and A. Abur, "Multi area state estimation using synchronized phasor measurements," *IEEE Transactions on Power Systems*, vol. 20, no. 2, pp. 611–617, 2005.

[6] F. Pasqualetti, R. Carli, A. Bicchi, and F. Bullo, "Distributed estimation and detection under local information," in *IFAC Workshop on Distributed Estimation and Control in Networked Systems*, Annecy, France, Sep. 2010, pp. 263–268.

[7] K.-K. Oh, M.-C. Park, and H.-S. Ahn, "A survey of multi-agent formation control," *Automatica*, vol. 53, pp. 424–440, 2015.

Spectral identification in networks of pulse-coupled oscillators

Marvyn Gulina and Alexandre Mauroy
Namur Institute for Complex Systems (naXys) and Department of Mathematics,
University of Namur, Rue de Bruxelles 61, B-5000 Namur, Belgium
Email: marvyn.gulina@unamur.be and alexandre.mauroy@unamur.be

1 Spectral identification of networks

Spectral network identification aims at estimating the eigenvalues of the network Laplacian matrix from data. This framework allows to infer global network information (e.g., mean node degree, bounds on minimal and maximal degrees, etc.) from local observations at a small number of nodes. It was initially developed for networks of diffusive-coupled units [3], [4], and has not be used for applications that require other types of coupling. In this work, we fill this gap by considering spectral identification in the case of pulse-coupled oscillators, which is the prototypical model in neuroscience.

2 Pulse-coupled oscillators

We consider a network of N identical weakly pulse-coupled phase oscillators $\theta_i \in \mathbb{S}$ described by the dynamics

$$\dot{\theta}_i = \omega + \varepsilon \sum_{j=1}^{N} \sum_{k\in\mathbb{N}} \boldsymbol{A}_{ij} Z(\theta_i(t))\, \delta(t-\tau_j^{(k)}), \;\; i=1,\dots,N \quad (1)$$

where ω is the natural frequency, $\boldsymbol{A}_{ij}$ are the entries of the network adjacency matrix $\boldsymbol{A}$, $Z:\mathbb{S}\to[0,2\pi[$ is the so-called phase response curve (PRC), and $\{\tau_j^{(k)}\}_{k\in\mathbb{N}}$ is a sequence of firing (i.e., spiking) times such that $\theta_j(\tau_j^{(k)})=0$. Moreover, we assume that the coupling is weak, i.e., $\varepsilon \ll 1$, and that the oscillators synchronize, i.e., $\lim_{t\to\infty}\theta_j(t)=\theta^*(t)$ for all j (with $\dot{\theta}^*=\omega$).

We measure spiking times series $\{\tau_j^{(k)}\}_{k\in\mathbb{N}}$ for a few nodes j and we aim at estimating (some information on) the eigenvalues of the network Laplacian matrix $\boldsymbol{L}$ (i.e., $\boldsymbol{L}=\boldsymbol{D}-\boldsymbol{A}$, where $\boldsymbol{D}$ is the matrix of in-degrees).

3 Stroboscopic map and weak coupling

Denote $\bar{\theta}_i[k] := \theta_i(kT)$ and define the stroboscopic map $\boldsymbol{S}:\mathbb{S}^N\to\mathbb{S}^N$ such that

$$\bar{\theta}_i[k+1] = \boldsymbol{S}_i(\bar{\theta}_1[k],\dots,\bar{\theta}_N[k]).$$

Under the weak coupling assumption, we can use averaging techniques to approximate the Jacobian matrix of the stroboscopic map by

$$\boldsymbol{J} = \boldsymbol{I} + \varepsilon Z'(0)\boldsymbol{L}. \quad (2)$$

It follows that we can recover the spectrum of L from the spectrum of J.

4 Numerical experiments

In practice, the procedure consists of three main steps:

1. Estimate the sequence of phases from measured spiking time sequences.
2. Estimate the eigenvalues of the Jacobian matrix by using the DMD algorithm [2] with the approximated phases.
3. Identify the eigenvalues of the Laplacian matrix using equation (2).

This procedure will be illustrated on synthetic spiking time series generated by the dynamics (1). In particular, we will report on preliminary results such as estimating the number of clusters in networks of varying sizes using the spectral gap of the identified Laplacian spectrum.

These early findings open the door to applications in neuroscience, e.g., performing the spectral identification on pulse-coupled FitzHugh – Nagumo neurons [1].

References

[1] R. FitzHugh, "Impulses and physiological states in theoretical models of nerve membrane," *Biophysical Journal*, vol. 1, no. 6, pp. 445–466, Jul. 1961. DOI: 10/dmw38k.

[2] P. J. Schmid, "Dynamic mode decomposition of numerical and experimental data," *Journal of Fluid Mechanics*, vol. 656, pp. 5–28, Jul. 2010, ISSN: 1469-7645. DOI: 10/frnm7m.

[3] A. Mauroy and J. Hendrickx, "Spectral identification of networks using sparse measurements," *SIAM Journal on Applied Dynamical Systems*, vol. 16, no. 1, pp. 479–513, Jan. 2017, ISSN: 1536-0040. DOI: 10/f9336p.

[4] M. Gulina and A. Mauroy, "Spectral identification of networks with generalized diffusive coupling," *IFAC-PapersOnLine*, vol. 55, no. 30, pp. 492–497, 2022. DOI: 10/grjq2t.

Frequency domain parametric estimation of fractional order impedance models for Li-ion batteries

Freja Vandeputte* Noël Hallemans*,** Nessa Fereshteh Saniee**
Widanalage Dhammika Widanage** John Lataire*

*ELEC, Vrije Universiteit Brussel
Pleinlaan 2, 1050 Brussel, Belgium

**WMG, University of Warwick
7AL-CV4 Coventry, United Kingdom

Email: Freja.Vandeputte@vub.be

1 Introduction

Electrochemical impedance spectroscopy (EIS) is a powerful data-driven technique for estimating the impedance of a Li-ion battery from current and voltage measurements. In classical EIS, as implemented in commercial cyclers and potentiostats, the battery impedance is estimated *nonparametrically*, i.e. in a discrete set of excited frequencies. The nonparametric impedance estimate is then often interpreted by means of an equivalent electrical circuit model (ECM), whose components relate to the physical processes occurring in the battery. The idea of this research however, is to estimate the battery impedance *parametrically*, by using such an ECM as underlying parametric model. Therefore, we propose a consistent parametric estimation algorithm in the frequency domain, based on a fractional order model of the battery impedance. The parametric impedance estimate has the advantage that it can be evaluated in every frequency of the frequency band of interest. Moreover, we are not limited to a single sine or odd random phase multisine excitation signal. Instead, the parametric estimation algorithm works for any persistently exciting signal, like for example a Gaussian white noise excitation signal. The parametric estimation algorithm is first validated on simulations and then applied to measurements of commercial Samsung 48X cells.

2 Impedance based battery model

A Li-ion battery can be modelled as a voltage source, called the open circuit voltage (OCV), in series with the impedance. The measured input and output signals are then respectively the current through and the voltage over the battery. For now, the battery impedance is assumed to be a linear time-invariant (LTI) system. In practice, this means that we have to measure in steady state, so after relaxation, with a small amplitude zero mean excitation signal. Indeed, since the relationship between the current and the voltage in a battery is inherently slightly nonlinear, the amplitude of the excitation current must be kept sufficiently small to satisfy the linearity assumption. If, in addition, the excitation current is also zero mean, the state of charge (SOC) of the battery will remain approximately constant after relaxation, such that the time-invariance assumption is fulfilled as well.

The battery impedance can be modelled parametrically by a Randles ECM with a Warburg element to model the diffusion, which is the main physical process in a battery at low frequencies. The Warburg impedance, and thus also the total battery impedance, are functions of the Warburg variable $\sqrt{s}$, where s denotes the Laplace variable. Hence, in the frequency domain, diffusion results in a rational transfer function in $\sqrt{s}$. In the time domain, this corresponds to a so-called fractional differential equation (FDE) [1].

3 Parametric estimation algorithm

The equation error of the FDE, computed in the frequency domain, is linear in the parameters, so that its minimisation becomes a total least squares (TLS) problem, which can be solved with the singular value decomposition of the regression matrix. Weighting the regression matrix with the variances of the equation error makes the estimation consistent.

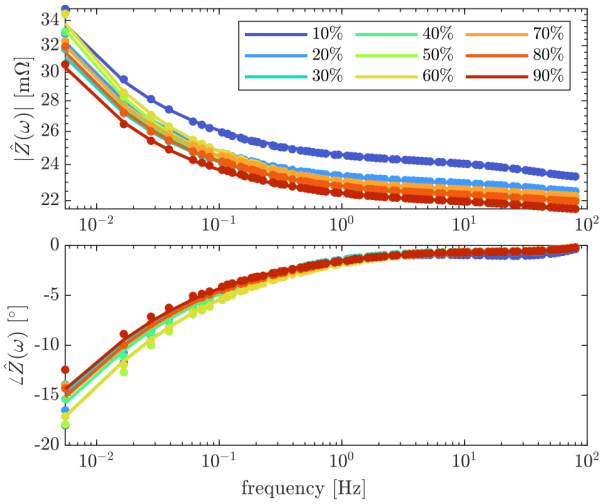

Figure 1: Bode plot of the nonparametric (dots) and parametric (lines) impedance estimates at different SOC levels.

References

[1] R. Pintelon, J. Schoukens, L. Pauwels, and E. Van Gheem, Diffusion systems: Stability, modeling, and identification, *IEEE Transactions on Instrumentation and Measurement*, 54, 2005.

Learning physical models using Hamiltonian Neural Networks with output error noise models

Sarvin Moradi[a,c] s.moradi@tue.nl
Nick Jaensson[b,c] n.o.jaensson@tue.nl
Roland Tóth[a,c,d] r.toth@tue.nl
Maarten Schoukens[a,c] m.schoukens@tue.nl

[a]Control Systems, [b]Processing and Performance of Materials Group, Eindhoven University of Technology, Eindhoven, Netherlands
[c]Eindhoven Artificial Intelligence Systems Institute, Eindhoven, Netherlands
[d]Systems and Control Laboratory, Institute for Computer Science and Control, Budapest, Hungary

1 Introduction

Hamiltonian neural networks (HNNs) [1] are a physics-based modeling tool in which Hamiltonian mechanics are embedded as prior knowledge in the neural network. Although HNNs have been successfully applied to model a wide range of academic examples, their application in modeling engineering systems remains challenging. In the HNN approach, it is assumed that noiseless data records of the state and its time derivatives are available, and that the system is energy conservative. However, real-life engineering systems are, in most cases, subjected to inputs, the measured data records are noisy and they are also energy dissipative. The current study addresses modeling physical systems with inputs and noisy measurements. In order to handle the noise in the measurements properly, an output-error model structure is introduced in the HNN approach, which results in the so-called output-error Hamiltonian neural network (OE-HNN) method. In addition, the introduction of the generalized Hamiltonian theory to OE-HNNs enables us to include external inputs into the approach [2].

2 Proposed method

In Hamiltonian mechanics, the total energy of the system E_{tot} is conserved and defined as the Hamiltonian of the positions $\mathbf{q}(t)$ and momenta $\mathbf{p}(t)$. In the generalized version of Hamiltonian theory, the inputs $\mathbf{u}(t)$ are added to the relation with $\mathbf{G}$ as the input matrix

$$\dot{\mathbf{q}} = \frac{\partial H}{\partial \mathbf{p}}, \quad \dot{\mathbf{p}} = -\frac{\partial H}{\partial \mathbf{q}} + \mathbf{G}\mathbf{u}(t). \tag{1}$$

We consider systems with continuous-time state-space equations as

$$\begin{aligned} \dot{\mathbf{x}}(t) &= f(\mathbf{x}(t), \mathbf{u}(t)), \\ \mathbf{y}(t) &= \mathbf{C}\mathbf{x}(t) + \mathbf{v}(t), \end{aligned} \tag{2}$$

in which $\mathbf{x}(t) = (\mathbf{q}(t), \mathbf{p}(t))^\top$, and f describes the evolution of $\mathbf{x}$, i.e., the dynamics of the system. The output measurements $\mathbf{y}(t)$ are contaminated by $\mathbf{v}(t)$, a zero-mean i.i.d. (white) noise with finite variance. It is assumed that $\mathbf{C} = \mathbf{I}$. Here, the goal is to train the neural network which represents the parameterized Hamiltonian H_θ. During the training of the neural network via backpropagations, derivatives of the neural network (H_θ) with respect to states, $\mathbf{x}$, are calculated via automatic differentiation resulting in the state time derivatives. These state derivatives are fed into an ODE-solver to predict the states at the next time step. The details of the training procedure are depicted in Figure 1 in which the loss function is defined as

$$\begin{aligned} &\min_\theta \sum_{k=1}^{N} \frac{1}{N} \left\| \mathbf{y}(kT_s) - \hat{\mathbf{y}}(kT_s) \right\|_2 \\ &\text{s.t.} \quad \dot{\hat{\mathbf{x}}}(t) = \mathbf{J}\frac{\partial H_\theta}{\partial \hat{\mathbf{x}}}(t) + \mathbf{G}\mathbf{u}(t) \\ &\qquad \hat{\mathbf{y}} = \mathbf{C}\hat{\mathbf{x}}(t), \end{aligned} \tag{3}$$

where $\hat{\mathbf{y}}(kT_s)$ is the the simulated model output with T_s as sampling rate, and $\mathbf{J} = \begin{bmatrix} \mathbf{0} & \mathbf{I} \\ -\mathbf{I} & \mathbf{0} \end{bmatrix}$.

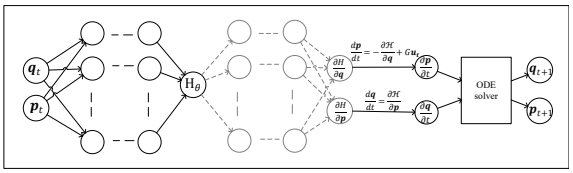

Figure 1: Output-error Hamiltonian neural network.

3 Example

In order to illustrate the performance of the proposed OE-HNN approach, two connected spring-mass systems subjected to a multisine input is studied. In Figure 2, the competency of the proposed approach in simulating the system is evident.

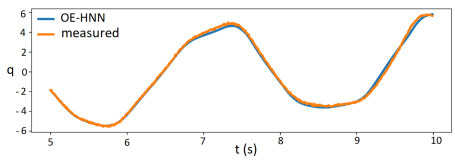

Figure 2: Simulated vs measured position of the second mass (q_2).

This work is part of the DAMOCLES research project, which received funding from the Eindhoven Artificial Intelligence Systems Institute, as part of the EMDAIR funding program.

References

[1] Greydanus, S. J., Dzumba, M., Yosinski, J., "Hamiltonian Neural Networks," *Proc. of the 33rd Conference on Neural Information Processing Systems*, Vancouver, Canada, 2019.
[2] Moradi, S, Jaensson, N., Tóth, R., Schoukens, M., "Physics-Informed Learning Using Hamiltonian Neural Networks with Output Error Noise Models," *under review at IFAC 2023.*

Connection between DTLS as an MEVP and as a Riemannian SVD

Sem Viroux and Bart De Moor, *Fellow IEEE, SIAM, IFAC*
Center for Dynamical Systems, Signal Processing, and Data Analytics (STADIUS),
Department of Electrical Engineering (ESAT), KU Leuven, 3001 Leuven, Belgium
sem.viroux@esat.kuleuven.be, bart.demoor@esat.kuleuven.be

1 Introduction

Previous work of our research group has shown how the least-squares optimal realisation of an autonomous linear time-invariant (LTI) system can be obtained by solving a multiparameter eigenvalue problem (MEVP) [3]. The globally optimal solution(s) of the non-convex optimisation problem can be found via the eigentuples of the MEVP. An alternative formulation of the problem, based on a structured total least-squares problem [1], is given by a so-called Riemannian singular value decomposition (SVD), which can be solved using a heuristic method [2]. We compare both approaches, investigate how they relate to each other, and try to extend the latter such that global optimality is guaranteed.

2 Dynamic total least squares (DTLS)

Given a sequence of single-input single-output (SISO) data $\boldsymbol{w} = \begin{bmatrix}\boldsymbol{u}^\mathsf{T} & \boldsymbol{y}^\mathsf{T}\end{bmatrix}^\mathsf{T} \in \mathbb{R}^{2N}$, we wish to identify an LTI model that has $\hat{\boldsymbol{w}} = \begin{bmatrix}\hat{\boldsymbol{u}}^\mathsf{T} & \hat{\boldsymbol{y}}^\mathsf{T}\end{bmatrix}^\mathsf{T} \in \mathbb{R}^{2N}$, an approximation of the observed data, in its behaviour (i.e., $\hat{\boldsymbol{w}}$ exactly satisfies the model equations). The model is chosen so that the 2-norm of the misfit $\tilde{\boldsymbol{w}} = \boldsymbol{w} - \hat{\boldsymbol{w}}$ is minimised.

The dynamic total least squares (DTLS) realisation problem is formulated as follows:

$$\begin{aligned} \min_{\boldsymbol{a},\boldsymbol{b}} \quad & \sigma^2 = \|\tilde{\boldsymbol{u}}\|_2^2 + \|\tilde{\boldsymbol{y}}\|_2^2 = \|\boldsymbol{u} - \hat{\boldsymbol{u}}\|_2^2 + \|\boldsymbol{y} - \hat{\boldsymbol{y}}\|_2^2 \,, \\ \text{s.t.} \quad & \sum_{i=0}^{n} a_i \hat{y}_{k+n-i} = \sum_{i=0}^{n} b_i \hat{u}_{k+n-i} \quad k = 0, \ldots, N-n-1 \,, \\ & a_0 = 1 \,, \end{aligned} \tag{1}$$

where $\boldsymbol{a}, \boldsymbol{b} \in \mathbb{R}^{n+1}$ contain the coefficients of the nth order difference equation governing the dynamics of the LTI model. This model class is a special case of the misfit-versus-latency framework [4]. Figure 1 schematically illustrates the relations given in (1).

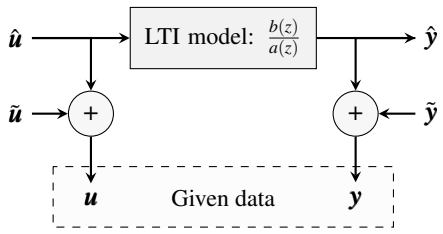

Figure 1: Schematic overview of the identification problem. The given input/output data $(\boldsymbol{u}, \boldsymbol{y})$ is decomposed in a regular part $(\hat{\boldsymbol{u}}, \hat{\boldsymbol{y}})$ that satisfies the LTI model, and a misfit part $(\tilde{\boldsymbol{u}}, \tilde{\boldsymbol{y}})$, the 2-norm of which is to be minimised.

3 MEVP

Notice that the DTLS problem of (1) is of multivariate polynomial nature: the objective function is a sum of squares, and all the constraints are multivariate polynomials in the unknowns ($\hat{\boldsymbol{u}}$, $\hat{\boldsymbol{y}}$, $\boldsymbol{a}$, and $\boldsymbol{b}$). Upon invoking Lagrange multipliers, the first order necessary conditions for optimality can be composed. This results in a system of multivariate polynomial equations, which can be reformulated as an MEVP, the eigentuples of which characterise all the stationary points of the identification problem [3]. After evaluation of the eigentuples in the objective function, the globally optimal solution(s) can be identified.

4 STLS & Riemannian SVD

An alternative, but equivalent, approach to solve the DTLS problem is given by approximating a "double Hankel" matrix $\mathbf{A} = \begin{bmatrix}\mathbf{Y} & \mathbf{U}\end{bmatrix}$ constructed from the observed data by a rank deficient matrix $\mathbf{B}$, which has the same affine matrix structure as $\mathbf{A}$, such that the objective σ^2 in equation (1) is minimal. The minimising matrix $\mathbf{B}$ is related to the singular triplet $(\boldsymbol{u}, \tau, \boldsymbol{v})$ with smallest singular value of the so-called Riemannian SVD [2]:

$$\begin{aligned} \mathbf{A}\boldsymbol{v} &= \mathbf{D}_{\boldsymbol{v}}\boldsymbol{u}\tau \,, \quad \boldsymbol{u}^\mathsf{T}\mathbf{D}_{\boldsymbol{v}}\boldsymbol{u} = 1 \,, \\ \mathbf{A}^\mathsf{T}\boldsymbol{u} &= \mathbf{D}_{\boldsymbol{u}}\boldsymbol{v}\tau \,, \quad \boldsymbol{v}^\mathsf{T}\mathbf{D}_{\boldsymbol{u}}\boldsymbol{v} = 1 \,, \end{aligned}$$

where τ is the (unknown) singular value and $\boldsymbol{u}$ and $\boldsymbol{v}$ are the corresponding singular vectors. The latter corresponds to the model parameters: $\boldsymbol{v} = \begin{bmatrix}\boldsymbol{a}^\mathsf{T} & \boldsymbol{b}^\mathsf{T}\end{bmatrix}^\mathsf{T}$. The positive definite matrices $\mathbf{D}_{\boldsymbol{v}}$ and $\mathbf{D}_{\boldsymbol{u}}$ are nonlinear weighting matrices, with elements quadratic in the components of resp. $\boldsymbol{v}$ and $\boldsymbol{u}$.

We derive the connection between both formulations and investigate whether we can we use root-finding algorithms to solve for the smallest singular triplet of the Riemannian SVD, leading to the globally optimal solution(s) of the DTLS problem.

Acknowledgements

This work was supported in part by the KU Leuven: Research Fund (project C16/15/059), and several Leuven Research and Development bilateral industrial projects, in part by Flemish Government agencies: FWO (EOS project G0F6718N (SeLMA), and PhD grant SB/1SA1319N), EWI (Flanders AI Research Program), and in part by the European Commission (EU Research Council under the European Union's Horizon 2020 research and innovation programme (ERC Adv. Grant) under grant 885682).

References

[1] B. De Moor. Structured total least squares and l2 approximation problems. *Linear algebra and its applications*, 188(C):163–205, 1993.
[2] B. De Moor. Dynamic total linear least squares. *IFAC Symposium on System Identification*, 3(10):159–164, 1994.
[3] B. De Moor. Least squares optimal realisation of autonomous LTI systems is an eigenvalue problem. *Comm. in Inf. and Systems*, 20(2):163–207, 2020.
[4] P. Lemmerling and B. De Moor. Misfit versus latency. *Automatica*, 37:2057–2067, 2001.

Local Network Identifiability: Path Conditions

Antoine Legat and Julien M. Hendrickx*
ICTEAM Institute, UCLouvain, B-1348 Louvain-la-Neuve, Belgium.
Email: { antoine.legat, julien.hendrickx } @uclouvain.be

1 Introduction

We consider the identifiability of a network matrix $G(q)$, where the network is made up of n node signals stacked in the vector $w(t) = [w_1(t) \quad w_2(t) \ \cdots \ w_n(t)]^\top$, known external excitation signals $r(t)$, measured node signals $y(t)$ and unmeasured noise $v(t)$ related to each other by:

$$\begin{aligned} w(t) &= G(q)w(t) + Br(t) + v(t) \\ y(t) &= Cw(t), \end{aligned} \tag{1}$$

where matrices B and C are binary selections indicating respectively the n_B excited nodes and n_C measured nodes, forming sets $\mathscr{B}$ and $\mathscr{C}$ respectively.

The nonzero entries of the transfer matrix $G(q)$ define the network topology: $G_{ij}(q)$ is the transfer function from node j to node i, represented by an edge (j,i) in the graph. Some of those transfer functions are known and collected in matrix $G^\bullet(q)$, and the others are unknown, collected in matrix $G^\circ(q)$, such that $G(q) = G^\bullet(q) + G^\circ(q)$.

We assume that *the input-output relations between the excitations r and measurements y have been identified*, and that the network topology is known. From this knowledge, we aim at recovering an entry of $G^\circ(q)$, or a subset of them.

Example 1.

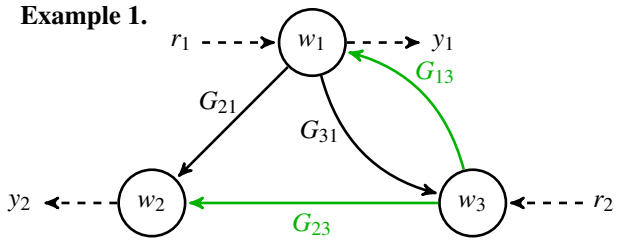

$$G^\circ = \begin{bmatrix} 0 & 0 & G_{13} \\ 0 & 0 & G_{23} \\ 0 & 0 & 0 \end{bmatrix}, \quad G^\bullet = \begin{bmatrix} 0 & 0 & 0 \\ G_{21} & 0 & 0 \\ G_{31} & 0 & 0 \end{bmatrix}, \ B = \begin{bmatrix} 1 & 0 \\ 0 & 0 \\ 0 & 1 \end{bmatrix},$$

$$C = \begin{bmatrix} 1 & 0 & 0 \\ 0 & 1 & 0 \end{bmatrix} \qquad G_{13} \text{ and } G_{23} \text{ are identifiable.}$$

A first line of work extends the classical closed-loop identification techniques to identify a single module, see e.g. [1]. A recent approach employs graph-theoretical tools to derive identifiability conditions on the graph of the network. Using this approach, [2] addresses the particular case where all nodes are excited/measured. In the general case of partial measurement *and* excitation, [3] introduces a local version of identifiability and derives algebraic necessary and sufficient conditions. In this work, we consider local identifiability with partial excitation and measurement. From the conditions of [3], we derive a path conditions which generalize the results of [2] when not all nodes are excited/measured.

* Work supported by the "RevealFlight" ARC at UCLouvain, and by the MIS grant "Learning from Pairwise Data" of the F.R.S.-FNRS.

2 Problem reformulation

Starting from the definition of a network system in (1), we first define $T(q) \triangleq (I - G(q))^{-1}$, which is assumed to be proper and stable. The input-output model of (1) is:

$$y(t) = C\,T(q)\,B\,r(t) + \tilde{v}(t),$$

where $\tilde{v}(t) \triangleq CT(q)v(t)$. We assume that $r(t)$ is sufficiently rich so that, for any B and C, $CT(q)B$ can be consistently estimated from $\{y(t), r(t)\}$ data. From the knowledge of $CT(q)B$, the aim is to identify $G^\circ(q)$. This motivates the following definition, which restricts the usual generic identifiability from [2] to non-discrete sets of solutions.

Definition 1. *The module G_{ij} is* locally identifiable *at G from excitations $\mathscr{B}$ and measurements $\mathscr{C}$ if there exists $\varepsilon > 0$ such that for any $\tilde{G}$ with same zero and known entries $G^\bullet$ as G satisfying $||\tilde{G} - G|| < \varepsilon$, there holds*

$$C\tilde{T}(q)B = CT(q)B \Rightarrow \tilde{G}_{ij} = G_{ij}, \tag{2}$$

where $\tilde{T}(q) = (I - \tilde{G})^{-1}$. G_{ij} is generically locally identifiable *if it is locally identifiable at* almost all *G.*

3 Results

In [3], a linearization of (2) yields a necessary and sufficient condition for generic local identifiability, based on the generic rank of a matrix K constructed from B, C and T.

In this work, we show how the generic rank of K relies on the generic rank of certain particular transfer matrices. Besides, we know from [2] that the generic rank of a transfer matrix can be characterized as paths in the network graph.

Combining those results allows to derive a necessary condition and a sufficient one for generic local identifiability in terms of paths in the network, which will pave the way for further developments in the subject.

References

[1] Van den Hof, P. M., Dankers, A., Heuberger, P. S., Bombois, X. "Identification of dynamic models in complex networks with prediction error methods—Basic methods for consistent module estimates," in *Automatica*, 2013.
[2] Hendrickx, J. M., Gevers, M., and Bazanella, A. S. "Identifiability of dynamical networks with partial node measurements," in *IEEE Trans. on Automatic Control*, 2018.
[3] Legat, A. and Hendrickx, J.M. "Local network identif with partial excitation and measurement," *IEEE CDC*, 2020.

Identifiability of diffusively coupled linear networks with partial instrumentation[1]

E.M.M. Kivits and P.M.J. Van den Hof
Control Systems Group, Department of Electrical Engineering
Eindhoven University of Technology, P.O. Box 513, 5600 MB Eindhoven, The Netherlands.
Email: e.m.m.kivits@tue.nl and p.m.j.vandenhof@tue.nl

1 Problem description and research questions

For analysing the identifiability of a network, we typically assume that all node signals can be measured [1]. However, some node signals might be unmeasurable. Sometimes, the dual case is studied, in which it is assumed that all node signals can be excited. This results in dual identifiability results, but also in very expensive experiments (as actuation is usually more expensive then sensing). Similar as before, it might be impossible to excite some node signals. To consider networks with unmeasurable and unexcitable node signals, we need to be more flexible in the experimental setup.

Our main research question is

Question 1: What conditions are needed to obtain identifiability of a diffusively coupled linear network?

In this general setting, we avoid the assumption that all node signals are measured or that all node signals are excited [2]. The identifiability conditions will include restrictions on the number (and possibly locations) of actuators and sensors. Therefore, we can also answer the question

Question 2: Where to place the instruments to obtain identifiability of a diffusively coupled linear network?

2 Diffusively coupled linear network

A diffusively coupled network is characterized by symmetric interconnections and therefore, it is typically represented by an undirected graph. This network is modelled as

$$A(q^{-1})w(t) = B(q^{-1})r(t) + v(t), \quad y(t) = C(q^{-1})w(t), \quad (1)$$

with node signals $w(t)$; excitation signals $r(t)$; process noises $v(t) = F(q)e(t)$ modelled as filtered white noise; measured signals $y(t)$; with symmetric polynomial matrix $A(q^{-1}) = \sum_{k=0}^{n_a} A_k q^{-k}$ with A_0 typically not equal to I and $A^{-1}(q^{-1})$ stable; polynomial matrices $B(q^{-1})$ and $C(q^{-1})$; and delay operator q^{-1}, i.e. $q^{-1}w(t) = w(t-1)$. The symmetry of the diffusive couplings is incorporated in the model (1) by the symmetry of $A(q^{-1})$.

[1] This project has received funding from the European Research Council (ERC), Advanced Research Grant SYSDYNET, under the European Union's Horizon 2020 research and innovation programme (grant agreement No 694504).

The input-output mapping of (1) is given by

$$y(t) = T_{yr}(q)r(t) + \bar{v}(t), \quad \bar{v}(t) = T_{ye}(q)e(t), \quad (2)$$

with rational transfer function matrices

$$T_{yr}(q) = C(q^{-1})A^{-1}(q^{-1})B(q^{-1}),$$
$$T_{ye}(q) = C(q^{-1})A^{-1}(q^{-1})F(q).$$

3 Approach

To analyse the identifiability of the network, we consider the uniqueness of the network model in the selected network model set. In other words: What conditions are needed to obtain a unique network model from experimental data? To answer this question, we analyse the input-output mapping (2), while making extensive use of the symmetric nature of the interconnection structure.

4 Result

Result 1: Identifiability conditions for of a diffusively coupled linear network.

The obtained identifiability conditions are much simpler than the ones for directed or nonsymmetric networks, due to the symmetry of the couplings that significantly reduce the degrees of freedom in the network model.

Result 2: A very simple instrumentation placement condition for identifiability of a diffusively coupled network.

Moreover, the identifiability conditions (and thus also the condition for actuator and sensor placement) can also be applied to a (diffusively coupled linear) subnetwork or single interaction.

References

[1] E.M.M. Kivits and P.M.J. Van den Hof, "Identification of diffusively coupled linear networks through structured polynomial models," To appear in IEEE Trans. Automatic Control, June 2023, ArXiv: 2106.01813.

[2] E.M.M. Kivits and P.M.J. Van den Hof, "Identifiability of diffusively coupled linear networks with partial instrumentation," Submitted to 22nd IFAC World Congress, 9-14 July 2023, Yokohama, Japan.

Nonlinear network identification: the static case

Renato Vizuete and Julien M. Hendrickx
ICTEAM, UCLouvain, 1348 Louvain-la-Neuve, Belgium
Email: {renato.vizueteharo, julien.hendrickx}@uclouvain.be

1 Introduction and problem formulation

Traditionally, the network identification problem has been mainly restricted to linear transfer functions. However, most of the networked dynamical system are characterized by nonlinear interactions among the nodes (e.g., neural networks, power networks) and hence conditions for the network identification need to be derived for the nonlinear case.

For a network composed by n nodes, we consider that the output of each node i is given by:

$$y_i(k) = \sum_{j \in \mathcal{N}_i} f_{ij}(y_j(k-1)) + u_i(k-1), \text{ for all } i \in \{1, \dots, n\}, \tag{1}$$

where f_{ij} is a nonlinear function, $\mathcal{N}_i$ is the set of in-neighbors of node i, and u_i is an external excitation signal. Notice that when the nonlinear functions f_{ij} are polynomial, the model (1) is an approximation of the well-known Volterra-series formulation since each $y_j(k-1)$ can also be considered as an input for the node i [1].

We assume that all the nodes are excited and the topology of the network is known; this implies that we know which nodes are connected by nonzero functions. The objective is to determine which nodes need to be measured to identify all the nonlinear functions in the network.

2 Path graph

To highlight the difference with the linear identification problem, we focus on a path graph due to its importance in the determination of conditions for the identifiability of linear networks [2], [3]. We consider the path graph with 3 nodes presented in Fig. 1. We excite all the nodes (u_1, u_2, u_3) and measure only the sink (y_3). It is well known that in the linear case, for this graph topology we only need to measure the sink to identify all the transfer functions of the network thanks to the superposition principle [2]. However, this is not true for the nonlinear case.

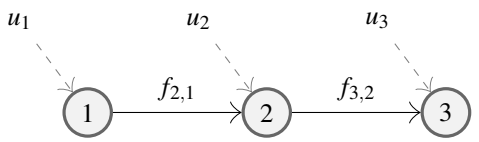

Figure 1: Nonlinear functions in a path graph with 3 nodes.

Let us assume that the function $f_{32}(x) = a_2 x$ is linear, and the function f_{21} is analytic and $f_{21}(0) \neq 0$ (e.g., $\cos(x)$, e^x). Thus, the function f_{21} can be expressed as $f_{21}(x) = a_1 + p(x)$, where $p(x)$ corresponds to the higher order terms of the Taylor series associated with f_{21}.

Based on the excitation signals and the measurement of the sink, we assume that a perfect identification of the function F is obtained:

$$y_3(k) = F(u_1(k-1), \dots, u_1(k-m_1), \dots, u_3(k-1), \dots, u_3(k-m_3)).$$

In our case, we get:

$$y_3(k) = u_3(k-1) + a_2 u_2(k-2) + a_2 g(u_1(k-3)) + a_1 a_2. \tag{2}$$

Unfortunately, due to the linear function f_{32}, the constant $a_1 a_2$ cannot be identified since it could be part of f_{21} or f_{32} or both. For instance, the alternative functions $\hat{f}_{21}(x) = p(x)$ and $\hat{f}_{32}(x) = a_2 x + a_1 a_2$ would generate the same nonlinear function (2). Although this analysis was performed in a path graph with 3 nodes, it is valid for any path graph with $m > 2$ nodes. This shows that unlike the linear case, in a path graph there exist nonlinear functions that cannot be identified by only measuring the sink.

Since the presence of constant factors in the nonlinear functions makes a network not identifiable, it is necessary to restrict the identification problem to a class of functions satisfying $f(0) = 0$. Finally, it is possible that the nonlinearities in the functions generate a unique flow of information through each path in a network, providing conditions for the identification that differ with respect to the linear case.

3 Acknowledgements

This work was supported by F.R.S.-FNRS via the *KORNET* project and via the Incentive Grant for Scientific Research (MIS) *Learning from Pairwise Comparisons*, and by the *RevealFlight* Concerted Research Action (ARC) of the Fédération Wallonie-Bruxelles.

References

[1] O. Nelles, *Nonlinear System Identification*. Springer, 2020.

[2] J. M. Hendrickx, M. Gevers, and A. S. Bazanella, "Identifiability of dynamical networks with partial node measurements," *IEEE Transactions on Automatic Control*, 2019.

[3] A. Legat and J. M. Hendrickx, "Path-based conditions for local network identifiability," in *IEEE CDC*, 2021.

Corridor Partitioning for Motion Planning in Structured Environments

Sonia De Santis, Joris Gillis, Wilm Decré and Jan Swevers
MECO Research Team, Department of Mechanical Engineering, KU Leuven, Belgium
Flanders Make@KU Leuven, Belgium
Email: sonia.desantis@kuleuven.be

1 Introduction

Developing optimized motion planning algorithms is a central topic in the robotics field. Among the possible applications, industrial ones largely benefit from fast optimized trajectory planning algorithms, as they play a significant role in improving efficiency, energy consumption, safety, etc.
This work targets motion planning in highly structured environments. Currently employed approaches tend to be cautious and conservative, allowing only motion with limited speeds and along predefined paths. On the other hand, optimization-based methods are typically too computationally intensive for cost-effective real-time implementation.
The purpose of this work is to develop a strategy that provides optimal solutions with respect to economic objectives (such as time, energy consumption, footprint) at a low computational cost. Furthermore, predictability of the solution should be enforced, as well as the possibility of shaping the trajectory based on the application at hand.

2 Proposed approach

The proposed approach breaks down the motion planning problem into three main strategies:

1. A set of application-specific motion primitives is devised offline to obtain predictable and human like trajectories;
2. A high-level optimal routing strategy is in charge of finding a globally optimal motion corridor;
3. A low-level optimal motion planner determines the optimal trajectory by partitioning the corridor in segments and, for each of them, deciding whether to assign a motion primitive or to solve a full-blown optimal control problem, where most effective.

3 Current work

A preliminary study is performed to address the corridor partitioning task. Initially, the time-optimal trajectory within an L-shaped corridor (see Figure 1) is analyzed, to devise a smart partition for this kind of corridors. We assume that the start and final position are given, with free orientation. A kinematic bicycle model describes the robot motion, where the control inputs are the velocity v and the steering angle δ, both upper and lower limited. The problem is formulated as a multi-stage optimal control problem, where the corridor is defined by two orthogonal rectangles and the

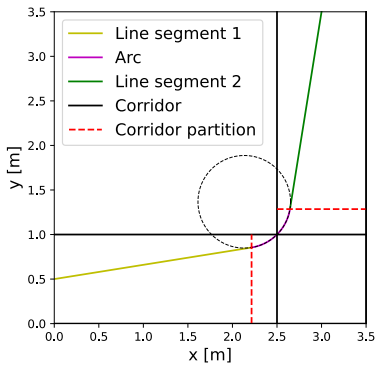

Figure 1: Path obtained by solving an optimal control problem within a corridor. A possible partition includes three segments, where three primitives can be selected.

condition to remain within their bounds is modeled as done in [1]. The solution turns out to be the sequence of three trajectory pieces: (1) a line segment with $\delta(t) = 0$, $v(t) = v_{max}$ for $t \in [t_0, t_1)$, (2) a circular arc with $\delta(t) = \delta_{max}$, $v(t) = v_{max}$ for $t \in [t_1, t_2)$, and (3) a second line segment for $t \in [t_2, t_f]$. Such solution can be derived analytically, since the second trajectory piece is part of a circle whose center and radius can be computed, knowing the parameters of the bicycle model and the size of the corridor. Then, the entire trajectory is constructed as: a line segment passing through the initial point and tangent to the circle, an arc belonging to the circle, and a line segment passing through the final point and tangent to the circle.
In future work, more complex scenarios and robot models will be considered and the influence on the solution of different applications will be investigated.

4 Acknowledgments

This work has been carried out within the framework of Flanders Make's SBO project ARENA (Agile & Reliable Navigation). Flanders Make is the Flemish strategic research centre for the manufacturing industry.

References

[1] M. Bos, W. Decré, J. Swevers and G. Pipeleers, "Multi-stage Optimal Control Problem Formulation for Drone Racing Through Gates and Tunnels," 2022 IEEE 17th International Conference on Advanced Motion Control (AMC), Padova, Italy, 2022, pp. 376-382

An efficient iterative scheme to compute an FIR filter

R. Haasjes[1]
r.haasjes@utwente.nl

A.P. Berkhoff[1,2]
a.p.berkhoff@utwente.nl

[1]University of Twente ET-AMDA, Drienerlolaan 5, 7522 NB Enschede (NL)
[2]TNO Acoustics and Sonar, Oude Waalsdorperweg 63, 2597 AK Den Haag (NL)

1 Introduction

Acoustic anechoic chambers are designed to absorb acoustic waves at its boundaries. In practice, low-frequency sound will be reflected at the walls due to limitations of the passive absorption measures. Active noise control is effective at lower frequencies, which makes this a promising addition to the passive wall absorption. Typical chamber dimensions are large, requiring a larger number of sources and sensors for satisfactory performance. The computational complexity increases rapidly for growing system sizes. This work proposes an efficient scheme to compute a finite impulse response controller, demonstrated by a multichannel example.

2 Approach

The proposed scheme is based on the work presented in [1], but substituted with the frequency-domain derived filters from [2], to reduce computational complexity. This results in the scheme as shown in Fig. 1.

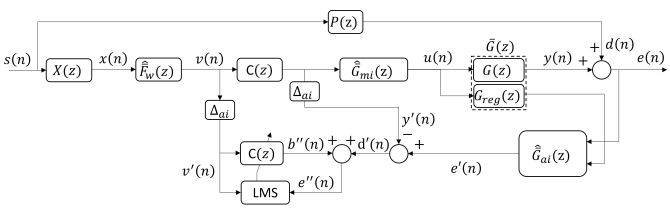

Figure 1: Block-scheme of the proposed algorithm [3].

The filter $\hat{\bar{F}}_w(z)$ is the prewhitening filter that applies prewhitening and decorrelation. The filter $\hat{\bar{G}}_{mi}(z)$ is the preconditioning filter, and the filter $\hat{\bar{G}}_{ai}(z)$ is the adjoint, which together decouple the system. These filters need an appropriate number of delay samples in order to ensure causality.

3 Simulation

The performance of the algorithm is shown using a 4-channel setup. The objective of the system is to reduce the reflections from the walls of the chamber, with the idea of improving an acoustic anechoic chamber. The decoupling of the plant for the first two channels is shown in Fig. 2. It can be seen that the plant is effectively diagonalized.

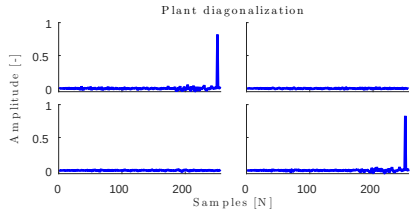

Figure 2: Decoupling of the plant using the filters $\hat{\bar{G}}_{mi}(z)$ and $\hat{\bar{G}}_{ai}(z)$.

The convergence of the algorithm is shown for the first two channels in Fig 3, where the controller converged to 13 dB reduction on the first channel and 14 dB on the second channel.

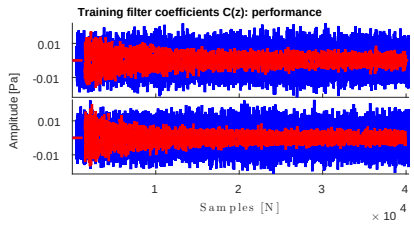

Figure 3: Convergence of the controller performance while running the proposed scheme.

4 Acknowledgements

This research is funded by TNO. The support and funding from TNO are gratefully acknowledged.

References

[1] A.P. Berkhoff and G. Nijsse. "A rapidly converging filtered-error algorithm for multichannel active noise control". In: Journal of Adaptive Control and Signal Processing (2007), pp. 556-569.

[2] M.R. Bai, S.J. Elliott. "Preconditioning multichannel adaptive filtering algorithms using EVD- and SVD-based signal prewhitening and system decoupling". In: Journal of Sound and Vibration 270 (2004), pp. 639-655.

[3] R. Haasjes and A.P. Berkhoff, "An efficient scheme to compute an FIR controller for active reduction of acoustic reflections in an anechoic chamber". In: Journal of Acoustical Society of America, submitted (2022).

Online constraint removal in MPC, satisfying constraints without imposing them

S.A.N. Nouwens
TU Eindhoven
s.a.n.nouwens@tue.nl

M.M. Paulides
TU Eindhoven

W.P.M.H. Heemels
TU Eindhoven

1 Introduction and problem description

Model predictive control (MPC) is a widely adopted optimization-based control strategy, where at each time instance a receding-horizon optimal control problem is solved to obtain the control input. Reducing the computation time of the receding-horizon optimal control problem is a well-established field of research. However, for a large class of control problems, where the system is constrained by many state constraints, the existing techniques are typically not highly effective in obtaining a real-time feasible control law. To fill this gap, we propose a new online constraint removal framework: constraint-adaptive MPC (ca-MPC). In so-called *exact* ca-MPC, we adapt the imposed constraints by removing, at each time-step, a subset of the state constraints in order to reduce the computational complexity of the receding-horizon optimal control problem, while ensuring that the closed-loop behavior is *identical* to that of the original MPC law.

To obtain an *exact* ca-MPC scheme, we seek state-dependent index sets $\mathbb{A}_i : \mathbb{R}^n \rightrightarrows \mathbb{N}_c$ (i.e., $\mathbb{A}_i(\boldsymbol{x}_k) \subseteq \{1,2,\dots,n_c\} =: \mathbb{N}_c$, where n_c denotes the number of state constraints) for each step in the horizon $i \in \mathbb{N}_N$, such that the minimizer of

$$\underset{\boldsymbol{u}_{i-1|k},\, i\in\mathbb{N}_N}{\text{minimize}} \sum_{i\in\mathbb{N}_N} \boldsymbol{x}_{i|k}^\top \boldsymbol{Q}\boldsymbol{x}_{i|k} + \boldsymbol{u}_{i-1|k}^\top \boldsymbol{R}\boldsymbol{u}_{i-1|k}, \tag{1a}$$

$$\text{subject to} \quad \boldsymbol{x}_{i|k} = \boldsymbol{A}\boldsymbol{x}_{i-1|k} + \boldsymbol{B}\boldsymbol{u}_{i-1|k}, \qquad i \in \mathbb{N}_N, \tag{1b}$$

$$\boldsymbol{f}_j \boldsymbol{x}_{i|k} \le h_j, \qquad j \in \mathbb{A}_i(\boldsymbol{x}_k), \quad i \in \mathbb{N}_N, \tag{1c}$$

$$\boldsymbol{u}_{i-1|k} \in \mathbb{U} \subseteq \mathbb{R}^m, \qquad i \in \mathbb{N}_N. \tag{1d}$$

is equivalent to the minimizer of (1) when choosing $\mathbb{A}_i(\boldsymbol{x}_k) = \mathbb{N}_c$. In (1), $\boldsymbol{x} \in \mathbb{R}^n$, $\boldsymbol{u} \in \mathbb{R}^m$ denote the state and input, $\boldsymbol{Q}$, $\boldsymbol{R}$, $\boldsymbol{A}$, $\boldsymbol{B}$ denote positive definite cost matrices and state space matrices of appropriate dimension, and $\boldsymbol{f}_j$, h_j denote the j-th state constraint.

Ideally, the cardinality of $\mathbb{A}_i(\boldsymbol{x}_k)$ is low, thereby, achieving a large reduction in state constraints, and, thus, a reduction in computational complexity. Note, in order to reduce the computational complexity of (1), computing the sets $\mathbb{A}_i(\boldsymbol{x}_k)$, $i \in \mathbb{N}_N$ themselves must be computationally cheap.

2 Methods and results

By exploiting forward and backward reachability, and the optimization-based nature of (1), we can bound the predicted states by p ellipsoids [1], i.e., $\boldsymbol{x}_{i|k} \in \bigcap_{j\in\mathbb{N}_p} \mathscr{E}_{i,j}(\boldsymbol{x}_k)$ for $i \in \mathbb{N}_N$. Here, $\mathscr{E}_{i,j}(\boldsymbol{x}_k) \subset \mathbb{R}^n$ denotes an ellipsoid that depends on the current state (and possibly more data available at time step k).

Given p ellipsoids that bound the predicted states, we define the index sets $\mathbb{A}_i(\boldsymbol{x}_k)$ as

$$\mathbb{A}_i(\boldsymbol{x}_k) = \{l \in \mathbb{N}_c \mid \exists x \in \mathscr{E}_{i,j}(\boldsymbol{x}_k),\ j \in \mathbb{N}_p,\ \text{s.t. } \boldsymbol{f}_l \boldsymbol{x} > h_l\}. \tag{2}$$

Intuitively, (2) removes all state constraints that cannot be violated by any state for some ellipsoidal bound $\mathscr{E}_{i,j}(\boldsymbol{x}_k)$. For example, any state constraint that is not forward reachable subject to the system dynamics and input constraints can be removed. Note that (2) admits a closed-form solution that computationally cheap to check [1], which is crucial to obtain a real-time feasible ca-MPC scheme.

We applied our ca-MPC scheme to an MPC controlled hyperthermia treatment using virtual population model [2]. Loosely speaking, a hyperthermia treatment aims to heat the tumor with external actuators while keeping healthy tissue temperatures below a certain threshold. Hence, each discrete location in the patient model has temperature upper bound, resulting in 10^5 state constraints for each step in the horizon. Figure 1 shows the percentage of state constraints included in the ca-MPC problem over the duration of a treatment for a horizon $N = 5$. Note that only a small percentage of the state constraints are required to obtain the exactly the same minimizer as for the full MPC problem. Moreover, the time required to obtain the control input is approximately 5 seconds using our ca-MPC setup, while the original MPC problem was intractable.

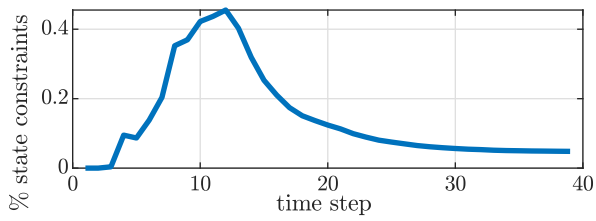

Figure 1: Percentage of total state constraints included in the ca-MPC optimization problem over the duration of the simulated hyperthermia treatment.

3 Conclusion

Online constraint removal for MPC is shown to be an effective strategy to accelerate the optimization problem without sacrificing performance with respect to the original MPC setup. In our hyperthermia case-study, we obtained a constraint reduction of more than 99.5%, yielding a tractable large-scale MPC feedback law.

References

[1] Nouwens, S. A. N., de Jager, B., Paulides, M. M., and Heemels, W. P. M. H. (2021) *Constraint Removal for MPC with Performance Preservation and a Hyperthermia Cancer Treatment Case Study* CDC, 4103-4108

[2] Paulides M. et al. (2021) *ESHO benchmarks for computational modeling and optimization in hyperthermia therapy* Int. J. Hyperthermia, 38:1425-1442

Robust Constrained Optimal Control for Uncertain Linear Systems With Adjustable Uncertainty Sets*

Yun Li[a], Neil Yorke-Smith[b], and Tamas Keviczky[a]

[a] Delft Center for Systems and Control, Delft University of Technology, Delft, the Netherlands
Email: y.li-39@tudelft.nl, T.Keviczky@tudelft.nl
[b] STAR lab, Delft University of Technology, Delft, the Netherlands
Email: n.yorke-smith@tudelft.nl

1 Introduction

Robust optimal control has been proved to be effective in many applications. Designing robust optimal controller for uncertain linear systems usually entails computing optimal control actions and/or control policies to immunize against all possible uncertainties. It should be pointed that most of the existing robust optimal control schemes consider the case that uncertainties reside in fixed uncertainty sets and also assume perfect state measurement. However, in several domains, especially in operating modern energy and building systems, the admissible region of uncertainties is unknown and adjustable. In addition, perfect state measurement is also not practical in reality for some applications.

In this work, we investigate the robust optimal control for uncertain linear systems with uncertain measurement errors and additive disturbances, which all reside in adjustable sets. Under the restriction of linear constraints and objective functions, two types of feedback control policies are investigated, and a bilinear optimization problem is formulated to compute the optimal size/shape of the adjustable uncertainty sets and the corresponding robust optimal control policy.

2 Problem Formulation

Consider the robust optimal control problem for the following linear uncertain systems:

$$x_{k+1} = Ax_k + Bu_k + w_k \tag{1}$$

where $x_k \in \mathbb{R}^{n_x}$ is the system state, $u_k \in \mathbb{R}^{n_u}$ is the control input, and $w_k \in \mathbb{R}^{n_w}$ is the unknown disturbance. The objective function is $J = \sum_{t=0}^{N-1} l_t(x_{t+1}, u_t)$, where $l_t(x_{t+1}, u_t)$ is a linear function in x_{t+1} and u_t. In our design, it is assumed that system state x_k cannot be accurately measured, and its measurement is denoted as $\hat{x}_k$. The measurement error is defined as $e_k := x_k - \hat{x}_k$. In addition, we assume that the uncertain disturbance w_k is not measurable, and its estimation is computed as $\hat{w}_k := \hat{x}_{k+1} - A\hat{x}_k - Bu_k$.

* The work was supported by the Brains4Buildings project under the Dutch grant programme for Mission-Driven Research, Development and Innovation (MOOI).

Under the restriction that the system state and input constraints and the adjustable uncertainty sets of the measurement error $\mathscr{E}$ and the additive disturbance $\mathscr{W}$ are polyhedra, we investigated two types of control laws: affine state feedback control policy u^{sf} and affine disturbance feedback control policy u^{df}, which are defined as

$$u_t^{\text{sf}} = \sum_{k=0}^{t} L_{t,k}\hat{x}_k + g_t,\ t = 0, \cdots, N-1 \tag{2}$$

$$u_t^{\text{df}} = \sum_{k=0}^{t-1} M_{t,k}\hat{w}_k + v_t,\ t = 0, \cdots, N-1 \tag{3}$$

where $L_{t,k} \in \mathbb{R}^{n_u \times n_x}$, $g_t \in \mathbb{R}^{n_u}$, $M_{t,k} \in \mathbb{R}^{n_u \times n_w}$ and $v_t \in \mathbb{R}^{n_u}$ are design parameters to be determined. Our design objective is to compute the optimal shape/size of the admissible uncertainty sets $\mathscr{E}$ and $\mathscr{W}$ while determining the corresponding optimal control policy so that the system constraints are satisfied for all admissible uncertainties $e_k \in \mathscr{E}$ and $w_k \in \mathscr{W}$.

3 Contribution

The contributions of our work are summarized as follows:

- Firstly, it is proved that the state feedback control policy (2) and the disturbance feedback control policy (3) are equivalent. Put differently, the feasible set of initial states for both two control policies are identical. Also, given a feasible state feedback policy u^{sf}, an equivalent feasible disturbance feedback policy u^{df} exists to give the same state and input sequences.
- Secondly, a bilinear optimization problem is formulated based on the duality of linear optimization to compute the optimal size/shape of the adjustable uncertain sets $\mathscr{W}$ and $\mathscr{E}$ while simultaneously computing the corresponding robust optimal control law u_t^{df}.
- Finally, the proposed design is illustrated in a case study of building temperature control to validate its effectiveness.

Please refer to [1] for the details of our proposed design.

References

[1] Y. Li, N. Yorke-Smith, and T. Keviczky, "Robust Optimal Control With Inexact State Measurements and Adjustable Uncertainty Sets", Under Review.

Efficient Scenario-based Control for Piecewise Affine Systems

Francesco Cordiano Matin Jafarian Bart De Schutter
Mekelweg 2, 2628 CD Delft, The Netherlands
Email: {f.cordiano, m.jafarian, b.deschutter}@tudelft.nl

1 Introduction

Dealing with uncertainty is one of the major challenges in control of dynamical systems. Various techniques, ranging from robust to stochastic control, have been proposed to take into account the uncertainty in the controller design. For example, stochastic model predictive control (SMPC) considers constraints that have to be satisfied with a desired level of probability (also known as chance constraints). However, SMPC problems are usually challenging to solve analytically, as they require the computation of multivariate integrals over the distribution of the uncertain parameter.

Randomized algorithms, such as the scenario approach [1], have received a lot of attention, as they allow to solve stochastic programs in an efficient manner. In the next sections, we highlight the main results for the scenario approach, and discuss its implementation in control algorithms for piecewise affine (PWA) systems, considered as they are the simplest extension of linear models that allows to capture nonlinearities in the system dynamics. Including uncertainty in PWA models is however challenging, so we present some open problems in SMPC for PWA systems.

2 The scenario approach

The scenario approach is a randomized method to solve stochastic programs. By drawing a number N of samples of the uncertain parameter, a chance constraint is replaced by a set of N deterministic constraints, leading to a deterministic scenario program. In [1], a lower bound on the number of samples is provided, so that a feasible solution for the scenario program is also feasible for the original problem with high probability, independently of the actual distribution of the uncertain parameter. Furthermore, although the original results in [1] are valid for convex constraints only, some recent works have extended the validity of the method to non-convex programs as well.

3 Scenario-based control of piecewise affine systems

A chance-constrained optimal control problem can be computationally intractable as soon as the uncertainties follow a non-Gaussian distribution, or nonlinearities occur in the dynamics. This is the case for PWA systems as well. An optimal control problem for a PWA system is in general non-convex, and the computational complexity can rapidly grow as the prediction horizon, state and input dimension grow. When the system is affected by uncertainty, analytical solutions to the stochastic control problem are in general not possible due to the nonlinear nature of the system dynamics. Randomized algorithms represent an appealing tool to provide tractable solutions to SMPC of PWA systems, leveraging in particular some recent results on the scenario approach for stochastic non-convex programs [2].

4 Open issues and research directions

The ultimate goal of our research is the derivation of an efficient scenario-based stochastic control algorithm for PWA systems capable of handling various sources of uncertainties in an efficient manner.

Some of the main challenges are the following. First of all, the scenario-based control algorithm must provide guarantees for chance constraint satisfaction, despite the presence of non-convex constraints originating from the hybrid nature of the system. The second aspect is that the computational burden of the scenario program should still be suited for online optimization, and the solution should not be overly conservative. For this, some inherent properties of PWA systems might play an important role to derive the least conservative bound on the number of samples required to obtain chance constraint satisfaction. Third, we may consider to trade off mathematical guarantees in favor of saving computational resources, in case the resulting scenario-based SMPC problem is not amenable for online optimization. To tackle this point, we plan to leverage clustering algorithms, scenario reduction techniques, or importance sampling algorithms, to define sets of representative scenarios with a lower sample complexity than the original scenario program.

References

[1] G. C. Calafiore, M. Campi, "The scenario approach to robust control design". IEEE Transactions on Automatic Control, vol. 51, no. 5, pp. 742-753, 2006.

[2] P. M. Esfahani, T. Sutter, J. Lygeros, "Performance bounds for the scenario approach and an extension to a class of non-convex programs". IEEE Transactions on Automatic Control, vol. 60, no. 1, pp. 46-58, 2014.

Acknowledgements

This research has received funding from the European Research Council (ERC) under the European Union's Horizon 2020 research and innovation program (Grant agreement no. 101018826 - ERC Advanced Grant CLariNet).

Integrated human-cyber-physical framework for temperature control in buildings

S. Ahmed, J.E.M. Martinez, A. A. Hoekstra, J.M.A. Scherpen
Faculty of Science and Engineering, University of Groningen, The Netherlands
{s.ahmed,j.e.machado.martinez,j.m.a.scherpen}@rug.nl, a.a.hoekstra@student.rug.nl

1 Motivation

Climate change and recent geopolitical implications increase the awareness of residential thermal energy consumption, thereby boosting the interest in optimizing heating, ventilation, and air conditioning (HVAC) systems that provide heating in residential buildings

2 Building Thermal Dynamics

The thermal dynamics of a building can be modeled with the electrical analogy of a resistance-capacitance circuit, with heat flow instead of the flow of charge [1]. To this end, consider a building with multiple zones $i = 1, ..., n$ as shown in Figure 1. The zones are divided into two groups. The first group consists of zones equipped with a (variable air volume (VAV) box. The second group is other spaces, like walls, windows, empty rooms, and furniture. The overall heat flow balance for both groups can, respectively, be described by

$$C_i\dot{T}_i = \frac{T_a - T_i}{R_i} + \sum_{j\in\mathcal{N}_i} \frac{T_j - T_i}{R_{ij}} + a_i(T_i^s - T_i)m_i + q_i$$

and

$$C_i\dot{T}_i = \frac{T_a - T_i}{R_i} + \sum_{j\in\mathcal{N}_i} \frac{T_j - T_i}{R_{ij}},$$

where T_i is the temperature of zone i, T_j the temperature of adjacent zones, R_i and R_{ij} are the resistances between the ambiance and zone i and between zone i and j, respectively, T_s is the temperature of the supplied heat, a_i is specific heat of the supplied air, m_i is the mass flow rate, and q_i is the heat gain from external factors like humans. The collective dynamics results in a bilinear model that severely complicates the design of computationally tractable controllers. To address this issue, we replace the terms $a_i(T_i^s - T_i)m_i$ with linear terms $a_i(T_i^s - \hat{T}_i)m_i$ where $\hat{T}_i$ is the initial condition for the temperature of zone i. The dynamics of the approximated system in matrix form is then

$$C\dot{T} = RT_a\mathbf{1} - (R + L)T + BG(\hat{T})m + Bq, \quad (1)$$

where T, q and m are collections of T_i, q_i, and m_i, respectively.

3 Optimization Problem

The optimization problem to be solved includes thermal comfort of occupants $||T - r||^2$ and energy minimization $f(m)$, i.e.,

$$\min_{T,m} \quad ||T - r||^2 + f(m),$$

subject to the steady state of the building's thermal dynamics 1, where r is the temperature setpoint which is a random variable coming from a probability distribution approximated by data from end users [2].

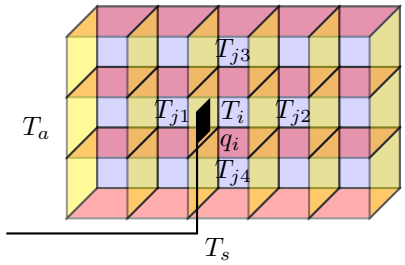

Figure 1: Basic topology of a building

4 Methodology and Outlook

Currently, we are exploring two techniques to solve the optimization problem with stability guarantees. One of the possible solutions is using a model predictive control framework and exploiting the turnpike property due to the strict dissipativity of the thermal dynamics. Another solution includes formulating the problem as a port-Hamiltonian system (or Brayton Moser system) and using equilibrium-independent passivity properties to establish the desired results.
As a future prospect, we also plan to incorporate the human model described by human values and behaviors toward the consumption of energy in the system from an environmental psychology point of view.

References

[1] T. Hatanaka, X. Zhang, W. Shi, M. Zhu, and N. Li, "An integrated design of optimization and physical dynamics for energy efficient buildings: A passivity approach", in *2017 IEEE Conference on Control Technology and Applications (CCTA)*, IEEE, 2017, pp. 1050–1057.

[2] M. Namazkhan, C. Albers, and L. Steg, "The role of environmental values, socio-demographics and building characteristics in setting room temperatures in winter", *Energy*, vol. 171, pp. 1183–1192, 2019.

Complexity-Fixed Relaxed Dynamic Programming

Ruben Beumer, René van de Molengraft and Duarte J. Antunes
Control Systems Technology
Eindhoven University of Technology
P.O. Box 513, 5600 MB Eindhoven, The Netherlands
Email: {r.m.beumer,m.j.g.v.d.molengraft,d.antunes}@tue.nl

1 Introduction

Dynamic programming has been applied to a wide variety of problems in several areas. However, the curse of dimensionality limits the applicability of this idea. One of the approximate methods that have been proposed is relaxed dynamic programming (RDP) [1], which relaxes the demand for optimality in order to reduce the complexity. It provides a method to approximate the optimal value function with a guarantee that the resulting (suboptimal) solution is within a prespecified factor from the optimal one. Such a suboptimal policy results from a parameterized approximate cost-to-go,

$$V_k(x) = \min_{p \in \mathcal{J}_k} p(x), \tag{1}$$

and the complexity of this cost-to-go determines the complexity of the policy. Typically the more stringent the factor from the optimal cost is, the larger the complexity. However, RDP does not give any theoretical guarantees on the complexity, which might grow unbounded. To tackle this issue, we propose to rather find the best constant factor away from optimality for an a priori complexity bound. We show that for a large class of problems where the cost-to-go is the minimum of a set of quadratic functions, this factor can be found by solving LMIs. Through a numerical method we show the effectiveness of our policy.

2 Proposed approach

Different forms of $p(x)$ are considered for several types of applications: (i) switched linear systems with quadratic costs [1], (ii) linear time-invariant (LTI) systems with piecewise linear costs [1], (iii) partially observable Markov decision processes (POMDPs) with finite state, control and observation spaces with piecewise linear costs [1], (iv) optimal joint maximum a posteriori probability (JMAP) estimation of the state and mode of a Markov jump linear system (MJLS) with quadratic costs [2] and (v) linear quadratic control problems with discretized input. These value functions can all be written in one general form:

$$V_k(x) = \min_{(P,q,r) \in \mathcal{J}_k} x^\top P x + q^\top x + r \tag{2}$$

for which the complexity can be decreased by constructing a pruned version $\mathcal{J}_k^p$ of the set of tuples $\mathcal{J}_k$.

This research is part of the research program SYNERGIA (project number 17626), which is partly financed by the Dutch Research Council (NWO).

We can initialize $\mathcal{J}_k^p$ as an empty set, or with the members of $\mathcal{J}_k$ for which $V(x)$ achieves the minimum value for a selected set of points $x_s \in X$. Then, for original RDP, if $\exists (P^*, q^*, r^*) \times x^* \in \mathcal{J}_k \times X \mid x^{*\top} P^* x^* + q^{*\top} x^* + r^* + \varepsilon < \min_{(P,q,r) \in \mathcal{J}_k^p} x^{*\top} P x^* + q^\top x^* + r$ with a predefined $\varepsilon \geq 0$, add $(\underline{P}, \underline{q}, \underline{r}) = \arg\min_{(P,q,r) \in \mathcal{J}_k} x^{*\top} P x^* + q^\top x^* + r$ to $\mathcal{J}_k^p$ and repeat this step. If not, the pruning procedure is completed. As a result, the costs are guaranteed to be within ε of the optimal value. Because in general the costs can be negative, ε is additive, similar to [3], instead of multiplicative [1], but both cases can be covered in the notation explained below.

Instead of predefining ε as an optimality guarantee, we only add a predefined number of tuples (P, q, r) to the pruned set $\mathcal{J}_k^p$ to have a complexity guarantee. Various methods can be applied to efficiently select this limited amount of elements. A sufficient condition to add a new tuple $(P^*, q^*, r^*) \in \mathcal{J}_k$ to $\mathcal{J}_k^p$ would for original RDP be if $\exists x^* \in X$ for which

$$x^{*\top} P(\varepsilon) x^* + q(\varepsilon)^\top x^* + r(\varepsilon) < \sum_{i=1}^{n} \alpha_i \left(x^{*\top} P_i x^* + q_i^\top x^* + r_i \right) \tag{3}$$

with $n = |\mathcal{J}_k^p|$, $0 \leq \alpha_i \leq 1 \; \forall i \in \{1, \ldots, n\}$ and $\sum_{i=1}^{n} \alpha_i = 1$. $P(\varepsilon) = P^*$, $q(\varepsilon) = q^*$ and $r(\varepsilon) = r^* + \varepsilon$ for the additive factor and $P(\varepsilon) = \varepsilon P^*$, $q(\varepsilon) = \varepsilon q^*$ and $r(\varepsilon) = \varepsilon r^*$ for the multiplicative factor. The condition for when the tuple would not be added can hence be written as an LMI (details are omitted here). The minimum value of ε for which all other tuples would not be added to the pruned set according to this LMI, provides a (conservative) indication for how far from optimal the solution will at most be.

References

[1] B. Lincoln and A. Rantzer, "Relaxing dynamic programming," *IEEE Trans. on Automatic Control*, vol. 51, no. 8, pp. 1249–1260, Aug 2006.

[2] A. R. P. Andriën and D. J. Antunes, "Near-optimal map estimation for markov jump linear systems using relaxed dynamic programming," *IEEE Control Systems Letters*, vol. 4, no. 4, pp. 815–820, 2020.

[3] D. J. Antunes, R. M. Beumer, M. J. G. van de Molengraft, and W. P. M. H. Heemels, "Adaptive sampling and actuation for pomdps: Application to precision agriculture," in *2022 IEEE 61st Conference on Decision and Control (CDC)*, 2022, pp. 2399–2404.

Robustness Benchmark of Prediction Models for Automated Driving

Manuel Muñoz Sánchez[1], Emilia Silvas[1,2], Jos Elfring[1,3], René van de Molengraft[1]
[1]Department of Mechanical Engineering, Control Systems Technology Group,
Eindhoven University of Technology, Eindhoven, The Netherlands
[2]Department of Integrated Vehicle Safety, TNO, Helmond, The Netherlands.
[3]VDL CropTeq Robotics, Eindhoven, The Netherlands
Email: m.munoz.sanchez@tue.nl

1 Introduction

Accurate and robust trajectory predictions of road users (RUs) are needed to enable safe automated driving. To do this, heavily processed datasets are used to develop machine learning models that leverage as much information as possible about the environment (e.g. surrounding RUs and road infrastructure [2]). The original dataset used during training is later modified synthetically introducing new or faulty data to evaluate the robustness of the prediction models.

2 Perturbations for Trajectory Prediction Robustness

Perturbations introduce synthetic variations to the dataset to simulate unrecorded situations or lower data reliability in order to evaluate and increase robustness of prediction models. For instance, [1] shows how the removal of irrelevant RUs (e.g. parked vehicles) impacts predictive accuracy. Increasing robustness towards perturbations is often addressed introducing similar perturbations to the data used for training the models [1]. However, if the perturbations applied to the dataset are not representative of what one will encounter in reality, the models can present erratic behavior (Fig. 1).

3 Methodology & Experiments

To identify the potential performance degradation of prediction models when deployed in a real vehicle, two common baselines (Constant Velocity and LSTM) [2] and two state-of-the-art models (MotionCNN [3] and MultiPath++ [4]) are compared under harsh, yet possible perturbations. Such perturbations are illustrated in Fig. 1 and are unavailability of road information, late detections, and highly noisy heading angle measurements, which could be given by faulty sensors or adverse weather conditions [5]. Additionally, the effectiveness of introducing similar perturbations during model development is investigated.

4 Results & Future Work

Results show that harsh perturbations significantly degrade performance, with errors increasing up to +1444.8% in common trajectory prediction evaluation metrics. Introducing perturbations during training mitigates this performance degradation, with error increases of up to +87.5%. We argue that despite being an effective mitigation strategy, perturbations during training do not guarantee robustness, since identification of all possible on-road complications is unfeasible. Furthermore, severe data degradation (e.g. road information removal) frequently leads to more accurate predictions, suggesting that the models are unable to learn the true relationships between the different elements in the data. Future work will focus on further analysis of these cases.

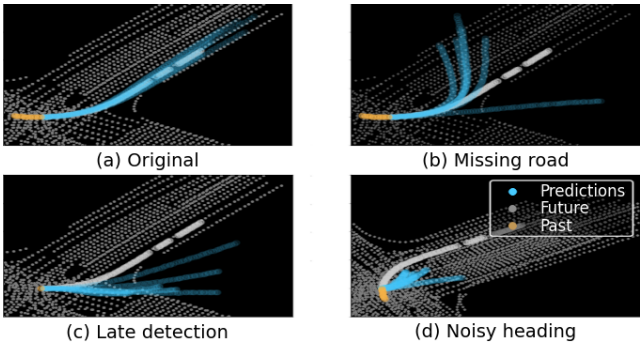

Figure 1: Example of vehicle predictions at an intersection using original (clean) data and perturbed (noisy) data.

Acknowledgement: This work was supported by the SAFE-UP project under EU's Horizon 2020 research and innovation programme, grant agreement 861570.

References

[1] R. Roelofs et al., "CausalAgents: A Robustness Benchmark for Motion Forecasting using Causal Relationships", *arXiv preprint arXiv:2207.03586*, 2022.

[2] M. Muñoz Sánchez et al. "Scenario-based Evaluation of Prediction Models for Automated Vehicles", ITSC, 2227–2233, 2022.

[3] S. Konev et al., "MotionCNN: A Strong Baseline for Motion Prediction in Autonomous Driving", *arXiv preprint arXiv:2206.02163*, 2021.

[4] S. Konev, "MPA: MultiPath++ Based Architecture for Motion Prediction", *arXiv preprint arXiv:2206.10041*, 2022

[5] S. Zang et al., "The Impact of Adverse Weather Conditions on Autonomous Vehicles: How Rain, Snow, Fog, and Hail Affect the Performance of a Self-Driving Car". IEEE Vehicular Technology Magazine, 103–111, 2019.

Leveraging Large Language Models for Visual Target Navigation

Bangguo Yu, Hamidreza Kasaei, Ming Cao
Faculty of Science and Engineering, University of Groningen
Nijenborgh 4, 9747 AG Groningen, The Netherlands
Email: {b.yu, hamidreza.kasaei, m.cao}@rug.nl

1 Introduction

This work focuses on the problem of visual target navigation, which serves as a key functionality for autonomous robots as it is the foundation of high-level tasks. To find a specific predefined object in unknown environments, classical and learning-based approaches are fundamental components of navigation that have been investigated thoroughly in the past. However, due to the difficulty in the representation of complicated scenes and prior and accumulated knowledge, previous methods are still not adequate, especially for large unknown scenes. To address this deficiency, we propose a novel framework for visual target navigation using the Large Language Model (LLM). In this proposed framework, visual observation is used to construct the real-time semantic map and extract the frontiers. Based on the frontiers and target object, the most relevant frontier is selected by the prediction of LLM as a long-term goal to explore the environment efficiently. We evaluate our framework on the simulation platform Habitat [1] and in real world settings. In sharp contrast to many other map-based methods, our framework selects the long-term goal from the score of LLM, which is a strong prior knowledge for the exploration.

2 Method

In the visual target navigation task, the agent should navigate to find an object as the appointed category in a scene. The overall framework is shown in Figure 1.

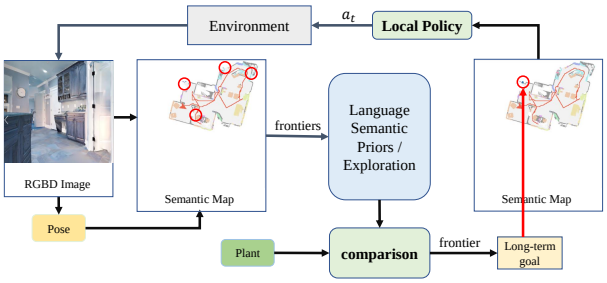

Figure 1: The overall architecture of the target navigation framework. This framework uses as input the RGB-D images to generate the semantic and frontier maps, and selects the long-term goal via the score of LLM. After getting the long-term goal, the local policy then guides the final action for the robot.

2.1 Map Representation

Given the sensory input, the semantic map is built based on RGBD images and the position of the agent. We denote the semantic map by a $K \times M \times M$ matrix, where $M \times M$ denotes the map size, and $K = C_n + 2$ is the number of channels. C_n is the number of semantic categories, and the first two channels represent the obstacle and explored map. For the frontier map, the explored edge is extracted by finding maximum contours from the explored map, and the frontier map can be represented by the differences between explored and obstacle maps.

2.2 Language Model for Exploration

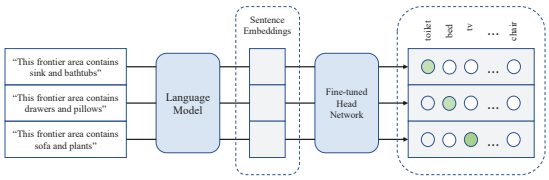

Figure 2: The query string contains the observation of the frontier is embedded by a pre-trained language model. Then, a fine-tuned neural network determines a distribution over the target object labels given that embedding.

The process of the selection of the frontier using LLM is shown in Figure 2. After obtaining the current semantic and frontier map at each step, we collect all the semantic categories around each frontier area and fill the labels into the query strings separately. Each string is then fed into a language model to produce a summary enbedding vector. Finally, all the embeddings are fed into a fine-tuned neural network head, which produces an $(F_n \times C_n)$-dimensional matrix of prediction logits corresponding to the object labels, with the inferred frontier area being the one corresponding to the maximum value of the output in the target object column. The centroid of the inferred frontier area can be extracted as the long-term goal. The path planning method is then used to guide the robot to explore around the long-term goal.

References

[1] M. Savva, A. Kadian, O. Maksymets, Y. Zhao, E. Wijmans, B. Jain, J. Straub, J. Liu, V. Koltun, J. Malik, D. Parikh, and D. Batra, "Habitat: A Platform for Embodied AI Research," in *2019 IEEE/CVF International Conference on Computer Vision (ICCV)*, vol. 2019-Octob, pp. 9338–9346, IEEE, oct 2019.

Path Tracking Controller for Reverse Driving Articulated Vehicle

Viral Gosar
v.v.gosar@tue.nl

Mohsen Alirezaei
m.alirezaei@tue.nl

I.J.M. Besselink
I.J.M.Besselink@tue.nl

1 Abstract

The most challenging part of the parking/docking of articulated vehicles at distribution centers is reverse driving due to the unstable dynamics of the trailer. This paper presents a cascade feedback-feedforward approach for the path-tracking of tractor semi-trailers while reversing. The controller developed is validated with a simulation model and scaled vehicle experiments.

2 Model and Controller Objective

The tractor semi-trailer under consideration is modeled as a function of traveled distance along the path (s_t) :

$$x'(s_t) = f(x(s_t), u(s_t)) \tag{1}$$

With states $x(s_t) = (\gamma(s_t)\ y_e(s_t)\ \psi_e(s_t))^T$ and using $'$ for $\frac{d}{ds_t}$. The error dynamics in Figure 1 (y_e and ψ_e) are defined using coordinate transformation, similar to [1]. Considering a feasible reference path is provided by the path planner.

$$x_r'(s_r) = f(x_r(s_r), u(s_r)) \tag{2}$$

The objective of the path-following controller is to control the tractor semi-trailer states such that the reference path is executed with zero tracking error:

$$\lim_{s_t \to \infty} ||x_r(s_r(s_t) - x(s_t)|| = 0 \tag{3}$$

In this work, The objective of the path-following controller is to ensure that the semi-trailer follows the reference path while reversing and achieving zero tracking error. The control input along with a complimentary feedforward δ_{ff} action thus reads:

$$u(s_t) = K_\gamma \gamma(s_t) + K_y y_e(s_t) + K_\psi \psi_e(s_t) + \delta_{ff}(\kappa_r(s_t)) \tag{4}$$

3 Preliminary Results

The path-tracking controller has been implemented on 1:13 scaled tractor semi-trailers, see Figure 2. The closed-loop response of the tractor-semitrailer tracking a straight line reference while driving in reverse with an initial lateral offset of 0.25m, in both simulation and scaled environment is shown in Figure 3

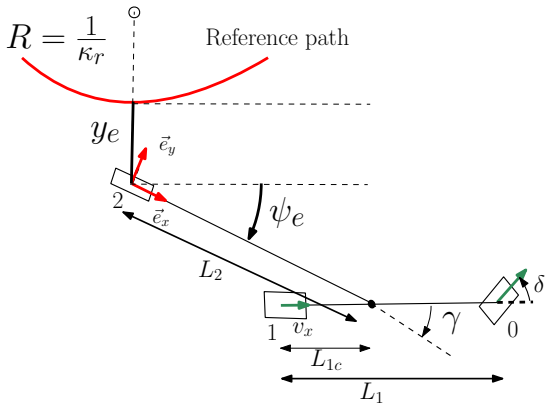

Figure 1: Vehicle-road error model

Figure 2: Distribution center scaled setup at TU/e

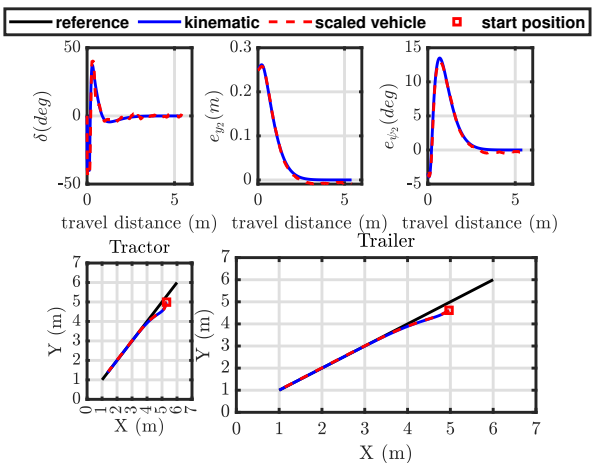

Figure 3: Closed loop response of the simulation model and scaled vehicle

References

[1] Y. Kanayama, Y. Kimura, F. Miyazaki and T. Noguchi, "A stable tracking control method for an autonomous mobile robot," Proceedings., IEEE International Conference on Robotics and Automation,1(384-389),1990.

Vision-based localization and parking space detection for the truck-trailer Autonomous Mobile Robot

Shuhao Zhang, Bastiaan Vandewal, Mathias Bos, Wilm Decré and Jan Swevers
MECO Research Team, Department of Mechanical Engineering, KU Leuven, Belgium
Flanders Make@KU Leuven, Belgium
shuhao.zhang@kuleuven.be

1 Introduction

In the field of autonomous driving, fully autonomous parking is one of the most important features that has received a lot of attention recently from both industry and academics. Parking space detection, path planning, and path tracking are the three basic steps that fully automated parking (FAP) entails. Among them, accurate parking space detection is a crucial task, as it determines the effectiveness of autonomous parking path planning and tracking efforts.

Parking space detection can be categorized into free-space-based approaches and vision-based approaches, depending on the on-board sensors. A free-space-based approach makes use of range-finding sensors to identify an available vacant space between vehicles. As a result, it cannot be used in an open area or parking lot where there are no other vehicles around. A vision-based approach locates parking slot markings from wide field-of-view image sensors. The performance of vision-based approaches is more accurate in most cases and is independent of nearby vehicles [1].

An autonomous truck-trailer parking maneuvering approach based on model predictive control was proposed [2], as well as a linear stabilizing feedback controller for path tracking. With an external positioning system and in a known parking space setting, this work demonstrates convincing experimental outcomes for autonomous parking. To achieve fully autonomous parking, it is necessary to develop on-board localization and parking space detection methods for the truck-trailer Autonomous Mobile Robot (AMR).

2 Vision-based localization and parking space detection

Using on-board image sensors, the truck-trailer AMR in this work locates itself and recognizes parking space online. This results in fully autonomous parking after combining with parking maneuvering and tracking methods in [2].

2.1 Hardware and software

The truck-trailer AMR is the in-house developed test setup driven by a KELO-wheel. Two RealSense T265 Tracking Cameras—one in the front of the truck and the other at the back of the trailer—provide image and visual-odometry sensing data. An angle encoder is attached to the hitching point of the truck for measuring the angle between the truck and the trailer. Vision-based localization and parking space detection algorithms are executed on a Jetson TX2 with a Robot Operating System (ROS) framework. Two projectors installed on the ceiling render the parking space environment on the lab floor.

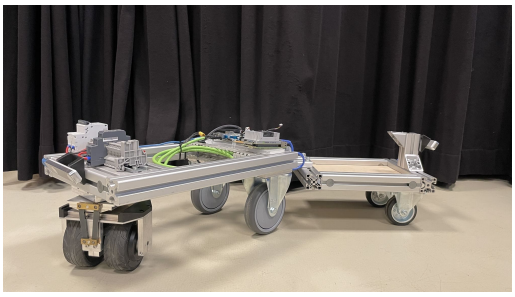

Figure 1: Truck-trailer AMR for lab experiments.

2.2 Localization and parking space detection

After converting the original images to Bird's Eye View (BEV) images, parking spaces are detected in a fashion of semantic segmentation, i.e., the pixels representing the parking spaces are segmented from BEV images first, a set of lines that can denote parking space markings are extracted from segmented pixels, and finally, the coordinates of parking space are inferred from extracted line sets.

To localize the truck-trailer AMR itself, the average of the visual-odometry data are calculated. After combining localization and parking space detection results at each timestamp, a map of the parking space can be built.

References

[1] Y. Ma, Y. Liu, L. Zhang, Y. Cao, S. Guo, and H. Li, "Research Review on Parking Space Detection Method," Symmetry, vol. 13, no. 1, p. 128, Jan. 2021.

[2] M. Bos, B. Vandewal, W. Decré, and J. Swevers, "MPC-based Motion Planning for Autonomous Truck-Trailer Maneuvering," in *IFAC World Congress 2023*, 2023, submitted.

Acknowledgement This work has been carried out within the European Union's Horizon 2020 research and innovation programme under the Marie Skłodowska-Curie grant agreement ELO-X No.953348 and the framework of Flanders Make SBO ARENA: Agile and Reliable Navigation.

Safety Regulation for Constrained Reinforcement Learning

Shuhao Qi, and Zhiyong Sun
Control Systems Group, Eindhoven University of Technology,
Eindhoven, The Netherlands
Email: s.qi@tue.nl

1 Introduction

Although reinforcement learning (RL) algorithms have achieved impressive results in games (e.g., Go and Atari games), they are rarely applied to real-world systems like autonomous driving. The main reason is that typical RL algorithms maximize the cumulative reward by continuous trial and error, and do not consider the satisfaction of constraints, especially safety constraints, during the exploration process. It is still an open problem to rigorously guarantee constraint satisfaction throughout training for RL algorithms. This paper will leverage popular tools in control theory, including control barrier function (CBF) and model predictive control (MPC), to design a regulation module to make sure RL algorithms explore only in the safe space/set. The proposed method will be applied to the obstacle avoidance task for autonomous vehicles based on several RL baseline algorithms.

2 Problem description

Typical autonomous vehicles can be formulated as the simplified bicycle model based on the no-slip assumption,

$$\begin{aligned} \dot{p_x} &= vcos(\theta) \\ \dot{p_y} &= vsin(\theta) \\ \dot{\theta} &= \tfrac{v}{l}tan(\delta) \\ \dot{v} &= a \end{aligned} \tag{1}$$

where (p_x, p_y) and v denote the 2-dimension position and linear velocity of the rear wheel of the vehicle, θ and l denote the direction and the length of the vehicle. δ and a denote steering angle and acceleration. This model can be written in the form of a nonlinear control affine system $\dot{x} = f(x) + g(x)u$, where $x = [p_x, p_y, \theta, v]$ and $u = [a, tan(\delta)]$. We assume an accurate model and state estimate are available in this work. In addition, robots should stay in collision-free space $x_t \in X_{free}$ constrained by obstacles under input limits $u_t \in U$. Therefore, the notion of safety is formalized based on the concept of set invariance such that hard constraints can be always satisfied.

Definition 1 (Invariance & Safty) *A set S is forward invariant if for every $x_0 \in S$, it holds $x_t \in S$ for all $t \in I(x_0)$. The system is safe with respect to the set S if the set S is forward invariant.*

The definition implies that a system remains safe under a particular control policy only if all solutions that begin in the safe set remain in the safe set. It is significant to have the set invariance property when RL algorithms are applied on safety-critical systems. Since RL algorithms generate actions (inputs) u_{RL} randomly to collect more data. To avoid catastrophic exploring, a safety regulator is designed to enable RL policy to explore only in the safe set.

3 Approaches

To regulate actions generated by RL algorithms in the safe invariant set, two promising tools can be utilized, which are control barrier function (CBF) [1] and predictive safety filter (PSF) [2]. The effectiveness of the two methods to regulate RL algorithms will be demonstrated in the case study of autonomous vehicles in cluttered environments.

3.1 Control Barrier Function

Definition 2 *Let $C \subset D \subset \mathbb{R}^n$ be the super level set of a continuously differentiable function $h : D \to \mathbb{R}$. Then h is a control barrier function if there exists an extended class K_e function α such that for the nonlinear control affine system:*

$$\sup_{u \in U} \left[L_f h(x) + L_g h(x) u \right] \geq -\alpha(h(x)).$$

for all $x \in D$.

CBF can directly generate an admissible input set S_{cbf} which can empower set invariance property. Therefore, a regulator based on CBF can be formulated as

$$\begin{aligned} \min_{u_0} \quad & \|u_0 - u_{RL}\| \\ \text{s.t.} \quad & u_0 \in S_{cbf}, \\ & u_0 \in U. \end{aligned} \tag{2}$$

3.2 Predictive Safety Filter

Unlike CBF, PSF utilizes the superiority of model predictive control on dealing with constraints to implicitly define a safe set, whose formulation is based on the discretization of the system (1)

$$\begin{aligned} \min_{x_k, u_k} \quad & \|u_0 - u_{RL}\| \\ \text{s.t.} \quad & \forall k \in I_{[0,N-1]} : \\ & x_{k+1} = f(x_k, u_k) \\ & x_k \in X_{free} \\ & u_k \in U, \\ & x_N \in S^t. \end{aligned} \tag{3}$$

The main challenge in designing PSF is the construction of the terminal set S^t which certifies the set invariance.

References

[1] A. D. Ames, S. Coogan, M. Egerstedt, G. Notomista, K. Sreenath, and P. Tabuada, "Control barrier functions: Theory and applications," in *European Control Conference*, pp. 3420–3431, 2019.

[2] K. P. Wabersich and M. N. Zeilinger, "A predictive safety filter for learning-based control of constrained nonlinear dynamical systems," *Automatica*, vol. 129, p. 109597, 2021.

On the continuity of a closed-form solution for the control allocation of surface vessels

Frank Mukwege, Emanuele Garone
SAAS - Université libre de Bruxelles
50, av. F.D. Roosevelt, CP 165/55
1050 Bruxelles
Belgium
Email: [frank.mukwege,emanuele.garone]@ulb.be

1 Introduction

For marine crafts, tasks such as station-keeping, path- or trajectory-tracking under weather disturbances depends on the ability to produce the appropriate forces and torques through the available set of actuators. A classical control architecture for surface vessels is usually composed of i) a top-level part computing the forces and moments needed to meet the control requirements and ii) a low-level part which handles the actuator dynamics. The link between these 2 components is the control allocation (CA) which translates the forces and moments vector τ into actuators inputs u. Sometimes, the allocation can be incorporated within the high-level control. Having the control allocation done separately enables modular design in the control scheme since all actuator's constraints can be efficiently handled within the CA.

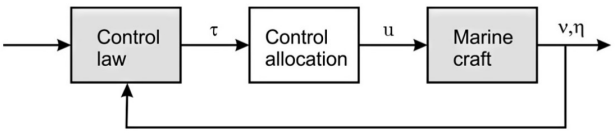

Figure 1: Typical control architecture for a marine craft [1]

In the case of an overactuated system, the allocation becomes an optimization problem depending on the designer objectives, such as fuel consumption or wear-and-tear under the actuators constraints [2]. Overactuation occurs for a surface vessel (SV) with 2 azimuth thrusters - thruster units that can be rotated by an angle θ about the z axis and produce a thrust T in a given direction.

2 Problem statement

A marine craft with 2 azimuth thrusters located at $p_i = [l_{x,i} l_{y,i}]^T$ in a classical 3DOF surge-sway-yaw model is considered. The approach chosen here is tackling the control allocation problem (CAP) at its core by considering it in its initial form with no saturation and angle rate constraints on the thrusters. The mapping between each single actuator's thrust and angles and τ is $\tau = M(p_i)F$

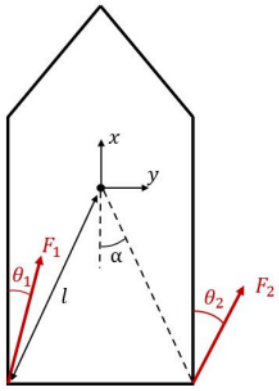

Figure 2: Representation of the SV with 2 orientable thrusters

where $F = [F_{xi}, F_{yi}]^T$ is the vector of the forces produced by the i-th actuator on the xy axes and M is the mapping matrix between the generalised forces and these forces to be produced.

In this form, the CAP is a unconstrained least-squares problem whose solution is given by the Moore-Penrose pseudoinverse. Unfortunately, this solution is discontinuous in the angles θ_i and cannot be applied as it in practice due to the actuator dynamics. The aim of the research is to come up with a solver-free and systematic way to build a sub-optimal solution that ensures the continuity of the solution.

References

[1] Thor I. Fossen and Tor A. Johansen. A survey of control allocation methods for ships and underwater vehicles. In 2006 14th Mediterranean Conference on Control and Automation, pages 1–6, 2006.

[2] Tor Arne Johansen, Thor I Fossen, and Stig P Berge. Constrained nonlinear control allocation with singularity avoidance using sequential quadratic pro- gramming. IEEE Transactions on Control Systems Technology, 12(1):211–216, 2004.

Experimental Evaluation of the Safety Shell with CARLA

Caspar Hanselaar[1], Yuting Fu[3], Andrei Terechko[3], Jochen Seemann[3],
Tim Beurskens[3], Emilia Silvas[1,2] and Maurice Heemels[1]
[1]Department of Mechanical Engineering, CST group, Eindhoven University of Technology;
[2]TNO, Dutch Organization for Applied Scientific Research; [3]NXP Semiconductors N.V

1 Introduction

Automated Vehicles (AVs) may help reduce the number of traffic deaths (the 8th cause of death annually worldwide) and accelerate adoption of sustainable transportation, via e.g, Mobility as a Service. However, to allow AV adoption, they need to first be safe. Research in [1] shows that the dominant reason for supervised AV test disengagement is the occurrence of a Functional Insufficiency (FI). FIs encompass deviating function behaviour (possibly in absence of faults), that leads in turn to unsafe vehicle behaviour in relevant circumstances, e.g, failing to slow down. To increase safe behaviour without reducing Automated Driving System (ADS) availability, the Safety Shell was developed [2]. The Safety Shell uses multiple heterogeneous channels, as shown in Fig. 1 to cross-compare the world model (WM) and motion planning (MP) results of each channel (Ch.), to obtain a risk estimation for each channel's plan. This is used to feed an Arbiter algorithm that weighs safety, availability and preference to select the channel used for driving. Though [2] showed promise in controlled simulation environments, it remains an open question whether the Safety Shell architecture is an effective solution when applied to more complex traffic situations with e.g, noisy sensor models and unpredictable occurrences of FIs. In addition, one of the key questions regarding the benefit of heterogeneity is whether heterogeneous channels will not make the same mistakes at the same time in more realistic circumstances, robbing the Safety Shell from its benefits. Therefore, in this paper we set out to test the Safety Shell algorithm in more realistic simulation environments.

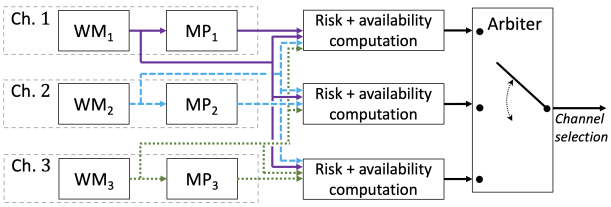

Figure 1: The basic architecture layout of the Safety Shell for a 3-channel system, adapted from [2]

2 Method

The open source CARLA simulator was selected to generate realistic simulations. The choice for CARLA was based, among other reasons, on its active competition with open source ADS channel submissions. Of those open source ADS channels, [3, 4] were used as channels in the Safety Shell architecture, next to [5]. Through an AD testbed developed by NXP, we were able to integrate these channels, as shown in Fig 2. A proof-of-concept route in a CARLA environment is tested, both with the Safety Shell and with single-channel control (by fixing the channel selector in Fig. 2). AV behaviour performance is evaluated with respect to travel time on a fixed route (lower is better), collisions and red light violations.

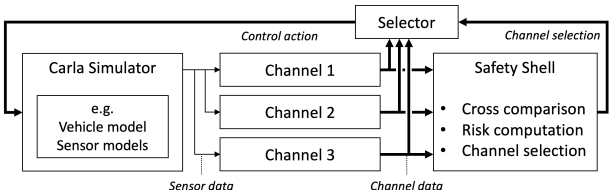

Figure 2: Schematic diagram of the used system.

3 Preliminary results

Independently, two channels [4, 5] complete the 1 km urban test route quickly, but cause collisions. Two channels violate red light rules (1x [3] and 8x [5]). The three-channel equipped Safety Shell completes the route without collisions or red light violations 15% faster than the safest individual channel [3]. Though preliminary, these results vindicate the potential benefit of the Safety Shell concept.

References

[1] Y. Fu, A. Terechko, C.A.J. Hanselaar, E. Silvas, and M. Heemels. Characterization and mitigation of limitations in automated driving systems. *27th ESV Conference*, 2023.

[2] C.A.J. Hanselaar, E. Silvas, A. Terechko, and W.P.M.H. Heemels. Detection and mitigation of functional insufficiencies in autonomous vehicles: The safety shell. *Intelligent Transporation Systems*, 2022.

[3] Dian Chen and Philipp Krähenbühl. Learning from all vehicles. In *Proceedings of the IEEE/CVF Conference on Computer Vision and Pattern Recognition*, pages 17222–17231, 2022.

[4] Kashyap Chitta, Aditya Prakash, Bernhard Jaeger, Zehao Yu, Katrin Renz, and Andreas Geiger. Transfuser: Imitation with transformer-based sensor fusion for autonomous driving. *arXiv preprint arXiv:2205.15997*, 2022.

[5] Autoware Foundation. https://www.autoware.auto, 2022.

Boosting the Kernel-induced Kalman Filter for Relative Localization of Micro Air Vehicle Swarms with Ultra-wideband Ranging

Changrui Liu[1], Sven Pfeiffer[2], Bart De Schutter[1], and Guido C.H.E. de Croon[2]

[1] Delft Center for Systems and Control (DCSC), Delft University of Technology

[2] MAVLab, Faculty of Aerospace Engineering, Delft University of Technology

Emails: {c.liu-14, s.u.pfeiffer, b.deschutter, g.c.h.e.decroon}@tudelft.nl

1 Introduction

Micro Air Vehicles (MAVs), with higher agility and a lighter design, hold a lot of potential for real-world operations such as surveillance, exploration, and indoor detection. MAV swarms can further compensate for the limited power and mobility of a single MAV. Successful operation of MAV swarms requires an accurate relative localization scheme that provides position feedback among agents for performing higher-level tasks collaboratively.

Infrastructure-free relative localization schemes using only onboard sensors are favorable due to their simple setup and low cost. Ultra-wideband (UWB) has recently drawn a lot of attention in aerial robot localization tasks [1] owing to its superior communication capabilities and accurate distance measurements. Therefore, equipping MAVs with UWB is a lightweight and economic solution for the relative localization purpose in swarming. However, in indoor cluttered environments, the UWB noise is *heavy-tailed* due to non-line-of-sight and multi-pathing effects, which degrade the localization performance. The kernel-induced Kalman filter [2] has demonstrated its effectiveness in handling heavy-tailed noise, thus applying it to solve the state estimation problem in relative localization using UWB has great potential.

2 Problem formulation

An agent i in the swarm is required to estimate the relative position $\mathbf{p}_{ij} = [x_{ij}, y_{ij}, z_{ij}]^\top$ of its neighboring agent j in the *body-centered horizontal frame* of agent i using the inter-distance y_{ij} measured by UWB two-way ranging and the velocities $\mathbf{v}_i$ ($\mathbf{v}_j$) in the body-centered horizontal frame of agent i (j). In addition, the relative heading ψ_{ij} is also included to characterize the coordinate transformation between different body frames. The system governing the relative motion is

$$\dot{\mathbf{x}}_{ij} = \begin{bmatrix} \dot{\psi}_j - \dot{\psi}_i \\ \mathbf{R}(\psi_{ij})\mathbf{v}_j - \mathbf{v}_i - \dot{\psi}_i S \mathbf{p}_{ij} \end{bmatrix}, \quad y_{ij} = \|\mathbf{p}_{ij}\|_2 + \nu,$$

where the state is $\mathbf{x}_{ij} = [\psi_{ij}, \mathbf{p}_{ij}^\top]^\top$, the inputs are the heading rate $\dot{\psi}_i$ ($\dot{\psi}_j$) and velocity $\mathbf{v}_i$($\mathbf{v}_j$) which are all perturbed by additive Gaussian noise, and the output is y_{ij} which is affected by the heavy-tailed UWB noise ν. The matrices

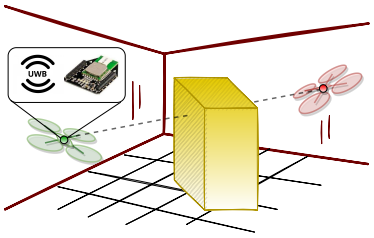

Figure 1: Peer-to-peer relative localization of MAVs in indoor cluttered environments using UWB ranging

$\mathbf{R}(\psi_{ij})$ and S are given as

$$\mathbf{R}(\psi_{ij}) = \begin{bmatrix} \cos(\psi_{ij}) & -\sin(\psi_{ij}) & 0 \\ \sin(\psi_{ij}) & \cos(\psi_{ij}) & 0 \\ 0 & 0 & 1 \end{bmatrix}, \; S = \begin{bmatrix} 0 & -1 & 0 \\ 1 & 0 & 0 \\ 0 & 0 & 0 \end{bmatrix}.$$

Note that the system is nonlinear. Now the main goal is to design a computationally efficient nonlinear filtering algorithm that can run online and provide accurate state estimation in the presence of heavy-tailed measurement noise.

3 Open issues

The kernel-induced Kalman filter [2] modifies the basic Kalman filter by introducing a *kernel-induced error* to replace the mean squared error used in the Kalman filter. The resulting algorithm requires an inner-loop fixed-point iteration to compute the posterior estimate. Monte Carlo simulations have shown that the Versoria kernel-based extended Kalman filter (EKF) provides more accurate localization than the standard EKF in various flight conditions. The next topics for future research are parametric kernel design and online adaptive kernel tuning which aim to deal with continuous changes in the environment. Besides, to reduce the computational complexity, an event-triggered mechanism can be leveraged as the posterior state update is only necessary when the estimates significantly deviates from the erroneous measurements.

References

[1] Ledergerber, Anton, Michael Hamer, and Raffaello D'Andrea. "A robot self-localization system using one-way ultra-wideband communication." 2015 IEEE/RSJ International Conference on Intelligent Robots and Systems (IROS). IEEE, 2015.

[2] B. Chen, X. Liu, H. Zhao, and J. C. Principe, "Maximum correntropy Kalman filter," Automatica, vol. 76, pp. 70–77, 2017.

Experimental Validation of Reference Spreading Control for Dual-Arm Robotic Manipulation under Simultaneous Impacts

Jari van Steen, Gijs van den Brandt, Nathan van de Wouw, Alessandro Saccon
Eindhoven University of Technology (e-mail: j.j.v.steen@tue.nl)

1 Introduction

Being able to utilize intentional impacts in robotic manipulation can allow for faster execution of tasks where humans currently excel in terms of speed, such as depalletizing. In this work, we propose and experimentally validate a novel control framework for dual-arm robotic manipulation of objects under nominally simultaneous impacts. This framework is built on earlier works on reference spreading, introduced in [1] and extended in [2] and references therein.

2 Approach

In this work, we consider time-based tracking control of both robot arms using position and velocity feedback, as well as a feedforward wrench. Both the velocity reference and the desired wrenches experience jumps at the nominal impact time, which is inevitably different from the actual impact time. To avoid peaks in the input signals as a result of a mismatch in impact times, the velocity reference and desired wrench are extended around the nominal impact time to create a separate ante- and post-impact reference, which overlap around the nominal impact time. This is used to control the setup through three distinct control phases. First is an ante-impact phase, using the extended ante-impact reference. This is followed by an interim phase, which initially disables velocity feedback and takes a convex combination of the ante- and post-impact desired wrench. Finally, a post-impact phase is entered, which uses the extended post-impact reference. By switching from the ante-impact phase to the interim phase based on impact detection, and by initially disabling velocity feedback in the interim phase, input peaks resulting from a mismatch in real and nominal impact times or unexpected separated impacts are avoided.

3 Experimental results

Validation is performed using a setup consisting of two Franka Emika Research 3 robots with flat silicone end effectors, as is shown in Figure 1. In Figure 2, the velocity signal and input force can be seen for one of the robots under naive tracking without reference spreading, under reference spreading control without entering an interim mode, and on the proposed approach, reference spreading with an interim mode. The results show that around the impact time, when the velocity v_y jumps, the proposed approach only shows a minor jump in input force f_y compared to the other two baseline approaches, showing the effect of our control strategy.

Figure 1: Depiction of the dual-arm setup, image taken from [3].

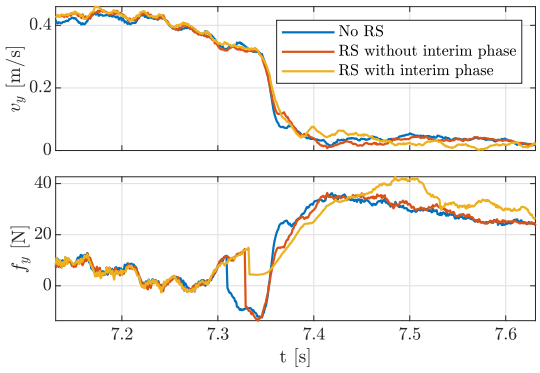

Figure 2: Normal velocity and input force of one of the robots during experiments with different control strategies

Acknowledgment

This work was partially supported by the Research Project I.AM. through the European Union H2020 program under GA 871899.

References

[1] A. Saccon, N. van de Wouw, and H. Nijmeijer, "Sensitivity analysis of hybrid systems with state jumps with application to trajectory tracking," in *Conference on Decision and Control*, pp. 3065–3070, IEEE, 2014.

[2] J. J. van Steen, N. van de Wouw, and A. Saccon, "Robot Control for Simultaneous Impact Tasks via Quadratic Programming Based Reference Spreading," in *American Control Conference*, IEEE, 2022.

[3] M. J. Jongeneel, S. Dingemans, and A. Saccon, "The Impact-Aware Robotics Database." hal-03900923, 2022.

Assistive shared control for interacting with articulated objects

Santiago Iregui, Joris De Schutter, Erwin Aertbeliën
Robotics Research Team, KU Leuven
Flanders Make@KU Leuven
Celestijnenlaan 300 - box 2420, 3001 Leuven, Belgium
Email: santiago.iregui@kuleuven.be

1 Introduction

In order to perform daily-living tasks, humans need to constantly interact with articulated objects (i.e. objects composed of a set of bodies connected by joints) such as doors, drawers, laptops, jars, etc. Performing these tasks is especially difficult for users with motor impairments. Assistive robotic solutions often rely on teleoperation joysticks that allows users to control 2 DoF or 3 DoF at a time. Nevertheless, these solutions are known to require a lot of effort from the users, especially during tasks that involve the interaction with articulated objects. Thus, in this work, we present a shared control method for interacting with articulated objects, targeted for people with motor impairments.

2 Methodology

In this work we adopt ideas of the *task frame* formalism [1] in order to propose a shared control method that can assist users during teleoperation of articulated objects with *unknown* geometric properties, by means of a 6 DoF joystick. Our method leverages an online (discrete) classifier to determine the type of articulated object and an online (continuous) *interactive perception* algorithm to estimate the position and the orientation of the corresponding joint. A task frame is then selected so that it is attached to the moving body, its origin is located at the estimated position, and one of its axes is aligned with the joint axis. The proposed shared control method then keeps the resulting velocity in this joint axis and downscales the rest. Initially no downscaling (i.e. no assistance) is applied, and while gathering additional information gradually more downscaling is applied to achieve seamless assistance. In this way we attempt to reduce the cognitive load and improve the performance of people while interacting with such objects during daily-living tasks.

This work fits within a constraint-based reconfigurable and adaptable framework for assistive robotics that we introduced in [2]. Thus, additional assistive strategies to the ones described in this text can be also be added.

3 Results

We performed two preliminary experiments where we compared the execution without assistance and with assistance. In both cases one inexperienced user interacted with the lid of a light-weight cardboard box (not fixed to the table) and the force/velocity commands were executed by means of a velocity-resolved admittance controller that uses force and torque measurements.

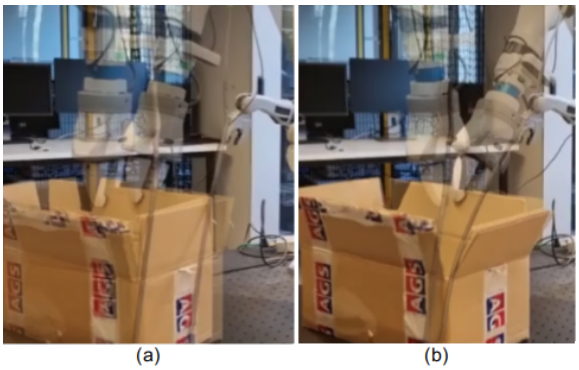

Figure 1: Preliminary experiments with a box as the articulated object (a) without assistance and (b) with assistance.

The comparison showed two performance improvements: *i)* a higher interaction velocity could be obtained by the user, and *ii)* the box did not move with respect to the table as it was intended. Fig. 1 shows two overlapping snapshots for each of the experiments. It can be observed that without the assistance the box was constantly dragged around the table as a result of non-accurate motions performed by the user. We plan to perform more rigorous experiments with objects with prismatic and revolute joints as future work.

Acknowledgements: All authors gratefully acknowledge the financial support provided by the Flanders Make projects Proud_SBO and SmartHandler_ICON, and the KU Leuven C1 project "Neurophysiological investigations of the human and nonhuman primate brain: from perception to action" (3M180301).

References

[1] H. Bruyninckx and J. De Schutter, Specification of force-controlled actions in the task frame formalism - a synthesis, IEEE Transactions on Robotics and Automation, vol. 12, no. 4, pp. 581589, 1996.

[2] S. Iregui, J. De Schutter, and E. Aertbeliën, Reconfigurable constraint-based reactive framework for assistive robotics with adaptable levels of autonomy, IEEE Robotics and Automation Letters , vol. 6, no. 4, pp. 73977405, 2021.

Achieving adaptive grip through compliant mechanical design and neuromorphic reflexes

Benn W.B. Proper, Irene A. Kuling, and Yoeri B. van de Burgt
Department of Mechanical Engineering
Eindhoven University of Technology
P.O. Box 513, 5600MB Eindhoven
The Netherlands
Email: b.w.b.proper@tue.nl

1 Abstract

Adaptive grip is an important part of robotic grippers to allow for the successful manipulation of irregularly shaped objects with (possibly unknown) material properties. Currently, external microprocessors with neural networks (NNs) can be used to train and optimize gripping behavior to complete tasks. However, these systems use standard CMOS-architectures, which are both time- and energy-inefficient for the training and operation of NNs. This results in a requirement of sufficient computational power and an external power source for basic operation and subsequently online training would be impossible on such a system.

Neuromorphic engineering is a developing field focussing on the development of systems mimicking biological neural systems such as brains and nerves [1, 2]. To reduce the computational and power load on the system to allow for local training on mobile systems, organic electrochemical transistors (OECTs) can be used to develop neuromorphic systems. OECT technology has not matured as much as standard CMOS-based systems, however, these systems are both time- and energy-efficient for use with NNs due to their internal memory and their application in analog calculation, allowing them to be used as nodes in neural network layers with analog matrix calculation. We aim to leverage this technology into developing 'reflex modules' that allow for reflexive responses to properties of held objects. These reflex modules can be trained locally to respond to individual stimuli, and a decision structure can assess the individual responses and map them to a change in the reference. The proposed control architecture can be viewed in Figure 1.

Considering that OECTs as a technology has not matured as much as the more developed field of CMOS-based architectures, we also aim to decrease the required computational complexity needed to control the system. We can achieve this by combining rigid and soft structures into the design of a robotic gripper finger. This semi-soft approach uses several soft actuators that share a pressure channel, if a phalange of the finger is blocked the rest of the finger can still form around the object. Additionally, if the tip of the finger is loaded, a pinch grip can be performed instead. Neither grips requires a special control task, as the compliant design automatically adjusts its strategy. The premise behind this functionality can be seen in Figure 2. The rigid structures aid in fixing the out-of-plane DOF, improving gripping stability.

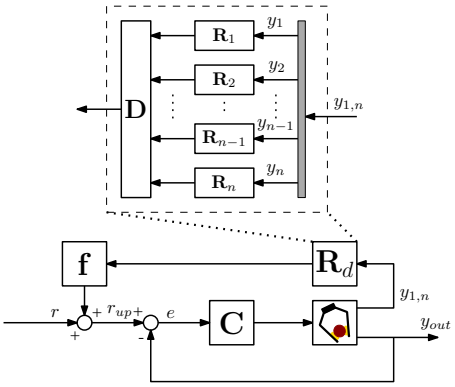

Figure 1: Control architecture with reflex modules that assess measurement data and map a response to a change in the reference signal.

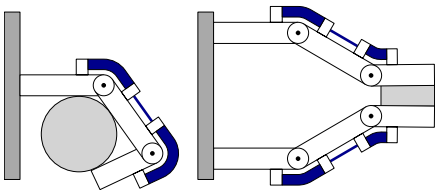

Figure 2: Semi-soft adaptive gripper with rigid links and soft pneumatic actuation.

References

[1] C. Mead. Neuromorphic electronic systems. *Proceedings of the IEEE*, 78(10):1629–1636, October 1990.

[2] Yeongjun Lee, Jin Young Oh, and Tae-Woo Lee. Neuromorphic Skin Based on Emerging Artificial Synapses. *Advanced Materials Technologies*, 7(12):2200193, December 2022.

Distance-based Rigid Formation-Motion Control for Unicycle Agents

Jin Chen, Bayu Jayawardhana
Jan C. Willems Center for Systems and Control, University of Groningen,
9747 AG Groningen, The Netherlands
jin.chen@rug.nl, b.jayawardhana@rug.nl

Hector Garcia de Marina
Department of Computer Engineer, Automation and Robotics, and with CITIC,
the University of Granada, Spain
hgdemarina.@ugr.es

1 Introduction

This paper studies the formation motion problem with nonholonomic constraints. We propose a gradient-based distributed formation control law for unicycle agents. In our control approach, without orientation measurement, all agents are assumed to agree *apriori* on the desired speed and are supposed to move under a distance-rigid formation in a same velocity. In addition, we provide rigorous stability analysis of the asymptotic behavior of the n-agent closed-loop system. Finally, we show numerically the convergence property of the unicycle agents which eventually form a desired rigid formation and realize orientation consensus.

2 Problem Formulation

In this paper, we utilize unicycle models in the 2D plane to describe the dynamics of agents. For our control design and analysis, we define the unit vector of the unicycle heading $h_i \in \mathbb{R}^2$ and its orthonormal vector $h_i^{\perp} \in \mathbb{R}^2$ in the global coordinate frame. Accordingly, we use the vectors $z_k \in \mathbb{R}^2$, $e_k \in \mathbb{R}$ and $e_k^{\theta} \in \mathbb{R}$ to represent the relative position vector, the distance error and the angular error, respectively, on the edge $\mathscr{E}_k = (i, j)$.

We assume that the agents share the information of the speed v^* with its neighbors which is easily achievable in several multi-agent applicable scenarios, like vehicle platooning and UAV swarm, by communication. For the multi-agent unicycle systems A_i, $i = 1, \ldots, n$, without heading angle measurement, the object of this paper is to design a distributed control law $\left[\begin{smallmatrix} v_i \\ \omega_i \end{smallmatrix}\right]$ for agents A_i such that $\left[\begin{smallmatrix} e_k(t) \\ e_k^{\theta}(t) \end{smallmatrix}\right] \to 0$ as $t \to \infty$ for all $\mathscr{E}_k \in \mathscr{E}$.

3 Distributed Formation-Motion Control of Unicycles

Using the kinematic offset points [2], we develop the distributed control law where the inputs are decomposed into the longitudinal velocity input (e.g., the velocity in the agent's direction) and the tangential velocity input (orthogonal to the longitudinal one). Applying the standard distance-based formation gradient control [1] to these inputs, the distributed control law for agents A_i, $i = 1, \ldots n$ is given by

$$\begin{aligned} v &= -D_{(h^{\top})} \bar{B} D_{z_r} e_r + v^* \mathbf{1}_{n \times 1} \\ \omega &= -\frac{1}{r} D_{((h^{\perp})^{\top})} \bar{B} D_{z_r} e_r \end{aligned} \tag{1}$$

where $h^{\top}, (h^{\perp})^{\top} \in \mathbb{R}^{|\mathscr{E}|}$ are the stacked vectors of $h_k^{\top}$'s and $(h_k^{\perp})^{\top}$'s, respectively for all $k \in 1, \ldots, |\mathscr{E}|$, B is the incidence matrix, r, z_r, e_r are the distance, the relative position, the distance error between offset points, respectively.

4 Simulation Results

In this simulation, we consider the formation of four unicycle agents. The trajectories of unicycle agents with the proposed distributed control are shown in Figure 1 where the agents are moving in the 2D-plane (x, y).

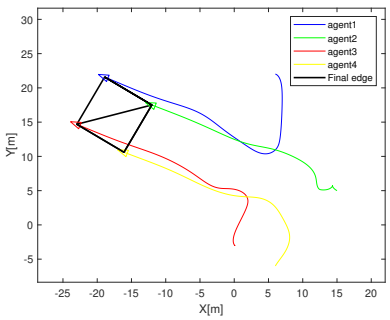

Figure 1: The plot of trajectories of four unicycle agents with the distributed control.

References

[1] Hector Jesús Garcia de Marina Peinado. "Distributed formation control for autonomous robots". PhD thesis. University of Groningen Groningen, 2016.

[2] Umit Ozguner, KA Unyelioglu, and C Hatipoglu. "An analytical study of vehicle steering control". In: *Proceedings of International Conference on Control Applications*. IEEE. 1995, pp. 125–130.

A novel biologically-inspired soft gripper driven by a dielectric elastomer actuator

Jiahao Pan
University of Groningen
The Netherlands
Email: j.pan@rug.nl

Raffaella Carloni
University of Groningen
The Netherlands
Email: r.carloni@rug.nl

1 Introduction

Soft grippers are in high demand in robotic applications as they promise to safely handle complex and fragile objects [1]. Origami, a traditional art of folding paper, is now attractive to researchers because it can provide elegant solutions for practical engineering problems [2]. Smart materials have been used to drive origami structures in place of conventional motors and pumps, which presents opportunities to make systems more compact and dexterous. Dielectric elastomers are smart materials and can deform under electrical stimuli. Dielectric elastomers have many advantages such as fast response and high strain [3], which make them suitable for gripper applications.

2 The biologically-inspired soft gripper

In this work, we present the design of a novel biologically-inspired soft gripper, whose structure mimics the Venus flytrap plant, as shown in Figure 1. The soft gripper is realized by combining an origami structure and a dielectric elastomer actuator. Specifically, the actuator is a minimum energy structural dielectric elastomer actuator [3], which is embedded in the structure of the soft gripper and drives it. The actuator consists of a pre-stretched dielectric elastomer film (3M VHB 4905) and a flexible frame (polyethylene terephthalate, thickness of 180 μm).

3 The fabrication of the soft gripper

The fabrication of the soft gripper is shown in Figure 2. First, the dielectric elastomer film is stretched with a stretch ratio of 3×3, and a rigid frame is attached to the pre-stretched film to keep it stretched. The flexible frame is then attached to the film with the shape of a hollow square. After that, the electrodes (carbon grease) are applied on both sides of the hollow area and the lead wires are connected to the electrodes. Stiffening frames (polyethylene terephthalate, thickness of 300 μm) are used to constrain the deformation of the flexible frame. The origami structure is attached to the actuator. When the gripper is released from the rigid frame, the elastic restoring force of the film bends the frame to its minimum energy state and makes the gripper open. When an electric field is applied, the DE film expands and the frame flattens from its initial bent state, allowing the gripper to close. When the electric field is off, the restoring force of the film makes the gripper open again. The design of the soft gripper is such that it can (i) clamp objects and (ii) wrap around objects like a flytrap. In addition, this gripper works in a continuous manner which provides protection for fragile objects. The prototype of the gripper has been built and tested with objects of different shapes and weights.

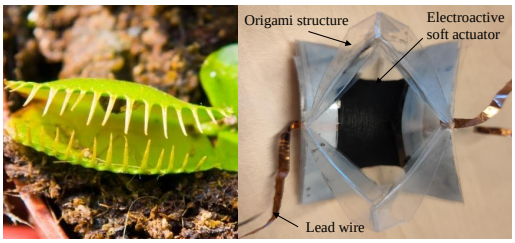

Figure 1: The Venus flytrap and the proposed soft gripper.

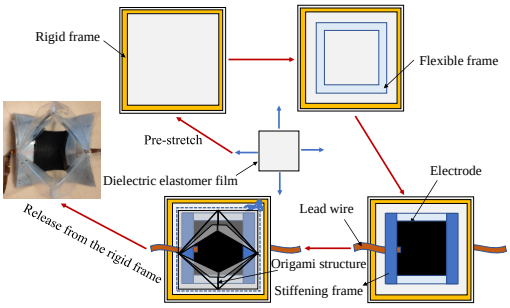

Figure 2: The fabrication steps of the soft gripper.

References

[1] X. Chen, X. Zhang, Y. Huang, L. Cao, and J. Liu,"A Review of Soft Manipulator Research, Applications, and Opportunities," Journal of Field Robotics, vol. 9, issue 3, 2022.

[2] L.M. Fonseca, G.V. Rodrigues, and M.A. Savi, "An Overview of the Mechanical Description of Origami-inspired Systems and Structures," International Journal of Mechanical Sciences, vol. 223, 2022.

[3] Y. Li, and T. Zhang, "Modeling and Characterizing Two Dielectric Elastomer Folding Actuators for Origami-Inspired Robot," IEEE Robotics and Automation Letters, vol. 2, issue 4, 2022.

Compliant grasping with a 2-DOF flexure-based gripper

Mohaddese Hazini, Janset Dasdemir, Wouter Hakvoort , Jan J. de Jong
University of Twente, Faculty of Engineering Technology
m.hazini@utwente.nl, j.dasdemir@utwente.nl, w.b.j.hakvoort@utwente.nl, j.j.dejong@utwente.nl

1 Introduction

Grasping deformable objects of different sizes, shapes or stiffness is one of the challenging problems in agricultural robotics. The guiding idea of this research is to design and control an under-actuated compliant grasping mechanism where the joints of the gripper are based on flexures instead of conventional ones. Although these types of joints reduce the uncertainties due to friction, backlash, or hysteresis and provide quite predictable dynamic behavior, external force measurements are still required in order to design a high-performance closed-loop interactive control algorithm. However, in some applications, it is difficult or costly to use a force sensor on the interaction surface. Therefore, it is highly desirable to design a control algorithm with a minimal sensing approach. In this study, we discuss the results of the proposed contact force and contact point estimation method on a compliant gripper mechanism.

2 System model

Consider a 2-DOF, finger-based gripping mechanism with two rigid links connected by flexure joints.The equation of motion of the system can be represented as

$$M\ddot{q}+C\dot{q}+Kq=\tau \tag{1}$$

where q is the joint position vector, M is the inertia matrix, C and K are damping and stiffness matrices respectively.

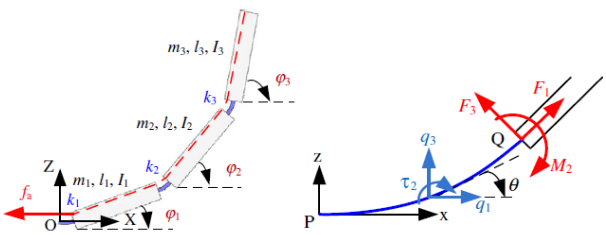

Figure 1: Schematic of a gripper with flexure joint [4]

3 Approach

The available grippers are mostly designed based on a quasi-static motion model, which results in slow grasping strategies[1]. One of the goals of this research is to speed up the process by considering dynamic grasping. On the other hand, the estimation of contact force during dynamic grasping without the use of a force sensor is a challenging task as contact force is required in interaction control strategies. Four different estimation algorithms were presented to estimate the contact stiffness and damping of the environment during the constraint motion [2]. The identified contact stiffness was then used to modify the desired end-effector trajectory during the contact, and impedance control was used to regulate the position and contact force according to the target impedance. However, in this work, the contact point was assumed to be known and a force sensor at the contact point was used to measure the force. In our proposed method, we applied an estimaon strategy to estimate the contact a force and point. By considering the contact force as an unknown disturbance on the system, the aim is to use disturbance observers to estimate the contact force through its effect on the joints as residual torques. The next step is to calculate the normal contact force as well as the position of the contact point on the gripper. The pseudo-inverse of the Jacobian matrix is used to map residual joint torques to normal contact force and estimate the contact point as in [3].

References

[1] Qiao, S., Zhang, L., Li, B., Liu, R., Guo, H. and Deng, Z., 2021. Coupled Bending Inwards Motion and Control Strategy Analysis of a Cable-Driven Underactuated Finger. IEEE Access, 9, pp.133902-133913.

[2] Erickson, D., Weber, M. and Sharf, I., 2003. Contact stiffness and damping estimation for robotic systems. The International Journal of Robotics Research, 22(1), pp.41-57.

[3] D'Ippolito, F., Alonge, F. and Cucco, E., 2014. Contact estimation in robot interaction. International Journal of Advanced Robotic Systems, 11(7), p.96.

[4] Guo, J. and Lee, K.M., 2013. Compliant joint design and flexure finger dynamic analysis using an equivalent pin model. Mechanism and Machine Theory, 70, pp.338-353.

Iterative Learning Control Applied to Explicit Co-simulation

Laurane Thielemans [1,2], Francisco Gonzalez [3], Laurens Jacobs [2,4], Jan Swevers [2,4], Roland Pastorino [1]
[1] Siemens Digital Industries Software, 3001 Leuven, Belgium
[2] MECO Research Team, Department of Mechanical Engineering, KU Leuven, Belgium
[3] Laboratorio de Ingeniería Mecánica, University of A Coruña, 15403 Ferrol, Spain
[4] Flanders Make@KU Leuven, Belgium
laurane.thielemans@siemens.com

1 Introduction

Co-simulation has become a cornerstone method for model-based system development. It constitutes an intuitive approach to model large and complex systems by dividing them into subsystems that are easier and faster to integrate. The simulation of these interconnected subsystems requires discrete-time communication, i.e., the exchange of the inputs and outputs of the subsystems (the coupling variables) at specific time instants. This exchange is the task of the co-simulation manager, which not only handles the communication between subsystems, but also compensates for any inaccuracies. In most cases, this manager contains an extrapolation algorithm. When the outputs of a subsystem directly depend on its inputs, direct feedthrough is present, resulting in an algebraic loop. This algebraic loop can be resolved by the co-simulation manager either iteratively or by extrapolating the unknown inputs. However, the latter can cause accuracy loss and stability issues. This has led researchers to investigate methods to monitor and correct co-simulation errors, e.g., by adapting the communication step size of the problem [1, 2]. If adapting the step size is not possible and some or all subsystems are 'black boxes', control algorithms using only the available coupling data can compensate for the chosen extrapolation methods, [3, 4].

2 A novel ILC-based approach

In this paper we propose a novel, twofold approach to correct coupling errors in explicit co-simulation. We formulate the co-simulation as a control problem, where the manager, containing the extrapolation method, is the system to be controlled. Firstly, we propose an Iterative Learning Control (ILC) method, which consists of performing a sequence of consecutive co-simulation runs. A correction is added to the co-simulation after every run, based on the information collected during the run. This yields a correction approach that does not require using implicit methods, adapting the communication step size, or modifying interface variables during runtime, which makes this approach compatible with real-time execution. In the case of co-simulation, however, a reference is not available, because the analytic and the monolithic (numerical) solutions, which could be used to determine the correctness of co-simulation results, are not available in most applications of interest. As a consequence, appropriate assumptions have to be made to provide a valid reference for the ILC in co-simulation experiments.

This choice of assumption is the second part of the approach: instead of using an extrapolation method, we assume that the co-simulation manager delays the output of the subsystem with direct feedthrough with one time step. This delay leads to a larger error in the uncorrected co-simulation, but the resulting system is easier to correct with ILC. A reference for the ILC now becomes available: the desired subsystem output value, or the output without time delay. This means that in the controller we need a time prediction of one time step, or a non-causal controller, for which ILC is perfectly suited. If the co-simulation is using an extrapolation method instead of the proposed time delay, for example zero-order-hold (ZOH) extrapolation, the exact subsystem output is not available anymore as a reference signal for the ILC scheme. The ILC sequence of co-simulations can still converge to zero tracking error but with an incorrect reference. Calculating another ILC reference that exactly compensates for the ZOH error is generally not possible, since the subsystems' internals are not accessible.

3 Simulation example

To demonstrate our novel twofold approach, we use a popular benchmark problem, the linear oscillator [3]. We study the ILC performance and how it compares to the uncorrected co-simulation. In the presentation, we will show that the ILC-compensated co-simulation achieves the same accuracy level as the monolithic co-simulation and thereby outperforms all alternatives. For the sake of completeness, we will also demonstrate the performance in a case where our main assumption does not hold.

References

[1] S. Sadjina, E. Pedersen. Energy conservation and coupling error reduction in non-iterative co-simulations. Engineering with Computers, 36:1579–1587, 2019.

[2] M. Benedikt, D. Watzenig, J. Zehetner, A. Hofer. NEPCE - A nearly energy-preserving coupling element for weak-coupled problems and co-simulation. In NAFEMS World Congress, Salzburg, Austria, 2013.

[3] B. Rodríguez, A. J. Rodríguez, B. Sputh, R. Pastorino, M. Á. Naya, F. González. Energy-based monitoring and correction to enhance the accuracy and stability of explicit co-simulation. Multibody System Dynamics, 55(1-2):103-136, 2022.

[4] W. Chen, S. Ran, C. Wu, B. Jacobson. Explicit parallel co-simulation approach: analysis and improved coupling method based on H-infinity synthesis. Multibody System Dynamics, 52(3):255–279, 2021.

Acknowledgment The financial support from the Flemish Agency for Innovation and Entrepreneurship (VLAIO, project HBC.2020.2880) is gratefully acknowledged.

Alternating projection-based optimal ILC for linear systems with non-uniform trial lengths under input constraints

Zhihe Zhuang
Jiangnan University
China
z.h.z.zhuang@tue.nl

Max van Meer
TU/e
Netherlands
m.v.meer@tue.nl

Hongfeng Tao
Jiangnan University
China
taohongfeng@hotmail.com

Dianqing Zhou
TU/e
Netherlands
d.zhou1@tue.nl

Tom Oomen
TU/e
Netherlands
t.a.e.oomen@tue.nl

1 Introduction

Iterative learning control (ILC) improves tracking performance trial by trial. In practical applications of ILC, the repetitive process may end up early by accident and the actual trial length varies. The ultimate goal of dealing with non-uniform trial lengths in ILC is to try to make the tracking performance as good as the identical case. In other words, try to increase the convergence speed along the trial axis in view of less information for learning. In this paper, the optimal ILC framework is employed to solve this issue. The alternating (successive) projection method is modified to adapt to the trial-varying situation with input constraints.

2 Problem Formulation

The illustration of the non-uniform trial lengths in ILC is as follows. The actual trial length N_k is set to vary in $\{N_-, N_- + 1, \ldots, N\}$, where N_- and N respectively denote the minimum and maximum lengths that occur in a particular application.

The lifted model with the same trial length N is employed, i.e.

$$y_k = Gu_k + d_k, \tag{1}$$

where G and d_k represent the system model and the effect of the initial conditions respectively. The discrete-time input and output sequence $u_k \in \mathbf{R}^{\ell N}$ and $y_k \in \mathbf{R}^{\mathrm{m}N}$. Define $y_d \in \mathbf{R}^{\mathrm{m}N}$ as the desired output. The tracking error vectors of systems with non-uniform trial lengths can be written as

$$e_k = F_k\left(y_d - y_k\right), \tag{2}$$

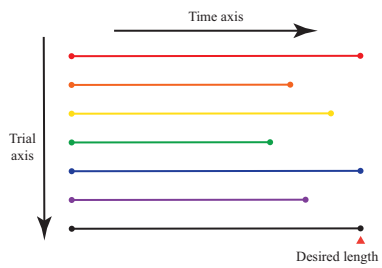

Figure 1: The illustration of the non-uniform trial lengths in ILC.

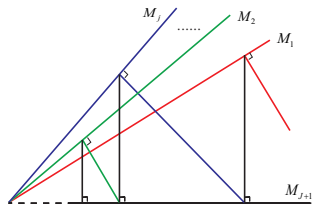

Figure 2: The illustration of designed alternating projections.

where

$$F_k = \begin{bmatrix} I_{N_k} \otimes I_{\mathrm{m}} & 0 \\ 0 & 0 \otimes I_{\mathrm{m}} \end{bmatrix}, \tag{3}$$

and I_l denotes the identity matrix with dimensions $l \times l$, and $\otimes$ denotes the Kronecker product.

3 Alternating Projection Design

Different from [1], multiple sets are introduced to represent the actual dynamics of the varying trial lengths. The ILC problem is equivalent to iteratively finding a point in the intersection of the following multiple sets in Hilbert space H

$$M_j = \left\{(e,u) \in H : e = F_j(y_d - y), y = Gu + d\right\}, \tag{4}$$

$$M_{J+1} = \left\{(e,u) \in H : e = 0, u \in \Omega\right\}, \tag{5}$$

where M_j and M_{J+1} respectively represent system dynamics and the tacking objective. Ω is the input constraint set. Then, the projection order is designed as (6) and the illustration can be seen in Fig. 2.

$$M_{j_k} = \begin{cases} M_j \in \{M_1, M_2, \ldots, M_J\}, & k \text{ is odd}, \\ M_{J+1}, & k \text{ is even}. \end{cases} \tag{6}$$

4 Ongoing Research

Future work includes the implementation of projections and developing optimal ILC algorithms for systems with non-identical trial lengths under input constraints.

References

[1] Y. Chen, B. Chu, and C.T. Freeman, "Generalized Iterative Learning Control Using Successive Projection: Algorithm, Convergence, and Experimental Verification," *IEEE Trans. Control Syst. Technol.*, vol. 28, no. 6, pp. 2079-2091, 2020.

Collision avoidance for UAV system using switching forces: Average dwell time analysis

Oscar Fabian Archila [1,2], Alain Vande Wouwer [1], and Johannes Schiffer [2]
[1]System, Estimation, Control and Optimization (SECO), University of Mons, Mons, Belgium
[2]Control Systems and Network Control Engineering, BTU Cottbus-Senftenberg, Cottbus, Germany
[1,2]Co-tutelle BTU and UMONS
Email: archilac@b-tu.de, alain.vandewouwer@umons.ac.be, schiffer@b-tu.de

1 Introduction

In UAV systems, a crucial requirement to attain autonomy is to ensure the security of the flight by avoiding unexpected obstacles. On the other hand, a collision avoidance algorithm should respond in a short time, maintaining a low computational cost. A method that aligns with these constraints is the artificial potential field forces based on simple geometrical calculations. However, depending on the position of the obstacle and the UAV, this strategy generates oscillations in the trajectory or dead zones. We propose to represent the attractive and repulsive forces as a switched system. The switching system is finally analyzed using the average dwell time that restricts the switching time.

2 Artificial forces as a switching system

The artificial potential field forces approach for collision avoidance problems is a strategy based on a virtual force $F_i = F_{att} + F_{rep}$ $(i = 1, \ldots, n)$ that depends on the sum of the attraction and repulsion forces [1]. This force returns the desired direction to avoid obstacles. We propose a modification of artificial forces by segmenting the workspace in the XY plane and establishing individual forces on each segment. Figure 1 shows an example of a UAV and an obstacle with four segments.

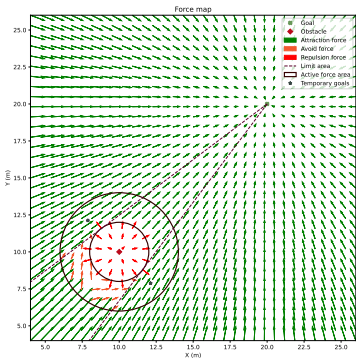

Figure 1: Force map for switching force approach.

Figure 1 presents three attractive forces and a fourth repulsive one around the obstacle. The switching of the force depends on the position of the UAV and the two circular areas around the obstacle.

3 Average dwell time analysis

The average dwell time is used to analyze the stability of the switched system [2]. If the number of switchings $N_\sigma(\tau,t)$ over an interval $[\tau,t)$ for a given previous value N_0 satisfies

$$N_\sigma(\tau,t) \leq N_0 + \frac{t-\tau}{\tau_a}, \tag{1}$$

where τ_a is the average dwell time, then the switched system is exponentially stable. By controlling N_σ and adding rules for the switching, we can ensure that the response of the system is bounded, and in a combination with the artificial forces the UAV reaches the goal objective while avoiding collisions. Figure 2 shows an example.

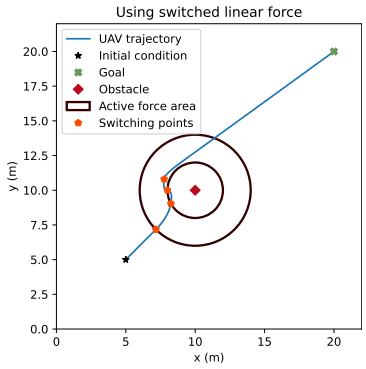

Figure 2: Average dwell time simulation for a UAV and an obstacle.

References

[1] L. Garcia-Delgado, A. Dzul, V. Santibáñez, and M. Llama, "Quad- rotors formation based on potential functions with obstacle avoidance," IET Control Theory & Applications, vol. 6, no. 12, pp. 1787–1802, 2012.

[2] G. Zhai, B. Hu, K. Yasuda, and A. N. Michel, "Stability analysis of switched systems with stable and unstable subsystems: an average dwell time approach," International Journal of Systems Science, vol. 32, no. 8, pp. 1055–1061, 2001.

Fueling and Density Control in Fusion Tokamaks using Mixed-Integer MPC

C. A. Orrico
Eindhoven University of Technology
c.a.orrico@tue.nl

D. Krishnamoorthy
Eindhoven University of Technology
d.krishnamoorthy@tue.nl

M. van Berkel
Dutch Institute for Fundamental Energy Research
m.vanberkel@differ.nl

1 Abstract

Core fueling and density control is essential to maximizing the power production and ensuring safe operation of fusion reactors [1]. Current development in the control of tokamak core fueling and density is limited due to the complexity of the problem. The primary actuators are frozen hydrogen fuel pellets fired into the tokamak plasma core [2, 3]. This results in a mixed logical dynamic (MLD) system as the controller must decide whether to launch a pellet or not (i.e., a discrete actuator). Edge density limits are safety critical, leading to plasma disruptions if violated [4]. Complicating matters further, modeling plasma core density and temperature requires continuous nonlinear coupled drift-diffusion partial differential equations (PDEs) [5]. Finally, to achieve real-time feedback control, maximum computation time of the controller cannot exceed the repetition rate of the pellet injection system ($\sim$ 100ms) [6].

In this work, a mixed-integer (MI) receding horizon control framework is proposed. State dynamics are discretized into a system of ordinary differential equations (ODEs) from the system of coupled nonlinear PDEs using the finite difference method. The fuel pellets are incorporated into this model as a fixed point source near the plasma edge. The optimal control problem is formulated as a model predictive control (MPC) algorithm over a prediction horizon N, where the $x_k \in \mathbb{R}^{n_x}$ denotes system state (electron density and temperature) at discrete time k and $u_k \in \{0,1\}$ denotes the binary control decision of whether to fire (1) or not fire (0) a hydrogen fuel pellet:

$$\min J(x(k),u_k)_{u_k} := \sum_{i=0}^{N} \|(x_{i|k} - x^r_{i|k})\|^2_Q + \sum_{i=0}^{N-1} \|u_{i|k}\|^2_R$$

$$\text{s.t.}$$

$$\begin{aligned} x_{i+1|k} &= f(x_{i|k}, u_{i|k}) \quad \forall i \in \{0,...,N-1\} \\ Gx_{i|k} &\leq n_{Gw} \quad \forall i \in \{0,...,N\} \\ u_{i|k} &\in \{0,1\} \quad \forall i \in \{0,...,N-1\}, \end{aligned}$$

where Q and R are weighting matrices. The ODE describing state dynamics $f(x_{i|k}, u_{i|k})$ is linearized around a desired control trajectory $x^r_{i|k}$. The MI-MPC problem is solved using the `Gurobi` solver. To improve performance, the optimization problem is reformulated as a penalty term homotopy (PTH) MPC problem [7], compatible with a quadratic programming (QP) solver.

Both the MI-MPC and PTH-MPC algorithms achieved good reference tracking for all prediction horizons tested without violating path constraints. While both methods meet computational requirements, the PTH-MPC algorithm consistently outpaces MI-MPC in terms of maximum computational time. Future work will apply both the PTH-MPC and MI-MPC algorithms to an experimentally validated transport model [8]. Next, the pellet control decision set will be extended to incorporate variable pellet size, frequency, and fuel composition. As this will significantly increase computational costs for the MI control problem, further measures will be explored to increase algorithm efficiency.

References

[1] L.R. Baylor et al., Nucl. Fusion 47, (2007) 443

[2] P.T. Lang et al., 2012 Nucl. Fusion 52 (2012) 023017

[3] S. K. Combs & L. R. Baylor, Fusion Sci. and Technol. 73:4, (2018) 493–518

[4] M. Greenwald et al., Nucl. Fusion 28, (1988) 2199

[5] Freidberg, J. *Plasma Physics and Fusion Energy*. Cambridge: Cambridge University Press, 2007. 453.

[6] Baylor, L. R. et al., IEEE Trans. Plasma Sci. 44:9, (2016) 1489–1495

[7] S. Sager. Numerical methods for mixed-integer optimal control problems. Lübeck: Der Andere Verlag, 2005.

[8] T.C. Blanken et al., Fusion Eng.and Des. 126, (2018) 87–103

Efficient Implementation of Model Predictive Control for Water Distribution Networks

Peter Verheijen
Control Systems group
Eindhoven Univ. of Tech.
The Netherlands
p.c.n.verheijen@tue.nl

Mircea Lazar
Control Systems group
Eindhoven Univ. of Tech.
The Netherlands
m.lazar@tue.nl

Dip Goswami
Electronic Systems group
Eindhoven Univ. of Tech.
The Netherlands
d.goswami@tue.nl

1 Introduction

Water distribution networks (WDNs) are large–scale systems that supply drinking water to consumers over a large area. The goal of the operation management is to distribute the water over the network to sustain local consumer demand, while continuously keeping the network pressurized and minimizing distribution cost. Additionally, the control action must anticipate on the nonlinear dynamical response and respect the (nonlinear) system constraints [1]. Model predictive control (MPC) provides a combination of open–loop constrained optimization over a prediction horizon and active feedback according to the receding horizon principle. In contrary to off–line optimization, which is currently still widely employed as the standard controller for WDNs, the active feedback prevents drift between the predictions and the measurements in real–time.

2 Approach

A water distribution network can be represented as a large set of interconnected hydraulic elements. The model can be defined as 3 equations, representing the dynamical part, the conservation of mass and the conservation of energy, respectively [1]:

$$\mathbf{h}(k+1) = \mathbf{h}(k) + A_q\mathbf{q}(k) + B_q\mathbf{u}(k) \tag{1a}$$
$$\mathbf{0} = G_q\mathbf{q}(k) + G_u\mathbf{u}(k) + G_d\mathbf{d}(k) \tag{1b}$$
$$\mathbf{0} = F_h\mathbf{h}(k) + \Phi(\mathbf{q}(k), \mathbf{u}(k)). \tag{1c}$$

Next, the cost function of the MPC controller for WDNs classical consists of 3 elements. First, the safety guarantee of water in the tanks, i.e.

$$l_1(k+i) = \begin{cases} \|\mathbf{h}_{i+1|k} - \mathbf{h}_S\|_2^2, & \text{if } \mathbf{h}_{i+1|k} \leq \mathbf{h}_S, \\ 0, & \text{else.} \end{cases} \tag{2}$$

Secondly, increasing longevity of the actuator components by penalizing fast switches, i.e.

$$l_2(k+i) = \|\mathbf{u}_{i|k} - \mathbf{u}_{i-1|k}\|_2^2 \tag{3}$$

The last term is to minimize overall distribution cost. The distribution cost can be expressed as $l_3(k+i) = (\alpha_1 + \alpha_{2,k})\|\mathbf{u}_{i|k}\|_2^2$, where α_1 and $\alpha_{2,k}$ are terms computed from the head of the pump, the efficiency and pump tariff, which varies over time.

The resulting nonlinear MPC problem is solved using a tailored sequential quadratic programming (SQP) algorithm, which exploits the specific model (1) and cost function $l_1 + l_2 + l_3$. SQP solves a nonlinear problem by successively linearizing it into a sequence of quadratic programs (QPs), which can be solved using standard solvers. With the proper linearization and guess of the initial point, SQP can compute the optimal nonlinear solution in a few QPs [2].

3 Results

For this simulation, we considered a small water networks, with 3 tanks, 2 pumps and 2 demand locations. The MPC has a sampling period of T_s =30 minutes and must regularize the volumes in the tanks (h_5 and h_6) with respect to a (partially uncertain) demand flow using pump flows q_{12} and q_{26} as control parameters. See Fig. 1 for the simulation result over a 4 day period.

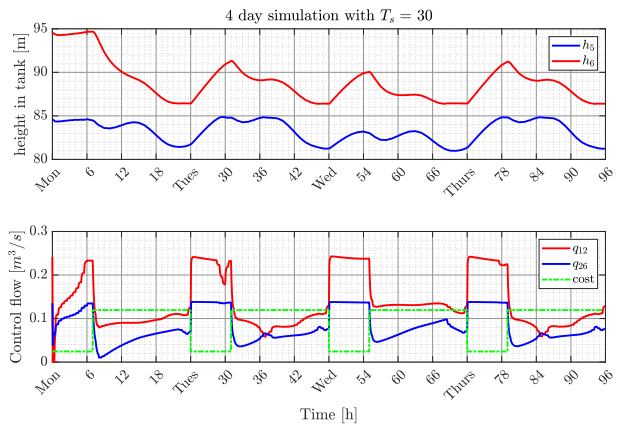

Figure 1: Simulation results of the SQP-MPC controller, with the pumping price in green

References

[1] Y. Wang, V. Puig and G. Cembrano, "Non–linear economic model predictive control of water distribution networks," Journal of Process Control, 2017.

[2] S. Gros, M. Zanon, R. Quirynen, A. Bemporad and M. Diehl, "From linear to nonlinear MPC: bridging the gap via the real-time iteration," Int. Journal of Control, 2016.

MIMO gas injection control of the electron density and NII impurity emission front position in TCV

J.T.W. Koenders[1,3], A. Perek[2], C. Galperti[2], B.P. Duval[2], O. Février[2], C. Theiler[2], M. van Berkel[1], and the TCV Team*

[1] DIFFER - Dutch Institute for Fundamental Energy Research, Eindhoven, The Netherlands

[2] Ecole Polytechnique Fédérale de Lausanne (EPFL), Swiss Plasma Center (SPC), Lausanne, Switzerland

[3] Eindhoven University of Technology, Control Systems Technology, Eindhoven, The Netherlands

* See author list of H. Reimerdes et al., 2022 Nucl. Fusion 62, 042018

Introduction

The EUROfusion consortium has identified seven challenges to be solved before commercial tokamak fusion reactors can be realized [1]. One of these challenges is the tokamak heat and particle exhaust. Without mitigation, the expected exhaust power leaving the high temperature plasma will exceed present-day material engineering limits [2]. The main approach considered for exhaust mitigation is the injection of several gas species in the tokamak exhaust region [3], called the *divertor*. Real-time control algorithms that actively assess the exhaust plasma state are required to continuously adjust the gas injection rates to evolving reactor conditions and disturbances. Control of the plasma exhaust with a single gas species has been performed on practically all operational tokamaks, see e.g. [4, 5, 6]. However, for reactor relevant mitigation, multiple gas species injection must be performed simultaneously. Two species will, at the least, be required: fueling of hydrogen isotopes to increase neutral pressure, and impurity species seeding that radiates strongly in the plasma edge region outside the last closed flux surface. In the envisioned demonstration powerplant called DEMO, a significant amount of the fusion power must be radiated from the core, probably requiring a third gas species which strongly radiates within the confined plasma's last closed flux surface. The required multiple gas species injection makes exhaust control in fusion reactors inherently a MIMO control problem.

Design and demonstration of a MIMO gas injection controller on the TCV tokamak

In this contribution we systematically design a two-gas MIMO controller for the TCV tokamak [7]. We demonstrate the control of the N-II emission front position L_{pol} and the line averaged electron density $\bar{n}_e$ using a combination of D_2 and N_2 gas injection in the divertor. The N-II emission front position and the line-averaged electron density are control variables related to plasma exhaust mitigation (detachment) and the core plasma performance respectively. The N-II emission front position is tracked by a real-time image processing algorithm [8] applied to spectrally filtered images from the multi-spectral imaging diagnostic MANTIS [9]. The line-averaged electron density is measured using a vertical Far InfraRed interferometer (FIR) intersecting the current centroid of the core plasma. The designed MIMO controller uses a decoupling matrix as a pre-compensator that mitigates interaction around the control loop bandwidth. The pre-compensator is based on a suitable transfer function structure for gas injection response in TCV [10] regressed on system identification results [11]. We demonstrate the MIMO gas injection controller performance with experiments on the TCV tokamak.

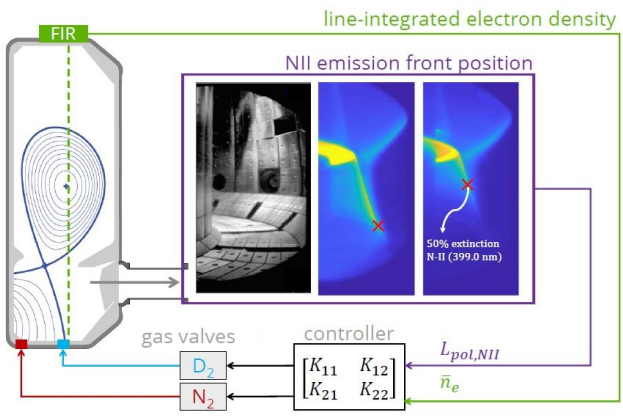

Figure 1: Overview of the control problem, using FIR for electron-density measurement, and multispectral camera MANTIS to identify the NII emission front.

References

[1] T. Donné et al., Roadmap to Fusion Energy, EUROfusion (2018)
[2] R. Pitts et al., Nucl. Mat. Ener. **20**, (2019)
[3] A. Kallenbach et al., Plasma Phys. Control. Fusion **55**, (2013)
[4] D. Eldon et al., Nuclear Fusion **57**, (2017)
[5] M. Bernert et al., Nuclear Fusion **61**, (2021)
[6] T. Ravensbergen et al., Nat. Commun. **12**, (2021)
[7] H. Reimerdes et al., Nucl. Fusion **52**, (2022)
[8] T. Ravensbergen et al., Nucl. Fusion **60**, (2020)
[9] A. Perek et al., Rev. Sci. Instrum. **90**, (2019)
[10] Koenders et al., Nucl. Fusion **62**, (2022)
[11] Koenders et al., Nucl. Fusion **63**, (2023)

A Framework for Data-Driven Time Series Forecasting for Model Predictive Control of Vessel Energy Systems

Esma Özdemir, Andrea Coraddu, Rudy R. Negenborn
Marine and Transport Technology, Delft University of Technology
Email: {e.ozdemir-1, a.coraddu, r.r.negenborn}@tudelft.nl

1 Background and Motivation

Marine Energy and Power Management Systems are systems in which numerous complex components interact to coordinate operations with various distributed energy resources, energy storage systems, and power grids to assure power delivery while minimising overall energy consumption, achieving tracking efficiency, ensuring reliability, health, and safety of the main onboard systems [1]. As a result, enhanced control strategies are necessary. While traditional methods (e.g., rule-based control [2], PID-based control [3]) are easy and intuitive to implement, they are limited by the fact that they cannot be applied to evaluate processes over a certain time horizon. However, employing traditional approaches to obtain accurate forecasting is rather difficult and requires advanced strategies. Model Predictive Control (MPC) is a control method that determines the best control input by considering predicted future system responses over a limited time horizon. The prediction of the system response is hard, as there are numerous time-varying constraints that need to be held. More accurate forecasting would result from leveraging historical operational data, Machine Learning (ML) algorithms together with time series (TS), and combining it with system-specific physical knowledge.

2 Proposed Framework

The objective of MPC considered optimisation problem is the minimisation of energy load (i.e., the feature to forecast over the time horizon) while being constrained by factors such as time and ensuring the health and safety of primary onboard systems. This work focuses on the predictor of the energy load of the MPC framework depicted in Figure 1, leveraging historical and real-time operational data. The combined controller and plant modelling framework is given in Figure 1 and explained as follows. First, model selection and error estimation [4] will be carried out for the predictive feature. Several state-of-the-art ML methods (e.g., kernel, ensemble, and neural methods) will be applied to identify the best-performing algorithm considering accuracy and computational requirements. In fact, the further the forecasts happen in time, the lower the accuracy is. Therefore, two new hyperparameters need to be learnt: the optimal amount of historical data to include in the learning phase (Δ^-) and the maximum horizon (Δ^+) that can be predicted

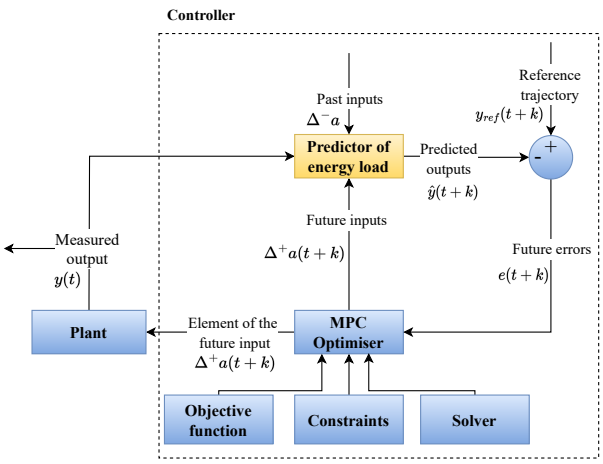

Figure 1: Combined MPC and plant modelling framework.

without compromising the accuracy. Subsequently, the predictor is included in the MPC framework. At each time step, the prediction $\hat{y}(t+k)$ is compared with the reference trajectory value $y_{ref}(t+k)$, and their difference is used to determine an error value $e(t+k)$. To maintain the process as close to the reference trajectory as possible, the error is integrated into the optimisation problem. Then the optimiser determines a new control variable $\Delta^+ a(t+k)$ for the next step. Results on operational data coming from a real vessel demonstrate that the proposed data-driven TS forecasting leads to a negligible loss in accuracy, at a minimal computational burden to forecast the energy load with a horizon Δ^+ of a number of minutes to be exploited in the MPC framework.

3 Acknowledgement

This research is supported by the Rijksdienst voor Ondernemend funded research project Sustainable Hydrogen Integrated Propulsion Drives (SH2IPDRIVE).

References

[1] C. Wei, X. Bai, and T. Kim. Advanced control and optimization for complex energy systems. *Complexity*, 2020, 2020.

[2] M. Casini. Building automation systems. *Journal: Construction*, 4:525–581, 2022.

[3] A. Visioli. *Practical PID control*. Springer Science & Business Media, 2006.

[4] L. Oneto. *Model selection and error estimation in a nutshell*. Springer, 2020.

The scenario approach to stochastic barrier functions

[1]Frederik Baymler Mathiesen, [2]Licio Romao, [1]Simeon C. Calvert, [2]Alessandro Abate, [1]Luca Laurenti
[1]Delft University of Technology, The Netherlands [2]Oxford University, England

1 Introduction

Many autonomous systems such aircrafts and autonomous vehicles are safety-critical. Consequently, they require formal assurances on their safety. Unfortunately, guaranteeing safety for non-linear stochastic systems remains an open question that has received much attention [1], [2], but a gap remains with respect to conservativity and scalability. We certify probabilistic safety for the system using Stochastic Barrier Function (SBF) for a system model that includes both epistemic (lack of knowledge) and aleatoric (inherent randomness) uncertainty. The SBF is found using robust convex optimization and the scenario approach.

2 Theory

Consider the following uncertain stochastic system

$$\mathbf{x}[k+1] = f(\mathbf{x}[k], \lambda) + \mathbf{v}[k] \quad \text{for } x_k \in q_i \tag{1}$$

where $\mathbf{x}[k] \in \mathbb{R}^n$ is the state of the system at time k, $q_i \subseteq \mathbb{R}^n$ is a polyhedron, and the epistemic uncertainty is represented by the parameter λ, which belongs to e.g. a hyperrectangle or the standard simplex. $\mathbf{v}[k]$ is an independent random variable capturing the aleatoric uncertainty.

Problem 1 (Probabilistic Safety)**.** Given a safe set $X_s \subset \mathbb{R}^n$, a finite time horizon $K = \{0, 1, \ldots, H\}$, and an initial set of states $X_0 \subseteq X_s$, compute probabilistic safety defined as

$$P_s(X_s, X_0, H) = \inf_{x_0 \in X_0} P(\forall k \in K, \mathbf{x}[k] \in X_s \mid \mathbf{x}[0] = x_0).$$

To certify safety, we employ SBFs [3, Thm. 2], which we assume to belong to the family of Piece-wise Affine (PWA) functions, motivated by the fact that a PWA function with arbitrarily many regions can approximate any continuous function. Let $Q = \{q_1, \ldots, q_m\}$ denote the set of regions.

$$B(x) = B_i(x) = u_i^\top x + v_i, \quad \text{for } x \in q_i \tag{2}$$

To find a SBF of this form, we use the scenario approach and prove it reduces to solving a robust linear program.

Theorem 1. *Let $\varepsilon \in (0,1)$ and N iid. samples $(v_l)_{l=1}^N$ of $\mathbf{v}$ be given and assume $\delta \geq \varepsilon\,[\sup_{x \in \mathbb{R}^n} B(x)]$. Let $\gamma, \beta \geq 0$ and define $q_{ij} = \{x \in q_i \mid f(x, \lambda) + v_l \in q_j\}$,*

$$h_{ij}(y, \lambda, v_l) = \sup_{x \in q_{ij}} B_j(f(x, \lambda) + v_l) + \frac{-B_i(x) - \beta + \delta}{1 - \varepsilon}.$$

Let $y^\star$ be the solution to the following program with $y = (\gamma, \beta, u_1, v_1, \ldots, u_m, v_m) \in \mathbb{R}^d$

$$\begin{aligned} \min_y \quad & \gamma + \beta H \\ & \left[\sup_{x \in q_i} -B_i(x)\right] \leq 0, && \forall i, \\ s.t. \quad & \left[\sup_{x \in q_i \cap X_0} B_i(x)\right] \leq \gamma, && \forall i, q_i \cap X_0 \neq \emptyset, \\ & B_i(x) = 1, && \forall i, q_i \cap X_u \neq \emptyset, \\ & h_{ij}(y, \lambda, v_l) \leq 0, && \forall i, j, \forall 1 \leq l \leq N \end{aligned} \tag{SBP}$$

Then, it holds that

$$P_s(X_s, X_0, H) \geq 1 - (\gamma^\star + \beta^\star H).$$

with a probability of at least $1 - \sum_{i=0}^{d-1} \binom{N}{i} \varepsilon^i (1-\varepsilon)^{N-i}$.

The idea to prove this theorem is to formulate the search for a SBF as a chance-constrained program. Then by showing convexity and applying the scenario approach, the optimal solution to the scenario program is, with a lower-bounded confidence, a valid stochastic barrier function, which lower bounds the probability of safety by $1 - (\gamma^\star + \beta^\star H)$.

3 Results

Table 1 shows scenario barrier functions for a drone, a vehicle and a Neural Network Dynamical Model (NNDM). The empirical results show that our method generates non-conservative certificates and is computationally tractable.

Table 1: Examples of Scenario Barrier Functions.

System	$P_s(X_s, X_0, H)$	Comp. time
Drone	99.5%	8.03s
Vehicle in wind	99.5%	32.56s
NNDM (inv. pendulum)	91.1%	6.49s

References

[1] T. Badings *et al.*, *Probabilities are not enough: Formal controller synthesis for stochastic dynamical models with epistemic uncertainty*, 2022.

[2] C. Knuth *et al.*, *Planning with learned dynamics: Probabilistic guarantees on safety and reachability via lipschitz constants*, 2020.

[3] C. Santoyo *et al.*, "A barrier function approach to finite-time stochastic system verification and control," *Automatica*, 2021.

Support system for active and passive design of sustainable buildings

Esteban Camilo Lage Cano
Eindhoven University of Technology
e.c.lage.cano@tue.nl

Christian Portilla Caicedo
Eindhoven University of Technology
c.r.portilla@tue.nl

Jairo José Espinosa Oviedo
Universidad Nacional de Colombia
jespinov@unal.edu.co

1 Abstract

In this work, a tool developed with the objective of providing support to the active and passive design of a construction is presented. Passive design focuses on the passive modules of the building, that is, on the construction components and materials, the windowing, the glazing, the orientation and the geographical location. Active design is a broad term that includes the characteristics and operation of all devices that consume electrical energy for their operation or those that generate electrical energy. This tool uses the thermal resistance and capacitance modeling methodology to estimate the thermal and the energy dynamics of a building. The support consists of providing suggestions to the professional designer mainly on the passive design of the construction. These suggestions are produced by solving a simulation-based multi-objective optimization problem, in which the initial investment cost of building materials, comfort, and energy consumption are optimized. The optimization method is developed by integrating the differential evolution algorithm programmed in Python with OpenModelica as the construction simulation software. This tool uses the Aixlib and Buildings libraries developed within the framework of the IEA EBC Annex 60 project in the Modelica language [2]. The summary of the framework is shown in the Figure. 1.

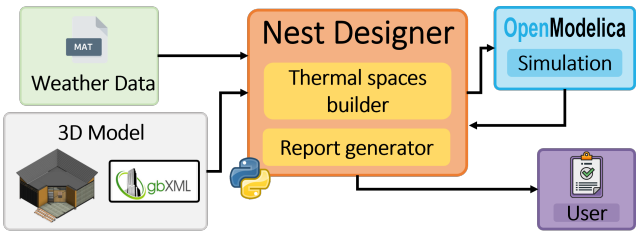

Figure 1: Nest Designer software framework

This methodological tool is applied to the case study established in Section 5.2.1 of the ANSI/ASHRAE 140-2001 standard, Test Case 600. In the optimization method, orientation, inclusion or exclusion of sunblinds, the thermal properties of the building envelope and the size and thermal properties of the windows are taken as decision variables. As an objective function to optimize comfort, the PPD index developed by Fanger is used [1]. To quantify energy consumption, annual cooling and heating loads are used. To optimize the initial investment in the cost of materials, a data set was constructed with their estimated costs and thermal properties. After using the tool in the study case, a saving of 72% in the cooling load and 83% in the heating load were obtained, with respect to the initial configuration, intervening only in the passive design of the construction. The heating and cooling loads are presented in the Figure 2. The red triangles and asterisk represent the heating and cooling load of the initial scenario of the study case respectively. The blue triangles and asterisk represent the heating and cooling load of the optimal scenario of the study case respectively, according to the methodology.

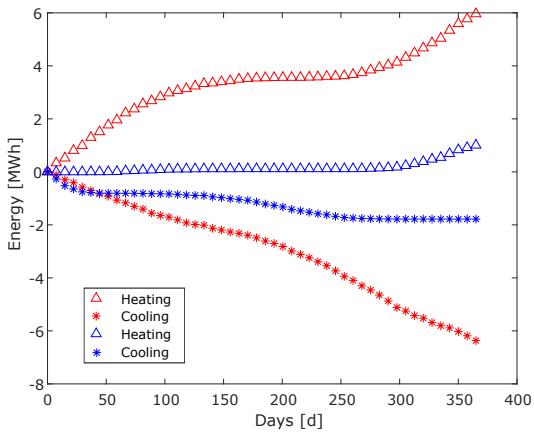

Figure 2: Comparison between the thermal loads between the initial configuration (red) and the configuration obtained from the methodology (blue) with a rotation in the azimuth angle of 60 degrees.

References

[1] Fanger, Povl O.: Calculation of Thermal Comfort, Introduction of a Basic Comfort Equation. En: Ashrae Transactions 73 (1967)

[2] AixLib - An Open-Source Modelica Library within the IEA-EBC Annex 60 Framework. Müller D., Lauster M., Constantin A., Fuchs M., Remmen P.. BauSIM 2016, p.3–9, September 2016.

Visibility-based Marching Methods: An Exact Solution to the Eikonal Equation for Path Planning on Cartesian Grids

Ibrahim Ibrahim, Joris Gillis, Wilm Decré, and Jan Swevers
MECO Research Team, Department of Mechanical Engineering, KU Leuven, Belgium
Flanders Make@KU Leuven, Belgium
ibrahim.ibrahim@kuleuven.be

Fast Marching Methods (FMM) constitute a class of algorithms that can be used in motion planning to compute optimal time-of-arrival values at all points in a Cartesian grid by efficiently propagating the frontline of one or more waves originating at one or more sources respectively [1]. At its core, this class of algorithms is driven by solving the Eikonal Equation, which is a particular Hamilton-Jacobi non-linear first order partial differential equation (PDE) that governs the monotonic evolution of wave frontlines,

$$1 = F(X)||\nabla T(X)|| \tag{1}$$

where $F(X)$ and $T(X)$ are the expansion speed of the wave and its time-of-arrival respectively, as a function of the position $X \in \mathbb{R}^n$.

A solution of (1) has been outlined in [2] by discretizing the gradient and solving it via entropy-satisfying upwind schemes. The result is a non-decreasing, local-minima-free function that can be initiated at any source point of interest. The optimal shortest path between the source and any point may then be obtained using gradient descent (GD). However, FMM solutions are not exact as they entail finite difference approximations of gradients. Moreover, FMM have been greatly optimized, yet they remain computationally demanding. Lastly, GD is required to obtain the optimal path from such algorithms.

In this work, an exact solution to (1) is proposed. The solution consists of utilizing the notion of visibility - the existence of an unobstructed line-of-sight between two points - to anchor pivots that ensure exact and uninterrupted wave propagation until it covers the whole grid. There have been approaches to quantify visibility - synonymously, accessibility - between two points, but they either entail approximations and simplifications, or are computationally expensive. In this work, we solve the visibility problem by advecting the visibility quantity, in a novel way, using a linear first-order hyperbolic PDE of the form

$$\frac{\partial u(x,y)}{\partial y} + c(x,y)\frac{\partial u(x,y)}{\partial x} = 0 \tag{2}$$

where $u(x,y)$ is the visibility at every grid position (x,y) and $c(x,y)$ is a field describing rays starting from the source and going out in all directions. Our approach employs an entropy-satisfying upwind scheme that converges to the true visibility polygon as the step size goes to zero. Lastly, our algorithm embeds the global shortest path from the source to every single grid-point, eliminating the need for GD backtracking.

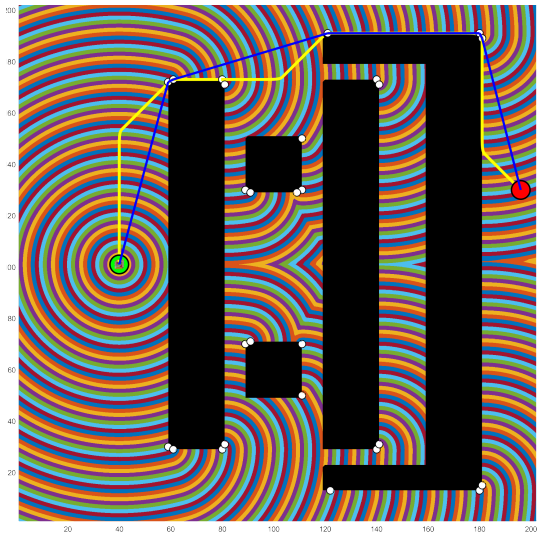

Figure 1: Sample wave propagation using our proposed method. The wavefront contour bands can be seen in color-scale.

A sample simulation result is presented in Fig. 1. We show the wave starting point in green, sample target point in red, pivot points around which the wave turns in white, and lastly, the obstacles in black. The accompanying shortest path result is obtained directly from the algorithm and is shown in blue. For comparison, GD shortest path is shown in yellow.

References

[1] M. S. Hassouna and A. A. Farag, "MultiStencils fast marching methods: A highly accurate solution to the Eikonal equation on cartesian domains," in IEEE Transactions on Pattern Analysis and Machine Intelligence, vol. 29, no. 9, pp. 1563-1574, Sept. 2007.

[2] S. Osher and J. A. Sethian, "Fronts propagating with curvature-dependent speed: Algorithms based on Hamilton-Jacobi formulations," Journal of Computational Physics, vol 79, no 1, pp. 12-49, 1988.

Acknowledgement This work has been carried out within the framework of Flanders Make's SBO project ARENA (Agile & Reliable Navigation). Flanders Make is the Flemish strategic research centre for the manufacturing industry.

Robust Tube MPC in an environment with state-dependent uncertainty

Filip Surma
Delft, 2628 CD
f.surma@tudelft.nl

1 Abstract

Model predictive control (MPC) is a common control method used in industrial applications [1]. MPC solves an optimization problem within a given prediction window and in a loop. Under the assumption of a perfect prediction model and lack of unmodelled disturbances, MPC finds an optimal within the prediction window control input sequence given a cost function and constraints. However, the assumption of the perfect model is hardly ever valid, constraints may be violated in the implementation of the control inputs determined by MPC. Robust MPC (RMPC) was designed to ensure the feasibility of the solution even in a worst-case scenario. RMPC assumes that disturbunce affecting system belongs to a bounded set and as long as it is true, the constraints will not be violated.

The original min-max RMPC is usually too conservative. To reduce conservatism, optimization over the parameters of a feedback policy instead of constant values was proposed but finding a solution was often not possible in real-time implementation. Therefore, to deal with this problem, robust tube MPC (TMPC) was proposed [2]. TMPC determines a tube offline, where the center of this tube corresponds to the nominal trajectory of the system determined by regular MPC, and auxiliary control law ensures the realized state trajectory would not leave the tube. Since for TMPC, most heavy computations are done offline the complexity of solving the optimization problem is similar to that of the regular MPC.

A main shortcoming of TMPC is that the MPC solver does not have any knowledge about the real state, which becomes especially important when the disturbances are state-dependent. In such cases, standard TMPC is formulated with the largest possible disturbances which yield overly conservative solutions. Some ideas on how to solve this issue have already been proposed in the literature. The algorithm in [3] was implemented in the real world in 2022 and achieved better performance than state of the art algorithm.

The current approaches can be divided into two ways. Some authors assume that the state-dependent bounds of the disturbance are known. In these papers, the authors often introduce additional properties of these bounds. This allows them to implement robust TMPC without increasing the online computation too much. Other authors use a machine learning approach to learn these bounds from data. The most common machine learning approaches are neural networks and Gaussian processes. In my work, I plan to use a fuzzy inference system because it could allow me to use both expert knowledge and data to design a model, but the results still need to be tested.

To implement TMPC, constraint tightening needs to be done. In state-dependent TMPC, this has been done in two ways. It can be done offline using disturbance properties or with an iterative algorithm that samples the state space. In this way, the computational complexity of the online approach is not much higher than that of standard TMPC. Other authors use a dynamic tube that evolves during the optimization process. This has been achieved by smart parametrization of a tube (e.g., as an incremental Lyapunov function) or by using neural networks to learn the error dynamics of the system.

In my work, I design a new nonlinear state-dependent TMPC for nonlinear systems. In my talk, I will explain the ideas from the literature and compare them with each other so that it will be possible to understand their advantages and disadvantages. I will also briefly present my ideas on how to contribute to the field.

References

[1] Michael G. Forbes, Rohit S. Patwardhan, Hamza Hamadah, R. Bhushan Gopaluni (2015) Model Predictive Control in Industry: Challenges and Opportunities.

[2] Raković S.V. and Mayne D.Q. (2005) A simple tube controller for efficient robust model predictive control of constrained linear discrete time systems subject to bounded disturbances

[3] R. Soloperto and M.A. Müller and S. Trimpe and F. Allgöwer (2018), Learning-Based Robust Model Predictive Control with State-Dependent Uncertainty

An Efficient Constrained Dynamics Algorithm based on an Equivalent LQR Formulation using Gauss Principle of Least Constraint

Ajay Suresha Sathya, Herman Bruyninckx[1], Wilm Decre and Goele Pipeleers[2]
Division RAM, Dept of Mechanical Engineering, KU Leuven, Leuven, Belgium.
Flanders Make@KU Leuven, Leuven, Belgium.
Additional affiliations: [1] TU Eindhoven, Netherlands, [2] Materialise NV, Leuven, Belgium
{ajay.sathya, firstname.lastname}@kuleuven.be

1 Introduction

Efficient constrained dynamics algorithms [1], necessary and useful in optimal control and reinforcement learning applications, are usually complex and used as black-box tools by most robot control engineers, due to which they are unable to adapt the algorithms to the problems at hand. We formulate constrained dynamics as an equality-constrained linear quadratic regulator (LQR) problem using Gauss principle of least constraint and solve it using dynamic programming (DP) making dynamics algorithms accessible to a wider audience including control and optimization researchers. This approach for fixed-base chains gives the pioneering (but largely unknown) $O(n)$ solver by Popov and Vereshchagin (PV), for which we provide an expository derivation and further extend it to floating-base kinematic trees with constraints on any link and propose further algorithm optimizations. We show the dual Hessian of the LQR problem is the inverse operational space inertia matrix, leading to a novel recursive $O(n)$ algorithm. Our numerical benchmarking shows the computational superiority of derived algorithms compared to the SOTA algorithms.

2 Problem formulation

The equality-constrained quadratic program whose minimizer is the solution to the fixed-base serial chain constrained multi-body dynamics with a constrained end-effector is

$$\underset{\mathbf{a}_1,\ldots,\mathbf{a}_n,\ddot{q}}{\textbf{minimize}} \quad \sum_{i=1}^{n} \frac{1}{2}(\mathbf{a}_i - H_i^{-1}\mathbf{f}_i)^T H_i (\mathbf{a}_i - H_i^{-1}\mathbf{f}_i), \tag{1a}$$

$$\textbf{subject to} \quad \mathbf{a}_i = \mathbf{a}_{i-1} + S_i\ddot{\mathbf{q}}_i + \mathbf{a}_{b,i}, \quad i = 1,2,\ldots,n, \tag{1b}$$

$$K_n\mathbf{a}_n = \mathbf{k}_n, \quad \mathbf{a}_0 = -\mathbf{a}_{\text{grav}}, \tag{1c}$$

which is structurally analogous to the LQR problem where the link accelerations $\mathbf{a}_i$ and joint accelerations $\ddot{\mathbf{q}}_i$ resemble the state and controls respectively. This problem is solved similarly to the textbook LQR derivation using DP on the Lagrangian similarly to derive a SOTA constrained dynamics algorithm. With minor modifications to the problem in 1, we extend the algorithm to include floating-base robots and kinematic trees in [2] as well as soft constraints similar to the approach followed in MuJoCo.

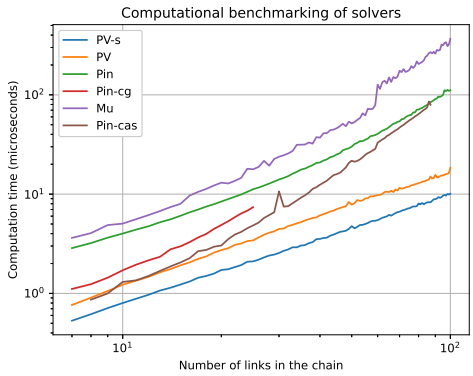

Figure 1: Benchmarking computational scaling w.r.t the number of links for a fixed-base chain and a constrained end effector.

3 Results and future work

The derived algorithm for fixed-base serial chain robots with fully constrained end-effector is compared against SOTA implementations of constrained dynamics in the popular software toolboxes Mujoco (Mu), Pinocchio (Pin), Pinocchio with CppADCodeGen (Pin-cg), Pinocchio with CasADi C-code generation (Pin-cas) in Fig. 1, where the proposed PV solver is also CasADi C-code generated. Apart from the applications in robot control, trajectory optimization and reinforcement learning, future exciting directions involve extensions to unilateral contact constraints, analytical gradients and uncertain dynamics.

Acknowledgement: The authors gratefully acknowledge support from Flanders Make through the Flanders Make SBO project - MULTIROB and from the Research Foundation Flanders (FWO) through the project G0D1119N.

References

[1] R. Featherstone, *Rigid body dynamics algorithms*. Springer, 2014.

[2] A. S. Sathya, H. Bruyninckx, W. Decre, and G. Pipeleers, "An Efficient Constrained Dynamics Algorithm based on an Equivalent LQR Formulation using Gauss' Principle of Least Constraint," Oct. 2022. [Online]. Available: https://doi.org/10.5281/zenodo.7243050

Preserving the Convex-Over-Nonlinear Structure of Varying-Radius Tunnel-Following Constraints

Alejandro Astudillo[1*], Wilm Decré[1], Jan Swevers[1]
[1]MECO Research Team, Dept. of Mechanical Engineering, KU Leuven, Leuven, Belgium.
[1]Flanders Make@KU Leuven, Belgium.
[*]Email: alejandro.astudillovigoya@kuleuven.be

1 Introduction

The tunnel-following nonlinear model predictive control (NMPC) scheme [1] is an extension of the path-following scheme where a (link of a) robot is allowed to deviate from a path reference up to certain user- or task-defined tolerance $\rho_\bullet \in \mathbb{R}_{>0}$, which defines the radius of the tunnel. Following a constrained-based task specification approach, a robot can be instructed to follow a tunnel by including the constraint

$$\|e_\bullet(x,s)\|^2 \leq \rho_\bullet^2 + l_\bullet, \tag{1}$$

in the optimal control problem (OCP) underpinning the tunnel-following NMPC scheme, whose transcription into a nonlinear program (NLP) is defined as

$$\min_{w} \quad \phi_0(c_0(w)) \tag{2a}$$

$$\text{s.t.} \quad \phi_i(c_i(w)) \leq 0, \; i = 1,\ldots,n_g, \tag{2b}$$

where $w \in \mathbb{R}^{n_w}$ is the vector of decision variables. In (1), the squared ℓ_2-norm of an error measurement $e_\bullet(x,s)$, which depends on the robot state $x \in \mathbb{R}^{n_x}$ and the path-progress variable $s \in \mathbb{R}_{[0,1]}$, is upper-bounded by $\rho_\bullet^2$ plus a slack variable $l_\bullet \in \mathbb{R}_{\geq 0}$ that relaxes the constraint to preserve feasibility of the solution of the OCP. While the robot is free to move within the tunnel, any excursion beyond $\rho_\bullet$ is discouraged by heavily penalizing the ℓ_1-norm of $l_\bullet$ in the objective function of the OCP. Note that the left-hand side of constraint (1) has a convex-over-nonlinear structure with $\phi(c) := c^2$ being the outer convex function and $c(x,s) := \|e_\bullet(x,s)\|$ being the inner nonlinear function.

2 Problem

The convex-over-nonlinear structure in (1) is exploited by the sequential convex quadratic programming (SCQP) method to solve OCP (2) while achieving fast convergence to a local minimizer w^* of (2) by using a computationally inexpensive approximation of the Hessian of the Lagrangian

$$B^{\text{SCQP}}(w,\mu) := B_0(w) + \sum_{i=1}^{n_g} \mu_i B_i(w), \tag{3}$$

where $B_i(w) := \frac{\partial c_i}{\partial w}(w)^\top \nabla^2_{c_i}\phi_i(c_i(w))\frac{\partial c_i}{\partial w}(w), \; \forall i \in [0,n_g]$. For a varying-radius $\rho_\bullet(s) : \mathbb{R}_{[0,1]} \to \mathbb{R}_{>0}$, however, the convex-over-nonlinear structure of (1) is broken, since (1) becomes

$$\|e_\bullet(x,s)\|^2 - \rho_\bullet(s)^2 \leq l_\bullet, \tag{4}$$

whose left-hand side has an outer function $\phi(c) := c$ and inner nonlinear function $c(x,s) := \|e_\bullet(x,s)\|^2 - \rho_\bullet(s)^2$. Since $\phi(c)$ is linear for this case, the SCQP method becomes equivalent to the generalized Gauss-Newton (GGN) method with Hessian approximation $B^{\text{GGN}}(w) := B_0(w)$, which may lead to unstable iterations of the SQP method.

3 Approach

By using the following reformulation of the varying-radius tunnel constraint (4),

$$\left\|\rho_\bullet(s)^{-1} e_\bullet(x,s)\right\|^2 \leq 1 + \bar{l}_\bullet, \tag{5}$$

which is relaxed by the slack variable $\bar{l}_\bullet \in \mathbb{R}_{\geq 0}$, we preserve the original convex-over-nonlinear structure with a nonlinear but convex outer function $\phi(c) := c^2$. This improves the local convergence of the solution of the OCP by allowing the exploitation of second-order information of the constraints in the Hessian approximation (3), as shown in Fig. 1 for an implementation of a bin-picking application performed with a Franka Panda robot manipulator [2].

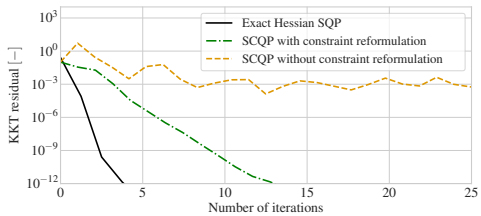

Figure 1: Comparison of the convergence of the SQP method with exact Hessian, and the SCQP method with and without reformulation of the tunnel constraints.

Future research directions involve the generalization of the SCQP method to handle constraints that have convex-over-nonlinear plus nonlinear, possibly concave, functions.

Acknowledgement This research is supported by the Flanders Make SBO projects MULTIROB: "Rigorous Approach for Programming and Optimal Control of Multi-Robot Systems" and DIRAC: "Deterministic and Inexpensive Realizations of Advanced Control".

References

[1] N. van Duijkeren, "Online motion control in virtual corridors - for fast robotic systems," Ph.D. Thesis, Department of Mechanical Engineering, KU Leuven, 2019.

[2] A. Astudillo, G. Pipeleers, J. Gillis, W. Decré, and J. Swevers, "Varying-radius tunnel-following NMPC for robot manipulators using sequential convex quadratic programming," in IFAC-PapersOnLine, 55 (37), pp. 345-352, 2022.

Online Parallel Trajectory Optimization Using GPU Acceleration

Fatemeh Rastgar[1,2], Arun Kumar Singh[2], and Jan Swevers[1,3]

[1] MECO Research Team, Department of Mechanical Engineering, KU Leuven, Leuven, Belgium
[2]Dept. of Science and Technology, University of Tartu, Tartu, Estonia
[3]Flanders Make, Leuven, Belgium
Email: fatemeh@ut.ee, arun.singh@ut.ee jan.swevers@kuleuven.be

1 Introduction

One of the well-known techniques for motion planning problems is formulating it as an optimal control problem (OCP) since encoding high-level robot behaviors through cost and constraints functions. Unfortunately, due to the presence of obstacles, most OCPs are non-convex. Non-convex optimization problems are challenging to be solved because they are prone to get stuck in local minima, and their solutions depend heavily on the initial guess used [1]. A potential solution to deal with this issue is providing multiple initial guesses for the trajectory optimization problem, solving them in parallel over multiple processors, and then choosing the best answer. However, implementing this trick is not straightforward. For example, off-the-shelf optimizers such as sequential quadratic programming (SQP) run on CPU threads, but the number of CPU cores is typically limited; hence the number of initial guesses is limited. While GPUs are typically available in very large quantities, e.g., thousands of cores, finding an implementable structure over GPU for most optimizers such as SQP is still an open problem [2]. Based on the above discussion, we aim to provide an efficient trajectory optimizer with a batchable structure over GPUs in this study.

2 Our Method

This work presents an online trajectory optimization method that is efficient for multiple instances in parallel over GPUs. To accomplish this, we change the OCP structure by providing a polar representation for the robot's trajectory (see [1]- [2]) and dividing the problem into several smaller convex sub-problems using Alternating Methods of Multipliers. Then, we show that for each instance, the obtained sub-problems can be converted into just computing vector-matrix production for which GPU implementation is available. After computing all the trajectories in parallel, we rank them based on collision avoidance and other robot constraints, such as maximum velocity or smoothness. Finally, the best trajectory is the one with the highest rank.

3 Results and Future Works

We implemented our trajectory optimizers in Python using JAX [3] library as our GPU-accelerated linear algebra back-end. The number of initial guesses is 200. The robot's LIDAR continuously observes the environment and sends the obstacle positions as point clouds to the optimizer. Then, for each instance, the optimizer obtains multiple candidate trajectories in parallel, sorts them based on collision avoidance and other constraints, and chooses the best trajectory to move forward. Fig. 1 shows top-ranked trajectories obtained by our optimizer at two different time instances. Also, it should be mentioned that the computation time for each instance is about 0.08s.

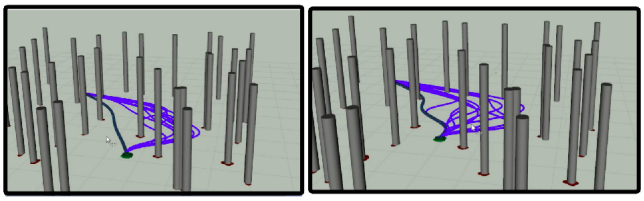

Figure 1: Qualitative result of our MPC batch optimizer. The purple trajectories represent the various locally optimal solutions obtained using our batch optimizer, while the black trajectories show the positional traces of the robot. The red points on the edges of spheres are point clouds detected as obstacles by the LIDAR.

References

[1] F. Rastgar, A. K. Singh, H. Masnavi, K. Kruusamae, and A. Aabloo, "A novel trajectory optimization for affine systems: Beyond convex- concave procedure," in 2020 IEEE/RSJ International Conference on Intelligent Robots and Systems (IROS). IEEE, 2020, pp. 1308–1315.

[2] F. Rastgar, H. Masnavi, J. Shrestha, K. Kruusamäe, A. Aabloo, and A. K. Singh, "Gpu accelerated convex approximations for fast multi- agent trajectory optimization," IEEE Robotics and Automation Letters, vol. 6, no. 2, pp. 3303–3310, 2021

[3] J. Bradbury et al., "JAX: Composable transformations of Python+NumPy programs," 2018. [Online]. Available: http://github.com/google/jax

Acknowledgement

This work is supported by European Social Fund through IT Academy Program in Estonia under Grant PSG753 from Estonian Research Council. It also contributes to the objectives of the Flanders Make SBO project Arena: Agile and Reliable Navigation.

Elastic metamaterials from control perspective

Marcin B. Kaczmarek
m.b.kaczmarek@tudelft.nl

S. Hassan HosseinNia
s.h.hosseinniakani@tudelft.nl

Precision and Microsystems Engineering, Delft University of Technology, Mekelweg 2, 2628 CD, The Netherlands

Motivation

Active elastic metamaterials promise a new solution for damping and vibration isolation in thin machine elements. Metamaterials are materials engineered to have properties not occurring in nature, that derive their properties not from the properties of the base materials, but from the designed repeating structures. While the potential of metamaterials has been demonstrated, the lack of systematic analysis of their dynamics hampers the development and use in applications.

Metamaterial as a feedback system

A simple 1D elastic metamaterial is presented in Fig. 1. The chain of masses m_p connected with stiffness k_p and damping c_p constitutes the base structures of the metamaterial. To each of the masses, a resonator, here characterized by m_r, k_r and c_r, is attached. The interaction between the base structure and the resonators leads to the unique properties of elastic metamaterials. Especially, the bandgaps, i.e. regions of lowered vibration transmissibility can be created at much longer wavelengths than the lattice size. The term *metamaterial* often corresponds to the transmission of waves in infinite chains. Finite chains with specific boundary conditions are described as *metastructures*.

Transmission of vibrations between consecutive masses can be represented as a feedback interconnection

$$u_n = Tu_{n-1} + Tu_{n+1},$$
$$T(s) = \frac{u_n(s)}{u_{n-1}(s)} = \frac{u_n(s)}{u_{n+1}(s)} = \frac{P(s)}{1+P(s)R(s)},$$

of with $P(s) = \frac{1/2}{(s/\omega_p)^2+2\zeta_p(s/\omega_p)+1}$ representing the base chain and the resonator $R(s) = \frac{K_R(s/\omega_r)^2(2\zeta_r(s/\omega_r)+1)}{(s/\omega_r)^2+2\zeta_r(s/\omega_r)+1}$. Transmissibility of a chain of 10 unit cells is presented in Fig. 2. When integer order resonators are used, not only the bandgap region but also undesired resonance peaks are created. If damped resonators are used, the undesired peaks are removed by a price of shallowing the bandgap.

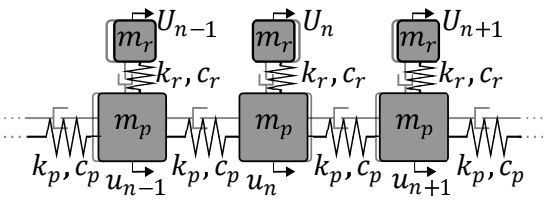

Figure 1: Schematic of a 1D elastic metamaterial.

The loop-shaping analysis of $T(s)$ reveals that the undesired resonances are created because of low phase margins. The problem can be alleviated by replacing $R(s)$ with commensurate-order $R_\alpha(s) = \frac{K_R\left(s/\omega_r\right)^{2\alpha}}{(s/\omega_r)^{2\alpha}+2\zeta_\alpha(s/\omega_r)^\alpha+1}$ or with power-law $\tilde{R}_\alpha(s) = \frac{K_R\left(s/\omega_r\right)^{2\alpha}}{\left((s/\omega_r)^2+2\tilde{\zeta}_\alpha(s/\omega_r)+1\right)^\alpha}$ fractional-order resonators. The use of fractional-order elements enables the use of simple analytical tools, varying the phase at low frequencies and maintaining the high resonance peak of the resonator. The corresponding transmissibilities are presented in Fig. 2. For both fractional elements, the depth of the bandgap is preserved, while the undesired peaks are removed. This demonstrates that the use of simple concepts from control engineering may lead to significant improvements in the performances of metastructures.

Open problems

To improve system properties different, possibly active resonators can be used. The existing literature is dominated by *ad hoc* designs and tools for systematic analysis are missing. In the case of active metamaterials, assuring stability is an important issue. For finite metastructures, standard tools can be used. In the infinite case, the problems become more involved. While the tools from infinite-dimensional systems theory may be useful, specific results are not available. Finally, practical realization leads to additional challenges. Since an integrated and compact solution is desired, often actuation and measurements of the relative position of subsequent masses are only possible. This makes the use of existing techniques, e.g. vehicle platooning, not trivial.

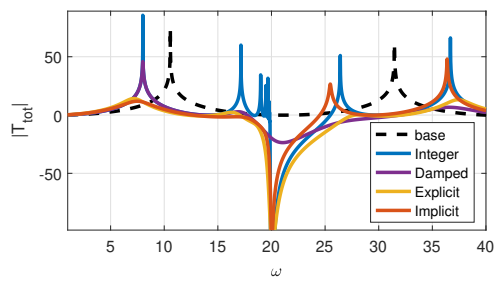

Figure 2: Transmissability of a metastructure with 10 cells and different resonators.

Computing the $\mathscr{H}_2$-norm of delay differential algebraic systems using a pseudospectral discretization

Evert Provoost and Wim Michiels
NUMA, Department of Computer Science, KU Leuven, Belgium
Email: {evert.provoost, wim.michiels}@kuleuven.be

1 Background

When modelling networks of complex systems, one often considers a collection of delay differential equations linked by algebraic constraints. These kinds of models give rise to delay differential algebraic equations (DDAEs), of the form

$$\begin{aligned} E\dot{\mathbf{x}}(t) &= \sum_{k=0}^{m} A_k \mathbf{x}(t-\tau_k) + B\mathbf{u}(t), \\ \mathbf{y}(t) &= C\mathbf{x}(t), \end{aligned} \tag{1}$$

where $0 \leq \tau_0 < \tau_1 < \cdots < \tau_m < +\infty$ and E is, in general, singular. These models generalize both delay differential equations of the retarded and neutral type, and differential algebraic equations (Michiels and Niculescu 2014).

In this work we propose a method to compute the norm of the transfer function of this system in the Hardy space $\mathscr{H}_2$, a robustness and performance measure which is often used in robust and optimal control.

The $\mathscr{H}_2$-norm of a stable, input-output system can be interpreted as a measure for the overall amplification over all frequencies, and is given by

$$\|T\|_{\mathscr{H}_2}^2 := \frac{1}{2\pi}\int_{-\infty}^{+\infty} \mathrm{Tr}\big(T(\omega i)^* T(\omega i)\big)\,\mathrm{d}\omega\,,$$

where i is the imaginary unit and

$$T(s) = C(sE - \textstyle\sum_{k=0}^{m} A_k e^{-\tau_k s})^{-1} B$$

is the transfer function of the system.

Determining whether this norm is finite is a challenge in its own right. If the system is unstable, the norm will be infinite (or is undefined, depending on the used definition) as T has a singularity in the right half plane. As the transfer functions of systems with delay can have infinitely many poles, special techniques are required to check for stability (Michiels and Niculescu 2014).

In the presence of a feedthrough the transfer function won't go to zero at infinity, also yielding an infinite norm. The challenge in (D)DAE's are hidden feedthroughs. As E can be singular it is possible for $\mathbf{y}(t)$ and $\mathbf{u}(t)$ to be directly coupled, even though there is no explicit feedthrough term present in (1), *e.g.* by including $0 = x_3(t) - u_2(t)$ and $y_1(t) = 3x_3(t)$, which imply $y_1(t) = 3u_2(t)$.

Finally both stability and the presence of hidden feedthrough can be highly dependent on the delays, where sometimes even an infinitesimal perturbation can render a system unstable or generate a feedthrough.

In recent work by Mattenet et al. (2022), they provided sufficient and necessary conditions for hidden feedthroughs and introduce the notion of the strong $\mathscr{H}_2$-norm, which is robust against infinitesimal delay perturbations. We build on these results to provide a computationally tractable method to compute the (strong) $\mathscr{H}_2$-norm.

2 A pseudospectral based approach

Similar to what Breda, Maset and Vermiglio (2005) introduced for non-algebraic delay differential equations, we use a pseudospectral discretization to arrive at an approximation of the system without delays. We can show that this discretization does not introduce feedthrough. Additionally, we show that in the rare case where, unlike the original system, the discretization is unstable, it can be made stable using only a few rank one updates to the discretization, without significantly impacting accuracy.

We can show that the differential algebraic equation, which we get after discretization, is equivalent to an ordinary differential equation of which we can finally compute the $\mathscr{H}_2$-norm using the usual Lyapunov equations.

Finally we characterize the method's convergence, and describe how to derive expressions for the derivative of the $\mathscr{H}_2$-norm with respect to system parameters, useful for optimal control.

References

Breda, D., S. Maset and R. Vermiglio (2005). "Pseudospectral Differencing Methods for Characteristic Roots of Delay Differential Equations". In: *SIAM Journal on Scientific Computing* 27.2, pp. 482–495.

Mattenet, Sébastien M. et al. (2022). "An improved finiteness test and a systematic procedure to compute the strong $\mathscr{H}_2$ norm of differential algebraic systems with multiple delays". In: *Automatica* 144, p. 110495. ISSN: 0005-1098.

Michiels, Wim and Silviu-Iulian Niculescu (2014). *Stability, Control, and Computation for Time-Delay Systems*. Philadelphia, PA: Society for Industrial and Applied Mathematics.

Cooperative situational awareness of multi-UAV system based on improved D-S evidence theory

Zirui Liao
Department of Electrical Engineering
Eindhoven University of Technology
P.O. Box 513, 5600 MB Eindhoven
The Netherlands
Email: z.liao@tue.nl

Zhiyong Sun
Department of Electrical Engineering
Eindhoven University of Technology
P.O. Box 513, 5600 MB Eindhoven
The Netherlands
Email: z.sun@tue.nl

1 Introduction

We consider the cooperative situational awareness (CSA) problem of multi-UAV system crossing three-dimensional obstacle belt without any priori information of obstacles. The main contributions are: (1) A CSA method of multi-UAV system is developed to improve the accuracy of information acquisition; (2) Multiple uncertainties are modeled and characterized; and (3) The conventional D-S evidence theory is modified to solve high evidence conflict. Pearson coefficient is utilized to measure the correlation between evidence and define the credibility. Subsequently, the uncertainty based on interval probability is introduced to modify the reliability and obtain the weight. Lastly, the original evidence is weighted and averaged, and the D-S combination rule is adopted for synthesis. Compared with other improved methods, our method can identify the correct propositions more accurately.

2 CSA based on D-S evidence theory

Notably, achieving CSA is challenging due to the randomness of obstacle distribution and detection uncertainties [1]. In this part, an information fusion method is adopted by introducing and modifying the traditional D-S evidence theory, which is presented in Fig. 1.

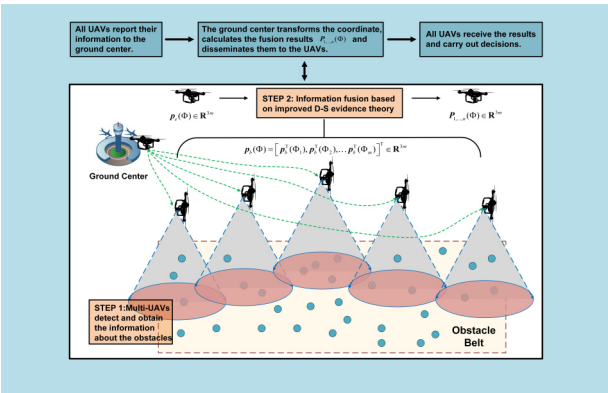

Fig. 1. Schematic diagram of the CSA method.

3 Method improvements

In this study, Pearson coefficient is adopted to build the correlation measure between evidence and determine the evidence credibility [2], whereas evidence uncertainty is evaluated comprehensively. Additionally, this study combines the credibility and uncertainty to determine the weight coefficient of the evidence, revise the original evidence, average the BPA of the revised evidence, and then use the Dempster combination rule to fuse it, so as to solve the evidence conflict. The flow chart of the improved method is illustrated in Fig. 2.

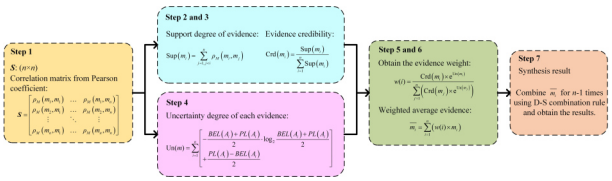

Fig. 2. The flow chart of improved combination method.

4 Conclusion

Based on the background of UAV detection, this study applies the improved D-S evidence theory to CSA of multi-UAV system to conduct the information fusion detected by airborne sensors. Our CSA scheme of mutli-UAV system can significantly detect more obstacles while being aware of the obstacles more accurately. Additionally, compared to existing modified D-S evidence theory methods, our improvement is superior in improving the detection accuracy and achieving an accurate CSA of multi-UAV system.

References

[1] C. Kwon, I. Hwang, Sensing-based distributed state estimation for cooperative multiagent systems, IEEE Transactions on Automatic Control 64 (6) (2018) 2368–2382.

[2] M. Radman, M. Moradi, A. Chaibakhsh, M. Kordestani, M. Saif, Multi-feature fusion approach for epileptic seizure detection from EEG signals, IEEE Sensors Journal 21 (3) (2020) 3533–3543.

Time-delayed Controller Design for Non-collocated Vibration Suppression

Adrian Saldanha and Wim Michiels
NUMA, Department of Computer Science
KU Leuven
Celestijnenlaan 200a 3001 Leuven
Belgium
Email: adrian.saldanha@kuleuven.be, wim.michiels@kuleuven.be

Tomas Vyhlidal
Faculty of Mechanical Engineering, CTU,
166 36 Prague 6
Czechia
Email: tomas.vyhlidal@fs.cvut.cz

1 Introduction

An established approach to suppress harmonic vibrations in mechanical structures consists of placing a so-called absorber at the position where vibrations need to be annihilated. Often however, in practical applications, it is not possible to attach an absorber directly at the desired point of suppression. In such cases, we can possibly silence disturbances of a desired harmonic frequency by designing an output feedback controller such that a pair of closed-loop transmission zeros of the transfer function G, constructed from the external force to the position of the target mass lie on the imaginary axis at the desired frequency ω i.e. $G(j\omega) = 0$.

2 Problem Setting

We consider an LTI model described by its state-space equation

$$\begin{aligned} \dot{x}(t) &= Ax(t) + B_1 u(t) + Bw(t) \\ y(t) &= C_1 x(t) \\ z(t) &= Cx(t), \end{aligned} \tag{1}$$

where x is the state vector, u the control input, y the measured output used for feedback and z, the system output. Input w represents a periodic disturbance force acting on the system with $w(t) = F\cos\omega t$, F being the magnitude of the disturbance and ω the excitation frequency, $u(t)$ represents the control input. The objective here is to completely suppress vibrations of frequency ω at the target position, represented by z while simultaneously maximizing the stability margin.

3 Solution Approach

We use a delay-based controller of the form

$$u(t) = \Sigma_{i=1}^{N} K_i^T y(t - \tau_i), \tag{2}$$

where $K_i \in \mathbb{R}^{q\times 1}$ is the gain matrix corresponding to fixed point wise delays τ_i, $i = 1,\ldots,N$. The controller utilizes static output feedback from the available outputs combined with intentionally introduced multiple fixed delays. The advantage of using multiple delays in the controller structure is that for systems with only a limited number of available output measurements, the presence of delays provides for greater number of free parameters which in turn can be utilized for achieving the desired control objective.

The requirement of maximizing the stability margin of the closed-loop system combined with ensuring zero displacement at the target location at frequency ω can be formulated as

$$\begin{aligned} \min_{K} \quad & \alpha(K) \\ \text{s.t}: \quad & G(j\omega; K) = 0, \end{aligned} \tag{3}$$

where $\alpha(K)$ is the spectral abscissa function of the resulting closed-loop system and $K = [K_1 \cdots K_N]$.

The objective function in (3) is typically non-convex and non-smooth while the constraints can be shown to be linear in K. To solve this, we remodel the system of equations with the controller as a Delay Differential Algebraic Equation (DDAE). Remodelling the system of equations in this form enables us to reduce the controller equation to one which resembles a static output feedback controller. Additionally, by obtaining the set of equations in the form of a DDAE, we can utilize the available routines from the `TDS-CONTROL` package. Once the equations are in the desired form, we use constraint elimination to convert the constrained optimization problem into an unconstrained one by exploiting the affine nature of the constraints in K.

References

[1] P. Appeltans, H. Silm, and W. Michiels, "TDS-CONTROL: A MATLAB Package for the Analysis and Controller-Design of Time-Delay Systems" IFAC-PapersOnLine 55.16, 272-277, Jul. 2022.

[2] A. Saldanha, H. Silm, W. Michiels, and T. Vyhlídal, "An Optimization-Based Algorithm for Simultaneous Shaping of Poles and Zeros for Non-Collocated Vibration Suppression," IFAC-PapersOnLine 55.16, 394–399, Jul. 2022.

Kalman filtering of a diffusion system with pointwise measurement

Anthony Hastir, Judicaël Mohet and Joseph Winkin
Department of Mathematics and Namur Institute for Complex system (naXys),
University of Namur, Rue de Bruxelles 61, B-5000, Namur, Belgium
Email: anthony.hastir@unamur.be, judicael.mohet@unamur.be and joseph.winkin@unamur.be

1 General Framework

The Kalman filter problem (KFP) received a lot of attention for many decades. It consists in solving an optimal state estimation problem whose solution is a Luenberger-type state observer. In the classical approach, the optimal output injection operator is related to the solution of an operator Riccati equation. In [2], we describe an algorithm for solving the KFP with a frequency domain approach for a class of dynamical systems whose dynamics generators are self-adjoint and Riesz-spectral operators A defined on the Hilbert space $X_{\frac{1}{2}} := D((\mu I - A)^{\frac{1}{2}})$ for some $\mu \geq 0$ such that $\sigma(\mu I - A) \subseteq \mathbb{R}_0^+$. It appears that the opposite of a Sturm-Liouville operator[1] fits the subsequently mentioned class of operators, under classical assumptions. This algorithm is applied to solve the KFP for a one-dimensional diffusion system on the interval $[0,1]$ with mixed boundary conditions.

2 Kalman Filtering Algorithm

We consider, for $t \geq 0$, the one-dimensional diffusion system governed by the (abstract) differential equation (corresponding to a partial differential equation)

$$\begin{cases} \dot{x}(t) = Ax(t) + C^* w(t), x(0) = x_0 \\ y(t) = Cx(t) + \eta(t), \end{cases} \tag{1}$$

where $Ax = \frac{d^2x}{dz^2}$, $x \in D(A) \subseteq X_{\frac{1}{2}} = D((-A)^{\frac{1}{2}})$ with

$$D(A) = \{x \in H^2(0,1) \colon \tfrac{dx}{dz}(0) = \chi_0 x(0), \tfrac{dx}{dz}(1) = -\chi_1 x(1)\}, \tag{2}$$

for positive constants χ_0 and χ_1, and where $w(t)$ and $\eta(t)$ are real-valued square-integrable disturbance signals. The operator A is self-adjoint and of Riesz-spectral type. Its eigenvalues and its eigenfunctions are denoted by $\{\lambda_n\}_{n\geq 1}$ and $\{\phi_n\}_{n\geq 1}$, respectively. As observation operator C, we consider the evaluation at $z = 0$ on $X_{\frac{1}{2}}$, i.e. $Cx = x(0)$. In our particular setting, the space $X_{\frac{1}{2}}$ is the Sobolev space $H^1(0,1)$ which is a reproducing kernel Hilbert space. This entails that the operator $C \in \mathscr{L}(X_{\frac{1}{2}}, \mathbb{R})$, i.e. C is linear and bounded, and that $Cx = \langle c_0, x\rangle_{\frac{1}{2}}$ for all $x \in X_{\frac{1}{2}}$ and some $c_0 \in X_{\frac{1}{2}}$. In addition, $-A$ is a Sturm-Liouville operator. Hence, the solution of the KFP is given by the Luenberger-like observer

$$\begin{cases} \dot{\tilde{x}}(t) = A\tilde{x}(t) + L(\tilde{y}(t) - y(t)), \\ \tilde{y}(t) = C\tilde{x}(t), \end{cases} \tag{3}$$

where $L \colon = \ell \in X_{\frac{1}{2}}$ is the optimal output injection. Our algorithm gives the components of ℓ in the orthonormal basis $\{\phi_n\}_{n\geq 1}$, and, for the diffusion system, it consists of three steps :

1. Compute the (stable) transfer function $\hat{g}(s) = \langle c_0, (sI - A)^{-1} c_0\rangle \colon = \frac{\hat{n}(s)}{\hat{d}(s)}$ of the system (1)-(2).
2. Compute the stable zeros $\{\mu_n\}_{n\geq 1}$ of the Popov function $\hat{f}(s) \colon = \hat{n}(s)\hat{n}(-s) + \hat{d}(s)\hat{d}(-s)$
3. Compute the components of ℓ using the formula

$$\ell_n = \frac{\mu_n - \lambda_n}{\langle c_0, \phi_n\rangle_{\frac{1}{2}}} \prod_{\substack{k=1 \\ k\neq n}}^{\infty} \frac{\lambda_n - \mu_k}{\lambda_n - \lambda_k}, \ \forall n \geq 1. \tag{4}$$

The formula (4) follows from duality arguments with respect to what is done in [1]. It is based on the spectral factorization problem of the Popov equation[2]. This problem is solved by using the symmetric extraction method developed in [3] which leads to the infinite product form $\hat{R}(s) = \prod_{n=1}^{\infty} \frac{s-\mu_n}{s-\lambda_n}$. The corresponding sequence of finite products converges to $\hat{R}$ in the Wiener class $\mathscr{A}(\sigma)$, where σ is negative and satisfies $2|\sigma| \leq \min(|\mu_n|, |\lambda_n|)$, see [2] and [3]. This implies that the infinite product in (4) can be truncated in order to get a good approximation of ℓ_n. Note that the algorithm for the general case of a self-adjoint and Riesz-spectral operator on $X_{\frac{1}{2}}$ is available in [2], together with numerical results.

References

[1] Callier, F.M, Winkin, J.J., 1992. LQ-optimal control of infinite-dimensional systems by spectral factorization. Automatica 28, 757-770

[2] Hastir, A., et. al., 2023. A frequency domain approach to Kalman filtering on Hilbert spaces: application to Sturm-Liouville systems with pointwise measurement. Submitted.

[3] Winkin, J., et. al., 2004. Spectral factorization by symmetric extraction for distributed parameter systems. SIAM Journal on Control and Optimization 43, 1435-1466.

[1] That is an operator of the form $(Af)(z) = -\frac{1}{\rho(z)}\left(\frac{d}{dz}\left(-p(z)\frac{df}{dz}\right) + q(z)f(z)\right)$, for $z \in [a,b]$, where $p, \frac{dp}{dz}, q$ and ρ are real-valued and continuous functions with $\rho > 0$ and $p > 0$.

[2] i.e. finding a spectral factor $\hat{R}$ of $\hat{f}$, i.e. an invertible stable transfer function such that $\hat{R}(\infty) = 1$ and $\hat{f}(s) = \hat{R}(s)\hat{R}^*(-\bar{s})$

State-Space Modeling of Charge-Carrier Dynamics for the Oxygen Evolution Reaction in Water Splitting

Bart van den Boorn[1] b.f.h.vandenboorn@differ.nl
Matthijs van Berkel[2] m.vanberkel@differ.nl
Anja Bieberle-Hütter[1] a.bieberle@differ.nl

[1]DIFFER - Electrochemical Materials and Interfaces, De Zaale 20, 5612 AJ Eindhoven, The Netherlands
[2]DIFFER - Energy Systems and Control, De Zaale 20, 5612 AJ Eindhoven, The Netherlands

1 Introduction

Hydrogen can provide a key contribution to the increased need for energy storage in the shift towards renewables. This requires sustainable production of hydrogen, such as by water-splitting in a photo-electrochemical cell. However, these cells are not yet able to achieve the efficiencies required for commercial use. The reaction that generates oxygen at the photo-anode, the oxygen evolution reaction (OER), is commonly regarded as the performance limiting reaction. Modeling of the OER provides an opportunity to investigate the processes and variables that are difficult to obtain from experiments, such as the surface coverage of the intermediate OER reaction species at the semiconductor-electrolyte interface. This work focuses on improving the current time-dependent non-linear state-space model of the OER, by the addition of spatially dependent charge carrier dynamics represented by a set of partial differential equations.

2 Oxygen evolution reaction model

A preliminary state-space model of the OER has previously been developed. [1] This model consists of two parts: (1) A microkinetic model of the reaction kinetics at the semiconductor-electrolyte interface. The model equations describe the evolution of the intermediate species under illumination and applied potential. (2) A simple description of the charge-carrier transport dynamics at the surface of the semiconductor material.

3 Model extension

In this work, we show the development and implementation of a new description of the charge-carrier dynamics. The description in the original model was limited to the evolution of the two charge carriers, electrons and holes, at the surface of the semiconductor. In this work, also processes in the bulk of the semiconductor are included, through addition of a space-dependency of the charge carriers in the semiconductor. The advantage is that we can fully include the following processes that are relevant for the evolution of the charge carriers: drift-diffusion effects, charge transfer at the interface, electron-hole pair generation and the recombination processes at the interface and in the bulk of the semiconductor. The resulting partial differential equations are connected to the state-space system of the reaction kinetics through semi-discretization in the spatial dimension.

The presentation highlights the new charge carrier dynamics description and its integration in the original model. Through the combination of the spatio-temporal description of the charge carrier dynamics and the microkinetic model, we aim to gain a realistic insight into the processes of the OER. This can be used in optimizing the OER, and in turn the performance of photo-electrochemical water-splitting.

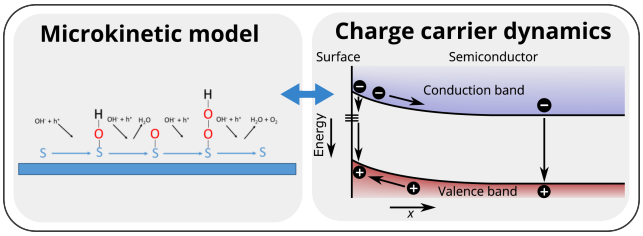

Figure 1: Model of the oxygen evolution reaction consisting of two parts: (1) The microkinetic model of the reaction kinetics and (2) the spatially-dependent charge carrier dynamics in the semiconductor. Electrons are indicated by (-) and holes by (+).

[1] K. George, T. Khachatrjan, M. van Berkel, V. Sinha, and A. Bieberle-Hütter. In: *ACS Catal.* 10.24 (2020), pp. 14649–14660.

Low order approximation of mechanical systems

S. Fatemeh Sharifi†
Department of Applied Mathematics, University of Twente
P.O. Box 217, 7500 AE Enschede, The Netherlands.
Email s.f.sharifi@utwente.nl

Daniël Veldman
Department of Data Science, FAU Erlangen-Nürnberg
Cauerstrasse 11, 91058 Erlangen, Germany.
Email: d.w.m.veldman@gmail.com

Hans Zwart†
Department of Applied Mathematics, University of Twente
P.O. Box 217, 7500 AE Enschede and
Technische Universiteit Eindhoven, Department of Mechanical Engineering,
P.O. Box 513, 5600 MB Eindhoven, The Netherlands
Email: h.j.zwart@utwente.nl, h.j.zwart@tue.nl

1 Abstract

Control design for linear, time-invariant mechanical systems typically requires an accurate low-order approximation in the low frequency range, for example a series expansion of the transfer function around zero consisting of a mass, velocity, and compliance term, see e.g. [1]. The transfer function of a mechanical system containing rigid body modes, from a force input to a position output typically includes a double-integrator-part. Thus it is of the form

$$G(s) = \frac{G_2}{s^2} + \frac{G_1}{s} + G_0 + G_{st}(s).$$

where G_2^{-1}, G_1, and G_0 denote the mass, velocity, and compliance terms , respectively, and $G_{st}(s)$ captures the remainder of order $O(s)$. The mass and velocity part are typically related to the rigid body modes, and $G_{flex}(s) = G_0 + G_{st}(s)$ captures the flexible part related to the (possibly infinitely many) non-rigid modes. When the transfer function of the system is available, then G_2, G_1, and G_0 can be directly obtained from it by taking an expansion of $G(s)$ around $s = 0$. However, in many situations a closed-form expression of the transfer function is not available. Therefor we propose a time-domain approach based on the step response of the system associated to the transfer function $G(s)$. In particular, let $y(t)$ denote the step response of the system. The inverse Laplace transform of $Y(s) = G(s)\frac{u_0}{s}$ equals

$$y(t) = G_2 u_0 \frac{t^2}{2} + G_1 u_0 t + G_0 u_0 + \omega_{st}(t),$$

where $\omega_{st}(t)$ is the inverse Laplace transform of $G_{st}(s)\frac{u_0}{s}$. Since G_{st} is stable and $G_{st}(0) = 0$, $\omega_{st}(t)$ converges to zero as $t \to \infty$. The compliance function can thus be determined from the static part of the step response. We show that for mechanical systems described by partial differential equations with distributed control and/or control at the spatial boundary, G_2, G_1 and G_0 can also be determined by assuming the following expression for the step response

$$y(t) = \omega_2 \frac{t^2}{2} + \omega_1 t + \omega_0 + \omega_{st}(t),$$

with $\omega_{st}(t)$ is stable, i.e. $\omega_{st}(t) \to 0$ for $t \to \infty$. For models in which it is impossible to obtain the exact expression of the transfer functions, closed form expressions, can be obtained for G_2, G_1, and G_0. For higher spatial dimensions even this can be too hard, but in these cases numerically simulation of the step response leads to the answer. For instance, ω_2, ω_1, and ω_0 can be determined from snapshots of the step response $y(t)$. In particular, let $t_1 < t_2 < \ldots < t_n$ be time instances that are so large that $\omega_{st}(t_i)$ are small. Then

$$\begin{bmatrix} y(t_1) \\ \vdots \\ y(t_n) \end{bmatrix}^T \approx \begin{bmatrix} \omega_2 & \omega_1 & \omega_0 \end{bmatrix} \begin{bmatrix} \frac{1}{2}t_1^2 & \frac{1}{2}t_2^2 & \cdots & \frac{1}{2}t_n^2 \\ t_1 & t_2 & \cdots & t_n \\ 1 & 1 & \cdots & 1 \end{bmatrix}.$$

Estimates for ω_2, ω_1, and ω_0 can thus be determined by minimizing the residue in the above equation.

Acknowledgement: †Members of the ITN network ConFlex. Their research has received funding from the European Union's Horizon 2020 research and innovation programme under the Marie Sklodowska-Curie grant agreement No. 765579.

References

[1] Kontaras, N., Heertjes, M.F., and Zwart, H.J. (2016). Continuous compliance compensation of position dependent flexible structures. *IFAC-PapersOnLine*, vol. 49, No. 13, pp. 76-81.

Tube MPC For Mission Planning of Search-and-Rescue Robots in Uncertain Dynamic Environments

Mirko Baglioni
Control and Operations
Delft University of Technology
Kluyverweg 1, 2629 HS Delft
The Netherlands
Email: M.Baglioni@tudelft.nl

1 Introduction

Human-induced and natural disasters require fast and effective responses from search-and-rescue (SaR) crews. In recent years, the use of SaR robots has been growing for assisting humans to speed up finding the victims. Therefore, the robots need effective mission planning approaches that determine an optimal trajectory to the victims, while dealing with uncertainties present in SaR scenarios. In this research, I introduce a path planning approach based on model predictive control (MPC) for an indoor SaR environment, where the robot should follow and reach the moving victims.

2 Background

Determining feasible and optimal trajectories autonomously and tracking the victims despite uncertainties are major challenges of SaR robots [1]. Therefore, the control system for mission planning of SaR robots should be robust to such uncertainties. Furthermore, established robust MPC methods exist [2] that, if adopted for SaR robots, will significantly improve the control performance in presence of uncertainties. Despite these potential benefits regarding optimality, constraint incorporation, and predictive decision making, the use of MPC for systematic exploration of SaR environments in the literature, is very limited. The SaR missions may be categorized as coverage-oriented or target-oriented. The most commonly used coverage-oriented approaches for mission planning of SaR robots include heuristics techniques, while optimization-based control approaches, including MPC, are often used in target-oriented SaR. The use of MPC in coverage-oriented SaR is very limited and, in particular, MPC is used for reference tracking [3].

3 Proposed approach

I have developed a path planning approach based on MPC for a SaR robot, and a corresponding case study. The algorithm is both target-oriented, in order to reach the trapped victims in the environment and the exit point, and coverage-oriented, to perform larger exploration of the area. The controller of the robot is based on a robust tube model predictive control approach. This algorithm determines the optimal velocity and heading angle of the robot, while optimizing the objective function, that includes reducing the mission time, maximizing the intersection of the robot perception field and the areas where the victims are supposed to be located, increasing the area coverage and going to the exit. The optimization is performed in presence of constraint which include robot dynamics, obstacles and moving victims avoidance, physical constraints of the robot in terms of velocity and orientation angle. The uncertainties that are taken into account in this approach are the unknown position of the target victims and the non-smoothness of the ground that acts as an external disturbance in the robot position. I consider a movement model for the victims based on a crowd evacuation model, therefore the target victims are dynamic targets and the non-target victims are dynamic obstacles.

4 Case study

In the case study, developed using Matlab, ROS and Gazebo simulator, the performance of the proposed approach is evaluated and compared to other four state-of-the-art path planning approaches, two coverage oriented and two target-oriented, and I show how the proposed method outperforms the other four in victims detection, area coverage and mission completion time, while being robust to uncertainties.

References

[1] F. Colas, S. Mahesh, F. Pomerleau, M. Liu, and R. Siegwart, "3D path planning and execution for search and rescue ground robots," 2013 IEEE/RSJ International Conference on Intelligent Robots and Systems, 2013.

[2] D. Q. Mayne, M. M. Seron and S. V. Raković, "Robust model predictive control of constrained linear systems with bounded disturbances," Automatica, 2005.

[3] M. Khadem, J. O'Neill, Z. Mitros, L. Da Cruz, and C. Bergeles, "Autonomous steering of concentric tube robots via nonlinear model predictive control," IEEE Transactions on Robotics, 2020.

Asynchronous NMPC with Variable Update Time (ASAP-MPC)

Dries Dirckx, Mathias Bos, Bastiaan Vandewal, Wilm Decré, Jan Swevers
MECO Research Team, Department of Mechanical Engineering, KU Leuven
Flanders Make@KU Leuven, Leuven, Belgium
Email: dries.dirckx@kuleuven.be

1 Introduction & Problem Setting

Nonlinear Model Predictive Control (NMPC) for trajectory planning is a topic that currently receives a widespread interest from the (robotics) research community. Classical NMPC schemes are supposed to stabilise a nonlinear system, reject disturbances to it and lead to agile control of that system which requires high NMPC update rates. The control inputs are computed by solving an Optimal Control Problem (OCP), minimising an objective e.g. time of the total trajectory or distance to be travelled to reach a target, subject to constraints such as collision avoidance, a model of the system dynamics, actuator limits, etc.

For nonlinear systems in complex environments or with limited onboard computation power, e.g. drones or autonomous vehicles, reaching high update rates and guaranteeing feasibility is often intractable. A widely used approach to reduce computational complexity is the Real-Time Iterations (RTI) technique [1]. RTI applies only the first iteration of an optimization solver to the system. It does not guarantee constraint satisfaction and can lead to collisions and infeasible controls that do not satisfy the modelled nonlinear system dynamics.

We propose an alternative NMPC strategy - Asynchronous NMPC (ASAP-MPC) - that deals with finite computation times that can extend over multiple update intervals but guarantees feasibility with respect to the constraints by solving the OCP to convergence. A low-level stiff feedback controller is added to guarantee that the actual state $x(t)$ tracks the computed NMPC solution such that $x(t) \approx \hat{x}(t)$. The expected finite computation time is maximally m samples.

2 Asynchronous NMPC

Figure 1 shows the principle for a one-dimensional example. Suppose at time t_i, a new solution A is available. Since a finite computation delay is expected, based on solution A and the current on-trajectory state $\tilde{x}(t_i)$, an estimation of the future on-trajectory state $\hat{x}(t_{i+m})$ is made. The next solution B is constrained to start from this future point. Awaiting solution B, solution A (red) is tracked up to m samples in the future. Once computed, solution B is stitched to A at $\hat{x}(t_{i+m})$.

If solution B arrives earlier at $t_j < t_{i+m}$, solution A is still tracked up to t_{i+m} after which the newly computed solution B is tracked up to t_{j+m}. Suppose the next solution (C) arrives just-in-time after m samples at $t_k = t_{j+m}$, solution C is stitched to solution B and immediately tracked. The future trajectory from solution B is discarded. Repeating this update procedure leads to a continuous trajectory in time for $x(t)$, constructed by asynchronously stitching new solutions to each other.

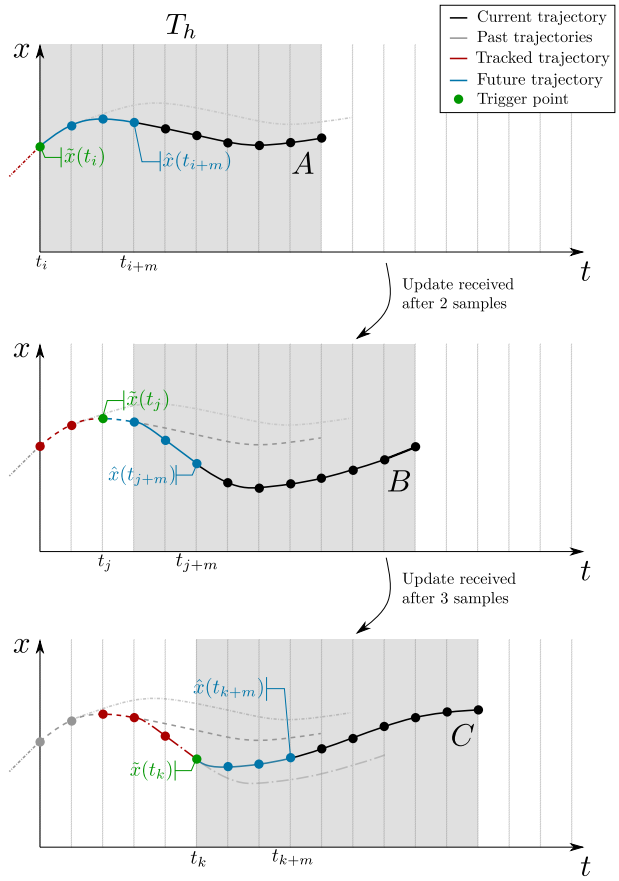

Figure 1: Working principle of the update strategy in ASAP-MPC, illustrated for a one-dimensional example.

References

[1] M. Diehl, R. Findeisen, F. Allgöwer "A Stabilizing Real-Time Implementation of Nonlinear Model Predictive Control," Real-Time PDE-Constrained Optimization, 2007.

Acknowledgement This research is supported by Flanders Make ICON FROGS: Flexible and Robust Robotic Gripping Solutions. Flanders Make is the Flemish strategic research centre for the manufacturing industry.

Relaxed Stability Condition for FeLMS based Adaptive Active Vibration Isolation Control

Sil Spanjer, Hakan Köroğlu, Wouter Hakvoort
Department of Mechanics of Solids, Surfaces and Systems (MS3), University of Twente
Email: {s.t.spanjer, h.koroglu, w.b.j.hakvoort}@utwente.nl

1 Introduction

Active Vibration Isolation Systems (AVIS) can be used to improve the performance of passive vibration isolation [1]. Several effective control methods are available, including disturbance feedforward. The performance of disturbance feedforward can be guaranteed under parameter variations and uncertainty by using an adaptive algorithm. For AVIS, the Filtered error Least Mean Square (FeLMS) algorithm is particularly appealing for its efficient computation.
The stability of the FeLMS algorithm is typically proven by the conservative SPR condition [1]. However, in most practical applications the condition is not satisfied, due to the typical high-frequency parasitic dynamics of mechanical systems, while the FeLMS is still stable. Hence, no formal stability guarantee can be given for practical systems. This work therefore proposes to append the SPR condition with a frequency-dependent weighting to reduce the conservatism of the stability condition.

2 Extended stability condition

The general control structure of an AVIS can be seen in figure 1. The output (k) of the feedforward controller is given by

$$(k) = \quad (\ _0(k)) \quad (k), \tag{1}$$

where (k) is the regressor matrix. The parameters (k) are updated with the FeLMS alogrithm as

$$(k+1) = \quad (k) - \mu(k)\,[\quad (q) \quad (k)]^T \quad (k). \tag{2}$$

Here $\mu(k)$ is the step size, (q) the noise shaping filter, $(k) = \quad (q)\ \hat{}_2^{-1}(q)\,\hat{}_1(k)$, and $\hat{}_2$ the model of $_2$. The SPR stability condition is

$$\left(\hat{\mathbf{P}}_{\mathbf{2}}^{-1}\left(e^{j\omega}\right)\mathbf{P_2}\left(e^{j\omega}\right)\right) \quad + \hat{\mathbf{P}}_{\mathbf{2}}^{-1}\left(e^{j\omega}\right)\mathbf{P}_2\left(e^{j\omega}\right) \succ 0. \tag{3}$$

This stability condition can be relaxed under the slow parameter adaptation assumption to

$$\frac{1}{2\pi}\int_{-} \mathrm{Tr}\left\{\mathbf{S}_{\xi}\left(e^{j\omega}, \tilde{}\right)\left[\left(\hat{\mathbf{P}}_{\mathbf{2}}^{-1}\left(e^{j\omega}\right)\mathbf{P_2}\left(e^{j\omega}\right)\right) + \hat{\mathbf{P}}_{\mathbf{2}}^{-1}\left(e^{j\omega}\right)\mathbf{P}_2\left(e^{j\omega}\right)\right]\right\}\mathrm{d}\omega > 0, \tag{4}$$

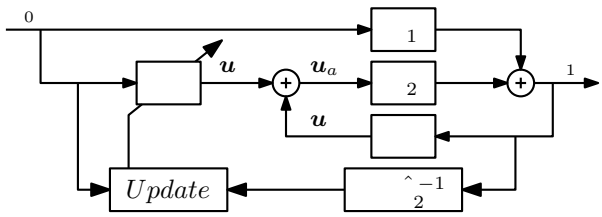

Figure 1: Blockscheme of FeLMS based AVIS, with the floor acceleration $_0 \in \mathbb{R}^n$, the payload acceleration $_1 \in \mathbb{R}^{n_y}$ and actuator input $_a \in \mathbb{R}^n$

where $\mathbf{S}_{\xi}\left(e^{j\omega}, \tilde{}\right)$ is the power spectrum of $\boldsymbol{\xi}(k) = (\hat{}(k))\tilde{}$. A similar condition can be found in [1] but is not used. It can be seen that this condition is satisfied if the SPR is satisfied. Due to the slow adaptation assumption, $\mathbf{S}_{\xi}\left(e^{j\omega}, \tilde{}\right)$ can be evaluated for a given $\tilde{} = \tilde{}(k_0)$, which is the frozen parameter error, and hence it can be determined if this point belongs to the domain of attraction. Note that (q) is a design parameter and can be chosen to satisfy condition 4 based on the measured FRF.

3 Conclusion and Results

For the numerical validation, equation (4) is checked for a SISO path of the system in [1], for the relevant parameter range. The new stability condition correctly predicted the observed convergence of the system, where SPR condition did not, while keeping the favourable frequency domain definition. There is still some conservatism left, which is due to the specific choice of the Lyapunov function [2]. However, from a practical point of view, this conservatism is not restrictive.

References

[1] M. Beijen, M. Heertjes, J. Van Dijk, and W. Hakvoort, "Self-tuning mimo disturbance feedforward control for active hard-mounted vibration isolators," *Control engineering practice*, vol. 72, pp. 90–103, 2018.

[2] R. Fraanje, M. Verhaegen, and S. J. Elliott, "Robustness of the filtered-x lms algorithm - part i: Necessary conditions for convergence and the asymptotic pseudospectrum of toeplitz matrices," *IEEE transactions on signal processing*, vol. 55, no. 8, pp. 4029–4037, 2007.

Conditions for Lossless State Space Reduction of Stopping Time Problems

Menno van Zutphen, Duarte J. Antunes, and Maurice Heemels
Control Systems Technology, Eindhoven University of Technology
Postbus 513, 5600 MB Eindhoven, The Netherlands
Email: {m.j.t.c.v.zutphen, d.antunes, w.p.m.h.heemels}@tue.nl

1 Introduction

[1] Decision problems concerning the question when to best terminate a stochastic process in order to minimize costs, *stochastic optimal stopping time problems*, are a subset of dynamic programming problems. This type of problems naturally arises in a wide range of fields, from pricing of financial derivatives [1] to connection scheduling in ad-hoc networks [2]. Our application domain is precision farming, where farmers must, *e.g.*, decide when best to apply herbicides to their fields [3]. A major complication that arises when solving this particular decision making problem, is the size of the state space $|\mathscr{X}| = |\{0,1\}^N| = 2^N$ growing exponentially with the number of (sub)fields $N \in \mathbb{N}$ considered in the problem. This effect renders such stopping time problems intractable for farms with many fields $N \gg 10$.

This paper proposes (i) conditions on stochastic optimal stopping time problems that enable lossless state space reduction, and (ii) related approximate methods enabling far greater (lossy) state space reductions. The approximate methods can be used to generate upper- and lower bounds on the optimal cost and a tractable, approximate policy that is within a constant factor of the optimal policy.

2 Problem formulation

Consider a standard stochastic stopping time problem with full state information in a discrete finite space $x_k \in \mathscr{X} := \{1,2,\dots,n\}$

$$\min \mathbb{E}[\sum_{k=0}^{\tau-1} g(x_k)], \tag{1}$$

with $P = [p_{ji}]$, $p_{ji} = \text{Prob}[x_{k+1} = j | x_k = i]$. For simplicity assume that $\tau \leq \bar{h} \in \mathbb{N}$.

To reduce the complexity of this problem (when $n \gg 1$), we are interested in finding a map (projection) $\phi : \mathscr{X} \to \mathscr{Y}$, where $\mathscr{Y} := \{1,2,\dots,m\}$ with $m < n$, that is able to group states into equivalence classes. The map ϕ thereby defines an *equivalence relation*: states $i \in \mathscr{X}$ and $j \in \mathscr{X}$, denoted by $i \sim j$, are equivalent if $\phi(i) = \phi(j)$. We search for conditions on the stopping time problem (1) for which we can work on the quotient space $\mathscr{X}/\sim$ of this equivalence relation, *i.e.*, work with m states rather than n states, without losing optimality.

[1]This research is part of the research program SYNERGIA (project number 17626), which is partly financed by the Dutch Research Council (NWO)

3 Conditions for lossless state space reduction

Let us define m equivalence classes $\mathscr{A}_j := \{i \in \mathscr{X} \mid \phi(i) = j\}$, $j \in \{1,\dots,m\}$. Consider the following two conditions

$$\text{(i)} \quad g(i) = g(j), \qquad \forall i,j \in \mathscr{X}, \text{ s.t. } i \sim j,$$

$$\text{(ii)} \quad \sum_{\ell \in \mathscr{A}_j} p_{\ell i} = \sum_{\ell \in \mathscr{A}_j} p_{\ell r}, \quad \forall i,r \in \mathscr{X}, \forall j \in \mathscr{Y}, \text{ s.t. } i \sim r.$$

We have shown that if these two conditions are met, the optimal costs-to-go $J_k(i)$ and optimal policy $\mu_k(i)$, $k \in \{0,1,\dots,\bar{h}\}$, $i \in \mathscr{X}$, satisfy $J_k(i) = J_k(j)$ and $\mu_k(i) = \mu_k(j)$ if $i \sim j$, which means we can restrict the treatment to a single representative from each class $\mathscr{A}_j$ for $j \in \{1,2,\dots,m\}$ when running the DP algorithm, reducing the number of operations from order n to order m.

4 Upper- and lower bounds

Some problems might not contain many states for which conditions (i) and (ii) hold, whereby $m \approx n$. Suppose we have an approximate version of such problem that can be proven to have a lower (or higher) optimal cost than the optimal cost of the original problem. If the P matrix (and $g(i)$) of the approximate problem is such that large groups of equivalent states satisfy the equivalence relation, then solving these problems on the highly reduced feature space $m \ll n$ enables cheap computation of lower- and upper bounds on the original problem. This can yield both bounds on the optimal cost, and an approximate policy that is within a constant factor of the optimal one.

References

[1] J. Tsitsiklis and B. van Roy, "Optimal stopping of Markov processes: Hilbert space theory, approximation algorithms, and an application to pricing high-dimensional financial derivatives," *IEEE Transactions on Automatic Control*, vol. 44, no. 10, pp. 1840-1851, 1999.

[2] D. Zheng, W. Ge, and J. Zhang, "Distributed Opportunistic Scheduling for Ad Hoc Networks With Random Access," *IEEE Transactions on Information Theory*, vol. 55, no. 1, pp. 205-222, 2009.

[3] D. Antunes, R. Beumer, M. van de Molengraft, and W. Heemels, "Adaptive Sampling and Actuation for POMDPs: Application to Precision Agriculture," Preprint at heemels.tue.nl/content/papers/AntBeu_CDC22a.pdf, 2022.

Interaction-aware Model Predictive Control for Autonomous Driving

Renzi Wang Mathijs Schuurmans Panagiotis Patrinos
KU Leuven, Department of Electrical Engineering ESAT-STADIUS
Kasteelpark Arenberg 10, bus 2446, B-3001 Leuven, Belgium
Email: {renzi.wang, mathijs.schuurmans, panos.patrinos}@kuleuven.be

1 Introduction

Lane changing remains a challenging task for autonomous driving, due to the strong interaction between the controlled vehicle and the uncertain behavior of the surrounding traffic participants. The interaction induces a dependence of the vehicles' states on the (stochastic) dynamics of the surrounding vehicles, increasing the difficulty of predicting future trajectories. Furthermore, the small relative distances cause traditional robust approaches to become overly conservative, necessitating control methods that are explicitly aware of inter-vehicle interaction. Towards these goals, we propose an interaction-aware stochastic model predictive control (MPC) strategy integrated with an online learning framework, which adaptively estimates the surrounding vehicles cooperation level through a parameterized state-dependent distribution.

2 Target vehicle behavior modelling

We model the uncertain behavior of the target vehicle (TV) as a randomized control policy $\kappa^{\mathrm{TV}} : \mathbb{R}^{n_z} \times \Xi \to \mathbb{R}^2$, where the finite set $\Xi := \{1, \dots, d\}$ denotes maneuver indices. The maneuver selection $\xi_t \in \Xi$ is made randomly according to

$$P(z_t) = (\mathbb{P}\{\xi_t = i \mid z_t\})_{i \in \Xi}, \tag{1}$$

which depends on the (joint) state $z_t = \left[(z^{\mathrm{E}})^\top \ (z^{\mathrm{TV}})^\top\right]^\top = \overline{f}(z_{t-1}, u_{t-1}, \xi_{t-1})$ of ego vehicle (E) and TV.

3 Optimal control problem

Consider an arbitrary N-step policy $(\mu_k)_{k=0}^{N-1} \in \Pi$. Since Ξ is finite, all realizations of the stochastic process $(z_k, u_k)_{k=1}^{N}$ satisfying dynamics $\overline{f}$ with $u_k = \mu_k(z_k)$, and z_0 known can be represented on a scenario tree [1] as illustrated in Fig. 1. Given $\bar{z}$ and θ, the optimal control problem is:

$$\begin{aligned}
\underset{\boldsymbol{u} \in \mathbb{R}^{n_u M}}{\text{minimize}} \quad & J_N(\boldsymbol{u}, \theta) && \text{(2a)}\\
\text{s.t.} \quad & z^{(\iota_+)} = \overline{f}\left(z^{(\iota)}, u^{(\iota)}, \xi^{(\iota_+)}\right) \ \forall \iota_+ \in \operatorname{ch} \iota, && \text{(2b)}\\
& \mathbb{P}\{G\left(z^{(\iota_+)}\right) \geq 0 \mid z^{(\iota)}\} \leq \gamma, \ \forall \iota_+ \in \operatorname{ch} \iota && \text{(2c)}\\
& u_k^{(\iota)} \in U, \ z_k^{(\iota)} \in Z, \ \forall \iota \in \operatorname{nod}(0, N-1), && \text{(2d)}\\
& z^{(0)} = \bar{z}, \ z^{(\iota_N)} \in Z, \ \forall \iota_N \in \operatorname{nod} N && \text{(2e)}
\end{aligned}$$

where $\operatorname{ch} \iota$ means children of node ι and $\operatorname{nod} k$ represents all nodes at step k. (2c) is the collision avoidance constraint. U and Z denote bound for input and states, respectively.

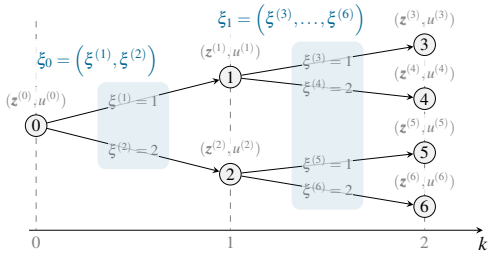

Figure 1: A fully branching scenario tree of horizon $N = 2$.

4 Online parameter estimation

A multinomial logistic regression scheme is used to learn the distribution $P(z)$. We introduce a parameterized model $\hat{P}(z; \theta)$ with parameter matrix $\theta = \left[\theta_1 \ \cdots \ \theta_d\right] \in \mathbb{R}^{n_\theta \times d}$. A moving horizon estimation update is used to adapt θ online. At each time step t, we compute a new estimate

$$\theta_t \in \underset{\theta}{\operatorname{argmin}} \, \lambda \rho(\theta, \theta_{t-1}) - \sum_{k=t-L+1}^{t} \log \hat{P}_{\xi_k}(z_k; \theta), \tag{3}$$

where $\lambda > 0$ is a fixed regularization constant for penalty term $\rho(\theta, \theta')$ and $L \in \mathbb{N}$ is a fixed window length.

5 Experiment result

We test our framework with different types of prediction scheme. Details of the result can be found in [2].

Acknowledgement This work was supported by the Research Foundation Flanders (FWO) research projects G081222N, G033822N, G0A0920N; European Unions Horizon 2020 research and innovation programme under the Marie Skodowska-Curie grant agreement No. 953348; Ford KU Leuven Research Alliance Project KUL0075; Research Council KU Leuven C1 project No. C14/18/068; Fonds de la Recherche Scientifique-FNRS the Fonds Wetenschappelijk Onderzoek-Vlaanderen under EOS project no 30468160 (SeLMA).

References

[1] G. C. Pflug and A. Pichler, *Multistage Stochastic Optimization*, ser. Springer Series in Operations Research and Financial Engineering. Cham: Springer International Publishing, 2014.

[2] R. Wang, M. Schuurmans, and P. Patrinos, "Interaction-aware model predictive control for autonomous driving," 2022. [Online]. Available: https://arxiv.org/abs/2211.17053

Autonomous interaction aware lane changing using optimal control through time-varying free spaces

Mathias Bos, Wilm Decré, Jan Swevers
MECO Research Team, Department of Mechanical Engineering, KU Leuven, Belgium
Flanders Make@KU Leuven, Belgium
Email: mathias.bos@kuleuven.be

1 Introduction

Autonomously performing lane changes on highways is challenging, especially when another vehicle approaches from behind on the lane into which the ego vehicle wants to insert. In literature, sometimes adding communication between vehicles is suggested [1]. However, this is not a viable strategy in the scenario where both human drivers and autonomous vehicles share the highways. This scenario requires a strategy to balance between assertively inserting in front of the approaching vehicle, expecting it to adapt to the ego behavior, and on the other hand adjusting the ego actions in order to safely comply with the behavior of the approaching vehicle, without forcing it into abrupt maneuvers.

To this end, we present a motion planning strategy to plan the lane switching maneuver through available convex free spaces, while taking the effect of the ego vehicle behavior on the actions taken by the other vehicles into account in a simplified manner.

2 Methods

The motion planning problem is formulated as an optimal control problem (OCP), using the multi-stage formulation for motion planning through subsequent convex spaces or corridors that is presented in [2]. The work presented here adds the movement and reshaping of the corridors over the prediction horizon, along with the movement of the other vehicles. Additionally, the expected future state of the other vehicles is taken into account in the OCP by adding the acceleration, velocity, and position of the corridor edges as controls and states.

The objective function is formulated as

$$T + \sum_{k=0}^{N} w_1 (v_k - v_{des})^2 + w_2 a_k^2 + w_3 \delta_k^2 + w_4 \dot{\delta}_k^2 + w_5 (v_{t,k} - v_{t,des})^2 + w_6 a_{t,k}^2,$$

in which the top line minimizes the time T to execute the lane changing maneuver, with regularization of the effort of the ego vehicle, which is represented by the deviation between the actual velocity v and the desired velocity v_{des}, the acceleration a, the steering angle input δ and its derivative $\dot{\delta}$. The bottom line of the objective adds the effort of the approaching vehicle, being its deviation between the actual velocity v_t and the desired velocity $v_{t,des}$, and the acceleration a_t. It is assumed that the vehicle in front does not accelerate or decelerate. The weights w_i determine the relative influence on the cost of each term. Hence, the choice of w_5 and w_6 determines the extent to which the ego vehicle takes the effort of the approaching vehicle into consideration.

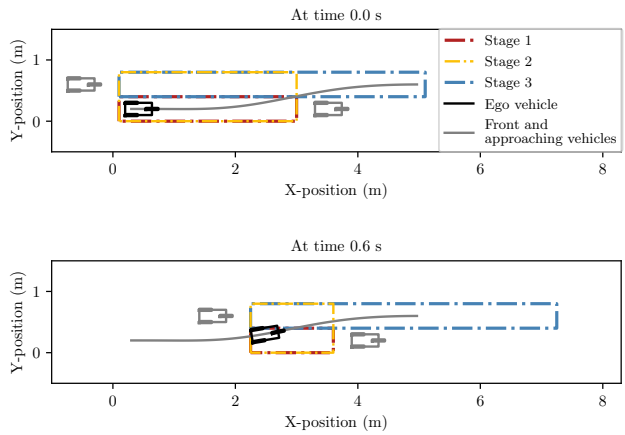

Figure 1: Illustration of an OCP solution to the lane change problem.

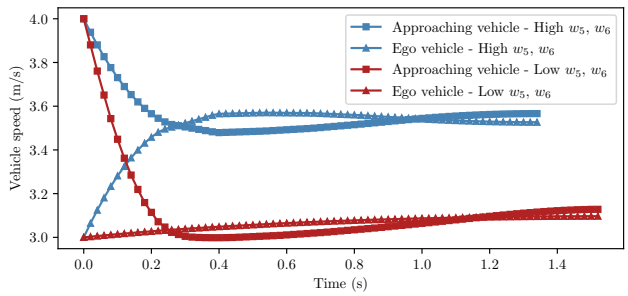

Figure 2: Influence of w_5 and w_6 on the planned ego vehicle and approaching vehicle velocity.

3 Results

Figure 1 illustrates the moving corridors during the execution of a lane changing maneuver, with the stage-dependent, time-varying box constraints. Figure 2 clearly shows the effect of the weights w_5 and w_6: when they are high, the ego vehicle accelerates strongly in order to reduce the required braking action of the approaching vehicle; when they are low, the approaching vehicle is expected to brake strongly, allowing the ego vehicle to accelerate only mildly.

References

[1] S. Dixit, S. Fallah *et al.*, "Trajectory planning and tracking for autonomous overtaking: State-of-the-art and future prospects," *Annual Reviews in Control*, vol. 45, pp. 76–86, 2018.

[2] M. Bos, W. Decré, J. Swevers, and G. Pipeleers, "Multi-stage optimal control problem formulation for drone racing through gates and tunnels," in *2022 IEEE 17th International Conference on Advanced Motion Control (AMC)*, 2022, pp. 376–382.

Acknowledgement This work has been carried out within the framework of projects Flanders Make SBO FLEXMOSYS: Flexible Multi-Domain Design for Mechatronic Systems and Flanders Make SBO ARENA: Agile and Reliable Navigation.

Towards experimental validation of an adaptive MPC scheme for systems with variable topologies

Taranjitsingh Singh, and Frederik Debrouwere
Flanders Make
Lommel, Belgium
Email: `firstname.lastname@flandersmake.be`

1 Introduction

Systems with variable topology, which occur during system operation, have a significant impact on the overall system dynamics, hence the control should be adaptive with respect to these topology changes. This article shows experimental validation of control for pneumatic systems with varying topologies with an adaptive MPC scheme.

2 Approach

The proposed approach presented in this article consists of first developing a 2-stage model: (i) a model of the subsystems of the system and (ii) a model of the possible interconnections. By adapting the state of the interconnections in the second part of the model, a certain system topology is modelled using graph theory [1]. The introduction of the Laplacian matrix $\mathscr{L} = \mathscr{D} - \mathscr{A} = [L_{ij}]$ as a parameter in the system allows us to adaptively switch the topology during the MPC loop, without the need for rewriting all system equations. $\mathscr{D}$ is the Degree matrix and $\mathscr{A}$ the Adjacency matrix, and undirected communication is assumed. This allows to very efficiently model all possible topologies. This limits furthermore the number of identifications required. Next, an MPC controller is designed which takes this 2-stage model into account, allowing for very efficient adaptation to the system topology by adapting the connection model during operation, once a topology change has been detected.

3 Results

For the considered pneumatic system, there exists a pressure control valve is present in the system that acts as the control input u that can operate in the range of 0-10V. The system also consists of discrete valves that controls the flow direction of the compressed air. There are also two tanks that acts as accumulators which can store compressed air. There is finally a pressure sensor which is the measured output in the system under consideration.

Figure 1 shows two possible topologies with the two tanks considered. The tanks are considered as first-order systems identified from experiments. The systems S_i and *Out* are virtual subsystems that are basically one sample delay. The output pressure is measured at *Out* using a pressure sensor, where we want to maintain a desired pressure. In order to design our adaptive MPC scheme, we extract the Laplacians $\mathscr{L}$ for these two topologies. We preformed experiments on

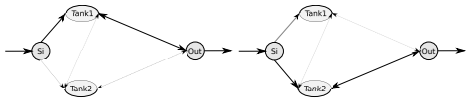

(a) Topology 1 (b) Topology 2

Figure 1: Considered topologies for the pneumatic system in experiments with (—-) represents connected links while (*gray*$\cdots$) represents disconnected links

the pneumatic setup, with online adaptive MPC on a real-time hardware which takes the Laplacian as a parameter. Figure 2 shows experimental results as compared to a robust and a scheduled aggressive PI controllers, with change in topology around 74s, when we switch to Topology 2. The controlled designed using our approach outperformed other controllers in reducing overshoot and achieving bandwidth.

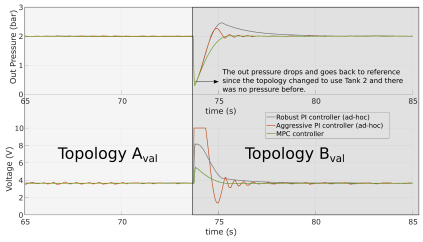

Figure 2: Experiment result for adaptive MPC for pneumatic system with variable topology compared with two (ad-hoc) tuned PI controllers

References

[1] G. Xie and L. Wang. Consensus control for a class of networks of dynamic agents. *International Journal of Robust and Nonlinear Control: IFAC-Affiliated Journal*, 17(10-11):941–959, 2007.

Acknowledgement: This work is supported by Flanders Make project: ICON ID2CON: Integrated Identification to Control.

Real-Time Optimal Control for Eco-Driving and Powertrain Energy Management [1]

N.A. Smit Y.J.J. Heuts O.F. Hulsebos M.C.F. Donkers
Department of Electrical Engineering, Control Systems Group
Eindhoven University of Technology, P.O. Box 513, 5600 MB Eindhoven
Email: {y.j.j.heuts, m.c.f.donkers}@tue.nl, nick.smit@nobleo.nl, O.Hulsebos@VDLETS.nl.

1 Introduction

Eco-driving and energy management can drastically reduce the power consumption of vehicles, [1]. As horizon-lengths increase and more sophisticated models are used for components, this leads to a larger computational load on the on-board computer. As a consequence, the optimization solver does not keep up with the rate of control inputs. In this work, methods for reducing computation time, while still obtaining comparable energy savings are applied to the problem.

2 Problem formulation

For the vehicle model, a series hybrid heavy-duty vehicle is considered. The interconnection is formulated as a second-order cone program. In order to do so, quadratic and hyperbolic equality constraints are relaxed into inequality constraints to fit this model formulation. We show numerically that the optimal solution lies on the equality and therefore the relaxation is exact. By applying receding-horizon control and move-blocking, i.e., fixing control inputs for multiple steps, the computational times can be reduced while still obtaining a close-to-optimal solution. The method has been tested on a 60km drive-cycle with large differences in elevation.

3 Results

In figure 1, the distance of the problem is fixed and the computational times for five horizon compositions with varying coarseness are shown. Case 1 has the largest horizon of length 2500, and case 5 has length 450 steps. It has been shown that computation times can be reduced without experiencing large increases in energy consumption. For figure 1, three cases are shown with equal horizon length, but with varying distance per case. It has been observed that under the same number of samples, horizons with a longer distance span but a lower average resolution due to blocked inputs, outperform horizons that have a shorter span with fewer inputs blocked concerning the energy consumption. This improvement in fuel economy has been attributed to the ability of the horizon to be able to detect upcoming events earlier and react appropriately. Conversely, lowering the number of samples leads to shorter horizon spans and increased energy consumption. Despite the observed increase in energy consumption that has arisen in the second case study, it can be concluded that the combined eco-driving and powertrain energy management solution, solved within 0.53 [s] on average, provides additional energy savings when compared to the full horizon solution, leading to a reduction in fuel consumption of 33.7 %.

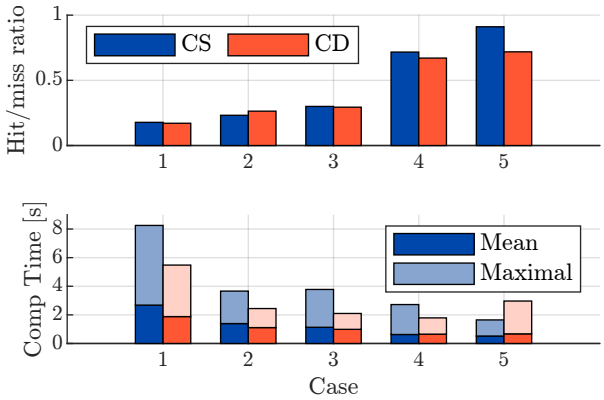

Figure 1: Fixed distance, increasing coarseness per case. Horizon lengths of $N = [2500, 1025, 795, 530, 450]$ respectively.

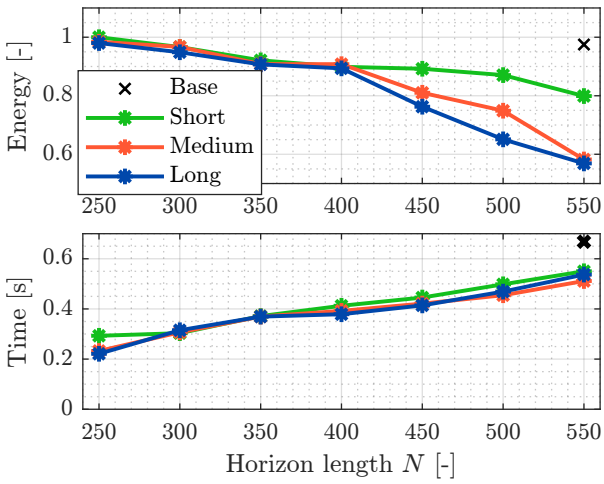

Figure 2: Varying distance, constant decision variables. Simulated distance is $d = [20N, 52N, 64N, 68N]$.

References

[1] E. Hellström, J. Aslund, and L. Nielsen, "Management of kinetic and electric energy in heavy trucks." SAE.

[2] N.A. Smit, Y.J.J. Heuts, O.F. Hulsebos, M.C.F. Donkers, "Real-Time Optimal Control for Eco-Driving and Powertrain Energy Management" *submitted*

[1] This work has received financial support under the grant LONGRUN.

Model Predictive Control of District Heating Networks with Decentralized Storage: A Framework for Optimization

Max Sibeijn
Delft Center for Systems and Control
Delft University of Technology
Mekelweg 2
2628 CD Delft
The Netherlands
Email: m.w.sibeijn@tudelft.nl

Tamas Keviczky
Delft Center for Systems and Control
Delft University of Technology
Mekelweg 2
2628 CD Delft
The Netherlands
Email: t.keviczky@tudelft.nl

Abstract

Real-time optimization for district heating networks (DHN) is becoming increasingly relevant for industrial applications, mainly due to increased use of highly intermittent renewable energy sources, which offers many challenges and opportunities from an operational perspective [1]. Specifically, more advanced control methods offer the potential to improve synergy among energy resources and to better exploit the flexibility available in the network. To optimally regulate these systems, mathematical models are used to optimize the set of possible operations for the system (i.e., boilers, heat pumps, pumps, and other control devices) according to some cost function.

Preferably, we consider mathematical models that approximate the real system as accurately and precisely as possible. However, non-linearities and non-convexities, caused in part by the bi-linear nature of heat transfer and discrete decision variables, increase the computational complexity of an already sizeable optimization problem (due to a large number of decision variables). Hence, in general we refrain from using highly detailed numerical techniques from thermo- and fluid dynamics, and instead opt for more simple representations of the systems at hand.

Different approaches to modeling DHNs exist, earlier works consider approximate pipe dynamics using a linearized solution of the partial differential equation (PDE) with constant time delays [2]. More recent works consider spatial and temporal discretization schemes of the PDEs suitable for real-time optimization [1]. Furthermore, the authors of [3] consider the inclusion of storage into the network and derive a dynamical model for the network. That said, they do not propose any optimization based control strategies.

In this work, we introduce a framework for real-time optimization of a DHN with storage capabilities, see Figure 1. In contrast to [3], we separate the pipe dynamics from the storage dynamics to retain a simple but modular structure which is suitable for optimization purposes. Here, we intend to evaluate different operational control scenarios with the aim of improving flexibility and resilience of the network. Furthermore, we also compare centralized and distributed approaches for their performance and computational tractability. To this end, we test the proposed control methods on GridPenguin [4], a DHN simulator designed for simple but accurate simulation of thermal dynamics. As part of future work, firstly, we will deal with the issue of feasibility versus performance by taking into account uncertainty and adopting either stochastic or robust control approaches. Secondly, we want to integrate flexibility from the electricity grid (i.e., from heat pumps) into the framework.

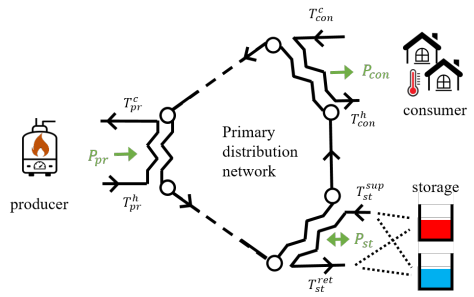

Figure 1: Example of a network configuration with producer, consumer, and storage components.

References

[1] R. Krug, V. Mehrmann, and M. Schmidt. "Nonlinear optimization of district heating networks." Optimization and Engineering 22.2, 2021. 783-819.

[2] G. Sandou, et al. "Predictive control of a complex district heating network," IEEE Conference on Decision and Control, 2005.

[3] J.E. Machado, M. Cucuzzella, and J.M.A. Scherpen."Modeling and passivity properties of multi-producer district heating systems." Automatica 142, 2022.

[4] J. Wu, R. Everhardt, K. Stepanovic, M.M. de Weerdt."GridPenguin: A District Heating Network Simulator." Conference Proceedings New Energy for Industry, 2022.

Optimal $\mathscr{H}_2$ and $\mathscr{H}_\infty$ Control of Bilinear Positive Systems with Uncertain Evolutionary Dynamics

Sanaz Akbarisisi
NUMA, Department of Computer Science, KU Leuven, Belgium
Email: sanaz.akbarisisi@kuleuven.be

1 Introduction

Positive systems arise in the modeling of various applications, such as epidemiology, power networks, etc. In such systems, the state variables remain non-negative in response to non-negative initial conditions and non-negative inputs. An important class of positive systems consists of bilinear systems. The richly available optimal policies for linear time-invariant positive systems cannot be applied to bilinear positive systems that will be studied in this presentation. More precisely, optimal $\mathscr{H}_2$ and $\mathscr{H}_\infty$ control problems of bilinear positive systems in the presence of uncertain evolutionary dynamics will be addressed. It will be proved that the semi-infinite min-max optimization problem can be modeled as a finite min-max convex optimization problem. Next, an iterative algorithm based on minimizing the partial cutting plane of the objective function will be applied. It is worth mentioning that global convergence to the optimum is guaranteed in this approach.

2 Problem Setting

Consider the following bilinear dynamics

$$\begin{aligned} \dot{x}(t) &= (A+K(u))x(t)+w(t), \\ z(t) &= x(t), \end{aligned} \tag{1}$$

where $x \in \mathbb{R}^n$ represents the states of the controlled system, $u \in \mathbb{R}^m$ denotes the constant control input, $w \in \mathbb{R}^n$ is the disturbance signal, and $z \in \mathbb{R}^n$ is the performance output. The matrix $K(u) \in \mathbb{R}^{n\times n}$ is a diagonal matrix defined as $K(u) = diag(Du)$. The matrix $D \in \mathbb{R}^{n\times m}$ is a constant matrix obtained from the practical investigation. Matrix A is Metzler and symmetric. Thus, the described system in (1) is positive [1]. Due to the uncertain nature of the model, matrix A is uncertain, and it is an unknown member of the convex polytopic set $\Omega = \left\{\sum_{i=1}^h \gamma_i A_i \,|\gamma_i \geq 0,\ \sum_{i=1}^h \gamma_i = 1\right\}$. The $\mathscr{H}_\infty$ norm is given as $J_\infty(u,A) = \underset{\omega\in\mathbb{R}}{\text{Sup}}\ \bar{\sigma}\left[\left(j\omega I - A - K(u)\right)^{-1}\right]$, and the square of the $\mathscr{H}_2$ norm is given as $J_2(u,A) = \int_0^\infty \text{trace}\left(e^{(A+K(u))t}e^{(A+K(u))^T t}\right)dt$. The optimal control problem can be formulated as

$$\begin{aligned} &\underset{u}{\text{Minimize}}\ \underset{A\in\Omega}{\text{Max}}\ J_*(u,A)+\Psi(u), \\ &\text{Subject to } A+K(u) \text{ is Hurwitz} \quad \forall A \in \Omega, \end{aligned} \tag{2}$$

where $\Psi(u)$ is an arbitrary convex constraint on u and $*$ can either be 2 or ∞.

3 Proposed Method

With considering the mathematical properties of positive systems, it will be shown that function $\mathscr{F}_*(u)$ defined as $\mathscr{F}*(u) = \underset{A\in\Omega}{\text{Max}}\ J_*(u,A)$ is convex. Consequently, the optimization problem (2) becomes a semi-infinite convex problem. Next, it will be proved that under the assumption that matrix A is invertible, the semi-infinite convex problem is equivalent to a finite min-max convex problem; it is sufficient to only solve the problem over the vertices of the polytopic set rather than all the infinite members of the polytopic set.

The primary concern of solving the developed problem by a descent algorithm is the non-smooth nature of it. Thus, an iterative descent algorithm relying on minimization of the partial cutting plane will be applied [2]. The cutting-plane approach with a bundling scheme iteratively refines a feasible set. As a main advantage of the partial cutting plane approach, the descent algorithm can be carried out with incomplete knowledge of the objective function. In fact, with the proposed algorithm there is no need to evaluate the objective function in all the trial points.

Finally, the effectiveness of the proposed strategy is studied for the case study of human immunodeficiency virus therapy. The performance of this method will be compared with the graident descent method. The results verify the importance of considering the uncertainty in the treatment design.

Acknowledgement

The talk concerns the author's results from her master's thesis work under the supervision of Dr. Maryam Babazadeh in the department of Electrical Engineering at Sharif University of Technology.

References

[1] V. Jonsson, N. Matni, and R. M. Murray, "Reverse engineering combination therapies for evolutionary dynamics of disease: An H_∞ approach," in Proc. 52nd IEEE Conf. Decis. Control, Dec. 2013, pp. 2060–2065

[2] C. Tang, J. Jian and G. Li, "A proximal projection partial bundle method for convex constrained min-max problems", *Journal of Industrial and Management Optimization*, vol. 15, no. 2, pp. 757–774, 2019.

Bayesian Optimiziation Applied to Calibration of Electron Microscope

Jilles van Hulst[1,*], Roy van Zuijlen[1], Duarte Antunes[1], and Maurice Heemels[1]

[1]Control Systems Technology Section, Dept. of Mechanical Engineering, Eindhoven University of Technology, The Netherlands
[*]Email: j.s.v.hulst@tue.nl

1 Introduction

Electron Microscopes (EMs) can create images at atomic level which continue to enable breakthroughs in a multitude of scientific fields. The quality of the images is a direct result of the quality of the electron beam focus. This focus quality is often imperfect due to fundamental physical limitations. These imperfections can be quantified and are referred to as aberrations. Hardware components can be introduced to compensate the aberrations, but this results in an increased number of calibration parameters, which in turn introduces the need for frequent and lengthy re-calibration by an expert operator. This motivates the need for automatic calibration.

2 Problem Formulation

The aim of this research is to automate the EM calibration process based on its output, which are images. This goal is challenging since these images are high-dimensional and the output is a non-injective mapping of the aberrations. This means that one image can correspond to different aberration configurations.

3 Approach

The proposed method consists of two steps: interpretation of the images, and decision-making based on the interpretation. The first step is performed by feature extraction based on physical insights, which reduces the high-dimensionality of the images first to a low-dimensional vector of features, and then to a scalar cost, similar to [1]. The second step uses Bayesian optimization (BO) [2] with a Gaussian process (GP) estimate to simultaneously estimate and optimize the unknown cost function. The GP uses data gathered from the EM to estimate the cost as a smooth function, while BO selects where to sample next based on the expected improvement which can be computed from the GP estimate.

4 Results

When applying the proposed method to a dataset of synthetic images produced by a high-fidelity model, we verify that the cost function produced by the first step is smooth, symmetrical, and has a unique global minimum. Fig. 1 shows that the cost function is well-estimated in very few samples and that the sample selection converges to the minimizer after initially exploring. In fact, the proposed method is able to calibrate two aberrations in 100% out of 50 attempts, and in 10 or fewer samples 92% of the time.

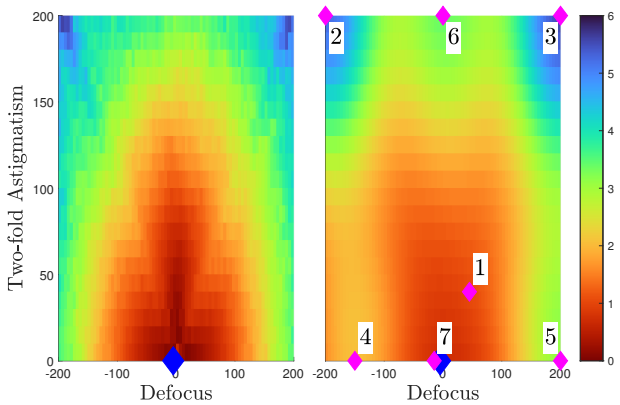

Figure 1: On the left: cost function resulting from feature extraction with minimizer (♦). On the right: GP approximation of the cost function. The indexed sample locations (♦) are selected using BO.

5 Conclusion and Outlook

This research introduces a method for the automatic calibration of EMs that interprets the microscope images and makes decisions that balance improving estimates and exploiting promising current beliefs. Future research avenues include automating the feature extraction process, incorporating more prior knowledge into the optimization scheme, and analyzing the stochastic optimization problem.

References

[1] M. Rudnaya, "Automated focusing and astigmatism correction in electron microscopy," PhD thesis, Eindhoven University of Technology, Eindhoven, 2011.

[2] D. R. Jones, M. Schonlau, and W. J. Welch, "Efficient Global Optimization of Expensive Black-Box Functions," *Journal of Global Optimization 1998 13:4*, vol. 13, no. 4, pp. 455–492, 1998.

Adaptive Difference-Of-Bundles algorithm with extrapolation for DC programming with linear constraints

Guillaume Van Dessel, François Glineur
ICTEAM, UCLouvain, 1348 Louvain-la-Neuve, Belgium
Email: {guillaume.vandessel, françois.glineur}@uclouvain.be

1 Introduction

During the last decades, many dedicated techniques were developed to speed-up the solving of convex optimization problems. Among most successful ones we find Nesterov's *momentum*, the *non-monotone backtracking line-search* and the use of *cutting-plane models*. Each of those relies on exogenous information about the structure at hand, either stemming from the objective function or the involved convex constraints. In this work, we propose to combine these techniques all at once in the following non-convex setting: difference of convex (DC) optimization with linear constraints. Akin to [1], our formulation is as follows for $F := f_1 - f_2$

$$F^* = \min_{x\in\mathbb{R}^d} \left\{ f_1(x) - f_2(x) : x \in \mathcal{P} := \{x \,|\, Ax \leq b\} \right\} \quad (1)$$

with $A^T = (a_1, \dots, a_m) \in \mathbb{R}^{d\times m}$, $b \in \mathbb{R}^m$, $f_1 \in \mathcal{C}_L^{1,1}(\mathcal{P})$ and f_2 continuous proper convex functions, $F^* > -\infty$.

Example 1. (ℓ_∞ proximity constrained clustering) One aims at minimizing the average $\mu > 0$ smoothed L_2 distance of points $\{\omega_i\}_{i=1}^N$ from $\mathbb{R}^w$ to their closest centroid from $\{c^{(s)}\}_{s=1}^D$ while choosing a center $c^{(0)}$ from which centroids must be within $r > 0$ in ℓ_∞ distance.

$$\min_{\mathbf{c}\in\mathbb{R}^{(1+D)\times w}} \frac{1}{N}\sum_{i=1}^N \left(\sum_{s=1}^D \sqrt{\mu^2 + ||\omega_i - c^{(s)}||^2} - \max_{s'=1,\dots,D} \sum_{s=1,\, s\neq s'}^D \sqrt{\mu^2 + ||\omega_i - c^{(s')}||^2} \right)$$
$$\text{s.t.} \quad ||c^{(s)} - c^{(0)}||_\infty \leq r \qquad \forall s \in \{1,\dots,D\} \quad (2)$$

2 Algorithmic approach

Our main contribution consists in a novel algorithm, *Adaptive Difference-Of-Bundles with extrapolation* (ADOBe), tackling problem (1), that mixes three powerful concepts already applied in the convex realm. At each iteration, we perform the following four steps.

1. Non-monotone line-search. A local smoothness parameter $\hat{L} > 0$ is updated based on the previous estimation $\tilde{L}$, e.g. $\hat{L} = \tilde{L}/\rho$ with $\rho \geq 1$.

2. Momentum. Inspired from [4], at the light of $\tilde{L}$, we deduce a suitable candidate extrapolation parameter $\hat{\beta} \in [0, 1[$. Then, given previous iterates $(\tilde{x})_+$ and $\tilde{x}$, with $d = \pm(\tilde{x} - (\tilde{x})_+)$ we compute (in closed-form)

$$\beta^* = \max\{\beta \,|\, x + \beta\, d \in \mathcal{P},\, \beta \leq \hat{\beta}\}$$
$$y = x + \beta^*(x - \tilde{x})$$

3. Cutting-plane models. Using past collected first-order information, we define bundles as in [3],

$$\mathcal{B}_b := \{(\tilde{f}_{b,1}, g_{b,1}), \dots, (\tilde{f}_{b,n_b}, g_{b,n_b})\}, \qquad b \in \{1,2\}$$
$$f_b(u) \geq \ell_b(u) := \max_{(\tilde{f},g)\in\mathcal{B}_b} \langle g, u\rangle + \tilde{f} \qquad \forall u \in \mathcal{P}$$

Solving the polyhedral DC subproblem:

$$x_+ \in \arg\min_{u\in\mathcal{P}} \ell_1(u) - \ell_2(u) + \frac{\hat{L}}{2}||u - y||^2$$

requires (among others), for $g_2 \in \partial f_2(x)$, the solution:

$$(x)_+ = \min_{u\in\mathcal{P}} \ell_1(u) - [f_2(x) + \langle g_2(x), u - x\rangle] + \frac{\hat{L}}{2}||u - y||^2$$

4. *Lyapunov*-check: With $\rho \in (0,1)$, $\kappa \in (0, 1/2)$, let

$$\Delta = \left(F(x) + \frac{\tilde{L}}{2}||(\tilde{x})_+ - \tilde{x}||^2\right) - \left(F(x_+) + \frac{\hat{L}}{2}||(x)_+ - x||^2\right)$$

If $\Delta < (1-\rho)/2\,||d||^2 + \kappa\,\hat{L}\,||x_+ - y||^2$ then $x_+ \leftarrow x$.

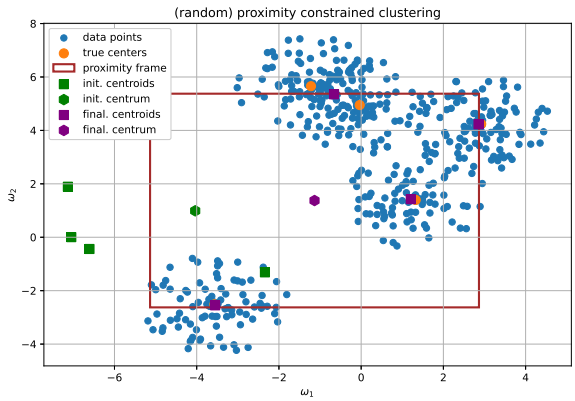

3 Results

We prove that ADOBe converges to *critical* points of (1). We present extensive numerical experiments on practical DC fitting, constrained trust-region and clustering problems, highlighting its performance in comparison with algorithms from [1, 3, 4]. We also implement a post-process from [2] to drive ADOBe towards stronger *d-stationary* points as depicted in the picture above.

References

[1] F.J. Aragon-Artacho, R. Campoy and P.T. Vuong, *The Boosted DC Algorithm for Linearly Constrained DC Programming*, Set-Valued Var. Anal 30 (2022), pp. 1265-1289

[2] A. Beck and N. Hallak, *On the Convergence to Stationary Points of Deterministic and Randomized Feasible Descent Directions Methods*, SIAM. J. Optim. 30 (2019), pp. 56-79

[3] S. Ksenia, W. de Oliveira and W. van Ackooij, *Minimizing the difference of convex and weakly convex via bundle method* (2023).

[4] S. Takahashi and M. Fukuda and M. Tanaka, *New Bregman proximal type algorithms for solving DC optimization problems*, Comput. Optim. Appl. 83 (2022), pp. 893–931

IMPACT: a toolchain for fast specification, prototyping, and deployment of model predictive control

Alvaro Florez[1*], Alejandro Astudillo[1], Wilm Decré[1], Jan Swevers[1] and Joris Gillis[1]
[1]MECO Research Team, Department of Mechanical Engineering, KU Leuven, Belgium
[1]Flanders Make@KU Leuven, Belgium
[*]Email: alvaro.florez@kuleuven.be

1 Introduction

Model predictive control (MPC) is a control methodology that uses a system model to predict future dynamics, and an optimization problem is solved to find the control sequence that minimizes a user-defined cost function. The first value of such sequence is applied to the system being controlled, and the process starts again, shifting the prediction horizon one sample time. MPC can be used to solve a wide range of increasingly complex control problems.The implementation and development of nonlinear MPC (NMPC) can be costly and time-consuming for engineers. Additionally, there is a lack of accessible tools for quickly prototyping and deploying NMPC solvers, which has restricted the widespread use of NMPC in complex and fast mechatronic applications. Here, we present IMPACT, an open-source toolchain that aims to facilitate the workflow of specification, prototyping, and deployment of NMPC.

2 Optimal Control Problem formulation

For a time horizon $t \in [t_0,\ t_\mathrm{f}]$, state vector $\mathbf{x}(t) \in \mathbb{R}^{n_\mathbf{x}}$, input vector $\mathbf{u}(t) \in \mathbb{R}^{n_\mathbf{u}}$, and algebraic state vector $\mathbf{z}(t) \in \mathbb{R}^{n_\mathbf{z}}$, in IMPACT we consider general OCP formulations of the canonical form

$$\begin{aligned}
\underset{\mathbf{x},\mathbf{u},\mathbf{z}}{\text{minimize}} \quad & \int_{t_0}^{t_\mathrm{f}} V(\mathbf{x}(t),\mathbf{u}(t),\mathbf{p},t)\mathrm{d}t + V_f(\mathbf{x}(t_\mathrm{f}),\mathbf{p}) && \text{(1a)}\\
\text{subject to} \quad & B(\mathbf{x}(t_0),\mathbf{x}(t_f),\mathbf{p}) \leq 0, && \text{(1b)}\\
& \dot{\mathbf{x}}(t) = \xi(\mathbf{x}(t),\mathbf{u}(t),\mathbf{z}(t),\mathbf{p}), \quad t \in [t_0,t_\mathrm{f}], && \text{(1c)}\\
& \Gamma(\mathbf{x}(t),\mathbf{u}(t),\mathbf{z}(t),\mathbf{p}) = 0, \quad t \in [t_0,t_\mathrm{f}], && \text{(1d)}\\
& h(\mathbf{x}(t),\mathbf{u}(t),\mathbf{p}) \leq 0, \quad t \in [t_0,t_\mathrm{f}], && \text{(1e)}
\end{aligned}$$

where $V(\cdot)$ and $V_\mathrm{f}(\cdot)$ in (1a) are smooth nonlinear functionals, $\mathbf{p}$ is a parameter vector that typically contains a vector of state measurements or estimates $\mathbf{x}_\mathrm{meas} \in \mathbb{R}^{n_\mathrm{meas}}$, (1b) defines a boundary constraint that typically takes the form of $\mathbf{x}(t_0) = \mathbf{x}_\mathrm{meas}$, (1c) and (1d) define a system of differential-algebraic equations representing the system model, and (1e) represent path constraints.

3 Toolchain Workflow

Let us now present the outline of the IMPACT workflow, which allows the user to define and deploy an NMPC. A general overview of the workflow is depicted in Fig.1.

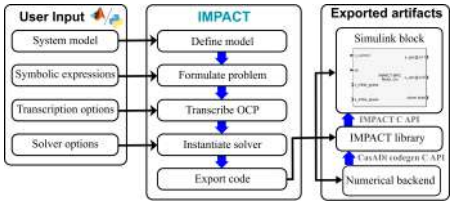

Figure 1: Overview of the workflow of the IMPACT toolchain.

4 Application Example Using IMPACT

We illustrate the use of IMPACT by controlling the point-to-point motion (angular position) of a DC motor using a Speedgoat SN7233 real-time target machine. The control scheme estimates a constant disturbance that represents unmodeled dynamics – e.g., input disturbances and static friction –, and counteracts its effect.

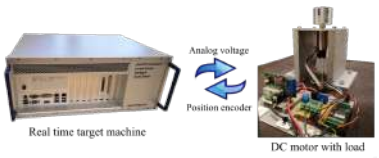

Figure 2: Overview of the system.

By following the workflow in Fig. 1, the motor model, transcription options, and solver were defined using the IMPACT syntax. The code was then exported and the Simulink block artifact was generated. Combining this artifact with the use of Simulink Speedgoat tools, the controller was easily deployed on the hardware resulting in a successful implementation.

5 Conclusions

We introduced IMPACT, a toolchain that simplifies the engineering process from specifying the problem to deploying the NMPC solution. An example of an application in real-time hardware was depicted. Future research directions include testing the toolchain in scenarios involving complex nonlinear (robotic) applications and embedded targets.

Acknowledgement This work is supported in part by Flanders Make SBO DIRAC "Deterministic and Inexpensive Realizations of Advanced Control" and in part by KUL-C1: KU Leuven Research project C14/15/067 "B-spline based certificates of positivity with applications in engineering".

Automated Performance Estimation for non convex optimization via a novel approach for function interpolation

Anne Rubbens and Julien Hendrickx
ICTEAM institute, UCLouvain, 1348 Louvain-la-Neuve, Belgium.
Email: {anne.rubbens, julien.hendrickx} @uclouvain.be

1 Introduction

The *Performance Estimation Problem* (PEP) was recently developed to automatically compute tight worst-case bounds on the performance of a wide class of first-order optimization algorithms designed for given classes of functions [1].
This framework relies on the interpolation problem of function classes: what necessary and sufficient conditions must a set of data satisfy to ensure the existence of a function of the class defined on the whole space and interpolating the data? The derivation of such conditions is crucial in the PEP framework since, to render the infinite-dimensional problem of computing the worst-case function of a given class tractable, one imposes conditions on a finite set of data for it to be consistent with a function class. In particular, a priori tight performance guarantees can only be obtained for function classes whose interpolation conditions are known, since if the condition imposed is only necessary, the worst-case data on which the bound on the performance is based might not correspond to any function of the analysed class.

2 Contribution

To provide tight analysis of methods applied to new classes, we propose a novel approach to analyze conditions, based on the *pointwise extensibility* of the condition to any arbitrary new point instead of its interpolability by a function defined on the whole space. Under reasonable continuity assumptions, we show that extensibility is equivalent to interpolability, even tough this approach allows one to get rid of all analytic properties of the function class to work only at an algebraic level.
Presently, interpolation conditions are available mostly for either variations of smooth strongly convex functions [1] or functions satisfying some Lipschitz condition [2]. However, nonsmooth and nonconvex functions, such as weakly convex functions (that is functions convex up to the addition of a quadratic term), while widespread in a large range of large-scale data applications such as robust PCA, phase retrieval or covariance matrix estimation, often lack of a characterization in terms of interpolation conditions. Since classical algorithms such as the subgradient method do not converge on the class of weakly convex functions, other assumptions are often added to the weak convexity. Relying on our extensibility approach, we provide interpolation conditions for weakly convex functions along with two of those classical assumptions: sharpness of the function, which ensures linear convergence of the subgradient method, and boundedness of the quasi-gradient of the function. Hence, our approach allows to get rid of conservativeness in performance analysis for new classes of functions.
The interpolation condition for the class of weakly convex sharp functions is the following classical definition:

$$\begin{cases} f(x) \geq f(y) + \langle g(x), x_i - x_j \rangle - \mu \frac{||x-y||^2}{2} \\ f(x) - f^* \geq B||x - x^*||, \end{cases}$$

where f^* is the minimum of the function and x^* is the projection of x onto the set of minima.
On the other hand, usually, weakly convex functions with bounded quasi-subgradients convexity are defined and analysed using the following condition:

$$\begin{cases} f(x) \geq f(y) + \langle g(y), x - y \rangle - \frac{\mu}{2}||x-y||^2 \\ ||g(x)|| \leq B. \end{cases}$$

However, this condition is not interpolable, so that any analysis based on it is a priori not tight. We thus propose a new condition, equivalently defining the class but holding as an interpolation condition:

$$\begin{cases} f(y) \geq f(x) + \langle g(x), y - x \rangle - \frac{\mu}{2}||x-y||^2 + \frac{\mu}{2}||y - z_{xy}||^2 \\ ||g(x)|| \leq B \end{cases}$$

where $z_{xy} = \min_{z \in \mathbb{R}^d:\ ||g(x)+x-z|| \leq B} ||y - z||^2$.
We show that performance analysis based on this condition is tighter for this class of functions, demonstrating the impact of our novel approach.

3 Acknowledgments

A. Rubbens is supported by the French Community of Belgium through a FNRS fellowship and a L'Oréal-UNESCO For Women in Science fellowship.

References

[1] A. B. Taylor, J.M. Hendrickx, F. Glineur, "Smooth strongly convex interpolation and exact worst-case performance of first-order methods", *Math. Prog.*, 2017.

[2] H. Whitney, "Analytic extensions of differentiable functions defined in closed sets", *Transactions of the American Mathematical Society*, 1934.

Meta-state-space: A new perspective on representing and identifying stochastic systems

Gerben I. Beintema[a], Roland Tóth[a,b], Maarten Schoukens[a]
[a]Control Systems Group, Electrical Engineering, Eindhoven University of Technology
[b]Systems and Control Laboratory, Institute for Computer Science and Control, Budapest, Hungary.
Emails: g.i.beintema@tue.nl, r.toth@tue.nl, m.schoukens@tue.nl

1 Introduction

Stochastic systems are often represented by either state-space equations with unknown stochastic signals [1] (e.g. $x_{t+1} = f_x(x_t, u_t, e_t)$ where e_t is unknown) or by the propagation of state probability distributions $p(x_t)$ subject to some conditional state transition probability $p(x_{t+1}|x_t, u_t)$ [2]. The identification of stochastic systems using either of these representations is challenging since it requires an estimate of the stochastic signals for consistent estimation or since it requires significant assumptions on the type of probability distribution (e.g. Gaussian distribution). We present a new representation of stochastic systems which allows for computationally efficient identification even with the presents of non-Gaussian state and output distributions.

2 Meta-state-space representation

The novel meta-state-space representation of stochastic systems has the form of

$$z_{t+1} = f_z(z_t, u_t), \tag{1a}$$
$$y_t \sim p(y_t|z_t, u_t). \tag{1b}$$

where $z_t \in \mathbb{R}^{n_z}$ is the meta-state, $u_t \in \mathbb{R}^{n_u}$ is the input, $y_t \in \mathbb{R}^{n_y}$ is the output, f_z is a static deterministic meta-state transition function and $p(y_t|z_t, u_t)$ is the conditional output probability.

One way to interpret and derive the existence of the meta-state-space representation is by taking the meta-state as a parameterization of the state distribution such that $p(x_t) = p(x_t|z_t)$ for all t. The existence of a parameterization of $p(x_t)$ with z_t directly implies the existence of f_z and $p(y_t|z_t, u_t)$. Thus the set of stochastic systems which can be represented by (1) is at least the set represented by probability distributions [2]. A small overview of this interpretation can be viewed in Figure 1.

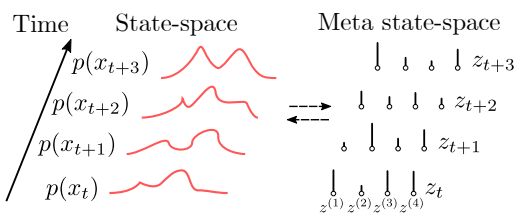

Figure 1: Overview of the meta-state-space representation.

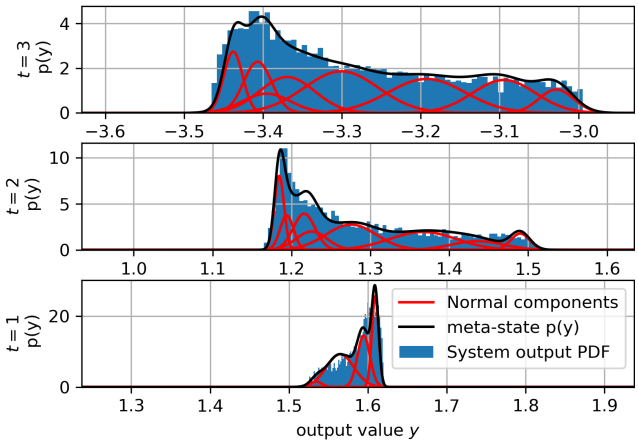

Figure 2: Comparison of output distributions of the meta-state-space model from identification to the system.

3 Meta-state-space identification

Since the meta-state-space representation (1) is deterministic in its dynamics it is well suited for identification. For instance, using Maximum A Posteriori (MAP) criterion the following identification problem is obtained

$$\min_{\theta, \hat{z}_1} \quad -\frac{1}{N}\sum_{t=1}^{N} \log(p_\theta(y_t^*|\hat{z}_t, u_t)) \tag{2a}$$
$$\text{s.t.} \quad \hat{z}_{t+1} = f_\theta(\hat{z}_t, u_t) \tag{2b}$$

where y_t^* are the measurements, f_θ is parameterized by a small ANN and $p_\theta(y_t|z_t, u_t)$ is a weighted sum of Gaussians with ANN parameterized weights, means and standard deviations. We apply this to a numerical system with very non-linear stochastic noise of the form

$$x_{t+1} = \left(0.7\exp\left(-(x_t + e_t)^2\right) + 0.3\right)x_t + u_t \tag{3}$$

where $y_t = x_t$, $p(e_t) = U(-0.5, 0.5)$. The results as seen in Figure 2 show that the obtained probability distributions from the meta-state-space identification are very similar in shape and amplitude compared to the PDF histogram obtained by repeated sampling of the considered system.

References

[1] T. Katayama *et al.*, *Subspace methods for system identification*, vol. 1. Springer, 2005.

[2] T. B. Schön, A. Wills, and B. Ninness, "System identification of nonlinear state-space models," *Automatica*, vol. 47, no. 1, pp. 39–49, 2011.

About (Rectangular) Multiparameter Eigenvalue Problems

Christof Vermeersch, Sarthak De, and Bart De Moor, *Fellow, IEEE & SIAM & IFAC*
Center for Dynamical Systems, Signal Processing, and Data Analytics (STADIUS),
Dept. of Electrical Engineering (ESAT), KU Leuven
{christof.vermeersch,sarthak.de,bart.demoor}@esat.kuleuven.be

1 Introduction

In the 19th century, the idea of considering eigenvalue problems with multiple spectral parameters came forth quite naturally from the classical problem of solving boundary-value problems for partial differential equations via a separation of variables [1]. For example, the two-dimensional Helmholtz equation, which arises when modeling the vibration of a two-dimensional membrane, leads to the study of a pair of ordinary differential equations, both of which share two spectral parameters [3]. This problem is a two-parameter eigenvalue problem, and, in the last two decades, a renewed interest in this topic has led to new approaches to solve boundary-value problems by computing the eigentuples of multiparameter eigenvalue problems (MEPs) [3]. More recently, we have shown that the identification of linear time-invariant models is, in essence, also a (rectangular) MEP [2, 4]. We currently investigate the properties of MEPs, especially the rectangular MEPs that arise in a system identification context, and research solution methods.

2 Research overview

Contrary to one-parameter eigenvalue problems, an MEP consists of one or more matrix equations with multiple eigenvalues combined into eigentuples $\lambda = (\lambda_1, \ldots, \lambda_n)$. Several manifestations of MEPs appear in the literature, but we focus in our research mainly on rectangular MEPs, which consist of one matrix equation with rectangular coefficient matrices, i.e.,

$$\left(\sum_{\{\omega\}} A_\omega \lambda^\omega\right) z = 0, \tag{1}$$

where $z \in \mathbb{C}^{l\times 1} \setminus \{0\}$ is the eigenvector that belongs to an eigentuple λ and $A_\omega \in \mathbb{C}^{k\times l}$ are the rectangular coefficient matrices ($k \geq l+n-1$). The multi-index $\omega = (\omega_1, \ldots, \omega_n)$ in the summation runs over the different monomials $\lambda^\omega = \prod_{i=1}^n \lambda_i^{\omega_i}$ and coefficient matrices $A_\omega = A_{\omega_1 \cdots \omega_n}$.

However, while a lot is known about one-parameter eigenvalue problems (and even about square MEPs), the available literature about rectangular MEPs and their solution methods is quite limited. Recently, some interesting new results on (rectangular) MEPs have been attained, including bounds on the number of solutions, solution methods, relations between the square and rectangular manifestation, and several interesting (system identification) applications [5].

3 Presentation outline

In our presentation, we will introduce MEPs and discuss their use within a system identification context. Furthermore, the presentation will contain some recent results about (rectangular) MEPs and will present the available tools to solve them. Numerical examples will motivate the perspectives and difficulties in system identification applications.

Acknowledgments

This work was supported in part by the KU Leuven: Research Fund (projects C16/15/059, C3/19/053, C24/18/022, and C3/20/117), Industrial Research Fund (fellowships 13-0260, IOFm/16/004, and IOFm/20/002), and several Leuven Research & Development industrial projects; in part by Flemish Government agencies: FWO (EOS project G0F6718N, SBO project S005319, Infrastructure project I013218N, TBM project T001919N), EWI (Flanders AI Research Program), and VLAIO (mandates COT.2018.018, HBC.2019.2204, and HBC.2019.2209); and in part by the European Commission: ERC Adv. Grant (grant 885682). The work of Christof Vermeersch was supported by the FWO Strategic Basic Research fellowship (SB/1SA1319N).

References

[1] Frederick V. Atkinson. Multiparameter spectral theory. *Bull. of the American Mathematical Society*, 74(1):1–27, 1968.

[2] Bart De Moor. Least squares optimal realisation of autonomous LTI systems is an eigenvalue problem. *Communications in Information and Systems*, 20(2):163–207, 2020.

[3] Bor Plestenjak, Călin I. Gheorghiu, and Michiel E. Hochstenbach. Spectral collocation for multiparameter eigenvalue problems arising from separable boundary value problems. *Journal of Computational Physics*, 298:585–601, 2015.

[4] Christof Vermeersch and Bart De Moor. Globally optimal least-squares ARMA model identification is an eigenvalue problem. *IEEE Control Systems Letters*, 3(4):1062–1067, 2019.

[5] Christof Vermeersch and Bart De Moor. Two double recursive block Macaulay matrix algorithms to solve multiparameter eigenvalue problems. *IEEE Control Systems Letters*, 7:319–324, 2023.

Subspace Methods for the Block Macaulay Matrix Framework

Sarthak De, Christof Vermeersch, and Bart De Moor, *Fellow*, *IEEE & IFAC & SIAM*
Center for Dynamical Systems, Signal Processing, and Data Analytics (STADIUS),
Department of Electrical Engineering (ESAT), KU Leuven
{sarthak.de,christof.vermeersch,bart.demoor}@esat.kuleuven.be

1 Introduction

Many system identification problems, like the least-squares identification of linear time-invariant models [1] and the globally optimal identification of autoregressive moving-average models [3], can be rephrased as rectangular multi-parameter eigenvalue problems (RMEPs). Their coefficient matrices are generated using the observed data to which we want to fit the model. The solutions of these RMEPs correspond to the stationary points of the optimization problems and can be computed by solving a set of standard eigenvalue problems (SEPs) that follows from a multidimensional realization problem in the null space of the block Macaulay matrix (BMM) [4].

The BMM method, however, scales poorly with respect to the size of the generating RMEP, which is proportional to the number of observed data points in the related system identification problem. Current BMM methods compute all the solutions of the RMEP, which remains computationally intensive and is often unnecessary. Since we are often only interested in a subset of the solutions, we take inspiration from subspace methods to solve SEPs and square MEPs prevalent in the numerical linear algebra literature [2], and we develop for the first time subspace methods for the BMM framework.

2 Subspace methods for RMEPs

RMEPs are defined in a single matrix pencil format as

$$M(\lambda)\mathbf{z} = \left(\sum_{\{\omega\}} \mathbf{A}_\omega \lambda^\omega\right)\mathbf{z} = \mathbf{0}, \quad \|\mathbf{z}\| = \mathbf{1}, \tag{1}$$

where $\mathbf{A}_\omega \in \mathbb{C}^{k\times l}$ are the coefficient matrices (with $k \geq l + n - 1$) and $\lambda^\omega = \prod_{i=1}^n \lambda_i^{\omega_i} = \lambda_1^{\omega_1}\cdots\lambda_n^{\omega_n}$ are the monomials. We call the n-tuples $\lambda = (\lambda_1, \ldots, \lambda_n) \in \mathbb{C}^n$ and vectors $\mathbf{z} \in \mathbb{C}^{l\times 1}\backslash\{0\}$ the eigentuples and eigenvectors of the RMEP, respectively.

Subspace methods to solve large SEPs and square MEPs consist of two alternating steps [2], which can also be developed for RMEPs in the BMM framework: (i) An *extraction* step, in which we project the large problem onto a smaller problem via approximation and projection spaces. In every extraction step, the basis of the approximation space helps to evaluate an approximation to the eigenvector of the original RMEP (1). The residual associated with the approximation is projected in a Petrov–Galerkin sense over the projection space, resulting in the new smaller problem. (ii) An *expansion* step, in which we use the right and left singular vectors associated with the eigentuple that makes the original pencil the most rank deficient, in order to expand the basis of the approximation and projection space, respectively. These two steps are applied in an alternating fashion until the convergence to an eigentuple of the original problem.

3 Presentation outline

In our presentation, we will start with a brief overview of RMEPs and the BMM method. Then, a detailed discussion regarding the two steps of the subspace methods for RMEPs will be provided. Finally, the convergence behavior and observed speed-up of the proposed subspace methods will be illustrated using numerical experiments.

Acknowledgements

This work was supported in part by the KU Leuven: Research Fund (projects C16/15/059, C3/19/053, C24/18/022, and C3/20/117), Industrial Research Fund (fellowships 130260, IOFm/16/004, and IOFm/20/002), and several Leuven Research & Development industrial projects; in part by Flemish Government agencies: FWO (EOS project G0F6718N, SBO project S005319, Infrastructure project I013218N, TBM project T001919N), EWI (Flanders AI Research Program), and VLAIO (mandates COT.2018.018, HBC.2019.2204, and HBC.2019.2209); and in part by the European Commission: ERC Adv. Grant (grant 885682). The work of Christof Vermeersch was supported by the FWO Strategic Basic Research fellowship (SB/1SA1319N).

References

[1] B. De Moor. Least squares optimal realisation of autonomous LTI systems is an eigenvalue problem. *Communications in Information and Systems*, 20(2):163–207, 2020.

[2] M. E. Hochstenbach, T. Kosir, and B. Plestenjak. A Jacobi–Davidson type method for the two-parameter eigenvalue problem. *SIAM Journal on Matrix Analysis and Applications*, 26(2):477–497, 2004.

[3] C. Vermeersch and B. De Moor. Globally optimal least-squares ARMA model identification is an eigenvalue problem. *IEEE Control Systems Letters*, 3(4):1062–1067, 2019.

[4] C. Vermeersch and B. De Moor. Two complementary block Macaulay matrix algorithms to solve multiparameter eigenvalue problems. *Linear Algebra and its Applications*, 654:177–209, 2022.

Data-driven state-space identification of nonlinear feedback systems

Merijn Floren[1,2,*], Jean-Philippe Noël[1], and Jan Swevers[1,2]

[1]MECO Research Team, Department of Mechanical Engineering, KU Leuven, Belgium
[2]Flanders Make@KU Leuven, Belgium
[*]Corresponding author. Email: merijn.floren@kuleuven.be

1 Background

Many nonlinear systems can be represented as linear time-invariant (LTI) systems with a static nonlinear function in the feedback path (see Fig. 1). As for system identification, modelling of the nonlinear function is particularly challenging since this typically requires prior system information, expert knowledge and/or engineering judgement. Another issue in identification of nonlinear systems is that the optimisation algorithm may converge to a local minimum of the typically non-convex cost function.

2 Problem statement

Consider the discrete-time state-space representation of a nonlinear feedback system

$$\begin{aligned} x_{k+1} &= Ax_k + Bu_k + w_k, \\ y_k &= Cx_k + Du_k, \end{aligned} \tag{1a}$$

where A, B, C and D are the linear state, input, output, and direct feedthrough matrices, respectively. Moreover, x_k is the latent state vector and u_k and y_k are the measured inputs and outputs, respectively, at discrete time instant k. The nonlinear function is represented by an additional multivariate input w_k, which is modelled as a feedforward neural network with one hidden layer:

$$\begin{aligned} w_k &= W_w \sigma(W_z z_k + b_z) + b_w, \\ z_k &= Ex_k + Fu_k + Gy_k, \end{aligned} \tag{1b}$$

where W_z and W_w are the inner and outer weights of the neural net, respectively, and b_z and b_w their associated biases. Any suitable nonlinear activation function $\sigma(.)$ can be chosen. The neural net input is z_k, which is comprised of a linear combination of the states, inputs, and outputs, through coefficient matrices E, F and G, respectively. The aim of this work is to first infer the nonlinear input w_k and the latent state x_k in the time domain, such that their functional mapping in the form of a neural net can be learnt afterwards.

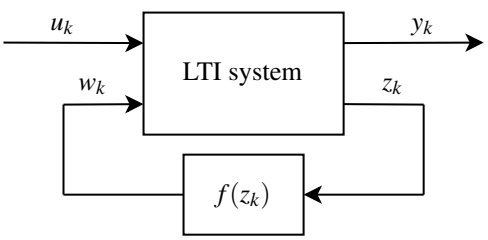

Figure 1: Block-diagram of a nonlinear feedback system.

3 Method

Based on the measured input-output data only, the identification procedure consists of four steps:

1. Initialise A, B, C and D, through the best linear approximation (BLA) [1]. This facilitates the ability to gather crucial data about the system, such as the order of its dynamic behaviour.
2. Use the BLA and the input-output data to find w_k in the time domain by solving a convex optimisation problem similar to unconstrained model predictive control [2]. Here, the reference that we track is the original output data y_k, while the original input data u_k is treated as a known disturbance. This step automatically yields an estimate of the latent state x_k.
3. Define E, F and G; decide on the activation function and the number of neurons; possibly perform some dimensionality reduction on z_k and w_k; and train the feedforward neural net (1b).
4. Perform final optimisation on all model parameters to further reduce the simulation error.

Steps 1-3 thus serve as an initialisation of the final optimisation step, and are meant to mitigate the risk of getting stuck in a local minimum. The considered method also requires almost no prior system knowledge, therefore overcoming one of the main challenges in nonlinear system identification.

4 Results

The effectiveness of the proposed method is evaluated on a number of nonlinear benchmark data sets (from www.nonlinearbenchmark.org), including the Silverbox system and the Bouc-Wen hysteric system.

References

[1] R. Pintelon and J. Schoukens, *System identification: a frequency domain approach*. John Wiley & Sons, 2012.

[2] E. F. Camacho and C. B. Alba, *Model predictive control*. Springer science & business media, 2013.

Learning non-linearities in the 2-layer decoupling problem using structured PARATUCK2 decomposition

Joppe De Jonghe, Peter Karsmakers, Mariya Ishteva
KU Leuven, Department of computer science
joppe.dejonghe@student.kuleuven.be, peter.karsmakers@kuleuven.be, mariya.ishteva@kuleuven.be

1 Introduction

To compress neural (sub)networks into a single layer with flexible activation functions methods based on the decoupling of multivariate polynomials [1] have recently been used [2]. Unfortunately, compression to a single hidden layer is currently the only possibility. However, more flexibility in the number of hidden layers in the compressed network might be desired when considering larger (sub)networks.

Providing compression to more than one hidden layer corresponds to approximating a solution of a multi-layer decoupling problem. In this work we approximate a solution of the 2-layer decoupling problem using a structured PARATUCK2 decomposition.

2 Problem description

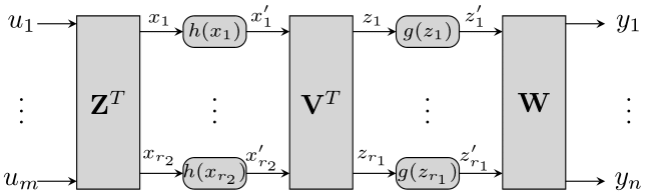

Figure 1: 2-layer decoupling problem. Given a function $\mathbf{f}(\mathbf{u})$, find $\mathbf{W}$, $\mathbf{V}$, $\mathbf{Z}$ and the coefficients of the g_i and h_j.

The 2-layer decoupling problem is defined analogously to the decoupling problem as defined by Dreesen et al. in [1] but generalised to the 2-layer case as shown in figure 1. The 2-layer decoupled representation is then written as

$$\mathbf{f}(\mathbf{u}) = \mathbf{W}\mathbf{g}(\mathbf{V}^T\mathbf{h}(\mathbf{Z}^T\mathbf{u})).$$

3 Proposed approach

The first-order information of $\mathbf{f}$ in the 2-layer decoupling problem is given by the Jacobian

$$\mathbf{J}(\mathbf{u}) = \mathbf{W}\, diag(g'_{i_1}(\mathbf{v}_{i_1}^T\mathbf{h}(\mathbf{Z}^T\mathbf{u})))\, \mathbf{V}^T diag(h'_{i_2}(\mathbf{z}_{i_2}^T\mathbf{u}))\, \mathbf{Z}^T.$$

As a result, the frontal slices of the tensor $\mathscr{J}$ as constructed in [1] follow the structure of a PARATUCK2 decomposable tensor. Combining this insight with the *coupled matrix tensor factorization* (CMTF) method proposed by Zniyed et al. in [2] leads to the following optimization problem

$$\min_{\substack{\mathbf{W},\mathbf{D_g},\mathbf{V},\\ \mathbf{D_h},\mathbf{Z},\mathbf{H}}} \sum_{i=1}^{N} \|\mathbf{J_i} - \mathbf{W}\cdot diag(\mathbf{D_g}^{(i)})\cdot\mathbf{V}^T\cdot diag(\mathbf{D_h}^{(i)})\cdot\mathbf{Z^T}\|^2 + \lambda\cdot\|\mathbf{F}-\mathbf{W}\cdot\mathbf{H^T}\|^2$$

$$\begin{aligned} s.t. \quad & \mathbf{D_h}^{(:,\mathbf{j_1})} = \mathbf{X_{j_1}}\cdot\mathbf{c^h_{j_1}} \quad for\ j_1 = 1,2,\ldots,r_2 \\ & \mathbf{D_g}^{(:,\mathbf{j_2})} = \mathbf{X_{j_2}}\cdot\mathbf{c^g_{j_2}} \quad for\ j_2 = 1,2,\ldots,r_1 \\ & \mathbf{h_{j_3}} = \mathbf{Y_{j_3}}\cdot\mathbf{c^g_{j_3}} \quad for\ j_3 = 1,2,\ldots,r_1 \end{aligned}$$

with N the number of sampling points in which the Jacobian of $\mathbf{f}$ is evaluated, $\mathbf{F}$ containing zeroth-order information of $\mathbf{f}$ and the constraints on $\mathbf{D_h}^{(:,\mathbf{j_1})}$, $\mathbf{D_g}^{(:,\mathbf{j_2})}$ and $\mathbf{h_{j_3}}$ analogous to those given in the CMTF method from Zniyed et al. We solve this optimization problem using a projection strategy as defined in [2] to satisfy the constraints.

4 Results

The proposed algorithm was used to approximate simple non-linearities consisting of multivariate polynomial functions containing either a sine, cosine or hyperbolic tangent. An example approximation that was found by the proposed algorithm for $\mathbf{f}(\mathbf{u}) = [f_1(\mathbf{u})\ f_2(\mathbf{u})]^T$ with $\mathbf{u}\in\mathbf{R}^2$, $f_1 = 2.5 + sin(0.2\cdot\pi\cdot(u_1+u_2))$ and $f_2 = -5 + tanh(u_1+u_2)$ is shown in figure 2.

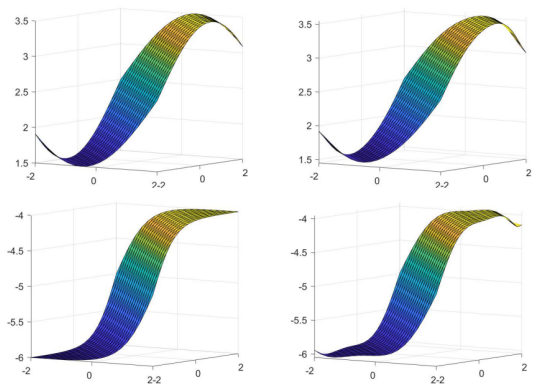

Figure 2: The left column shows $f_1(\mathbf{u})$ and $f_2(\mathbf{u})$, the right column the found approximations.

References

[1] P. Dreesen et al. "Decoupling multivariate polynomials using first-order information," *SIAM J Matrix anal. Appl.*, 36(2):864–879, 2015.

[2] Y. Zniyed et al. A tensor-based approach for training flexible neural networks. In *2021 55th Asil. Conf. Signals, Systems, and Comp.*, 1673–1677. IEEE, 2021.

Non-parametric Continuous-time System Identification with Lebesgue-sampled Output Measurements

Rodrigo A. González
TU/e
r.a.gonzalez@tue.nl

Koen Tiels
TU/e
k.tiels@tue.nl

Tom Oomen
TU/e and TUD
t.a.e.oomen@tue.nl

1 Background

Event-based sampling schemes in control design can lead to improvements in overall performance and resource efficiency [1], with applications in, e.g., network control and incremental encoders [2]. One of the most popular event-based sampling methods is Lebesgue sampling, which consists of sampling the continuous-time signal whenever it crosses fixed thresholds in the amplitude domain.

The problem that is addressed in this work is the estimation of non-parametric continuous-time models from Lebesgue-sampled output data. To this end, we seek an estimator that can 1) provide a *continuous-time* impulse response estimate from possibly noisy and short data records, and 2) exploit the entirety of the information contained in the irregular sampling instants and the bounded intersample behavior.

2 Problem formulation

Consider a linear and time-invariant, continuous-time system G (with impulse response $g(t)$), excited by a known input $u(t)$. The noisy output $z(t)$ is Lebesgue-sampled, as in Figure 1. In practice, $z(t)$ is fastly-sampled every Δ [s] and samples are retrieved only when $z(i\Delta)$ crosses a threshold level. Thus, we have access to $y(i\Delta)=[\eta_i, \eta_i+h]$, where η_i is the lower threshold at time $i\Delta$ and h is the threshold amplitude. This setup is presented in Figure 2.

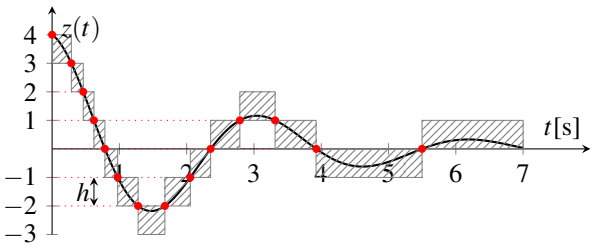

Figure 1: Lebesgue sampling of $z(t)$, with threshold amplitude h=1.

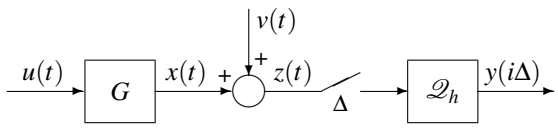

Figure 2: Block diagram of the Lebesgue-sampling scheme. The $\mathscr{Q}_h$ block delivers a set-valued signal y.

The goal is to derive an identification method that estimates $g(t)$ using $\{u(t)\}_{t\in[0,\Delta N]}$ and $\mathbf{y}_{1:N} = \{y(i\Delta)\}_{i=1}^{N}$.

3 Approach

By adopting a kernel-based approach, the goal is to find a regularized estimator of the form

$$\hat{g} = \arg\min_{g\in\mathscr{G}} \left(-\log \mathrm{p}(\mathbf{y}_{1:N}|g) + \gamma\|g\|^2_{\mathscr{G}}\right),$$

where $\mathrm{p}(\mathbf{y}_{1:N}|g)$ is the likelihood function, and $\mathscr{G}$ is a reproducing kernel Hilbert space (RKHS). The impulse response $\hat{g}$ can be obtained via a *finite-dimensional* optimization problem thanks to the Representer Theorem. The finite-dimensional problem that is derived is solved with MAP-EM (MAP Expectation-Maximization), which provides closed-form iterations that are shown to converge to the global optimum if adequately initialized.

Any kernel-based estimator will depend on the choice of hyperparameters. These are computed with Empirical Bayes in this work, from which MAP-EM iterations are also derived. This time the iterations require computing the second moment of a high-dimensional truncated Gaussian. Such matrix can be estimated with Monte Carlo sampling methods.

4 Results

We consider $G(s) = 1/(0.05s^2 + 0.2s + 1)$. The proposed approach exploits the output intersample knowledge to deliver more accurate models than the standard kernel (Riemann) approach [3], for all values of h.

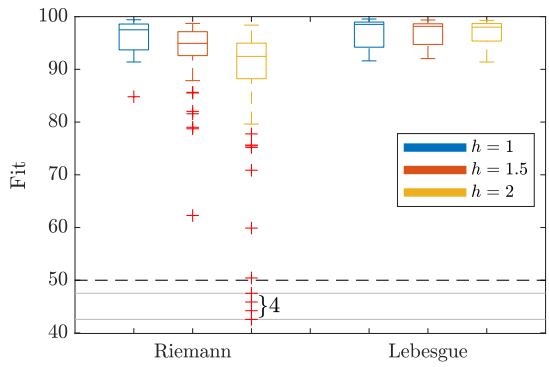

Figure 3: Fit boxplots for the standard Riemann approach (left), and the proposed method (Lebesgue, right) for different values of threshold amplitude h.

Acknowledgments

This work is part of the research program VIDI with project number 15698, which is (partly) financed by NWO.

References

[1] K. J. Åström, and B. Bernhardsson. Systems with Lebesgue sampling. In *Directions in Mathematical Systems Theory and Optimization*, pp. 1–13. Springer, 2003.

[2] N. Strijbosch and T. Oomen. "Iterative learning control for intermittently sampled data: Monotonic convergence, design, and applications". *Automatica*, Article 110171, 2022.

[3] G. Pillonetto and G. De Nicolao. "A new kernel-based approach for linear system identification". *Automatica*, 46(1), pp. 81–93, 2010.

Kernel-Based Sparse Identification and Variable Selection of Nonlinear Systems Through Linearization

Sadegh Ebrahimkhani, John Lataire
ELEC dept., Vrije Universiteit Brussel, Pleinlaan 2, Brussels, Belgium.
Email: Sadegh.Ebrahimkhani@vub.be

1 Motivation

Kernel-based identification of a class of nonlinear (NL) systems is considered. While the structure of the NL system is unknown, we reconstruct the structure of the system through the identification of the linearized model. When the analytical equations of the nonlinear system are available finding the system's linearization is straightforward. While the focus of the present paper is to regenerate the nonlinear model through the identification of its linearization. Two of our main motivations for nonlinear reconstruction through linearization are: the large and often infeasible problem of the unknown NL system identification will be decomposed into simpler subproblems. And also, we will show that there are some structural relations in the linearized model which can be exploited for the estimation.

2 Problem statement

Consider a NL dynamical system described by the following equation:

$$f\left(y(t),\ldots,y^{(n_a)}(t),u(t),\ldots,u^{(n_b)}(t)\right)=0 \qquad (1)$$

where $u(t)$ and $y(t)$ are the input and output of the system, $\bullet^{(n)}$ denotes the nth derivative with respect to t, and $f(\bullet)\in C^2$ is a NL static function of the instantaneous values of $(y(t),\ldots,y^{(n_a)}(t),u(t),\ldots,u^{(n_b)}(t))$.

Consider one stable trajectory of the nonlinear system:

$$p_L(t)=(y_L(t),\ldots,y_L^{(n_a)}(t),u_L(t),\ldots,u_L^{(n_b)}(t)) \qquad (2)$$

Then a small-fast input perturbation ($\tilde{u}(t)$) is used to perturb the system trajectory slightly. Using the Taylor series expansion, the behaviour of (1) can be approximated locally around the trajectory (2) [1]:

$$\sum_{n=0}^{n_a}\alpha_n(p_L(t))\frac{d^n\tilde{y}(t)}{dt^n}+\sum_{m=0}^{n_b}\beta_m(p_L(t))\frac{d^m\tilde{u}(t)}{dt^m}=0 \qquad (3)$$

Where $\tilde{y}(t)$ is the small-fast output corresponding to $\tilde{u}(t)$, and the coefficients $\alpha_n(.)$ and $\beta_m(.)$ are the partial derivatives of (1) with respect to its arguments. Indeed, (3) is a linear parameter-varying (LPV) system scheduled by the trajectory. The main problem of the present work is to regenerate (1) through the identification of (3) with few parameters and a structure which is as simple as possible. Note that the scheduling variable is the system trajectory, which in some cases will be a high dimensional vector, and in many cases the nonlinear system (1) is not a function of all its arguments but a subset of (2). So, the summations in (3) will not be complete and some are zero and the coefficients are functions of a subset of (2). Then the main problem is the sparse identification of (3) with variable selection. This leads to a simpler and more interpretable model.

3 Proposed approach

The PV coefficients in (3) are partial derivatives of (1):

$$\begin{cases}\alpha_n(p_L(t))=\frac{\partial f}{\partial y^{(n)}}|_{p_L(t)}\\ \beta_m(p_L(t))=\frac{\partial f}{\partial u^{(m)}}|_{p_L(t)}\end{cases} \qquad (4)$$

So in order to recover (1) one can obtain the LPV model in (3) via an LPV identification procedure, and by integration reconstruct (1). To ensure the integrability of the LPV and reconstruction of the NL from LPV, we will show that the parametrization of the vector of PV coefficients must satisfy a specific structure (curl-free constraint).

The partial derivative of a function with respect to each of its arguments measures the rate of change of the function in that direction. We make use of this fact to measure the dependency of each PV coefficient of the LPV on the elements of (2). We will prove that these partial derivatives are the elements of a Hessian matrix. The sparsity of the LPV model can be cast as the minimization of the L_1 norm. Finally, we exploit the obtained structural relations for the LPV parametrization and variable selection via regularization. The reconstructed LPV model is the integral of the PV coefficients of the LPV. Hence, the LPV and NL models are related through a linear transformation, which is the last structural relation we impose on the model structure.

This research was supported by the Fund for Scientific Research (FWO Vlaanderen, grant G005218N) and by the Flemish Government (Methusalem Grant METH1).

References

[1] John Lataire, Rik Pintelon, Tom Oomen, "An LTV Approach to Identifying Nonlinear Systems-with Application to an RRR Robot", IFAC-PapersOnLine, 54 (7), pp. 445-450, 2021

Safety Assurance Framework for Connected, Automated Mobility Systems

Nishant Rajesh[1,2], Mohsen Alirezaei[1,2], Erjen Lefeber[2], and Nathan van de Wouw[2]

[1]Siemens Digital Industries Software, Helmond, The Netherlands
[2]Dept. of Mechanical Engineering, Eindhoven University of Technology, Eindhoven, The Netherlands
Email addresses: {n.rajesh, m.alirezaei, a.a.j.lefeber, n.v.d.wouw}@tue.nl

1 Introduction

In the recent years, there have been significant strides in the development of Automated Vehicles (AVs), giving rise to a requirement for a standardised verification and validation framework to ensure safety of AVs. Real-world testing of AVs through test drives alone is not a feasible solution, as it would require billions of kilometers of testing [1]. Scenario-based testing in simulation is an attractive potential alternative for the safety assurance of autonomous vehicle functions.

Safety in road vehicles is covered by ISO 26262 which addresses functional safety, or the safety of the system under malfunctioning behaviour of Electrical and/or Electronic (E/E) safety-related systems [2]. Additionally, with respect to AVs in particular, hazardous situations caused by functional insufficiencies, or reasonably foreseeable misuse, are also of importance, and are covered by Safety Of The Intended Functionality (SOTIF) as described in ISO 21448 [3]. SOTIF assessment focuses on identifying hazardous events, caused by a combination of unsafe scenarios and hazardous behaviour. This is done by classifying the set of possible scenarios as known or unknown, and safe or unsafe. The goal is the identification of unsafe and unknown scenarios, and systematically reducing the probability of unsafe-unknown scenarios.

For a scenario-based assessment of AVs, the following requirements need to be fulfilled:

- The scenarios need to be representative of situations which the AV is expected to encounter in the real-world.
- The scenario subset needs to consist of a diverse range of scenarios, which span the entire possible scenario space, and subject the AV to a wide range of possible test cases.
- In line with the SOTIF assessment methodology, the focus is on 'unsafe' and 'unknown' scenarios, therefore requiring metrics for measurement of criticality and novelty of scenarios.

2 Approach

The above task of finding critical, novel and diverse scenarios for the validation of AVs can be formulated as an optimization problem. The optimization problem has the following characteristics:

- The degree of criticality and novelty of the scenario need to be modeled as independent objectives.
- The objective functions require the simulation of an entire traffic scenario, and therefore the problem is non-linear, non-convex, and expensive to evaluate.
- Depending on the type of the scenario being modelled, there may be integer or discrete variables in addition to continuous variables, leading to a mixed discrete-continuous optimization problem.
- A diverse set of possible critical scenarios need to be identified. As opposed to traditional optimization problems, where the goal is to isolate a single global minimum, here the requirement is to isolate multiple local minima, and differentiate and categorise them.

In order to solve the optimization problem in a manner which deals with the above requirements, we need to use a global optimization algorithm, which can deal with the existence of multiple local minima, as well as with multiple objective functions.

References

[1] N. Kalra and S. M. Paddock, "Driving to safety: How many miles of driving would it take to demonstrate autonomous vehicle reliability?," *Transportation Research Part A: Policy and Practice*, vol. 94, no. C, pp. 182–193, 2016.

[2] "Road vehicles — Functional safety," standard, International Organization for Standardization, Dec. 2018.

[3] "Road vehicles — Safety of the intended functionality," standard, International Organization for Standardization, June 2022.

Online Unit Commitment Problem Solving using Dynamic Programming

Wim Van Roy*, Joris Gillis, Goele Pipeleers and Jan Swevers
MECO Research Team, KU Leuven DMMS lab, Flanders Make
*Email: wim.van.roy@kuleuven.be

1 Overview

Unit Commitment problems (UCMs) are problems in which a set of generators need to work together to achieve a common goal. Examples of such problems are the energy grid, heating systems or production of compressed air. The nature of these problems are NP-hard as it combines nonlinearities together with discrete states of the generators[1]. Due to this complexity, achieving the global optimum often takes a very long time and warmstarting is often impossible making the solvers limited to offline scheduling approaches. This abstract proposes a new solution technique based on Dynamic Programming (DP), a recursive solution technique. The technique can achieve a near-optimal solution in short amount of time making it feasible to run online on embedded targets.

2 Background

The goal of a UCM is to generate a demand flow of electricity, heat or air as efficiently as possible over a given time horizon using the given set of generators. Equation 1 [2] formulates the UCM for a horizon of T and a set of generators $\mathbb{G}$.

$$\begin{aligned} \min \sum_{g\in\mathbb{G}} \sum_{t=0}^{T} & p_g(c_{g,t}, s_{g,t}) \\ \text{s.t.} \sum_{g\in\mathbb{G}} & q_g(c_{g,t}, s_{g,t}) = D(t) \quad \forall t \in [0,1,...,T] \\ & (c_{g,t}, s_{g,t}) \in \Pi_g(t) \qquad \forall g \in \mathbb{G}, \\ & \qquad \forall t \in [0,1,...,T] \end{aligned} \tag{1}$$

In this equation $c_{g,t}$ and $s_{g,t}$ are the capacity and the machine state of generator g at time t. The consumed power and the produced flow of the generator g are given by p_g and q_g. The machine state can be *on*, *off* or *idling* and are constraint by the feasible set Π_g. The demand flow is given by $D(t)$. In literature, both the consumed power and produced flow formulas are often simplified to piecewise linear functions[1]. As a result, this formulation becomes a Mixed Integer Linear Problem (MILP). Existing solvers for MILP-problems are often hard to warmstart and take a long calculation time, especially when there are many feasible solutions.

3 Contribution

The proposed DP solution technique divides the original problem from Equation 1 into smaller subproblems for which the state and the capacity for each generator only has to be solved for one time instance given the required costs to go to a next iteration. Each iteration solves the problem given by Equation 2.

$$\begin{aligned} \min \sum_{g\in\mathbb{G}} & p_g(c_{g,t_i}, s_{g,t_i}) \\ & + C_{g,t_{i+1}}(s_{g,t_i}) + C_{g,t_{i-1}}(s_{g,t_i}) \\ \text{s.t.} \sum_{g\in\mathbb{G}} & q_g(c_{g,t_i}, s_{g,t_i}) = D(t_i) \\ & (c_{g,t_i}, s_{g,t_i}) \in \Pi_g(t_i | c_{g,t_{i-1}}, s_{g,t_{i-1}}) \quad \forall g \in \mathbb{G} \end{aligned} \tag{2}$$

In this equation a lumped cost to go to the next state is given by $C_{g,t_{i+1}}$ as well as an additional cost $C_{g,t_{i-1}}$ due to the state of a previous time step. The feasible set of states for the generator is based on the previous time step. The algorithm alternately solves these subproblems in a backwards sweep and updates the feasible set of states for the generators in a forward sweep in time. This process continues until no further improvements can be made. After each iteration, the solvers guaranties a feasible solution. Since the algorithm can be stopped at any given time after the first iterate and allows warmstarting, it is able to run in an online system. A comparison with MILP-based approaches from literature is performed. The results show that the proposed technique achieves a near-optimal solution while reducing the calculation time. The proposed technique can run in an online system.

References

[1] Tiwari, S., Dwivedi, B., Dave, M. P., Shrivastava, A., Agrawal, A., & Bhadoria, V. S. (2021). Unit commitment problem in renewable integrated environment with storage: A review. *International Transactions on Electrical Energy Systems*, e12775.

[2] Knueven, B., Ostrowski, J., & Watson, J. P. (2020). On mixed-integer programming formulations for the unit commitment problem. *INFORMS Journal on Computing*, 32(4), 857-876.

Electric Autonomous Mobility-on-Demand: Joint Optimization of Routing and Charging Infrastructure Siting

Fabio Paparella, Karni Chauhan, Theo Hofman, Mauro Salazar
Control System Techonology
Eindhoven University of Technology
5600 MB Eindhoven
The Netherlands
Email: {f.paparella,k.s.chauhan,t.hofman,m.r.u.salazar}@tue.nl

1 Abstract

The advent of vehicle autonomy, connectivity and electric powertrains is expected to enable the deployment of Autonomous Mobility-on-Demand systems. Crucially, the routing and charging activities of these fleets are impacted by the design of the individual vehicles and the surrounding charging infrastructure [1] which, in turn, should be designed to account for the intended fleet operation [2]. This paper presents a modeling and optimization framework where we optimize the activities of the fleet jointly with the placement of the charging infrastructure. We adopt a mesoscopic planning perspective and devise a time-invariant model of the fleet activities in terms of routes and charging patterns, explicitly capturing the state of charge of the vehicles by resampling the road network as a digraph with iso-energy arcs. Then, we cast the problem as a mixed-integer linear program that guarantees global optimality and can be solved in less than 10 min. Finally, we showcase two case studies with real-world taxi data in Manhattan, NYC: The first one captures the optimal trade-off between charging infrastructure prevalence and the empty-mileage driven by the fleet. The jointly optimized infrastructure siting significantly outperforms heuristic placement policies, and that increasing the number of stations is beneficial only up to a certain point. The second case focuses on vehicle design and shows that deploying vehicles equipped with a smaller battery results in the lowest energy consumption: Although necessitating more trips to the charging stations, such fleets require about 12% less energy than the vehicles with a larger battery capacity.

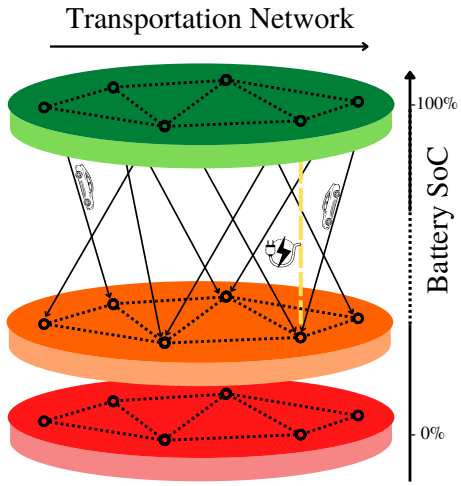

Figure 1: Multi-layer digraph schematically representing an E-AMoD system. Each layer is a battery state-of-charge (SoC). Nodes on the same vertical line represents the same geographic location. The yellow arc indicates a charging station.

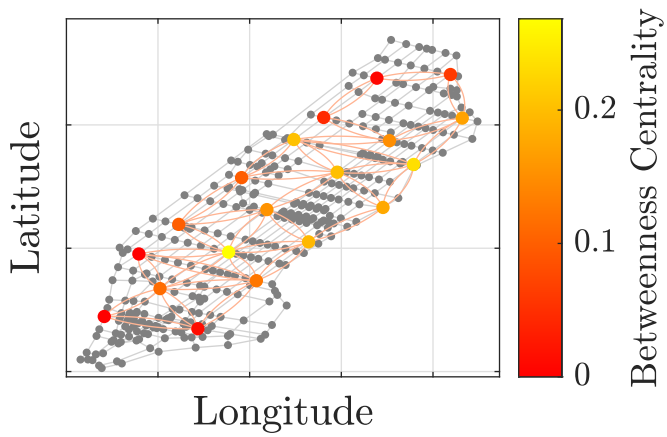

Figure 2: Road graph of Manhattan (grey). Reduced iso-energy graph (colored). Each orange arc has a weight equal to the unit energy or an integer multiple.

References

[1] F. Rossi, R. Iglesias, M. Alizadeh, and M. Pavone, "On the interaction between Autonomous Mobility-on-Demand systems and the power network: Models and coordination algorithms," *IEEE Transactions on Control of Network Systems*, vol. 7, no. 1, pp. 384–397, 2020.

[2] J. Luke, M. Salazar, R. Rajagopal, and M. Pavone, "Joint optimization of electric vehicle fleet operations and charging station siting," in *Proc. IEEE Int. Conf. on Intelligent Transportation Systems*, 2021, in press.

Modeling Hysteresis and Current-Direction Dependence in Li-Ion Batteries using Linear Parameter-Varying Framework

A.M. Ahmad, H.J. Bergveld, M.C.F. Donkers
Control Systems Group – Eindhoven University of Technology – The Netherlands
Email: {a.m.a.sheikh,h.j.bergveld,m.c.f.donkers}@tue.nl

1 Introduction

Lithium-ion batteries have been at the forefront of the recent global research activities to achieve the rapid electrification of various transport systems. An essential component of such battery-powered systems is the Battery Management System (BMS) which ensures safe and efficient battery operation using appropriate battery models. Due to their ease of parameterization and reduced computational complexity, the empirical models, such as the equivalent circuit models (ECMs) are the preferred choice in the BMS environment over the high-fidelity first-principles models. Quite understandably, more accurate and versatile ECMs remain the focus of the current research so that the battery state estimation can be reliably achieved over a wide range of operation.

2 Problem statement and Approach

During the formulation of the ECMs, the battery electromotive force (EMF), also known as the open-circuit voltage, is generally considered as a static nonlinear function of the battery state-of-charge (SOC). However, the presence of the hysteresis phenomenon in various battery chemistries, such as lithium iron phosphate, renders the EMF as a path-dependent battery characteristic [1]. In addition, the battery has been shown to exhibit current-direction-dependent [2] as well as SOC-dependent dynamics. While there exist various approaches in the literature to model such battery behaviors separately, mainly using the linear time-invariant (LTI) models, a systematic approach to incorporating them in a single framework is currently lacking.

In this work, we propose a novel model structure based on the linear parameter-varying (LPV) framework that can incorporate the hysteresis, the current-direction dependence, and the SOC dependence in a unified manner. Essentially, we present a multiple-input single-output LPV model which incorporates the hysteresis nonlinearity as an additional model input besides the battery current. Furthermore, we define the so-called scheduling variable to comprise of the battery SOC as well as a cycling-direction variable δ, which accordingly takes care of the SOC and the current-direction dependence.

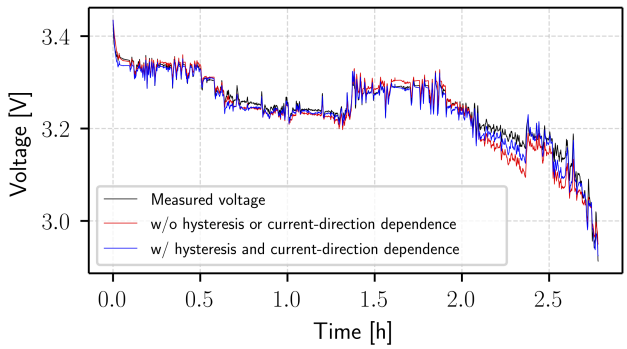

Figure 1: Validation results comparing the voltage predictive capability of two LPV models.

3 Results and Conclusions

The parameter estimation procedure for the proposed model structure was carried out by formulating a linear regression problem with the ARX noise structure. Subsequently, the voltage-predictive capability of two LPV models was analyzed, where the first model incorporates only the SOC dependence, and the second model additionally includes the hysteresis and the current-direction dependence. Figure 1 shows the obtained validation results using a real drive-cycle profile with a 2.5 Ah LFP cell. The RMSE values associated with the first and the second model were found out to be 21.165 mV and 12.559 mV, respectively. It can be concluded that the proposed model structure demonstrates an intuitive approach to incorporate novel battery characteristics, thereby enhancing the model applicability over a wide range of the battery operation. Furthermore, it also offers flexibility to downgrade to a *submodel* depending on the quality of the available identification dataset, and the intended model application.

References

[1] Barai, Anup, et al. "A study of the open circuit voltage characterization technique and hysteresis assessment of lithium-ion cells." J. Power Sources (2015).

[2] Christophersen, Jon P., et al. "Pulse resistance effects due to charging or discharging of high-power lithium-ion cells: A path dependence study." J. Power Sources (2007).

Energy-aware Time-optimal Routing of Battery-electric Trolley Trucks

Finn Vehlhaber, Mauro Salazar
Eindhoven University of Technology
PO Box 513, 5600 MB Eindhoven
The Netherlands
Email: {f.n.vehlhaber,m.r.u.salazar}@tue.nl

Abstract

Dynamic charging has attracted interest for its potential to decarbonize heavy-duty road transport with battery-electric trolley trucks (BETTs). A study on its feasibility finds that for the best immediate impact, it should be first installed on the most frequented highway segments [1]. In this work, we show that this placement can enable long-haul deliveries that are not yet feasible with current battery-electric truck (BET) models. To this end, we formulate a vehicle routing problem as a network flow model, introducing an efficient implementation of battery constraints to ensure path feasibility.
First, we devise a weighted second-order cone optimization problem in the space domain [2] with two objectives - time and battery energy - to obtain optimal drive cycles for a given road topography. This way, we can trade time for energy and possibly avoid otherwise necessary charging stops.

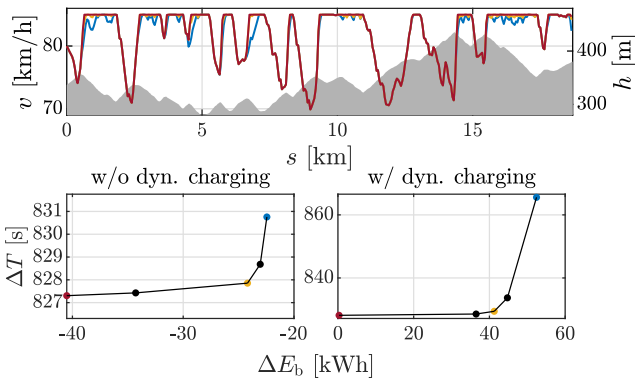

Figure 1: Drive cycles and Pareto fronts for a selected road segment. Colored dots correspond to drive cycle in the same color.

We obtain Pareto fronts like those in Fig. 1 and leverage them in a routing problem [3]. We relate the energy expenditure on a traversed edge to the vehicle's state of charge at each node, obtaining a mixed-integer linear problem that accurately respects battery path constraints and can be solved rapidly.
The results in Fig. 2 show that few strategically placed dynamic charging roads lead to a significant decrease in travel time for the BETT compared to the BET.

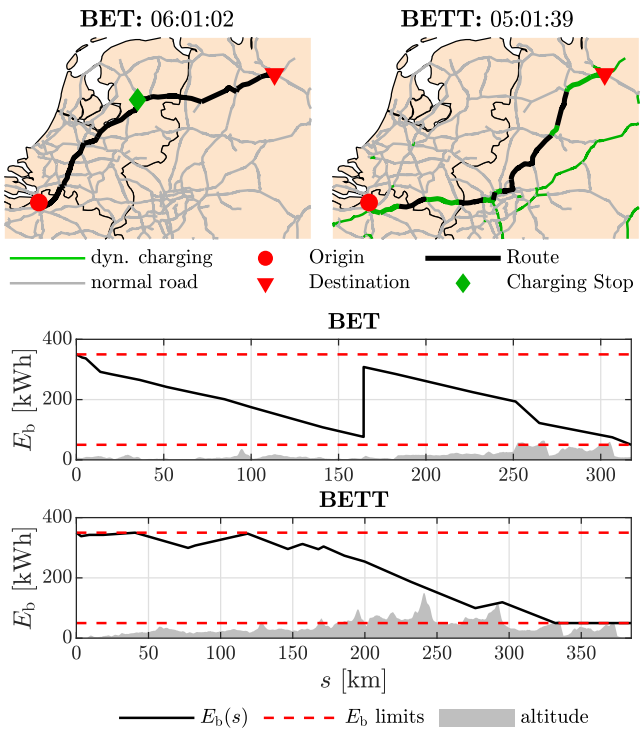

Figure 2: Route comparison from Antwerp to Bremen and battery discharge trajectories.

For most origin-destination pairings, the BETT can match the time required by a diesel truck, spurring a switch to more environmentally friendly freight transport options.

References

[1] M. Wietschel *et al.*, "Electric trolley trucks—a techno-economic assessment for germany," *World Electric Vehicle Journal*, vol. 10, no. 4, 2019.

[2] J. van Kampen, T. Herrmann, and M. Salazar, "Maximum-distance race strategies for a fully electric endurance race car," *European Journal of Control*, 2022, in press. Available online at https://arxiv.org/abs/2111.05784.

[3] M. Salazar, A. Houshmand, C. G. Cassandras, and M. Pavone, "Optimal routing and energy management strategies for plug-in hybrid electric vehicles," in *Proc. IEEE Int. Conf. on Intelligent Transportation Systems*, 2019.

Extremum-seeking control for settling time optimization*

Wouter Weekers[†,**] Dragan Kostić[‡] Alessandro Saccon[†] Nathan van de Wouw[†]

[†] Eindhoven University of Technology, Department of Mechanical Engineering, P.O. Box 513, 5600 MB Eindhoven, The Netherlands

[‡] ASMPT, Center of Competency, Platinawerf 20, 6641 TL Beuningen, The Netherlands

[**] Email: w.weekers@tue.nl

1 Introduction

Mechatronic systems typically show variations in dynamic responses due to, e.g., different disturbance situations. However, since individual controller design is time-consuming, generally one controller is designed for a group of these systems, causing a loss of individual system performance. Automated controller tuning methods such as Iterative Feedback Tuning (IFT) [1] and Extremum-Seeking Control (ESC) [2] facilitate individual controller tuning, yet are ineffective in minimizing the settling time t_s, which is essential for large system throughput. The reason for this is twofold: 1) standard IFT and ESC typically minimize an error norm, which does not guarantee minimization of t_s, and 2) t_s is a discontinuous function of controller parameters, hence standard gradient-based IFT and ESC methods cannot be applied. Moreover, standard IFT and ESC do not guarantee crucial closed-loop stability and its robustness. In this work, we present an alternative ESC-based tuning approach that optimizes t_s and warrants robust closed-loop stability.

2 Problem formulation and approach

We consider the feedback interconnection of a plant P performing repeated point-to-point motions between positions p_0 and p_f, and a feedback controller $C_{fb}(\theta)$ with parameters θ. Each motion profile defined on the time interval $[0,T]$ consists of 1) a motion phase of length t_m, during which the system moves from p_0 to p_f, or vice versa, 2) a settling phase of length $t_s := \max\{s \in [0, T-t_m] : |e(t_m+s)| > e_b\}$, during which the servo error e converges until it satisfies the error bound e_b at the end of the time interval, and 3) a process phase of length $t_p = T - t_s - t_m$, during which it is crucial that e respects $|e| \leq e_b$ to perform the machine operation. Our goal is to maximize throughput by solving $t_s^* := \min_{\theta\in\Theta} t_s$ s.t. $|e(t)| \leq e_b, \forall t \in [t_m+t_s, T]$, where Θ is the set of all θ resulting in robust closed-loop stability.

Since t_s is a discontinuous function of θ, we introduce an additional optimization variable τ and reformulate the problem of minimizing t_s as the continuous problems $\tau^* := \min_{\tau\in[0,\mathrm{T}-\mathrm{t_m}]} \tau$ s.t. $\mathrm{J}^*(\tau) \leq \mathrm{e_b}$ and $J^*(\tau) := \min_{\theta\in\Theta} \sup_{t\geq 0} |w(t;\tau)e(t)|$, where $w(t;\tau)$ equals one if $t \in [t_m+\tau, T]$ and zero otherwise. We repeatedly search for θ^* corresponding to $J^*(\tau)$ using the DIRECT algorithm [3], and use $J^*(\tau)$ to update τ in a bisection search to find τ^*. To ensure $\theta \in \Theta$, motion experiments are only performed if for θ the closed-loop is asymptotically stable with a peak sensitivity below a given bound, which is automatically verified based on the Nyquist criterion and FRF data of P. Otherwise, $w(t;\tau)e(t)$ is replaced by a high penalty value.

3 Results

In a case study with a wire bonder system, the proposed approach (ESC) achieves comparable performance to (in practice time-consuming and thus infeasible) *dedicated* controller tuning using manual loop-shaping (LS) and an industrial tuning algorithm (FBA), as shown in Figure 1.

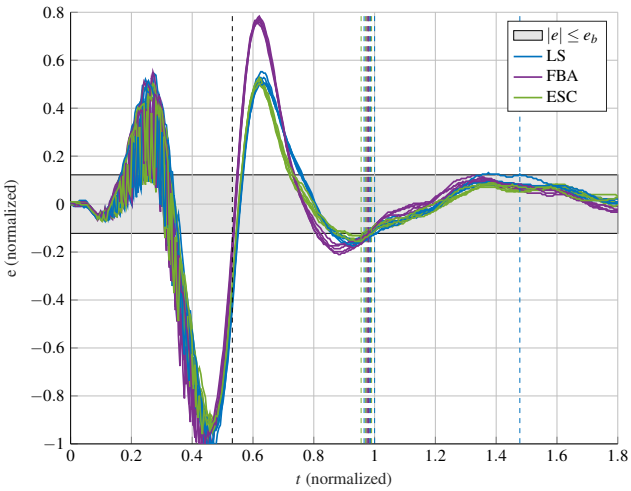

Figure 1: Servo error comparison for the three controllers. Dashed lines indicate t_m (black) and $t_m + t_s$ (colored).

References

[1] H. Hjalmarsson, "Iterative feedback tuning - an overview," *Int. J. Adapt. Control Signal Process.*, vol. 16, no. 5, pp. 373–395, 2002.

[2] Y. Tan, W. H. Moase, C. Manzie, D. Nešić, and I. M. Y. Mareels, "Extremum seeking from 1922 to 2010," in *Proc. 29th Chin. Control Conf.*, pp. 14–26, IEEE, 2010.

[3] D. R. Jones, C. D. Perttunen, and B. E. Stuckman, "Lipschitzian optimization without the Lipschitz constant," *J. Optim. Theory Appl.*, vol. 79, no. 1, pp. 157–181, 1993.

*This work is part of the project Digital Twin with project number P18-03 of the research programme TTW Perspective which is (partly) financed by the Dutch Research Council (NWO).

A data-based real-time system for the management of urban traffic networks.

Christian Portilla
The Eindhoven University of Technology
c.r.portilla@tue.nl

Andrés Acosta
Universidad Nacional de Colombia
afacostag@unal.edu.co

Jairo Espinosa
Universidad Nacional de Colombia
jespinov@unal.edu.co

1 Introduction

Sustainable urban mobility in modern cities is a major concern for authorities since it has to consider aspects such as congestion, road safety, infrastructure planning, public and alternative transportation, social inclusion, and the environment, among others. Particularly, the increasing number of private vehicles has led to negative externalities associated with congestion such as increments of pollution, noise, and travel time, affecting the quality of life of citizens. In this sense, it is necessary to generate alternatives for managing the vehicular traffic network by taking advantage of the available infrastructure resources. However, the urban traffic network is a large-scale system with high complexity with signalized intersections that interact with agents with different priorities: public and private vehicles, cyclists, and pedestrians. In this work, we present a based-data decision-making system to reduce congestion and pollution in middle and big cities. This system fuses the available data and proposes optimal traffic light plans that can be used in real-time based on the current traffic conditions. This system was implemented in the city of Medellín - Colombia in real-time for 35 signalized intersections reducing the travel time by 15% and the pollution by 10%.

2 Methodology

The management system contains monitoring and control traffic modules, as well as a configuration file. **The monitoring module** is in charge of collecting the available data and fusing it to increase its reliability and estimate the variables in roads without measurements. Since the data is coming from different sources is usual to find heterogeneous data, i.e., the combination of different variables or sample times. Therefore, the monitoring system unifies the variables using mathematical relationships, for instance, relating speed and flow through the fundamental diagram or the data-based models. On the other hand, **the control module** clusters the recurrent traffic conditions in the network and finds the best traffic light plans via optimization. This is an offline process where there are as many clusters as traffic light plans for each intersection. Using the pre-calculated clusters and the optimal traffic light plans, the system selects, in real-time, the best traffic light plans based on the current traffic conditions. Finally, **the configuration file** must contain the information about the road (length and the number of lanes, road identifiers, connections (turns), and allowed vehicles), the traffic lights(green, red, and amber time of each traffic light planning throughout the day), and the databases (mapping between the information of databases and the road description). The testing and validation of the system were performed using SUMO (Simulation of Urban MObility) which is an open-source simulator developed by the Institute of Transportation Systems at the German Aerospace Center [1].

3 Results

The management system of urban traffic networks was implemented and validated in 35 signalized intersections of the city of Medellín-Colombia as is shown in Figure 1.

Figure 1: FLEXI GUI showing the interactive map.

As a result of this implementation, the travel times and the pollution were reduced by 15% and 10% respectively.

References

[1] Krajzewicz, D., Erdmann, J., Behrisch, M., & Bieker, L. (2012). Recent development and applications of SUMO-Simulation of Urban MObility. International journal on advances in systems and measurements, 5(3&4).

Predictable error decay model predictive control

Johan Ubbink, Wilm Decré, Joris De Schutter
Department of Mechanical Engineering, KU Leuven
Flanders Make@KU Leuven
Belgium
Email: johan.ubbink@kuleuven.be

1 Introduction

In sensor-based robotics applications, it is desirable to control a manipulator arm to interact with the environment, such as maintaining a desired force or distance from an object. Predictability is often favored in these scenarios. For safety reasons, it is helpful to know how fast the controller will try to decrease some task errors (for instance, the speed at which the robot is moving toward a human operator). Additionally, it is not practical to accurately model everything in the robot-environment system. For example, any real system is subjected to actuator and/or sensor bandwidth limits. Therefore, we want to limit the closed-loop bandwidth of the controller.

Some classical robot control techniques, such as the constraint-based task specification framework eTaSL [1], can account for this. In this framework, which is based on the task function approach [2], the task error e, as a function of the state x, is controlled to zero with a defined control law

$$\frac{\mathrm{d}}{\mathrm{d}t}e(x) = -Ke(x) \tag{1}$$

where K is a user-selected feedback gain. This gain is directly interpretable: (1) the time constant K^{-1} provides insight into how quickly the error will decay, and (2) it can be selected to limit the closed-loop bandwidth of the controller.

However, this approach is purely instantaneous and therefore sub-optimal. It is known that incorporating a prediction horizon through model predictive control (MPC) improves the performance of the controller, allowing it to better anticipate geometric/kinematic constraints (workspace limits) and dynamic constraints (actuator limits). In MPC, an optimal control problem (OCP) is solved at every time step for a horizon into the future. Although there is no "standard" MPC formulation, it is common to specify an objective function inspired by the linear quadratic regulator (LQR) formulation

$$J_{\mathrm{MPC}} = \int_{t_k}^{t_k+T_n} e(x)^\intercal Q e(x) + u^\intercal R u \,\mathrm{d}t \tag{2}$$

where the objective function trades off the task error e with the control input u, weighted with Q and R respectively. Choosing the appropriate values for Q and R is not always obvious, and how fast the error should decay cannot be directly observed. In contrast, with the control law in (1), the gain K provides direct information on how the error should decay.

In this research, we extend the instantaneous formulation of [1] to include a prediction horizon. This provides a way to design MPC controllers with a predictable response, which can be selected to limit the closed-loop bandwidth. The research is presented in the context of robot task control, but the formulation might be relevant for MPC practitioners controlling other systems, where selecting objective function gains is also difficult.

2 Predictable error decay MPC

The key idea is that rather than penalizing the error directly within the objective function, deviation from the desired control behavior in terms of desired error decay is penalized. This is achieved by introducing a new error function

$$\varepsilon(x,u) = \frac{\mathrm{d}}{\mathrm{d}t}e(x) + Ke(x) \tag{3}$$

$$= \frac{\partial e}{\partial x} f(x,u) + Ke(x), \tag{4}$$

which represents the deviation from a first-order decay, where the time derivative of the error can be expanded using the chain rule and substituting in the system dynamics $\dot{x} = f(x,u)$. The new objective function becomes

$$J = \int_{t_k}^{t_k+T_n} \varepsilon(x,u)^\intercal Q \varepsilon(x,u) + \mu[u^\intercal R u] \,\mathrm{d}t. \tag{5}$$

As before, the control inputs are still penalized within the objective. However, it is multiplied by a very small weighting factor μ. Therefore, the dominant term in the objective is the deviation from the desired error decay. Choosing K determines how fast the error decays, Q adjusts the priority of conflicting constraints, and R adjusts the null space motion (e.g. for redundant robot systems).

References

[1] E. Aertbeliën, and J. De Schutter, "eTaSL/eTC: A constraint-based task specification language and robot controller using expression graphs" IEEE IROS, 2014.

[2] C. Samson, M. Le Borgne, and B. Espiau, "Robot Control, the Task Function Approach," Clarendon Press, 1991.

This research was supported by project G0D1119N of the Research Foundation - Flanders (FWO - Flanders).

Safe Unicycle Robot Navigation via Feedback Motion Prediction

Aykut İşleyen and Nathan van de Wouw and Ömür Arslan
Department of Mechanical Engineering
Eindhoven University of Technology
P.O. Box 513, 5600 MB Eindhoven, The Netherlands
Email: {a.isleyen, n.v.d.wouw, o.arslan}@tue.nl

1 Introduction

Due to their simplicity and high maneuverability, differential drive robots that can be modelled as a kinematic unicycle become a standard choice as a mobile robot base in logistics and service robotics. Safe and smooth robot navigation around obstacles is an essential skill for mobile robots to perform diverse tasks in complex cluttered environments. In this paper, we introduce a new conic feedback motion prediction method for bounding the close-loop motion trajectory of a unicycle robot under a standard unicycle motion control approach. We apply unicycle feedback motion prediction for safety assessment and mobile robot navigation.

2 Unicycle Motion Control

Consider a kinematic unicycle robot, with position $\mathrm{x} \in \mathbb{R}^2$ and orientation $\theta \in [-\pi, \pi)$, whose equations of motion are

$$\dot{\mathrm{x}} = v \begin{bmatrix} \cos\theta \\ \sin\theta \end{bmatrix} \quad \text{and} \quad \dot{\theta} = \omega \tag{1}$$

where $v \in \mathbb{R}$ and $\omega \in \mathbb{R}$ are the linear and angular velocity control inputs, respectively. Based on a standard unicycle control approach [1], we construct a unicycle forward motion controller, denoted by $\mathrm{u_y}(\mathrm{x}, \theta) = (v_\mathrm{y}(\mathrm{x}, \theta), \omega_\mathrm{y}(\mathrm{x}, \theta))$, that moves the unicycle robot in the forward direction towards any given goal position $\mathrm{y} \in \mathbb{R}^2$ as

$$v_\mathrm{y}(\mathrm{x}, \theta) = \kappa_v \max\left(0, \begin{bmatrix} \cos\theta \\ \sin\theta \end{bmatrix}^\mathrm{T} (\mathrm{y} - \mathrm{x})\right) \tag{2a}$$

$$\omega_\mathrm{y}(\mathrm{x}, \theta) = \kappa_\omega \operatorname{atan2}\left(\begin{bmatrix} -\sin\theta \\ \cos\theta \end{bmatrix}^\mathrm{T} (\mathrm{y} - \mathrm{x}), \begin{bmatrix} \cos\theta \\ \sin\theta \end{bmatrix}^\mathrm{T} (\mathrm{y} - \mathrm{x})\right) \tag{2b}$$

where $\kappa_v > 0$ and $\kappa_\omega > 0$ are positive scalar control gains.

3 Unicycle Motion Prediction

Since the Euclidean distance of the robot to the goal is non-increasing under the unicycle motion control in (2), the unicycle motion trajectory can be bounded by a circle.

Proposition 1 *Starting at $t = 0$ from any initial unicycle pose $(\mathrm{x}_0, \theta_0) \in \mathbb{R}^2 \times [-\pi, \pi)$, the unicycle position trajectory $\mathrm{x}(t)$ under the unicycle forward motion control $\mathrm{u_y}$ in (2) towards a given goal $\mathrm{y} \in \mathbb{R}^2$ satisfies*

$$\mathrm{x}(t) \in \mathrm{B}(\mathrm{y}, \|\mathrm{y} - \mathrm{x}_0\|) \qquad \forall t \geqslant 0, \tag{3}$$

where $\mathrm{B}(\mathrm{c}, \rho) := \{\mathrm{z} \in \mathbb{R}^2 \big| \|\mathrm{z} - \mathrm{c}\| \leqslant \rho\}$ is the Euclidean closed ball centered at $\mathrm{c} \in \mathbb{R}^2$ with radius $\rho \geqslant 0$.

Moreover, since the unicycle motion control in (2) constantly adjusts the robot orientation towards the goal, the unicycle motion can be more accurately bounded by a cone.

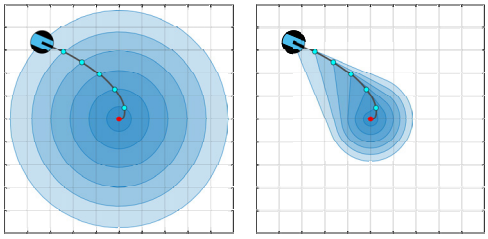

Figure 1: Unicycle feedback motion prediction that bounds the close-loop unicycle motion trajectory (black line) towards a given goal position (red point): (left) Circular motion prediction, (right) Conic motion prediction.

Proposition 2 *For any goal position $\mathrm{y} \in \mathbb{R}^2$ and any initial pose $(\mathrm{x}_0, \theta_0) \in \mathbb{R}^2 \times [-\pi, \pi)$ at $t = 0$, the unicycle position trajectory $\mathrm{x}(t)$ under the forward motion control $\mathrm{u_y}$ in (2) is bounded for all future times $t \geqslant 0$ as*

$$\mathrm{x}(t) \in \begin{cases} \mathrm{C}(\mathrm{x}, \mathrm{y}, d_\mathrm{y}(\mathrm{x}, \theta)) & \text{, if } \begin{bmatrix} \cos\theta \\ \sin\theta \end{bmatrix}^\mathrm{T} (\mathrm{y} - \mathrm{x}) \geqslant 0 \\ \mathrm{B}(\mathrm{y}, \|\mathrm{y} - \mathrm{x}\|) & \text{, otherwise} \end{cases} \tag{4}$$

where $\mathrm{C}(\mathrm{a}, \mathrm{b}, \rho) := \{\mathrm{a} + \alpha(\mathrm{z} - \mathrm{a}) \big| \alpha \in [0, 1], \mathrm{z} \in \mathrm{B}(\mathrm{b}, \rho)\}$ is a bounded cone and $d_y(\mathrm{x}, \theta) := \left| \begin{bmatrix} -\sin\theta \\ \cos\theta \end{bmatrix}^\mathrm{T} (\mathrm{y} - \mathrm{x}) \right|$ is the perpendicular alignment distance to the goal.

4 Unicycle Motion Planning

In Fig. 2, we apply unicycle feedback motion prediction for safe robot navigation using a reference governor [2]. We observe in our numerical studies that accurate unicycle motion prediction is key for safe and fast robot navigation.

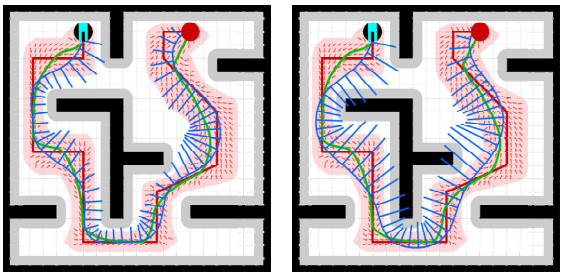

Figure 2: Safe unicycle robot navigation using (left) circular and (right) conic unicycle motion prediction and a reference governor, where the unicycle speed is indicated by blue bars and the reference path is shown in red.

References

[1] Ö. Arslan and D. E. Koditschek, "Sensor-based reactive navigation in unknown convex sphere worlds," *The International Journal of Robotics Research*, vol. 38, no. 2-3, pp. 196–223, 2019.

[2] A. İşleyen, N. van de Wouw, and Ö. Arslan, "Safe robot navigation using motion prediction and reference governor," *IEEE Robotics and Automation Letters*, vol. 7, no. 4, pp. 9715–9722, 2022.

Manipulation tasks as geometric constraint sets

P. van Dooren, H. C. Bruyninckx, M. J. G. van de Molengraft
Eindhoven University of Technology, Control Systems Technology group
p.v.dooren@tue.nl

Figure 1: A human operator uses two hands to box rice. One hand uses a non-prehensile grip to push the boxes against each other while the other hand supports the task by counteracting the pushing force

1 Introduction

We are currently examining how to describe motion plans for manipulation tasks where the task involves making deliberate contact with the environment. We will examine how to formulate these tasks and provide an example as to how one can go from the task specification to a robot motion for a robot packing boxes.

In robot manipulation the goal is to alter the poses and configurations of objects in the robots environment. Robots are becoming more able to perform human like manipulation tasks. Examples are picking fruit, handling deformable and fabric-like materials and handling heterogenous products. As a result we are now looking at applications for robotics in the agro food industry (Van Henten 2017). A requirement for a robot working with food products is situational awareness. The robot must be aware of the contacts it is making with the environment, how much force it is exerting on the environment and how much force is appropriate on that particular part of the environment. Figure 1 shows one such task.

2 Method

In our approach we aim to carefully consider which geometric relations are relevant to the current task. By carefully switching the relation to be controlled we hypothesise to be much more robust against the geometric uncertainty inherent in manipulation tasks.
We furthermore acknowledge that not all tasks require the same accuracy, therefore rather than specify one setpoint value that the relation must have we will aim to specify constraints on the geometric relations. This allows us to verify if a task is complete and it allows us to compose multiple constraints originating from different subtasks.
We will also utilise contacts as a geometric relation which gives a high degree of certainty. In many tasks the goal will be to make contact between two pieces of the environment.

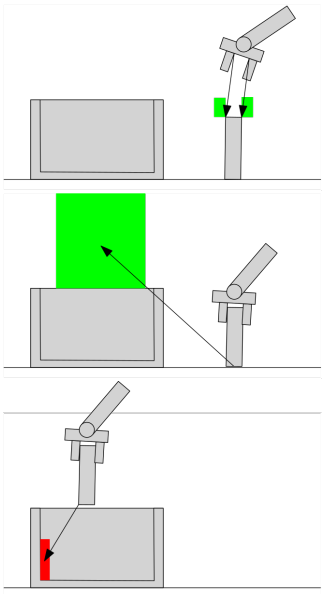

Figure 2: Relative positions used in three subtasks of packaging a box. Arrows indicate the relation of relevance. Green area indicates a region of acceptable positions for the origin of the arrows. A red area indicates a desired contact situation.

3 conclusion

We propose a method to define the goals of a manipulation task as a set of relative positions and contact situations. In the coming time we will test this hypothesis on the task of packaging.

References

Van Henten, E.J. (2017). "Project proposal: Cognitive Robots for Flexible Agro Food Technology (FlexCRAFT)". In: p. 5600.

A multi-agent robotic system for bricklaying

Zemerart Asani[1, 2], Michele Ambrosino[2], Bram Vanderborght[1], Emanuele Garone[2]
Brubotics, Vrije Universiteit Brussel, and IMEC, Belgium[1]
SAAS, Université Libre de Bruxelles, Belgium[2]
Emails: zemerart.asani@vub.be; michele.ambrosino@ulb.be; bram.vanderborght@vub.be; egarone@ulb.be

1 Introduction

Multi-agent cooperative control of two heterogenous construction agents for heavy construction tasks is the focus of this study. These two agents have complementary capabilities. The rigid robotic arm is used to achieve the needed precision during the fine placement, and the hoisting mechanism to support the majority of the block's weight (1).

The dynamic model of the multi-agent robotic system can be written in a compact form:

$$\begin{cases} M(q)\ddot{q}+C(q,\dot{q})\dot{q}+g(q)=u+A^T(q)\lambda \\ h(q)=0 \end{cases}, \qquad (1)$$

where, $A(q)=\frac{\partial h(q)}{\partial q}\in\mathbb{R}^{6\times 11}$ represents the Jacobian of the constraints, $u=\left[u_r^T,\,0,\,0,\,u_{cp},\,0,\,0,\,0\right]^T\in\mathbb{R}^{11}$ is the control input vector ($u_r\in\mathbb{R}^5$ are the robot control inputs and $u_{cp}\in\mathbb{R}^1$ is the lifting mechanism control input), $\lambda\in\mathbb{R}^6$ is the vector of Lagrange multipliers, and the matrices $M(q)\in\mathbb{R}^{11\times 11}$, $C(q,\dot{q})\in\mathbb{R}^{11\times 11}$, and $g(q)\in\mathbb{R}^{11}$ represent the joint-space inertia matrix, centripetal-Coriolis matrix, and gravitational vector, respectively.

In this work, we propose a control strategy that ensures: (i) correct cooperation between the robot and the lifting mechanism in order to move the brick to the desired position; and (ii) safe cooperation between the two robotic systems, such that the robot is never overloaded.

2 Application and results

Based on the model, we designed a controller. The stability of this control scheme is proved using the LaSalle's invariance principle.

We implemented this controller to an experimental setup consisting of an in-scale lifting mechanism and a Kuka YouBot (a mobile manipulator). In the experiment, we used a brick weighing **1.0 kg**, which exceeded the maximum payload of **0.5 kg** that can be handled by the Kuka YouBot by itself. Through this experiment, we can show that based on an offline trajectory evaluation with the proposed control scheme, the multi-robot system is able to safely and precisely place the blocks.

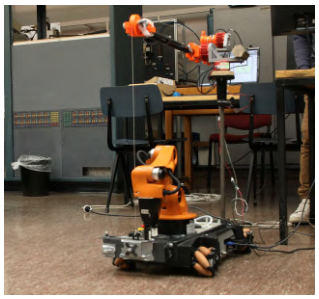

Figure 1: The multi-robot system.

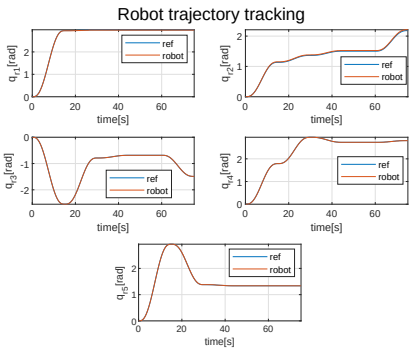

Figure 2: Robot joint positions.

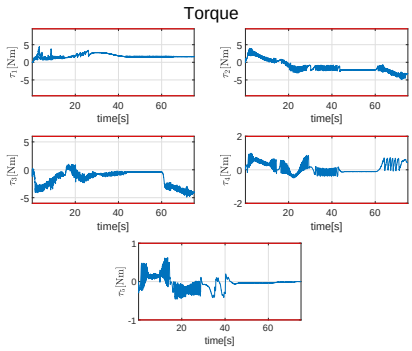

Figure 3: Robot joint torques.

References

[1] Ambrosino, M., Delens, P., and Garone, E. (2021a). Control of a multirobot bricklaying system. Advanced Control for Applications, 3(4), e90.

Addition of absolute localization measurements to SLAM

Kurt Geebelen, Ferran Gebelli and Ellen van Nunen
Core Lab MotionS, Flanders Make VZW
Gaston Geenslaan 8, 3001 Leuven, Belgium
Email: kurt.geebelen@flandersmake.be

1 Introduction

Autonomous vehicles working in industrial environments require accurate and robust localization for their navigation. However, industrial environments can present specific challenges for localization, including complex environments, dynamic objects and changing environments, and high installation costs for external localization systems. Existing solutions for localization can be split into two categories: absolute (e.g. GNSS, ultra-wideband, visual markers) and relative localization methods (e.g. camera- or lidar-based SLAM). By combining both types of localization, it is possible to increase the robustness and reliability of localization while also reducing installation costs, resulting in a high availability and high accuracy localization solution that requires minimal infrastructural changes.

2 Approach

Absolute localization measurements, such as GNSS, ultra-wideband and visual markers, provide precise, absolute position and/or orientation information that can be used to correct errors and drift in SLAM-based localization methods, even if the absolute measurements do not cover the complete environment.

By integrating absolute localization measurements into a SLAM-based localization framework, we show it is possible to significantly improve the robustness and accuracy of the localization system, particularly in large environments or in the presence of dynamic objects or changing conditions.

To realize this, we extended RTAB-Map[1] to support the use of absolute measurements. RTAB-Map is structured as a graph-based SLAM algorithm, in which the nodes of the graph represent the robot's poses at different points in time, and the edges represent the relative motion between poses. By default, RTAB-Map only supports relative pose measurements, e.g. coming from visual odometry or loop-closure detections. We extended RTAB-Map to support generic measurements, such as range measurements from an ultra-wideband system and the corner measurements from a visual marker detection.

3 Results

Figure 1 shows a mapping of the ground floor of the Flanders Make building in Leuven. In the environment, five visual markers are placed and their absolute position measured. Four of these markers are located in the area in the bottom right, while one of them is located about halfway in the corridor. The left figure shows the result of the standard RTAB-Map in which the visual markers are not used. In the figure on the right, we enable our additions for visual markers with a known absolute pose. Quantitatively, it is clear that the overall drift in the map building is significantly reduced. During the presentation, we show similar results for the addition of ultra-wideband and GNSS measurements.

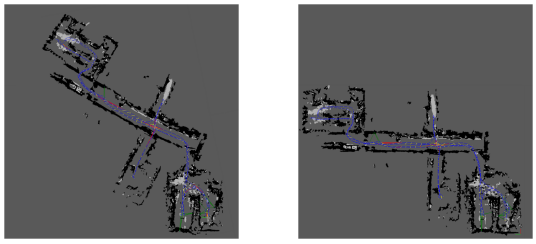

(a) Map without absolute localization information.

(b) Map with absolute localization information.

Figure 1: Comparison of map built with/without absolute localization information.

4 Conclusion

In conclusion, the combination of absolute localization measurements with SLAM-based methods can significantly improve the accuracy and robustness of localization in industrial environments. By integrating GNSS, ultra-wideband, and visual marker measurements into a SLAM framework, we were able to reduce drift and error accumulation, resulting in a high-quality localization solution that is resistant to the challenges commonly encountered in industrial environments. Our approach, which extends the RTAB-Map algorithm to support the use of absolute measurements, provides a flexible and effective method for integrating multiple types of localization into a single framework. Our results demonstrate the potential of this approach to significantly improve the performance of autonomous vehicles in a wide range of industrial applications.

References

[1] M. Labbé and F. Michaud,"Long-term online multi-session graph-based SPLAM with memory management," in Autonomous Robots, vol. 42, no. 6, pp. 1133-1150, 2018. (Springer)

Initializing UWB anchors based on visual SLAM odometry

Miel Van der Wilt, Kurt Geebelen and Ellen van Nunen
Core Lab MotionS, Flanders Make VZW
Gaston Geenslaan 8, 3001 Leuven, Belgium
Email: miel.vanderwilt@flandersmake.be

1 Introduction

Accurate localization is essential for navigation of autonomous vehicles working in industrial environments. Two main types of localization solutions exist: absolute (e.g. GNS, ultra-wideband (UWB), visual markers) and relative (e.g. camera- or lidar-based SLAM). Combining these two methods by adding range-only constraints (e.g. UWB) to SLAM can help mitigate drift errors due to noisy odometry and increase robustness. Here, we focus on the range-only constraint coming from an UWB system. In this presentation, we present a method to initialize the position of UWB anchors for use in a SLAM-based localization framework.

2 Approach

The SLAM-based localization framework we use is RTAB-Map [1], a graph-based SLAM algorithm. Here each node of the graph represents a pose of the robot or a landmark such as an UWB anchor. Each edge represents a measurement between two nodes, this can be an odometry measurement between robot poses or a range measurement between an UWB anchor and a robot pose.

Traditionally in an UWB systems the anchors are carefully placed around the area where localization info is needed. The UWB measurements can then be added to the graph as 3D absolute localization measurements or as 1D range-constraints. However, this assumes that the coordinates of all the anchors are known in advance. To add the UWB measurements to the graph when there is no prior information on the anchors, the anchors need to be initialized before they can be added to the graph.

Each range measurement constrains the position of the anchor to a sphere around the current robot position. In theory, having 4 such measurements would result in a unique position for the anchor. However, in practice, multiple solutions may exist for a given set of more than four ranges. Two cases of ambiguous situations are given below:

- Collinearity: A set of poses on a straight line ranging to a single anchor will have a solution space on a circle around the straight line of the poses
- Coplanarity: A set of poses which lie in the same plane ranging to a single anchor will have at least two solutions. One above the plane and one mirrored solution below the plane.

In practice measurement noise also impacts the solution. In the case where the robot drives on a perfect line, in practice it will not be a perfect line due to the measurement noise. In this case, localization will be very sensitive to the noise on both the robot position and on the range measurements. Including range measurements of an ambiguous case to the graph makes the problem ill-conditioned which can cause instability of the solver and divergence of the solution resulting in poor localization performance. To mitigate these effects first an initial guess of an anchor is made using MDS (multidimensional scaling), then the PDOP (position dilution of precision) of this initial guess is checked before accepting the initial guess. Once an anchor passes the initialization phase, it is added to the graph along with all its range measurements. This additional information allows the optimization of the pose estimate to become more accurate.

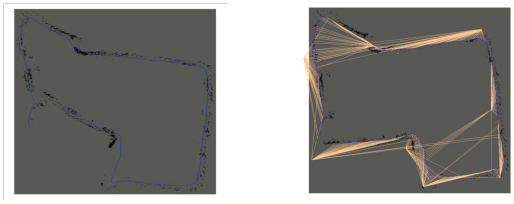

(a) Map without ultrawideband measurements.

(b) Map with ultrawideband measurements.

Figure 1: Comparison of map built with/without ultrawideband measurements.

3 Results

Figure 1 shows a mapping of the parking lot of the Flanders Make building in Leuven. Eight UWB anchors are placed around the environment. The left figure shows the result of the standard RTAB-Map in which the UWB measurements are not used. In the figure on the right, we enable our additions for UWB measurements without priors on the anchor coordinates. From these figures, it is clear that the overall drift in the map building is reduced.

4 Conclusion

In conclusion, after carefully initializing the UWB anchors the UWB measurements can be added to the problem. Using the UWB measurements without priors on the anchors reduces the drift caused by the odometry significantly.

References

[1] M. Labbé and F. Michaud,"Long-term online multi-session graph-based SPLAM with memory management," in Autonomous Robots, vol. 42, no. 6, pp. 1133-1150, 2018. (Springer)

Acknowledgements: This work has been carried out within the framework of Flanders Make's ICON project 'Marloc' (Mixed Absolute and Relative Localization), funded by the agency Flanders Innovation & Entrepreneurship (VLAIO) and Flanders Make. Flanders Make is the Flemish strategic research centre for the manufacturing industry

Obstacle Avoidance of Soft Robots using Virtual Force Field and Null-Space Projection

Mahboubeh Keyvanara
Dynamics and Control Group
Mechanical Engineering Department
Eindhoven University of Technology
The Netherlands
m.keyvanara@tue.nl

Irene Kuling
Dynamics and Control Group
Mechanical Engineering Department
Eindhoven University of Technology
The Netherlands
i.a.kuling@tue.nl

1 Abstract

Tasks such as moving, packing and transporting products are examples in industry that require automation. Redundant robots are some of the best manipulators that can help with this type of automation. For these tasks, accurate trajectory tracking control along with obstacle avoidance is a critical requirement. Extra degrees of freedom (DoF) of redundant manipulators, such as soft robots, help in achieving secondary task objectives such as obstacle avoidance [1].
Inspired by biological systems, soft robotics is a branch of robotics in which use of soft materials enhances robot's dexterity and enables a wide variety of motion primitives. Animals' bodies are comprised of soft materials, giving them the ability to adapt to a variety of environments. Hence, the ability of these robots to bend at any point of their body gives them the potential to perform tasks that are not feasible with their rigid counterparts. Due to their continuum change of shape and high degrees of freedom (DoF), these robots are usually known to be redundant. These robots belong to the domain of continuum mechanics and therefore their dynamics is formulated as Partial Differential Equations (PDE). Using model reduction techniques, newly developed reduced-order ODE models can be used for model-based control. One of the best known methods of spatial reduction techniques is the so called Peicewise Constant Curvature (PCC) model, where the robot is divided into smaller parts, each part with constant curvature. Using this formulation, through model-based control, the robot can be controlled to perform different tasks.
In this research, we investigate the problem of trajectory tracking in task space of a redundant soft robot with the secondary goal of obstacle avoidance. Tracking control and obstacle avoidance are known to be challenging problems individually [2], combining these two into one single framework along side of complexity of soft robots will become an even more complicated technical challenge. For this reason, a multi-segment soft robot is chosen and modeled using the PCC modeling and a task space controller is designed to control the position of the end-effector on the desired trajectory. As the robot is chosen to have redundancy, the null-space of the Jacobian of the end-effector is chosen for tasks with second priority, here the obstacle avoidance. To design the obstacle avoidance algorithm, virtual resistant forces and damping forces are inserted from the obstacles to the body of the robot with the aim of preventing the body of the robot getting close to obstacle. They are exerted from different points on the obstacle that are closest to the body, and are distributed on different points on the body of the robot to create a smooth force field (Fig.1). Multiple scenarios such as constant obstacles and also dynamic (moving) obstacles, both in 2D and 3D, are simulated using this algorithm.

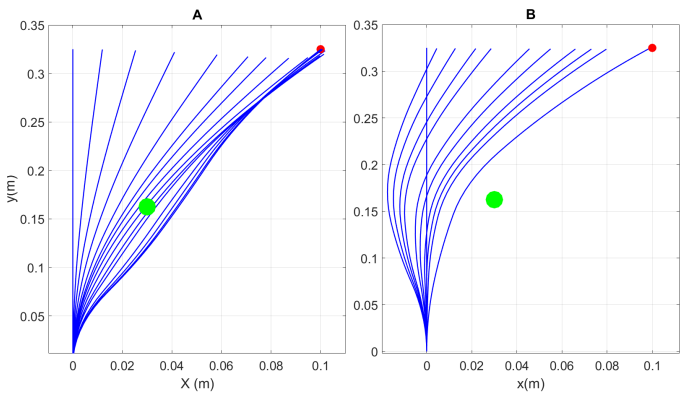

Figure 1: Obstacle avoidance algorithm for a 5 segment soft robot. (A) the robot does not have any obstacle and it is controlled only using a task space control. (B) The obstacle avoidance algorithm is added as the second task to the controller of the robot. The red dot is the desired end point and the green dot is the obstacle. Both simulations have an initial condition of zero state (vertical line).

References

[1] L. Jin, S. Li, X. Luo, Y. Li, and B. Qin, "Neural dynamics for cooperative control of redundant robot manipulators," IEEE Trans. Ind. Informat., vol. 14, no. 9, pp. 3812–3821, Sep. 2018.

[2] Z. Zhang, S. Chen, X. Zhu, and Z. Yan, "Two hybrid end-effector posture-maintaining and obstacle-limits avoidance schemes for redundant robot manipulators," IEEE Trans. Ind. Informat., to be published, doi: 10.1109/TII.2019.2922694.

Adaptive Nonsingular Terminal Sliding Mode Control for Unmanned Surface Vehicles

Alejandro Gonzalez-Garcia[1,2*] and Herman Castañeda[2]
[1]MECO Research Team, Department of Mechanical Engineering, KU Leuven, Belgium.
[1]Flanders Make@KU Leuven, Belgium
[2]Tecnologico de Monterrey, School of Science and Engineering, Monterrey, Mexico.
*Email: alex.gonzalezgarcia@kuleuven.be

1 Introduction

Since Unmanned Surface Vehicles (USVs) are susceptible to uncertainty and external disturbances, robust control methods are desired to counteract such effects. Sliding mode control is robust, but the common chattering effect imposes a challenge for practical implementation. In consequence, adaptive sliding mode (ASM) has been proposed to attenuate chattering and keep the robust performance. Then, this work proposes leveraging the chattering attenuation from adaptive sliding mode, combined with the finite-time convergence of terminal sliding surfaces. Thus, the proposed adaptive nonsingular sliding mode (ANTSM) controller achieves practical finite-time convergence, which results in accurate and robust trajectory tracking for USVs.

2 Methodology

First, consider a second-order nonlinear uncertain system:

$$\dot{x}_1 = x_2;\ \dot{x}_2 = f(x_1,x_2) + g(x_1,x_2)u - \delta \tag{1}$$

where x_1, x_2 are the states, $f(x_1,x_2)$ and $g(x_1,x_2)$ are continuous functions, u is the control input, and δ contains the disturbances and uncertainty. δ is assumed to be continuous, and bounded. Then, the error variables are established, $e_1 = x_{1d} - x_1$; $e_2 = x_{2d} - x_2$, where x_{1d}, x_{2d} are the reference states. Now, a sliding variable s following a nonsingular terminal sliding mode strategy is introduced, $s = e_1 + \beta\,\mathrm{sign}(e_2)|e_2|^{\gamma}$. Now, the control u is designed as:

$$u = \frac{1}{g(x_1,x_2)}[\dot{x}_{2d} - f(x_1,x_2) + \frac{1}{\beta\gamma}\mathrm{sign}(e_2)|e_2|^{2-\gamma} - u_a] \tag{2}$$

where u_a is an auxiliary control, taken by the adaptive sliding mode strategy:

$$u_a = -K_1|s|^{1/2}\mathrm{sign}(s) - K_2 s \tag{3}$$

with the following adaptive gain dynamics:

$$\dot{K}_1 = \begin{cases} K_3\mathrm{sign}(|s| - \mu), \text{ if } K_1 > K_{\min} \\ K_{\min}, \text{ if } K_1 \leq K_{min} \end{cases} \tag{4}$$

where $K_{\min}$ maintains a non-zero adaptive gain, K_3 regulates the adaptation rate, and μ detects the loss of the real sliding mode dynamics. In this sense, when the sliding variable s is larger than the threshold μ, the adaptive gain K_1 increases to reject disturbances and uncertainty. In contrast, if s is lower than μ, K_1 decreases to reduce control effort and chattering amplitude.

3 Results

By implementing the proposed controller into the hand-position-based model from [1], using the VTec S-III parameters [2], the simulation results are shown in Fig. 1. Here, an improved tracking accuracy from the proposed ANTSM is depicted. Furthermore, the ANTSM achieved a mean square error of 0.002 m, in contrast to the larger 0.0095 using the algorithm from [1]. Likewise, the control effort was lower, achieving 1604.8 N in surge and 154.2 Nm in yaw, lower than the control effort of [1] of 2145.7 N and 180 Nm.

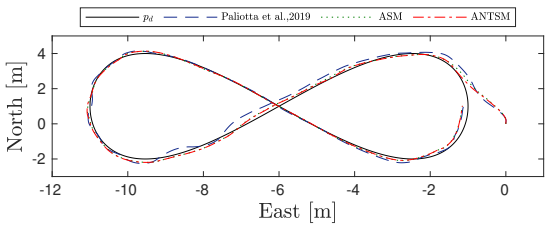

Figure 1: Reference versus USV trajectories.

4 Acknowledgement

This work was done at the Robotics National Laboratory of the ITESM-CONACyT, and we acknowledge the funding within the framework of Flanders Make's SBO project ARENA (Agile & Reliable Navigation).

References

[1] C. Paliotta et al., "Trajectory Tracking and Path Following for Underactuated Marine Vehicles," IEEE Transactions on Control Systems Technology, 2019.

[2] A. Gonzalez-Garcia and Herman Castañeda, "Guidance and Control Based on Adaptive Sliding Mode Strategy for a USV Subject to Uncertainties," IEEE Journal of Oceanic Engineering, 2021.

Higher-Order Sinusoidal-Input Describing Function Analysis for MIMO Reset Systems

Luke F. van Eijk[1,2] l.f.vaneijk@tudelft.nl
Dragan Kostić[2] dragan.kostic@asmpt.com
S. Hassan HosseinNia[1] s.h.hosseinniakani@tudelft.nl

[1] *Department of Precision and Microsystems Engineering, Delft University of Technology, Delft, The Netherlands*
[2] *Center of Competency, ASMPT, Beuningen, The Netherlands*

1 Introduction

Ever-growing demands on speed and accuracy of motion systems, makes it increasingly difficult to achieve desired performance specifications using linear time-invariant (LTI) feedback control. LTI control is subject to inherent limitations due to the well-known waterbed effect. Reset control is a nonlinear control technique that can overcome these limitations, and is considered as a potential alternative due to its many similarities with LTI control. Essentially, a reset controller is an LTI controller which resets (part of) its states when its input is equal to zero. However, this means that the reset controller's output is non-sinusoidal for a sinusoidal input, unlike an LTI controller. The controller output also contains higher-order harmonics of the sinusoidal input – caused by the nonlinear nature of the reset controller – where each harmonic has its own magnitude- and phase-characteristics, the so-called higher-order sinusoidal-input describing functions (HOSIDFs). These frequency-domain properties have been derived for reset controllers in [1], an example of which is depicted in Fig. 1 for a resetting integrator.

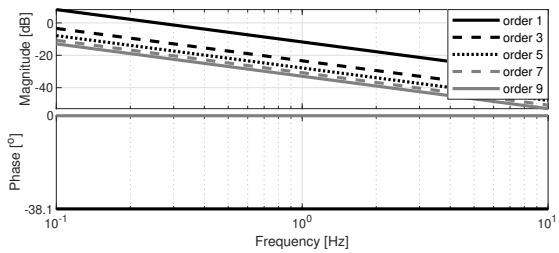

Figure 1: HOSIDFs of a reset integrator.

The HOSIDF-based open-loop frequency-domain properties of single-input single-output (SISO) reset control systems have also been derived in [1], which can be computed based on a (measured) frequency-response function (FRF) of the plant. However, these frequency-domain properties are not yet investigated for reset control systems with multiple-input multiple-output (MIMO) LTI plants.

2 Main result

In this work we extend the open-loop frequency-domain properties of SISO reset control systems to the case with MIMO LTI plants, as depicted in Fig. 2. We prove that, given a combination of sinusoidal inputs $e(t) = [\sin(\omega_1 t), ..., \sin(\omega_M t)]^T$, the plant outputs converge to a unique solution

$$y_k(t) = \sum_{i=1}^{M} \sum_{n=1}^{\infty} |L_{k,i}^n(\omega_i)| \sin\left(n\omega_i t + \angle L_{k,i}^n(\omega_i)\right), \qquad (1)$$

where M is a number of plant in-/outputs, $k \in [1, M]$, n is the number of the higher-order harmonic, and the open-loop frequency-domain properties for the MIMO reset control system are given by $L^n(\omega) = P(nj\omega) \cdot \mathrm{diag}(H_1^n(\omega), ..., H_M^n(\omega))$, where H_k^n is the nth-order SIDF corresponding to reset element R_k, as derived in [1]. This means that the frequency-domain properties can be visualized using an $M \times M$ grid of characteristics similar to Fig. 1.

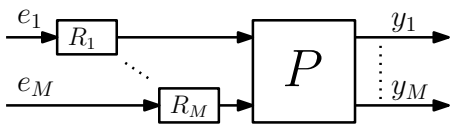

Figure 2: Open-loop system with a MIMO LTI plant and multi-loop SISO reset controllers.

3 Conclusion

In this work we have proven that the outputs of MIMO LTI plants, controlled by multi-loop SISO reset controllers, converge to a unique solution when subject to sinusoidal inputs. This property still holds when sinusoidal signals are simultaneously applied to multiple inputs. The MIMO open-loop HOSIDFs provide a thorough, yet still intuitive, way to design reset controllers for MIMO LTI plants.

References

[1] N. Saikumar, K. Heinen, and S. H. HosseinNia, "Loop-shaping for reset control systems: A higher-order sinusoidal-input describing functions approach". In: *Control Engineering Practice* 111 (2021), p. 204808.

Inversion-based data-driven output feedback control using Gaussian process regression

Hamin Chang
Bernoulli Institute for Mathematics, CS and AI
University of Groningen
Nijenborgh 9, 9747 AG Groningen
The Netherlands
Email: h.chang@rug.nl

1 Introduction

We propose data-driven output feedback controller for a class of nonlinear systems based on the inverse dynamics model identified by Gaussian process regression (GPR). Since our approach is based on input/output inversion, we assume that the system is of minimum phase and has relative degree one.

2 Problem Formulation

Consider a single-input single-output (SISO) nonlinear discrete-time control-affine system with relative degree one in Byrnes-Isidori normal form:

$$y(t+1) = f(z(t), y(t)) + g(z(t), y(t))u(t) \tag{1a}$$
$$z(t+1) = h(z(t), y(t)) \tag{1b}$$

where $u(t) \in \mathbb{R}$ is the input, $z(t) \in \mathbb{R}^{n-1}$ is the state of the zero dynamics, and $y(t) \in \mathbb{R}$ is the output. It is assumed that the functions $f(\cdot,\cdot)$, $g(\cdot,\cdot)$, and $h(\cdot,\cdot)$ are unknown and only the input/output of the system are available as measurements. In addition, the following assumption is given.

Assumption 1 *The system* (1) *satisfies the followings:*

(a) The system has global relative degree one, or equivalently, $g(z,y) \neq 0$ for all $(z,y) \in \mathbb{R}^n$. Also, the system dimension n and the global relative degree one are known.

(b) The internal dynamics (1b) *is input-to-state stable with the input being y.*

(c) There exists a smooth function $\theta : \mathbb{R}^{2(n-1)} \times \mathbb{R} \to \mathbb{R}^{n-1}$, such that the state $z(t)$ of (1) *is given by*

$$z(t) = \theta(\zeta_0(t), y(t)),$$

where $\zeta_0(t) := [y_{[t-n+1,t-1]}; u_{[t-n+1,t-1]}] \in \mathbb{R}^{2(n-1)}$, for all time step t.

3 Design of Output Feedback Controller

Let us consider a stable reference model given by

$$y_r(t+1) = f_r(y_r(t)) \quad \in \mathbb{R} \tag{2}$$

which satisfies the additional assumption that $y_r(t+1) = f_r(y_r(t)) + \eta(t)$ is input-to-state stable when η is viewed as an input. In order to make the controlled system (1) become the reference model (2), the controller should be

$$u(t) = \frac{f_r(y(t)) - f(z(t), y(t))}{g(z(t), y(t))}. \tag{3}$$

Let us define the vector $\zeta_1(t) := [\zeta_0(t); y(t)] \in \mathbb{R}^{2n-1}$ which is composed of an arbitrary input/output trajectory of the system (1).

Define $c : \mathbb{R}^{2n} \to \mathbb{R}$ as

$$c([\zeta_1(t); s]) := \frac{s - f(\theta(\zeta_0(t), y(t)), y(t))}{g(\theta(\zeta_0(t), y(t)), y(t))}.$$

Then, the ideal control (3) is generated by $u(t) = c([\zeta_1(t); f_r(y(t))])$. We finally design the output feedback controller by applying GPR to identify the function $c(\cdot)$ itself. This idea is feasible by treating $[\zeta_1(t); y(t+1)]$ as input data to the function c, and $u(t)$ as output data since $u(t) = c([\zeta_1(t); y(t+1)])$ from (1a). For later use, we define $\mathscr{C}$ as the set of all possible $[\zeta_1(t); f_r(y(t))]$ and denote $\hat{c}(\cdot)$ as the identification result of the function $c(\cdot)$ by GPR.

Theorem 1 *[1] Under Assumption 1, there exists a class-$\mathscr{K}$ function γ such that, if $\hat{c}$ satisfies*

$$|\hat{c}([\zeta_1; s]) - c([\zeta_1; s])| < \delta, \quad \forall [\zeta_1; s] \in \mathscr{C} \tag{4}$$

for a given $\delta > 0$, then, the closed-loop system (1) *with the controller $u(t) = \hat{c}([\zeta_1(t); f_r(y(t))])$ guarantees*

$$\limsup_{t\to\infty} \|[y(t); z(t)]\| < \gamma(\delta).$$

References

[1] H. Kim, H. Chang, and H. Shim, "Model reference Gaussian process regression: data-driven output feedback controller," 2022. http://arxiv.org/abs/1906.01404

Feedforward Tuning with Input Nonlinearities: Application to Magnetic Saturation in Wirebonders[1]

Maurice Poot[2,*], Jim Portegies[3], Tom Oomen[2,4]

[2]Control Systems Technology Group, Dept. of Mechanical Engineering, Eindhoven University of Technology, The Netherlands

[3]CASA, Dept. of Mathematics and Computer Science, Eindhoven University of Technology, The Netherlands

[4]Delft Center for Systems and Control, Delft University of Technology, The Netherlands

*Email: m.m.poot@tue.nl

1 Background

The increasing demands on throughput and accuracy of semiconductor manufacturing equipment necessitates accurate feedforward motion control that includes compensation of input nonlinearities. In [1], iterative learning control with polynomial basis functions (ILCBF) is introduced to enable extrapolation of the motion tasks. To achieve high tracking accuracy and task flexibility for nonlinear systems, extensions are necessary that compensate input nonlinearities, e.g., magnetic saturation in linear actuators [2].

2 Problem formulation

The aim of this research is to develop a data-driven feedforward tuning approach consisting of a Wiener feedforward, i.e., linear parameterization $F(\theta)$ with an output nonlinearity $h(\cdot,\phi)$, see Fig. 1, for Hammerstein systems.

3 Approach

The developed approach exploits norm-optimal iterative learning control (NOILC) to learn a feedforward signal from data that minimizes the error and utilizes a control-relevant cost function to learn θ,ϕ of the Wiener feedforward [3].

4 Results

Experimental results, see Fig. 2, on a wirebonder subject to magnetic saturation show a reduction in tracking error using the developed approach compared to the linear approach. Moreover, for motion tasks with varying maximum accelerations, the mass parameter is significantly more consistent in the developed approach, indicating task flexibility.

5 Conclusion and outlook

The developed Wiener feedforward approach achieves high tracking accuracy and task flexibility for Hammerstein systems. Ongoing research focuses on online learning in an ILC setting, extensions to non-parametric models for h, and analysis of position dependency of the magnetic saturation.

[1]This work is supported by ASM Pacific Technology. The authors thank Jilles van Hulst, Kelvin Kai Wa Yan, and Dragan Kostić for their contributions to this research.

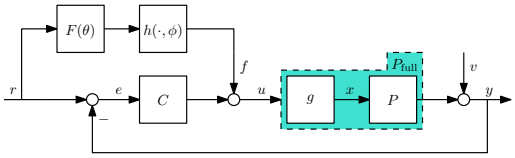

Figure 1: Proposed control scheme with Wiener feedforward $f = h(F(\theta)r,\phi)$.

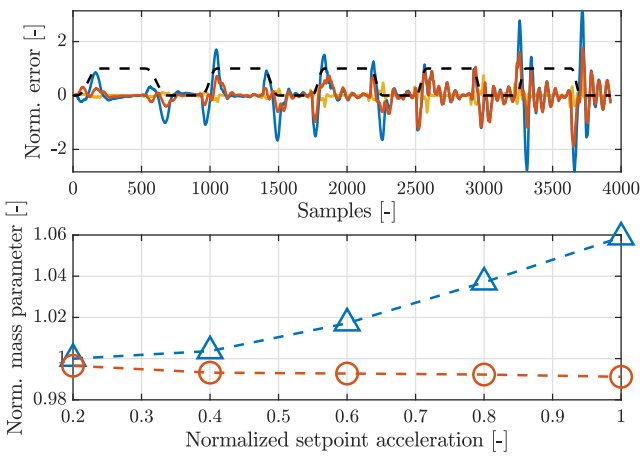

Figure 2: Top: error signals of linear (—), the developed (—), and NOILC (—) approach. Bottom: mass per setpoint acceleration of linear (-△-) and the developed (-⊖-) approach.

References

[1] J. van de Wijdeven and O. Bosgra, "Using basis functions in iterative learning control: analysis and design theory," *Int. J. Control*, vol. 83, no. 4, pp. 661–675, apr 2010.

[2] H. Polinder, "Modelling a linear PM motor including magnetic saturation," in *Int. Conf. Power Electron. Mach. Drives*, vol. 2002, no. 487. IEE, 2002, pp. 632–637.

[3] J. van Hulst, M. Poot, D. Kostić, K. W. Yan, J. Portegies, and T. Oomen, "Feedforward Control in the Presence of Input Nonlinearities: A Learning-based Approach," in *Model. Estim. Control Conf.*, Jersey City, New Jersey, 2022.

Frequency-domain Analysis Method for Reset Control Systems

Xinxin Zhang
Email: X.Zhang-15@tudelft.nl

S. Hassan HosseinNia
Email: S.H.HosseinNiaKani@tudelft.nl

Precision and Microsystems Engineering, Delft University of Technology, Mekelweg 2, 2628 CD, NL

1 Introduction & Problem Formulation

Reset control systems (RCSs) have demonstrated superior performance in the precision motion field compared to traditional linear control systems [1]. For instance, Fig. 1 presents a step response comparison of a DC (Direct Current) motor controlled by an RCS "PI+CI" (Proportional Integrator + Clegg Integrator) [2] and an integrator. The results illustrate the advantages of RCSs.

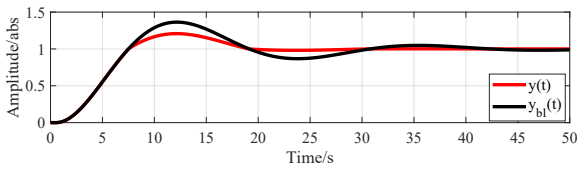

Figure 1: Step responses of a DC motor with two controllers: (a) a "PI+CI" $y(t)$ (red) and (b) an integrator $y_{bl}(t)$ (black).

In practice, the frequency-domain analysis technique is effective for quantifying the performance of control systems. The nonlinearity of RCSs makes it difficult to analyse them in closed-loop. For RCSs to be widely applicable in industries, a precise frequency-domain analysis method is needed.

2 New Analysis Model for Reset Control Systems

As shown in Fig. 2, the output $u_{ci}(t)$ of an open-loop CI with the input signal $e(t) = \sin(\omega t)$ is the summation of its base-linear output $u_i(t)$ and a square wave defined as $q_i(t)$.

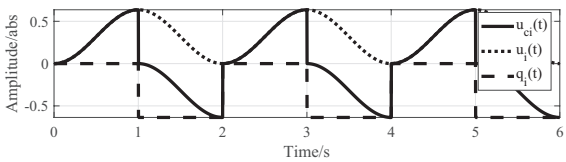

Figure 2: $u_{ci}(t)$ (solid line), $u_i(t)$ (dotted line), and $q_i(t)$ (dashed line) of CI in open-loop when $\omega = \pi$ rad/s and $\gamma = 0$.

Figure 3 (a) shows the block diagram of an RCS. Based on the CI model in Fig. 2, we develop a new block diagram for analysing RCSs with two reset instants per period, as shown in Fig. 3 (b).

In this new model, $u(t)$ is given by $u(t) = u_{bl}(t) + u_{nl}(t)$, where $u_{bl}(t)$ is the base-linear control input signal; and

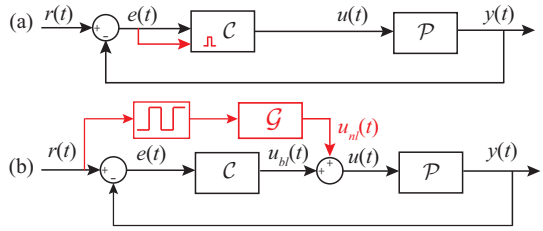

Figure 3: The block diagrams of the RCS, where the block C represents the reset controller including the resetting action, and P is the plant. $r(t)$ is the reference input signal, $e(t)$, $u(t)$, and $y(t)$ are the corresponding error, control intput, and output signals.

$u_{nl}(t)$ is a nonlinear signal generated by $r(t)$ going through a "Pulse Generator" and a transfer function $\mathscr{G}$.

3 Illustrative Example

The prediction error (PE) is defined as the difference between the model-predicted output and the simulated output. Figure 4 compares the PE of the new method with those of previous methods in an RCS. The new model has

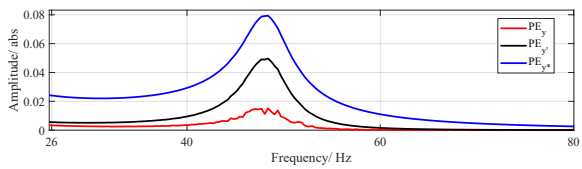

Figure 4: Prediction errors (PE) of $y(t)$ in an RCS, where PE_y (red) is from the new method, and PE'_y (black) and PE_y* (blue) are from the previous methods.

smaller prediction errors, thus providing us with a more precise frequency-domain analysis tool for RCSs. It may facilitate the design and implementation of RCSs in the industry.

References

[1] Ruud Beerens, Andrea Bisoffi, Luca Zaccarian, WPMH Heemels, Henk Nijmeijer, and Nathan van de Wouw. Reset integral control for improved settling of PID-based motion systems with friction. *Automatica*, 107:483–492, 2019.

[2] Alfonso Baños and Angel Vidal. Definition and tuning of a PI+ CI reset controller. In *2007 european control conference (ECC)*, pages 4792–4798. IEEE, 2007.

Extended Augmented Error Method for Designing an Output Feedback Adaptive Controller

S.S. Sheikh Aboumasoudi
University of Twente
BME and MS3 Department
Email: s.s.sheikhaboumasoudi@utwente.nl

Dr. Hakan Köroğlu
University of Twente
MS3 Department
Email: h.koroglu@utwente.nl

Prof. Dr. Ir. H. van der Kooij
University of Twente
BME Department
Email: h.vanderkooij@utwente.nl

Dr. Ir. Arvid Q.L. Keemink
University of Twente
BME Department
Email: a.q.l.keemink@utwente.nl

1 Introduction

Model Reference Adaptive Control (MRAC) is one of the most frequently used algorithms in adaptive control theory [1]. The *augmented error method* [2] is a technique for designing an Output Feedback MRAC, which is used when all states of the system are not measurable directly. In this work, we extend this method to relax its conditions and widen the choices of designs.

2 The Extended Augmented Error Method

In the existing method (Fig. 1), the regressor vector (ρ) is formed by combining the reference with filtered versions of the plant input (u) and the output (y). The input to the plant is generated as the inner product of this regressor vector with adapted controller parameters. Both the control input and the regressor vector are then processed further to generate a so-called augmented error (ε).

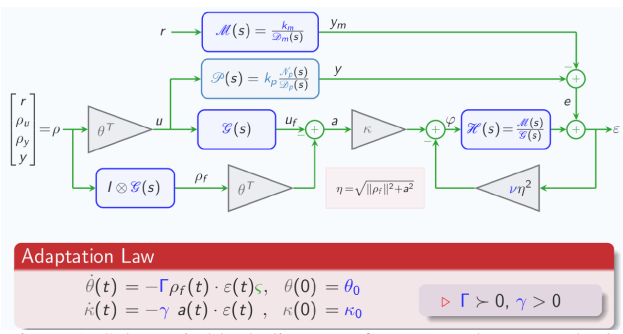

Figure 1: Schematic block diagram of augmented error method.

At the final stage of augmented error generation, an LTI filter $\mathscr{H}$ is used together with a nonlinear feedback. In the existing method, $\mathscr{H}$ is required to be strictly positive real, and strictly proper. In this work, we show that $\mathscr{H}$ can be chosen to be biproper as well, provided that the positive realness property is maintained. This also makes it possible to choose the numerator of $\mathscr{H}$ (and thus $\mathscr{G}$) based on the well-known positive realness LMI (with known A, B and to be determined C, D):

$$\begin{bmatrix} A^TP+PA & PB-C^T \\ B^TP-C & -D-D^T \end{bmatrix} \preceq 0, \quad P \succ 0.$$

Another contribution of this work is that φ can be generated more generally as

$$\varphi = \nu\eta^{\alpha+1}|\varepsilon|^{\alpha}\mathrm{sign}(\varepsilon), \quad \alpha > 0.$$

Note that the existing method is recovered with $\alpha = 1$.

3 Simulation results

Simulation results of the modified controller on a linear mass-spring-damper system show that the error convergence to zero can be improved with the proposed modifications. Results are shown in Fig. 2.

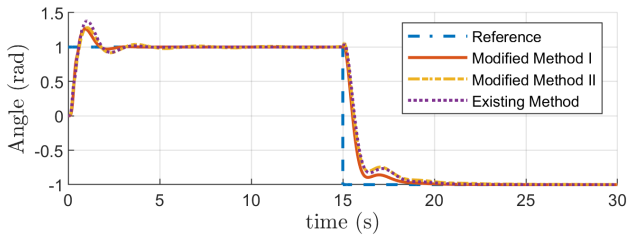

Figure 2: Modified Method I associates with a biproper LTI filter and Modified Method II associates with nonlinear feedback loop in which $\alpha = 0.5$. Adaptation gains are the same for all simulations.

4 Concluding Remarks

In this work, we proposed two alternative modifications to the augmented error method. We believe these to be promising modifications that would facilitate robust adaptive controller synthesis based on LMI optimization.

References

[1] Adaptive control design and analysis, G. Tao, Vol. 37, John Wiley & Sons, 2003

[2] Monopoli, R. (1974). Model reference adaptive control with an augmented error signal. *IEEE Transactions on Automatic Control, 19(5)*, 474-484.

Control of Power Flows under Stochastic Disturbances

Zhen Wang
Department of Applied Mathematics, Delft University of Technology,
Mekelweg 4, 2628CD Delft, The Netherlands, z.wang-21@tudelft.nl

1 Motivation of the Control Problem

At each power company and every five minutes, the company must decide how much power should be generated in each power node with power generators during the next five minutes such that the power network is as stable as possible in one hand and as cheap as possible in the other hand. Nowadays a considerable portion of the power supplies comes from renewable power sources. Due to the fluctuations of the energy of renewable power sources, the stability properties of the network are different from those of power systems during the 20th century. Hence current research on control of power systems should focus also on the stability of such a power systems. The lecture is based on joint research with Kaihua Xi and Aijie Cheng (Shandong University), and with Hai Xiang Lin and Jan H. van Schuppen (TUDelft).

2 The Control Problem

A power system is modelled as in frequency control, see [1], and the fluctuations of the energy of renewable power sources are modelled as a standard Brownian motion and regarded as an input to the power system. The nodes of the power network are partitioned into two groups: A group of nodes with power supply and a group of nodes with only power demand. It is assumed that the sum of the maximal available power supply over the first group of nodes is larger than the sum of the power demands of the second group of nodes. The output of the power system is defined as the vector of phase angle differences of each power line of the power network. The output of the stochastic linearized power system model is a Gaussian stochastic process, see [3]. Of primary interest is the output at a synchronous state.

The *control problem* is to determine a vector of power supplies which minimizes the above defined output of the power system. Define the optimization criterion of the control problem as the maximum over all power lines of the absolute value of the stationary phase angle difference plus two times its standard deviation: $|\theta_i^* - \theta_j^*| + 2\sigma_{ij}$. Based on an analysis of the power system in a synchronous state, the control objective function becomes,

$$f(p_1) \quad = \quad \|arcsin(|Ap_1 + Bp_{demand}|) + 2\sigma(p_1)\|_\infty.$$

In this function the matrices A, B are known from the power network, $p_1 \in \mathbb{R}^{n_1}$ is the vector of power supplies which is regarded as an input variable, and $p_{demand} \in \mathbb{R}^{n_2}$ is the vector of power demands. Denote the domain of the power supply vectors by $\mathbb{D}(p_1)$, which is constrained by the maximal power supply per node and by the condition that the total power supply is larger than the power demand and the power losses. Then that domain is a convex compact subset of $\mathbb{R}^{n_1}$ with linear constraints.

3 The Solution Procedure

From the property that a Lipschitz continuous function sends a compact convex set to a compact convex set, the value range of the objective function should be $[a,b] \subset \mathbb{R}^1$, where b should be less than $\pi/2$. A minimizer $p_1^* \in p^{+,max}$ of the objective function is then such that $f(p_1^*) = a$, in general a minimizer is not unique. Subgradient method is used to compute an approximation of a minimizer for the optimization problem.

4 Example

The following example of a power system illustrates the solution of the control problem. Nodes colored red supply only power and nodes colored blue only have power demand.

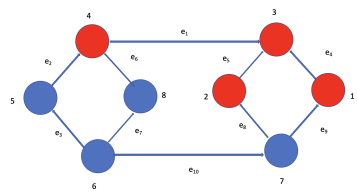

For the original network, we get $a = 0.5779$ and three critical lines: $4-8$, $2-7$ and $3-4$. If we add a line between the nodes $2-4$, then $a = 0.6142$ and the most vulnerable line is line $4-8$. If we double the capacity of line $3-4$, then $a = 0.6026$ and the most fragile line is line $4-8$.

References

[1] P. Kunder, *Power System Stability and Control,* New York: McGraw-Hill, 1994.

[2] S. Jafarpour, E. Y. Huang, K. D. Smith, F. Bullo, *Flow and Elastic Networks on the n− Torus: Geometry, Analysis, and Computation,* SIAM REVIEW, 64 (2022), pp. 59-104.

[3] Z.Wang, K.Xi, A.Cheng et al., *Synchronization of power systems under stochastic disturbances,* Automatica (2023) 110884, https://doi.org/10.1016/j.automatica.2023.110884.

Networks of memristors and the effective memristor

Anne-Men Huijzer, Arjan van der Schaft, Bart Besselink
Bernoulli Institute for Mathematics, Computer Science and Artificial Intelligence
CogniGron - Groningen Cognitive Systems and Materials Center
University of Groningen
m.a.huijzer@rug.nl, a.j.van.der.schaft@rug.nl, b.besselink@rug.nl

1 Introduction

The emerging field of neuromorphic computing aims to reduce the energy requirements of computing platforms. It is suggested that memristors will play an important role within the hardware of these new neuromorphic technologies. Memristors, originally introduced by Chua in [1], are resistors with a memory storage that can act as non-volatile memory. In this work, we introduce a mathematical framework to study the behavior of networks of memristors. We will use this framework to provide an alternative and more detailed proof of Chua's closure theorem that states that "a one-port containing only memristors in equivalent to a memristor" [1]. In addition, we can characterize this so-called *effective memristor* based on the individual memristors in the circuit. Furthermore, by using the monotonicity properties of the memristors in our network, we show how the characteristics of an individual device influence the characteristics of the effective memristor.

2 Main results

We will consider a connected memristor network with N nodes and B branches characterized through the incidence matrix $D \in \mathbb{R}^{N\times B}$, see Figure 1. Let $q \in \mathbb{R}^B$ and $\varphi \in \mathbb{R}^B$ denote the branch charges and fluxes, respectively. We model the memristors through the relation $M \subset \mathbb{R}^B \times \mathbb{R}^B$ as

$$(q,\varphi) \in M, \tag{ML}$$

see [1]. We assume that for all $(q,\varphi),(q',\varphi') \in M$

$$\begin{aligned}(q-q')^\top(\varphi-\varphi') \geq &(q-q')^\top \mathscr{A}(q-q') \\ &+ (\varphi-\varphi')^\top \mathscr{B}(\varphi-\varphi')\end{aligned}$$

is satisfied. Here, $\mathscr{A} = \mathrm{diag}(\alpha_1,\dots,\alpha_B)$ and $\mathscr{B} = \mathrm{diag}(\beta_1,\dots,\beta_B)$ are positive definite matrices. The parameters α_m and β_m correspond to the memristor on edge m in the network.

Furthermore, we assume that our circuit is attached to a port at node k and ℓ. We denote the port charge and port flux as $q_P \in \mathbb{R}$ and $\varphi_P \in \mathbb{R}$, respectively. We want to show that there is a relation between q_P and φ_P by utilizing integrated versions of Kirchhoff's voltage and current law, as in [2], and (ML). We note that the integrated version of Kirchhoff's current states that

$$D(q-q_0) = D_E(q_P - q_{P,0}) \tag{KqL}$$

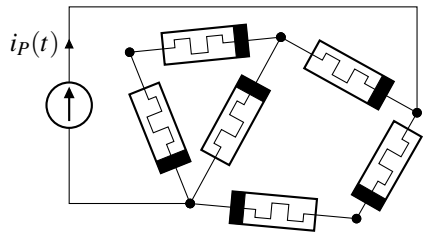

Figure 1: Network of memristors attached to a source applying an input $i_P(t) : [0,t] \to \mathbb{R}$, leading to $q_P(t) - q_P(0) = \int_0^t i(\tau)d\tau$, to the circuit.

and the integrated version of Kirchhoff's voltage law reads

$$\exists \psi \in \mathbb{R}^N \text{ s.t. } \begin{bmatrix}\varphi-\varphi_0 \\ \varphi_P - \varphi_{P,0}\end{bmatrix} = \begin{bmatrix} D^\top \\ (e_k - e_\ell)^\top\end{bmatrix}\psi. \tag{KφL}$$

Here, the notation was simplified by omitting time-arguments, e.g. $q(t) = q$ and $q_0 = q(0)$. For sake of simplicity we introduce the new notation

$$\delta q_P := q_P - q_{P,0} \text{ and } \delta\varphi_P := \varphi_P - \varphi_{P,0}.$$

We can now state the following theorem.

Theorem 2.1 *Consider a connected graph $\mathscr{G}(D)$ and assume $(q_0,\varphi_0) \in M$. Then there exists a relation $M_P(q_0,\varphi_0) \subset \mathbb{R}\times\mathbb{R}$ such that $(\delta q_P, \delta\varphi_P) \in M_P(q_0,\varphi_0)$ Moreover, there exist $\alpha_P > 0$ and $\beta_P > 0$ satisfying $\alpha_P\beta_P \leq 1$ such that*

$$\begin{aligned}(\delta q_P - \delta q_P')(\delta\varphi_P - \delta\varphi_P') \geq &\alpha_P(\delta q_P - \delta q_P')^2 \\ &+ \beta_P(\delta\varphi_P - \delta\varphi_P')^2\end{aligned}$$

for all $(\delta q_P, \delta\varphi_P), (\delta q_P', \delta\varphi_P') \in M_P(q_0,\varphi_0)$.

References

[1] L. Chua, "Memristor-the missing circuit element," *IEEE Transactions on Circuit Theory*, vol. 18, no. 5, pp. 507–519, 1971.

[2] F. Corinto and M. Forti, "Memristor circuits: Flux—charge analysis method," *IEEE Transactions on Circuits and Systems I: Regular Papers*, vol. 63, no. 11, pp. 1997–2009, 2016.

(γ,δ)-Abstraction for Hierarchical Control

Armin Pirastehzad Arjan van der Schaft Bart Besselink

Bernoulli Institute for Mathematics, Computer Science and Artificial Intelligence
University of Groningen
Email: a.pirastehzad@rug.nl,a.j.van.der.schaft@rug.nl,b.besselink@rug.nl

1 Introduction

Following the rapid growth of modern engineering systems in size, control synthesis for such systems has become increasingly challenging, as many existing design methods do not scale with the system dimension. This motivates abstraction-based hierarchical control techniques which refine the control input designed for a low-dimensional abstract system into the proper control input for the concrete system. We propose a notion of system abstraction and characterize the existence of the abstract system in terms of rank constrained linear matrix inequalities.

2 The notion of (γ,δ)-abstraction

Consider a *concrete* control system

$$\mathbf{\Sigma}_c : \begin{cases} \dot{x}_c = A_c x_c + B_c u_c + E_c w_c, \\ z_c = G_c x_c + H_c u_c + K_c w_c, \end{cases} \tag{1}$$

where $x_c \in \mathbb{R}^{n_c}$, $u_c \in \mathbb{R}^{m_c}$, $w_c \in \mathbb{R}^{q_c}$, and $z_c \in \mathbb{R}^{k_c}$ represent system state, control input, external input, and controlled output, respectively. We assume that (1) is asymptotically stable.

As many synthesis methods do not scale with the dimension of (1), we hierarchically control (1) by synthesizing a controller for a low-dimensional *abstract* control system which, in turn, provides the proper control input for (1). For this purpose, we consider an abstract system of the form

$$\mathbf{\Sigma}_a : \begin{cases} \dot{x}_a = A_a x_a + B_a u_a + E_a w_a, \\ u_c = C_a x_a + D_a u_a, \\ z_a = G_a x_a + H_a u_a + K_a w_a, \end{cases} \tag{2}$$

where $x_a \in \mathbb{R}^{n_a}$, $u_a \in \mathbb{R}^{m_a}$, $w_a \in \mathbb{R}^{q_a}$, and $z_a \in \mathbb{R}^{k_a}$. We also assume that (2) is asymptotically stable.

Definition 1. Given asymptotically stable dynamical systems $\mathbf{\Sigma}_c$ and $\mathbf{\Sigma}_a$, for $\gamma, \delta > 0$, the system $\mathbf{\Sigma}_a$ is said to be a (γ,δ)-abstraction of the system $\mathbf{\Sigma}_c$ if there exist constants $\varepsilon, \mu > 0$ such that for initial conditions $x_c(0) = 0$ and $x_a(0) = 0$ and for every external input $w_c, w_a \in \mathscr{L}_2$ and every control input $u_a \in \mathscr{L}_2$,

$$\|z_c - z_a\|^2 \leq \gamma \|w_c - w_a\|^2 + (\delta - \varepsilon) \left\| \begin{bmatrix} w_c \\ w_a \end{bmatrix} \right\|^2 + (\mu - \varepsilon) \|u_a\|^2 .$$

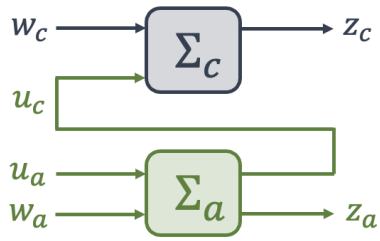

For any controlled-output trajectory of $\mathbf{\Sigma}_a$, determined by w_a and u_a, $\mathbf{\Sigma}_a$ generates a control signal u_c subject to which $\mathbf{\Sigma}_c$ admits a controlled-output trajectory which approximates that of $\mathbf{\Sigma}_a$.

3 Main Results

We characterize the existence of a (γ,δ)-abstraction of a concrete system as a rank-contratined LMI feasibility problem.

Theorem 1. Given a system $\mathbf{\Sigma}_c$, there exist a system $\mathbf{\Sigma}_a$ of the form (2) such that $\mathbf{\Sigma}_a$ is a (γ,δ)-abstraction of $\mathbf{\Sigma}_c$ if and only if there exist positive definite matrices X, Y, matrices W, Z and a positive scalar μ such that $Y - X \succcurlyeq 0$ and

$$\begin{bmatrix} XA_c^T + A_c X & E_c & XG_c^T \\ E_c^T & -(\gamma+\delta)I & K_c^T \\ G_c X & K_c & -I \end{bmatrix} \prec 0,$$

$$\begin{bmatrix} \langle A_c Y + W B_c^T \rangle_s & E_c & 0 & B_c Z \\ E_c^T & -(\gamma+\delta)I & \gamma I & 0 \\ 0 & \gamma I & -(\gamma+\delta)I & 0 \\ Z^T B_c^T & 0 & 0 & -\mu I \end{bmatrix} \prec 0,$$

$$\operatorname{rank} \begin{bmatrix} Y - X & W \end{bmatrix} = \operatorname{rank} Y - X,$$

$$\operatorname{rank} Y - X \leq n_a,$$

where $\langle M \rangle_s = M + M^T$.

4 Conclusion

The notion of (γ,δ)-abstraction relates to the hierarchical control problem as it measures to what extent the controlled-output trajectories of a concrete system are simillar to that of its abstraction. The existence of such an abstraction is characterized in terms of rank-constrained LMIs.

Control for implementation of assume-guarantee contracts

B. M. Shali
b.m.shali@rug.nl

A. J. van der Schaft
a.j.van.der.schaft@rug.nl

B. Besselink
b.besselink@rug.nl

Bernoulli Institute, University of Groningen, The Netherlands

1 Introduction

Simulation-based assume-guarantee contracts for linear dynamical systems are introduced in [1] as an alternative to traditional methods for expressing specifications in control, such as dissipativity theory and set invariance. These contracts have a couple of distinguishing features. First, they express specifications on the *dynamic* behaviour of a system. Second, they are tailored to support *modular* analysis and design of interconnected systems through notions of contract refinement and contract composition.

Here, we will consider the problem of controller design for contract implementation. In particular, we will provide necessary and sufficient conditions for the existence of a controller that turns a given plant system into an implementation of a given contract. We will also consider the problem of constructing such a controller.

2 Control for implementation

Consider a linear system of the form

$$\Sigma : \begin{cases} \dot{x} = Ax + Bu, \\ y = Cx + Du, \end{cases} \tag{1}$$

with state x, input u, and output y. The contracts in [1] express specifications on the dynamic behaviour of Σ. A characteristic feature of these contracts is that they take the environment of Σ explicitly into account. The environment of Σ is a linear system that generates input trajectories for Σ. The available information about the behaviour of this environment is captured by the *assumptions* A, defined as

$$\mathrm{A} : \begin{cases} \dot{x}_a = A_a x_a + G_a d_a, \\ u = C_a x_a. \end{cases} \tag{2}$$

with state x_a, driving variable d_a, and output u. That is, we know that the only input trajectories that Σ might receive are the ones that can be generated by the assumptions A. We obtain the interconnection $\mathrm{A} \wedge \Sigma$ by setting the output of A as input of Σ. We take both u and y as outputs of $\mathrm{A} \wedge \Sigma$.

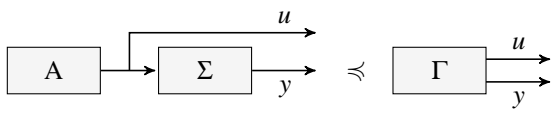

Figure 1: Contract implementation.

The desired dynamic behaviour of Σ is captured by the *guarantees* Γ, defined as

$$\Gamma : \begin{cases} \dot{x}_g = A_g x_g + G_g d_g, \\ u = C_g^u x_g, \\ y = C_g^y x_g, \end{cases} \tag{3}$$

with state x_g, driving variable d_g, and outputs u and y. A contract $\mathscr{C}$ is defined as a pair of assumptions and guarantees, that is, $\mathscr{C} = (\mathrm{A}, \Gamma)$. Then, contract implementation is defined using the notion of simulation. Roughly speaking, a system Ξ_1 is simulated by another system Ξ_2, denoted by $\Xi_1 \preccurlyeq \Xi_2$, if any output trajectory that Ξ_1 can generate is an ouptut trajectory that Ξ_2 can also generate.

Theorem 1. *A system Σ implements the contract $\mathscr{C} = (\mathrm{A}, \Gamma)$ if and only if $\mathrm{A} \wedge \Sigma \preccurlyeq \Gamma$.*

This means that Σ implements $\mathscr{C} = (\mathrm{A}, \Gamma)$ if any input-output trajectory generated by Σ, where the input trajectory is generated by A, can also be generated by Γ.

Now, suppose that we are given a plant system

$$\mathrm{P} : \begin{cases} \dot{x}_p = A_p x_p + B_p^u u + B_p^v v, \\ y = C_p^y x_p, \\ z = C_p^z x_p, \end{cases} \tag{4}$$

with state x_p, input u, control input v, output y, and control output z. Our goal is to design a controller

$$\mathrm{C} : \begin{cases} \dot{w} = Kw + Lz, \\ v = Mw + Nz, \end{cases} \tag{5}$$

with state w, input z, and output v, such that the interconnection $\mathrm{P} \wedge \mathrm{C}$ implements a given contract $\mathscr{C} = (\mathrm{A}, \Gamma)$. We can show that such a controller exists if and only if there exists a pair of subspaces that satisfy a set of conditions that are reminiscent of controlled-invariance and conditioned-invariance. Given such a pair of subspaces, we can explicitly construct a controller that achieves our goal. Fortunately, we can also derive a systematic procedure to obtain such a pair of subspaces whenever it exists.

References

[1] B. M. Shali, H. M. Heidema, A. J. van der Schaft, and B. Besselink, "Series composition of simulation-based assume-guarantee contracts for linear dynamical systems," in *Proceedings of the IEEE Conference on Decision and Control*, pp. 2204–2209, 2022.

Data-driven Synchronization of Network Systems

Yongzhang Li
University of Groningen
SCO-Bernoulli Institute
Nijenborgh 9, 9747 AG,
Groningen, The Netherlands
yongzhang.li@rug.nl

Kanat Camlibel
University of Groningen
SCO-Bernoulli Institute
Nijenborgh 9, 9747 AG,
Groningen, The Netherlands
m.k.camlibel@rug.nl

Harry Trentelman
University of Groningen
SCO-Bernoulli Institute
Nijenborgh 9, 9747 AG,
Groningen, The Netherlands
h.l.trentelman@rug.nl

1 Introduction

Network systems are widely applied in analysis and control of interconnected systems, such as multi-agent systems and smart grids. The synchronization problem, as a fundamental issue in the research of network systems, received considerable attention in the last two decades. Recently, in order to bypass the difficulty of system identification in the model-based control, data-driven control has been popularized in research of synchronization problems.

To necessarily design controllers directly from data that are not informative to identify the system model uniquely, the data informativity framework was proposed by van Waarde et. al. [1]. We will focus on solving synchronization problems of linear discrete-time homogeneous network system based on the informativity framework. In particular, we provide necessary and sufficient conditions that the data are informative for synchronization, and show how to design a controller achieving from the data.

2 Problem

We consider a linear discrete-time multi-agent system of the form

$$\xi(k+1) = [(I_p \otimes A_s) - (\mathscr{L} \otimes B_s K)]\xi(k), \tag{1}$$

where p is the number of agents, $(A_s, B_s) \in \mathbb{R}^{n\times m} \times \mathbb{R}^{n\times m}$ describe the node dynamic, K is the coupling matrix, and $\mathscr{L} \in \mathbb{R}^{p\times p}$ is the Laplacian matrix of a connected undirected simple graph. Let $0 < \lambda_1 \leqslant \lambda_2 \leqslant \cdots \leqslant \lambda_p$ be the eigenvalues of $\mathscr{L}$. It is well-known that the system (1) is synchronized if and only if $A_s - \lambda_i B_s K$ is Schur for all $i \in [2, p]$.

In this note, we want to study synchronization of the system (1) under the assumption that A_s and B_s are unknown but we can collect input/state data from the system

$$x(k+1) = A_s x(k) + B_s u(k). \tag{2}$$

Suppose that $T \geqslant 1$ and

$$U_- := \begin{bmatrix} u(0) & u(1) & \dots & u(T-1) \end{bmatrix}$$
$$X := \begin{bmatrix} x(0) & x(1) & \dots & x(T) \end{bmatrix}$$

are input/state data that are harvested from the system (2). We define the set of systems that explain the data (U_-, X) by

$$\Sigma := \left\{ (A,B) | X_+ = \begin{bmatrix} A & B \end{bmatrix} \begin{bmatrix} X_- \\ U_- \end{bmatrix} \right\},$$

where

$$X_+ := \begin{bmatrix} x(1) & x(2) & \dots & x(T) \end{bmatrix},$$
$$X_- := \begin{bmatrix} x(0) & x(1) & \dots & x(T-1) \end{bmatrix}.$$

Clearly, we have $(A_s, B_s) \in \Sigma$, and any system $(A,B) \in \Sigma$ can generate the data (U_-, X). Then we give the definition of synchronization as follows.

Definition 1 *We say that the data (U_-, X) are informative for synchronization if there exists K such that the multi-agent system (1) is synchronized for all $(A,B) \in \Sigma$.*

The problem is to find the necessary and sufficient conditions that the data (U_-, X) are informative for synchronization, and provide the design method of K.

3 Main Results

Theorem 1 *The data (U_-, X) are informative for synchronization of a discrete-time system, whose interconnection structure is an connected undirected simple graph, with control gain K if and only if the following conditions are satisfied.*

① *X_- is full row rank, and there exist $p-1$ right inverses $(X_-^\dagger)_2, (X_-^\dagger)_3, \dots, (X_-^\dagger)_p$ of X_- such that $X_+(X_-^\dagger)_i$ is Schur for all $i \in [2, p]$.*

② *$U_-(\lambda_i (X_-^\dagger)_j - \lambda_j (X_-^\dagger)_i) = 0$ for all $i, j \in [2, p]$.*

Moreover, if conditions ① and ② are satisfied, $K = -\frac{U_-(X_-^\dagger)_i}{\lambda_i}$ is the control gain that achieves synchronization.

References

[1] H. J. van Waarde, J. Eising, H. L. Trentelman and M. K. Camlibel, "Data Informativity: A New Perspective on Data-Driven Analysis and Control," in IEEE Transactions on Automatic Control, 2020.

Performance Shaping for Data-Driven Generalized plants

L.M. Spin[1], R. Tóth[1,2], N. Van de Wouw[3] and W. P. M. H. Heemels[4]

[1] Control Systems Group, Eindhoven University of Technology, Netherlands

[2] Systems and Control Lab, Institute for Computer Science and Control, Hungary

[3] Dynamics and Control Group, Eindhoven University of Technology, Netherlands

[4] Control Systems Technology Group, Eindhoven University of Technology, Netherlands

Email: {l.m.spin, r.toth, n.v.d.wouw, w.p.m.h.heemels}@tue.nl

1 Introduction

Nowadays data is more readily available than it used to be. Moreover, computers are able to store more data and their computational strength is still increasing according to Moore's law. There are increasing performance expectations in terms of accuracy, speed, and energy efficiency that drive machine designs to become more complex, making first principle modeling increasingly more challenging for these new designs. In modern control engineering, it is essential to learn a controller directly from the available data instead of designing a controller from data-based modeling. Firstly, the latter is computationally expensive, and secondly, this avoids losing information by imposing a model class and structure on the data.

Direct data-driven controller synthesis is achieved by viewing the data as a non-parametric representation of the actual system. This viewpoint stems from a result that has had enormous attention in the last few years. This result is known as Willems' Fundamental Lemma [1] provides a systematic way to represent the behavior of dynamical systems based on measured data. This Lemma state that given a measured input-output trajectory $\mathscr{D}_N = \{u_k^d, y_k^d\}_{k=0}^{N-1}$ with a sufficiently rich input, the output is also guaranteed to be informative as well. In [2] it derived that if the following rank condition

$$rank\left(\begin{bmatrix}\mathscr{H}_L(u^d)\\ \mathscr{H}_L(y^d)\end{bmatrix}\right) = \mathbf{m}(\mathfrak{B})L + \mathbf{n}(\mathfrak{B}) \tag{1}$$

holds, where $L \geq \ell(\mathfrak{B})+1$, then linear combinations of the columns span the finite behavior of the system. Here $\mathbf{m}(\mathfrak{B})$ is the input cardinality, $\mathbf{n}(\mathfrak{B})$ is the state-dimension and $\ell(\mathfrak{B})$ is the lag of the system, e.g. how many samples are required to uniquely determine the initial state condition.

The input-state measurement version of the Fundamental Lemma has been used for optimal controller design, see for instance [3]. Compared with model-based controller design, it is not yet clear how to use data-based controller synthesis results to guarantee certain performance in the time domain a priori.

2 Proposed approach

An intuitive tool to design model-based controllers with performance guarantees is mixed-sensitivity. This shaping framework is based on a powerful concept appropriately named generalized plants, see [4]. Generalized plants are able to specify a large generality of control problems. Generalized plants are augmented by weighting filters that encode desired time-domain performance criteria by shaping sensitivity functions. In this work, we propose to incorporate generalized plants into the data-driven framework.

First and foremost, the versatility of control configurations

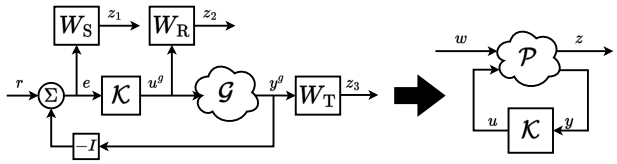

Figure 1: Data-driven control configuration

as block diagrams is investigated. A marriage of model-based representations and data-driven non-parametric representations is shown in Figure 1, here the rectangular blocks represent parametric models while the cloud-shaped blocks represent gathered data. The model-based weighting filters are seen as constraints on signals in the control configuration. A sketch of this marriage is provided in the following example where a filter is applied to the error signal in the figure.

$$\begin{aligned} z_1 = W_S(r-y^g) \Leftrightarrow A(\sigma)z_1(k) = B(\sigma)(r(k)-y^g(k)) \\ B(\sigma)y^g = \sum_{i=0}^{n} B_i\sigma^i y^g(k) = B\mathscr{H}_{n+1}(y^d)g \end{aligned} \tag{2}$$

where $B = [B_0, B_1, ..., B_n]$ which holds for some g if $n \geq \ell(\mathfrak{B})$. Now user-defined exogenous inputs w require initializing data for the augmented weighting filters. Incorporating weighting filters into the generalized plant allows for mixed-sensitivity shaping.

This transformation to a purely data-driven generalized plant allows for dissipativity analysis and synthesis for which some system norms, such as the $\mathscr{H}_\infty$-norm, arise as a particular choice of the supply function. The availability of only input-output data renders the construction of a storage function infeasible. As mentioned in [3] the past samples of inputs and outputs, e.g. the memory, can also be viewed as the state.

With this approach, we aim at generalizing control configurations, controller synthesis, and shaping methods for data-based representations that rival the performance achieved by sequential system identification and model-based controller design.

References

[1] J. C. Willems, P. Rapisarda, I. Markovsky, and B. L. De Moor, "A note on persistency of excitation," *Systems & Control Letters*, vol. 54, no. 4, pp. 325–329, 2005.

[2] I. Markovsky and F. Dörfler, "Identifiability in the behavioral setting," *IEEE Transactions on Automatic Control*, 2022.

[3] C. De Persis and P. Tesi, "Formulas for data-driven control: Stabilization, optimality, and robustness," *IEEE Transactions on Automatic Control*, vol. 65, no. 3, pp. 909–924, 2019.

[4] S. Skogestad and I. Postlethwaite, *Multivariable feedback control: analysis and design.* john Wiley & sons, 2005.

Computation of Admissible Reference Dependent Invariant Sets for Polynomially Feedback Linearizable Systems

Andres Cotorruelo
Université Libre de Bruxelles
andres.cotorruelo.jimenez@ulb.be

Emanuele Garone
Université Libre de Bruxelles
emanuele.garone@ulb.be

1 Introduction

Born with the inception of the study of dynamical systems, invariant sets are at the core of stability analysis. These sets can be defined using several pathways and mathematical concepts, but the most direct and intuitive definition is as follows: an invariant set $\mathcal{S}$ is a subset of the state space such that, once the state belongs to $\mathcal{S}$, it will remain therein for all future instants. Mathematically,

$$\mathcal{S} \text{ is invariant if } x(t_0) \in \mathcal{S} \Rightarrow x(t) \in \mathcal{S}\ \forall t \geq t_0.$$

The computation of this family of sets has been the subject of many a research line over the last two centuries, with the vast majority of them focusing on the computation of invariant sets *around a single point of equilibrium*. Such invariant sets are useful in the *regulation* problem, where the goal is to drive the state to a given point of equilibrium—typically the origin.

However, when tackling the *set-point regulation* problem, where the objective is to steer the state towards *any* given point of equilibrium within a variety of equilibria, these "static" invariant sets prove themselves ineffective. Indeed, in this setting, invariant sets need to be *reference dependent*: a set-valued function, $\mathcal{S}(r)$, that returns an invariant set for any admissible value of the reference, r.

Another aspect that fundamentally changes the computation of invariant sets is the presence of constraints. Undoubtedly, invariant sets need to be contained strictly within the constraint set for the state to never violate the constraints once it enters these sets. If indeed, a given invariant set is contained in the constraint set, it is said to be *admissible*.

This publication cover the computation of admissible reference dependent invariant sets for systems which can be feedback-linearized by a polynomial control law.

2 Problem statement and results

Consider the following constrained system

$$\delta x = f(x,u),$$
$$x \in \mathcal{X},\ u \in \mathcal{U},$$

with $x \in \mathbb{R}^n$, $u \in \mathbb{R}^m$, $\mathcal{X} \subseteq \mathbb{R}^n$, $\mathcal{U} \subseteq \mathbb{R}^m$, and where δx denotes the successor state in discrete time, and the time derivative in continuous time. It is assumed that a stabilizing polynomial control law $u(x,r) : \mathbb{R}^n \times \mathbb{R}^p \to \mathbb{R}^m$ is known such that

$$f(x,u(x,r)) = Ax + Br,$$

for some asymptotically stable $A \in \mathbb{R}^{n\times n}$ and $B \in \mathbb{R}^{n\times m}$. As the system is in linear form, it admits a reference dependent Lyapunov function of the form

$$V(x,r) = (x-\bar{x}_r)^{\mathrm{T}} P(r)\,(x-\bar{x}_r)\,,$$

in which $P(r)$ is a matrix of size $n \times n$ whose elements are polynomials in r, and $\bar{x}_r$ denotes the steady state associated to the reference r.

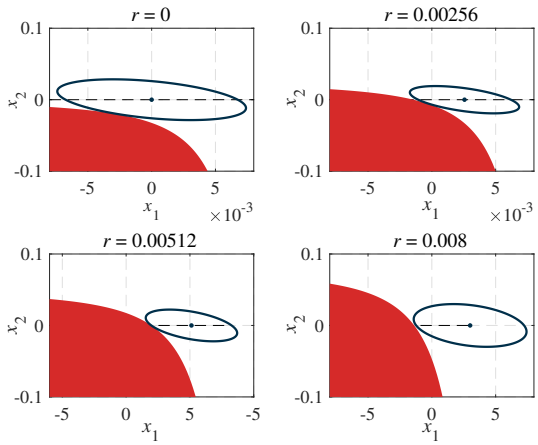

Figure 1: Visualization of the reference dependent invariant sets for different values of the reference.

By invoking the central theorem of [1] it is possible to use Semi-Definite Programming to compute the polynomial matrix $P(r)$, and consequently ellipsoidal invariant sets whose shape and center vary according to the reference. An example of this is presented in Figure 1, in which the constraint is depicted in solid red, the invariant set as a solid black ellipsoid, the steady state as a black dot, and the admissible variety of steady states as a black dashed line.

References

[1] A. Cotorruelo, M. Hosseinzadeh, D. R. Ramirez, D. Limon, and E. Garone. "Reference dependent invariant sets: Sum of squares based computation and applications in constrained control". Automatica, 129, 109614, 2021.

Time-Series Analysis Using Third-Order Recurrence Plots

Martijn Boussé, Philippe Dreesen, Pietro Bonizzi, Joël Karel, Ralf Peeters
Department of Advanced Computing Sciences
Maastricht University, Maastricht, The Netherlands
Email: m.bousse@maastrichtuniversity.nl

1 Introduction

Higher-order recurrence plots may enable us to reveal more structure than what is possible with traditional recurrence plots (RPs). While RPs attempt to detect recurrence relations by pair-wise comparison of time-delayed embeddings, given a time series, higher-order RPs may detect recurrences by comparing *multiple* time-delayed embeddings simultaneously. In this work, we limit ourselves to third-order recurrence plots (TORPs) for time series analysis, as they can still be graphed straightforwardly, and propose future directions.

2 Recurrence Plots & Existing Extensions

Recurrence plots (RPs) allow us to visualize recurrences in state-space trajectories, enabling us to deduce certain properties of the underlying system [1]. A recurrence is a point in the state space where the trajectory passes through at a time i and returns to at a later time j (up to some small error, say ε), i.e., recurrences are points where $\mathbf{x}^{(i)} \approx \mathbf{x}^{(j)}$ with $\mathbf{x}^{(i)}$ the state of the system at time i. More formally, thresholded RPs can be represented by an $N \times N$ matrix $\mathbf{R}$ defined element-wise as

$$r_{ij} = \begin{cases} 1 & \text{if dist}\left(\mathbf{x}^{(i)}, \mathbf{x}^{(j)}\right) \leq \varepsilon \\ 0 & \text{otherwise,} \end{cases}$$

for $1 \leq i, j \leq N$, where dist$(\cdot)$ is some distance metric — usually the Euclidean distance — and ε is the recurrence threshold. Given a time series $\mathbf{u}$, the state can be reconstructed via a time-delayed embedding defined as $\mathbf{x}^{(i)} = \begin{bmatrix} u_i & u_{i+\tau} & \cdots & u_{i+\tau(M-1)} \end{bmatrix}^{\mathrm{T}}$ with embedding dimension M and time delay τ. The matrix $\mathbf{R}$ can then be visualized in a 2D graph by plotting a black dot at coordinate (i, j) if $r_{ij} = 1$.

Higher-order extensions to RPs have been proposed, such as 'generalized' RPs — a.k.a. "recurrence hypercubes" — and 'generalized' recurrence networks [2, 3], that are tailored to spatial data. Recurrence hypercubes are constructed by pair-wise comparison (i.e., two orders) of spatial data (i.e., two orders), leading to a fourth-order tensor. A recurrence network represents the states by nodes and the recurrence relations by edges between nodes so that the network topology characterizes the recurrence patterns. Alternatively, multiple traditional RPs, obtained under varying parameter settings, can be 'stacked' into a third-order tensor as proposed in [4].

3 Third-Order Recurrence Plots & Time Series

We propose a straightforward generalization of traditional RPs as follows. We define a *third-order* recurrence plot, or TORP, that can be represented by an $N \times N \times N$ third-order tensor $\mathscr{R}$ defined element-wise, for $1 \leq i, j, k \leq N$, as

$$r_{ijk} = \begin{cases} 1 & \text{if dist}\left(\mathbf{x}^{(i)}, \mathbf{x}^{(j)}, \mathbf{x}^{(k)}\right) \leq \varepsilon \\ 0 & \text{otherwise.} \end{cases}$$

In contrast to traditional RPs, we require a distance metric that allows us to compare *three* time-delayed embeddings simultaneously instead of just two. There are many ways to do this. A TORP can then be visualized by plotting a colored dot at coordinate (i, j, k) if $r_{ijk} = 1$ in a 3D graph.

TORPs can be used for time series analysis. In Figure 1, we illustrate the unthresholded and thresholded TORP for a simple univariate and noisy time series that features three events. One can deduce the event times from the image. In this example, we used a generalization of the cosine similarity for the distance metric. Our approach can be extended easily to joint, cross, and fuzzy RPs, as well as recurrence quantification analysis, leading to new exciting directions for time-series analysis by means of higher-order RPs.

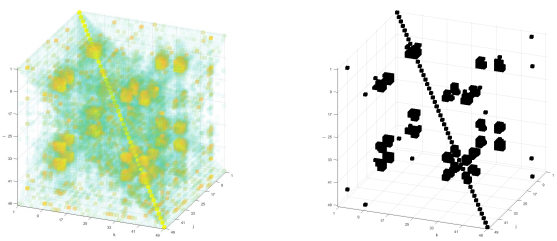

Figure 1: Unthresholded (left) and thresholded (right) TORP.

References

[1] J.-P. Eckmann, et al., "Recurrence Plots of Dynamical Systems," Europhysics Letters 4(9), pp. 973–977, 1987.

[2] N. Marwan, et al., "Generalised recurrence plot analysis for spatial data," Physics Letters, pp. 545–551, 2007.

[3] C.-B. Chen, et al., "Recurrence network modeling and analysis of spatial data," Chaos 28(8), 085714, 2018.

[4] T.D. Pham, et al., "Fuzzy cross recurrence analysis and tensor decomposition of major-depression time-series data," in proc. of DATA'21 (Jordan), pp. 28–34, 2021.

The Design and Optimization of an Aquaponics System Using Static and Dynamic Optimization

Joris Bergman
Mathematical and Statistical Methods (Biometris)
Wageningen University
P.O. Box 16, 6700 AC Wageningen
The Netherlands
Email: joris.bergman@wur.nl

1. Introduction

In the coming decades, a combination of a growing world population and growing income levels will increase the demand for animal proteins [1]. One source of high-quality animal protein is aquaculture, which makes up over 50% of global fish consumption. Current state of the art recirculating aquaculture systems (RAS), achieve high fish production rates, but produce a large amount of waste in the form of chemical oxygen demand (COD), total ammonium nitrogen (TAN), nitrate (NO_3^-) and phosphorus compounds (P) [2].

Aquaponics, the coupling of a RAS to a hydroponic system (HPS) can help solve this problem and achieve optimal nutrient use and recycling. The core system consists of a RAS which is connected one-way to an HPS system. Dissolved N and P flow from RAS to HPS, where the water leaves the system through evapotranspiration. Solid waste from the fish tank and from the HPS flows to an up-flow anaerobic sludge blanket (UASB) digester, where COD is removed and solid P and N are solubilized. Dissolved nutrients from the digester also flow to the HPS. Additional nutrients can be supplemented if required [2].

2. Problem Definition

The performance of the aquaponics system is evaluated by three key types of parameters:

1) Nutrient use efficiency (NUE) for P and N, defined as the percentage of nutrients coming into the system that end up in fish or in plants;
2) Water use efficiency (WUE), defined as the percentage of water that is not wasted through over-dilution;
3) Nutrient self-sufficiency (NSS) for P and N, defined as the percentage of nutrients that go to the HPS originating from the RAS.

KPI values depend in on the relative sizing of the RAS and HPS sub-systems and on the flows between these systems. Current systems are unbalanced, leading to unutilized waste streams and the need for nutrient supplementation. This can be improved by expanding the network with more nodes and by improving the dynamic operation of the system.

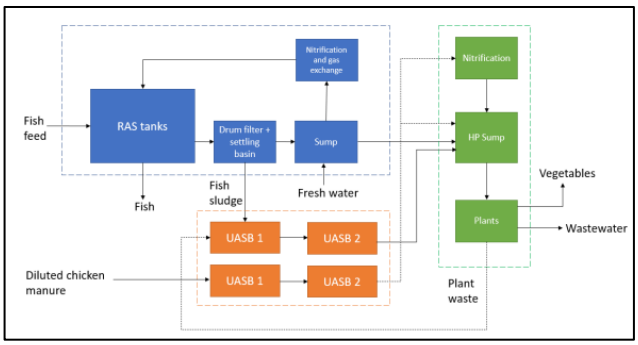

Figure 1: Optimal aquaponics system design

3. Research Methods

This research combined static and dynamic optimization techniques with previous modelling work to investigate a) which nodes to add to the system and b) the optimal control trajectory for the best system design found in part a). Static optimization was carried out in Matlab in four different seasons under natural and supplemented light conditions.

Of the four evaluated system designs, the design shown in figure 1 was evaluated under dynamic conditions using Tomlab, a Matlab extension for optimal control.

4. Key Findings

1) A chicken manure digester should be added to prevent nitrogen limitation;
2) Optimal control is able to achieve high simultaneous values for NUE, WUE and NSS for all nutrients, area remains a key design parameter;
3) Using optimal control, buffering of the system can take place in time, as the constraints on nutrient concentration allow for annual fluctuations.

5. References

[1] FAO. The Future of Food and Agriculture: Trends and Challenges [Internet]. 2017. Available from: https://www.fao.org/3/a-i6583e.pdf.
[2] Goddek S, Körner O. A fully integrated simulation model of multi-loop aquaponics: A case study for system sizing in different environments. Agricultural Systems. 2019;171:143–154.

A Size Independent Formulation for Automatic Performance Evaluation of Decentralized Optimization Algorithms

Sebastien Colla and Julien M. Hendrickx
ICTEAM Institute, UCLouvain, 1348 Louvain-la-Neuve, Belgium.
Email: { sebastien.colla, julien.hendrickx } @uclouvain.be

We develop a methodology that automatically provides numerically tight performance bounds for first-order decentralized methods, by solving a semidefinite program whose size is independent of the number of agents in the network [1].

In decentralized optimization, we consider a set of agents $\{1,\dots,N\}$, working together to minimize the average of their local functions $f(x) = \frac{1}{N}\sum_{i=1}^{N} f_i(x)$. This problem can be written using a separable function $F_s : \mathbb{R}^{Nd} \to \mathbb{R}$:

$$\min_{x_1\dots,x_N \in \mathbb{R}^d} \quad F_s(x_1,\dots,x_N) = \frac{1}{N}\sum_{i=1}^{N} f_i(x_i), \qquad (1)$$
$$\text{such that} \quad x_1 = \dots = x_N.$$

where $f_i : \mathbb{R}^d \to \mathbb{R}$ is the private function locally held by agent i and $x_i \in \mathbb{R}^d$ is its local decision variable. Each agent i performs local computations and exchanges local information with its neighbors to come to an agreement on the minimizer x^* of the global function f. Exchanges of information often take the form of an average consensus on some quantity, e.g., on the x_i. These consensuses can be represented using a multiplication by a matrix $W \in \mathbb{R}^{N\times N}$, typically assumed symmetric and doubly stochastic and characterized by its second largest eigenvalue λ.

In general, the quality of an optimization algorithm is evaluated *via* a worst-case guarantee. Accurate worst-case guarantees can be difficult to compute theoretically. Recently, an alternative computational approach, called Performance Estimation Problem (PEP), has been developed to automatically compute tight worst-case guarantees by solving an optimization problem [2]. A PEP is looking for the function and the initial point maximizing a given performance criterion when running K iterations of the algorithm. In our previous work [3], we have extended this PEP framework to decentralized optimization, resulting in problems whose size grows with the number of agents N. In our new work [1], we develop a new PEP formulation for decentralized optimization whose problem size is now independent of N, though N could still appear as a scaling coefficient in some cases. This allows to obtain worst-case guarantees valid for any number of agents N by solving compact problems.

This new PEP formulation takes a global view on the decentralized problem (1), by neglecting the separability of the function F_s, which a priori corresponds to a relaxation. The problem becomes then one of optimizing a function $F : \mathbb{R}^{Nd} \to \mathbb{R}$ over $\mathbf{x} \in \mathbb{R}^{Nd}$, under the constraint that $\mathbf{x}$ belongs to the consensus subspace (all $x_i \in \mathbb{R}^d$ are equal). This will admit a simple representation that only requires decomposing $\mathbf{x}$ into two blocks of components, respectively along the consensus subspace and along its orthogonal complement, as opposed to the N blocks of components along each x_i in [3]. See [1] for details about this new formulation.

We have demonstrated this new agent-independent PEP formulation on several examples (algorithms DGD, DIGing and EXTRA), and observe empirically its tightness for symmetric and generalized[1] doubly stochastic averaging matrices [1]. This tool allows to answer rapidly to a large diversity of questions about the performance of decentralized algorithms. For example, it can help in algorithm comparison: Figure 1 shows that EXTRA seems to perform better than DIGing for time-constant averaging matrices but is not robust to time-varying matrices.

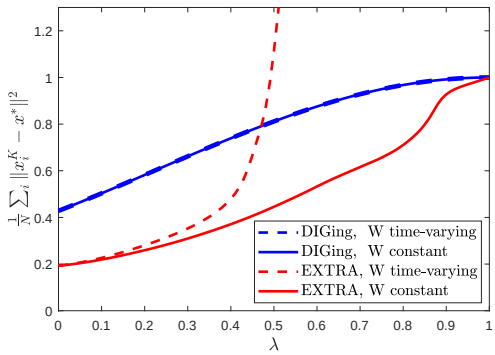

Figure 1: Comparison between algorithms DIGing and EXTRA for 10 iterations with constant and time-varying averaging matrices W, for different values of λ. Optimized step-sizes and f_i are 0.1-strongly convex and 1-smooth, for all i.

Acknowledgements

S. Colla is supported by the French Community of Belgium through a FRIA fellowship (F.R.S.-FNRS).

References

[1] S. Colla, J. M. Hendrickx, "Automated Performance Estimation for Decentralized Optimization via Network Size Independent Problems", *61th IEEE CDC*, 2022.

[2] A. B. Taylor, J. M. Hendrickx and F. Glineur, "Exact Worst Case Performance of First-Order Methods for Composite Convex Optimization," 2015.

[3] S. Colla, J. M. Hendrickx, "Automatic Performance Estimation for Decentralized Optimization", *Preprint*, 2022.

[1] A generalized doubly stochastic matrix has rows and columns that sum to one, without the need to be non-negative, see [3, Definition 2]

Feasible Real-Time Optimization for Nonlinear Model Predictive Control

David Kiessling, Alejandro Astudillo, Wilm Decré, Jan Swevers
MECO Research Team, Department of Mechanical Engineering, KU Leuven, Belgium
Flanders Make@KU Leuven, Belgium
Email: david.kiessling@kuleuven.be

1 Introduction

Nonlinear optimization methods such as Feasible Sequential Linear Programming (FSLP) [2] or Feasibility-Projected Sequential Quadratic Programming (FP-SQP) [4] iteratively find solutions to Nonlinear Programs (NLP) of the form:

$$\begin{aligned} \min_{x\in\mathbb{R}^n} \quad & f(x) \\ \text{s.t.} \quad & g(x) = 0, \\ & h(x) \leq 0. \end{aligned} \tag{1}$$

where $x \in \mathbb{R}^n$ is the vector of decision variables, $f\colon \mathbb{R}^n \to \mathbb{R}$ denotes the objective function, and $g\colon \mathbb{R}^n \to \mathbb{R}^m$, $h\colon \mathbb{R}^n \to \mathbb{R}^p$ denote the equality and inequality constraints, respectively. Particularly interesting is the fact that both methods keep all intermediate iterates feasible. Thus, the algorithms can be stopped at any feasible, suboptimal iterate. In applications, where calculation time is limited, such as Nonlinear Model Predictive Control (NMPC), this is beneficial. An NMPC controller solves a sequence of NLP (1) in a receding horizon fashion. Every NLP is solved within a given time window which must be shorter than the sampling time to allow real-time implementations.
The research proposed in this abstract aims at applying FSLP and FP-SQP in a real-time scenario. This includes embedding the algorithm and its ability to be stopped at a feasible point in a real-time setting. Additionally, the globalization strategy applied in FSLP and FP-SQP will be exploited for reliable convergence while ensuring fast execution time. The resulting algorithm will be tested on a challenging autonomous driving example.

2 Algorithmic Framework

FSLP shares the algorithmic core of FP-SQP, with linear problems being solved instead of quadratic programs. Therefore, the presentation below is limited to FP-SQP only. The algorithm of FP-SQP is depicted as follows. For every iteration, a quadratic program of the form

$$\begin{aligned} \min_{\Delta w} \quad & \nabla f(w)^\top \Delta w + \frac{1}{2}\Delta w^T H_k \Delta w \\ \text{s.t.} \quad & g(w) + \nabla g(w)^\top \Delta w = 0, \\ & h(z) + \nabla h(w)^\top \Delta w \leq 0, \\ & \|\Delta w\|_\infty \leq \Delta_k. \end{aligned} \tag{2}$$

is solved. The solution of (2), i.e., Δw_k, is used to perform a step $w_{k+1} = w_k + \Delta w_k$ towards the optimal solution. However, this iterate is in general not feasible with respect to the constraints of (1). Next, w_{k+1} is projected on the feasible set of (1). The trust-region combined with a merit function decides upon step acceptance. In [2], a feasibility projection strategy was introduced which is used in the real-time algorithm. The higher order terms of the constraints in (1) at w_{k+1} are corrected until a feasible iterate is reached.
In real-time optimization, the so-called Real-Time Iteration (RTI) scheme [1] is state-of-the-art. One SQP iteration, i.e., solving only one QP, per NMPC iteration is performed. In many applications this is sufficient to achieve a converging real-time algorithm.
The proposed algorithm starts from the RTI scheme by solving (2). The resulting iterate is projected on the feasible set. In certain cases, this already suffices to achieve recursive feasibility of the NMPC controller. An additional new approach will be to use the trust-region in (2) to guarantee global convergence for real-time optimization problems.

3 Outlook

A novel real-time algorithm which is based on FP-SQP is proposed. An additional globalization strategy is used to achieve global convergence. The algorithm will be demonstrated on an autonomous driving simulation example. Implementing the algorithm on real-time hardware will be subject of future research.

References

[1] S. Gros, M. Zanon, R. Quirynen, A. Bemporad, M. Diehl. "From Linear to Nonlinear MPC: Bridging the Gap via Real-Time Iteration" *International Journal of Control*, 2015.

[2] D. Kiessling, A. Zanelli, A. Nurkanović, J. Gillis, M. Diehl, M. Zeilinger, G. Pipeleers, and J. Swevers. "A feasible sequential linear programming algorithm with application to time- optimal path planning problems" *Proceedings of 61st IEEE Conference on Decision and Control*, 2022.

[3] M. Tenny, S. Wright "Nonlinear Model Predictive Control via Feasibility-Perturbed Sequential Quadratic Programming" *Computational Optimization and Applications*, 2004.

[4] S. Wright, M. Tenny "A feasible trust-region sequential quadratic programming algorithm" *SIAM Journal on Optimization*, 2004.

Acknowledgement: This work has been carried out within the framework of Flanders Make SBO DIRAC: DIRAC - Deterministic and Inexpensive Realizations of Advanced Control. Flanders Make is the Flemish strategic research centre for the manufacturing industry.

Optimal allocation under strategic attacks on uncertain systems

Sribalaji C. Anand
Department of Electrical Engineering,
Uppsala University, Sweden.
sribalaji.anand@angstrom.uu.se

André M. H. Teixeira
Department of Information Technology,
Uppsala University, Sweden
andre.teixeira@it.uu.se

1 Introduction

To mitigate cyber attacks on networked control systems (NCS), security measures (such as encryption) should be optimally allocated, such that the attack is effectively detected with minimal performance loss. To this end, we propose an allocation strategy for uncertain linear systems under sensor attacks [1]. We next explain the problem setup.

2 Problem Setup

We consider a DT LTI process with parametric uncertainty $\delta \in \Omega$, regulated by a full order controller and, a Kalman filter's residue-based anomaly detector as depicted in Figure 1. The NCS has good performance if the energy of the performance output $||y_p||^2_{\ell_2}$ is small (LQ control) and an anomaly is considered to be detected when the detector output energy $||y_r||^2_{\ell_2}$ is greater than a predefined threshold, say ε_r.

In the NCS, we consider an adversary injecting false data into the sensors (or actuators, but not both). The adversary disrupts the system's behavior while staying stealthy (contradictory objectives to the operator). Only the operator has an uncertain process model but the adversary has the exact process knowledge. This setup is far from reality but helps us study the worst case. Now, the main problem we study is to allocate the n_w security measures across n_y sensors where $n_w < n_y$ which can be formulated as

$$\mathscr{Q}_w^* = \arg\inf_{\mathscr{Q}_w} \mathrm{VaR}_\beta \left\{ \sup_{a \in \ell_{2e}} ||y_p(\delta)||^2_{\ell_2} \middle| \begin{array}{c} ||y_r(\delta)||^2_{\ell_2} \leq \varepsilon \\ \delta \in \Omega \end{array} \right\} \quad (1)$$

where $\mathscr{Q}_w \triangleq \{\mathscr{Q} | \mathscr{Q} \subset \mathscr{S}, |\mathscr{Q}| = n_w\}$, $\mathscr{S}$ is the set of sensors, and $\mathscr{Q}_w^*$ is the protected set of sensors, and VaR_β represents the Value-at-risk given $\beta \in [0,\ 1]$. Given a random variable X, $\mathrm{VaR}_\beta[X] \triangleq \inf\{x | \mathbb{P}_\Omega[X \leq x] \geq 1 - \beta\}$.

3 Contributions

Contribution 1*:* Given a set of protected sensors $\mathscr{Q}_w$, the problem of determining the VaR_β is computationally intense as Ω is continuous or discrete with large cardinality. Then, given ε_1 as the accuracy of approximation of $\mathbb{P}_\Omega$ in VaR, we show that the ε_1 approximate VaR_β can be determined by solving N_1 SDPs where $N_1 \propto \varepsilon_1^{-1}$ [1, Theorem 4.3].
Contribution 2*:* Using exhaustive search over the set $\mathscr{Q}_w$, we outline an algorithm to determine the set of protected sensors that minimizes the (approximate) VaR [1, Algorithm 1].

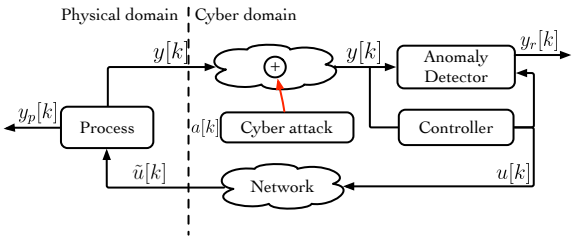

Figure 1: NCS under attack

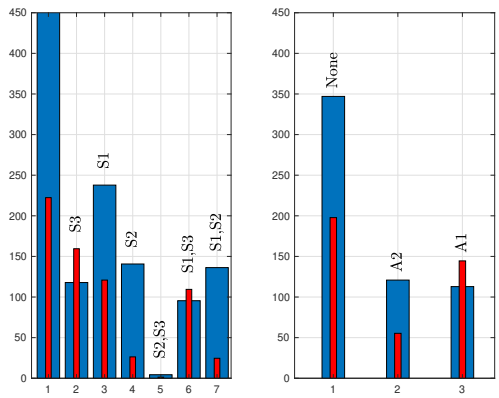

Figure 2: The $\mathrm{VaR}_{0.1}$ after protecting various combinations of sensors (actuators) are depicted on the left (right) figure in blue. The text on the top of each bar denotes the sensor (actuator) that is protected. The bar at position "1" of the figure on the left corresponds to the risk when none of the sensors are protected. The plots in red represent the impact on the nominal system after the security measures are allocated using the impact on the nominal system as a metric.

We numerically depict the difference when allocating using the impact on the nominal system in Figure 2 considering the system matrices in [1, Section VI].

Ongoing works

Some ongoing works include (*i*) considering CVaR as the risk metric, (*ii*) optimal design of controllers [2, 3], and (*iii*) considering an uncertain adversary [4].

References

[1] S. C. Anand, A. M. Teixeira, and A. Ahlén, "Risk assessment and optimal allocation of security measures under stealthy false data injection attacks," in *2022 IEEE Conf. on Control Technology and Appl. (CCTA)*, pp. 1347–1353, IEEE, 2022.

[2] S. C. Anand and A. M. Teixeira, "Joint controller and detector design against data injection attacks on actuators," *IFAC-PapersOnLine*, vol. 53, no. 2, 2020.

[3] S. C. Anand and A. M. H. Teixeira, "Risk-averse controller design against data injection attacks on actuators for uncertain control systems," in *2022 American Control Conference (ACC)*, pp. 5037–5042, 2022.

[4] S. C. Anand, A. M. Teixeira, and A. Ahlén, "Risk assessment of stealthy attacks on uncertain control systems," *arXiv preprint arXiv:2106.07071*, 2021.

Reformulations for data-driven stochastic optimization problems with structured ambiguity sets

Lotfi M. Chaouach[1], Dimitris Boskos[1], and Tom Oomen[1,2]

[1]Delft Center for Systems and Control, 2628CD, Delft, the Netherlands (e-mail: l.chaouach@tudelft.nl)
[2]Eindhoven University of Technology, the Netherlands

1 Introduction

Hedging against uncertainty in the choice of probability distributions is essential in data-driven stochastic optimization. Such choices need to account for limitations like the amount of available data, the dimensionality of the uncertainty, or the fact that the data might be corrupted, as these factors influence the accuracy of the inferred model and the reliability of the decision. Thus, it is required to derive trustworthy ambiguity sets from the available data, which contain the data-generating distribution with high probability. It is desirable to achieve this under the least possible amount of conservativeness and with tractability guarantees for the optimization problem.

2 Problem formulation

A typical data-driven distributionally robust optimization problem has the form

$$\min_{x\in\mathcal{X}} \max_{P_\xi\in\widehat{\mathcal{P}}^N} \mathbb{E}_{P_\xi}\left[f(x,\xi)\right], \tag{1}$$

where f is the cost function, x is the decision variable, $\xi\in\mathbb{R}^d$ is a random vector with distribution P_ξ, and $\widehat{\mathcal{P}}^N$ is an ambiguity set of distributions that is informed by N samples of ξ. A convenient choice to build $\widehat{\mathcal{P}}^N$ is by grouping the distributions around the empirical distribution P_ξ^N of the samples up to a given distance ε in the Wasserstein metric [2], which yields a ball $\mathcal{B}(P_\xi^N,\varepsilon)$. It is possible to tune the radius of this ball to guarantee that it contains the true distribution with prescribed confidence. However, this becomes very conservative when the dimension d of the uncertainty is high [1]. This curse of dimensionality can be overcome by exploiting independence between the lower-dimensional components of $\xi=(\xi_1,\dots,\xi_n)$ to build an ambiguity ball for each component and construct a product measure hyperrectangle

$$\mathcal{H}(\boldsymbol{P}_\xi^N,\boldsymbol{\varepsilon}) := \mathcal{B}(\hat{P}_{\xi_1}^N,\varepsilon_1)\otimes\ldots\otimes\mathcal{B}(\hat{P}_{\xi_n}^N,\varepsilon_n), \tag{2}$$

around the product of the empirical distributions of the components $\boldsymbol{P}_\xi^N$. Nevertheless, $\mathcal{H}$ is a non-convex set and tractable reformulations of (1) with $\widehat{\mathcal{P}}^N=\mathcal{H}(\boldsymbol{P}_\xi^N,\boldsymbol{\varepsilon})$ are only available when the cost is the sum or the product of functions that depend on the individual components $\xi_1,\dots,\xi_n$ [1].

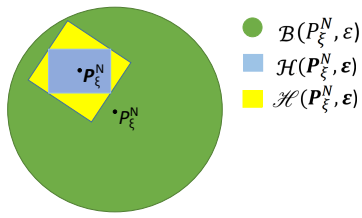

Figure 1: The multi-transport hyperrectangle contains the product measure hyperrectangle while enjoying the same statistical guarantees and similar size-reduction properties compared to the monolithic ambiguity ball.

3 Multi-transport ambiguity hyperrectangles

To obtain tractable reformulations for a broader class of functions, we propose another ambiguity set, which contains $\mathcal{H}$ without being much larger. Given a baseline measure μ and a vector of transport budgets $\boldsymbol{\delta}=(\delta_1,\dots,\delta_n)\in\mathbb{R}_+^n$, consider the set of transport plans

$$\Pi(\mu,\boldsymbol{\delta}) := \Big\{\pi\in\mathcal{P}_p(\mathbb{R}^d\times\mathbb{R}^d) : \mathrm{pr}_1(\pi)=\mu \\ \int \|\xi_k-\hat{\xi}_k\|^p d\pi(\hat{\xi},\xi)\le\delta_k,\ k=1,\dots,n\Big\}.$$

where $\mathcal{P}_p(\mathbb{R}^d\times\mathbb{R}^d)$ denotes the class of distributions on $\mathbb{R}^d$ with finite pth momen and $\mathrm{pr}_1(\pi)$ denotes the first marginal of π. We next introduce the *multi-transport* hyperrectangle

$$\mathscr{H}(\boldsymbol{P}_\xi^N,\boldsymbol{\varepsilon}) := \big\{P_\xi\in\mathcal{P}_p(\mathbb{R}^d) \text{ s.t } \exists\pi\in\Pi(\boldsymbol{P}_\xi^N,\boldsymbol{\varepsilon}) \\ \text{with marginal } P_\xi\big\}. \tag{3}$$

By exploiting the analysis in [2], we formulate a tractable dual problem for (1) with $\widehat{\mathcal{P}}^N=\mathscr{H}(\boldsymbol{P}_\xi^N,\boldsymbol{\varepsilon})$ and establish strong duality for any upper semi-continuous cost function f. In addition, $\mathscr{H}$ enjoys similar statistical properties to $\mathcal{H}$ with favorable size reduction rates (see Figure 1).

References

[1] Chaouach, L. M., Boskos, D., & Oomen, T., Uncertain uncertainty in data-driven stochastic optimization: Towards structured ambiguity sets. In 61st IEEE Conference on Decision and Control, Cancun, Mexico, 2022.

[2] J. Blanchet and K. Murthy, "Quantifying distributional model risk via optimal transport," Mathematics of Operations Research, vol. 44, no. 2, pp. 565–600, 2019.

Optimization Methods for Generalized Linear Models

Ousmane Diao
UCLouvain, Belgium
ousmane.diao@uclouvain.be

1 Introduction

One of the most important developments in statistics in the last few years has been the introduction and widespread use of *generalized linear models* (GLMs), as formulated by Nelder and Wedderburn [2].
A GLM respects the following steps:

- Random variable: $Y_t \sim f(Y_t;\mu_t)$, where Y_t is the explained variable with mean μ_t, f is the probability density or mass of an exponential family, and t is the observation time.
- Deterministic component: $\eta(X_t) = \sum_{j=1}^{k} \beta_j X_{tj}$, where η represents the linear predictor, X is the matrix of explanatory variables, the β_j's are regression coefficients, and k represents the number of explanatory variables.
- Link function
$$g(\mu_t) = \eta(X_t), \tag{1}$$
where g represents a transformer function, and depends on the probability distribution.

2 Methods

Consider the GLM with Poisson distribution which is probably the most used discrete distribution because of its simplicity [1]. It is often used to model the number of events occurring in a fixed period of time when the times at which events occur are independent. Its log-likelihood is

$$L(\beta, Y, X) = \sum_{t=1}^{n} \{Y_t \log(\mu_t) - \mu_t - \log(Y_t!)\}, \tag{2}$$

where $\mu_t = g^{-1}(\sum_{j=1}^{k} \beta_j X_{tj})$, according to (1). When $g = \log$, the Score function is $S(\beta) = X^T\{Y - \mu\}$, and the Hessian is $H(\beta) = -X^T W X$, where $W = \frac{\partial \mu}{\partial \eta}$ is the diagonal matrix with $[\frac{\partial \mu_t}{\partial \eta_t}]_{tt} = [\mu_t]_{tt} = [\exp(\eta_t)]_{tt}$ and called the iterative weights. We get the estimates denoted $\hat{\beta}$ by *maximum likelihood estimation*. Then, the *Newton-Raphson algorithm* [3] (method A) is commonly used to solve this kind of problem (i.e, root finding), which produces a sequence β_n according to

$$\beta_{n+1} = \beta_n - (H|_{\beta=\beta_n})^{-1} S(\beta_n) \tag{3}$$

until it stabilizes around a solution.

An alternative estimation method should be to compute $\hat{\beta}$ by applying the `scipy.optimize.fmin` method that uses the *downhill simplex algorithm* with the log-likelihood (2) as the objective function (method B).

3 Applications

The explained variable is malaria incidence ($Y_{o\{t\}}$) from the "Programme National de Lutte contre le Paludisme" (PNLP) of Senegal).[1] The explanatory variables are the rainfall (R), the temperature (T), the relative humidity (H) from meteoblue,[2] but also ($Y_{o\{t-1\}}$) and an artificial unity vector (I).

We conduct experiments to investigate the importance of the choice of the initial guess for method B. We observe that method B stays fixed when we initialize it with the outcome of method A and that it gives worse RMSE scores when initialized at others points; see Table 1. This suggests that the log-likelihood function (2) is a multimodal function with several local nonglobal minimizers.

Table 1: Results from the two methods in Dakar. RMSE_test is reported. The first part values is for A and the second for B (where β_init's and $\hat{\beta}$ (in dark) are reported).

β_R	β_T	β_H	$\beta_{Y_{o\{t-1\}}}$	β_I	RMSE
44.61	-134.89	52.75	0.41	-598.59	2689.7
44.61 **44.611**	-134.89 **-134.89**	52.75 **52.75**	0.41 **0.41**	-598.59 **-598.59**	**2689.7**
0 **45.79**	0 **-11.56**	0 **12.86**	0 **0.385**	0 **-52.64**	**2812.6**
2*44.61 **44.61**	-134.89*2 **-134.89**	2*52.75 **52.75**	2*0.41 **0.412**	-598.59*2 **-598.59**	**2689.7**
44.61^2 **13.24**	-134.89^2 **445.76**	52.75^2 **178.18**	0.41^2 **0.63**	-598.592^2 **-21179.73**	**5189.8**
44.61*10 **36.86**	-134.89*10 **-1616.72**	52.75*10 **136.07**	0.41*10 **1.22**	-598.59*10 **26872.21**	**3419.4**

References

[1] Sehlabana Makwelantle Asnath, Maposa Daniel, and Boateng Alexander. "Modelling Malaria Incidence in the Limpopo Province, South Africa: Comparison of Classical and Bayesian Methods of Estimation". In: *International Journal of Environmental Research and Public Health* 17.14 (2020). ISSN: 1660-4601.

[2] P.J Green and B.W. Silverman. "Nonparametric Regression and Generalized Linear Models". In: *Monographs on Statistics and Applied Probability*. 58. United States of America: CHAPMAN and HALL, 1994.

[3] Christian P. Robert and George Casella. "Deterministic numerical methods". In: *Monte Carlo Statistical Methods*. 2. New York, NY: Springer New York, 2004, p. 649. ISBN: 978-1-4757-4145-2.

[1] `https://www.dropbox.com/s/0p4uc2dihfhr9cb/Dakar.csv?dl=0`
[2] `https://www.meteoblue.com/historyplus`

Multi-period Optimal Bidding Policy with Energy Storage

Azin Khaleghi[1], Wouter Baar[1], Dario Bauso[1,2]
[1]Jan C.Willems Center for Systems and Control, ENTEG, Faculty of Science and Engineering, University of Groningen, 9747 AG, The Netherlands
[2]Dipartimento di Ingegneria, Università di Palermo, Palermo, 90128, Italy
Email: {a.khaleghi, w.baar, d.bauso}@rug.nl

1 Abstract

Motivated by the application in bidding in the two-settlement energy market, we formulate and solve the optimal bidding problem as a nonlinear constrained stochastic optimization problem. The novelty of our work is the usage of electricity storage devices in a multi-period bidding setting. In addition, we implement short-sighted versus far-sighted policies and investigate the impact of information on the risk-averse attitude of wind power producers.

2 Introduction

The large-scale integration of wind power into the electric grid is hampered by its inherent intermittency. A possible solution is letting wind power producers participate in the electricity pool, where participants have to offer bids on multiple forward (e.g. day-ahead) markets. The bids offered in such markets are financially binding and subject to penalties by the system operator for uninstructed deviations [1]. How should these bids be optimized to minimize quantity risk and maximize the expected profit of wind power producers? We answer this question by optimal bidding over a multi-period horizon and under uncertainty.

3 Problem Formulation

Let the finite sequence of wind outputs be given as $\{W(k), k = 0, \ldots, f-1\}$, where the wind output $W(k)$ is modelled as a stochastic variable characterized by Gaussian distribution. To characterize the expected profit, we must first consider the decision variable, which is the finite sequence of bids $C = \{C(k), k = 0, \ldots, f-1\}$ to be offered in a multi-period ahead market. The selling prices are denoted by the finite sequence $\{p_k, k = 0, \ldots, f-1\}$. The imbalance prices for the negative and the positive deviations from the offered bid in a multi-period ahead market are denoted by B and g, respectively. Let us define the storage dynamics as

$$\begin{cases} x(k+1) = x(k) + W(k) - C(k), \ \forall k = 0, \ldots, f-1, \\ x(0) = 0. \end{cases}$$

where $x(k)$ models the storage state in the interval k. The expected profit obtained by the wind power producer for the sequence of bids $C = \{C(k), k = 0, \ldots, f-1\}$ is given by

$$\mathbb{E}(\Pi(C)) = \sum_{k=0}^{f-1} p_k C(k) + \sum_{k=0}^{f} \mathbb{E}(B[x(k)]^- - [x(k)]^+). \qquad (1)$$

where $[y]^- := min\{y, 0\}$ and $[y]^+ := max\{y, 0\}$, $y \in \mathbb{R}$. The expected profit (1) consists of the revenue of selling electricity subtracted by the realized imbalances derived from the shortfall or the overage in the wind outputs. To maximize the expected profit (1), we have to find the optimal sequence of bids $C^* = \{C^*(k), k = 0, \ldots, f-1\}$ given by

$$C^* := \arg\max_{C \geq 0} \mathbb{E}(\Pi(C)).$$

To this aim, we consider three different decision-making policies, which we refer to as 'far-sighted', 'short-sighted', and 'short-sighted with information'. As the far-sighted policy decides for the whole horizon at once by maximizing (1) then the bid obtained by adopting this policy is optimal. On the other hand, the sequence $C^{sub(*)} = \{C^{sub(*)}(k), k = 0, \ldots, f-1\}$ which is returned by the short-sighted policy is sub-optimal as it maximizes (1) separately for every single interval k. An extension to the short-sighted policy is when the wind power producer has information on the storage state from the past interval.

4 Results

The following streamlines three main results of our work:

Theorem 1. *The following relation holds for the optimal and sub-optimal bids, respectively,*

$C^{sub(*)}(k) \geq C^*(k), \ \forall \ k = 0, ..., f-2,$

$C^{sub(*)}(f-1) \leq C^*(f-1).$

Theorem 2. *The following inequality holds for the expected profits of the far-sighted and the short-sighted policies:*

$\mathbb{E}(\Pi(C^*)) - \mathbb{E}(\Pi(C^{sub(*)})) \leq \bar{\beta}.$

Theorem 3. *The short-sighted policy with information is risk-averse; vice versa, the short-sighted policy is risk-tolerant.*

References

[1] D. Bauso, "Aggregate Energy Production in Wind Farms via Dynamic Robust Coalitional Games," in IEEE Control System Letters, vol. 6, pp. 55-60, 2022.

Model Predictive Control for Lane Merging Automation with Recursive Feasibility Guarantees

Merlijne Geurts*, Alexander Katriniok*,†, Emilia Silvas*,‡, Maurice Heemels*
*Eindhoven, University of Technology, Mechanical Engineering, Control Systems Technology, 5612 AZ, Eindhoven, The Netherlands,
†Ford Research & Innovation Center (RIC), Süsterfeldstraße 200, 52072 Aachen, Germany
‡TNO, Integrated Vehicle Safety, Automotive Campus 30, 5708 JZ, Helmond, The Netherlands
Email: {m.e.geurts, a.katriniok, e.silvas, m.heemels}@tue.nl

1 Introduction

Automated and cooperative driving holds the promise to improve road traffic by reducing traffic accidents, congestion, saving time and money for drivers and transportation companies, and by reducing pollution. The functionalities and algorithms that are needed in autonomous vehicles, need to cope with more complexity caused by mixed traffic (i.e. autonomous and manually driven cars), multiple road users interactions and prediction uncertainty. These challenges are observed in virtually all scenarios including lane merging scenarios. To address these aspects and improve vehicle safety, this paper will present a trajectory generation method that guarantees recursive feasibility in various lane merging scenarios.

2 Problem Formulation and Scenario

Current merging algorithms, using machine learning or optimization methods, are not always able to proactively make proper decisions, as they often exploit only knowledge about the current traffic situation and they do not use future predicted information about other road users. This may lead to conservative, uncomfortable or even unsafe behavior. Therefore, novel solutions are desired [1]. In this paper, safe trajectory generation algorithms for lane merging are introduced. The scenario, we are interested in considers an ego vehicle, which merges into a target lane with target vehicle, while keeping a safe distance depending on the ego vehicle position and speed (see Fig. 1).

3 Controller Design

In order to develop safe trajectory generation algorithms for merging, in this paper a model predictive controller (MPC) will be presented. It is assumed that we have perfect knowledge of the target vehicle's (future) trajectory (i.e. position, speed and acceleration). Further, the ego vehicle is only controlled longitudinally through its acceleration, while it moves along a priori known path. To ensure safe solutions, recursive feasibility guarantees are proven, by introducing a terminal set [2] depending on a lane merge in front or behind the target vehicle. Concluding, this will lead to a non-convex

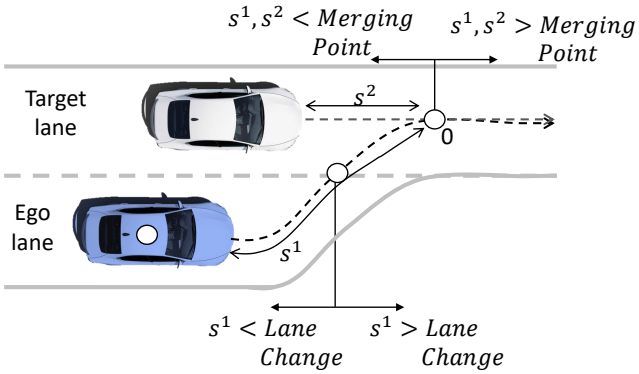

Figure 1: Set-up of the lane merging scenario.

mixed integer MPC optimization programs (MIQP-MPC) to be solved online, which is able to function during the longitudinal part of lane merge and continues with (Adaptive) Cruise Control-functionality ((A)CC) afterwards. The control scheme adheres to the safety constraints during the complete merging process.

4 Outlook

Future work will focus on considering different driving behavior of target vehicles with uncertainty regarding their predicted behaviors. In these scenarios we strive for guarantees regarding safe robust recursive feasibility.

Acknowledgment

This work is part of the research program AMADeuS with project number 18489, which is partly financed by the Netherlands Organisation for Scientific Research (NWO).

References

[1] M. Bouton, A. Nakhaei, D. Isele, K. Fujimura, & M.J. Kochenderfer (2020). Reinforcement Learning with Iterative Reasoning for Merging in Dense Traffic. In arXiv:2005.11895v1 [cs.AI] 25 May 2020.

[2] J. B. Rawlings, D. Q. Mayne, & M. Diehl, Model predictive control: Theory, computation, and design. Published 2017.

Adaptive Optimal Tracking Control of a Spacecraft with Constrained Inputs using Incremental Generalized Policy Iteration

Yifei Li
Section Control&Simulation
Delft University of Technology
Kluversweg 1, 2629HS Delft
The Netherlands
Email: Y.Li-34@tudelft.nl

Erik-Jan van Kampen
Section Control&Simulation
Delft University
Kluversweg 1, 2629HS Delft
The Netherlands
Email: E.van Kampen@tudelft.nl

1 Introduction

Exact modelling of a spacecraft is difficult because there are unknown uncertainties. Sloshing liquid fuel is one of the uncertainties that affect the motion of the spacecraft[1]. Current researches model the sloshing liquid as a pendulum analogous mechanical system, but controlling a spacecraft with sloshing liquid dynamics is still challenging. Incremental Generalized Policy Iteration(IGPI) is a model-free Reinforcement Learning(RL) method which can be used to design an adaptive optimal controller for nonlinear systems.

2 Spacecraft Model

The transitional models of rigid-body spacecraft and liquid fuel in longitudinal plane are derived by using Lagrange equations as in [1]. The control input forces and moments in the spacecraft attitude dynamical model are usually constrained because the actuators can only provide limited force and moment. As a result, the control performance degrades when the actuators can not provide enough controls.

3 Problem Formulation

The spacecraft dynamics can be modelled as a control-affine nonlinear dynamical system in discrete-time form as

$$x_{k+1} = f(x_k) + g(x_k)u(x_k) \tag{1}$$

where $x_k \in \mathbb{R}^n, f(x_k) \in \mathbb{R}^n, g(x_k) \in \mathbb{R}^{n\times m}$, and the input $u(x_k) \in \Omega_u$, where Ω_u is the compact of controls the actuator can provide. Assume that the system (1) is stabilizable on a prescribed compact set $\Omega \in \mathbb{R}^m$. The infinite-horizon cost function is given as

$$V(x_k) = \sum_{n=k}^{\infty} \left[Q(x_k) + u_k^T R u_k\right], \text{for all } \mathrm{x_k} \tag{2}$$

where $Q(x_k) > 0$ and $R > 0 \in \mathbb{R}^{m\times m}$.

4 Methods

To minimize the cost function in (2), the IGPI control algorithm is developed. Specifically, an incremental model of the nonlinear system is identified by using the Recursive Least Square(RLS) algorithm, then generalized policy iteration is used to numerically solve (2) until the solution converges to its local minimum. The critic and actor networks are used to approximate the cost function and control policy.

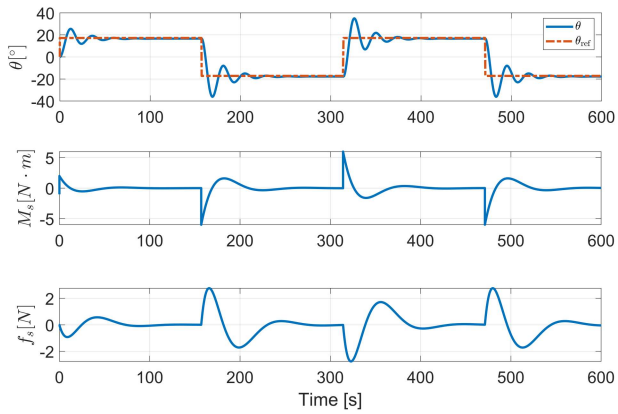

Figure 1: Pitch angle θ tracking and control inputs M_s and f_s

5 Results

Figure 1 shows that the pitch angle θ follows the reference in square-form θ_{ref} in 60s. When the sign of θ_{ref} turns, θ tracks θ_{ref} in less than 50s. The constrained inputs M_s and f_s change with the tracking error of θ. The bounds of constraints affect the tracking performance. This work considers the constraints in solving the constrained optimization problem in Eq.(1) and (2), leading to the fact that the control commands always satisfy the constraints, i.e. $u(x_k) \in \Omega_u$.

References

[1] Y.Zhou, E. van Kampen, Q.Chu. Incremental approximate dynamic programming for nonlinear adaptive tracking control with partial observability. Journal of Guidance, Control and Dynamics, 41(12), 2554-2567, 2018.

[2] R.S.Sutton, A.G.Barto. Reinforcement Learning: An Introduction, Cambridge, USA: The MIT Press, 1998.

Reinforcement learning-based method for automated calibration of an automotive thermal control system

Prasoon Garg* Lars Mulder* Emilia Silvas*,† Frank Willems*,†
*Dept. of Mechanical Eng., Eindhoven University of Technology, The Netherlands
†TNO Traffic and Transport, Helmond, The Netherlands (p.garg.1@tue.nl)

1 Introduction

Efficient operation of thermal systems in battery electric vehicles (BEVs) is necessary to maximize range of these vehicles. The state-of-the-art thermal system comprise of a heat pump system for battery heating and cooling, and heating, ventilation and air conditioning (HVAC) of the driver cabin [1]. Typically, classical feedback control is used for controlling actuators in the heat pump system such that the system efficiency characterized by coefficient of performance (COP) is maximized. The control parameters are tuned by experts, which requires large times and system knowledge due to a wide range of operating conditions. These conditions can be classified into several groups: 1) Ambient conditions such as temperature, pressure, humidity, 2) Driver settings such as cabin temperature and blower speed and 3) Vehicle speed. Moreover, system efficiency is limited due to the manual tuning process.

Reinforcement Learning (RL) is identified as a promising method for automating this calibration process, reducing the expert effort and maximizing system efficiency [2]. In RL, an agent interacts with the environment autonomously and learns to take actions that maximizes the control system performance. In this paper, an off-line calibration approach using RL is proposed to calibrate the reference setpoints for steady-state control of heat pump system in cabin cooling mode.

2 Method

The control scheme with RL-based calibration of reference setpoints is shown in Figure 1. A design

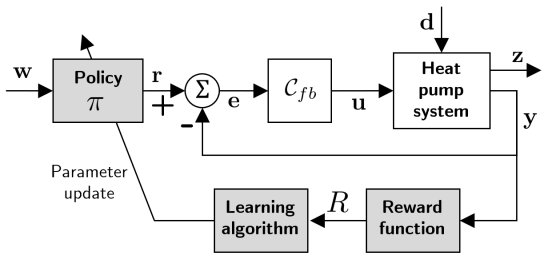

Figure 1: Proposed control system design. Components of RL-based method shown in gray.

process shown in Figure 2 is proposed to develop a RL-based calibration method. As a first step, the agent was trained in simulation environment assuming no noise in the signals. Thereafter, the impact of sensor noise is studied on the agent performance.

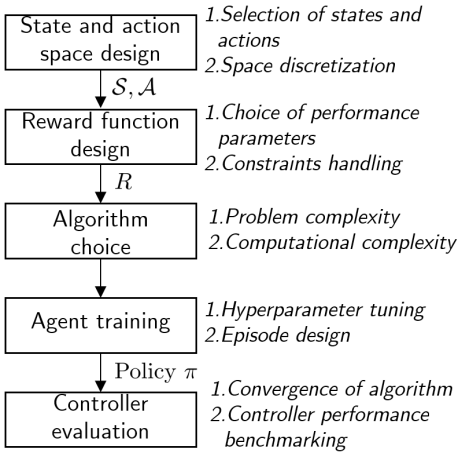

Figure 2: Main steps in the design of RL-based calibration method.

3 Results

For the studied 36 steady-state operating points, mean absolute error in COP reduced from 0.29 to 0.001 with respect to the achievable optimum COP by using the proposed RL-based calibration method in simulation. Moreover, the reference values are determined in an automated manner, therefore, significantly reducing the effort required by a calibration engineer.

In this paper, we will discuss the design process and the results of applying this method in the simulation environment. A comparison of system performance over a driving cycle and calibration effort is made between the developed method and the benchmark control system.

Acknowledgement

We thank DENSO for providing financial support and the Powertrain R&D team at DENSO Aachen Engineering Centre (AEC) for the constructive discussions for this study.

References

[1] M. Sukri, M. Musa, M. Senawi, and H. Nasution, "Achieving a better energy-efficient automotive air-conditioning system: a review of potential technologies and strategies for vapor compression refrigeration cycle," *Energy Efficiency*, vol. 8, no. 6, pp. 1201–1229, 2015.

[2] P. Garg, E. Silvas, and F. Willems, "Potential of machine learning methods for robust performance and efficient engine control development," *6th IFAC Conference on Engine Powertrain Control, Simulation and Modeling E-COSM*, vol. 54, no. 10, pp. 189–195, 2021.

Towards Self-learning Combustion Engines by Idealised Thermodynamic Cycle Tracking

Maarten Vlaswinkel* Frank Willems*,†
*Control Systems Technology, Eindhoven University of Technology (TU/e), The Netherlands
†TNO Automotive, Helmond, The Netherlands

1 Abstract

In the field of Internal Combustion Engines, the need for more efficient and cleaner engines is one of the main drivers for innovation. Roughly speaking, there are two ways to achieve this: 1) move to more efficient and cleaner combustion concepts, and 2) improve the control methods to become self-learning. In practice, these two approach are intertwined. More efficient and cleaner combustion concepts tend to be more sensitive to ambient conditions, fuel quality and engine operating conditions, which requires more advanced control concepts such as self-learning. On the other hand, integrating self-learning concepts into existing combustion concepts only increases efficiency by a limiting factor, which requires the development of more efficient and cleaner combustion concepts.

Current feedback control strategies are based on feedback signals related to intake s_{im} or exhaust manifold conditions (i.e., pressure or temperature), combustion phasing and power output [1]. Reference mappings for these references signals are determined by optimising the combusting process in a lab environment for a range of operating conditions given a total fuel energy Q_{fuel} as demanded by the driver. In turn, the reference signals, combined with feedback controller methods, are used to determine the fuel settings u_{fuel} (i.e., quantity and timing of injection). For more efficient combustion concepts, which are more sensitive to ambient conditions and fuel quality, this method becomes impracticable. It will take calibration experts too much time to calibrate a single engine [2]. Furthermore, directly relating the current feedback signals to efficiency and emissions is not trivial.

In this talk, we will presented a novel set of feedback signals $w(u_{\text{fuel}}, s_{\text{im}})$ that are based on the Principle Component Decomposition (PCD) of the measured cylinder pressure $p(\theta)$ [3]. These feedback signals give the opportunity to directly shape the heat release, hence they have a direct relation to efficiency and emissions. Fig. 1 shows the proposed control architecture. A quadratic cost function $J_{\text{ITC}}(w(u_{\text{fuel}}, s_{\text{im}}))$ with respect to $w(u_{\text{fuel}}, s_{\text{im}})$ will be formulated combing the PCD of $p(\theta)$ and an Idealised Thermodynamic Cycle (ITC) ($p_{\text{ITC}}(\theta, Q_{\text{fuel}})$ and $w_{\text{ITC}}(Q_{\text{fuel}})$) at a given Q_{fuel}. This cost function captures the theoretically possible efficiency gains. To guarantee mechanically safe operation, a set of linear inequality constraints in $w(u_{\text{fuel}}, s_{\text{im}})$ are included.

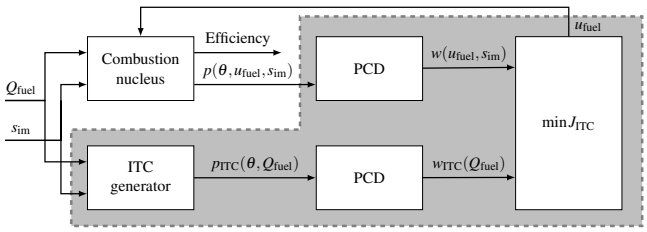

Figure 1: Schematic of the proposed fuel-path control architecture with Principle Component Decomposition (PCD) and an Idealised Thermodynamic Cycle (ITC) to regulate the combustion nucleus.

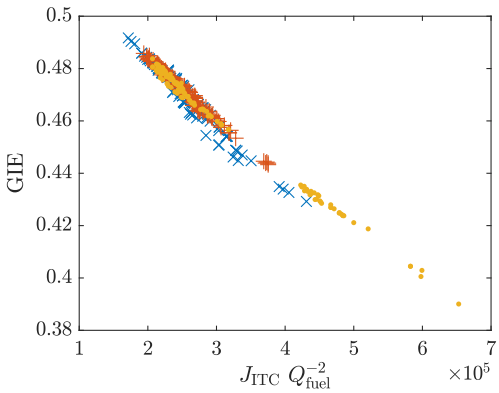

Figure 2: Cost function J_{ITC} scaled with squared fuel energy Q_{fuel}^2 against Gross Indicate Efficiency (GIE) with intake manifold pressures of (2.100 ± 0.025) bar ($\times$), (2.300 ± 0.025) bar ($+$), and (2.500 ± 0.025) bar ($\cdot$).

Fig. 2 shows J_{ITC} scaled with squared fuel energy Q_{fuel}^2 against the Gross Indicated Efficiency (GIE) for different intake manifold pressures and operating conditions. It shows that minimising J_{ITC} results in an increase of the efficiency. Therefore, we hypothesise that J_{ITC} and the novel feedback signals are a good candidate that brings us closer towards self-learning engines.

References

[1] J. Verhaegh, F. Kupper, and F. Willems, "Data-Driven Air-Fuel Path Control Design for Robust RCCI Engine Operation," Energies, vol. 15, no. 6, Art. no. 6, Jan. 2022, doi: 10.3390/en15062018.

[2] F. Willems, "Is Cylinder Pressure-Based Control Required to Meet Future HD Legislation?," IFAC-PapersOnLine, vol. 51, no. 31, Art. no. 31, Jan. 2018, doi: 10.1016/j.ifacol.2018.10.021.

[3] M. Vlaswinkel, B. de Jager, and F. Willems, "Data-Based In-Cylinder Pressure Model including Cyclic Variations of an RCCI Engine," IFAC-PapersOnLine, vol. 55, no. 24, pp. 13–18, 2022, doi: 10.1016/j.ifacol.2022.10.255.

Context-Aware Motion Planning: A Risk-Based Approach

C. van der Ploeg[1,2], E. Silvas[1,2], P. Mohajerin Esfahani[3], N. van de Wouw[2]

[1] Netherlands Organisation for Applied Scientific Research, Integrated Vehicle Safety Group, 5700 AT Helmond, The Netherlands

[2]Department of Mechanical Engineering, Technische Universiteit Eindhoven, P.O. Box 513, 5600 MB Eindhoven, The Netherlands

[3]Delft Center for Systems and Control, Delft University, Mekelweg 2, 2628 CD Delft, The Netherlands

Email: C.J.v.d.Ploeg@tue.nl

1 Introduction

At the core of safe autonomous driving lies the capability of an autonomous vehicle (AV) to make safe and responsible decisions while progressing toward a point of interest. In literature, multiple layers of planning are proposed, in this work we focus on the problem of local trajectory planning, i.e., planning a trajectory within a horizon of $3-10$s which respects the infrastructure, the surrounding (possibly dynamic) objects, and any other information which could improve the safety, acceptance, and efficiency of the planning result. This work suggests using contextual information, i.e., information that is not directly visible or measurable but can be derived using prior knowledge, such as explicit observations, traffic rules, or social norms. This information is deployed in the form of risk fields in a model-predictive control (MPC) planning framework.

2 Problem statement

Consider a risk-based model-predictive planner, as proposed in [1]. Limitations imposed on this work are clear, namely that the planned trajectory relies purely on explicit information, i.e., observations or predictions of the infrastructure and observable objects. In this work, we aim to incorporate contextual information, which borrows its definition from [2]: " *Any information that can be used to characterize the situation of an entity. An entity is a person, place, or object that is considered relevant to the interaction between a user and an application, including the user and applications themselves.*".

A first example of this implicit type of information is object context. Based on explicit observations of objects and their surroundings, one could deduce how to treat such an object. For example, within an urban area, it is acceptable to drive over a pile of leaves or a plastic bag. However, the observation of an elephant would be highly unlikely and should be treated with caution, hence, it would impose high risk. A second example of implicit information is the presence of unseen objects. In urban environments, many areas may be obstructed by other vehicles, parked objects or buildings. It is up to the AV to anticipate possible hidden objects, which could appear from obstructed areas. The primary research questions revolve around the methodology to deduce different types of contextual information, and how to capture them in the model-predictive risk-driven program.

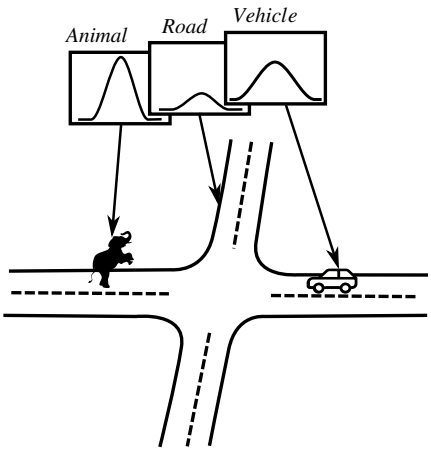

Figure 1: Depiction of entities and their induced risk within a trajectory generation problem.

3 Proposed solution

We propose to incorporate contextual information in the objective function of the MPC, by augmenting the risk fields from [1]. Each risk field, surrounding the infrastructure, observed objects, or spaces where hidden objects could reside, is characterized by the shape and size of the entity. The identification and characterization of risk-fields can be done by comprehending the situation and reasoning about its implications. Through discrete convolution of the entities shape with the proposed "*risk-kernel*" (as depicted in Fig. 1), a risk-field is obtained which can be incorporated in the model-predictive program.

References

[1] C van der Ploeg, R. Smit, A. Teerhuis, and E. Silvas. “Long Horizon Risk-Averse Motion Planning: A Model-Predictive Approach”. In: *2022 IEEE 25th International Conference on Intelligent Transportation Systems (ITSC)*. 2022, pp. 1–8.

[2] Anind K. Dey. “Understanding and Using Context”. en. In: *Personal and Ubiquitous Computing*. Vol. 5. 1. 2001, pp. 4–7.

Evaluation of Autonomous Driving Controllers for Human-like Performance

Flavia Sofia Acerbo[1,2,3], Jan Swevers[1,4], Tinne Tuytelaars[2] and Tong Duy Son[3]
[1] MECO Research Team, Department of Mechanical Engineering, KU Leuven, Belgium
[2] PSI Research Team, Department of Electrical Engineering, KU Leuven, Belgium
[3] Siemens Digital Industries Software, Leuven, Belgium [4] Flanders Make@KU Leuven, Belgium
Email: flavia.acerbo@siemens.com

1 Introduction

Autonomous driving controllers should be evaluated on their ability to imitate human-like characteristics that can influence passenger comfort and safety perception. This is especially important for imitation learning (IL) policies from human demonstrations. This work compares human lane keeping demonstrations to MPC-based IL policies by measuring average driver performance and analyzing derived motion cues.

2 Human-like Performance Metrics for Lane Keeping

We evaluate human-like performance on the closed-loop simulations by metrics such as:

1. **Imitation by closed-loop (CL) likelihood**: the human lateral deviation from the track centerline d^* is modeled as a Gaussian Process. Then, we compute the mean likelihood of each d point.
2. **Lateral deviation from the centerline** (d): mean and standard deviation, in meters.
3. **Steering Reversal Rate** (SRR): the number, per minute, of steering wheel angle reversals larger than 5 degrees, as defined by [1].

Then, we validate whether variations in the selected metrics are reflected onto human-perceivable variables on a hexapod driving simulator i.e., the platform roll angle computed by an adaptive washout motion cueing algorithm [2] from the high-fidelity simulated vehicle motion in Simcenter Amesim.

3 Evaluation of MPC-based Imitation Learning Policies

In Table 1 it can be seen that using a higher level neural network on top of MPC (NN-MPC) yields a more human-like d in its standard deviation, and more human-like SRR. However, when the prediction horizon of the MPC is reduced (d_{la}, in meters), *causal confusion* yields worse performance. To reduce this effect, we replace open-loop algorithms such as behavioral cloning (BC) or supervised learning (SL) with state cloning (SC), which employs the MPC model for closed-loop training on the states. In Figure 1 it is shown an example of the motion cueing roll angle transient behavior during a change in curvature: the MPC shows a steeper curve transient, which can be perceived as more aggressive, while the NNMPC policies show a smoother change, comparable to the human one.

Configuration			**Imitation**	**Human-like**	
IL Policy		d_{la}		d	SRR
MPC	BC	30	**0.92**	-0.44 $\pm$ 0.06	37.5
NN-MPC	SL	30	**0.98**	**-0.53 $\pm$ 0.29**	**25.83**
NN-MPC	SL	9.72	0.48	-0.50 $\pm$ 0.76	**17.50**
NN-MPC	SC	9.72	**0.93**	**-0.46 $\pm$ 0.17**	**23.33**
Human			1.22	-0.54 $\pm$ 0.39	19.5

Table 1: Evaluation metrics for different MPC-based policies and human demonstrations.

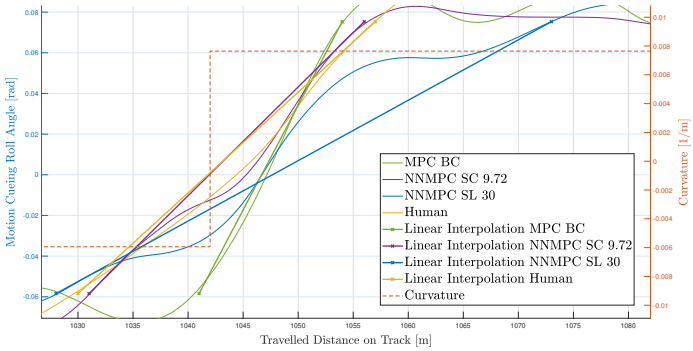

Figure 1: Motion cueing roll angle, highlighting the difference in the transient slopes through linear interpolation (lines with the same colors).

References

[1] Markkula, G. and Engström, J., "A steering wheel reversal rate metric for assessing effects of visual and cognitive secondary task load," Proceedings of the 13th ITS World Congress, 2006.

[2] Garrett, N. J., and Best, M., "Driving simulator motion cueing algorithms–a survey of the state of the art", Proceedings of the 10th International Symposium on Advanced Vehicle Control (AVEC), 2010.

This project has received funding from the Flemish Agency for Innovation and Entrepreneurship (VLAIO) under the Baekeland Mandaat No. HBC.2020.2263 (MIMIC) and has been supported by the European Union's Horizon 2020 research and innovation program under the Marie Skłodowska-Curie grant agreement No. 953348 (ELO-X).

Safety Envelope for Orthogonal Collocation Methods in Embedded Optimal Control

Jean Pierre Allamaa [1,2], Panagiotis Patrinos [2], Herman Van der Auweraer [1], Tong Duy Son [1]
[1] Siemens Digital Industries Software, 3001, Leuven, Belgium
[2] Dept. Electr. Eng. (ESAT) - STADIUS research group, KU Leuven, 3000 Leuven, Belgium
Email: jean.pierre.allamaa@siemens.com

1 Introduction

Orthogonal collocation methods are direct simultaneous approaches for solving optimal control problems (OCP). A high solution accuracy is achieved with few optimization variables, making it favorable for embedded NMPC applications. However, collocation approaches lack a safety guarantee as inequality constraints are only imposed on a finite number of points. In this work we propose a method to efficiently create a convex safety envelope containing the trajectory such that the solution spline satisfies the OCP constraints entirely. We show that our method, Spectral Orthogonal Collocation with Safety Envelope (SOCSE) has comparable computational performance to pseudospectral (PS) approaches and approximates the original OCP more accurately and 9 times faster than multiple-shooting for autonomous driving applications, without adding complexity.

2 Safety envelope through polynomial bounds

The collocation approach does not require an embedded ODE solver as we set the trajectories as a combination of orthogonal polynomials with basis $\mathscr{L}_k$, the Legendre polynomial of degree k to approximate the solution $\tilde{x}(\tau)$ and $\tilde{u}(\tau)$ by a Legendre-spline of degree M, by solving for α in:

$$\tilde{x}(\tau) = \sum_{j=0}^{M} \alpha_j \mathscr{L}_j(\tau) = \alpha^\top \mathbf{L}_M v(\tau), (\tau \in [-1,1]), \quad (1)$$

where $v(\tau) = \begin{bmatrix} 1 & \tau & \tau^2 & \cdots & \tau^M \end{bmatrix}^\top$. Let $P(t) = \sum_0^M a_j t^j$ be a polynomial with real coefficients a_j. It follows from [1] for the extrema $\underline{P}$ and $\overline{P}$ of $P(t)$, and for $j = 0,\ldots,M$:

$$\min\{b_j\} \leq \underline{P} \leq P(t) \leq \overline{P} \leq \max\{b_j\},\ 0 \leq t \leq 1 \quad (2)$$

The Bernstein extrema estimations b_j for $j = 0,\ldots,M$ are:

$$b_j = \sum_{k=0}^{M} a_j \binom{j}{k} \Big/ \binom{M}{k} \rightarrow b = \mathscr{B}a,\ \mathscr{B} \in \mathbb{R}^{(M+1)\times(M+1)} \quad (3)$$

The spline is contained in it's convex envelope defined by the maximum and minimum elements of $\mathscr{P}$:

$$\mathscr{P} = \mathscr{B}\mathscr{E}^\top \mathbf{L}_M^\top \alpha = \mathscr{C}_M \alpha. \quad (4)$$

$\mathscr{E}$ is a time domain transformation, $\mathbf{L}_M$ stacks the coefficients of $\mathscr{L}_k | k = 0,\ldots,M$, and $\mathscr{C}_M$ is computed offline.

Table 1: Comparison of the different methods for solving the OCP (MS: Multiple shooting, SS: Single shooting)

Method	Solve time (s)	Optimal cost error	ODE solution error
MS-50steps	0.876	1.978%	-
SS-50steps	5.668	1.978%	-
SOCSE $\mathscr{O}(5)$	**0.102**	**-0.009%**	**5.978e-04**

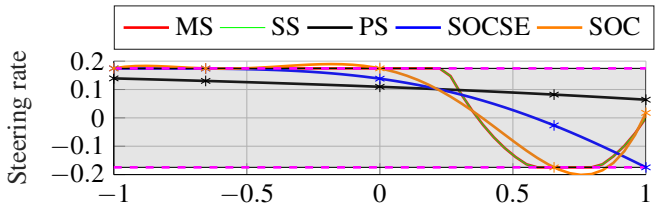

Figure 1: NMPC optimal control action spline (Blue: SOCSE degree 5 (our), Grey: convex safety envelope, Dashed pink: OCP bounds, collocation points in asterisk)

3 Real-time NMPC for autonomous valet parking

We validate our method in a valet parking autonomous driving, by setting a path following and position tracking formulation using an augmented dynamic bicycle model with 10 states and 2 control inputs. The horizon length is 3 seconds. The dynamic constraints are evaluated at the Legendre-Gauss-Lobatto spectral collocation points including the boundaries $[-1,1]$. The state and control inequality constraints are linear in the coefficients α as set in (4), and guarantee feasibility without analytical derivation of the extrema at runtime inside the NLP (e.g. $\underline{x} \leq \mathscr{C}\alpha \leq \bar{x}$). Without a safety envelope (SOC), the steering rate spline solution violates the boundaries between the last two collocation points, even though the OCP is feasible as in Figure 1. Our method solve this issue, and is order faster and more accurate than shooting methods with fine grid.

Acknowledgements

This project has received funding from the European Union's Horizon 2020 research and innovation programme under the Marie Skłodowska-Curie grant agreement ELO-X No 953348

References

[1] O. S. G. T. Cargo, "The Bernstein form of a polynomial," *Journal of Research of the Notional Bureau of Standard section B.*, vol. 70B, pp. 79–81, 1966.

Uniform stability of switched nonlinear systems : Toward a Lie-algebraic condition via the Koopman operator approach

Christian Mugisho Zagabe and Alexandre Mauroy
Namur Institute for Complex Systems (naXys), Department of Mathematics
University of Namur, Rue J. Grafé 2, B-5000 Namur, Belgium
Email: christian.mugisho@unamur.be and alexandre.mauroy@unamur.be

1 Introduction

Switched systems consist of a finite set of dynamical systems and a switching signal indicating which system is activated. Their stability properties are not intuitive. Indeed, with two individually stable systems, one can construct a signal that makes the whole system unstable. The main goal of uniform stability theory is to find sufficient (and/or necessary) conditions that make the whole system stable for all possible switching laws. In [1] it has been proved that for a switched linear system, the solvability property of the Lie algebra generated by Hurwitz matrices is a sufficient condition for global uniform asymptotic stability (GUAS). In [2], the author proposed an open problem to find which condition of the Lie algebra (of vector fields) can be used to guarantee the GUAS property of switched nonlinear systems.

The Koopman operator approach can be seen as a "global linearization" of nonlinear dynamics and therefore can be used to induce global properties such as global stability. Using the Koopman operator approach, we provide a partial answer to the open problem in [2]. Our result is related to the dynamics on the polydisc and shows that a sufficient condition for GUAS (on a specific invariant set) follows from the solvability of the Lie algebra generated by Hurwitz Jacobian matrices of the vector fields. More precisely, we construct a common Lyapunov function (CLF) for switched nonlinear systems, which is convergent in a specific region of the state space. See [5] for more details.

2 Preliminary concepts

The *Hardy space* on the polydisc $\mathbb{D}^n$ is the Hilbert space

$$\mathbb{H}^2(\mathbb{D}^n) = \left\{ f : \mathbb{D}^n \longrightarrow \mathbb{C}, \text{holomorphic} : \|f\|^2 < +\infty \right\},$$

with the norm $\|f\|^2 = \sum_{\alpha\in\mathbb{N}^n} |a_\alpha|^2$ and the scalar product $\langle f, g\rangle = \sum_{\alpha\in\mathbb{N}^n} a_\alpha \bar{b}_\alpha$ for $f(z) = \sum_{\alpha\in\mathbb{N}^n} a_\alpha z^\alpha$ and $g(z) = \sum_{\alpha\in\mathbb{N}^n} b_\alpha z^\alpha$. Note that $\mathbb{H}^2(\mathbb{D}^n)$ is a reproducing Kernel Hilbert space and its (Cauchy) Kernel allows us to define the *evaluation functional* $\langle k_z, f\rangle = f(z)$. See [4] for more details.

Consider a switched nonlinear system

$$\left\{ \dot{z} = F_i(z), \quad z \in \mathbb{D}^n, \quad F_i \in \mathscr{C}^1 \right\}_{i=1}^m, \tag{1}$$

where each vector field F_i generates a flow $\varphi_i^t : \mathbb{D}^n \to \mathbb{D}^n$, with $t \in \mathbb{R}^+$. For a fixed F_i, the *semigroup of Koopman operators* on $\mathbb{H}^2(\mathbb{D}^n)$ is the family of operators $(U_i^t)_{t\geq 0}$:

$$U_i^t : \mathbb{H}^2(\mathbb{D}^n) \to \mathbb{H}^2(\mathbb{D}^n) : U_i^t f = f \circ \varphi_i^t.$$

The *Koopman generator* of $(U_i^t)_{t\geq 0}$ is the operator

$$L_{F_i} f = F_i \cdot \nabla f, \; f \in \mathscr{D}_i \subset \mathbb{H}^2(\mathbb{D}^n),$$

where the domain $\mathscr{D}_i = \left\{ f \in \mathbb{H}^2(\mathbb{D}^n) : F_i \cdot \nabla f \in \mathbb{H}^2(\mathbb{D}^n) \right\}$ is dense on $\mathbb{H}^2(\mathbb{D}^n)$. The Koopman operator U_i^t and its associated Koopman generator L_{F_i} are both linear on $\mathbb{H}^2(\mathbb{D}^n)$. The corresponding *Koopman switched system* of (1) is the switched linear infinite-dimensional system defined by

$$\left\{ \dot{f} = L_{F_i} f, \quad f \in \mathscr{D} = \bigcap_{i=1}^m \mathscr{D}_i \right\}_{i=1}^m. \tag{2}$$

In this study we assume that the origin 0 is the unique (hyperbolic) equilibrium point in $\mathbb{D}^n$ and that $\mathbb{D}^n$ is forward invariant with respect to the flow φ_i^t of F_i.

3 Brief description of the main result

Under some technical assumptions on F_i, our main result is summarized with the following main steps :

- Thanks to the Koopman operator approach, a given dynamics (1) on $\mathbb{D}^n$ is turned into the dynamics (2) on $\mathbb{H}^2(\mathbb{D}^n)$.
- The solvability assumption on the Lie algebra generated by Hurwitz Jacobian matrices $JF_i(0)$ implies there exists a common infinite invariant flag (generated by the monomials $\{z^\alpha : \alpha \in \mathbb{N}^n, |\alpha| \geq 1\}$) of the ajoints $L_{F_i}^*$ of L_{F_i}.
- With the infinite invariant flag, we can construct a CLF of (2) and
- the evaluation functional k_z allows us to obtain a CLF of (1) on a specific polydisc $\mathbb{D}^n(0,\rho) = \{z \in \mathbb{C}^n : |z_i| < \rho, i = 1, \cdots, n\}$ with $\rho \in]0,1]$. Therefore, we prove the GUAS property of (1) on $\mathbb{D}^n(0,\rho)$.

From the main result, two specific cases are studied in practice. First, we may determine the GUAS property with $\rho = 1$ when F_i in (1) are polynomials. Second, the GUAS property can be obtained with $\rho \in]0,1[$ when a diagonal dominance condition is assumed on the Jacobian matrices of analytic (in general) F_i.

References

[1] D. Liberzon, J. Hespanha and A. Morse, *Stability of switched linear systems: a Lie-algebraic conditions*. Systems and Control Letters, vol. 37, pp. 117-122, 1999.

[2] D. Liberzon, *Lie algebras and stability of switched nonlinear systems*, in *Unsolved problems in mathematical systems and control theory*, 203–207, 2004, Princeton University Press Princeton, NJ/Oxford.

[3] A. Mauroy, I. Mezić and Y. Susuki, *The Koopman Operator in Systems and Control Concepts, Methodologies and Applications*, Springer, 2020.

[4] W. Rudin, *Function Theory in Polydiscs*, Benjamin, New York, 1969.

[5] C. M. Zagabe and A. Mauroy, *Global uniform stability of switched nonlinear systems in the Koopman operator framework*, https://doi.org/10.48550/arXiv.2301.05529.

Nonlinear singular switched systems in discrete-time: solution theory and (incremental) stability under fixed switching signals

Sutrisno[1], Hao Yin[2], Stephan Trenn[1], Bayu Jayawardhana[2]
[1]Bernoulli Institute for Mathematics, CS and AI, University of Groningen, The Netherlands
[2]Engineering and Technology Institute, University of Groningen, The Netherlands
Email: [s.sutrisno, hao.yin, s.trenn, b.jayawardhana]@rug.nl

1 Introduction

We consider the homogeneous nonlinear singular switched system (NSSS) in discrete time of the form

$$E_{\sigma(k)}x(k+1) = F_{\sigma(k)}(x(k)), \tag{1}$$

where $k \in \mathbb{N}$ is the time step/instant, $x(k) \in \mathbb{R}^n$ is the state, $\sigma : \mathbb{N} \to \{0,1,2,...,\mathrm{p}\}$ is the switching signal determining which mode $\sigma(k)$ is active at time instant k, $E_i \in \mathbb{R}^{n\times n}$ are singular, and $F_i(x) = (f_{1,i}(x), f_{2,i}(x), ..., f_{n,i}(x))^\top$ are vector valued functions of nonlinear functions $f_{j,i} : \mathbb{R}^n \to \mathbb{R}$. Define $\mathscr{S}_i := \{x \in \mathbb{R}^n : F_i(x) \in \operatorname{im} E_i\}$. Inspired by the solution theory for singular linear switched systems in [1], we study the solution theory and (incremental) stability for this system class under the following assumption.

Assumption 1.1. *$\mathscr{S}_i$ are subspaces in $\mathbb{R}^n$.*

2 Solution Theory

We consider the following solvability notion in studying the solution of (1) as well as the stability analysis.

Definition 2.1. *The NSSS* (1) *is* solvable *w.r.t. a fixed and known switching signal σ if, for all $k_0, k_1 \in \mathbb{N}$, $k_1 > k_0$ and for all $x_{k_0} \in \mathscr{S}_{\sigma(k_0)}$ there exists a unique solution of* (1) *under σ considered on $[k_0, k_1]$ with $x(k_0) = x_{k_0}$.*

The solvability notion above requires a unique solution for any time interval, and, in particular, the state at the current time instant depends only on the past states i.e. causal. The following theorem provides a necessary and sufficient for the solvability of system (1) where the proof relies on the projector lemma in [2].

Theorem 2.2. *The NSSS* (1) *under Assumption 1.1 is solvable w.r.t. a fixed and known switching signal $\sigma : \mathbb{N} \to \{0,1,...,\mathrm{p}\}$ if, and only if,*

$$\mathscr{T}_{\sigma(k)} \subseteq \mathscr{S}_{\sigma(k+1)} \oplus \ker E_{\sigma(k)} \quad \text{for } k = 0,1,2,\dots \tag{2}$$

where $\mathscr{T}_i = \{E_i^+ F_i(\varsigma) | \varsigma \in \mathscr{S}_i\}$. Furthermore, if solvable, its solution satisfies the surrogate ordinary switched system

$$x(k+1) = \Phi_{\sigma(k+1),\sigma(k)}(x(k)),\ \forall k \in \mathbb{N} \tag{3}$$

where $\Phi_{i,j}(x(k)) := \Pi_{\mathscr{S}_i}^{\ker E_j} E_j^+ F_j(x(k))$, E_j^+ is a generalized inverse of E_j and $\Pi_{\mathscr{S}_i}^{\ker E_j}$ is the canonical projector from $\mathscr{S}_i \oplus \ker E_j$ to $\mathscr{S}_i$.

3 (Incremental) Stability

By utilizing the surrogate switched system (3), we provide the following theorem and conjecture for Lyapunov stability and incremental stability analysis of system (1).

Theorem 3.1 (Lyapunov stability)**.** *Consider the NSSS* (1) *under Assumption 1.1 with a fixed and known switching signal σ via its surrogate ordinary switched system* (3)*, and assume $x = 0$ is its equilibrium. Assume for all $i \in \{0,1,...,\mathrm{p}\}$, $\Phi_i : \mathscr{S}_i \to \mathbb{R}^n$ is continuous on $\mathscr{S}_i \subsetneq \mathbb{R}^n$ and each mode is (asymptotically) stable with corresponding Lyapunov function V_i. If the following conditions hold:*

(i) $V_i(x) = V_j(x)\ \forall x \in \mathscr{S}_i \cap \mathscr{S}_j,\ \forall i,j \in \{0,1,...,\mathrm{p}\}$

(ii) $V_{\sigma(k+1)}(\Phi_{\sigma(k+1),\sigma(k)}(x)) - V_{\sigma(k)}(x)(<) \le 0,\ \forall x \in \mathscr{S}_{\sigma(k)} - \{0\},\ k = 0,1,...$

then $x = 0$ is (asymptotically) stable w.r.t. σ.

Definition 3.2. *The NSSS* (1) *is called* locally asymptotically incrementally stable *on $\mathscr{S}_{\sigma(0)}$ w.r.t. the fixed switching signal σ if there exists $\beta \in \mathscr{KL}$ such that*

$$||x'(k;x_0') - x''(k;x_0'')|| \le \beta(||x_0' - x_0''||, k) \tag{4}$$

for all $x_0', x_0'' \in \mathscr{S}_{\sigma(k_0)}$ and all $k \ge 0$.

Conjecture 3.3 (Incremental stability)**.** *Consider the NSSS* (1) *under Assumption 1.1. Assume each mode is locally asymptotically incrementally stable on $\mathscr{S}_i$ with the corresponding incremental Lyapunov function $V_i : \mathscr{S}_i \times \mathscr{S}_i \to \mathbb{R}_{\ge 0}$ and class-$\mathscr{K}_\infty$ functions α_{1i}, α_{2i} and α_{3i} satisfying, for each $i \in \{0,1,\dots,\mathrm{p}\}$,*

$$\alpha_{1i}(||x' - x''||) \le V_i(x', x'') \le \alpha_{2i}(||x' - x''||),$$
$$V_i(\Phi_i(x'), \Phi_i(x'')) - V_i(x', x'') \le -\alpha_{3i}(||x' - x''||).$$

for all $x', x'' \in \mathscr{S}_i$. If the following conditions hold:

1. *For all $x, x', x'' \in \mathscr{S}_i \cap \mathscr{S}_j$ and all $i, j \in \{0,1,...,\mathrm{p}\}$,*
$$V_i(x', x'') = V_j(x', x''),\ \alpha_{1i}(x) = \alpha_{1j}(x),$$
$$\alpha_{2i}(x) = \alpha_{2j}(x),\ \alpha_{3i}(x) = \alpha_{3j}(x)$$
2. *For $k = 0,1,...,$*
$$V_{\sigma(k+1)}(\Phi_{\sigma(k+1),\sigma(k)}(x'), \Phi_{\sigma(k+1),\sigma(k)}(x''))$$
$$-V_{\sigma(k)}(x', x'') \le -\alpha_3(||x' - x''||)\ \forall x', x'' \in \mathscr{S}_{\sigma(k)}$$
$$\text{with } \alpha_3 : \mathbb{R}^n \to \mathbb{R},\ \alpha_3(x) = \begin{cases} \alpha_{3i}(x) & \text{if } x \in \mathscr{S}_i \\ 0 & \text{otherwise} \end{cases}$$

then system (1) *is* locally asymptotically incrementally stable *on $\mathscr{S}_{\sigma(0)}$ w.r.t. σ.*

References

[1] Pham Ky Anh, et al. "The one-step-map for switched singular systems in discrete-time." *Proc. 58th IEEE Conf. Decision Control (CDC) 2019.*

[2] Sutrisno, Stephan Trenn. "Nonlinear Switched Singular Systems in Discrete-time: The One-step Map and Stability Under Arbitrary Switching Signals." *Preprint.*

Embedding of Polynomial Nonlinear Systems into Finite Dimensional Koopman Representations

Lucian Cristian Iacob[a], Maarten Schoukens[a] and Roland Tóth[a,b]
[a]Control Systems Group, Eindhoven University of Technology, Eindhoven, The Netherlands
[b]Systems and Control Laboratory, Institute for Computer Science and Control, Budapest, Hungary
Email: {l.c.iacob, m.schoukens, r.toth}@tue.nl

1 Introduction

Recent work in the field of control of nonlinear systems focuses on embedding the nonlinear dynamics into linear representations, to make use of the simple and powerful control tools available for linear systems. One such technique is based on the Koopman framework, where the states of the nonlinear system are lifted through nonlinear functions (called observables) to a higher dimensional, but linear space. The main limiting factor is that the transformation is generally infinite dimensional and the choice of the observables is ad-hoc. In this work, we show that for a class of continuous-time polynomial nonlinear systems there always exists a finite dimensional Koopman embedding that can fully represent the dynamics of the original system.

2 Embedding approach

Consider a continuous-time nonlinear system:

$$\dot{x} = f(x), \tag{1}$$

where $x(t)$ is the state at time $t \in \mathbb{R}$ and $f : \mathbb{R}^{n_x} \to \mathbb{R}^{n_x}$ is a nonlinear vector field. In the Koopman framework, the lifting is done through continuously differentiable scalar observable functions $\phi : \mathbb{R}^{n_x} \to \mathbb{R}$, and $\phi \in \mathcal{F}$, where $\mathcal{F}$ is a Banach function space. In continuous time, the dynamics of the observables is described using the Koopman generator $\mathcal{L}$ as follows:

$$\dot{\phi} = \frac{\partial \phi}{\partial x} f = \mathcal{L}\phi, \tag{2}$$

which is a linear, but infinite dimensional representation of (1). If a finite dimensional Koopman invariant subspace exists $\mathcal{F}_{n_f} \subseteq \mathcal{F}$, for $\phi_i \in \mathcal{F}_{n_f}$ and $\Phi = [\phi_1 \cdots \phi_{n_f}]^\top$, it holds that $\forall \phi \in \Phi$, $\mathcal{L}\phi \in \text{span}\{\Phi\}$. Thus, the lifted representation of (1) is described by $\dot{\Phi}(x) = A\Phi(x)$, with $A \in \mathbb{R}^{n_f \times n_f}$ being the Koopman matrix. Furthermore, to explicitly express the LTI dynamics of the Koopman representation of (1), let $z(t) = \Phi(x(t))$, giving the following form:

$$\dot{z} = Az, \quad \text{with } z(0) = \Phi(x(0)). \tag{3}$$

Consider now that the nonlinear system (1) is polynomial with the following structure:

$$\begin{aligned} \dot{x}_1 &= a_1 x_1 & &\dots \\ \dot{x}_2 &= a_2 x_2 + f_2(x_1) & \dot{x}_n &= a_n x_n + f_n(x_1, \dots, x_{n-1}), \end{aligned} \tag{4}$$

This work has received funding from the European Research Council (ERC) under the European Union's Horizon 2020 research and innovation programme (grant agreement nr. 714663) and from the European Union within the framework of the National Laboratory for Autonomous Systems (RRF-2.3.1-21-2022-00002).

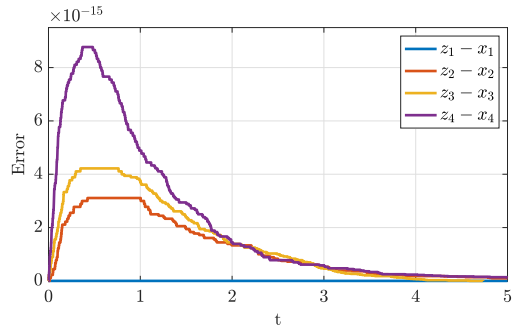

Figure 1: Error between the state trajectories of (6) and the associated Koopman embedding (3).

where f_n is given by:

$$f_n(x_1, \dots, x_{n-1}) = \sum_{j_1=0}^{d_n} \dots \sum_{j_{n-1}=0}^{d_n} \alpha^n_{j_1 \dots j_{n-1}} \prod_{i=1}^{n-1} x_i^{j_i} \tag{5}$$

and α^n denotes the coefficients. For such a system, as detailed in [1], the following theorem holds:

Theorem 1. *For an autonomous continuous-time nonlinear system that has a polynomial state-space representation in the form of* (4)*, there exists an exact finite-dimensional lifting* $\Phi : \mathbb{R}^{n_x} \to \mathbb{R}^{n_f}$*, containing the states* x_i*, with* $i \in \{1, \dots, n\}$*, such that* $\dot{\Phi} \in span\{\Phi\}$ *holds true.*

Proof. See [1] for the proof. Moreover, as the proof is constructive, it can be used as an algorithm to compute the observables. □

Consider the following example:

$$\begin{aligned} \dot{x}_1 &= a_1 x_1 & \dot{x}_3 &= a_3 x_3 + \alpha^3_{11} x_1 x_2 + \alpha^3_{02} x_2^2 \\ \dot{x}_2 &= a_2 x_2 + \alpha^2_3 x_1^3 & \dot{x}_4 &= a_4 x_4 + \alpha^4_{111} x_1 x_2 x_3. \end{aligned} \tag{6}$$

The lifting observable functions are computed based on the algorithm developed in [1] and are the following: $W_1 = \{x_1\}$, $W_2 = \{x_2, x_1^3\}$, $W_3 = \{x_3, x_1x_2, x_2^2, x_1^4, x_1^3x_2, x_1^6\}$, and $W_4 = \{x_4, x_1x_2x_3, x_1^4x_3, x_1^2x_2, x_1x_2^3, x_1^5x_2, x_1^4x_2, x_1^8, x_1^7x_2, x_1^{10}\}$ and the entire lifting set is $\Phi = \text{vec}(W_1, W_2, W_3, W_4)$. Consider $a_i = -0.5$, all $\alpha^i = -0.2$ and $x(0) = [1\ 1\ 1\ 1]^\top$. As depicted in Fig. 1, the Koopman model can exactly capture the solution trajectories of the original system ($\{z_i\}_{i=1}^4$ correspond to $\{x_i\}_{i=1}^4$), and the error is purely numerical (around 10^{-15}).

References

[1] L. C. Iacob, M. Schoukens and R. Tóth, *Finite Dimensional Koopman Form of Polynomial Nonlinear Systems*, Submitted to the IFAC World Congress, 2023

A Koopman-based method to approximate basins of attraction

François-Grégoire BIERWART and Alexandre MAUROY
Namur Institute for Complex Systems (naXys), Department of Mathematics, UNamur, Belgium
Email : {francois-gregoire.bierwart, alexandre.mauroy}@unamur.be

1 Introduction

Global stability analysis of equilibria is a challenging topic in nonlinear systems theory. It usually relies on the design of a Lyapunov function, which is a demanding task. In this context, investigating the Koopman operator appears as a relevant tool which allows to linearize systems in an infinite dimensional space. In particular, this linear framework is amenable to systematic stability analysis since stability is directly related to specific eigenfunctions of the Koopman operator [1].

Here we extend a numerical method developed in [2] to compute an approximation of the basin of attraction of equilibria

2 The Koopman operator

Consider the dynamical system

$$\dot{x} = F(x), \quad x \in \mathbb{X} \subset \mathbb{R}^n$$

where $\mathbb{X}$ is a compact set. Let $\varphi^t(x) : \mathbb{R}^+ \times \mathbb{X} \to \mathbb{X}$ be the associated flow map and assume $\mathscr{F}$ to be a Banach space of *observable* functions. We define the Koopman semi-group of linear operators as the family $\{\mathscr{K}_t\}_{t\geq 0}, \mathscr{K}_t : \mathscr{F} \to \mathscr{F}$ such that

$$\mathscr{K}_t f \;=\; f \circ \varphi^t, \quad \forall f \in \mathscr{F}.$$

The function $\phi_\lambda \in \mathscr{F}$ is an eigenfunction of the Koopman operator if

$$\mathscr{K}_t \phi_\lambda \;=\; e^{\lambda t}\phi_\lambda, \quad t \geq 0$$

where $\lambda \in \mathbb{C}$ is the associated eigenvalue. Eigenfunctions associated to eigenvalues with strictly negative real part capture stability properties. Indeed, it is shown in [1, 2] that these eigenfunctions allow to construct a generic Lyapunov function

$$\mathscr{V}(x) \;=\; \left(\sum_{i=1}^{n} c_i \left|\phi_{\lambda_i}\right|^p\right)^{1/p}, \quad \forall x \in \mathbb{X} \tag{1}$$

where λ_i are the eigenvalues of the Jacobian matrix of F evaluated at the fixed point.

The eigenfunctions are not easy to identify and it is common to compute their approximation on a finite dimensional subspace spanned by a finite set of basis functions. The approximation of the eigenfunctions is then obtained by computing right eigenvectors of the matrix approximation of the Koopman operator on the subspace [3]. Then, an approximation $V(x)$ of the Lyapunov function (1) can be obtained with these approximated eigenfunctions associated to eigenvalues with strictly negative part. The approximate basin of attraction is given as the largest sublevel set of $V(x)$ lying within the region $\dot{V}_{<0} \;=\; \{x \in \mathbb{X} \mid \dot{V}(x) < 0\}$.

3 Choice of basis functions

We investigate the effect of the Koopman operator approximation (e.g. choice of projection and basis functions) on the approximation of the basin of attraction. To this end, we implement the generic method developed in [2] with several sets of basis functions, including Gaussian radial basis functions that had not been considered before. We perform numerical experiments on several systems, including three dimensional ones and show that good performance is obtained, in particular in the case of radial basis functions.

4 Stability guarantee

The Lyapunov function V computed in the previous section relies on an approximation and has to be validated in a rigorous way. In the case of a monomial basis, we evaluate $\dot{V}$ on a grid and provide a criterion that ensures that the sign of $\dot{V}$ remains unchanged over a grid cell. We also develop an adaptive grid scheme for numerical efficiency. Moreover, we show that LaSalle theorem can be applied to deal with regions characterized by $\dot{V}(x) > 0$.

References

[1] Mauroy A. & Mezić I. *Global stability analysis using the eigenfunctions of the Koopman operator*. IEEE Transactions on Automatic Control, vol. 61(11), pp. 3356-3369, 2018.

[2] Mauroy A., Susuki Y. & Mezić I. *Koopman operator in systems and control*. Berlin: Springer International Publishing, 2020.

[3] WILLIAMS M.O., KEVREKIDIS I.G. & ROWLEY C.W. *A data-driven approximation of the Koopman operator: Extending dynamic mode decomposition*. ArXiv e-prints, 2014.

Formal Synthesis of Path-Complete Lyapunov Functions on Neural Templates

Virginie Debauche[1], Alec Edwards[2], Stella Simic[2], Raphaël M. Jungers[1,2], and Alessandro Abate[2]

[1]ICTEAM Institute, UCLouvain, B-1348 Louvain-la-Neuve, Belgium
[2]Department of Computer Sciences, University of Oxford, United Kingdom

1 Introduction

We study the stability analysis of discrete-time switched systems on $M \in \mathbb{N}$ modes of the form

$$x(k+1) \;=\; f_{\sigma(k)}(x(k)), \tag{1}$$

where the state $x(k) \in \mathbb{R}^n$ for any $k \in \mathbb{N}$, and the switching signal $\sigma : \mathbb{N} \to \{1,\ldots,M\}$ determines the current dynamics at each time step. In particular, we study the stability *under arbitrary switching*, i.e. when there is no constraints on the switching signal. In this work, we merge two recently introduced tools; the path-complete Lyapunov framework [1] (PCLF) which is a graph-based generalization of the multiple Lyapunov function approach for switched systems, and FOSSIL [2] a software for the formal synthesis of Lyapunov functions based on neural networks.

On one side, the PCLF framework generalizes multiple Lyapunov functions for switched systems, and involves two structural parameters. First, a labeled and directed *graph* whose edges encode the Lyapunov inequalities, and a *template* which defines the search space for the Lyapunov functions as quadratic functions for instance. This framework provides in particular a characterization of the validity of a graph-based certificate thanks to the *path-completeness* property. Therefore, this formalism offers a large range of stability certificates, and the question of finding the best ones among them is still the focus of active research [3].
On the other side, FOSSIL [2] is a sound counterexample-guided inductive synthesis (CEGIS) method which is used to find one Lyapunov function for general dynamical systems. This software features two main components as illustrated in Figure 1: as a first step, the *learner* suggests a candidate Lyapunov function valid over a finite sets of points to the *verifier* which checks the validity of the function over the whole domain. If the verifier finds a point where the Lyapunov constraints are not satisfied, the point is added to the training set and the algorithm loops. Otherwise, the algorithm stops and produces a valid Lyapunov stability certificate. In FOSSIL, the learner trains a neural network while the verifier is an SMT solver.

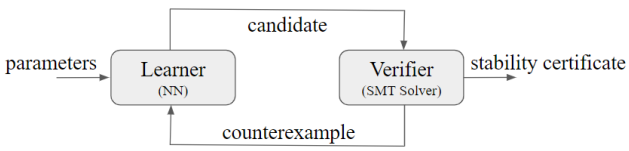

Figure 1: CEGIS loop of the FOSSIL software [2].

2 Results

In this work, we managed to adapt the FOSSIL architecture to graph-based stability certificates for switched systems in order to synthesize path-complete Lyapunov functions where the template is a neural network.

Concluding, the adaptation of the software FOSSIL to PCLF certificates allows to fully exploit the flexibility of both formalisms. In the future, we plan to leverage this flexibility in order to develop further the comparison of PCLF certificates in terms of performance by studying the modifications on the Lyapunov function when we add new layers, new neurons or when we modify the graph.

Acknowledgements

RJ is a FNRS honorary Research Associate. This project has received funding from the European Research Council (ERC) under the European Union's Horizon 2020 research and innovation programme under grant agreement No 864017 - L2C.

References

[1] A.A. Ahmadi, R.M. Jungers, P.A. Parrilo and M. Roozbehani (2014). *Joint spectral radius and path-complete graph Lyapunov functions*. SIAM Journal on Control and Optimization, 52(1), pp. 687–717.

[2] A. Abate, D. Ahmed, A. Edwards, M. Giacobbe, & A. Peruffo (2021). *FOSSIL: a software tool for the formal synthesis of lyapunov functions and barrier certificates using neural networks*. Proceedings of the 24th ACM International Conference on Hybrid Systems: Computation and Control, pp. 1–11.

[3] V. Debauche, M. Della Rossa and R.M. Jungers, (2022). *Comparison of path-complete Lyapunov functions via template-dependent lifts*. Nonlinear Analysis: Hybrid Systems, vol. 26, p.101237.

Soft-Reset Control with Max-of-Quadratics Lyapunov Certificates

R. Bertollo
TU/e (Eindhoven, NL)
rbertollo@gmail.com

A.R. Teel
UC (Santa Barbara, USA)
teel@ucsb.edu

L. Zaccarian
UniTN (Trento, IT),
LAAS-CNRS (Toulouse, FR)
zaccarian@laas.fr

1 Abstract

After being introduced by Clegg [1] in 1958, the control strategy known as *reset control* received renewed interest in the early 2000 [2] for its ability to overcome the intrinsic limitations of classical feedback laws [3]. The key idea in modern reset control architectures known as FORE (*first-order reset element*) is to apply an exponentially unstable first-order continuous control, suitably resetting the input to zero to obtain overall converging (hybrid) trajectories. While it is proven that the FORE outperforms classical continuous-time controllers in stabilizing relatively simple linear plants (essentially removing the phase lag introduced by regular integrators) [3], it still presents some issues, such as *i*) the existence of "pathological" discrete non-converging solutions to the closed-loop dynamics *ii*) the generation of discontinuous control inputs. To deal with *i*), a regularization of the dynamics is proposed in [4]; concerning *ii*), some different control solutions borrow some ideas from reset control to improve the performance, while still generating a continuous-time control input, see e.g. [5].

In this extended abstract, extracted from [6], we analyze a continuous-time implementation of a reset-control-based closed loop, known as *soft-reset* architecture. In particular, given a planar reset control dynamics

$$\begin{cases} \dot{x} = Ax, & x \in C := \{x \in \mathbb{R}^n : x^\top Mx \leq 0\}, \\ x^+ = Rx, & x \in D := \{x \in \mathbb{R}^n : x^\top Mx \geq 0\}, \end{cases} \tag{1}$$

we consider the following soft-reset implementation

$$\dot{x} \in Ax + \gamma\Big(\mathrm{SGN}\left(x^\top Mx\right) + 1\Big)(Rx - x), \tag{2}$$

where SGN is the Krasovskii regularization of the sign function. This formulation switches to a (more widely known) continuous-time dynamics, where the tuning knob $\gamma > 0$ allows adjusting how closely the solutions of (2) resemble the solutions of (1). Moreover, the non-converging discrete solutions are automatically excluded by the soft-reset implementation. Indeed, the following assumption is sufficient to certify global exponential stability (GES) of the origin for (2)

Assumption 1. *There exists a Lipschitz, homogeneous of degree 2, positive definite, strongly convex $V : \mathbb{R}^n \to \mathbb{R}$ s.t.*

$$\exists \varepsilon > 0 : \langle \nabla V(x), Ax \rangle \leq 0, \quad \textit{for almost all } x \in C_\varepsilon \tag{3}$$

$$V(Rx) - V(x) \leq 0, \quad \textit{for all } x \in D, \tag{4}$$

where $C_\varepsilon := \{x \in \mathbb{R}^n : x^\top Mx \leq \varepsilon x^\top x\}$, and no continuous solution to (1) *keeps V constant and nonzero. Additionally, $x \in D$ implies $Rx \in C$ in* (1).

Assumption 1 holds for most systems involving reset controllers, however it does not guarantee their convergence to zero, as it does not rule out the discrete nonconverging solutions. Conversely, we can prove the following result

Theorem 1. *Under Assumption 1, the origin of* (2) *is GES for γ large enough. Moreover, if* (3) *holds for almost all $x \in \mathbb{R}^n$, the origin is GES for any $\gamma > 0$.*

Since V is not required to be smooth, and it is known that many reset-control-based systems do not admit a qudratic Lyapunov function, we check Assumption 1 using a max-of-quadratics Lyapunov function V. In particular, we propose BMI (*bilinear matrix inequalities*) conditions, associated to polynomial multipliers, to check Assumption 1 using an SOS (*sum of squares*) numerical formulation (classical numerical techniques based on constant multipliers proved to be too conservative here). Moreover, we provide an iterative algorithm to automatically synthesize a max-of-quadratics Lyapunov function that satisfies Assumption 1. Laslty, we use the proposed algorithm to certify exponential stability of some simple examples and of an interesting mechatronics case study: the control of a precision positioning system.

References

[1] J. C. Clegg. *A nonlinear integrator for servomechanisms.* Transactions of the American Institute of Electrical Engineers, 77(1):41-42, 1958.

[2] A. Baños, A. Barreiro. *Reset control systems.* Springer, 2011.

[3] O. Beker et al. *Plant with an integrator: an example of reset control overcoming limitations of linear feedback.* IEEE TAC, 46:1797-1799, 2001.

[4] D. Nesic et al. *Stability and performance of SISO control systems with first order reset elements.* IEEE TAC, 56(11):2567-2582, 2011.

[5] D. A. Deenen et al. *Projection-based integrators for improved motion control: Formalization, well-posedness and stability of hybrid integrator gain systems.* Automatica, 133:109830, 2021.

[6] R. Bertollo et al. *Soft-Reset Control with Max-of-Quadratics Lyapunov Certificates.* IEEE TAC, 2022.

Minimum-Dissipation Driving of Physical Systems

Léopold Van Brandt and Jean-Charles Delvenne
Institute for Information and Communication Technologies,
Electronics and Applied Mathematics (ICTEAM)
Université catholique de Louvain,
Belgium
leopold.vanbrandt@uclouvain.be
jean-charles.delvenne@uclouvain.be

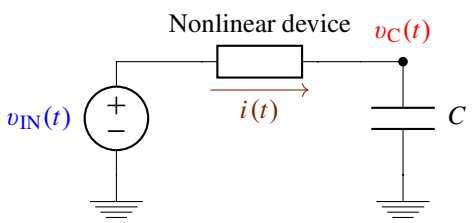

Figure 1: DRAM Bit Cell.

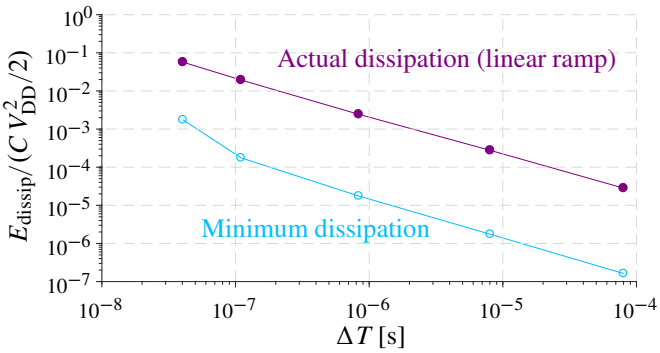

Figure 2: DRAM bit switching: dissipation vs response time ΔT.

1 Introduction

With a view to a large class of nonlinear physical systems made of both dissipative and energy-story components, we propose in this work an analysis of the dissipation in a general nonlinear electronic circuit whose schematic is depicted in Figure 1). This architecture exploits the charge $q(t)$ as state variable on a capacitor to represent a logical 0 (no charge) or a logical 1 (charge Q).

This works focuses on the bit switching ("$0 \to 1$") and notably to the dissipation inherent to this charging process. The nonlinear device between the energy source and the capacitor has indeed a finite conductance and is thereby dissipative. An important design issue is to minimize this purely dissipation consumption, that we propose to analyse in this work. We illustrate it for the writing operation of Dynamic Random-Access Memory (DRAM) bitcell. We expect the fundamental result to be valuable for all driving processes in port-Hamiltonian physical systems.

2 Analysis of the Dissipation

Our goal is to bring a charge Q on the capacitor in a time ΔT. The *energy dissipation* is defined as

$$E_{\text{dissip}} = \int_{t_0}^{t_0+\Delta T} (v_{\text{IN}}(t) - v_{\text{C}}(t))\, i(t)\, \mathrm{d}t \qquad (1)$$

The efficiency of the operation can be discussed by invoking a fundamental lower bound for the dissipation:

$$E_{\text{dissip}} \geq E_{\text{dissip,min}} \equiv \frac{Q^2}{\overline{G}\,\Delta T}, \qquad (2)$$

$\overline{G}$ may be interpreted as the *average* conductance of the nonlinear device over the whole charging time interval. Remarkably, the bound is tight, i.e. the bit switching is energetically optimal if the voltage difference across the nonlinear device is constant.

In Figure 2 we compare for a state-of-the-art DRAM cell the actual dissipation, as extracted from SPICE simulations, to the derived lower bound. The charging process is ensured by a linear input voltage ramp. The discrepancy is more than two orders of magnitude which reveals that as of it, the linear profile for $v_{\text{IN}}(t)$ results in a highly inefficient switching process in terms of dissipation.

3 Perspectives

Applied to more general port-Hamiltonian systems, we believe that the theoretical minimum dissipation is a useful tool to quantitatively assess the energy yield of any dynamic driving operation.

Spatial computational design synthesis for vehicle powertrain systems

Jorn van Kampen
Control Systems Technology
Eindhoven University of Technology
Email: j.h.e.v.kampen@tue.nl

Mauro Salazar
Control Systems Technology
Eindhoven University of Technology
Email: m.r.u.salazar@tue.nl

Theo Hofman
Control Systems Technology
Eindhoven University of Technology
Email: t.hofman@tue.nl

1 Abstract

The design of mechatronic systems, such as electric vehicle powertrains, is challenging due to the large complexity. Key performance indicators such as the overall powertrain efficiency and cost are influenced by both the components and the system architecture, resulting in the need for a holistic approach. Such a holistic approach typically aims at finding the optimal topology, being the one-dimensional component or sub-system connections, through computational design synthesis methods [1]. However, once a suitable topology is found, there exists an almost infinite amount of possible physical implementations. In addition, the physical placement of the components once again influences the overall performance. In case of a powertrain, the component placement directly affects the vehicle weight distribution and lengths of component connections, which in turn affects the total vehicle weight and thereby the energy consumption. Furthermore, a more compact placement of the components can increase passenger space within the vehicle, thereby improving comfort. Therefore, it is important to consider the spatial system design within the holistic design approach.

In previous research, spatial model-based design synthesis was applied to small systems, such as a gearbox [2] or an air-compressor [3]. However, these studies only optimized the placement for a fixed component orientation. In addition, the studies optimized single systems, whereas the vehicle powertrain typically includes multiple system levels that should be jointly optimized.

This work presents an optimization model of the two-dimensional spatial placement and orientation of components within a multi-level powertrain system, for a given component library and (sub-)system topology. Although the problem is highly combinatorial, it is still tractable due to the multi-level approach. We generate constraints on the component position, orientation or alignment purely based on the component properties (such as size and energy domain) and connections, resulting in a modular framework. Finally, we jointly optimize sub-systems, such as the battery pack, in terms of size and location, together with the complete powertrain system. A preliminary result is shown in Fig. 1 where the connection lengths and sub-system sizes are minimized. In this topology, the sub-systems were the battery pack, consisting of battery modules, and the transmission at the rear wheels, consisting of several gears. All mechanical connections (shafts) are automatically axially aligned, whereas the electrical connections (cables) are free. Overall, this framework can simplify the design of complex mechatronic systems and bring new insights to design engineers.

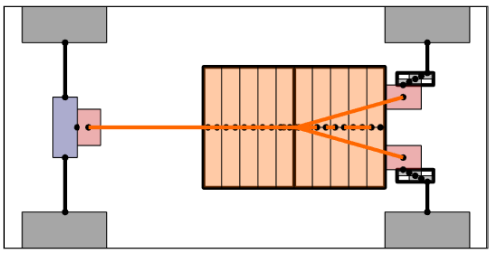

Figure 1: Preliminary results for the optimal spatial powertrain design consisting of a differential (violet), electric motors (red), gears (gray) and battery modules (orange).

References

[1] J. Wijkniet and T. Hofman, "Modified computational design synthesis using simulation-based evaluation and constraint consistency for vehicle powertrain systems," *IEEE Transactions on Vehicular Technology*, vol. 67, no. 9, pp. 8065–8076, 2018.

[2] K. Berx, K. Gadeyne, M. Dhadamus, G. Pipeleers, and G. Pinte, "Model-based gearbox synthesis," in *Mechatronics Forum International Conference*, 2014.

[3] A. Rosich, K. Berx, and G. Pinte, "Model-based design synthesis: application to optimal air-compressor system design," in *IFAC Symp. on Mechatronic Systems*, 2016.

Towards Experimental Validation of Cooperative Adaptive Cruise Control for Heterogeneous platoons

Redmer de Haan, Tom van der Sande, Erjen Lefeber
Eindhoven University of Technology
{r.d.haan, t.p.j.v.d.sande, a.a.j.lefeber}@tue.nl

1 Introduction

Research on autonomous driving aims to automate vehicles to outperform the human driver. Potential benefits of vehicle automation are, among others, increased road capacity and safety. By adding vehicle-to-vehicle (V2V) communication to automated vehicles, the collective behavior of a group of vehicles can be controlled to further improve the collective performance of the interconnected system of vehicles [1]. For example, Adaptive Cruise Control (ACC) automates the longitudinal behavior of the vehicle by using on-board forward looking sensors to control the distance to a preceding vehicle. Cooperative Adaptive Cruise Control (CACC) uses V2V communication in addition to the sensor set from ACC, and is able to reach the same level of disturbance attenuation through the vehicle string at significantly shorter inter-vehicle distances when compared to ACC [2].

2 Heterogeneous platoon controller design

Consider a platoon (i.e., closely packed formation) of vehicles as depicted in Figure 1 where the longitudinal dynamics of an individual vehicle are modeled according to

$$\begin{aligned} \dot{q}_i(t) &= v_i(t) \\ \dot{v}_i(t) &= a_i(t) \qquad\qquad i = 1,2,\dots,m, \\ \dot{a}_i(t) &= -\frac{1}{\tau_i}a_i(t) + \frac{1}{\tau_i}u_i(t) \end{aligned} \tag{1}$$

where τ_i is a time constant associated with the driveline, and q_i, v_i, a_i and u_i are the position, velocity, acceleration and input of vehicle i respectively, for $m \in \mathbb{N}_+$ vehicles in the platoon.

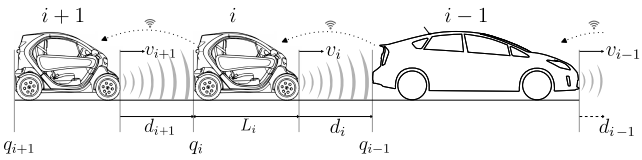

Figure 1: Platoon of vehicles equipped with CACC.

The objective for each individual vehicle in the platoon is to follow its predecessor at a constant headway h_i in seconds. This objective is captured by the constant timegap policy that defines the desired distance $d_{r,i}$ to the preceding vehicle as

$$d_{r,i}(t) = r_i + h_i v_i(t), \quad 2 \le i \le m, \tag{2}$$

where r_i is the desired standstill distance in meter. Using (2), the position error e_i for vehicle i in the platoon from Figure 1 is defined as

$$\begin{aligned} e_i(t) &= d_i(t) - d_{r,i}(t) \\ &= (q_{i-1}(t) - q_i(t) - L_i) - (h_i v_i(t) + r_i), \end{aligned} \tag{3}$$

where L_i is the length of vehicle i. Lefeber et al. [3] show that a change of input to the system according to

$$u_i = \frac{\tau_i}{h_i}a_{i-1} + \left(1 - \frac{\tau_i}{h_i}\right)a_i + \frac{\tau_i}{h_i}\xi_i, \tag{4}$$

results in a system where where any controller that stabilizes the error dynamics can be used for the new input ξ_i.

3 Open work

The control strategy from (4) has the major benefit it enables heterogeneous platooning, because no knowledge of the drive-line dynamics of the preceding vehicle is required. However, both the ego- and preceding- vehicle's acceleration are directly present in the controller output. Measured accelerations are typically signals with a low signal-to-noise-ratio that potentially contain a bias. Experimental results show the high noise levels are not beneficial for the passenger comfort. Additionally, the bias can have negative impact on the safety characteristics of the platoon. Therefore, an observer design will be investigated to obtain a bias-free acceleration signal with better signal-to-noise characteristics.

References

[1] J. Ploeg and R. de Haan, "Cooperative automated driving: from platooning to maneuvering," *VEHITS 2019 - Proceedings of the 5th International Conference on Vehicle Technology and Intelligent Transport Systems*, pp. 5–10, Jan. 2019.

[2] J. Ploeg, B. T. M. Scheepers, E. van Nunen, N. van de Wouw, and H. Nijmeijer, "Design and experimental evaluation of cooperative adaptive cruise control," *2011 14th International IEEE Conference on Intelligent Transportation Systems (ITSC)*, pp. 260–265, 2011.

[3] E. Lefeber, J. Ploeg, and H. Nijmeijer, "Cooperative adaptive cruise control of heterogeneous vehicle platoons," *IFAC-PapersOnLine*, vol. 53, pp. 15217–15222, Nov. 2020.

Verification and validation of Autonomous Driving Systems - Scenario modeling and criticality measures

Kevin Tom Kurian[1], Mohsen Alirezaei[1,2] , Erjen Lefeber[2], and Igo Besselink[2]
[1] Siemens Digital Industries Software, Helmond, The Netherlands
[2] Eindhoven University of Technology, Eindhoven, The Netherlands
Email: {k.tom.kurian, m.alirezaei, a.a.j.lefeber, i.j.m.besselink}@tue.nl

1 Introduction

Safe operation of Multi-Agent Systems (MAS) involving humans and robot agents is a complex problem. The tasks of evaluating risk, coordination with other entities, and decision-making are crucial to the safe operation of MASs. These tasks are typically classified as the 'situational awareness' of an agent. Developing a framework for MAS modeling which incorporates 'situational awareness' of autonomous robots and human agents collaborating in dynamically changing outdoor environments is an open challenge. This is particularly relevant for the verification, and validation of Autonomous Driving Systems (ADS).

The approach to verification and validation of an ADS includes test driving in a real-world environment. The tests are based on the number of kilometers driven, during which the ADS is exposed to different scenarios. A scenario is defined as a temporal development between several scenes, where a scene is a snapshot in time of the environment [1]. Depending on the type of scenario, it can be characterized using parameters and their probability distributions [2].

Given the time-consuming and expensive nature of real-world testing, virtual testing of these systems through Hardware-in-Loop (HiL) simulations is preferred. Hence, scenario-based testing methods are employed, which recreate the real-world scenarios encountered by an ADS in a virtual environment. Often, a smaller set of relevant scenarios are evaluated for an ADS. These scenarios are made representative of real-world conditions by basing them on measured data or expert knowledge.

The SOTIF (ISO 21448) standard pertains to retaining the safe functioning of an ADS in the event of a foreseeable failure within its Operational Design Domain (ODD) [3]. This involves a systematic identification of unknown-unsafe scenarios in the ODD. Optimization methods [4] can be used for this systematic identification. The novelty and the criticality of a scenario are considered the two objectives for optimization. Thereby, a set of novel, critical scenarios can be compiled for the virtual verification and validation of an ADS using scenario-based testing.

2 Problem statement

The overall problem consists of multiple facets as follows:

- The existing definitions of a scenario in literature are varied and application-specific. This makes the comparison of different scenario-based testing approaches for ADS systems difficult. Hence, a widely applicable framework for the abstraction/modeling of a scenario is to be developed.
- Currently available measures of the criticality of a scenario are scenario-specific. Hence, new criticality measures which are applicable to different MAS scenarios are required from an optimization standpoint.
- Key performance indicators of the abstraction technique depicting how well the abstracted model can represent real actor interactions are to be developed. The proposed framework and KPI's need to be evaluated for their feasibility and effectiveness by implementation in vehicle-in-loop testing.
- An equivalent measure of the 'number of kilometers driven' based on the chosen set of test scenarios for the ADS is to be realized. This is relevant for statements of safety comparing ADS with human drivers.

References

[1] S. Ulbrich, T. Menzel, et al., "Defining and substantiating the terms scene, situation, and scenario for automated driving," in 2015 IEEE 18th International Conference on Intelligent Transportation Systems, pp. 982–988, IEEE, 2015

[2] T. Menzel, G. Bagschik, and M. Maurer, "Scenarios for development, test and validation of automated vehicles," in 2018 IEEE Intelligent Vehicles Symposium (IV), pp. 1821–1827, IEEE, 2018

[3] "Road vehicles- Safety Of The Intended Functionality,", International Organization for Standardization (ISO), June 2022.

[4] M. Klischat and M. Althoff, "Generating critical test scenarios for automated vehicles with evolutionary algorithms," in 2019 IEEE Intelligent Vehicles Symposium (IV), pp. 2352–2358, IEEE, 2019

Risk in Stochastic and Robust Model Predictive Control for Vehicular Motion Planning

Leon Tolksdorf[1, 2], Arturo Tejada[1, 3], Nathan van de Wouw[1], and Christian Birkner[2]

[1]*Department of Dynamics and Control, Eindhoven University of Technology, P.O. Box 513, 5600 MB Eindhoven, The Netherlands, e-mail:* {l.t.tolksdorf, a.tejada.ruiz, n.v.d.wouw}@tue.nl

[2]*CARISSMA Institute of Safety in Future Mobility, Technische Hochschule Ingolstadt, Esplanade 10, Ingolstadt, Germany, e-mail:* {leon.tolksdorf, christian.birkner}@thi.de

[3]*TNO, Integrated Vehicle Safety, 5700 AT Helmond, The Netherlands, e-mail:* arturo.tejadaruiz@tno.nl

1 Introduction

In autonomous driving, risk is a quantity describing potential harm to passengers of an autonomous vehicle (AV) and other road users. Recent studies on human driving behavior, as well as safety standardization, suggest embedding risk into a motion planning algorithm of an AV. This yields an optimization problem balancing reward, i.e., reaching a desired goal sufficiently fast with potential risk. To archive this, we define a stochastic risk measure and introduce it into both robust and stochastic nonlinear model predictive path-following controllers (RMPC and SMPC, respectively) as a constraint and compare the performance.

2 Risk Definition

Within a specific driving scenario, the occurrence of a harm-inducing event $\mathscr{E}$ at time k can be identified by ascertaining whether specific conditions between kinematic variables associated with the actors of the scenario are fulfilled. These conditions can, for example, evaluate if the physical boundaries of actors overlap, representing a collision. Let $z_k \in \mathbb{R}^{n_{\mathscr{E}}}$ denote the values of the kinematic variables at time k required to determine the occurrence of an event $\mathscr{E}$. Denote $\mathscr{B}_{\mathscr{E},k}$ the subset of vectors in $\mathbb{R}^{n_{\mathscr{E}}}$ that satisfy the conditions used to identify the occurrence of $\mathscr{E}$ at time k. In general, z_k is a random vector with associated probability density function $p_{z,k}$, due to uncertainties involved in measuring or estimating the kinematic variables of interest. Lastly, let $s : \mathscr{B}_{\mathscr{E},k} \to \mathbb{R}_{+,0}$ denote a function that assigns the severity to every element of $\mathscr{B}_{\mathscr{E},k}$. Then we can define the risk R_k at time k as

$$R_k := \mathbb{E}[s(z_k)] = \int_{\mathscr{B}_{\mathscr{E},k}} s(z) p_{z,k}(z) \mathrm{d}z,$$

that is, R_k can be interpreted as the expected severity of an event $\mathscr{E}$ at time k. To constrain the risk at every time step, we introduce the risk tolerance $\varepsilon \in \mathbb{R}_+$, such that $R_k \leq \varepsilon$ represents an explicit risk constraint.

3 Problem Formulation

Suppose that within a configuration space only exist one AV, referred to as the ego vehicle, and one other vehicle referred to as the object. The ego vehicle is provided with a time-independent reference path and reference velocity. The ego vehicle is tasked with planning its own motion online to minimize the error w.r.t to the references within some finite horizon. However, the exact reference following may lead to collisions. To avoid collisions, we introduce a risk constraint that forces the controller to deviate from the references, requiring a balancing of reference following and potential risk online by the controller. As such, the controller does online motion planning for the ego vehicle based on the following objectives: (i) minimize the error to the reference path and velocity, (ii) constraint satisfaction, explicitly including a risk constraint that enforces safety.

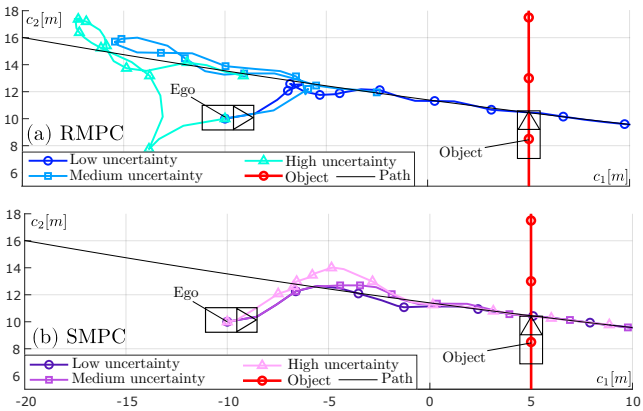

Figure 1: RMPC and SMPC comparison for three different uncertainties.

4 Approach

We approach our problem by employing a RMPC and SMPC controller. We model the uncertainty with truncated Gaussians in the (given) predictions of the future position and velocity of the object. The ego vehicle motion is modeled with a unicycle model, and an absolute kinetic energy model models the collision severity.

5 Results

In Figure 1 the ego vehicle is displayed at $k = 0s$ and the object at $k = 9s$. The dots represent a time difference of $1.5s$. One can see that the RMPC (a) takes significant deviations from the reference, increasing with the level of uncertainty for both risk tolerance settings. For all cases, the RMPC avoids a collision. On the other hand, the SMPCs (b) error towards references is smaller and leaves less distance to the object while, in all cases, successfully avoiding a collision. Further, the SMPC leaves less distance to the object when the risk threshold increases. Also, under increasing uncertainty, the SMPC leaves more distance to the object. Overall, the RMPC's behavior appears to be overly conservative.

Dynamic life-cycle assessment of emissions in the battery supply chain

Maurizio Clemente, Mauro Salazar, Theo Hofman
Eindhoven University of Technology
PO Box 513, 5600MB
Eindhoven, The Netherlands
m.clemente@tue.nl

Abstract

Electric powertrains have the potential to lower the environmental impact of the transport sector, which in 2021 contributed to 16% of the emissions, for a total of 5.8 equivalent Gigatonnes of CO_2. Despite the diffusion of this technology there has also been a surge in battery demand and production. In fact, in just five years, between 2015 and 2020, the battery demand increased by a factor of six. Furthermore, according to the IEA outlines for a Sustainable Development Scenario (SDS), this number will continue to grow: In 2030 the annual global battery demand for EVs is expected to reach 3.3 TWh of storage capacity. While some authors have focused on the economic impact of this production ramp-up, the environmental impact of such a dramatic change in battery production is still uncertain, yet so critical for our society.

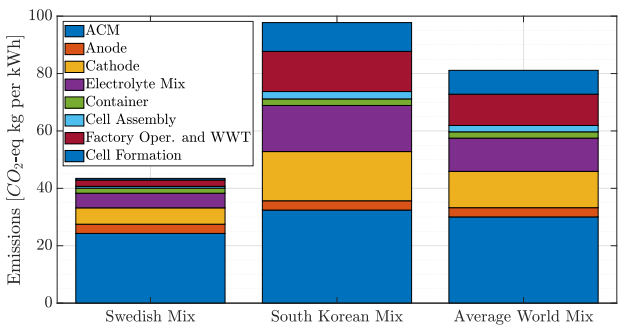

Figure 1: Contributes to the total equivalent CO_2 emissions considering different energy mixes.

In this paper, we make use of Life Cycle Assessment (LCA) to determine the total emissions per kWh generated during the production of a battery, from the raw material extraction to the final assembly of the battery (cradle to gate). The results shown in Figure 1 outline a heavy influence of the energy mix on emissions. While some of the processes, like material extraction, use heavy machinery running on diesel or other hydrocarbons, the other production steps could use electrical power coming from renewable sources. We also take into account the technological learning taking place during the scaling-up, identifying the influence of production volumes through different learning effects, such as learning-by-doing and learning-by-searching [1]. The implementation of learning methods on an LCA framework considers the manner in which the processes change over time, known in the literature as dynamic LCA (DLCA) [2]. The learning effects are taken into account using two different strategies: single-factor and multi-factor learning. The single-factor approach considers one single overall learning rate for the product, while the multi-factor approach distinguishes different learning rates for each constituent. The multi-factor approach provides more insights on where exactly the learning happens in the supply chain, and is more suitable to take into account physical limits of individual components compared to the single-factor, as shown in Figure 2. On the other hand it is difficult to gather the data needed to accurately identify a learning coefficient for every process, resulting in higher uncertainty.

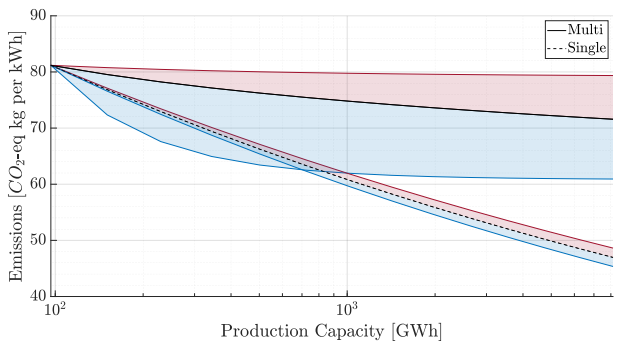

Figure 2: Evolution of equivalent CO_2 emission per kWh considering single-factor and multi-factor approaches.

References

[1] Martin Weiss, Andreas Zerfass, and Eckard Helmers. "Fully electric and plug-in hybrid cars - An analysis of learning rates, user costs, and costs for mitigating CO_2 and air pollutant emissions". In: Journal of Cleaner Production 212 (Mar. 2019), pp. 1478–1489. ISSN: 0959-6526. DOI: 10.1016/J.JCLEPRO.2018.12.019.

[2] Joshua Sohn et al. "Defining Temporally Dynamic Life Cycle Assessment: A Review". In: Integrated Environmental Assessment and Management 16.3 (2019), p. 314. DOI: 10.1002/ieam.4235.

Reference Governor in the Zonotopic Framework applied to a Quadrotor under an INDI Control Strategy

G. Delansnay, A. Vande Wouwer
System, Estimation, Control and Estimation (SECO), University of Mons, Belgium
Email: gilles.delansnay@umons.ac.be

1 Introduction

We investigates the combination of incremental nonlinear dynamic inversion (INDI) control with a reference governor scheme, i.e., a specific control scheme that enables constraint and limit protection handling, developed in a zonotopic framework. The zonotopic representation of the safe flight envelope is simple and computationally efficient for real-time implementation. The global scheme consisting of INDI and reference governor ensures safe flight under disturbances and constraints, as illustrated with numerical tests using the Parrot Mambo simulator provided in the Mathworks Simulink environment.

2 Incremental nonlinear dynamic inversion

The Incremental Nonlinear Dynamic Inversion (INDI) controller is a feedback linearization controller [1] which uses derivatives of the system states as an input. It allows achieving a closed-loop linear systems (Fig. 1).

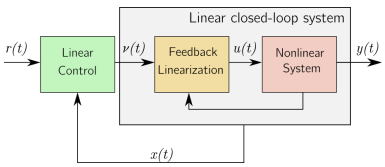

Figure 1: Feedback linearization principle

3 Reference governor

The reference governor [2] is an intermediary system that transforms a reference $r(t)$ generated by a high-level guidance system into a new reference $v(t)$ which is more suitable with respect to the dynamics of the closed-loop system and the constraints imposed on the system (Fig. 2).

Constrained zonotopes are selected for the convex set representation in the reference governor, as they have been proven suitable even for high-dimensional systems. Moreover, efficient algorithms are available for their computation, [3].

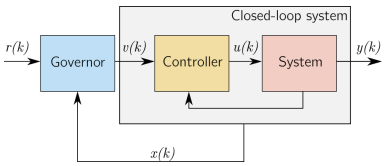

Figure 2: Reference governor structure

4 Results

Fig. 3 shows first results. An initial trajectory (blue doted line) is given to the UAV. When adding a constraint, the reference governor creates a new trajectory (red dotted line) for the closed-loop system such that it lies within the constraint. The resulting trajectory of the system (yellow line) is tracking the new reference while ensuring no constraint violation.

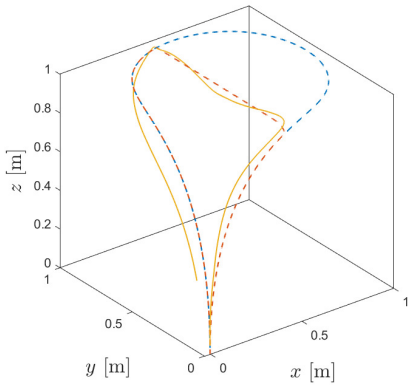

Figure 3: Constrained response (constraint $x < 0.5$) of the Mambo mini drone

References

[1] E. J. J. Smeur, Q. Chu, G. C. H. E. de Croon, Adaptive incremental nonlinear dynamic inversion for attitude control of micro air vehicles, Journal of Guidance, Control, and Dynamics 39 (3) (2016) 450–461. doi:10.2514/1.g001490.

[2] Reference and command governors for systems with constraints: A survey on theory and applications, Automatica 75 (2017) 306–328. doi:10.1016/j.automatica.2016.08.013.

[3] M. Althoff, Reachability analysis and its application to the safety assessment of autonomous cars, Ph.D. thesis, Lehrstuhl für Steuerungs- und Regelungstechnik, Technische Universität Müunchen, Germany (2010).

A Flexible Lab Setup and Software Framework for Developments in Motion Planning and Control

Bastiaan Vandewal, Mathias Bos, Wilm Decré and Jan Swevers
MECO Research Team, Department of Mechanical Engineering, KU Leuven, Belgium
Flanders Make@KU Leuven, Belgium
Email: bastiaan.vandewal@kuleuven.be

1 Introduction

Online (optimal) motion planning is a strongly researched field which receives a lot of attention from both industry and academia. It is a powerful method to navigate vehicles safely through complex cluttered environments, increasing the degree of autonomy of these vehicles in warehouses, greenhouses and on factory floors. Merging data from different sensors for localization and environment recognition, deploying various motion planning algorithms, and controlling the vehicle require a user-friendly framework.

Our proposed flexible software framework for motion planning and control facilitates fast testing and deployment, both for simulation purposes and for experimental work. Additionally, it allows students in control courses to implement and validate their motion planning, state estimation and state feedback algorithms.

2 Hardware Description

We developed a truck-trailer test setup as shown in Fig. 1. The truck is driven by a KELO drive [1] and executes the velocity inputs as calculated by the motion planner and feedback algorithms, as discussed in [2]. Onboard sensor measurements are processed by an Odroid XU4. A tracker of the HTC Vive virtual reality gaming console is used to localize the vehicle with high accuracy [3] which provides 6D pose estimates at a rate of 100 Hz. The tracker is mounted above the trailer axle's center point, and directly measures the trailer's state. An angle encoder is mounted on the hitching point of the truck and measures the relative angle between truck and trailer. Together, these sensors measure full state information.

Multiple projectors project the environment on the lab floor, allowing the visualization of (rapidly) changing environments. In addition to a road map, (virtual) obstacles or other environmental features, the visualization tool Rviz can also display planned and traveled trajectories, velocity vectors, and other useful debugging information, as shown in Fig. 1. These features make this setup visually attractive and ideal for development and demonstrative purposes.

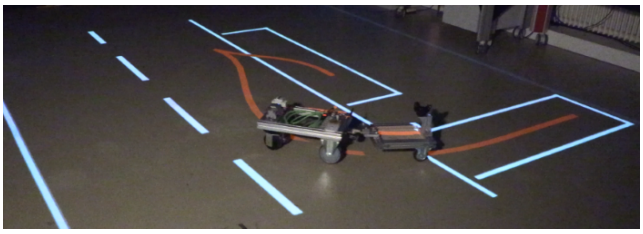

Figure 1: Lab setup with the truck-trailer, projected environment and planned trajectory.

3 Software Framework

The flexible software framework is built using Robot Operating System (ROS), because ROS inherently handles threading of parallel operations through its nodal structure, it easily handles network communication between independent devices (offboard laptop, onboard computer, etc.), and there is a vast supply of packages available from the ROS community that are interfaced in a plug-and-play manner. The onboard deployed software consists of the interface for the actuated wheel and for the onboard sensor. The offboard deployed software is a finite-state machine for discrete switching between tasks, the motion planning algorithm, the controller, the localization interface, and visualization tools. Additionally, the software configuration entails the feature that the physical vehicle with actuator and sensor interfaces can easily be replaced by an equivalent simulation node, without any changes in the remainder of the framework. This interchangeability makes the setup ideal for fast offline testing and debugging using the simulator, and direct deployment on the physical setup afterwards.

Acknowledgement This work has been carried out within the framework of Flanders Make SBO project ARENA (Agile and Reliable Navigation). Flanders Make is the Flemish strategic research centre for the manufacturing industry.

References

[1] KELO Robotics, Our technologies. https://www.kelo-robotics.com/technologies/. Accessed on: Jan. 12, 2023.

[2] M. Bos, B. Vandewal, W. Decré, J. Swevers. MPC-based Motion Planning for Autonomous Truck-Trailer Maneuvering. arXiv:2302.03474

[3] Okreylos, Lighthouse tracking examined. http://doc-ok.org/?p=1478. Accessed on: Jan. 12, 2023.

Improving position sensor calibration via Bayesian inference

Max van Meer[1] (m.v.meer@tue.nl), Emre Deniz[1], Gert Witvoet[2], Tom Oomen[1,3]
Control Systems Technology section[1], Dept. of Optomechatronics[2], Delft Center for Systems and Control[3]
Eindhoven University of Technology, PO Box 513, 5600MB, the Netherlands[1],
TNO, Delft, the Netherlands[2], Delft University of Technology, the Netherlands[3]

1 Background

The performance of mechatronic systems is limited by the accuracy of the position sensors used for feedback. These sensors require accurate calibration, which is achieved using test beds that, in turn, require even more accurate calibration [1]. Due to this cascade of calibration steps, see Figure 1, modeling errors in individual calibration steps can compound and limit the achieved accuracy of the position sensor calibrated last. This compounding of calibration errors is especially problematic when limited data is available due to the high costs of manual calibration.

2 Problem formulation

The aim is to find an accurate mapping of a low-cost, relatively inaccurate sensor S_1, to a highly accurate manual instrument S_3. To this end, a test bed, equipped with sensor S_2, is calibrated on S_3 once. Subsequently, a large range of different products, each with its own sensor S_1, is calibrated automatically on this test bed.

3 Cascaded calibration via Bayesian inference

The key idea is to model the intermediate sensor calibration model $f_{2\to3}$ as a Gaussian Process (GP), where

$$y_3 = f_{2\to3}(y_2), \tag{1}$$

such that when the two sensors are aligned, the sensors S_2, S_3 each measure positions y_2, y_3. By collecting a data-set $\mathcal{D}$ from the sensors and modeling $f_{2\to3}$ as GPs, the posterior model variance $\mathrm{cov}(\hat{f}_{2\to3})$ can be computed. Indeed, when readings of a low-cost sensor S_1 are then compared on the intermediate calibration model and stored as $\hat{D}$, the total calibration model is affected by the model uncertainty of the intermediate calibration model:

$$\hat{y}_3 = \mathbb{E}(\hat{f}_{1\to3}(y_1)) = g(y_1, \mathrm{cov}(\hat{f}_{2\to3}), \mathcal{D}, \hat{\mathcal{D}}). \tag{2}$$

Crucially, (2) provides an expression for the expected true position of the mechatronic system as a function of the reading of low-cost sensor S_1, and the variance of the intermediate calibration model. This expression can be evaluated online to correct for repeatable sensor inaccuracies.

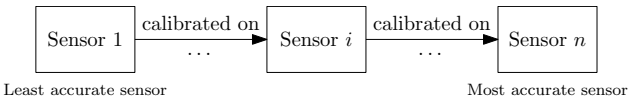

Figure 1: When multiple sensors are calibrated on each other, any calibration error is propagated down the chain.

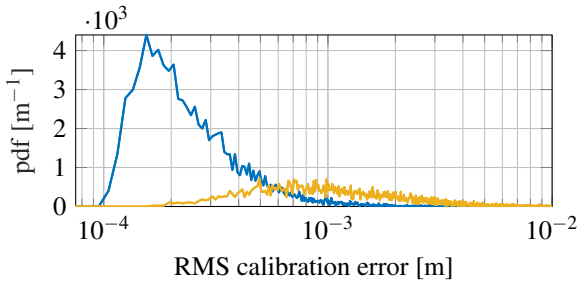

Figure 2: Normalized probability density function of the calibration error. The developed approach (—) achieves more accurate calibration than a lookup table with linear interpolation (—).

4 Simulation results

Monte Carlo simulations with 5000 scenarios are performed. In each scenario, $f_{1\to2}$ and $f_{1\to3}$ are generated randomly from a fourier basis. Figure 2 compares the resulting calibration errors $\|\hat{y}_3 - y_{\text{true}}\|_2/\sqrt{N}$ of the developed calibration approach with a lookup table with linear interpolation. The developed approach leads to significantly more accurate calibration, because (i) the chosen model structure is better suited for extrapolation, and (ii) model uncertainty of the intermediate calibration model is taken into account, such that in these regions the prior is trusted more than the model.

5 Conclusion

A cascaded calibration method is developed to accurately model position sensor inaccuracies, enabling more accurate calibration of mechatronic systems with fewer resources.

References

[1] M. Dresscher, J. D. Human, G. Witvoet, N. Van Der Heiden, R. Den Breeje, S. Kuiper, E. C. Fritz, C. W. Korevaar, N. C. Van Der Valk, T. J. De Lange, R. Saathof, N. Doelman, W. E. Crowcombe, C. M. Duque, and H. De Man. Key Challenges and Results in the Design of Cubesat Laser Terminals, Optical Heads and Coarse Pointing Assemblies. *2019 IEEE International Conference on Space Optical Systems and Applications, ICSOS 2019*, 2019.

A distributed sensor fault diagnosis scheme for the navigation of autonomous surface vessels

Abhishek Dhyani, R.R. Negenborn and Vasso Reppa
Department of Maritime and Transport Technology, Delft University of Technology, The Netherlands.
Emails: {a.dhyani-1, r.r.negenborn, v.reppa}@tudelft.nl [1]

1 Introduction

Autonomous surface vessels (ASVs) are predicted to be one of the key technological trends within the maritime sector owing to their promising merit of increased safety levels in the maritime ecosystem. However, since ASVs will extensively rely upon sensor measurements for navigating through oceans and inland waterways, it poses new challenges to the safety of the vessel. A fault in one or more of these sensors may have a severe consequence such as damage to the vessel, infrastructure, or a human injury. It is therefore critical that a fault in the navigational sensors must be detected and isolated quickly and accurately.

The current research on the model-based fault diagnosis of ASVs mainly focuses on the diagnosis of actuator faults while assuming the occurrence of a single fault. However, the sensor fault detection and isolation problem is equally crucial, owing to the harsh marine environment which may additionally contribute to the sensor degradation, for instance, due to the presence of salt spray and moisture [1]. In this work, we propose a model-based distributed two-level scheme for the detection and isolation of multiple sensor faults occurring in an ASV. In the proposed approach, the sensors being monitored are decomposed into multiple local sensor sets, to facilitate the isolation of multiple sensor faults and recognise the propagating sensor faults. The local monitoring modules consist of extended state observers (ESO) that can simultaneously estimate the sensor measurements as well as the external torque acting on the vessel due to wind. The various local monitoring modules are also capable of exchanging measurements and detecting the occurrence of a fault based upon a computed set of analytical redundancy relations (ARRs). Furthermore, the faulty sensor is isolated based upon a combinatorial decision logic - at the first level by each of the local monitoring modules, followed by a global monitoring module at the second level. This two-level scheme provides an improved isolability of the faulty sensors [2].

We consider a 3 DOF maneuvering model to describe the dynamics of an ASV. The vessel is considered to be equipped with multiple redundant sensors, including a GPS/GNSS sensor for the measurement of the vessel's position, an IMU sensor- constituting of a gyrocompass and accelerometer, for measuring the vessel's heading and velocity, an anemometer for measuring the wind speed and a weather vane for measuring the wind direction.

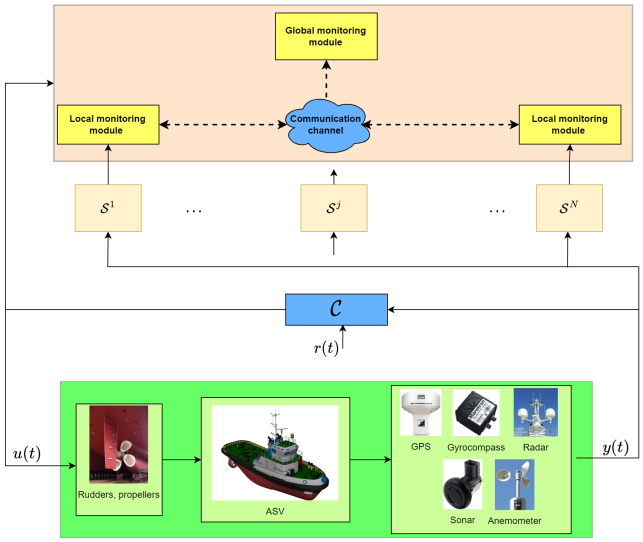

Figure 1: Proposed architecture for the FDI of ASVs

The proposed scheme is verified through simulations performed on a vessel model for the case of the vessel tracking a desired trajectory.

References

[1] Z. Liu, Y. Zhang, X. Yu, and C. Yuan, "Unmanned surface vehicles: An overview of developments and challenges," *Annual Reviews in Control*, vol. 41, pp. 71–93, 2016.

[2] V. Reppa, M. M. Polycarpou, and C. G. Panayiotou, "Distributed sensor fault diagnosis for a network of interconnected cyberphysical systems," *IEEE Transactions on Control of Network Systems*, vol. 2, no. 1, pp. 11–23, 2014.

[1] The research leading to these results has received funding from the European Union's Horizon 2020 research and innovation programme under the Marie Skłodowska-Curie grant agreement No 955.768 (MSCA-ETN AUTOBarge). This publication reflects only the authors' view, exempting the European Union from any liability. Project website:http://etn-autobarge.eu/.

Feedforward Control for an Interventional X-ray: A Physics-Guided Neural Network Approach

Johan Kon[i,*], Dennis Bruijnen[ii], Jeroen van de Wijdeven[iii], Marcel Heertjes[i,ii], and Tom Oomen[i,iv] [1]

1 Background

Interventional X-ray systems (IXs) are a key technology in healthcare that improve treatment quality through visualization of patient tissue. This enables minimally invasive therapies, resulting in faster patient recovery. To guarantee both high imaging quality as well as patient and operator safety, accurate feedforward control is essential during operation of an IX. A typical IX is visualized in Fig. 1.

2 Problem Formulation

The tracking performance of feedforward controllers based on first-principles modeling is limited by hard-to-model dynamics in the IX, such as the configuration-dependent cable forces and nonlinear friction characteristics in the guidance.

Instead, the goal of this work is to learn these hard-to-model dynamics from input-output data of the IX through capturing their contributions to the equations of motion using neural networks as flexible function approximators.

3 Physics-Guided Neural Network Feedforward

To compensate the hard-to-model dynamics, the feedforward controller is parametrized as a parallel combination of a physical model and neural network g_ϕ such that the feedforward f for reference θ_d is given by

$$f(\theta_d(k)) = M\ddot{\theta}_d(k) + mgh(\theta_d(k)) + g_\phi(T(\theta_d(k)), \quad (1)$$

where M and $mgh(\theta)$ represent the inertia and gravity contribution derived from first-principles, and

$$T(\theta_d(k)) = \begin{bmatrix}\theta_d(k) & \dot{\theta}_d(k) & \ddot{\theta}_d(k) & \text{relay}(\theta_d(k))\end{bmatrix}^T \quad (2)$$

represents is a physics-guided input transformation.

The parameters M, m, ϕ are learned from input-output data $\{u(k), y(k)\}_{k=1}^N$ through inverse system identification, i.e., by regressing the feedforward output $f(y(k))$ on $u(k)$ as

$$\sum_{k=1}^N (u(k) - f(y(k)))^2 + R(\phi). \quad (3)$$

$R(\phi)$ represents orthogonal projection-based regularization [1] to ensure that g_ϕ does not learn modeled effects, such that the physical model remains interpretable.

[1]This work is supported by Topconsortia voor Kennis en Innovatie (TKI), and ASML and Philips Engineering Solutions.
[i]Control Systems Technology Group, Eindhoven University of Technology, P.O. Box 513, 5600 MB Eindhoven, The Netherlands. [ii]Philips Engineering Solutions, High Tech Campus 34, 5656 AE Eindhoven, The Netherlands. [iii]ASML, De Run 6501, 5504 DR Veldhoven, The Netherlands. [iv]Delft University of Technology, P.O. Box 5, 2600 AA Delft, The Netherlands. [*]Email: j.j.kon@tue.nl

4 Results

The feedforward controller is validated experimentally on the IX setup of Fig. 1. Fig. 2 shows the resulting tracking errors. The proposed feedforward controller (—) compensates almost all dynamics, resulting in a tracking error of a few encoder counts. In contrast, the physical-model-based feedforward controller (—) improves upon the feedback only case (—), but still contains predictable errors from uncompensated dynamics. Overall, the tracking error is reduced from 0.095 to 0.020 deg in mean absolute sense by the inclusion of a neural network.

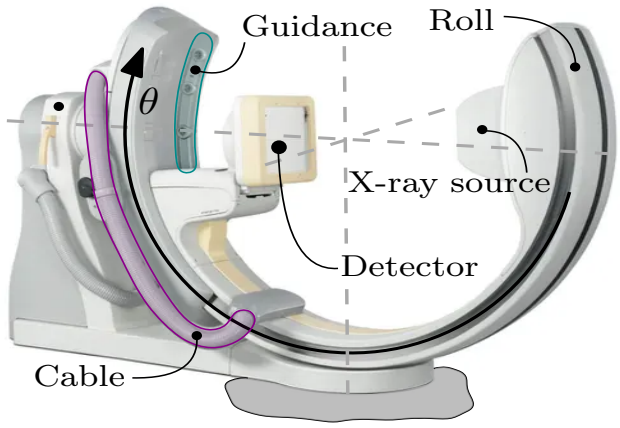

Figure 1: Interventional X-ray system positioning the X-ray source and detector through rotating, i.a., the roll axis.

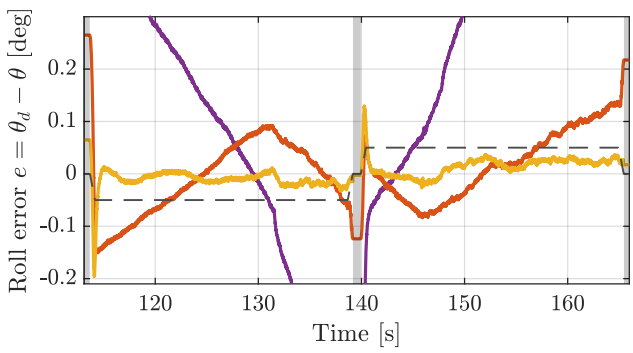

Figure 2: Error signals for proposed (—) and physical-model-based (—) feedforward controller compared to the feedback only case (—) with scaled velocity reference (- -).

References

[1] J. Kon, D. Bruijnen, J. van de Wijdeven, M. Heertjes, and T. Oomen, "Physics-guided neural networks for feedforward control: An orthogonal projection-based approach," in *Proc. Am. Control Conf.*, 2022.

On Nullspace-based Fault Diagnosis of Complex Mechatronic Systems

Koen Classens[1], W.P.M.H. (Maurice) Heemels[1] and Tom Oomen[1,2]

[1]Dept. of Mechanical Engineering, Eindhoven University of Technology, The Netherlands
[2]Delft Center for Systems and Control, Delft University of Technology, The Netherlands
{K.H.J.Classens,W.P.M.H.Heemels,T.A.E.Oomen}@tue.nl

1 Background

The economic value of high-tech production equipment is proportional to productivity. Key enablers are fast and accurate positioning systems which rely on a refined mechanical design and effective control algorithms. Despite incredible progress over the past decades, high-tech production equipment still breaks down. To minimize downtime, fault diagnosis systems are crucial to facilitate optimal and targeted maintenance such that productivity is maximized [1].

2 Problem

Fault detection and isolation (FDI) for large scale closed-loop controlled multi-input multi-output (MIMO) systems is challenging and successful application to complex mechatronic production equipment remains to be proven. For this purpose, accurate fault diagnosis system of low computational complexity are required, enabling to isolate a large number of possible actuator and sensor faults.

3 Approach

The proposed approach integrates prior information, i.e., accurate models available from controller design, with posterior information in the form of experimental input/output data during normal operating conditions. The fault diagnosis system, see Fig. 1, is based on an accurate low-order MIMO model and is synthesized by means of a numerically reliable nullspace-based FDI approach [2]. The residual signals, denoted by ε, are invariant to exogenous disturbances r, d, and w, and allow to isolate the root-cause fault f, highlighted in real-time in a digital counterpart (×), see Fig. 2.

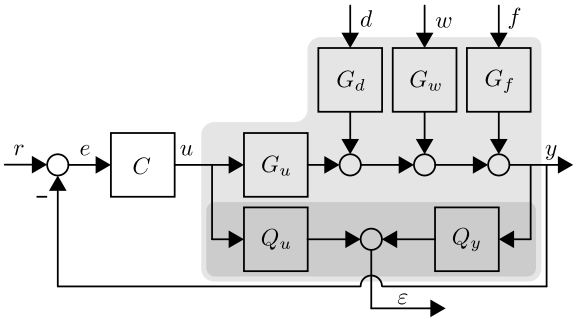

Figure 1: Closed-loop controlled system with augmented residual generator, highlighted in (■).

4 Results

It is shown that effective fault diagnosis filters can be synthesized which solve the FDI problem. By means of a numerical case study and experimental validation on a next-generation prototype wafer stage, see Fig. 2, its effectiveness is illustrated. The fault diagnosis system guarantees fault detection and isolation of a large number of imposed actuator and sensor faults.

5 Outlook

The main focus of this abstract is on successful application to a large scale MIMO industrial setup. Next, more emphasis will be put on incorporating modeling uncertainty into the synthesis tools to provide robustness guarantees.

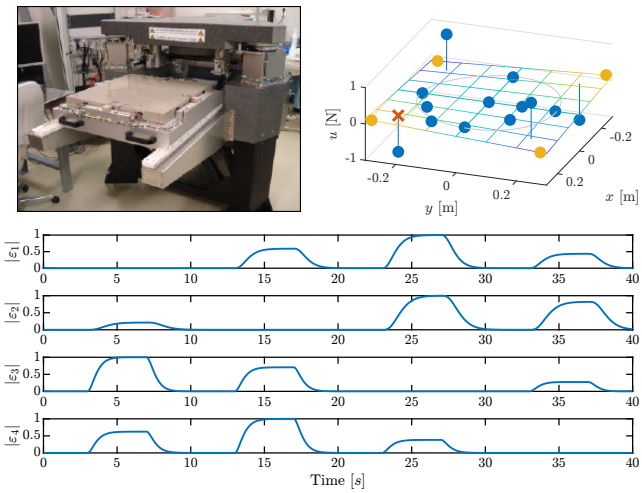

Figure 2: FDI on a prototype wafer stage with 4 sensors (●) and 13 actuators (●). To this end, a bank of 13 residuals signals ε are used, of which 4 are depicted. These signals allow to isolate the root-cause of the faulty system, highlighted in real-time by (×).

References

[1] K. Classens, W. P. M. H. Heemels, and T. Oomen, "Digital Twins in Mechatronics: From Model-based Control to Predictive Maintenance," in *2021 IEEE International Conference on Digital Twins and Parallel Intelligence*, Beijing, China, 2021.

[2] A. Varga, *Solving Fault Diagnosis Problems*. Springer International Publishing, 2017.

This work is supported by Topconsortia voor Kennis en Innovatie (TKI), and is supported by ASML Research, Veldhoven, The Netherlands.

www.SystemIdentification.be

Johan Schoukens
Vrije Universiteit Brussel
johan.schoukens@vub.be

1 Introduction

System Identification deals with data driven modeling of dynamic systems. It is a well established theory and many text books are available [1, 2, 4]. However, the threshold to work on this material is quite high and many potential users are lacking the time and/or the background to study the theory in detail. Alternative educational material to lower the threshold was developed using Matlab® exercises [3]. Because the reader has still to do all the programming work, it still might take a lot of time to absorb all the information.

On the website www.systemidentification.be we offer in the Hands-On section an alternative online book using Matlab® live scripts. The material is organized in an extensive set of Hands-On exercises that explain and illustrate each time a sub-topic of the system identification theory. 'Simple' but generic examples provide a deeper understanding of the explained theory, combined with a hands-on experience. General conclusions and user guidelines are provided at the end of each section. References are given to guide the reader to the literature. The book can be used for self-study or as additional material in courses on data driven modeling. In the presentation, we will discuss and illustrate in more detail the goals and philosophy of this project.

2 Outline

The Hands-On are organized along the following chapters:
- Statistics Refresher
- System Identification
- Design of Excitation Signals
- Nonparametric Identification
- Identification of Linear Systems
- Identification in the Presence of Nonlinear Distortions
- Identification of Nonlinear Systems.

An overview of the material already available can be found in the table of contents:
https://www.systemidentification.be/?page_id=1140

3 Illustration

We selected an example from the Hands-On *Matching the Model to the Data: Choice of the Error Signal and Cost Function*. In this Hands-On, the likelihood function concept is introduced and next it is illustrated on a number of examples. For this abstract, we selected a part of the discussion on the estimation of the mean and median. The underlying Matlab code can be visualized and accessed in the Matlab Live Script files that are downloadable from the website.

Exercise 1 Illustration of the different cost functions

In this exercise, the behavior of the different cost functions is illustrated for a data set with only 3 points: $[-1\ x\ 1]$. The value of x is randomly generated in [-1 1]. In the figure, the following cost functions are plotted (the standart deviation is put equal to one: $\sigma = 1$):

- $V_{LS}(\theta) = \sum_{k=1}^{N}(y(k)-\theta)^2$ with the mean value as the minimizer,
- $V_{LAV}(\theta) = \sum_{k=1}^{N}|y(k)-\theta|$ with the median as the minimizer,
- $V_p(\theta) = \sum_{k=1}^{N}(y(k)-\theta)^p$, and the normalized version $V_p(\theta) = \left(\sum_{k=1}^{N}(y(k)-\theta)^p\right)^{1/p}$ to give a better view of the cost function. For p becoming large, the midrange estimator is retrieved. The reader can set the value of p.

Run the exercise a few times for different values of p and observe the variations of the different cost functions and their minimizers. $V_{LAV}(\theta)$ is minimized in x, and $V_p(\theta)$ is minimized at $\theta = 0$ which is the midrange of [-1 1].

The sample mean (minimizer of $V_{LS}(\theta)$) is $\hat{\mu} = \frac{-1+x+1}{3} = \frac{x}{3}$; the median is $\hat{m} = x$.

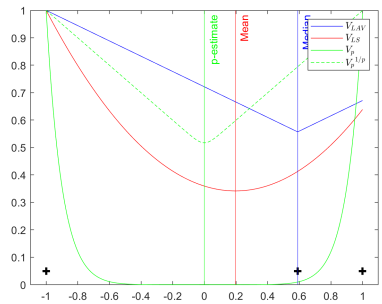

4 Long term perspective

The development of this website is a long-term project. We intend to expand/update gradually the information in the coming years. We decided to make the website publicly accessible in this period, even if it is far from being finished. It is our strong believe that also the partial information can be very useful for many readers. Moreover, the feedback that we get from these early experiences provides very valuable inputs for the further development of our project.

References

[1] Ljung, L. (1999). System Identification: Theory for the User. Prentice Hall.

[2] Pintelon, R. and Schoukens, J. (2012). System Identification: A Frequency Domain Approach. Wiley-IEEE Press.

[3] Schoukens, J., Pintelon, R., and Rolain, Y. (2012). Mastering System Identification in 100 Exercises. Wiley-IEEE Press.

[4] Söderström, T. and Stoica, P. (1989). System Identification. Prentice Hall International.

Spatio-Temporal Modeling for Next-Generation Motion Control

Paul Tacx[1], Matthijs Teurlings[1], Gert Witvoet[1,4], Marcel Heertjes[1,3], Tom Oomen[1,2]
[1]Eindhoven University of Technology, Department of Mechanical Engineering
[2]Delft University of Technology, Delft Center for Systems and Control, Delft, The Netherlands
[3]ASML, Mechatronic Systems Development, Veldhoven, the Netherlands
[4]TNO, Optomechatronics Department, Delft, the Netherlands
Email: p.j.m.m.tacx@tue.nl, t.a.e.oomen@tue.nl

1 Background

Flexible dynamics in next-generation motion systems lead to inherent spatio-temporal system dynamics. Inevitably, next-generation control techniques increasingly rely on accurate modeling techniques that capture the spatio-temporal nature of the flexible dynamic behavior [1]. Two case studies are being investigated: adaptive optics and mechanical stage control.

2 Problem Formulation

A key challenge for next-generation motion systems is the modeling of the spatio-temporal flexible dynamics. Traditional parametric and nonparametric identification approaches aim to identify the temporal behavior of the flexible dynamics. As a result, the flexible dynamic behavior is estimated at a limited spatial grid which limits the understanding of the position-dependency of the flexible dynamic behavior[2]. The aim of this paper is to identify and reconstruct the spatio-temporal behavior for spatio-temporal control of next-generation motion systems with a large number of spatially distributed actuators.

3 Approach

Given a motion system $G_m : [u_1 \dots u_{n_a}]^\top \mapsto [y_1 \dots y_{n_s}]^\top$ with a large amount n_a of spatially distributed actuators and a limited amount of n_s sensors, i.e. $n_s \ll n_a$. The aim is to model the spatio-temporal nature of the flexible dynamic behavior. The approach includes the identification of modal models [2]. The modal system description is exploited by including mechanical systems knowledge [3]. The proposed approach allows enhancing the estimation of the spatial system behavior [4].

4 Results

The proposed approach is illustrated on an experimental beam setup, see Figure 1. The approach proposed in this paper allows identifying the full response G_m while only having access to the first sensor by exploiting the proposed approach. In particular, the approach allows analyzing the spatio-temporal behavior with limited sensing capabilities, see Figure 2. In particular, the full system G_m is identified while only having access to the first sensor.

This work is part of the research programme VIDI with project number 15698, which is (partly) financed by the Netherlands Organisation for Scientific Research (NWO).

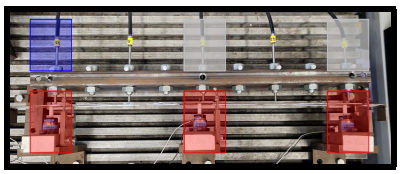

Figure 1: Experimental overactuated beam setup. The three voice-coil actuators are indicated in red. The flexible beam system G_m is actuated by three voice coil actuators (red) and the displacement is measured by three sensors (blue and grey). The proposed method only considers the first sensor (blue) to estimate the full system G_m.

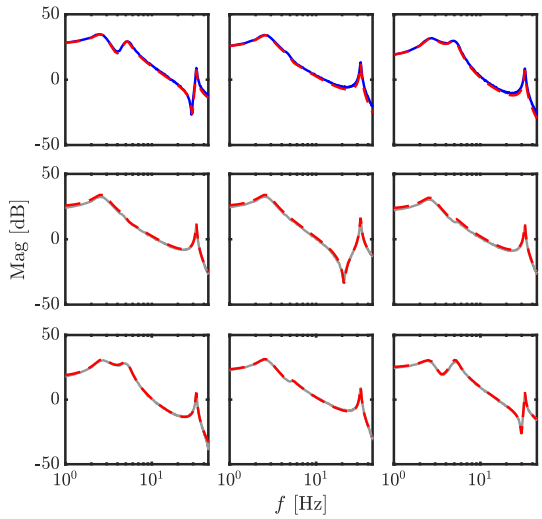

Figure 2: Element-wise Bode magnitude plot of the non-parametric estimate of the full system G_m (grey), the non-parametric estimate of subsystem G_o (blue), and extended plant G_m (dashed red).

References

[1] T. Oomen, R. van Herpen, S. Quist, M. van de Wal, O. Bosgra, and M. Steinbuch, "Connecting system identification and robust control for next-generation motion control of a wafer stage," IEEE Trans. on Contr. Sys. Tech., vol. 22, no. 1, pp. 102–118, 2013.

[2] R. Voorhoeve, R. de Rozario, W. Aangenent, and T. Oomen, "Identifying position-dependent mechanical systems: A modal approach applied to a flexible wafer stage," IEEE Trans. on Contr. Sys. Tech., vol. 29, no. 1, pp. 194–206, 2020.

[3] A. Ghali and A. Neville, "Structural Analysis: A unified classical and matrix approach," CRC Press, 1981.

[4] P Tacx, R. Habraken, M. Teurlings, G. Witvoet, M. Heertjes, T. Oomen, "Spatio-Temporal Analysis of Overactuated Motion Systems: A Mechanical Modeling Approach," Under review.

A design space specification language for production system topology

N. Paape*, J.A.W.M. van Eekelen, and M.A. Reniers
Control Systems Technology, Eindhoven University of Technology
Email corresponding author*: n.paape@tue.nl

The design process of a production system can be an intricate process, with many iterations of (re)design. The field of design space exploration (DSE) deals with automatically exploring the solution space of feasible designs to identify and analyze the differences between design alternatives. Examples of DSE frameworks are found in the fields of vehicle powertrains [1] and embedded systems [2]. As noted in [2], an effective DSE framework must describe methods for *representation*, *analysis*, and *exploration* of the design space.

Our previous work in [3] describes a simulation-based method for exploration and analysis in DSE of production systems. Here we focus on representation of the design space. A formal language is presented for specification of the design space of a production system topology. This language uses unambiguous syntax with natural language expressions. Using this language, design constraints can be described with the same level of expressiveness as first-order logic. Because it is a formal language, all feasible designs can be generated from the design space specification, which facilitates automated DSE. The expressiveness of the language and the ability to use it to generate designs have been validated through an adaptation of an industrial case study.

From a product flow perspective, a production plant consists of machines and products which flow between these machines. Thus, the functional design of a production plant can be considered to consist of components (machines) and the connections between them (e.g., a conveyor bringing products from machine A to machine B). The proposed formal design space specification language has been described using Extended Backus-Naur Form (EBNF) [4]. It supports specification of (1) which types of components can be used in the design, (2) which instances of these component type there must be, and (3) design constraints, such as: how many of a component type are used, or how a component must be connected. The EBNF notation has been omitted for brevity.

Figure 1 shows an example of a design space specification written using this specification language. The example shows how the language can be used to specify component types, instances and constraints. Figure 2 shows one of the feasible designs of this design space. Note that not all instances which are allowed to be present in a design need to be defined explicitly; machineA1, machineB1, and machineB2 are not specified but are present in the design.

An algorithm has been developed for generating all feasible designs. In this algorithm, potential designs are constructed,

Component types
- There is component type **Infeed** with output ports [out]
- There is component type **MachineA** with input ports [in] and output ports [out1, out2]
- There is component type **MachineB** with input ports [in] and output ports [out]
- There is component type **Outfeed** with input ports [in]

Component instances
- infeed1 is an instance of Infeed
- outfeed1 is an instance of Outfeed

Constraints
- #Components(MachineA) ≤ 1 AND #Components(MachineB) ≤ 2
- For all instances iN of Infeed: There exists an instance iA of MachineA: iN.out connects to iA.in
- For all instances iB of MachineB: There exists an instance iO of Outfeed: iB.out connects to iO.in

Figure 1: Formal specification of the design space.

and the designs are then checked to validate if the given constraints are adhered to. However, for a design space with many constraints, this could require many iterations before all feasible designs are found. The next step in future work is to achieve a more efficient method for generating feasible design candidates from the design space specification, and to integrate this into the DSE methods described in [3].

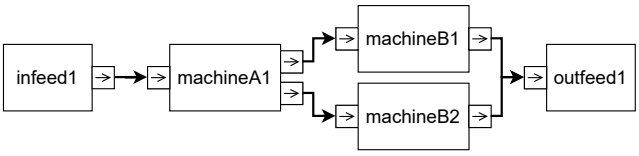

Figure 2: Instantiation of a feasible design.

References

[1] Kort, A.J., Wijkniet, J., Serebrenik, A., and Hofman, T. (2020). Automated Multi-Level Dynamic System Topology Design Synthesis. Vehicles, 2(4), 603–624.

[2] Kang, E., Jackson, E., and Schulte, W. (2011). An Approach for Effective Design Space Exploration. In Foundations of Computer Software. Modeling, Development, and Verification of Adaptive Systems. Monterey Workshop 2010. Lecture Notes in Computer Science, vol 6662 (pp. 33–54). Springer Berlin Heidelberg.

[3] Paape, N., van Eekelen, J., and Reniers, M. (2022). Design space exploration of a poultry fillet processing system using discrete-event simulation. Proceedings of FOODOPS 2022. Preprint.

[4] Scowen, R. S. (1993). Extended BNF - A generic base standard. Proceedings of SESS 1993, 25–34.

Joint Physics-Based and Kernel-Regularized LPV Feedforward

Max van Haren
TU/e
m.j.v.haren@tue.nl

Lennart Blanken
Sioux Technologies and TU/e
lennart.blanken@sioux.eu

Tom Oomen
TU/e and Delft University of Technology
t.a.e.oomen@tue.nl

1 Background

Increasing demands for motion control result in a situation where Linear Parameter-Varying (LPV) dynamics have to be taken into account. Inverse-model feedforward for LPV systems is challenging since the inverse is often dynamically dependent. The aim of this paper is to develop an identification approach that directly identifies dynamically scheduled feedforward controllers for LPV systems from data.

2 Problem Formulation

The goal is to create LPV feedforward controller F_{LPV} to reduce tracking error $e = r - y$ for LPV system G_{LPV}. The closed-loop setup considered is shown in Figure 1.

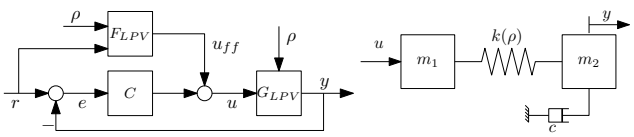

Figure 1: Left: Feedforward structure considered. Right: Example system that can be represented as (1).

The class of LPV systems considered are statically dependent on the scheduling variable with the following representation

$$G_{LPV} : \textstyle\sum_{i=-2}^{n_a} a_i(\rho(t))y^{(i)}(t) = \sum_{j=0}^{n_b} b_j(\rho(t))\frac{d^j}{dt^j}\iint u(t)\,dt^2, \quad (1)$$

with $\cdot^{(i)}$ the i'th derivative if $i \geq 0$ or the i'th integral if $i < 0$. The inverse dynamics, i.e., the dynamics from y to u, are dynamically dependent on ρ, due to the second integral.

Example 1. Consider the system in Figure 1, where the input-output behavior from input u to output y is given by

$$\left(m_2 m_1 \tfrac{d^2}{dt^2} + c m_1 \tfrac{d}{dt} + (k(\rho)(m_1+m_2))\right) y + k(\rho) c \textstyle\int y\,dt = k(\rho)\iint u\,dt^2.$$

The inverse dynamics are given by

$$u = \tfrac{m_2 m_1}{k(\rho)} y^{(4)} + \tfrac{c m_1}{k(\rho)} y^{(3)} + (m_1+m_2)\ddot{y} + c\dot{y} + \frac{\frac{2\rho^2 k'^2(\rho)}{k(\rho)} - \rho^2 k''(\rho) - \rho k'(\rho) - 2\rho k'(\rho)}{k^2(\rho)} f(y,\dot{y},\ddot{y}),$$

with $f(y,\dot{y},\ddot{y}) = m_1 m_2 \ddot{y} + c m_1 \dot{y} + k(\rho)(m_1+m_2)y$ and k' and k'' the derivatives of k with respect to ρ. ■

3 Approach

The approach uses a basis function approach with LPV feedforward parameters, where the parameters are learned using data with kernel-regularized least-squares. The feedforward controller is parameterized as

$$F_{LPV} : w_{ff} = \sum_{i=1}^{n_\theta} \theta_i(\rho)\psi_i\left(\frac{d}{dt}, I\right) r, \quad (2)$$

where the second integral is applied such that the dynamic dependence on the scheduling sequence is compensated for. The input applied to the system is calculated as $u_{ff} = \frac{d^2}{dt^2} w_{ff}$. The parameters $\theta_i(\rho)$ are identified using kernel-based regularization similar to [1] as follows

$$\hat{\Theta} = \arg\min_{\Theta} \|\bar{w} - \Phi\Theta\|^2 + \gamma\|\Theta\|_{\mathcal{H}}^2, \quad (3)$$

where Θ, $\bar{w}$ and Ψ are matrices or vectors of θ_i, w and ψ_i and $\mathcal{H}$ denotes the squared induced norm on the reproducing kernel Hilbert space, where $\|\Theta\|_{\mathcal{H}}^2 = \Theta^\top K^{-1}\Theta$. The kernel K incorporates prior knowledge of the feedforward parameters, such as smoothness or periodicity.

4 Results

Tracking performance of the system in Figure 1 with $k(\rho) = EA/(\rho(L-\rho))$ is compared for traditional LTI feedforward and the developed approach and is seen in Figure 2.

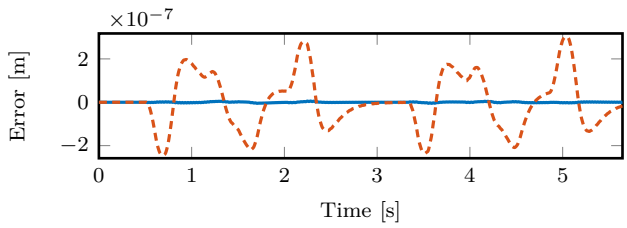

Figure 2: Error for LTI (- -) and developed (—) feedforward.

Significant tracking performance is achieved by the developed approach compared to LTI feedforward. The error 2-norm $\|e\|_2$ reduces from $4.2 \cdot 10^{-6}$ m to $5.8 \cdot 10^{-8}$ m.

Acknowledgments

This research has received funding from the ECSEL Joint Undertaking, grant agreement 101007311 (IMOCO4.E).

References

[1] G. Pillonetto, F. Dinuzzo, T. Chen, G. De Nicolao, and L. Ljung, "Kernel methods in system identification, machine learning and function estimation: A survey," *Automatica*, vol. 50, no. 3, pp. 657–682, 2014.

Mutual Information-based Feature Selection for the Inverse Mapping Parameter Updating Method

Bas Kessels, TU/e*
b.m.kessels@tue.nl

Adarsh Subrahamanian Moosath, TU/e*
a.subrahamanian.moosath@student.tue.nl

Rob Fey, TU/e*
r.h.b.fey@tue.nl

Nathan van de Wouw, TU/e*
n.v.d.wouw@tue.nl

1 Introduction

A digital twin of a (controlled) physical system allows engineers to efficiently optimize the design of the physical system and both optimize its performance and monitor its health in real-time. Since a model (i.e., a digital twin) is typically not an exact representation of a measured physical system, the digital twin cannot be exploited to its full potential. Therefore, model parameter updating is employed to minimize the mismatch between the model and the measured system. To make model parameter updating generally applicable in an online, digital twin context, the updating method should be: 1) applicable in (near) real-time, 2) applicable to nonlinear models, and 3) physically interpretable. To satisfy these requirements, the Inverse Mapping Parameter Updating (IMPU) method is proposed [1] which maps a set of features to corresponding parameter values. Since many distinct features can be extracted and using too many features may lead to deteriorating accuracy and computational efficiency, a Feature Selection (FS) technique is applied.

2 Inverse mapping parameter updating

In this research, the IMPU method is used to update physically interpretable parameter values $\boldsymbol{p}$ of a first-principles based (nonlinear dynamics) parametric (forward) model. This is achieved by using the inverse relation between $\boldsymbol{p}$ and a set of features $\boldsymbol{\psi}$ as extracted from output responses that are obtained for user-defined initial conditions and excitation signals, see Figure 1. This inverse relation is captured in an Inverse Mapping Model (IMM):

$$\hat{\boldsymbol{p}} = \mathcal{I}(\bar{\boldsymbol{\psi}}). \tag{1}$$

The IMM is constituted by an ANN that is trained offline using simulated training data $\{\boldsymbol{p}_s, \boldsymbol{\psi}_s\}$, where $s = 1, \ldots, n_s$, such that it learns an accurate mapping. Then, in an online phase, measured sets of features are used as input to the already trained ANN such that the parameter estimates are typically obtained in approximately 5 milliseconds, allowing for real-time updating. In this method, features describe the transient output response of the system. As many different features can be extracted from output data, see [1], and too many features may deteriorate accuracy and training/inference time, FS is applied to obtain a more informative subset.

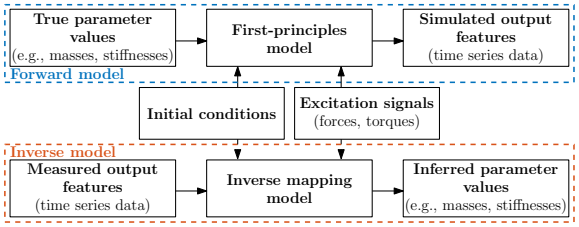

Fig. 1: Comparison of a first-principles forward model and an inverse mapping model with their inputs and outputs.

3 Feature selection using mutual information

To select a subset of features, the Mutual Information (MI) scores [2] between the different features and the different parameter values are used. Here, MI can be regarded as the entropy that represents the information contained within a variable (feature or parameter value). By calculating a MI score for each combination of features and parameters in the training data, the features are ranked and the features with the highest MI score are selected. By employing a subset of selected features as inputs to the ANN, it is observed that the accuracy of the parameter estimates is maintained or improved with respect to the use of the entire set of features, along with reduced training/inference time.

4 Conclusions

Using an IMM, constituted by an offline trained ANN, physically interpretable parameter values of nonlinear dynamics models can be updated in (near) real-time. To decrease training and inference time, and to potentially the increase accuracy of the estimated parameter values, MI-based FS is employed.

References

[1] B.M. Kessels, R.H.B. Fey, and N. van de Wouw, "Real-time parameter updating for nonlinear digital twins using inverse mapping models and transient-based features," *Nonlinear Dynamics* (Submitted for review), 2022.

[2] B. C. Ross, "Mutual information between discrete and continuous data sets," *PloS one*, vol. 9, no. 2, 2014.

*Eindhoven University of Technology, Department of Mechanical Engineering, Dynamics & Control Group

Gaussian Mechanism Design for Prescribed Privacy Sets in Data Releasing Systems

Teimour Hosseinalizadeh, Nima Monshizadeh

I. Introduction

Cyber-Physical Systems (CPSs) such as smart grids, intelligent transportation, and smart buildings provide better scalability, fault tolerance, and resource sharing compared to traditional systems. These come at the expense of sharing data and possibly losing privacy in the society and therefore require extra attention from researchers.

II. Problem formulation

We consider linear dynamical systems described by equations of the form

$$\begin{aligned} x(k+1) &= Ax(k) + Bu(k) \\ y(k) &= Cx(k) + Du(k), \quad k \in \mathbb{N}_0, \end{aligned} \tag{1}$$

with state $x \in \mathbb{R}^n$, input $u \in \mathbb{R}^m$ and output $y \in \mathbb{R}^p$. For this system, define

$$\begin{aligned} Y_{K-1} &\coloneqq \left[y^\top(0), y^\top(1), \ldots, y^\top(K-1)\right]^\top \in \mathbb{R}^{pK} \\ \mathcal{O}_K &\coloneqq \left[C^\top, (CA)^\top, \ldots, (CA^{K-1})^\top\right]^\top, \end{aligned}$$

for some $K \in \mathbb{N}$, and $\mathcal{W}_o = \mathcal{O}_K^\top \mathcal{O}_K$.

We are interested in the case where state variables or some of the state variables contain privacy-sensitive information when *1) everything except x_0 is publicly known and 2) system* (1) *is observable.*

A. Perturbing the initial state

As a solution for providing privacy for x_0, we first consider perturbing the initial condition x_0 itself. Assume $\tilde{x}_0 \coloneqq x_0 + v$, where v is a random variable with normal distribution $v \sim \mathcal{N}_n(0, \Sigma_v)$ and independent of x_0. In this case, the covariance of $\hat{x}_0$ as the maximum likelihood estimator is [1, p. 97]

$$\mathrm{Cov}(\hat{x}_0) = \mathbb{E}\left[(\hat{x}_0 - x_0)(\hat{x}_0 - x_0)^\top\right] = \Sigma_v. \tag{2}$$

It follows from (2) that adding noise directly to the initial state x_0 enables the designer to hide the true value of x_0 within a prescribed confusion set, characterized by Σ_v. Despite this advantage, perturbing the initial state is neither feasible nor desired in real-life processes such as a chemical reactor.

T. Hosseinalizadeh and N. Monshizadeh are with the Engineering and Technology Institute; University of Groningen, The Netherlands. Email: {t.hosseinalizadeh, n.monshizadeh}@rug.nl.

B. Perturbing the output measurements

Motivated by mentioned limitation, we consider instead perturbing the measurements of the system Y_{K-1} as

$$\tilde{Y}_{K-1} = Y_{K-1} + N_{K-1}, \tag{3}$$

where the added noise $N_{K-1} \sim \mathcal{N}_{pK}(0, \Sigma)$ is independent of Y_{K-1}. In this case, the covariance of $\hat{x}_0$ is

$$\mathrm{Cov}(\hat{x}_0) = \mathbb{E}\left[(\hat{x}_0 - x_0)(\hat{x}_0 - x_0)^\top\right] = \left(\mathcal{O}_K^\top \Sigma^{-1} \mathcal{O}_K\right)^{-1}. \tag{4}$$

A question that arises is that whether a Gaussian noise N_{K-1} can be found for the output mechanism (3) such that the optimal adversary encounters a prescribed confusion set Σ_v for x_0? Formally:

Problem 1. Find the covariance matrix $\Sigma \succ 0$ for the Gaussian mechanism in (3) such that for a given $\Sigma_v \succ 0$

$$\left(\mathcal{O}_K^\top \Sigma^{-1} \mathcal{O}_K\right)^{-1} = \Sigma_v. \tag{5}$$

III. Output Gaussian Mechanism

The following theorem addresses Problem 1 by providing results on existence and uniqueness of positive definite solutions Σ to (5).

Theorem 1. *Let $\Sigma_v \succ 0$ be the prescribed confusion set for x_0 in Problem 1. Consider the matrix equation*

$$(\mathcal{O}_K^\top X \mathcal{O}_K)^{-1} = \Sigma_v, \tag{6}$$

and the set

$$S_X \coloneqq \{X \in \mathbb{R}^{pK \times pK} |\ (6) \textit{ holds}\}. \tag{7}$$

Then, the following statements hold.

(i) The set S_X is nonempty and given by

$$S_X = \{N^\top N + R - MRM |\ R \in \mathbb{R}^{pK \times pK}\}, \tag{8}$$

where

$$M \coloneqq \mathcal{O}_K \mathcal{W}_o^{-1} \mathcal{O}_K^\top, \quad N \coloneqq \Sigma_v^{-1/2} \mathcal{W}_o^{-1} \mathcal{O}_K^\top. \tag{9}$$

(ii) The set

$$S_X^+ \coloneqq \{X \in S_X |\ X \succ 0\}, \tag{10}$$

is nonempty.

(iii) If $pK = n$, then the set S_X^+ is singleton and is given by $S_X^+ = \{N^\top N\}$. □

It follows from Theorem 1 that the solution to (6) is in general not unique, and hence it can be chosen optimally. The result for this part is dropped due to space limitation.

References

[1] T. Kailath, A. H. Sayed, and B. Hassibi, *Linear estimation*. Prentice Hall, 2000.

Data-driven discovery of nonlinear dynamical flame model

Roeland Wildemans[1]
Dynamics & Control, TU/e
Email: r.wildemans@tue.nl

Viktor Kornilov[1]
Power & Flow, TU/e
Email: v.kornilov@tue.nl

Philip de Goey[1]
Power & Flow, TU/e
Email: l.p.h.d.goey@tue.nl

Ines Lopez Arteaga[1,2]
Dynamics & Control, TU/e
Email: i.lopez@tue.nl

1 Introduction

Thermo-acoustic instabilities pose a severe challenge in the development of clean, stable burning techniques. These instabilities can typically be divided in two categories, namely unstable modes with a duct acoustic origin and a Intrinsic Thermo-Acoustic (ITA) origin. The first type of instability is caused by a feedback loop between the acoustics and the flames, while the ITA instabilities originate from an intrinsic feedback loop in the flame. Therefore, the latter type of modes reflect the pure flame dynamics. Flames are well known to exhibit a wide range of distinct nonlinear oscillations. However, accurate low-order models that describe the nonlinear flame dynamics are not available. Such models are essential in understanding the mechanisms of thermo-acoustic instabilities and developing successful mitigation strategies. In this research a low-order nonlinear dynamical flame model is discovered based on experimental data. Thereto, the Sparse Identification of Nonlinear Dynamics (SINDy) algorithm is used to discover the governing equations of the flame dynamics [1].

2 Data-driven model discovery

The dynamics of physical systems are often described by only a few relevant terms, which makes the dynamics sparse in a high-dimensional nonlinear function space. The SINDy algorithm uses sparsity promoting techniques to discover low-order dynamical models that describe the underlying time-series data of the state variables. First, the time history of the state variables is measured and stored in a data matrix $\mathbf{X} \in \mathbb{R}^{m\times n}$ in which m is the number of time samples and n the number of state variables. Next, a library is constructed that consists of different (non)linear candidate functions that are evaluated with the time history of the states which is typically denoted by $\Theta(\mathbf{X}) \in \mathbb{R}^{m\times p}$ with p the number of candidate functions. Furthermore, the time-derivatives of the state variables are numerically calculated and stored in a matrix $\dot{\mathbf{X}} \in \mathbb{R}^{m\times n}$. Finally, a sparse regression is executed to determine which functions from the library are required in the governing equations. This regression problem is given by $\dot{\mathbf{X}} = \Theta(\mathbf{X})\Xi$, in which $\Xi \in \mathbb{R}^{p\times n}$ is the matrix with the coefficients of the different candidate functions. The columns in this matrix select the active terms that are required to describe the evolution of the time-derivative of the corresponding state.

The SINDy algorithm is applied to experimentally obtained data of an unstable flame. The flame dynamics are typically described by the acoustic velocity just upstream of the flame and the heat-release rate. In Figure 1 the time-series of these state variables are shown for both a validation data set and a model simulation. It is shown that the discovered model describes the measured limit cycles accurately.

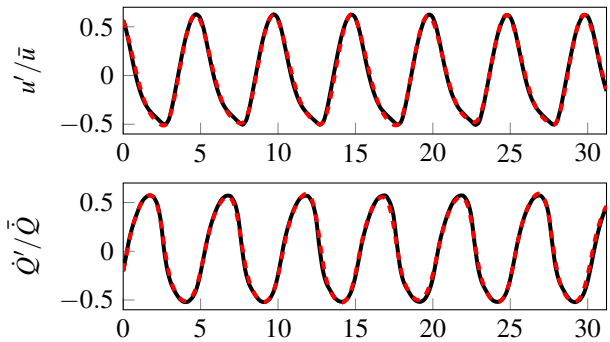

Figure 1: Comparison between experimental validation data (——) and model output (- - -) of the normalized acoustic velocity perturbations (top) and the heat-release rate perturbations (bottom).

3 Conclusions

In this research a low-order dynamical model of the flame dynamics is successfully discovered with the SINDy algorithm. This model will be used to investigate the interplay with the acoustic embedding of the flame and to develop new instability mitigation strategies.

References

[1] S.L. Brunton and J.N. Kutz, "Discovering governing equations from data by sparse identification of nonlinear dynamical systems" Cambridge University Press, 2019.

[1]Department of Mechanical Engineering, Eindhoven University of Technology, The Netherlands

[2]KTH Royal Institute of Technology, Department of Engineering Mechanics, Marcus Wallenberg Laboratory, Sweden

Identification and control of the divertor plasma in the General Atomics DIII-D tokamak

L. Ceelen[1,3], J.T.W. Koenders[1,3], D. Eldon[2], H. Anand[2], M. van Berkel[1], M.R. de Baar[1,3]

[1] DIFFER - Dutch Institute for Fundamental Energy Research, Eindhoven, Netherlands

[2] General Atomics, San Diego, CA 92186-5608, United States of America

[3] Eindhoven University of Technology, Control Systems Technology, Eindhoven, Netherlands

1 Introduction

One major challenge for tokamak fusion reactors is the mitigation of the paramount heat flux in the divertor exhaust [1]. A promising operational regime for heat flux mitigation is a detached divertor plasma, achieved with controlled injection of fuel and impurity gas [2]. The design of gas injection controllers for heat flux mitigation necessitates control-oriented dynamic models of the divertor plasma, which can only be verified with system identification experiments on present-day tokamaks. This contribution aims to progress the development of control-oriented dynamic divertor plasma models by performing system identification experiments on the mid-size DIII-D tokamak. The DIII-D tokamak has a considerably larger size and higher power than tokamaks on which identification experiments have been performed previously, for example, TCV [3]. Therefore, this study allows for a first assessment of a scaling of the divertor plasma dynamics across device size.

2 Experimental set-up

We identify the frequency response of the divertor plasma in DIII-D with multi-sine perturbations as in [4]. The perturbations are performed with deuterium (fuel) and nitrogen (impurity) gas injection. We measure the divertor plasma response using emitted Dα emission, mainly originating from the excitation and ionization of injected gas. Additionally, we measure the response of total radiated power, closely related to heat flux mitigation in the plasma edge. It has been observed on the DIII-D tokamak that the magnetic field direction affects how the divertor plasma progresses to the detached regime. Specifically, a jump-like event occurs from minor to substantial mitigation in the forward field direction, termed the detachment cliff. Therefore, we performed perturbative system identification experiments in both forward and reversed toroidal magnetic field directions, allowing us to investigate this effect on the measured divertor plasma dynamics.

3 Results

We find the divertor plasma response to be equal for deuterium and nitrogen gas injection in both field directions, suggesting the physics governing the measurements to be minorly affected by these condition changes. However, we find the dynamic response of divertor plasma radiated power is sensitive to the integrated amount of nitrogen injected, likely due to a change in the impurity concentration regime.

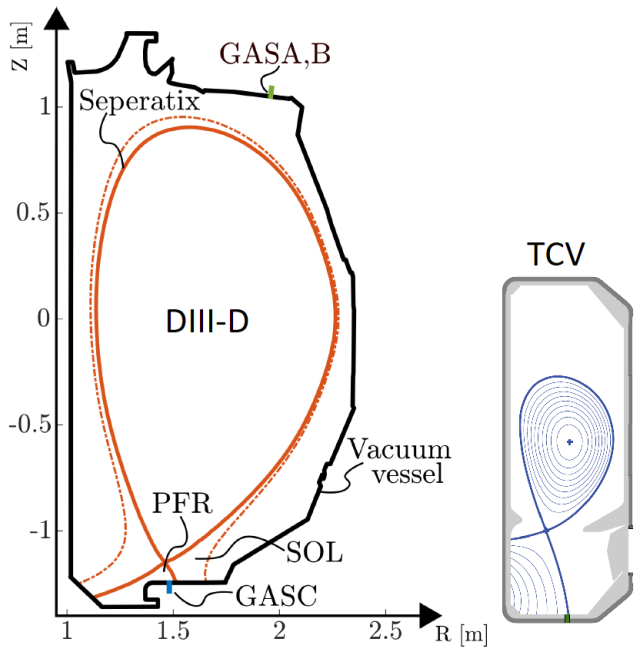

Figure 1: Left: an overview of the magnetic geometry on the DIII-D tokamak, including gas injection locations GAS A, B, and C. Right: example plasma geometry in the TCV tokamak [5] drawn to scale for comparison.

Additionally, we have exploited the system identification experiments to design an impurity injection controller. This controller has been demonstrated to adequately control the radiated power from the divertor plasma to mitigate the divertor heat flux in DIII-D and was used to support further experiments.

References

[1] R. Pitts et al., Nucl. Mat. Ener. **20**, (2019)
[2] D. Eldon et al., Nuclear Fusion **57**, (2017)
[3] Koenders et al., Nucl. Fusion **62**, (2022)
[4] M. van Berkel et al., PPCF **62**, (2020)
[5] H. Reimerdes et al., Nucl. Fusion **52**, (2022)

MIMO transfer function decoupling by Loewner tensorization

Philippe Dreesen
Maastricht University, DACS
philippe.dreesen@gmail.com

Mariya Ishteva
KU Leuven, CS/ADVISE-NUMA
mariya.ishteva@kuleuven.be

1 Problem statement and existing work

MIMO systems may have an underlying structure that is desirable to uncover during modeling or in applications [3, 5]. Here we consider a diagonal structure (Figure 1) written as

$$G(q) = WD(q)V^{\top}, \tag{1}$$

where the (static) mixing matrices W and V have sizes $p \times R$ and $m \times R$, and $D(q)$ is diagonal containing R SISO transfer functions $H_1(q), \ldots, H_R(q) \in \mathbb{C}$.

Existing approaches center around the matrix diagonalization of the frequency response matrix $G(q)$, such as the eigenvalue decomposition to diagonalize $G(q)$ at a single point, or the simultaneous diagonalization of multiple matrices $G(q_k)$ [4]. Because these approaches are agnostic about the mode containing the rational SISO transfer functions, the estimates of the functions $H(q_k)$ may be erratic.

2 Loewner-based tensorization

We present a tensor-based approach that jointly considers all available transfer function data while exploiting the structure of the rational functions [1, 6]. The proposed technique enables the use of tensor decomposition algorithms [7] that enjoy advantageous uniqueness properties.

Given are N samples of the $p \times m$ transfer function matrix $G(q)$ in the (complex) points $q_1, \ldots, q_N$, which are partitioned into two complementary sets $\{s_1, \ldots, s_{N/2}\}$ and $\{t_1, \ldots, t_{N/2}\}$. For convenience, we assume here that N is even and that both sets have $N/2$ elements. The frequency response data is then organized into a fourth-order Loewner tensor $\mathscr{L}$ of size $N/2 \times N/2 \times p \times m$ as

$$\mathscr{L}(i,j,k,l) = \frac{G_{kl}(s_i) - G_{kl}(t_j)}{s_i - t_j}.$$

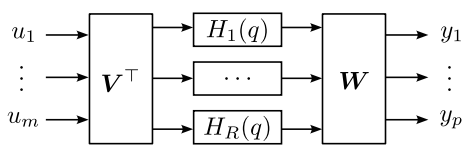

Figure 1: From a given MIMO transfer function matrix $G(q)$, we aim to extract a 'diagonal' decomposition into R SISO transfer functions $H_1(q), \ldots, H_R(q)$ with mixing matrices V and W at inputs and outputs.

The rank of a Loewner matrix $L(g)$ constructed from a rational function g is known to be equal to the degree of g, formally $\text{rank}(L) = \deg(g)$. The low-rank property of the Loewner matrix is generalized to a low (block-term) rank property of the tensor $\mathscr{L}$. In particular, $\mathscr{L}$ admits a block-term decomposition [2] in rank-$(\delta_r, \delta_r, 1, 1)$ terms as

$$\mathscr{L} = \sum_{r=1}^{R} L(H_r) \circ w_r \circ v_r = \sum_{r=1}^{R} (A_r B_r^{\top}) \circ w_r \circ v_r,$$

where A_r and B_r have sizes $N/2 \times \delta_r$ with $\delta_r = deg(H_r)$. The block-term decomposition of $\mathscr{L}$ returns the mixing matrices W and V (up to scaling and permutation), and a set of factors A_r and B_r modeling the low-rank Loewner matrices $L(H_r)$ from which the internal SISO transfer functions can be reconstructed [1, 6].

3 Discussion

Compared to the state-of-the-art approach [4], the proposed technique is able to guarantee the retrieval of the diagonal structure (1) for a larger number of internal SISO transfer functions. Furthermore, we observe that the method exhibits an improved ability to reject noise on the functions $H_r(q)$.

References

[1] Debals O., Van Barel M., De Lathauwer L., Löwner-based blind signal separation of rational functions with applications, IEEE Transactions on Signal Processing 64(8), 1909–1918, 2016.

[2] De Lathauwer L., Decompositions of a higher-order tensor in block terms — Part I: Lemmas for partitioned matrices, SIMAX, 30, 1022-1032.

[3] Hovd M., Braatz R.D., Skogestad S., SVD controllers for H_2, H_∞ and μ-optimal control, Automatica, 33(3), 433–439, 1997.

[4] Stoev J., Ertveldt J., Oomen T., Schoukens J., Tensor methods for MIMO decoupling and control design using frequency response functions, Mechatronics 45, 71–81, 2017.

[5] Vaes D., Optimal static decoupling for multivariable control design, PhD thesis, KU Leuven, Belgium, 2004.

[6] Verbeke D., Ishteva M., Dreesen P., MIMO transfer function decoupling by Loewner tensorization, IFAC World Congress 2023 (submitted), 2023.

[7] Vervliet N., Debals O., Sorber L., Van Barel M., De Lathauwer L., Tensorlab 3.0, available online at www.tensorlab.net, 2016.

Deep weather elements forecasting

Siamak Mehrkanoon
Department of Information and Computing Sciences, Utrecht University, Utrecht, The Netherlands.
Email: s.mehrkanoon@uu.nl

1 Introduction

A data-driven predictive model based on deep convolutional neural networks (CNN) is proposed for weather elements forecasting. The model exploits the spatio-temporal multivariate historical weather data to forecast weather elements for a number of user defined weather stations simultaneously in an end-to-end fashion. The embedded feature learning component of the model as well as coupling the learned features of different input layers have shown to have a significant impact on the prediction task. An experimental setup has been considered based on a high temporal resolution dataset collected from the National Climatic Data Center (NCDC) at five stations located in Denmark. The experiment concerns wind speed prediction at three weather stations located in Denmark for 6 and 12 hours ahead.

2 Formulation of the method

Let us assume that the number of weather stations is q, and the total number of weather elements (variables) is p. Furthermore, let $y_j^{s_i}(t)$ denotes the measurement corresponding to the j-th weather element of the i-th station at time t. If for instance we set the j-th weather element of the first station at time t as target variable, and also the lag parameter of both input and target signals to d, then one can construct the following regressor vector at time t: $z(t) = [y_1^{s_1}(t-1), \ldots, y_p^{s_1}(t-1), \ldots, y_1^{s_1}(t-d), \ldots, y_p^{s_1}(t-d), \ldots, y_1^{s_q}(t-1), \ldots, y_p^{s_q}(t-1), \ldots, y_1^{s_q}(t-d), \ldots, y_p^{s_q}(t-d)]$, which would be a vector of length $p \times q \times d$. Thus the problem is reduced to finding a right mapping from the input vector $z(t)$ to the desired target variable $y_j^{s_1}(t)$ as follows: $y_j^{s_1}(t) = f(z(t))$. In order to exploit the spatio-temporal structure of the input data, we first cast each regressor vector into a tensor with (stations, lags, variables) as (height, width, channel). Here we present a model that learns a bank of three dimensional kernels that are applied on the tensorial data containing the measurements of all the weather stations. The architecture of the proposed 3d-CNN model in [1], for weather forecasting is depicted in Figure 1. Here, the input data is fed to $(2 \times 2 \times 2)$-convolution layers with 10 filters followed by ReLU nonlinear activation function. The obtained feature maps are then flattened and the network is followed by fully connected layers with ReLU and linear activation functions respectively.

3 Experimental results

Our experiment concerns 6 and 12 hours ahead wind speed prediction for three weather stations located in Denmark.

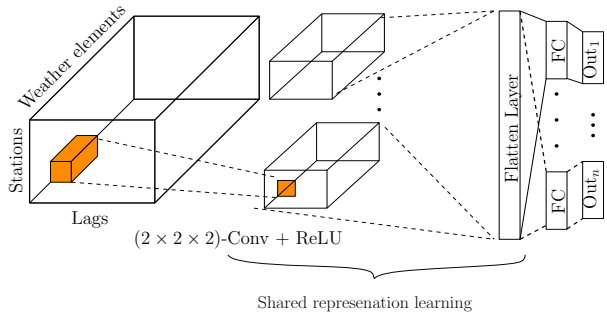

Figure 1: The 3d-CNN architecture proposed in [1] for weather elements forecasting.

Here the hourly historical data which include four weather elements including temperature, pressure, wind speed and wind direction from 2000-2010 are used. The performance of the proposed 1d-, 2d- and 3d-convolutional neural networks models for wind speed prediction is compared with those of NARX and LSTM networks. The test set consists of the last 10% of the data, while the remaining 90% percent of the data is used for training the models. For this dataset, the sequence length and the number of hidden units in the LSTM cell are set to four days (96 hours) of measurements and 200 respectively. The obtained results are shown in Fig. 2 and tabulated in Table 1.

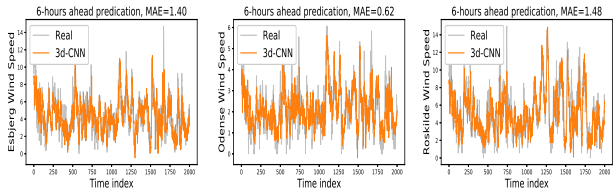

(a) (b) (c)

Figure 2: The Obtained 6-hours ahead wind speed forecasts for three stations.

Table 1: The MAEs (mean absolute errors) of the proposed models, the NARX and LSTM models.

		Method				
Hours ahead	**Station**	**3d-CNN [1]**	**2d-CNN [1]**	**1d-CNN [1]**	**NARX**	**LSTM**
6	Esbjerg	1.40	1.42	1.44	1.59	1.54
	Odense	0.62	0.63	0.63	0.68	0.86
	Roskilde	1.48	1.50	1.52	1.56	1.49
12	Esbjerg	1.71	1.75	1.75	1.81	1.77
	Odense	0.79	0.80	0.82	0.86	1.05
	Roskilde	1.84	1.90	1.92	1.96	1.79

References

[1] S. Mehrkanoon, *Deep shared representation learning for weather elements forecasting*, Knowledge-Based Systems, Vol 179, pp. 120-128, 2019.

A Differential Riccati Equation Approach to Prescribed-Time Regulation: Stability and Robustness

Amir Shakouri
Bernoulli Institute, University of Groningen, The Netherlands
a.shakouri@rug.nl

1 Introduction

In terms of the user's knowledge about the settling time, non-asymptotic controllers can be divided into three major categories of finite-time, fixed-time, and prescribed-time approaches. In finite-time schemes, it is only known that the system non-asymptotically converges at a finite time that is generally a function of the initial conditions. Fixed-time schemes provide an upper bound for the settling time, independently of initial conditions. However, in prescribed-time control, the settling time is commanded to the system, which means that the user is not only aware of the convergence moment but can arbitrarily specify it just by changing a parameter. Over the last few years, prescribed-time controllers have been developed in the literature for different types of systems (see [1–3]). It turns out that another interesting feature of prescribed-time controllers, apart from having an adjustable settling time, is their robustness to unknown dynamics for which no known bounds exist.

In this note, we discuss the capability of prescribed-time controllers in dealing with unknown systems. After introducing the basic definitions of prescribed-time convergence, a finite-time linear-quadratic regulator (LQR) is formulated to guarantee prescribed-time attractivity/stability for unknown linear and nonlinear systems. Next, the robustness of the proposed scheme over unknown dynamics is discussed in Proposition 1. Finally, Proposition 2 shows the interesting property of the proposed control gain in reaching the set of stabilizing constant gains for the uncertain system.

2 Results

In the context of prescribed-time control, we deal with the following type of closed-loop time-varying nonlinear systems

$$\dot{x} = f(x,t,\tau), \tag{1}$$

where $\tau > 0$ is a user-defined constant parameter, which affects the convergence behavior of the system. The following definitions are used in the sequel:

Definition 1 (see [2, Def. 3]). *System* (1) *is called "globally prescribed-time attractive" if, starting from any* $x(0) \in \mathbb{R}^n$, *the solution of the system satisfies* $\|x(t)\| \to 0$ *as* $t \to t_0 + \tau$ *for any* $\tau > 0$.

Definition 2 (see [2, Def. 3]). *System* (1) *is called "globally uniformly prescribed-time stable" if it is uniformly stable (in the sense of Lyapunov) and globally prescribed-time attractive.*

In this note, we consider a nonlinear system as follows:

$$\dot{x} = Ax + B(u + D(x)x), \tag{2}$$

where $A \in \mathbb{R}^{n\times n}$ and $B \in \mathbb{R}^{n\times m}$ are known, the pair (A,B) is controllable, and $D(x) \in \mathbb{R}^{m\times n}$ is an unknown (state-dependent) matrix satisfying the following assumption:

Assumption 1. *There exists (an unknown)* $\delta > 0$ *such that* $\|D(x)\| < \delta$ *for all* $x \in \mathbb{R}^n$.

Now, consider the following controller for system (2):

$$u = -R^{-1}B^\top \Theta^{-1}(t)x, \tag{3}$$

where the time-varying matrix $\Theta \in \mathbb{R}^{n\times n}$ is obtained via a backward integration of the following differential Riccati equation:

$$\dot{\Theta} = \Theta Q \Theta + \Theta A^\top + A\Theta - BR^{-1}B^\top,\ \Theta(t_0+\tau) = 0. \tag{4}$$

Proposition 1. *Suppose that Assumption 1 is satisfied. Then, system* (2) *under control law* (3) *is: (i) Globally prescribed-time attractive, and (ii) Globally uniformly prescribed-time stable and optimal (corresponding to the cost function* $J = \lim_{\alpha\to\infty}[\alpha\|x(t_0+\tau)\|^2 + \int_{t_0}^{t_0+\tau}(x^\top Qx + u^\top Ru)\mathrm{d}t]$*) if* $d(x) = 0$.

Proposition 2. *There exists* $\varepsilon > 0$ *such that the gain of the control law* (3) *at* $t = t_0 + \tau - \varepsilon$, *i.e.,* $K = -R^{-1}B^\top\Theta^{-1}(t_0 + \tau - \varepsilon)$, *is a globally asymptotically stabilizing gain for system* (2) *near the zero equilibrium.*

References

[1] Song, Y., Wang, Y., Holloway, J., Krstic, M., "Time-varying feedback for regulation of normal-form nonlinear systems in prescribed finite time" *Automatica*, vol. 83, 2017, pp. 243–251.

[2] Shakouri, A., Assadian, N., "Prescribed-time control for perturbed Euler-Lagrange systems with obstacle avoidance, *IEEE Transactions on Automatic Control*, vol. 67, no. 7, 2022, pp. 3754–3761.

[3] Shakouri, A., "On the prescribed-time attractivity and frozen-time eigenvalues of linear time-varying systems", *Automatica*, vol. 140, 2022, p. 110173.

Towards fast control of flexible robots with approximate NMPC

Shamil Mamedov[1⋆], Rudolf Reiter[2], Moritz Diehl[2], Jan Swevers[1]
[1]MECO Research Team, Dept. of Mechanical Engineering, KU Leuven, Leuven, Belgium
[1]DMMS Lab, Flanders Make, Leuven, Belgium
[2] Dept. of Microsystems Engineering, University Freiburg, Freiburg, Germany
⋆Email: *shamil.mamedov@kuleuven.be*

1 Introduction

Flexible robots are notoriously difficult to control due to oscillations and their infinite-dimensional state-space. Novel control strategies for such robots might advance industry by increasing payload-to-mass ratio of robot manipulators and improving human-robot collaboration.

For control purposes, partial differential equations governing the dynamics of the flexible robots are approximated with ordinary differential equation. In this work, we utilize an approximation method called modified rigid FEM (MRFEM) [1]. MRFEM, first, divides flexible links into n_{seg} and lumps their spring and damping properties at a point. Then, MRFEM isolates so-called rigid finite elements (rfes) between massless passive joints. For deriving the dynamics of serial chain flexible robots, MREFM can take advantage of existing tools for rigid body robots.

2 Approximating NMPC law

Nonlinear model predictive control (NMPC) has shown excellent performance in many fields of engineering including robotics. One of the limitations of the NMPC is long computation time, especially for system with high dimensional state-space such as flexible robots. To overcome this limitation, we propose to approximate the NMPC law with neural network (NN) using the imitation learning algorithm Dataset Aggregation (DAgger) [2]. In contrast to classical supervised learning algorithms, DAgger interacts with the environment using the current policy $\pi^i_{\text{NN}}(x)$ and queries the expert policy $\pi^\star(x)$ (NMPC) on visited states. Existing dataset $\mathscr{D}$ is complemented with a new dataset $\mathscr{D}_i = \{(x, \pi^\star(x))\}$ and new policy $\pi^{i+1}_{\text{NN}}(x)$ is trained on $\mathscr{D}$. Given enough time for interaction and training, DAgger can quite accurately imitate expert NMPC controller.

However, NN policy $\pi_{\text{NN}}(x)$ does not provide any safety guarantees necessary in robotics. To recover the safety, we leverage predictive safety filter (PSF) method [3]. PSF is an MPC scheme that receives a candidate input (from NN controller) and verifies if it can drive the system to a safe terminal set after applying the candidate input. If the answer is positive, the input is applied to the system; otherwise, it is modified as little as possible to ensure safety. Fig. 1 shows the complete pipeline for approximating NMPC law.

The proposed safe approximate NMPC controller has achieved a significant improvement in computational time, as demonstrated by experiments on a simulated three degrees of freedom flexible robot manipulator. On average, the computational time of the proposed controller is 3.6 ms, compared to the original NMPC's 11.8 ms.

Acknowledgement This research is supported by the Research Foundation Flanders (FWO-Vlaanderen) through SBO project Energy-efficient, Lightweight, safe Yet Strong manipulator Arm (ELYSA) for cobot applications (S001821N).

References

[1] E. Wittbrodt, I. Adamiec-Wójcik, and S. Wojciech, *Dynamics of flexible multibody systems: rigid finite element method*. Springer Science & Business Media, 2007.

[2] S. Ross, G. J. Gordon, and J. A. Bagnell, "A reduction of imitation learning and structured prediction to no-regret online learning," in *AISTATS*, 2011.

[3] K. P. Wabersich and M. N. Zeilinger, "A predictive safety filter for learning-based control of constrained nonlinear dynamical systems," *Automatica*, vol. 129, no. May, 2021.

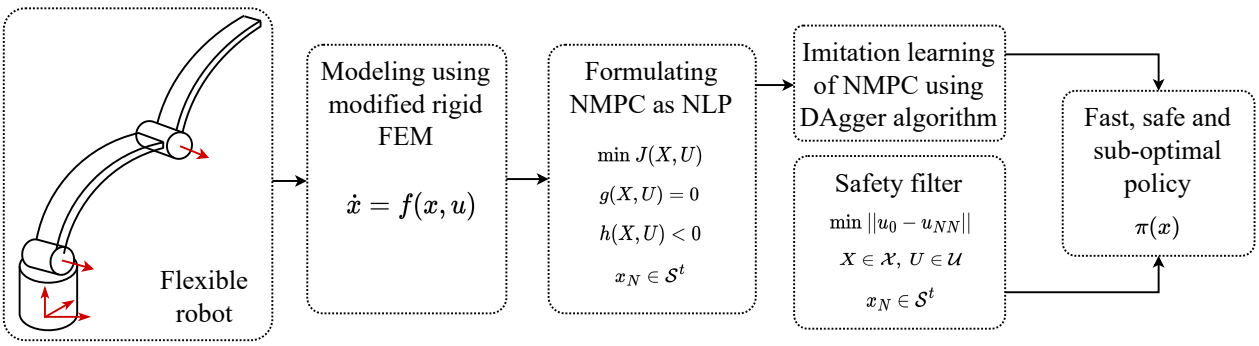

Figure 1: A pipeline for approximating NMPC law with safe NN policy

Flock Formation for Robot Navigation in a Large and Structured Environment

Koen de Vos, Elena Torta, César López Martinez, Herman Bruyninckx, René van de Molengraft
Control Systems Technology, Eindhoven University of Technology
P.O. Box 513. 5600 MB Eindhoven, The Netherlands
Email: k.d.vos@tue.nl

1 Introduction

Recent developments have allowed mobile robots to become more prevalent in a large number of industries and environments. Their application puts a requirement on their operation to be autonomous and safe. To achieve both, a popular approach is to make use of Model Predictive Control (MPC) techniques. However, due to their computational complexity, these approaches tend to be limited to small environments and a small number of agents. This while robots (likely) only need to communicate with a small subset of all agents which are currently relevant. Formation of these subsets was already shown in e.g. [1], which solved the problem of "when and with whom to communicate" using a Multi-Agent Reinforcement Learning approach. In our work we call the subsets of communicating agents flocks, and introduce an approach to form these based on our semantic knowledge of the environment.

2 Setting

A set of mobile robots is tasked with navigating in a structured environment, which consists of corridor-like spaces and intersections between those spaces. An example of such an environment is depicted in Figure 1. During the execution of their navigation task, the robots need to prevent collisions with obstacles, the environment and each other. As a human, we have a clear understanding how to behave in this environment. Furthermore, we know when and where to expect interactions with whom. When we approach an intersection, and see someone approaching the same intersection, we know that we should take them into account when planning our motion. People which we are not likely to meet in the near future do not need to be considered at this time.

3 Approach

We propose that robots can form flocks using similar insights as in the above. Robots communicate and collaborate only among their flock members. We hypothesise that using this approach performance is maintained, while the requirements on communication and computation can be drastically reduced. The first step in enabling robots to form flocks is to construct a world model which allows storage and retrieval of both semantic and spatial knowledge about the environment. Inspired by Deeken et al. [2], we combine a spatial database with a knowledge base. This allows reasoning about the connectivity of spaces and the agents contained within those space. For instance, agents contained within spaces with a topological distance smaller than a certain threshold form a flock, otherwise no communication is established. After the flock formation step, the next step is to generate a motion plan. The main requirement for this motion plan is making progress while satisfying the constraints. A natural framework to formulate the motion planning problem is through the use of (nonlinear) MPC, due to its ability to explicitly handle the constraints that follow from the problem formulation.

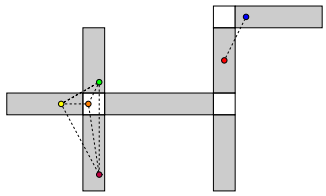

Figure 1: An example environment consisting of corridors (grey rectangles) and intersections (white rectangles). Robots (coloured dots) are grouped into flocks (dashed lines).

4 Conclusion

We propose that through the definition and formation of flocks MPC-like approaches can be applied in larger environments and among a larger number of agents. Our talk will discuss the creation and requirements of the world model, the MPC controller, and the overall approach in further detail.

References

[1] Á. Serra-Gómez, B. Brito, H. Zhu, J. J. Chung, and J. Alonso-Mora, "With whom to communicate: Learning efficient communication for multi-robot collision avoidance," *CoRR*, vol. abs/2009.12106, 2020.

[2] H. Deeken, T. Wiemann, and J. Hertzberg, "A spatio-semantic approach to reasoning about agricultural processes," *Applied Intelligence*, vol. 49, no. 11, pp. 3821–3833, 2019.

Minimalformulated nonlinear spatial rod models in Soft Robotics

Philipp Mitterbach, Dr. Alexander Pogromskiy, and Dr. ir. Irene Kuling
Dynamics and Control, Eindhoven University of Technology
p.mitterbach@tue.nl, a.pogromski@tue.nl, i.a.kuling@tue.nl

1 Introduction and Method

In literature, the most used model for soft robot rod structures is the Piecewise-Constant-Curvature (PCC) model. That approach keeps the rigid structure of the system mostly intact and substitutes the rigid links with links that are deformed in a specific constant curvature. Due to the low number of Degrees of Freedom $DOF = n - 1$ with n being the number of discrete points distributed over the continuum, the PCC model is a numerically effective solution. On the other hand, it is not particularly accurate when external forces or gravity influence the system, which can be seen in [2]. To describe the dynamics of soft actuators more accurately, a more advanced approach based on discretized continuum theories is necessary. The most accurate option for that problem is a Finite-Element formulation of a Cosserat rod, but that is also an expensive solution in terms of computational efficiency since the Degrees of Freedom grow with $DOF = 6n$. To be able to design a real-time control of soft robots, the computational efficiency of these models is an important factor. To reduce the order of the model and improve the computational accuracy of the continuum-based system, we propose a minimalformulation of a spatial Kirchhoff-Love rod, which is discretized based on the theory of isogeometric analysis with B-spline interpolation functions. That way we were able to reduce the number of DOFs for multi-segment continuum robot models by 33% to $DOF = 4n$, while maintaining the same accuracy and performance as the more expensive Finite-Element formulation of a Cosserat rod. The Kinematics of a spatial continuum rod are illustrated in Figure 1. This continuous rod theory

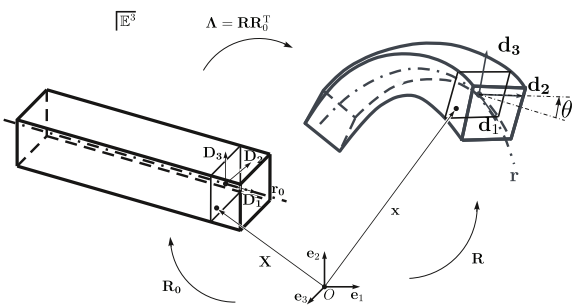

Figure 1: Kinematics of a nonlinear spatial Kirchhoff Love rod.

formulation is being derived from the principle of virtual work [1]. Afterwards, the rod is being discretized as a geometrically exact beam with B-spline curves in a Bubnov-Galerkin method, because the minimalformulation requires shape functions, which are at least C^1-continous globally over the whole domain. Typical Lagrange elements of FEM-discretizations for example are only C^0-continuous on the element boundaries and therefore can not represent the deformations of this rod formulation accordingly.

2 Validating Example

To validate the accuracy of the Kirchhoff-Love rod model based on B-splines, we analyze the numerical example of a multi-segment continuum manipulator, which is loaded with an increasing external force at the tip. By analysing the x-,y-,z-displacement of the end-effector we compare the minimalformulated Kirchhoff-Love rod with B-splines to a Cosserat rod with Lagrange elements and a Cosserat rod model in [3]. Figure 2 shows that the minimalformulation can achieve basically the same accuracy, while having 33% fewer $DOFs$ and therefore being a computationally less expensive model option for the control of soft robots.

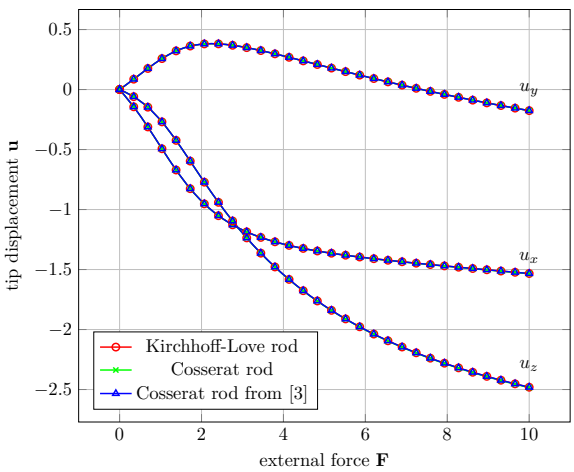

Figure 2: Performance of multi-segment continuum models.

References

[1] Eugster, S. On the Foundations of Continuum Mechanics and its Application to Beam Theories (2014).

[2] Neppalli, S., and Jones, B. A. Design, construction, and analysis of a continuum robot. IEEE/RSJ International Conference on Intelligent Robots and Systems (2007).

[3] Harsch, J., Capobianco, G., and Eugster, S. R. Finite element formulations for constrained spatial nonlinear beam theories. Mathematics and Mechanics of Solids (2021).

Control framework for precise robotic manipulation tasks for insect farming under the CoRoSect Horizon 2020 project

K. Bujnarowski, S. Grassi, L. Dahl, R. Möckel
Department of Advanced Computing Sciences
Maastricht University
Paul-Henri Spaaklaan 1, 6229 EN, Maastricht
The Netherlands
Email: k.bujnarowski@maastrichtuniversity.nl

1 Abstract

The environmental footprint of today's food production and concerns about self-sufficiency have created interest in producing proteins for feed and food by farming insects. To meet the required industrial scale in insect production, it is however necessary to enhance production efficiency, reduce labor intensity and thereby markedly decrease the production cost. The Horizon 2020 project 'Cognitive Robotics for automated and digitized Insect Farming' (CoRoSect) aims to introduce a digitized, integrated solution to insect farming where robots handle most of the challenging manipulation tasks. CoRoSect aims at pushing the state-of-the-art to a point where robots can manipulate objects they have not seen before and handle these objects without the involvement of writing or training new software. This is still an unsolved problem. However, if a robot would gain such abilities it would allow insect farms, but also other industrial and agricultural applications, to quickly exchange materials and objects to be handled.

Here we present preliminary work aiming at enabling a KUKA LBR iiwa 14 robot arm to automatically identify those grasping poses that would allow the robot arm to pick up and manipulate objects the robot arm has not encountered before. For this we equip the robot arm with a ZED2i stereo camera and a RG6 gripper from OnRobot. The control framework for the robot consists of the off-the-shelf path-planning system MoveIt! combined with a grasp synthesis algorithm. With the ZED2i stereo camera we register the workspace including those objects that should be manipulated as a 3D point cloud. With the robot arm we move the stereo camera to generate a point cloud from different perspectives. Still this point cloud provides an incomplete representation of the object to be manipulated due to occlusions and reflections forcing us to deal with challenging representations as we can expect from realistic scenarios inside insect farms. We transform the occupancy map into the robot's coordinate frame, and plan a series of waypoints using the Open Motion Planning Library (OMPL) in MoveIt!. Both joint space and Cartesian space are applicable, with inverse kinematics being performed on the proprietary robot controller. Preliminary results on processing time of path planning to random poses in joint space are calculated within a mean of 0.013s and a linear path in Cartesian space is calculated within a mean of 0.060s with an 80% success rate. Two methods have been further expanded upon with a focus on obtaining suitable grasping positions from the generated point clouds: a surface matching algorithm called LoCoMo [1], and a novel integration of LoCoMo with an end-to-end architecture based on PointNet++ [2]. PointNet++ is a deep neural network architecture specifically designed for processing 3D point clouds. LoCoMo has been modified to integrate the RG6 gripper and to return the possible grasping poses. LoCoMo was used to automatically label a simulated dataset to train the PointNet++ model. This model allows the robot to compute a grasping pose without the necessity of a priori obtained 3D models of objects. The two resulting approaches have been benchmarked on point clouds obtained from the YCB object and model dataset [3] and have been tested on real-world low-quality robot perceptions generated from the ZED2i stereo camera. PointNet++ demonstrated a fast grasp synthesis (with a median of 40ms) and 69% accuracy in collision prediction, even with objects partially invisible in the point cloud. LoCoMo proved its suitability, generating in median 32s a median of 651 possible grasping poses. In the end, for the KUKA LBR iiwa 14 robot arm, the control framework, combining the MoveIt! path planning, KUKA inverse kinematics controller, and grasping synthesis achieved 75% successful stable grasps in our tests. Several limitations in the training procedure and the architecture of our PointNet++ model have been identified convincing us that further improvements in accuracy will become possible in the future.

References

[1] M. Adjigble et al., "Model-free and learning-free grasping by local contact moment matching," 10 2018.

[2] C. R. Qi et al., "Pointnet++: Deep hierarchical feature learning on point sets in a metric space," 2017.

[3] B. Calli, et al., Benchmarking in Manipulation Research: Using the Yale-CMU-Berkeley Object and Model Set, in IEEE Robotics Automation Magazine, vol. 22, no. 3, pp. 36-52, Sept. 2015.

Learning Control for Vibration Free Flexible Object Handling with a Robot Manipulator.

Daniele Ronzani, Shamil Mamedov and Jan Swevers
MECO Research Team, Dept. of Mechanical Engineering, KU Leuven, Belgium
Flanders Make@KU Leuven, Belgium
deniele.ronzani@kuleuven.be

1 Introduction

Innovative solutions in many industries require lighter, more durable, and often, consequently, flexible material. Applying standard manipulation solutions to flexible materials can lead to large vibrations. Existing solutions that cope with flexibilities require accurate sensing of the vibrations using additional sensors, complex analytical or data-driven models and often lead to an increase of the task execution time. In this work we address the general problem of manipulating a flexible beam with a rigid robot arm. In this work, by exploiting the repetitive nature of many manipulation tasks, we focus on Iterative Learning Control (ILC) approach and, specifically, to a solution that does not use exteroceptive sensors to sens beam vibrations – such as external force-torque sensors at the end-effector or position tracking system – only a joint torque estimator, available in the manipulator software, is used. Additionally, the approach only employs a simple pendulum approximation of the flexible object. In contrast to the state-of-the-art, the proposed approach simultaneously designs the point-to-point (PTP) motion trajectory while accounting for residual vibrations, the nonlinear dynamics of the manipulator and hard joint constraints.

2 Algorithm

This work [1] presents a vibration suppression ILC for flexible object handling with a robot manipulator. The approach starts by deriving a simple yet effective model of the setup used for estimation and control. Namely: a double integrator to describe the robot dynamics; a pendulum dynamics approximation of the flexible object attached to the end-effector employing the forward kinematics; finally, a model of the external torque sensing that accounts for estimation errors. The ILC approach exploits the generic formulation of an explicit learning and control steps. The learning step consists of two estimation problems: the first, to learn the parameters of the above mentioned pendulum model considering the nonlinear kinematics of the robot manipulator; the second, to learn an equivalent output disturbance to account for residual dynamics. Finally, the control step, in which we formulate a vibration suppression Optimal Control Problem (OCP) for PTP motions that leverages the learned residual dynamics and exploit a time-optimal-like formulation to induce zero residual vibration.

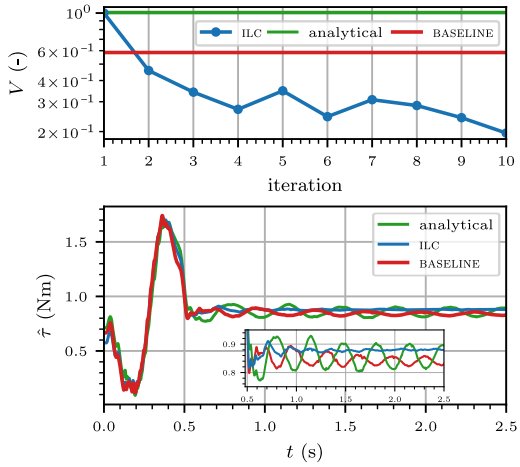

Figure 1: Top: Vibration suppression metric along the ILC iterations. Bottom: residual vibrations induced in the torque measurements $\hat{\tau}$ for the last iteration of the proposed ILC, an approach using ANALYTICAL, and the BASELINE state-of-the-art solution.

3 Experiments

The approach is experimentally validated on a 7-dof Franka Emika Panda robot arm manipulating a stainless steel flexible beam. A visual demonstration of the experiments can be found at https://youtu.be/c8vi91NDlkg. Figure 1 compares the superior vibration suppression performance of the proposed ILC method with a solution using model parameters obtained analytically and a state-of-the-art solution that exploits identified model parameters through ad-hoc experiments prior to the task.

References

[1] D. Ronzani, S. Mamedov, and J. Swevers, "Vibration Free Flexible Object Handling with a Robot Manipulator Using Learning Control," Nov. 2022, doi: 10.48550/arxiv.2211.11076.

Acknowledgement This research was supported by the FWO-Vlaanderen through SBO project ELYSA for cobot applications (S001821N).

Multi-agent control with hard constraints and lossy communications

Matthias Pezzutto, Emanuele Garone
Service d'Automatique et d'Analyse des Systèmes (SAAS) – Université Libre de Bruxelles (ULB)
email addresses: matthias.pezzutto@ulb.be, emanuele.garone@ulb.be

1 Introduction

Moving toward future industrial applications, mobile and cooperative robots are expected to substitute fixed single-robot systems aiming to achieve higher flexibility. Looking further, mobile cooperative robots can potentially cross factory boundaries to meet a large number of other applications, e.g., agriculture, construction, delivery, and autonomous operations in city environment. Such multi-agent systems are characterized by the *presence of constraints* and the *need for wireless communications*. On one side, constraints arise due to obstacles and coordination requirements, e.g., limits on the relative distance between the agents or on the stress applied to the load in cooperative object transportation tasks (see Figure 1). On the other side, wireless communications allow to connect mobile agents while avoiding annoying wires. Unfortunately, they introduce packet losses and delays in the loop. In the literature, several works have addressed the problem of constrained control in mobile robotics, both for single-agent and multi-agent systems. However, they mainly focus on obstacle avoidance and typically use soft constraints to ease the implementation. Similarly, control with lossy communications has been widely studied in the last twenty years. However, the interplay of lossy communications and constraints has been less studied, especially for the multi-agent case.

2 Problem formulation

Consider a system featuring N agents cooperating to accomplish a task. The overall system state is given by the concatenation of the states of the agents and possibly the state of the load, while the overall system input is given by the concatenation of the inputs of the agents. We assume that the agents and the load are equipped with an onboard sensor able to measure its own state. We assume that the overall system is linear and strictly stable, possibly thanks to low-level local feedback laws implemented on the agents. The objective is to design the input such that the overall system state always fulfils hard convex constraints and it eventually reaches a desired target state. We propose to solve the problem through a central control unit and to use a shared wireless network to connect the control unit with the agents. Specifically, the wireless network is used for transmissions of control packets (from the control unit to the agents, containing the new inputs), and of measurement packets (from the agent to the control unit, containing the current state and the current applied input). Unfortunately, the wireless network is unreliable and packets may be randomly lost.

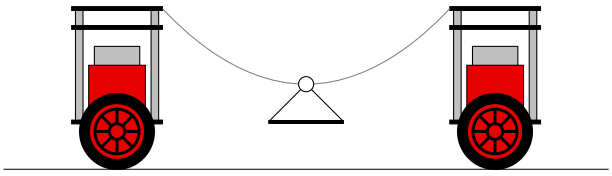

Figure 1: Two wheeled robots transporting a suspended load. Distance between the agents is limited to avoid that the load touches the floor or the rope is too stressed. Presence of both constraints and wireless communications poses new challenges. For instance, if two new inputs are admissible when both applied (e.g. two shifts ahead of 1m starting from an initial still position) but one packet is lost, the constraints will be violated.

3 Proposed solution

The considered problem has two critical issues. First, if new inputs are computed to be admissible if applied by all the agents, constraints may be violated in situations where the packets have been received and used only by some agents. Second, when a new input is sent but no information is received back at the control unit, the applied input is no more known and the number of possible states increases, possibly exponentially with the number of unknown past inputs.
To solve the first issue, we adopt an asynchronous approach where at each sampling instant only the new input of one agent is computed and transmitted. In this way, if the input is suitably computed, we are able to move among admissible configurations: if the control packet arrives, then the system moves to the new admissible configuration, while, if the packet is lost, the system remains in the current admissible configuration. To solve the second issue, we adopt a smart agent allocation mechanism to decide the agent whose input is computed. More specifically, the new input of an agent is computed and transmitted only if its current applied value is known by the central controller. In this way, the number of possible states is limited.
The proposed solution consists of a state estimator and a constrained controller. The estimator is designed to compute in an efficient way all the possible states. The controller is based on the Reference Governor over Lossy Channels [1]. The main idea is to enforce that the new computed input, if kept constant, satisfies the constraints for any arbitrary long period and for any state estimate provided by the estimator.

References

[1] M. Pezzutto, E. Garone, L. Schenato. "Reference Governor for Constrained Control over Lossy Channels." IEEE Control Systems Letters (2019)

Combined Approach for Achieving Both Task Flexibility and Higher Tracking Performance in ILC

Kentaro Tsurumoto
The University of Tokyo
tsuruken@koseki.t.u-tokyo.ac.jp

Wataru Ohnishi
The University of Tokyo
ohnishi@koseki.t.u-tokyo.ac.jp

Takafumi Koseki
The University of Tokyo
koseki@koseki.t.u-tokyo.ac.jp

1 Background

Basis Function Iterative Learning Control (B-ILC) enables task flexibility for ILC [1]. However, B-ILC has a compromise in achievable tracking performance when compared to other ILC frameworks such as frequency domain ILC (F-ILC). The aim of this paper is to develop an ILC framework combining the previous frequency domain design and basis function approach, enhancing the tracking performance against repeating tasks without losing task flexibility.

2 Problem Formulation

The control objective is to minimize the tracking error $e_j = r_j - y_j$ for trial j as possible for both when same tasks are repeated and tasks have been changed. The supposed close-loop setup and reference trajectories are shown in Figure 1.

3 Approach

As shown in Figure 1, the approach consists of parallel feedforward of basis function component f_j^θ and frequency domain design component f_j^{ILC}. H_θ is an optional filter which may be used to get desired error characteristic for latter (3).

3.1 Basis function component f_j^θ

Instead of minimizing e as the validation function, minimizing $e^\theta := e + SGf^{\mathrm{ILC}} = Sr - SGH_\theta F(\theta)r$ is proposed. Due to this modification, f^θ will be able to learn an accurate inverse model G^{-1} with less parameter estimation bias.

3.2 Frequency domain design component f_j^{ILC}

The feedforward update law is defined as

$$f_{j+1}^{\mathrm{ILC}} = Q(f_j^{\mathrm{ILC}} + Le_j) + H_\theta(f_j^\theta - f_{j+1}^\theta). \tag{1}$$

With an assumption of an asymptotic FF controller $F(\theta_\infty) = \lim_{j\to\infty} F(\theta_j)$ and

$$|Q(e^{i\omega})||1 - G(e^{i\omega})S(e^{i\omega})L(e^{i\omega})| < 1, \quad \forall\omega, \tag{2}$$

the asymptotic error $e_\infty = \lim_{j\to\infty} e_j$ for C-ILC becomes,

$$e_\infty = \frac{(1-Q)S}{1-Q(1-SGL)}(1 - H_\theta GF(\theta_\infty))\,r. \tag{3}$$

This achieves $(1 - H_\theta GF(\theta_\infty))$ times performance improvement against traditional F-ILC. Note that in this implementation f_{j+1}^{ILC} is reset to zero when task is changed.

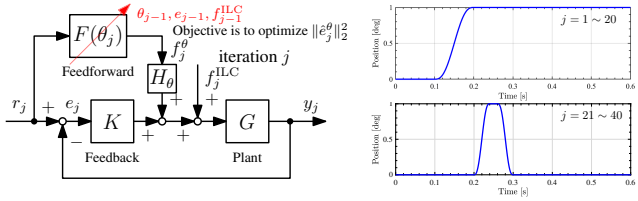

Figure 1: Left: Proposed Combined ILC (C-ILC) structure. f_j^θ and f_j^{ILC} each denote the basis function component and frequency domain design component respectively. Right: Given task r_j per each iteration.

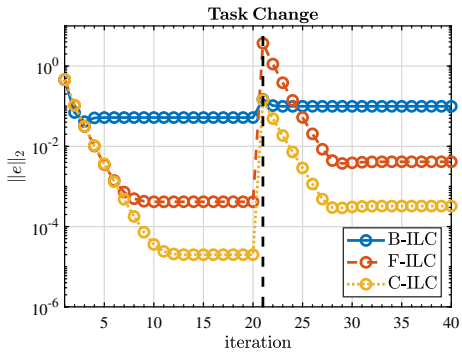

Figure 2: Comparison of F-ILC, B-ILC, and C-ILC performance.

4 Results

Tracking performance per iteration of C-ILC is compared with traditional F-ILC and B-ILC in Figure 2. From the result, C-ILC is able to exceed the performance of F-ILC for repeating tasks, while ensuring the same task flexibility as B-ILC.

5 Ongoing Research

Ongoing research is focused at experimental validation and the consideration of disturbance.

References

[1] L. Blanken, F. Boeren, D. Bruijnen, and T. Oomen, "Batch-To-Batch Rational Feedforward Control: From Iterative Learning to Identification Approaches, with Application to a Wafer Stage," *IEEE/ASME Transactions on Mechatronics*, 22(2), 826–837.

Privacy Analysis for Control Systems with a Stochastic Quantizer

Le Liu
DTPA Group
University of Groningen
Nijenborgh 4, 9747 AG Groningen
The Netherlands
Email: le.liu@rug.nl

Ming Cao
DTPA Group
University of Groningen
Nijenborgh 4, 9747 AG Groningen
The Netherlands
Email: m.cao@rug.nl

1 Introduction

Cloud computing and control improve the efficiency of modern industries, which also raise privacy concerns. The private information may be inferred by some adversaries for monitoring the activities of those agents that carry out computations or implement control actions. For instance, it has been shown that Google Map can be used to monitor an agent's movement[1]. Therefore, researchers have considered different mechanisms to guarantee privacy while ensuring the connectedness between network nodes. Quantization control has been shown to be an effective way to guarantee the privacy of initial states while stabilizing the systems[2]. Designing a stochastic quantizer to guarantee the privacy of the initial state is the main focus of this research.

2 Problem Formulation

Consider a discrete-time, linear, time-invariant system:

$$\begin{aligned} x(k+1) &= Ax(k), x(0) = x_0 \\ y(k) &= Cx(k). \end{aligned} \tag{1}$$

where $x \in \mathbb{R}^{n_1}$, and $y \in \mathbb{R}^p$. The matrix dimensions are compatible. Instead of directly sharing the outputs in the network, we propose to share quantized outputs, which is given in the following form:

$$v = \mathscr{Q}_v(y), \tag{2}$$

where $v \in \mathbb{R}^p$ and $\mathscr{Q}_v$ is a quantizer to be specified subject to communication capacity constraints and privacy requirements. In this work, we would like to design a quantizer $\mathscr{Q}_v$ that protects the privacy of initial state x_0.

The following definitions describe what we mean by differential privacy.

Definition 1 [3]: Given $\zeta > 0$, a pair of initial states $(x_0, x_0') \in \mathbb{R}^{n_1} \times \mathbb{R}^{n_1}$ is said to belong to the binary relation ζ-adjacency if $||x_0 - x_0'||_1 \leq \zeta$. The set of all pairs of the input data that are ζ-adjacent under the $1-$ norm is denoted by Adj_1^{ζ}.

Definition 2 [3]: Let $\left(\mathbb{R}^{(t+1)p}, \mathscr{F}, \mathbb{P}\right)$ be a probability space. The mechanism (2) is said to be (ε, δ)-differentially private for Adj_1^{ζ} at a finite time instant $t \in \mathbb{Z}_+$if there exist $\varepsilon > 0$ and $\delta \geq 0$ such that

$$\begin{aligned} &\mathbb{P}(\mathscr{Q}_v(O_t x_0) \in \mathscr{S}) \\ &\leq \mathrm{e}^{\varepsilon} \mathbb{P}\left(\mathscr{Q}_v(O_t x_0') \in \mathscr{S}\right) + \delta, \forall \mathscr{S} \in \mathscr{F} \end{aligned}$$

for any $(x_0, x_0') \in \mathrm{Adj}_1^{\zeta}$, where

$$O_t := [C^\top, (CA)^\top, ..., (CA^{t-1})^\top]^\top.$$

3 Stochastic Quantizer

The stochastic quantizer $\mathscr{Q}_v$ (function on each element of a vector) is designed by:

$$\mathscr{Q}_v(z+nd) = \begin{cases} nd, \text{with Prob. } 1 - \frac{z}{d} \\ (n+1)d, \text{with Prob. } \frac{z}{d} \end{cases} \quad z \in (0, d], n \in \mathbb{Z}, d > 0. \tag{3}$$

Then, we have the following main theorem:

Theorem: For a fixed time t and a given $r \in (0,1)$, $(0,r)$ differential privacy for Adj_1^{ζ} can be achieved if the quantizer $\mathscr{Q}_v$ in the form of (3) chooses the quantization level $d \geq \frac{||O_t||_1 \zeta}{r}$.

It can be concluded that with a coarser quantizer (a larger d), the initial state of the system is more private. The estimation and control performance with such quantizers can be further analyzed.

References

[1] Wang, G., Wang, B., Wang, T., Nika, A., Zheng, H., & Zhao, B. Y. (2016, June). Defending against sybil devices in crowdsourced mapping services. In Proceedings of the 14th annual international conference on mobile systems, applications, and services (pp. 179-191).

[2] Y. Kawano and M. Cao, "Effects of Quantization and Dithering in Privacy Analysis for a Networked Control System," 2021 60th IEEE Conference on Decision and Control (CDC), Austin, TX, USA, 2021, pp. 2758-2763.

[3] Y. Kawano and M. Cao, "Design of Privacy-Preserving Dynamic Controllers," in IEEE Transactions on Automatic Control, vol. 65, no. 9, pp. 3863-3878, Sept. 2020.

Physics–guided neural networks for feedforward control with input–to–state stability guarantees

Max Bolderman[1], Mircea Lazar[1] and Hans Butler[1,2]
[1] Control Systems Group, Eindhoven University of Technology, 5600 MB Eindhoven, The Netherlands
[2] ASML, 5504DR Veldhoven, The Netherlands.
Email: {m.bolderman, m.lazar, h.butler}@tue.nl

1 Introduction

High–performance feedforward controllers require flexible nonlinear models, such as physics–guided neural networks (PGNNs), for accurate identification of the (inverse) system dynamics [1]. However, the nonlinear model complicates the assessment of stability, which is crucial for safe operation. In this work, we derive stability conditions for nonlinear PGNN feedforward controllers via the discrete–time input–to–state stability (ISS) framework [2]. The conditions can be used to impose stability of the PGNN before training.

2 ISS of PGNN feedforward controllers

Consider the following PGNN feedforward controller

$$u_{\text{ff}}(k) = [\hat{a}^T, \hat{b}^T] \begin{bmatrix} \phi_r(k) \\ \phi_{u_{\text{ff}}}(k) \end{bmatrix} + f_{\text{NN}}\left(\hat{\theta}_{\text{NN}}, \begin{bmatrix} \phi_r(k) \\ \phi_{u_{\text{ff}}}(k) \end{bmatrix}\right), \quad (1)$$

where $\phi_{u_{\text{ff}}}(k) := [u_{\text{ff}}(k-1), \ldots, u_{\text{ff}}(k-n_b+1)]^T$ with $u_{\text{ff}}(k)$ the feedforward input, $\phi_r(k) := [r(k+n_k+1), \ldots, r(k+n_k-n_a+1)]^T$ with $r(k)$ the reference signal, and $k \in \mathbb{Z}_{\geq 0}$ the time instant. The function $f_{\text{NN}} : \mathbb{R}^{n_{\theta_{\text{NN}}} \times (n_a+n_b)} \to \mathbb{R}$ represents the neural network, and the parameters $\hat{\theta} := [\hat{a}^T, \hat{b}^T, \hat{\theta}_{\text{NN}}^T]^T$ are trained to have the PGNN approximate the inverse system on a data set. A state–space representation of the PGNN (1) can be obtained by defining $x(k) := \phi_{u_{\text{ff}}}(k)$, i.e.,

$$\begin{aligned} x(k+1) =& A(\hat{b})x(k) + B\Big(\hat{a}^T \phi_r(k) \\ &+ f_{\text{NN}}\left(\hat{\theta}_{\text{NN}}, [\phi_r(k)^T, x(k)^T]^T\right)\Big), \end{aligned} \quad (2)$$

where $B := [1,0]^T \in \mathbb{R}^{n_b-1}$, $A(\hat{b}) := \begin{bmatrix} \hat{b}^T \\ I \quad 0 \end{bmatrix} \in \mathbb{R}^{(n_b-1)\times(n_b-1)}$, and $\phi_r(k)$ is the external input. We pursue ISS of the PGNN (1), since this implies:

1. $x(k)$ remains bounded for bounded $\phi_r(k)$ and, consequently, $u_{\text{ff}}(k)$ remains bounded;
2. $x(k) \to 0$ for $\phi_r(k) \to 0$ and, consequently, $u_{\text{ff}}(k) \to 0$.

ISS conditions for (2) are derived in [1], which require that $\hat{b}$ is such that $A(\hat{b})$ is Hurwitz, and $\hat{\theta}_{\text{NN}} \in \Theta_{\text{NN}}$ with Θ_{NN} a predefined set. Moreover, in the situation that $A(\hat{b})$ is not Hurwitz, ISS of the PGNN (2) can be achieved via:

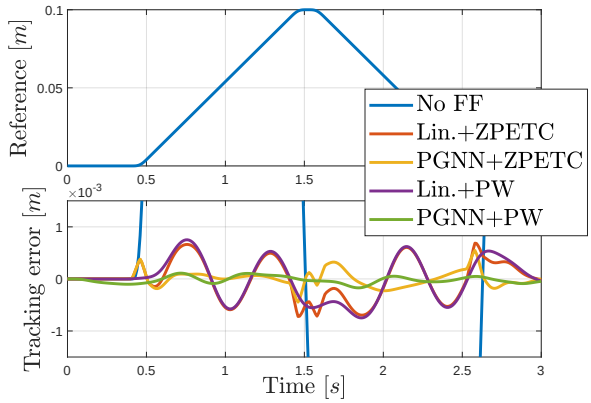

Figure 1: Reference (top window) and the tracking errors resulting from the different feedforwards (bottom window).

1. *Linear stable approximate inversion techniques* on the linear part of (1), such as ZPETC, or ZMETC;
2. *Increasing the preview window*, i.e., use $\phi_{u_{\text{ff}}} = [u_{\text{ff}}(k-1), \ldots, u_{\text{ff}}(k-n_b+1+n_{\text{us}})]^T$ and $\phi_r = [r(k+n_k+1+n_{\text{pw}}), \ldots, r(k+n_k-n_a+1)]^T$ with $n_{\text{us}} \in \mathbb{Z}_{\geq 0}$ the number of unstable eigenvalues of $A(\hat{b})$ and $n_{\text{pw}} \in \mathbb{Z}_{\geq 0}$ the extended preview window, and reidentify $\hat{\theta}$.

3 Nonminimum phase simulation example

Effectiveness of the PGNN is demonstrated on a nonminimum phase rotating–translating mass with nonlinear cogging force, see [1] for details. Fig. 1 shows the reference and the resulting tracking error achieved by linear and PGNN feedforward controllers stable approximated using ZPETC or a preview $n_{\text{pw}} = 20$. Due to the flexible model structure, the PGNN outperforms the linear feedforward controller.

References

[1] M. Bolderman, H. Butler, S. Koekebakker, E. van Horssen, R. Kamidin, T. Spaan–Burke, N. Strijbosch, M. Lazar, "Physics–guided neural networks for feedforward control with input–to–state stability guarantees," *arXiv:2301.08568*, 2023.

[2] Z.–P. Jiang, Y. Wang, "Input–to–state stability for discrete–time nonlinear systems," *Automatica*, vol. 37, no. 6, pp. 857–869, 2001.

Dynamic mathematical models of theory of mind for model-based control of socially assistive robots

Maria Morão Patrício
Faculty of Aerospace Engineering, TU Delft
M.L.MoraoPatricio@tudelft.nl

Anahita Jamshidnejad
Faculty of Aerospace Engineering, TU Delft
A.Jamshidnejad@tudelft.nl

1 Abstract

Socially assistive robots (SARs), i.e., robots that assist human users via social interactions [3], have shown the potential to improve the life quality of humans in the fields of health care, education, assistance of children with learning disabilities, and in-home-assistance. Despite their expected benefits, these robots do not yet have the capability to engage their users for long periods of time, since they lack social skills. Being able to keep the users interested indeterminately is of extreme importance given that, in the domains where SARs are expected to help humans, the capability of accompanying the users for long periods of time is of utmost importance [3]. Consequently, SARs do not yet assist humans in the real world.

The incapability of sustaining user engagement is intrinsically linked with the methods used to control the behavior of SARs. Model-based control methods, e.g., model predictive control, offer several benefits to SARs. Particularly, model predictive control is one of the most popular control methods that can explicitly cope with constraints, next to being able to deal with systems with multiple inputs, outputs, constraints, and conflicting control objectives. Most of the state-of-the-art controllers for SARs rely on black-box approaches, e.g., machine learning methods such as reinforcement learning, that are trained with the goal of maximizing the performance of the users in the task where the SAR must help the users with. Furthermore, these methods never attempt to model the cognition of the users. Nevertheless, understanding the users and their mental states is essential for SARs to behave humanly and socially [3]: when humans socially interact with each other, they create cognitive models of their peers and behave according to what these models estimate to be the mental states of their peers. This allows humans to steer their relationships with their peers. Logically, for SARs to behave humanly, they require similar models. Moreover, the existence of mathematical models of human cognition will enable SARs to use, for the first time, systematic model-based control methods, such as model predictive control.

Therefore, we propose a cognitive model of humans based on the findings from cognitive science research, and we formalize it mathematically as a dynamic representation of human cognition and behaviour. Given this formalization, it is possible to apply control theory and methods (e.g., model-based control) in order to use the model not only to estimate and predict the behaviour of humans, but also to control the behaviour of the robot in a predictive way based on the model of the human.

The framework selected to formalize the cognitive models was Theory of Mind, a framework proposed in the field of neuroscience that has been successfully used to generate computational models of human behaviour and cognition. Therefore, our model has been developed based on a simple computational Theory of Mind model proposed by Baker [1]. This model describes the actions of rational agents as a consequence of their beliefs and goals, and is formulated as a Partially Observable Markov Decision Process (POMDP). The model is able to make inferences regarding the beliefs and goals of agents given their actions using Bayesian inference [1]. In our proposed model, we have added certain elements (particularly emotions and biases) to the model by Baker [1]. These new elements have been shown by cognitive scientists to play a significant role in human cognition. An extensive mathematical formalization is presented, and the model is mathematically formulated using fuzzy variables and fuzzy cognitive maps [2]. The model was implemented in Python and its structure, formalization, and formulation were validated by using the model to predict the behaviour and estimate the intentions of human participants in a computer simulation. In the simulation, the participants were requested to make decisions in search and rescue scenarios regarding which human, animal, or object they would save in different circumstances.

References

[1] Chris L. Baker, Rebecca R. Saxe, and Joshua B. Tenenbaum. "Bayesian theory of mind: modeling joint belief-desire attribution". In: *Proceedings of the Annual Meeting of the Cognitive Science Society*. Boston, MA, USA, 2011, pp. 2469–2474.

[2] Bart Kosko. "Fuzzy cognitive maps". In: *International Journal of Man-Machine Studies* 24.1 (Jan. 1986), pp. 65–75.

[3] Maja J. Matarić and Brian Scassellati. "Socially Assistive Robotics". In: *Springer Handbook of Robotics*. 1st. Berlin, Heidelberg, Germany: Springer, 2016, pp. 1973–1993.

Disturbance-based control design in a gravitational wave detector: an $\mathscr{H}_2$-based dynamic error budgetted approach

Mathyn van Dael[1,2,*], Gert Witvoet[1,3], Bas Swinkels[2], Tom Oomen[1,4]
[1] Control Systems Technology, Eindhoven University of Technology, Eindhoven, The Netherlands
[2] Nikhef, Amsterdam, The Netherlands
[3] Optomechatronics Department, TNO, Delft, The Netherlands
[4] Delft Center for Systems and Control, Delft University of Technology, Delft, The Netherlands
*Email: m.r.v.dael@tue.nl

1 Introduction

Gravitational Wave detectors such as Virgo [1] (Fig. 1) utilize interferometry between two several kilometer long beams of light to detect fluctuations in *spacetime* in the order of 1×10^{-18} m. In this work, $\mathscr{H}_2$ synthesis is used to optimize one of the the control systems in Virgo. Experimental results of the new control design on the Gravitational Wave detector Virgo are furthermore presented.

2 Problem formulation

One of the degrees of freedom in Virgo is controlled using a set of three nested control loops. This control system is subject to various disturbances which couple through different disturbance paths to the output, making it difficult to determine which of the controllers to tune and how to improve the performance of the control system.

3 Approach

A dynamic error budget (see Fig. 2) of the control system is first used to identify the dominant disturbances and to determine which controller to tune. $\mathscr{H}_2$ optimization has then been used to redesign one of the controllers, using the dynamic error budget as weighting in the optimization scheme.

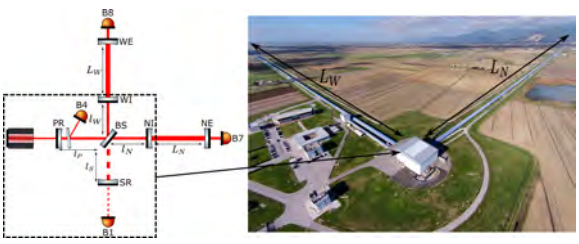

Figure 1: Optical layout of Virgo (left) and top view of Virgo (right). Two arms L_W and L_N are 3 km long.

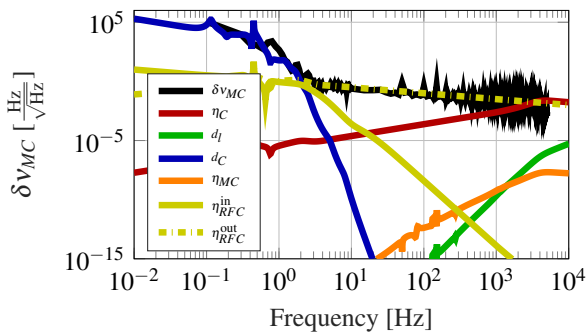

Figure 2: Dynamic error budget for one of the degrees of freedom in Virgo, illustrating the contributions of the different disturbances to the output of the control system.

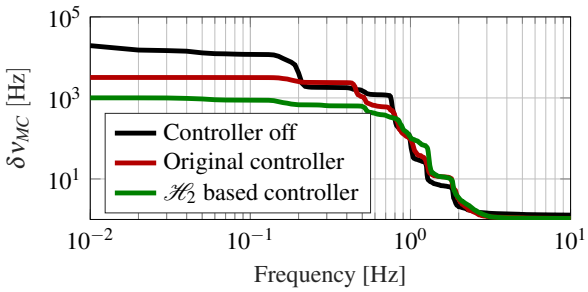

Figure 3: Comparison of the different control designs measured on Virgo. The $\mathscr{H}_2$ controller achieves lower RMS compared to the original controller.

4 Experimental results

In Fig. 3, a spectrum of the output of the control system measured on the Virgo detector is shown for the open-loop, old and newly presented control strategy. The $\mathscr{H}_2$ based control method is shown to achieve better performance compared to the old control design. In this talk, we will present a systematic design method using dynamic error budgetting and $\mathscr{H}_2$ synthesis to derive the presented control design and further elaborate on the experimental results.

References

[1] F. Acernese *et. al.*, "Advanced Virgo: a second-generation interferometric Gravitational Wave detector," Classical and Quantum Gravity, vol. 32, no. 2, p. 024001, 2014.

Plug-and-Play Secondary Control for Safety of LTI Systems under Attacks

Yankai Lin, Michelle S. Chong, and Carlos Murguia
Department of Mechanical Engineering
Eindhoven University of Technology
The Netherlands
Email: y.lin2@tue.nl, m.s.t.chong@tue.nl, and c.g.murguia@tue.nl

1 Introduction

We consider the problem of controller design for linear time-invariant cyber-physical systems (CPSs) controlled via networks. Specifically, we adopt the set-up that a controller has already been designed to stabilize the plant. However, the closed loop system may be subject to actuator and sensor attacks. To ensure the safety of the system, we choose a subset of sensors that can be locally secured. Using these limited resources, an extra controller is designed to enhance the safety of the new closed loop system. The safety of the system will be characterized by the notion of safe sets. Lyapunov based analysis is used to derive sufficient conditions that ensure the states always stay in the safe set. The conditions are stated as a convex optimization problem.

2 Problem formulation

We consider the setup in Figure 1, where the plant is modelled as a linear time-invariant (LTI) system. We also assume that there is already a controller stabilizing the plant,

$$\begin{aligned} \dot{x}_1 &= A_1 x_1 + B_1(y + a_y) \\ u_P &= C_1 x_1 + D_1(y + a_y) + a_u, \end{aligned} \tag{1}$$

which we call the *primary controller* of system. The signals a_u and a_y denote actuator and sensor attacks respectively. The secondary controller, taking the following form, uses a subset of the sensors and actuators, which are either available locally or known to be free of malicious manipulation.

$$\begin{aligned} \dot{x}_2 &= A_2 x_2 + B_2 y_S \\ u_S &= C_2 x_2 + D_2 y_S, \end{aligned} \tag{2}$$

where $y_S = C_S y$ is the set of sensors that are available to the secondary controller, and u_S is the control input signal. The goal of the secondary controller is to ensure that when the overall system with input (u_P, u_S) is subject to cyber attacks, the safety of the closed loop (1)-(2) can be ensured.

3 Main result

We synthesize the secondary controller to ensure safety using an optimization approach. The sensor selection matrix C_S is assumed to be pre-selected. Specifically, given C_S, we

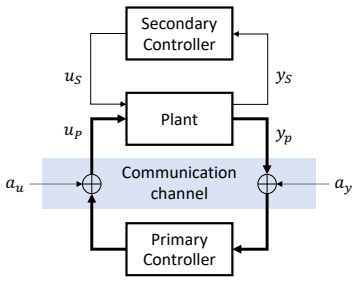

Figure 1: Ensuring safety with a secondary controller.

want to find $\kappa := (A_2, B_2, C_2, D_2)$ such that the size of the attack signal is maximized while there exists an invariant ellipsoid that is contained in the safe set (last condition in (3)). The synthesis problem can be formulated as follows.

$$\begin{aligned} \min_{P, R_a, \alpha, \beta, \kappa} \ & \mathrm{Tr}[R_a] \\ s.t. \ & -E_2 - \alpha F - \beta S \succeq 0 \\ & \mathscr{E}_P \subseteq \mathscr{E}(R_\zeta, \bar{\zeta}). \end{aligned} \tag{3}$$

The matrices containing both decision variables and system parameters E_2, F, and S are defined in [1]. The initial synthesis problem is not convex, but can be rendered so with a congruence transformation, which yields an LMI condition.

$$\begin{aligned} \min_{\eta, \alpha, \beta, \delta} \ & \mathrm{Tr}[R_a] \\ s.t. \ & \mathbf{E}_2 + \alpha \mathbf{F} + \beta \mathbf{S} \preceq 0 \\ & P(\eta) \succ 0 \\ & \mathbf{J} - \delta \mathbf{L} \preceq 0, \end{aligned} \tag{4}$$

where all matrices $\mathbf{E}_2, \mathbf{F}, \mathbf{S}, \mathbf{J}$, and $\mathbf{L}$ are shown to be linear in $\eta := (X, Y, \mathbf{A}, \mathbf{B}, \mathbf{C}, \mathbf{D})$ after change of variables. We verify the efficacy of the proposed design via a numerical example, where a secondary controller is designed to guarantee safety which can not be guaranteed by the primary controller alone.

References

[1] Y. Lin, M. S. Chong, and C. Murguia. "Plug-and-Play Secondary Control for Safety of LTI Systems under Attacks." arXiv preprint arXiv:2212.00593, 2022.

Predictive Control of Unknown Nonlinear Systems via Koopman Observables and Empirical Gramians

M. Bahadır Saltık Bayu Jayawardhana
Discrete Technology and Production Automation
University of Groningen
Nijenborgh 4
9747 AG Groningen
The Netherlands
Email: {m.b.saltik,b.jayawardhana}@rug.nl

Ashish K. Cherukuri
Optimization and Decision Systems
University of Groningen
Nijenborgh 4
9747 AG Groningen
The Netherlands
Email: a.k.cherukuri@rug.nl

1 Koopman Operator, Empirical Grammians and MPC Problem

Introduction: The aim of this work is to develop a model predictive controller (MPC) that controls an unknown nonlinear system along a trajectory. We make use of Koopman operator-based modeling ([1]) and empirical grammians ([2]) to approximate a prediction model. Recently Koopman operator is used for modeling nonlinear systems by transforming the state trajectories into the observables. Here the empirical controllability and observability grammians are calculated from the observable trajectories to generate a balanced linear state space system for the prediction model.

Mathematical Construction: Consider the reference tracking MPC problem for a nonlinear system as in $\mathscr{P}$:

$$\mathscr{P}: \begin{cases} \min & J^{MPC}, \\ J^{MPC} = & \sum_{j=0}^{N_p-1} \varepsilon_{j|k}^\top Q \varepsilon_{j|k} + \Delta u_{j|k}^\top R \Delta u_{j|k}, \\ x_{j+1|k} = & f(x_{j|k}, u_{j|k}),\ y_{j|k} = h(x_{j|k}), \\ \varepsilon_{j|k} = & y_{j|k} - r_{k+j},\ u_{j+1|k} = u_{j|k} + \Delta u_{j|k}, \\ & c_j(x_{j|k}, u_{j|k}) \leq 0. \end{cases} \tag{1}$$

We assume that state measurements are available, which defines the Koopman observables as $\chi_k = \Psi(x_k)$, where $\Psi(\cdot)$ are independent and invertible functions. The empirical grammians for the observables are defined as;

$$\begin{aligned} \hat{W}_c = & \frac{1}{|S_c|} \sum_{j=1}^{|S_c|} \sum_{m=1}^{M} \frac{1}{\varepsilon_j^c} \int_0^{t_f} \Phi_c^{jm}(t)dt \\ \hat{W}_o = & \frac{1}{|S_o|} \sum_{l=1}^{|S_o|} \sum_{n=1}^{N} \frac{1}{\varepsilon_o} \int_0^{t_f} \Phi_o^{ln}(t)dt \\ \text{where} \quad & \Phi_c^{jm} := (\chi_{jm} - \bar{\chi})(\chi_{jm} - \bar{\chi})^\top, \\ & \Phi_o^{ln} := (x_{ln} - \bar{x})(x_{ln} - \bar{x})^\top, \end{aligned} \tag{2}$$

in which the trajectories χ_{jm} and x_{ln} are generated from the same initial condition with perturbed input signal $u_{jm} = \bar{u} + \varepsilon_j^c e^m$ and from the same input with different initial conditions $\chi_0^{ln} = \bar{\chi}_0 + d_l e^n$, respectively. Lastly, $\bar{x}_k$ corresponds to the sample average of state trajectories within the state dataset at time k.

2 A Case Study and Conclusions

We consider the problem of controlling the levels of outputs in a 4-tank system. The system dynamics, the associated physical parameters and the MPC parameters can be found in [1]. For the Koopman observables, we make use of 5 distinct Gaussian kernels for each state dimension, with different centers around the average operating condition, and 100 different runs are stored to generate the average trajectories and the empirical grammians. Lastly we calculate the Hankel matrix, and resulting state-space realization, via the empirical grammians. The reference signal, constraints, and the resulting trajectories are given in Figure 1. The result

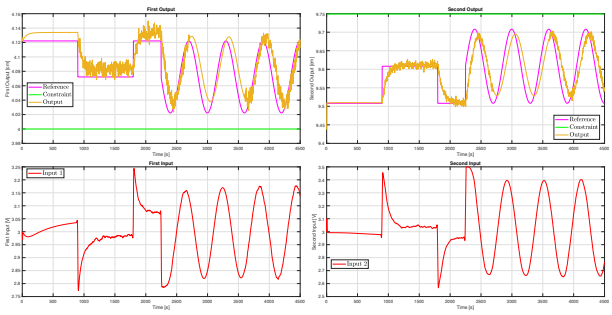

Figure 1: Output trajectories for the system controlled with MPC using model generated via Koopman observables and empirical grammians.

indicates that the system is controlled with acceptable accuracy. However, it is observed in different runs that the controlled trajectories are not guaranteed to satisfy the constraints, potentially due to plant-model mismatch.

References

[1] Saltık, M.B., Jayawardhana, B., Cherukuri, A. (2022). Koopman Operator based Iterative Learning and Model Predictive Control for Repetitive Nonlinear Systems. In 61st IEEE Conference on Decision and Control. IEEE.

[2] Himpe, C. (2018). emgr—the empirical gramian framework. Algorithms, 11(7), 91.

Improved Parameter Estimation of the Doyle-Fuller-Newman model by Incorporating Temperature Dependence

Francis Anne le Roux[1], Tijs Donkers[1], Henk Jan Bergveld[1,2]
[1] Control Systems Group, Eindhoven University of Technology, Netherlands
[2] NXP Semiconductors, Eindhoven, Netherlands
Email: f.a.l.le.roux@tue.nl

1 Introduction

Due to the complex electrochemical nature of Li-ion battery technology, modeling and control tools are needed to support the wide application of Li-ion batteries. Electrochemical models such as the Doyle-Fuller-Newman (DFN) model [1] are needed for more complex applications such as aging-aware charging or battery prognostics [3], as these applications require information on the internal states of the battery. Identifiability remains a key issue in estimating the model parameters of the Doyle-Fuller-Newman model. In this work, we aim to improve the identifiability and physical meaning of the model parameters by incorporating physics-based temperature relations.

2 Temperature-Dependent DFN Model

Based on literature, the temperature-dependent parameters of the DFN model are the Li-ion diffusion coefficient in the electrolyte D_e, the kinetic constants k_0, and the solid-phase Li-ion diffusion coefficients D_s [3]. We propose an adjusted DFN model which includes a temperature dependence that satisfies an Arrhenius relation, leading to

$$\hat{D}_e = \hat{D}_e^0 e^{-E_e^a/(RT)} \tag{1a}$$

$$\hat{D}_{s,i} = \hat{D}_{s,i}^0 e^{-E_{s,i}^a/(RT)} \tag{1b}$$

$$\hat{k}_{0,i} = \hat{k}_{0,i}^0 e^{-E_{0,i}^a/(RT)}, \tag{1c}$$

where $\hat{D}_e^0$, $\hat{D}_{s,i}^0$, and $\hat{k}_{0,i}^0$ are the pre-exponential factors and E_e^a, $E_{s,i}^a$, and $E_{0,i}^a$ are the activation energies of the electrolyte diffusion, the solid-phase diffusion and the reaction kinetics, respectively, in the different parts of the battery. R is the universal gas constant and T the temperature in Kelvin.

3 Parameter Estimation

The parameter estimation procedure of [2] was extended to perform parameter estimation over a wide temperature range. The parameter estimation procedure consists of a 3-step approach, determination of the electrode potentials, sensitivity analysis and estimation of model parameters. The sensitivity analysis is performed on the parameters to determine the sensitivity of the voltage output to each of the parameters. In case only a subset of the parameters is to be estimated to prevent overfitting, the most sensitive parameters should be estimated, while keeping the others constant

To investigate the effect of implementing temperature-dependencies in the DFN model, we analysed the change in Root Mean Square Error (RMSE) while estimating an increasing number of model parameters. Upon comparing the RMSE with an increasing number of parameters for the original and adjusted parameter estimation techniques Fig. 1, it was found that the implementation of physics-based temperature relations resulted in a parameter estimation technique which is robust and reliable.

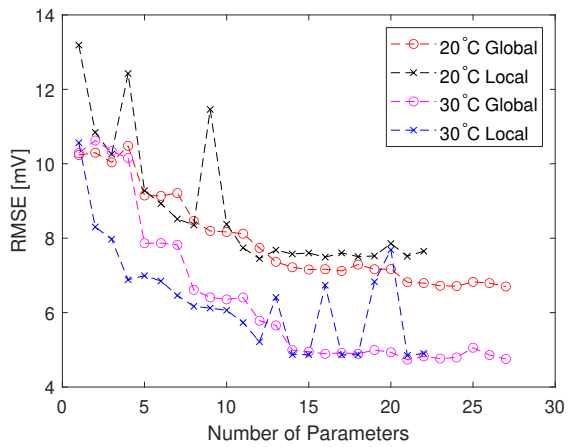

Figure 1: RMSE Response upon estimating an increasing number of model parameters

References

[1] Marc Doyle, Thomas F. Fuller, and John Newman. Modeling of galvanostatic charge and discharge of the lithium/polymer/insertion cell. *Journal of The Electrochemical Society*, 1993.

[2] Z. Khalik, M. C.F. Donkers, J. Sturm, and H. J. Bergveld. Parameter estimation of the doyle–fuller–newman model for lithium-ion batteries by parameter normalization, grouping, and sensitivity analysis. *Journal of Power Sources*, 2021.

[3] Changlong Li, Naxin Cui, Chunyu Wang, and Chenghui Zhang. Simplified electrochemical lithium-ion battery model with variable solid-phase diffusion and parameter identification over wide temperature range. *Journal of Power Sources*, 2021.

In-Flight Monitoring of an Aircraft Electromechanical Actuator

Benjamin Wauthion, Michel Kinnaert
SAAS, Université libre de Bruxelles
50, av. Roosevelt, 1050 Bruxelles, Belgique
Email: bewauthi@ulb.ac.be

Dan Telteu-Nedelcu, Paul Alexandre
Sté Anonyme Belge de Construction Aéronautique
Chaussée de Haecht 1470, 1130 Bruxelles, Belgium
Email: paul.alexandre@sabca.be

1 Introduction

In the framework of the "More Electric Aircraft", electromechanical actuators (EMAs) are further favored for the control of both primary and secondary aircraft flight surfaces [1]. Nonetheless, while EMAs could reduce weight and consumption, the reliability of the EMA technology is not yet established for critical applications. The degradation of mechanical parts specific to the EMA, i.e. gear teeth, ball bearings or nut/screw, is difficult to predict, and may lead to a significant mechanical backlash or jamming. As a consequence, it is required to develop a health monitoring system (HMS) that can ensure a proper predictive maintenance and hence the required level of reliability.

This abstract introduces a procedure for designing a monitoring algorithm able to perform early detection of degradations that may lead to jamming in an EMA used for the control surfaces of an aircraft. The challenge is to construct, without extra sensors, a detection algorithm performing an online monitoring while using realistic in-flight data.

2 The approach

In order to prevent jamming to happen, we propose to track the evolution of three parameters that characterize the internal friction of the EMA. These parameters describe the behavior of the dry, the load dependent, and the viscous friction. Based on this proposal, an online Fault Detection and Identification (FDI) procedure using in-flight data is constructed in three steps.

The detection of informative zones. During a flight, a control surface is subject to a wide variety of phenomena and excitations. However, the EMAs only move during a short duration in the different in-flight phases. It is thus necessary to identify the data subsets containing relevant information for the identification of at least some of the friction parameters. This first task is carried out through a sensitivity study which informs us when and which specific parameters can be identified.

The identification of the friction parameters. To this end a dual extended Kalman filter (DEKF) is exploted. A DEKF uses two separate filters, the first one is dedicated to the estimation of the states of the system, while the second one estimates the parameters of interest, i.e. the EMA friction parameters.

The computation and the analysis of residuals. The fault indicators or residuals, are obtained as the difference between the identified friction parameters and the predetermined healthy parameter values. An increase of friction is then detected when the confidence interval around the parameters identified online do not intersect anymore with the zone where the parameter values are associated to healthy operation.

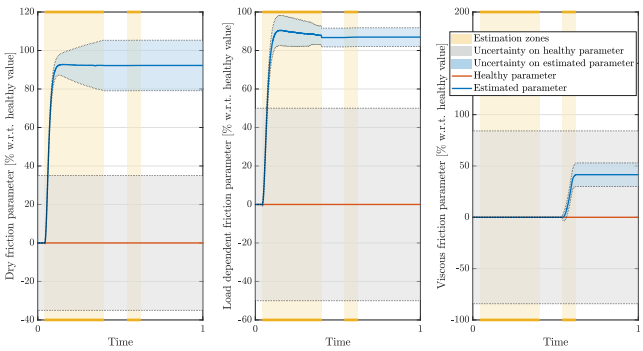

Figure 1: Friction parameters estimation. For confidentiality reasons the axis are normalized

As a matter of illustration Figure 1 shows the results of the parameter identification during a take-off phase (each subplot shows the estimation of one of the three friction parameters). The zones associated to informative data are highlighted by the yellow areas. The red line indicates the healthy value of the parameters; the grey area shows until which percentage the estimated parameter is considered as healthy. The blue curve is the ongoing estimation, to which is associated a 95% confidence interval (blue area). It appears that at the end of the take-off, the dry and load dependent parameters are faulty (no areas intersection), while the viscous friction parameter is still in the healthy zone.

3 Acknowledgement

This work is supported by the Brussels-Capital Region (Innoviris) through the MONISA project.

References

[1] D. Van Den Bossche, "The A380 flight control electrohydrostatic actuators, achievements and lessons learnt", 25th Inter. Congress of the Aeronautical Sciences, 2006.

Sensor Data Fusion in Electrochemical Applications: An Overview and its Application to Electrochlorination Monitoring

Ross, E.A.[1,2], Wagterveld, R.M. [1], Stigter, J.D. [2], Mayer, M. [3] and Keesman, K.J.* [1,2]

1. Wetsus, European Centre of Excellence for Sustainable Water Technology, Oostergoweg 9, 8911 MA, Leeuwarden, the Netherlands
2. Mathematical and Statistical Methods - Biometris, Wageningen University and Research, PO Box 16, 6700 AA, Wageningen, the Netherlands
3. EasyMeasure B.V., Breestraat 22, 3811 BJ, Amersfoort, the Netherlands

* Corresponding author: Karel Keesman, karel.keesman@wur.nl

Sensor Data Fusion (SDF) is a widely used means of monitoring electrochemical processes, such as the use of batteries and hydrogen production. The application of SDF contributes to solving challenges in process efficiency, control and reliability [1].

In the drinking water and food sectors, electrochlorination is an increasingly important means of disinfecting water. Due to stringent regulations regarding the formation of by-products such as chlorate and perchlorate, the real-time monitoring of this process has become desirable as well [2]. As there are no sensors for some of these oxychlorides, SDF is proposed as an alternative means of monitoring by-product concentrations [3].

To use SDF for the monitoring of by-product formation is a novel application of techniques that are already widely used. Therefore, it is worthwhile gain an overview of the adjacent applications where SDF has been researched and applied, as well as to understand what differences and similarities exist between these adjacent applications and the monitoring of by-product formation during electrochlorination, in order to learn how SDF can best be applied in this new case.

In electrochlorination, the main reason why a model, without the application of SDF, is insufficient, is due to the multidimensional, multiphase nature of the process. Due to a high overpotential, the mass transfer is expected to limit the by-product formation, at least in part. The mass transfer, in turn, depends highly on the degree of mixing that occurs due to bubble formation. Although empirical approximations of mass transfer due to bubble formation exist, this problem remains difficult to solve accurately, even with Computational Fluid Dynamics modeling. This means that with the current technology it is infeasible to accurately determine the bubble formation, and by extension the electrochemical reaction rates, in real-time. The present alternative is to employ a model that compromises on accuracy, which is then corrected through additional sensor data and a sensor data fusion (SDF) algorithm.

In addition, a significant challenge in the monitoring of by-product formation in general, is the relative lack of influence that the by-product concentration has on sensor data.

Four potential solutions are foreseen. One approach is to reconstruct the chlorate concentration from the small influence that the chlorate in the solution has on 'bulk' sensor readings, such as the electrical conductivity, through a first-principles model. A purely data-driven approach is also possible, by simply attempting to correlate sensor readings and process conditions with the chlorate concentration. A detectable first-principles model may devised, and finally, a hybrid solution may be possible, that can better balance data requirements, robustness and accuracy. Research specific to electrochlorination is required to determine whether these approaches are feasible.

References

[1] W. Waag, C. Fleischer and D. U. Sauer, "Critical review of the methods for monitoring of lithium-ion batteries in electric and hybrid vehicles," *Journal of Power Sources,* vol. 258, pp. 321-339, 2014.

[2] The European Parliament and The Council of the European Union, Directive (EU) 2020/2184 of the European Parliament and of the Council of 16 December 2020 on the Quality of Water Intended for Human Consumption (recast), 2020.

[3] D. L. Hall and J. Llinas, "An introduction to multisensor data fusion," in *Proceedings of the IEEE*, 1997.

On inventory control of perennial crop seeds

Robbert van der Kruk
Control Systems Technology, Faculty of Mechanical Engineering, University of Technology Eindhoven
P.O.Box 513, Eindhoven, 5600 MD, The Netherlands
r.j.v.d.kruk@tue.nl

Hybrid seed production of perennial crops requires a number of growth cycles before yearly production. Examples are Artichoke, Asparagus, Rhubarb, Strawberry and Rosemary. Large variations in the yield of these seeds, combined with the long time to harvest could lead to shortages or excess stock. Figure 1 shows the yearly planning cycle.

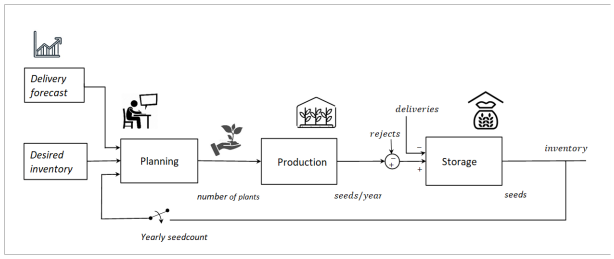

Figure 1: Manual production planning cycle to control inventory level

Since no literature exist on this topic a method to control the inventory level of perennial crop seeds is presented. A time discrete model of the seed production and inventory was derived and validated to describe the yearly cycle as demonstrated in Figure 2. The model is used as a predictor within

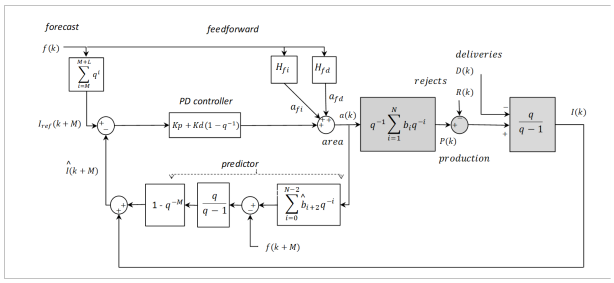

Figure 2: Feedback-feedforward control scheme with modified Smith predictor.

a Feedback-feedforward Controller and in a Model Predictive Controller designed to keep the inventory between limits. The methods were compared to historical data showing strong improvements related to cost of inventory as well as cost of non-deliveries as shown in Figure 3.
Large variations, dozens of years for experiments make it impossible to conduct research by experimental tests. Instead we used the statistics from the historical data for sensitivity analysis of the variations. The yearly planning cycle for planting, production and inventory could highly benefi-

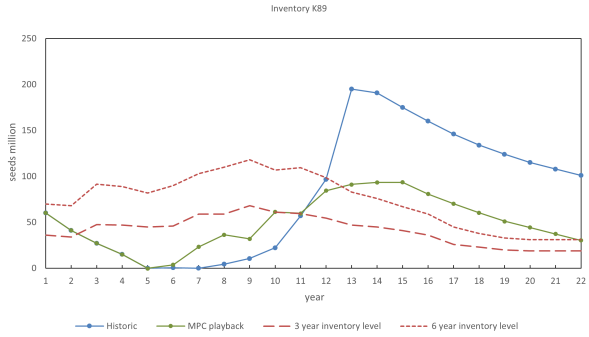

Figure 3: Historical inventory values and values from MPC play back

cially make use of the method by implementation of a semi-automatic MPC in an agricultural Customer Relationship Management system. Figure 4 depicts a view of the planting and inventory history. The flexibility of the method enables ease of use and stimulates craftsmanship of the planner. The

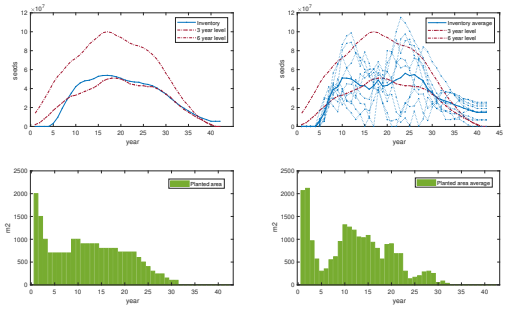

Figure 4: Simulated MPC inventory level and planting area for K832 variety during a life cycle. Right: variations in delivery (0.2 RSD) and yield (0.74 RSD). Left: no variations

significance of this paper is to prescribe the production planning and control of perennial crop seeds in a sustainable way to minimize the destruction of the plants. Finally, a short discussion of apparent future research directions completes this article.

Integrating Optimization- and Learning-Based Control for Large-Scale Hybrid Networks: Challenges and Opportunities

Samuel Mallick Azita Dabiri Bart De Schutter
Delft Center for Systems and Control, Delft University of Technology, The Netherlands
Email: {s.h.mallick, a.dabiri, b.deschutter}@tudelft.nl

1 Introduction

Critical infrastructure networks enabling the progress of modern society, e.g., road, railway, power, and water networks, are growing in scale and complexity as population and city sizes increase. These systems can be modelled as hybrid networks, i.e., models that describe interconnected components combining continuous and discrete dynamics. Continuous dynamics describe physical processes, such as traffic flow or power loss, while discrete dynamics capture discrete events, changes in modes of operation, and switches in network topology. Controlling hybrid networks is a nonlinear and non-convex problem containing continuous and discrete variables. On the scale of infrastructure systems this results in an explosion of computational complexity.

Current centralized control methods are no longer appropriate in this setting. Centralized computation becomes intractable, and presents a single point of vulnerability to critical failure [2]. Simultaneously, sensing and computation has become ubiquitous throughout infrastructure networks, enabling the application of small-scale intelligent controllers throughout the network, handling their own computation and communication with neighboring systems.

In this work we develop a control approach that integrates optimization- and learning-based control in a distributed fashion, as a solution to the hybrid network control problem. Optimization-based control offers hard guarantees on constraint satisfaction, ensuring safety. Learning-based control requires reduced online computation, suitable for the enormous decision spaces of large hybrid systems. Distributed control divides the computation between sub-systems, is robust to centralized failures, and naturally fits the geography of modern, computation equipped, infrastructure networks.

2 Optimization- and Learning-Based Control

Model Predictive Control (MPC) is an optimal control approach in which a model is used to predict future system behaviour, which is used to obtain an optimal control sequence over a finite horizon. The first element of the optimal sequence is then applied and the optimisation is repeated in the next time step. The advantages of MPC are explicit handling of constraints and theoretical guarantees on stability and performance. In MPC for hybrid networks [1], the control problem is a *mixed-integer* optimization with a complexity that typically grows exponentially with the number of discrete variables, unsuitable for control of large networks on fast time scales.

Reinforcement learning (RL) is a learning-based control approach where a control policy is learnt through simulation or experience [3]. RL can learn a control policy for very complex systems and environments with limited online computation. For safety critical systems however, RL cannot provide guarantees on performance, stability, and constraint satisfaction.

3 Research Directions

We consider potential research directions for combining MPC and RL in a distributed fashion to address control of large hybrid networks. Addressing the computational burden of hybrid MPC, partitioning the control problem is effective if it reduces the number of variables in each subproblem. Offline model-based RL could be used to learn control of the discrete components in the system, reducing online computation to a continuous MPC problem. Reduced fidelity prediction models can reduce the online computation in MPC, at the cost of performance. To compensate, RL methods could be applied to update a parameterized MPC model and cost, improving closed loop performance. In particular PWA systems are a candidate hybrid system model that provides a tuneable balance of accuracy and complexity.

Acknowledgement: This paper is part of a project that has received funding from the European Research Council (ERC) under the European Union's Horizon 2020 research and innovation programme (Grant agreement No. 101018826 - CLariNet).

References

[1] A. Bemporad and M. Morari. "Control of Systems Integrating Logic, Dynamics, and Constraints". In: *Automatica* 35.3 (1999), pp. 407–427.

[2] F. Lamnabhi-Lagarrigue et al. "Systems & Control for the Future of Humanity, Research Agenda: Current and Future Roles, Impact and Grand Challenges". In: *Annual Reviews in Control* 43 (2017), pp. 1–64.

[3] R. S. Sutton and A. G. Barto. *Reinforcement Learning: An Introduction*. MIT press, 2018.

Efficient online problem reformulation for adaptive gridding in optimal control problems

Louis Callens, Wilm Decré, Jan Swevers
MECO Research Team, Department of Mechanical Engineering, KU Leuven
Flanders Make@KU Leuven, Leuven, Belgium
Email: louis.callens@kuleuven.be

1 Introduction

Many different approaches exist to solve optimal control problems (OCPs). Typically, these problems have to satisfy continuous-time dynamics which make them difficult to solve. One such approach is a direct approach that solves OCPs by first discretizing the problem and subsequently solving the resulting nonlinear program (NLP). Adaptive gridding methods for OCPs try to produce a time grid on which the discrete problem can be solved efficiently [1]. Often, a user-specified accuracy requirement on the dynamical constraints needs to be satisfied while reducing the number of optimization variables as much as possible, reducing memory usage and computation time. Because the optimal discretization is not known a priori, adaptive gridding methods iteratively refine an initial coarse grid and hence solve multiple NLPs. These refinements require changing the constraints of the NLP, which introduces overhead both in computation time and memory allocation because expressions for consraint Jacobians and Langrangian Hessians have to be recomputed. For online use cases in which the same problem is solved many times, the overhead of changing the problem structure negates all adaptive gridding advantages. This explains the little number of online results using adaptive gridding in literature. Often, only a single refinement is done [2]. To overcome the hurdle of a changing problem structure, we propose to precompute building blocks to evaluate the constraints, their Jacobian and the contribution to the Hessian of the Langrangian. These building blocks can be computed using `CasADi` [3] and used to efficiently construct the problem to be passed to a solver.

2 Adaptive no-collision constraints

In many problems, it can be interesting to add and remove constraints such as some of the obstacle avoidance constraints that often are inactive. Instead of adding all constraints directly, an iterative strategy is proposed in which these constraints are only added if collisions are detected, to avoid irrelevant computations. Even though this adaptive approach requires solving multiple NLPs, it can still be significantly faster than solving the complete NLP once. Consider an example where a point mass moves in a plane from one point to another as fast as possible while avoiding obstacles. Its horizontal and vertical velocity are controlled. For this example, using the adaptive approach results in a speedup of 2 compared to solving the complete problem once when 100 time-steps are considered. A speedup of 3 is observed for 500 time-steps. Figure 1 shows the consecutive solutions. Note that in between iterations, there is no need to compute any Jacobian or Hessian expressions.

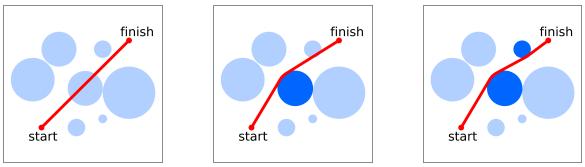

(a) Iteration 1 (b) Iteration 2 (c) Iteration 3

Figure 1: Adaptive addition of constraints

3 Adaptive discretization constraints

Imagine a point-mass that moves in one dimension. The acceleration is controlled. The objective is to cover a distance as fast as possible starting and ending with zero velocity. The optimal solution exhibits bang-bang control. If direct collocation is used to solve this problem, the jump in the control leads to a large discretization error in the approximation. By splitting intervals, the discontinuity can be placed at an interval edge which leads to highly accurate results. Using building blocks for collocation equations, intervals can be split efficiently. Solving the problem first with a single interval that is split using the building blocks after observing the discretization error, results in a speed-up of 1.5 compared to reconstructing the problem. When 9 intervals are used (of which only one is split), a speed-up of 3 is observed.

Acknowledgement This work has been carried out within the framework of Flanders Make SBO project ARENA (Agile and Reliable Navigation). Flanders Make is the Flemish strategic research centre for the manufacturing industry.

References

[1] A. V. Rao, M. A. Patterson, and W. W. Hager. "A ph collocation scheme for optimal control", Automatica, 2013.

[2] K. Lee, W. H. Moase and C. Manzie. "Mesh adaption in direct collocated nonlinear model predictive control," International Journal of Robust and Nonlinear Control, 2018.

[3] Joel A E Andersson and Joris Gillis and Greg Horn and James B Rawlings and Moritz Diehl, "A software framework for nonlinear optimization and optimal control," Mathematical Programming Computation, 2019

Optimised conversion of supplemental light energy into photosynthesis: a model based approach

Dominique Joubert
Dept. of Mathematical and Statistical Methods
Wageningen University and Research
P.O. Box 16, 6700 AV Wageningen
The Netherlands
Email: dominique.joubert@wur.nl

J.D. Stigter
Dept. of Mathematical and Statistical Methods
Wageningen University and Research
P.O. Box 16, 6700 AV Wageningen
The Netherlands

1 Introduction

Conventional greenhouse supplemental lighting practices are often guided by decreases in observed natural light. For such strategies however, the conversion of light energy into photosynthesis may not always be efficient.

Here, the inefficiency of photosynthesis is addressed using a model-based approach. More concisely, the addition of supplemental light is guided by a leaf's photosynthetic history and its effect on photosynthetic induction (the increase in photosynthesis following an increase in light).

2 The problem

Different photosynthetic induction responses (A_n) are compared in Fig.1. Initially subjected to different low levels of light, a leaf is suddenly subjected to 1000 $[\mu mol/m^2 s]$. The conversion of light energy into photosynthesis increases when a leaf is, *a priori*, subjected to higher levels of light. Induction is therefore directly related to both the level and duration of prior light.

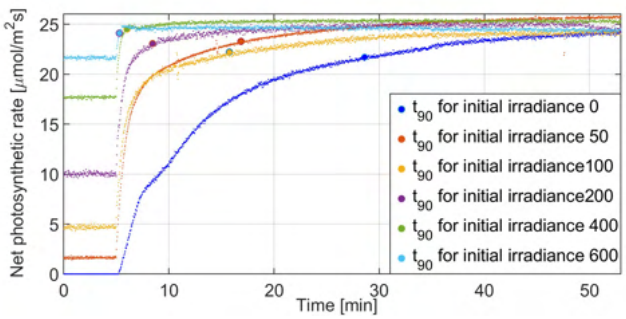

Figure 1: Induction curves of tomato leaves in different shade-sun transitions with the accompanying time taken for each to reach 90% of its steady-state photosynthesis.

Our aim is to optimise a leaf's photosynthetic efficiency under natural fluctuating light. This is achieved using a model-based control strategy that drives supplemental light. It is not guided by real-time light levels, but adopts as set point, a net photosynthetic rate inferred from Fig.1.

3 Results

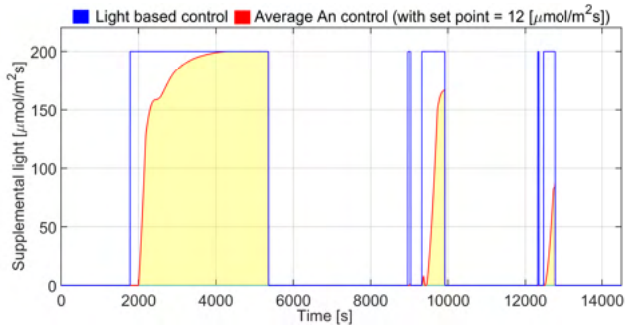

Figure 2: Comparing the predicted supplemental light required for both conventional light based control and photosynthesis based control with set point 12 $[\mu mol/m^2 s]$.

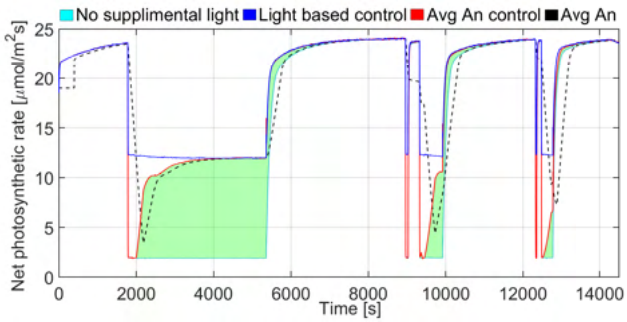

Figure 3: Comparing predicted photosynthesis under different light control strategies. Notice similar induction curves for both light and A_n based control when natural light increases (supplemental light is switched off in Fig.2).

4 Conclusion

Simulations suggest that a leaf's photosynthetic induction, the conversion of supplemental light energy into photosynthesis, can be increased whilst reducing the supplemental light required. Dimmable LEDs make this application feasible. The belief is that whilst both conventional and physiology driven lighting practices will produce similar crop yields, the latter will be associated with lower energy costs.

Virtual barriers to charge Li-ion battery cells using CCCVs: An experimental aging comparison

Alejandro Goldar, Maxime Bussios, Emanuele Garone
Service d'Automatique et d'Analyse des Systèmes - ULB
alejandro.goldar.davila@ulb.be,maxime.bussios@ulb.be, emanuele.garone@ulb.be

Most of the current commercial battery management systems (BMSs) charge Li-ion batteries based on logic-based charging algorithms, whose main appeals are the low computational complexity and the low cost of the power electronics required for their implementation.

The most common of such charging algorithms is the Constant Current – Constant Voltage (CCCV) protocol that consists of 2 charging stages. In the first stage, the battery is charged at constant current (CC) until the voltage reaches a pre-defined voltage threshold. During the second stage, such a voltage threshold is kept constant (CV) while the charging current is being progressively decreased until an end-of-charge current condition is reached (usually a current equivalent to 5% of the nominal capacity in 1 h).

The parameters of both CCCV stages are empirically selected aiming at achieving a pre-set performance criterion. The usage of high charging currents may reduce the charging time, but this is done at expenses of increasing cell temperature and impacting dramatically on the cell lifespan. On the other hand, low voltage thresholds for the CV stage also reduce the charging time to the detriment of reducing the stored energy. As such, the selection of CCCV parameters represents a trade-off between energy storage, aging, and charging time. In most commercial devices the CCCV values are pre-set by the developer, while in others (e.g. in batteries for drones) the selection of such parameters is often done by the users.

Most of the Li-ion cell manufacturers recommend, on their datasheets, that the charge should be carried out considering a CCCV with a charging current of around 1C (a ratio with respect to the cell nominal capacity), and a CV voltage between 4.1 - 4,2 V. Such a recommendation for the CCCV parameters, rather conservative, avoids both accelerating the aging, and increasing the surface temperature at expenses of long charging times.

Despite the increase of that conservative charging may intuitively reduce the charging time, experimental data from charge/discharge cycles with Sony VTC6 cells, Pareto's fronts of Figs. 1-2, show that there is a virtual barrier when increasing the CC current. Thus, beyond 3C, the reduction of the charging time is almost negligible, regardless the number of testing cycles.

The existence of this "virtual" barrier, that cannot be trespassed by simply increasing the charging current, is also observed even when the voltage threshold for the CV phase is reduced from 4.2 V to 4.1 V. Thus, the experimental data show that for the high-power Sony battery cells, there is no potential manner to further accelerate the charge of the battery by simply "playing" with the CCCV parameters without reducing either the lifespan or the amount of energy stored, or even both.

One of the safe ways to "go beyond" this barrier is by implementing model-based techniques able to monitor the state the battery and charge it accordingly. Therefore, instead of resorting to the knowledge of the user, an accurate characterization of both the electrochemical and thermal phenomena inside the battery cell, and the definition of a safe charging area allow charging faster a battery while exhibiting a degradation rate such as the rate shown by the recommended charge of the manufacturer (see red diamond on Pareto's plot).

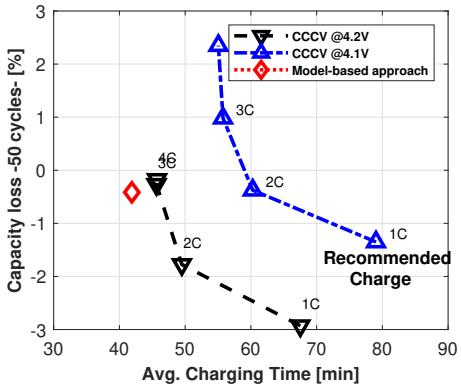

Figure 1: Average Charging Time vs. Capacity Loss for single Sony VTC6 cells after 50 cycles.[1]

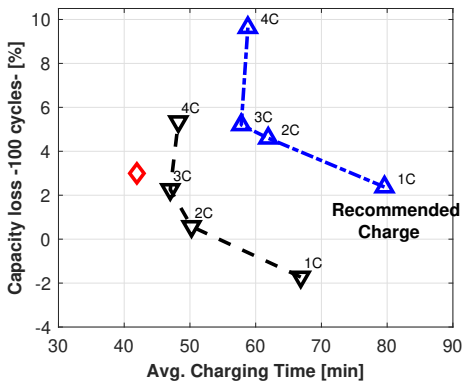

Figure 2: Average Charging Time vs. Capacity Loss for single Sony VTC6 cells after 100 cycles.[1]

[1]Note: For the sake of comparison, the capacity loss is computed w.r.t. the nominal capacity of the battery, that is why some values are lower than 0.

Cooperative Path Planning for Tethered Underwater Vehicles

Gianpietro Battocletti Dimitris Boskos Bart De Schutter
Delft Center for Systems and Control, Delft University of Technology, The Netherlands
Email: {g.battocletti, d.boskos, b.deschutter}@tudelft.nl

1 Introduction

Tethered Unmanned Underwater Vehicles (UUV) represent an effective approach to tackle a large number of underwater tasks. The cabled connection of a UUV to a surface boat can be used as a power source, communication channel, and to get access to additional computational power, significantly reducing some of the most critical issues of UUVs. However, this does not come without challenges. In fact, the tether cannot be controlled directly, and so it might get *entangled* with obstacles present in the environment or with itself, forming knots. In case of multi-agent systems, this problem is amplified as the tethers of different UUVs can also get entangled with each other. The most common approach to tackle this issue is through a suitable planning of the UUV's motion. Despite the attention given to this problem in the past, several questions are still open.

In this presentation we first review the existing research on motion planning for tethered UUVs. Next, we aim to improve on the current state of art in two ways: *(i)* by generalizing the definition of "entanglement" (in the literature, entanglement avoidance has been studied only with respect to specific tether configurations that have to be avoided) and *(ii)* by implementing and comparing multiple approaches to obtain a computationally efficient planning algorithm, including both online and offline solutions.

2 Entanglement and topological constraints

The presence of the tether adds a *topological* constraint to the motion planning problem. This affects the planning problem in two ways: in the first place the tether length must always be respected, resulting in a limited workspace. Additionally, the presence of obstacles gives rise to multiple *homotopy classes* (i.e., configurations with common endpoints that cannot be transformed into each other without passing through an obstacles) in which the tether can lie. Some points in the environment can be reached only if the cable lies in the correct homotopy class, and this renders the planning problem highly non-trivial. In addition to this, a *non-entanglement constraint* can be added to the problem.

In the existing literature, entanglement is defined either as simple contact between cables [1] or as a full loop of the tether around an obstacle [2]. In both cases, the planning algorithm must avoid the occurrence of entanglement during the motion from one point to another. These definitions, while effective, are either too broad (for simple contact) or too specific (for full looping), allowing the tethers to reach potentially critical configurations. To address this issue we seek to find novel and more general definitions of entanglement, including both definitions that avoid specific situations and others aimed at keeping the 'entanglement level' of the tether at a minimum. Moreover, we aim to implement a flexible framework in which different definitions of entanglement can be used depending on the needs.

3 Graph-based planning algorithm

In most of the existing literature, the motion planning problem for tethered robots is tackled as a graph search problem. To include the topological constraint posed by the presence of the tether, the graph is built with additional information stored in the nodes and in the edges [2]. During the creation of the graph, the non-entanglement constraint is also considered and nodes/edges that violate it are discarded. A significant issue of algorithms following this approach is the high computation time required to build the graph.

In the literature, different possible approaches have been considered to obtain a more efficient planning algorithm. Sampling-based methods represent a promising research direction. Several results are available regarding the properties of this class of planning algorithms in terms of optimality, completeness, and convergence [3]. In addition, variations of the algorithms have been developed to obtain online re-planning (in case of uncertain or dynamic environments) or anytime algorithms (that return a valid solution even if interrupted at any point of the computation). We aim to merge sampling-based approach with the existing tethered planning techniques to obtain an efficient and fast planning algorithm. Future research will focus on the extension of the planning algorithms to multi-agent systems.

Acknowledgments: This research has been supported by the funding from the European Union under grant agreements No 871295 (SeaClear) and No 101093822 (SeaClear2.0).

References

[1] S. Hert and V. Lumelsky, "Motion planning in $\mathbb{R}^3$ for multiple tethered robots," *IEEE Transactions on Robotics and Automation*, vol. 15, no. 4, pp. 623–639, 1999.

[2] S. Kim, S. Bhattacharya, and V. Kumar, "Path planning for a tethered mobile robot," in *2014 IEEE International Conference on Robotics and Automation (ICRA)*, pp. 1132–1139, 2014.

[3] S. Karaman and E. Frazzoli, "Sampling-based algorithms for optimal motion planning," *The International Journal of Robotics Research*, vol. 30, no. 7, pp. 846–894, 2011.

A high-order regularization method and approximate solution

Xinghua Liu
Engineering and Technology institute Groningen
University of Groningen
P.O. Box 72, 9700 AB Groningen
The Netherlands
Email: xinghua.liu@rug.nl

Ming Cao
Engineering and Technology institute Groningen
University of Groningen
P.O. Box 72, 9700 AB Groningen
The Netherlands
Email: m.cao@rug.nl

1 Introduction

A range of sensor network problems, such as localization problems [1, 2, 3], can be described using linear models; even when the original models are nonlinear, their linearized approximation can still lead to meaningful solutions. Consider a set of linear equations

$$Ax = b \tag{1}$$

where $x \in \mathbf{R}^n$, $A \in \mathbf{R}^{m\times n}$, $b \in \mathbf{R}^m$. The least square (LS) method and its variations are often used in solving such linear problems (1). However, it is more challenging when the matrix A is ill-conditioned ([4], Chapter 5.8); in this case, an approximate solution given by the Tikhonov regularization (TR) method [5] can be handy. A standard form of the TR solution can be found in [5], which is given by

$$x_{TR} = \left(A^T A + \lambda^2 I\right)^{-1} A^T b \tag{2}$$

where λ is a given regularization parameter. It is known, though, the TR solution can be overly smooth without a proper justification of adding a regularization term to the original problem (1).

2 The high-order regularization method

To find a relationship between the LS solution and the TR solution, and get a better explainable solution to the original problem (1), we propose a high-order regularization (HR) method that is described as follows

$$x_{HR} = \left(A^T A + R\right)^{-1} \sum_{l=0}^{k} \left(R\left(A^T A + R\right)^{-1}\right)^l A^T b \tag{3}$$

where the regularization matrix $R \in \mathrm{S}_+^n$ is a diagonal matrix and the matrix $\left(A^T A + R\right)$ is non-singular. When $k = 0$, the HR solution is equivalent to the TR solution with $R = \lambda^2 I$, and the condition $\rho\left(R\left(A^T A + R\right)^{-1}\right) < 1$ required in the matrix series can always be satisfied. In general, we can select $k = 1$, and for a diagonal regularization matrix, the HR solution can be simplified as

$$x_{HR} = \left(A^T A + R\right)^{-1} A^T b + \left(A^T A + R\right)^{-1} R \left(A^T A + R\right)^{-1} A^T b \tag{4}$$

which is a better solution than the TR solution in the sense of approximation of the inverse of the matrix $A^T A$.

3 Example

A mobile robot localization problem can be formulated into a matrix form like (1) with

$$A = \begin{bmatrix} (p_1 - p_{m+1})^T \\ \vdots \\ (p_m - p_{m+1})^T \end{bmatrix}, \; b = \begin{bmatrix} p_1^T p_1 - p_{m+1}^T p_{m+1} + d_{m+1}^2 - d_1^2 \\ \vdots \\ p_m^T p_m - p_{m+1}^T p_{m+1} + d_{m+1}^2 - d_m^2 \end{bmatrix} \tag{5}$$

where $A \in \mathbf{R}^{m\times 3}$, $p_i = (x_i, y_i, z_i)^T$, $i = 1, \ldots, m+1$ are positions of $m+1$ anchors with known given positions and d_i are distance measurements between the i-th anchor and the robot. Therefore, the position estimation of the robot can be given by the high-order regularization method (3).

4 Conclusion

In this work, we proposed a high-order regularization method to solve the linear sensor localization problem when the associated matrix is ill-conditioned. We show that the proposed method is superior to the Tikhonov regularization in approximating the inverse problem.

References

[1] Ali H Sayed, Alireza Tarighat, and Nima Khajehnouri. Network-based wireless location: challenges faced in developing techniques for accurate wireless location information. *IEEE signal processing magazine*, 22(4):24–40, 2005.

[2] Chen Wang, Handuo Zhang, Thien-Minh Nguyen, and Lihua Xie. Ultra-wideband aided fast localization and mapping system. In *2017 IEEE/RSJ international conference on intelligent robots and systems (IROS)*, pages 1602–1609. IEEE, 2017.

[3] Kexin Guo, Xiuxian Li, and Lihua Xie. Ultra-wideband and odometry-based cooperative relative localization with application to multi-uav formation control. *IEEE transactions on cybernetics*, 50(6):2590–2603, 2019.

[4] Roger A Horn and Charles R Johnson. *Matrix analysis*. Cambridge university press, 2012.

[5] Zhongxiao Jia. Regularization properties of lsqr for linear discrete ill-posed problems in the multiple singular value case and best, near best and general low rank approximations. *Inverse Problems*, 36(8):085009, 2020.

Multi-agents Source Seeking and Flocking Control with Connectivity Preservation and Collision Avoidance

Tinghua Li [1] t.li@rug.nl
Bayu Jayawardhana[1] b.jayawardhana@rug.nl

[1] DTPA, ENTEG, Faculty of Science and Engineering, University of Groningen, The Netherlands

1 Abstract

We present a distributed source seeking and flocking control method for networked multi-agent systems with nonholonomic constraint in an unknown cluttered environment. Based solely on identical on-board sensor systems, which measure the source local field, the group objective is attained by appointing a leader agent, which has the largest signal strength to the source (as a proxy to the distance to the source), to seek the source while the remaining follower agents form a cohesive flocking with the leader using a distributed flocking control law in a connectivity-preserved undirected network of multi-agent systems. To guarantee the safe separation and group motion for all agents and to solve the conflicts with the "cohesion" flocking rule of Reynolds, the distributed control algorithm is solved individually through quadratic-programming optimization problem with safety constraints, which guarantee the collision avoidance for inter-agents and obstacles in the cluttered environment. Stability analysis of the closed-loop system is presented and the efficacy of the methods is shown in simulation results.

2 Problem Formulation and Control Design

We consider an unknown concave function $J(x,y)$ where the source located at (x^*, y^*) with the maximum signal strength. The control objective of leader robot is to safely search the source's location by its own local measurements. In the meantime, all the followers in the group needs to realize a flocking by maintaining a desired gradient error $d^*_{\nabla J}$ with its neighbors' average while flocking with the source-seeking leader. The desired error $d^*_{\nabla J}$ is defined to be within the sensing interaction region (i.e. $d^*_{\nabla J} < r$).

Henceforth, in order to achieve the flocking task with safety and connectivity maintenance, the quadratic programming problem can be constructed based on the nominal source-seeking and flocking controller for leader $\mathscr{L}$ and follower agent $i \in \mathscr{V}_f$, respectively, as follows.

- Leader $\mathscr{L}$:

$$\begin{bmatrix} u^*_{\mathscr{L}} \\ R^*_{\mathscr{L}} \end{bmatrix} = \underset{u_{\mathscr{L}} \in \mathscr{U}_{\mathscr{L}}, R_{\mathscr{L}} \in \mathbb{R}^{N_{\mathscr{L}c}}}{\operatorname{argmin}} \frac{1}{2} \left(\left\| u_{\mathscr{L}} - \begin{bmatrix} \dot{v}_{\mathscr{L},s} \\ \omega_{\mathscr{L},s} \end{bmatrix} \right\|^2 + \|R_{\mathscr{L}} - R_\alpha\|^2 \right) \quad (1)$$

such that

$$L_f h_{\mathscr{L}}(\xi_{\mathscr{L}}) + L_g h_{\mathscr{L}}(\xi_{\mathscr{L}}) u_{\mathscr{L}} + \alpha(h_{\mathscr{L}}(\xi_{\mathscr{L}})) \geq 0 \quad (2)$$

$$L_f h_{\mathscr{L}j}(\xi_{\mathscr{L}}) + L_g h_{\mathscr{L}j}(\xi_{\mathscr{L}}) u_{\mathscr{L}} + \gamma_{\mathscr{L}j} \alpha(h_{\mathscr{L}j}(\xi_{\mathscr{L}})) \geq 0, \quad \forall j \in \mathscr{N}_{\mathscr{L}c} \quad (3)$$

- Follower i:

$$\begin{bmatrix} u^*_i \\ R^*_i \end{bmatrix} = \underset{u_i \in \mathscr{U}, R_i \in \mathbb{R}^{N_{ic}}}{\operatorname{argmin}} \frac{1}{2} \left(\left\| u_i - \begin{bmatrix} \dot{v}_i \\ \omega_i \end{bmatrix} \right\|^2 + \|R_i - R_\alpha\|^2 \right) \quad (4)$$

such that

$$L_f h_i(\xi_i) + L_g h_i(\xi_i) u_i + \alpha(h_i(\xi_i)) \geq 0 \quad (5)$$

$$L_f h_{ij} + L_g h_{ij} u_i + \gamma_{ij} \alpha(h_{ij}) \geq 0, \forall j \in \mathscr{N}_{ic} \quad (6)$$

3 Main Results

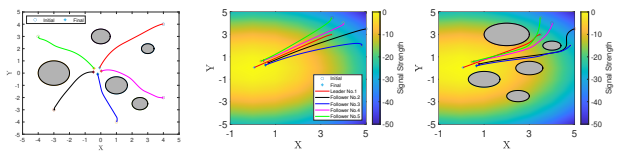

(a) (b) (c)

Figure 1: Simulation results of multi-agent flocking and source seeking with orientation-unconstrained controller u_i in the free and cluttered environment. Leader's trajectories are shown with red solid line and the others denote 4 follower agents'.

References

[1] T. Li, B. Jayawardhana, A. M. Kamat and A. G. P. Kottapalli, "Source-Seeking Control of Unicycle Robots With 3-D-Printed Flexible Piezoresistive Sensors," *IEEE Transactions on Robotics*, vol. 38, no. 1, pp. 448-462, 2022.

Risk-Aware Task Assignment with Formal Specifications for Heterogeneous Multi-Agent Systems

Zengjie Zhang, Zhiyong Sun, and Sofie Haesaert
Department of Electrical Engineering, Eindhoven University of Technology, The Netherlands
Email: {z.zhang3, z.sun, s.haesaert}@tue.nl

1 Introduction

In recent years, the conventional multi-agent systems that consist of homogeneous robot agents with identical structures and capabilities have not been able to satisfy the application of sophisticated engineering problems. Instead, the heterogeneous combination of robot agents with diverse dynamic models and various task-execution capabilities is increasingly needed. The differentiation among the capabilities of the robot agents makes it easier to realize the division of work, such that the resources can be deployed in an efficient manner [1]. On the other hand, the resulting heterogeneous multi-agent system faces additional challenges due to inconsistency and incompatibility among distinct agent features.

Dynamic task assignment is a typical high-level multi-agent system coordination problem that is dedicated to distributing a cluster of tasks to the agents in the system during the run-time [2]. For conventional multi-agent systems with homogeneous agents, the tasks can be allocated evenly, which results in trivial assignment schemes. For heterogeneous multi-agent systems, however, the task assignment problem becomes challenging due to the incorporation of diverse agent capabilities. The conventional multi-agent task assignment studies mainly focus on the task aspects without considering possible system risks, such as task failure, execution delay, or safety violation. Recent work starts to incorporate risk-handling into the task assignment process by encoding risky events to certain temporal logic specifications [3], rendering a higher demand on risk awareness [4].

Nevertheless, the existing solutions for the dynamic task assignment problem are still based on deterministic assignment models without incorporating stochastic uncertainties. This results in weak robustness of the system against external disturbance or internal random faults. Extending the current task assignment models to incorporate stochastic environmental uncertainties for heterogeneous multi-agent systems is still a challenging but necessary problem.

2 Problem Formulation

We consider a dynamic multi-agent task assignment problem that consists of a finite set of heterogeneous agents $A = \{A_1, A_2, \cdots, A_n\}$ together with a finite set of tasks $T = \{T_1, T_2, \cdots, T_s\}$ that is given in a temporal logic of choice. To execute a given task such as "to reach region A and then pick up package B", the agent needs to solve an optimal control problem to maximize some completeness metric, such as "to pick up the packages as firmly as possible", while satisfying some anti-risk or safe specifications, such as "to finish the task within a given time limit". The task execution is affected by the uncertainties of the environment, which is reflected by the influence of the stochastic disturbances on the behavior of each individual agent when executing the tasks. Thus, the capabilities of agents to maximize the task completeness metric while satisfying the required task specifications should be sufficiently robust to cope with the stochasticity of the individual agent dynamic models.

For any agent A_i and task T_j, $i = 1, 2, \cdots, n$, $j = 1, 2, \cdots, s$, the satisfaction of the anti-risk specifications is depicted as a stochastic variable. The completeness of all tasks while satisfying all these specifications is indicated by a binary variable $T_{\text{comp}} \in (0, 1)$. Then, the main target of the dynamic task assignment problem is to find a dynamic mapping $\mathscr{M} : A \times \mathbb{R}^+ \to T$ for all time $t \in \mathbb{R}^+$, such that the probability of the complete execution of all tasks is maximized,

$$\max_{\mathscr{M}} E(T_{\text{comp}}), \tag{1}$$

with all anti-risk specifications satisfied. The main challenge of this task assignment problem is the encoding of the stochasticity to the agent dynamic models, which renders a probabilistic planning problem. The critical technical point to solving this problem is converting it to an equivalent or slightly conservative deterministic programming problem.

References

[1] Haibo Du, Guanghui Wen, Di Wu, Yingying Cheng, and Jinhu Lü. Distributed fixed-time consensus for nonlinear heterogeneous multi-agent systems. *Automatica*, 2020.

[2] Amin Abbasi, Somaiyeh MahmoudZadeh, and Amirmehdi Yazdani. A cooperative dynamic task assignment framework for cotsbot auvs. *IEEE Transactions on Automation Science and Engineering*, 2020.

[3] Kevin Leahy, Zachary Serlin, Cristian-Ioan Vasile, Andrew Schoer, Austin M Jones, Roberto Tron, and Calin Belta. Scalable and robust algorithms for task-based coordination from high-level specifications (scratches). *IEEE Transactions on Robotics*, 2021.

[4] Lars Lindemann, George J Pappas, and Dimos V Dimarogonas. Reactive and risk-aware control for signal temporal logic. *IEEE Transactions on Automatic Control*, 2021.

Passivity-Preserving Model Reduction for Interconnected Systems

Luuk Poort
Eindhoven University of Technology*
l.poort@tue.nl

Bart Besselink
University of Groningen†
b.besselink@rug.nl

Rob Fey
Eindhoven University of Technology*
r.h.b.fey@tue.nl

Nathan van de Wouw
Eindhoven University of Technology*
n.v.d.wouw@tue.nl

1 Introduction

Physical systems, such as RLC networks or structural dynamics systems, can often be modeled appropriately as an interconnection of several subsystems. These subsystems are often naturally passive, i.e., the systems do not generate energy internally, leading to complex, passive, coupled models. The complexity of these models typically prevents efficient dynamic analysis. Model reduction is thus required to attain an accurate low-order model. Usually, this is performed on subsystem level, for example by Component Mode Synthesis (CMS). Unfortunately, subsystem reduction does not explicitly ensure accuracy of the interconnected system. While there exist reduction methods to focus on the accuracy of the reduced, interconnected model, passivity and stability of this model are generally not retained.

2 Research approach

We introduce the Passive Interconnected Balancing (PIB) method to reduce models of interconnected subsystems, approximating the input-output behaviour of the interconnection, while preserving both the interconnection structure and passivity of the model. Equivalently, this new method reduces the individual subsystems, based on the input-output behaviour of the interconnection, while preserving passivity of the subsystems and interconnection.

Our approach is based on the concept of balancing, where typically the controllability and observability Gramians of a system are equalized and diagonalized to sort states by their importance to input-output behaviour. Instead of the observability Gramian, we use the available storage per subsystem, as in Positive-Real Balancing (PRB), to guarantee passivity of the reduced subsystem model [1]. Moreover, instead of the subsystem controllability Gramian, we use a partition of the controllability Gramian of the interconnected system, as with Interconnection Structure-preserving Balancing (ISB) [2]. This combination of available storage and a partition of the coupled controllability Gramian provides both passivity guarantees and accuracy of the coupled system.

*Dynamics & Control, Mechanical Engineering, Eindhoven University of Technology, PO Box 513, 5600 MB Eindhoven, The Netherlands

†Bernoulli Institute for Mathematics, Computer Science and Artificial Intelligence, University of Groningen, P.O. Box 407, 9700 AK Groningen, The Netherlands

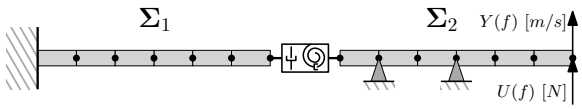

Figure 1: Schematic drawing of the coupled beam model.

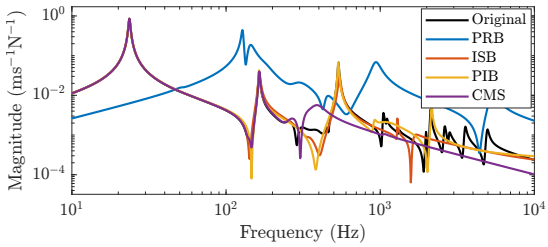

Figure 2: Magnitude plot of $|Y/U|$.

3 Numerical example

Observe the SISO system of two lightly damped Euler beams, in Figure 1, which are coupled by a translational and rotational damper. Both beam nodels consist of 24 states each and are reduced to 10 states each. Reduction is performed using (i) PRB, (ii) ISB, (iii), Craig-Bampton CMS reduction and (iv) the new PIB method. The resulting magnitudes of the collocated FRF is shown in Figure 2. PIB and ISB both show superior accuracy compared to the other methods. However, ISB does not preserve stability, whereas PIB preserves stability and passivity.

4 Conclusion and outlook

Passive Interconnected Balancing (PIB) both guarantees passivity preservation, interconnection-structure preservation and results in an accurate reduced coupled model. Further extensions will make it more computationally efficient, to also allow application to industry-relevant benchmarks.

References

[1] A. C. Antoulas, *Approximation of Large-Scale Dynamical Systems*, R. C. Smith, Ed. Philedelphia: Society for Industrial and Applied Mathematics, Jan. 2005.

[2] A. Vandendorpe and P. Van Dooren, "Model Reduction of Interconnected Systems," in *Model Order Reduction: Theory, Research Aspects and Applications*, 2008, pp. 305–321.

Modular Model Reduction of Interconnected Systems

Lars Janssen, TU/e*
Email: l.a.l.janssen@tue.nl

Rob Fey, TU/e*
Email: r.h.b.fey@tue.nl

Bart Besselink, RUG†
Email: b.besselink@rug.nl

Nathan van de Wouw, TU/e*
Email: n.v.d.wouw@tue.nl

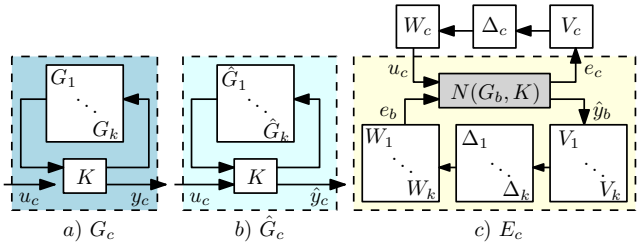

Fig. 1: Transfer functions of a) the high-order, b) the reduced-order interconnected models, and c) the RP perspective.

1 Introduction

Complex models of dynamic (multi-)physical systems are often based on an interconnection of subsystems with a high number of states. For such systems, model order reduction (MOR) is required to make controller synthesis, simulation and analysis computationally feasible. In modular MOR, each subsystem model is reduced individually. This preserves the interconnection structure of the model, and dividing the problem into multiple smaller problems avoids the computationally challenging reduction of one high-dimensional model. However, although modular MOR leads to accurate subsystem models, it does not guarantee the accuracy of the interconnected reduced-order model (ROM). We introduce a top-down method that allows translation of accuracy requirements on the interconnected ROM to a set of accuracy requirements for subsystem ROMs which allows for a completely modular approach.

2 Methodology

To model the system, we combine k linear time-invariant subsystems G_j in the transfer function $G_b = \mathrm{diag}(G_1, \ldots, G_k)$. Inputs u_b and outputs y_b of the subsystems are interconnected via the coupling matrix K. All subsystems are reduced to ROMs given by $\hat{G}_b = \mathrm{diag}(\hat{G}_1, \ldots, \hat{G}_k)$. The high-order interconnected model G_c and interconnected ROM $\hat{G}_c$ are then both given by a feedback of K with G_b and $\hat{G}_b$, respectively, external input u_c, and output y_c, as shown in Fig. 1a and 1b. In this work, we relate $E_j = G_j - \hat{G}_j$ to $E_c = G_c - \hat{G}_c$ by reformulating the problem such that the structured singular value μ, a tool from robust control [1], can be used. We define a weighted uncertain system for which $E_j = W_j \Delta_j V_j$. Then, we model E_c as a feedback of VNW and Δ as shown in Fig. 1c. Nominal system N is a function of G_b and K. $V = \mathrm{diag}(V_1, \ldots, V_k, V_c)$, $W = \mathrm{diag}(W_1, \ldots, W_k, W_c)$ and $\Delta = \mathrm{diag}(\Delta_1, \ldots, \Delta_k, \Delta_c)$.

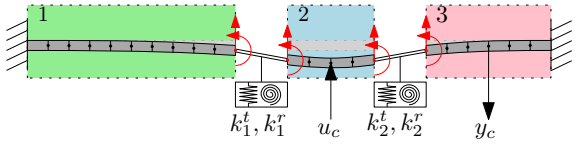

Fig. 2: : Example system: Three interconnected beams.

Theorem 1 *From robust performance (RP) [1], let $\omega \in \mathbb{R}$, for the system in Fig. 1c,*

$$|W_c(\omega)E_c(i\omega)V_c(\omega)| < 1, \textit{ for all } E_j(i\omega) \textit{ such that}$$
$$|W_j^{-1}(\omega)E_j(i\omega)V_j^{-1}(\omega)| \leq 1, \textit{ if and only if}$$
$$\mu_\Delta(V(\omega)N(i\omega)W(\omega)) < 1. \quad (1)$$

Given that $\mu_\Delta(V(\omega)N(i\omega)W(\omega)) < 1$ can be verified computationally, this relation can be used, given requirements on the interconnected ROM, to find a set of subsystem requirements in terms of $V_j(\omega)$ and $W_j(\omega)$ for any $\omega \in \mathbb{R}$. Then, the subsystems can be reduced completely individually, i.e., modularly. To illustrate how Theorem 1 can be used for modular MOR, we apply it to the system illustrated in Fig. 2. In this case, the subsystems are reduced as much as possible within the computed subsystem requirements using balanced truncation. The results are shown in Tab. 1.

Tab. 1: # states in the high-order model and for a ROM satisfying given accuracy requirements for all $30 \leq \omega \leq 10{,}000$.

Subsystem	G_1	G_2	G_3	G_c
High-order model	200	84	120	404
ROM: $\lvert E_c(i\omega)\rvert < 0.01\lvert G_c(i\omega)\rvert$	21	19	15	55
ROM: $\lvert E_c(i\omega)\rvert < 0.1\ \lvert G_c(i\omega)\rvert$	19	13	12	44

3 Conclusion

Modular MOR is a computationally efficient method that allows for the computation of ROMs of interconnected (multidisciplinary and multi-physical) subsystems. We introduce a mathematical relation between the accuracy of subsystem ROMs and the accuracy of the interconnected ROMs that allows for modular MOR with accuracy guarantees. We apply this to an example model, in which we reduce the interconnected system using modular MOR while guaranteeing different levels of accuracy for the ROM.

References

[1] Packard, A., & Doyle, J. (1993). The complex structured singular value. Automatica, 29(1), 71-109

*Eindhoven University of Technology, Department of Mechanical Engineering, Dynamics & Control Group
†University of Groningen, Bernoulli Institute for Mathematics, Computer Science and Artificial Intelligence

Balancing for nonlinear differential-algebraic systems

Arijit Sarkar, Yu Kawano and Jacquelien M.A. Scherpen

Abstract

Differential-algebraic equations can be utilized to model various systems in industrial applications. For example, in mechanics to model systems with holonomic or non-holonomic constraints, in circuit simulation, electric networks to cater to Kirchoff's current and voltage law, etc. These systems can be large-scale due to the complexity of the engineering applications. This demands a reduced-order model of a similar structure for fatser simulation and less-expensive controller design.

Balanced truncation is one of the well-known model reduction techniques based on the controllability and observability properties of the system and since its introduction in [1], various balancing theories have been studied for linear [2] and nonlinear [3], [4] differential systems. Balanced truncation was first introduced in [5] for differential-algebraic systems. Afterward, various balancing techniques have been studied for linear descriptor systems [6], [7]. However, balancing is not well-explored for nonlinear descriptor systems. In this work we propose controllability and observability functions associated with a nonlinear differential-algebraic system of the form (1) below. Moreover, we also show that they can be utilized to come up with a balanced realization of the system.

Let us consider a nonlinear differential-algebraic control system of the form

$$\Xi : \begin{cases} \dot{\widehat{E(x)}} = E'(x)\dot{x} = f(x) + g(x)u, \\ y = h(x), \end{cases} \tag{1}$$

where $x \in X$ is the generalized state, X is an n-dimensional differential manifold, $u \in \mathbb{R}^m$ is the control vector and $y \in \mathbb{R}^p$ is the output vector. We denote by TX the tangent bundle of X and by T_xX the tangent space of X at $x \in X$. $E, f : X \to \mathbb{R}^l$, $g : X \to \mathbb{R}^{l\times m}$ and $h : X \to \mathbb{R}^p$ are $\mathcal{C}^\infty$ - smooth maps. For each $x \in X$, $\frac{\partial E}{\partial x}(x) =: E'(x)$ induces a linear map from T_xX to $\mathbb{R}^l$. If X is an open subset of $\mathbb{R}^n$, then $E'(x) \in \mathbb{R}^{l\times n}$. The map E' is not necessarily a square matrix in general and even if $l = n$, E' can be singular in nature because of the presence of algebraic constraints associated with some generalized state variables and/or the external input. In this paper, we consider $X \subseteq \mathbb{R}^n$ and $l = n$. Now, consider M^* as the locally maximally controlled invariant submanifold around the origin. The controllability function associated with (1) is defined as

$$L_c(x_0) := \min_{\substack{u\in L_2(-\infty,0),\\ x(-\infty)=0, x(0)=x_0\in M^*}} \frac{1}{2}\int_{-\infty}^{0} ||u(t)||^2 dt.$$

The observability function is defined as

$$L_o(x_o) := \frac{1}{2}\int_0^\infty ||y(t)||^2 dt, x(0) = x_0 \in M^*, u(t) \equiv 0.$$

Let us assume $E(0) = 0$. If 0 is an asymptotically stable equilibrium of $f(x)$ on a neighbourhood U of 0, then it is possible to show that for all $x \in M^* \cap U$, $\bar{L}_o(E(x))$ is the unique smooth solution of

$$\frac{\partial \bar{L}_o(E(x))}{\partial E(x)} f(x) + \frac{1}{2} h^\top(x)h(x) = 0. \tag{2}$$

Also, for all $x \in U$, $\bar{L}_c(E(x))$ is the smooth solution of

$$\begin{aligned} &\frac{\partial \bar{L}_c(E(x))}{\partial E(x)} f(x) \\ &+ \frac{1}{2}\frac{\partial \bar{L}_c(E(x))}{\partial E(x)} g(x)g^\top(x) \frac{\partial^\top \bar{L}_c(E(x))}{\partial E(x)} = 0, \end{aligned} \tag{3}$$

such that 0 is an asymptotically stable equilibrium of $-f(x) - g(x)g^\top(x)\frac{\partial^\top \bar{L}_c(E(x))}{\partial E(x)}$ on $M^* \cap U$.

Moreover, one can show that there exist some functions $\bar{L}_o$ and $\bar{L}_c$ satisfying

$$\begin{aligned} L_o(x_0) &= \bar{L}_o(E(x_0)) \\ L_c(x_0) &= \bar{L}_c(E(x_0)). \end{aligned} \tag{4}$$

Based on this, we can guarantee the existence of a balanced realization.

A. Sarkar and J.M.A. Scherpen are with the Jan C. Willems Center for Systems and Control, Engineering and Technology Institute Groningen, Faculty of Science and Engineering, University of Groningen, Nijenborgh 4, 9747 AG Groningen, Netherlands. Y. Kawano is with Graduate School of Advanced Science and Engineering, Hiroshima University, Higashi-Hiroshima 739-8527, Japan. (Emails: {a.sarkar, j.m.a.scherpen}@rug.nl, ykawano@hiroshima-u.ac.jp.)
This publication is part of the project Digital Twin P18-03 project 1 of the research program Perspectief which is (partly) financed by the Dutch Research Council (NWO).

References

[1] B. C. Moore, "Principal compoent analysis in linear systems : Controllability, observability and model reduction," *IEEE Transactions on Automatic Control*, vol. 26, no. 1, pp. 17–32, 1981.

[2] A. C. Antoulas, *Approxiation of Large-scale Dynamical systems*. Society for Industrial and Applied Mathematics, 2005.

[3] J. M. A. Scherpen, "Balancing for nonlinear systems," *Systems and Control Letters*, vol. 21, no. 2, pp. 143–153, 1993.

[4] E. I. Verriest and W. S. Gray, "Flow balancing nonlinear systems," in *14th International Symposium on Mathematical Theory of Networks and Systems*, 2000.

[5] T. Stykel, "Gramian-based model reduction for descriptor systems," *Mathematics of Control, Signals and Systems*, pp. 297–319, 2004.

[6] T. Reis and T. Stykel, "Positive real and bounded real balancing for model reduction of descriptor systems," *International Journal of Control*, vol. 83, no. 1, pp. 74–88, 2010.

[7] T. Reis and E. Virnik, "Positivity preserving balanced truncation for descriptor systems," *SIAM Journal of Control and Optimization*, vol. 48, no. 4, pp. 2600–2619, 2009.

Globally optimal SISO H_2-norm model reduction

Sibren Lagauw and Bart De Moor, *Fellow IEEE, SIAM, IFAC*
Center for Dynamical Systems, Signal Processing, and Data Analytics (STADIUS),
Department of Electrical Engineering (ESAT), KU Leuven, 3001 Leuven, Belgium
sibren.lagauw@esat.kuleuven.be, bart.demoor@esat.kuleuven.be

1 Introduction

State-of-the-art methods for H_2-norm model reduction have demonstrated exceptional performance on large-scale problems [4], however, the methods are generally suboptimal as only local optimality can be guaranteed. The approach that we present is, by contrast, deterministic in the sense that it ensures to identify the globally optimal reduced model. We use the first-order necessary conditions for optimality of the single-input single-output (SISO) H_2-norm model reduction problem, which can be shown to be interpolatory conditions (Walsh's theorem), to reformulate the problem as a multivariate root-finding problem. While aiming for global optimality through this reformulation comes at the cost of a combinatorial growth of the problem complexity for increasing model orders, our methodology allows to tackle larger problems compared to the other globally optimal approaches described in the literature [1, 2].

2 H_2-norm model reduction

Given a 'higher-order' system $H(z) \in H_2$, with H_2 the class of stable and causal LTI models with real-valued impulse response:

$$H(z) = \frac{b(z)}{a(z)} = \frac{b_{n-1}z^{n-1} + \cdots + b_1 z + b_0}{z^n + a_{n-1}z^{n-1} + \cdots + a_1 z + a_0},$$

model reduction techniques search for a model $\hat{H}(z) \in H_2$ of order $m < n$, while minimizing the approximation error in some measure. We consider the H_2-norm:

$$\begin{aligned} \min_{\hat{H}(z)} \quad & J = \left\| H(z) - \hat{H}(z) \right\|_{H_2}^2 \\ & = \frac{1}{2\pi} \int_{-\pi}^{\pi} |H(e^{j\omega}) - \hat{H}(e^{j\omega})|^2 d\omega = \sum_{k=0}^{\infty} (h_k - \hat{h}_k)^2, \end{aligned}$$

with $\{h_k\}_{k=0,\ldots,\infty}$, $\{\hat{h}_k\}_{k=0,\ldots,\infty}$ the impulse response of $H(z)$ and $\hat{H}(z)$ respectively.

3 Walsh's theorem

Walsh's theorem originates from the field of rational approximation theory [9], but has also been derived in the context of systems and control [3, 6, 7]. The result states that in the stationary points of the model reduction problem $\hat{H}(z)$ satisfies:

$$H(z) - \hat{H}(z) = \frac{b(z)}{a(z)} - \frac{\hat{b}(z)}{\hat{a}(z)} = \left[\frac{\hat{a}_r(z)}{\hat{a}(z)}\right]^2 G(z),$$

with $G(z) \in H_2$ the z-transform of some real-valued, stable and causal signal and $\hat{a}_r(z)$ defined as $\hat{a}_r(z) = \hat{a}_0 z^m + \hat{a}_1 z^{m-1} + \cdots + \hat{a}_{m-1} z + 1$, the polynomial which has the reciprocals of the roots of $\hat{a}(z)$ as its roots.

4 Methodology

Manipulation of Walsh's relation allows to construct a square system of $n+m$ multivariate polynomial equations in the $2m$ decision variables $\{\hat{a}_i, \hat{b}_i\}_{i=0,\ldots,m-1}$ and $n-m$ auxiliary variables. After pruning the common-roots of the system (the $\{\hat{a}_i, \hat{b}_i\}_{i=0,\ldots,m-1}$ must be real-valued and $\hat{H}(z)$ stable), the globally optimal minimizer(s) of the model reduction problem can be selected by means of evaluation of J. The system contains one linear, one quadratic and $n+m-2$ cubic equations, the low degree of which is a major advantage as it keeps the complexity of the root-finding problem relatively low: other globally optimal approaches [1, 2] have been applied to setups with at most $(n,m) = (4,2)$, whereas e.g., the case $(15,4)$ seems feasible using our methodology.

Walsh's theorem has been considered in the context of the H_2-norm model reduction problem [6, 7], but, up to our knowledge, it has never been used to solve directly for the stationary points. We will present the theoretical machinery behind the novel methodology using a didactic toy problem and show how our approach, in combination with state-of-the-art root-finding methods [5, 8], can tackle numerical examples that were considered unfeasible before.

Acknowledgements

This work was supported in part by the KU Leuven: Research Fund (project C16/15/059), and several Leuven Research and Development bilateral industrial projects, in part by Flemish Government agencies: FWO (EOS project G0F6718N (SeLMA), and PhD grant SB/1SA1319N), EWI (Flanders AI Research Program), and in part by the European Commission (EU Research Council under the European Union's Horizon 2020 research and innovation programme (ERC Adv. Grant) under grant 885682). The work of S. Lagauw was supported by the FWO Fundamental Research PhD Fellowship, under Grant 11K5623N.

References

[1] O.M. Agudelo, C. Vermeersch, and B. De Moor. Globally optimal H_2-norm model reduction: A numerical linear algebra approach. *IFAC PapersOnLine (Special Issue: Proc. of MTNS 2020)*, 54(9):564–571, 2021.

[2] M.I. Ahmad, M. Frangos, and I.M. Jaimoukha. Second order $\mathscr{H}_2$ optimal approximation of linear dynamical systems. In *IFAC Proceedings Volumes*, volume 44, pages 12767–12771, Milano (Italy), 2011.

[3] P.R. Aigrain and E.M. Williams. Synthesis of n-reactance networks for desired transient response. *Journal of Applied Physics*, 20(6):597–600, 1949.

[4] A. C. Antoulas. *Approximation of Large-Scale Dynamical Systems*. Advances in Design and Control. Society for Industrial and Applied Mathematics, Philadelphia, PA USA., 2005.

[5] P. Breiding and S. Timme. HomotopyContinuation.jl: A package for homotopy continuation in julia. In *International Congress on Mathematical Software*, pages 458–465, 2018.

[6] B. De Moor, P. Van Overschee, and G. Schelfhout. H_2 model reduction for SISO systems. In *Proc. of the 12th IFAC World Congress*, pages 227–230, Sydney, Australia, July 1993.

[7] Phillip A. Regalia. *Adaptive IIR Filtering in Signal Processing and Control*. CRC Press, 1995.

[8] C. Vermeersch and B. De Moor. Two complementary block Macaulay matrix algorithms to solve multiparameter eigenvalue problems. *Linear Algebra and its Applications*, 654:177–209, 2022.

[9] J.L. Walsh. *Interpolation and Approximation by Rational Functions in the Complex Domain*, volume XX of *American Mathematical Society Colloquium Publications*. American Mathematical Society, 3th edition, 1960.

Predicting cell size distribution in balanced growth with constraint-based modelling

Michiel Busschaert
Department of Chemical Engineering, KU Leuven.
michiel.busschaert@kuleuven.be

Steffen Waldherr
Department of Functional and Evolutionary Ecology, University of Vienna.
steffen.waldherr@univie.ac.at

Flux Balance Analysis (FBA) [1] is a commonly used method to predict cell growth rate and intracellular reaction rates. The method consists of an maximization of the growth rate μ subject to biochemical constraints. Notably, the metabolic network is included to balance the production/consumption of metabolites due to metabolic reactions.

FBA typically assumes an average cell description, meaning that heterogeneity between cells is not modelled. This heterogeneity may present itself on the level of cell age, certain protein content, or, as discussed here, on the level of cell size. In this contribution, we propose an extended formulation of FBA in which cell size can be taken into account. An example in which this may proof useful, is when uptake kinetics or cell composition are influenced by cell size (conform surface-to-volume-ratio). This may provide a more detailed cell culture description compared to regular FBA.

To model the cell size heterogeneity, the deterministic framework of Population Balance Models (PBM) [2] is used. In PBM, the cell size distribution is represented by a number density function (NDF) $n(x)$. In balanced growth conditions, the shape of $n(x)$ is time-invariant, and can be shown to satisfy

$$\bar{\mu} n(x) = -\frac{\partial\left(\mu(x) x n(x)\right)}{\partial x} - \gamma(x) n(x) + \int_0^\infty \beta(x,x')\gamma(x')n(x')dx', \tag{1}$$

where $\bar{\mu}$ is a population-average growth rate. The right-hand side of (1) describes cellular dynamics, i.e. growth and cell division. In our proposed extended FBA, The population balance (1) acts as a constraint in the optimization of the average growth rate $\bar{\mu}$. Additional constraints describe e.g. intracellular metabolism. The solution of the extended FBA program is the average growth rate $\bar{\mu}$, the NDF $n(x)$ and the reaction fluxes per cell size.

We have applied our method to a core-carbon metabolic network of *Escherichia coli* [4], consisting of 95 reactions (including 1 biomass reacion) and 72 metabolites. Aerobic growth on glucose under limited oxygen availability is simulated (note, in this case the assumption of balanced growth only holds on a short time interval). The resulting cell size distribution by biomass is shown in Figure 1. The blue shaded area represents the existence of alternative solutions due to the existence of multiple optimal solutions.

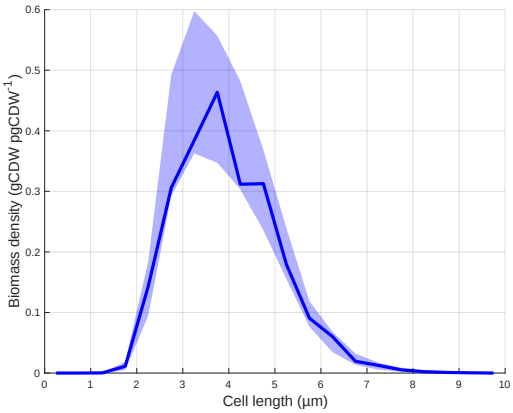

Figure 1: Prediction of cell biomass distribution under limited oxygen availability.

This example illustrates that the proposed extension may be implemented easily from existing FBA models. The prediction on cell size distribution may help in validating the model to experimental data. In addition, this framework may help in modelling cell division within the FBA framework, providing a better understanding of the cell cycle.

This work has been funded by Fonds voor Wetenschappelijk Onderzoek Vlaanderen (FWO), grant number G066621N.

References

[1] A. Varma and B. Ø. Palsson, "Metabolic flux balancing: Basic concepts, scientific and practical use," *Biotechnology*, vol. 12, pp. 994–998, 1994.

[2] D. Ramkrishna, "Population Balances: Theory and Applications to Particulate Systems in Engineering," 1st ed. Academic Press, 2000.

[3] A. Goelzer, V. Fromion, and G. Scorletti, "Cell design in bacteria as a convex optimization problem," *Automatica*, vol. 47, pp. 1210–1218, 2011.

[4] J. D. Orth, R. M. Fleming, and B. Ø. Palsson, "Reconstructionanduse of microbial metabolic networks: the core escherichia coli metabolic model as an educational guide," *EcoSal plus*, vol. 4, no. 1, 2010.

Improving breathing effort identification in respiratory patients: A linear regression perspective

Lars van de Kamp[1,2], Bram Hunnekens[2], Nathan van de Wouw[1,3], and Tom Oomen[1,4]
1 Department of Mechanical Engineering, Eindhoven University of Technology, Eindhoven
2 Demcon Advanced Mechatronics, Best
3 Department of Civil, Environmental and Geo-Engineering, University of Minnesota, Minneapolis, USA
4 Delft Center for Systems and Control, Delft University of Technology, Delft, The Netherlands
Email: l.g.j.v.d.kamp@tue.nl

Introduction

Mechanical ventilation is used in Intensive Care Units (ICUs) to save lives of patients who are not able to breath on their own. Mechanical ventilation supports patients by ensuring adequate oxygenation and carbon dioxide elimination via appropriate ventilator settings. To find these settings, information about the patient, e.g., the lung capacity, is required as well as the patient's breathing effort. Therefore, it is crucial to accurately estimate the information of the patient. We investigate the limits of accuracy of estimation for different setups of the identification problem. The main methodology is a linear regression framework.

Linear regression framework

A patient supported by a mechanical ventilator is modeled in the generic structure:

$$y(k) = G(\xi)\boldsymbol{u}(k) + d(k), \tag{1}$$

where $y(k)$ is a measured output, $G(\xi)$ the static linear function from $\boldsymbol{u}$ to y, which includes the unknown patient parameters $\xi \in \mathbb{R}^n_{>0}$, $\boldsymbol{u}(k)$ the measured input signals, and $d(k)$ the unknown exogenous disturbance, which is the breathing effort of the patient. The estimation goal is to accurately find estimates of the patient parameters ξ and the exogenous disturbances $d(k)$ in the chosen grey box model presented in (1) for a single breath of N samples. Based on a single breath, we define the following model structure:

$$\mathcal{M}_\beta : X \to Y, \quad Y = X\beta \tag{2}$$

with $Y := \begin{bmatrix} y(1) & \cdots & y(N) \end{bmatrix}^\top$, $X := \begin{bmatrix} \boldsymbol{u}(1) & \cdots & \boldsymbol{u}(N) \\ & I_N & \end{bmatrix}^\top$, and $\beta := \begin{bmatrix} \xi & d(1) & \cdots & d(N) \end{bmatrix}^\top$. The data set of a single breath is captured by $\mathcal{D} = \{X, Y\}$. We assume that the patient parameters ξ do not change over the data set $\mathcal{D}$. Note that there is no unique solution for β because the model structure $\mathcal{M}_\beta$ is not identifiable [1].

General approach

Incorporating prior knowledge on the exogenous disturbance is crucial to find a unique parameter vector β within the estimation problem. Prior knowledge can be incorporated by parameterization of the exogenous disturbance d over a single breath, i.e., $d(k) = \theta^\top q(k)$ like in [2] or by enforcing constraints on the exogenous disturbance d over multiple breaths, e.g., periodicity, variations. This is visualized in Figure 1.

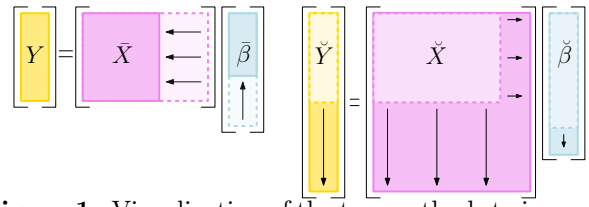

Figure 1: Visualization of the two methods to incorporate prior knowledge in the linear regression framework, i.e., parameterization of the exogenous disturbance or estimating over multiple breaths.

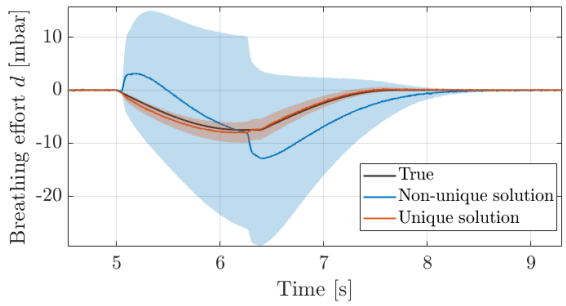

Figure 2: Simulation results of the breathing effort estimation in the linear regression framework. The not identifiable model structure leads to a non-unique breathing effort estimate (▬). Estimation over multiple breaths leads to identifiable structure and a unique breathing effort estimate (▬).

Results

Through a simulated case-study it is validated that estimation over multiple breaths is sufficient to obtain a unique solution, as shown in Figure 2. In a larger context, this shows that the linear regression framework as presented encompasses a large range of practically relevant solutions to solve the estimation problem and thereby improve the treatment of patients supported by mechanical ventilation.

References

[1] L. van de Kamp, B. Hunnekens, N. van de Wouw, and T. Oomen, "An Estimation Perspective on Breathing Effort Disturbances in Mechanical Ventilation", in proceedings of IFAC worlds 2023.

[2] J. Reinders, B. Hunnekens, N. van de Wouw, and T. Oomen, "Noninvasive breathing effort estimation of mechanically ventilated patients using sparse optimization", IEEE Open Journal of Control Systems.

Background study on the biology and mathematics behind the olfactory sense

Radu Cimpean, Alden Waters, Stephan Trenn
Bernoulli Institute
Nijenborgh 9, 9747 AG Groningen
The Netherlands
Emails: r.cimpean@rug.nl, a.m.s.waters@rug.nl, s.trenn@rug.nl

1 Introduction

Communication is a key aspect when it comes to the existence and functioning of systems. For the biological systems, neurons fulfil this role via chemical and electrical modes. There is an exchange of chemical substances that either excites or inhibits the relevant components till a spike, also called action potential, is reached and thus the neuron has relayed the information. As a system of interest, the research will focus further on the olfactory system.

2 Biological description and the mathematical model

The basic function of the aforementioned system is represented by the identification of odors as singular or mixed chemical compounds. For a better understanding, the case of human olfaction will be exemplified. The chemical molecules are entering the nasal cavity and reach the olfactory epithelium, where the binding to the Olfactory Receptor Neurons (ORN) occurs, triggering a two pathway response. The information is further relayed to the olfactory bulb (OB). The exchange occurs in ball shaped components called glomeruli, where the closely related ORN synapse with other neurons, called mitral cells (MC), one for each glomerulus. The MC have a major role in conveying the odor information, through a process called whitening. Since there can be a lot of redundancy in the information gathered in the glomeruli from the ORN, the OB performs the above mentioned process with the purpose of decorelating the activity patterns, aspect achieved via the interaction between the MC, which are excitatory by nature and granule cells (GC)/interneurons (IN), which are inhibitory. As a result, a preprocessed, decorelated pattern of signal activity is obtained, which is further fed to the higher areas of the brain for analysis and identification. Given the above brief biological description of the olfactory process, the interest of this research lies in the mathematical modeling. The base model is provided by [1] in the form of equations of motion:

$$\dot{X} = -H_0 G_Y(Y) - \alpha_x X + I$$
$$\dot{Y} = W_0 G_X(X) - \alpha_Y Y + I_c,$$

where X-signal from the MC; Y-signal from the GC; G_X, G_Y cell output as continuous functions, proportional to the cell firing frequency; H_0 - $n \times m$ matrix describing the synaptic connection MC $\rightarrow$ GC; W_0 - $m \times n$ matrix describing the synaptic connection GC $\rightarrow$ MC; I - input, result of the sniffing process; I_c - input control, coming from higher areas of the brain; α_X, α_Y - parameters. Moreover, [1] further indicates that the OB system may behave like a harmonic oscillator with damping, thus treating it as a group of coupled non-linear oscillators.

3 Current issues and research directions

By reducing the biological complexity of the OB to the damped harmonic oscillator approach, several issues arise. One such issue is that the model does not account for the whitening process. This aspect can be confirmed by observing the diagrams in [2] and [3]. The outcomes indicated there do not fully match the proposed oscillator model. Another issue concerns the parameters (α_X, α_Y) for the OB system. For instance, in [1], they are taken as fixed values related to the firing rate of the neurons.

Given these issues, several research directions are being explored. As a starting point, it would be of interest to account for the whitening process by providing a function based approach to the parameters (α_X, α_Y). This would entail modeling them as characteristic functions, and further considering obtaining a well-posedness result. Another key aspect is the optimization of the connectivity matrices H_0 and W_0, again towards the goal of expressing the whitening process more accurately.

References

[1] Z.Li and J.J.Hopfield, "Modeling the Olfactory Bulb and its Neural Oscillatory Processings,"Biol. Cybern. 61,379-392, 1989.

[2] A. Wanner and R.W. Friedrich, "Whitening of odor representations by the wiring diagram of the olfactory bulb," Nat Neurosci. 23(3), 433-442, 2020.

[3] M. Beyeler, F. Stefanini, H. Proske, G. Galizia and E.Chicca, "Exploring olfactory sensory networks: simulations and hardware emulation," Biomedical Circuits and Systems Conference (BioCAS), Paphos, Cyprus, 270-273, 2010.

Testing and preemptive quarantine for control of epidemics

Ouassim Benhamouche, Matthias Pezzutto, Nicolás Bono Rosselló, Emanuele Garone
SAAS, Universite Libre de Bruxelles,
50, av. Roosevelt, 1050 Bruxelles, Belgique
E-mails: ouassim.benhamouche@ulb.be, matthias.pezzutto@ulb.be,
nicolas.bono.rossello@ulb.be, emanuele.garone@ulb.be

1 Introduction

In the early stages of Covid–19 epidemic, generalized lockdown has been the only control measure to contain the diffusion of the disease. In later stages, epidemic control has relied on testing prior symptoms onset and preemptive quarantine for contacts of infected. Increasing the number of tests per day and the number of quarantined contacts improves the effectiveness of the strategy but results in a higher social-economical cost. Moreover, increasing the number of quarantined individuals might result in weaker compliance in the population and can compromise the control efforts. For this reason, it is important to properly assess the effects of testing and preemptive quarantine, taking into account the compliance of the individuals.

2 Main idea

We propose a novel compartmental model that encompasses different control actions available to the decision maker. We consider five compartments, the fist one for the susceptible individuals, the second one for the infected individuals, the third one for the recovered ones, the fourth one for the susceptible quarantined and the last one for the infected quarantined. We consider the actions aiming to reduce the disease transmissibility, either reducing the average number of contacts or reducing the transmission probability per contact , e.g. lockdown, curfew, mobility limitation, social distancing, use of personal protective equipment. More importantly, we propose a new model for detection and quarantining: rather than simple constant rates as in the [1], we propose a more elaborated rate depending on a weighted combination of the current state of all the compartments. Finally, we include in the model the compliance with preemptive quarantine by properly decreasing the probability of entering and remaining in quarantine with more traced contacts per detected.

3 Simulations and Results

We use the proposed compartmental model that takes into account testing, quarantine, and compliance with the applied measures, to study the effect of Non-Pharmaceutical Interventions (NPI) on the control and the eradication of the infectious disease.

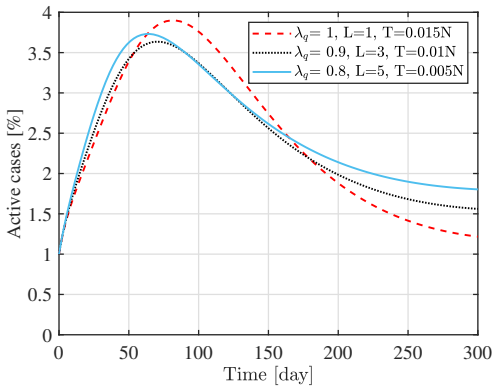

Figure 1: Evolution of the percentage of active cases.

We simulate our model and vary the number of test allocated T, the number individuals quarantined per detected L, and the compliance with the quarantine measure λ_q. The results are reported in Figure 1. We conclude:

- There is a trade-off between the resources allocated for increasing the number of tests and those allocated for affording an higher number of preemptively quarantined individuals. The best resource allocation might change depending on if the objective is the worst case or the steady state.
- Quarantining more individuals leads to a counter-effect that affects negatively the evolution of active cases, due to lower compliance associated to stronger interventions.

4 Acknowledgement

This work is supported by the Fonds de la Recherche Scientifique-FNRS under the grant 40003443 (Smart Testing)

References

[1] Giordano, G., Blanchini, F., Bruno, R., Colaneri, P., Di Filippo, A., Di Matteo, A., and Colaneri, M. (2020). Modelling the covid-19 epidemic and implementation of population-wide interventions in italy. Nature Medicine, 26(6), 855–860.

Derating control strategies impact on the lifetime fatigue loads of a wind turbine

Younes OUDICH[1], Anthony FEGHALY[1], Michel KINNAERT[1]
Department of Control Engineering and System Analysis (SAAS)[1]
Université Libre de Bruxelles
CP 165/55, 50 Av.F.D. Roosevelt B-1050 Brussels
Belgium
Emails: younes.oudich@ulb.be; anthony.feghaly@ulb.be; michel.kinnaert@ulb.be

1 Introduction

During this last decade, the exponential growth of renewable energy demand has led to a rapid expansion of wind power worldwide. This expansion motivates wind power plant owners to take part in frequency regulation, competing with traditional power plants. Nevertheless, the latter is challenging, because of the intermittence of the wind. Hence, a power reserve is needed. For wind farms, the power reserve can be realized thanks to derating strategies. Derating a turbine means that the extracted power from the wind is less than the available one, enabling the owners to have a power margin that can be used when it is needed. In this work, the comparison between two derating control strategies is assessed, in terms of lifetime damage equivalent load (DEL). The first strategy acts on the generator torque set point for derating the power while keeping the standard configuration of the pitch angle controller. The second strategy derates the wind turbine (WT) power thanks to the pitch controller while maintaining the standard tip speed ratio set point. These strategies were simulated in OpenFAST under different turbulent wind conditions, in order to assess their impact on the lifetime DEL of the WT.

The contribution of this research relies on introducing a simple pitch-based derating control strategy, and comparing it with the classical torque-based derating control approach in terms of lifetime DEL. The first strategy conserves the Standard Tip Speed Ratio values in the different operating regions of a WT, and is thus noted STSR. The second strategy will be noted as SP, referring to the conservation of the Standard Pitch control configuration while derating by acting on the torque. The Base Case control strategy aiming at maximum power point tracking (MPPT), hence no derating, will be referred as BC.

2 Application and results

In the present work, the focus is brought on three components of the 5MW-NREL WT[1]; the low-speed shaft bending moments noted SSTipMya and LSSTipMza; the edgewise and flapwise moments on the blades, noted RootMxb1 and RootMyb1, respectively; and the tower base edgewise and flapwise moments, noted RootMxb1 and RootMyb1, respectively. The resulting lifetime DEL are depicted in Figure 1, normalized on the BC. The STSR performs better than the SP, achieving derating while decreasing the lifetime DEL of the WT for all components. The latter conclusion is due to the low variations of the pitch angle, inducing lower thrust loads on the rotor.

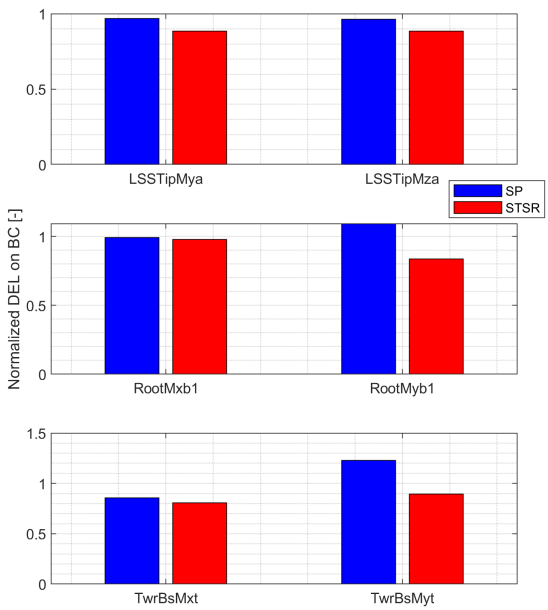

Figure 1: Lifetime DEL on different components of the WT, normalized on the basis of the BC strategy

3 Acknowledgement

This research is part of the Belgian PhairywinD project, funded by the Belgian FPS Economy.

References

[1] Jonkman J et al. 2009. Definition of a 5-MW Reference Wind Turbine for Offshore System Development. Technical Report NREL/TP-500-38060

$\mathscr{H}_\infty$ control with $\mathscr{D}$-unstable weighting filters and $\mathscr{D}$-stability constraints

Laurens Jacobs[1,2] and Jan Swevers[1,2]
[1]MECO Research Team, Dept. of Mechanical Engineering, KU Leuven, B-3001 Leuven
[2]Flanders Make@KU Leuven, B-3001 Leuven
laurens.jacobs@kuleuven.be

1 Introduction & problem definition

$\mathscr{H}_\infty$ control design is a popular and widely recognized approach for developing (in most cases linear) control systems with optimal performance and robustness as key requirements. Various design paradigms based on $\mathscr{H}_\infty$ norms, such as mixed-sensitivity, weighted-sensitivity, and multi-objective design have proven their value in practical applications. All these problem formulations can be solved through a wide variety of mathematical tools, including operator theory, polynomial methods, Riccati equations, linear matrix inequalities (LMIs), and descent-based methods for solving bilinear matrix inequalities (BMIs) or nonsmooth formulations. After more than 30 years of intensive research, a relatively generic problem formulation is regularly claimed to be formally solved these days [1].

In this work, the authors focus on a multi-objective weighted-sensitivity $\mathscr{H}_\infty$ control problem formulation with weighting filters $\mathbf{W}_\mathrm{i}$ and $\mathbf{W}_\mathrm{o}$ that are allowed to be $\mathscr{D}$-unstable, while still requiring the targeted controller to render the closed loop formed with the generalized plant $\mathbf{P}$ $\mathscr{D}$-stable. Using the control configuration depicted in Fig. 1, one can write this design problem as

$$\underset{\mathbf{K}}{\text{minimize}} \quad \sum_{i\in\mathbb{I}_\mathrm{o}} c_i \left\|\mathrm{MR}[\mathbf{T}_i]\right\|_\infty \tag{1a}$$

$$\text{subject to} \quad \left\|\mathrm{MR}[\mathbf{T}_j]\right\|_\infty \leq 1, \forall j \in \mathbb{I}_\mathrm{c} \tag{1b}$$

$$\mathrm{MR}[\mathscr{F}_l(\bar{\mathbf{P}},\mathbf{K})] \text{ is } \mathscr{D}\text{-stable} \tag{1c}$$

($c_i > 0$, $\mathbb{I}_\mathrm{o}, \mathbb{I}_\mathrm{c} \subset \mathbb{N}^+$) where $\mathrm{MR}[\cdot]$ denotes an observable and controllable realization and $\mathscr{F}_l(\bar{\mathbf{P}},\mathbf{K})$ represents the weighted feedback interconnection of the plant and the controller. This problem type is particularly relevant in motion and vibration control problems for uncertain systems with lightly damped modes. Consider, for example, these two cases that are often seen in mechatronic control problems:

- An integrator is required in the controller, which yields a weighting filter with at least one pole in 0.
- An inverted sharp (lightly damped) notch filter

$$W(s) = \frac{s^2 + 2\zeta_1\omega_n s + \omega_n^2}{s^2 + 2\zeta_2\omega_n s + \omega_n^2}$$

  is used as a weighting filter while a conflicting conic pole region ($\mathscr{D}$-stability) constraint is imposed by choosing

$$\mathscr{D} = \left\{ z \;\middle|\; z \in \mathbb{C},\ \sqrt{1-\zeta_\mathscr{D}^2}\,|\Im(z)| < -\zeta_\mathscr{D}\Re(z) \right\}$$

  (with $\zeta_\mathscr{D} > \zeta_2$) to enforce a minimal damping ratio of the closed-loop dynamics.

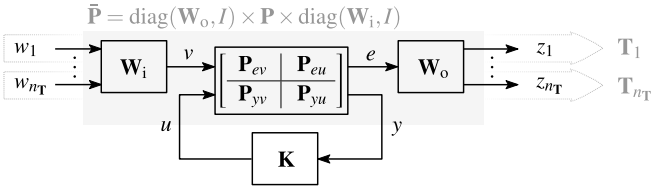

Fig. 1: Generalized control configuration associated with (1).

Previous approaches and extensions in the field of $\mathscr{H}_\infty$ control related to $\mathscr{D}$-stability, such as [2]–[3], have not been able to handle this problem type so far because the controller cannot $\mathscr{D}$-stabilize the $\mathscr{D}$-unstable modes of the weighting filters.

2 Solution approach

We build upon earlier results from related research to obtain a reformulation of problem (1) and show how a convex optimization approach or a nonsmooth optimization approach for an underlying standard $\mathscr{H}_\infty$ problem constitutes a generic solution procedure for (1). More specifically, our methodology is a straightforward extension of the results in [4], combined with the techniques advocated by [2]–[3] or by [5]–[6].

3 `sshinfcd`: a MATLAB implementation

In order to support practicing control engineers in implementing the solution that we present, we have developed a high-level software package in MATLAB: `sshinfcd`. It is freely available on GitHub [7] and comes with an extensive explanation and several examples.

References

[1] P. Apkarian and D. Noll (2012). "The $\mathscr{H}_\infty$ control problem is solved." https://www.math.univ-toulouse.fr/~noll/PAPERS/solved.pdf. Retrieved January 3, 2023.

[2] M. Chilali and P. Gahinet. "$\mathscr{H}_\infty$ design with pole placement constraints: An LMI approach". *IEEE Transactions on Automatic Control* 41 (3), pp. 358–367, 1996.

[3] C. Scherer et al. "Multiobjective output-feedback control via LMI optimization". *IEEE Transactions on Automatic Control* 42 (7), pp. 896–911, 1997.

[4] H. Köroğlu (2013)."$\mathscr{H}_\infty$ synthesis with unstable weighting filters: An LMI solution". 52nd IEEE Conference on Decision and Control (CDC), Florence, Italy.

[5] P. Apkarian and D. Noll. "Nonsmooth $\mathscr{H}_\infty$ synthesis". *IEEE Transactions on Automatic Control* 51 (1), pp. 71–86, 2006.

[6] P. Apkarian et al. (2014). "Multi-model, multi-objective tuning of fixed-structure controllers". 13th European Control Conference (ECC), Strasbourg, France.

[7] L. Jacobs (2023). "sshinfcd – State-space $\mathscr{H}_\infty$ control design for LTI systems'. https://github.com/meco-group/sshinfcd/. Retrieved January 5, 2023.

Acknowledgement Laurens Jacobs is financially supported by a postdoctoral fellowship from Flanders Innovation and Entrepreneurship (VLAIO) (grant HBC.2021.0200).

Reference Model based Data-driven Control of Power Amplifiers for High-precision Motion Systems

Duo Xu, Serban Popescu and Mircea Lazar
Control Systems Group, Eindhoven University of Technology, The Netherlands

1 Introduction

In order to achieve sub-nanometer position accuracy, the current provided by the amplifier must have a specific step response, which is represented as a desired reference model. This work deals with a data-driven control method for an industrial power amplifier. Given the reference model, the Virtual Reference Feedback Tuning (VRFT) method synthesizes fixed-order linear controllers based directly on data collected from the plant, such that the closed-loop response is as close as the desired reference model.

2 System model

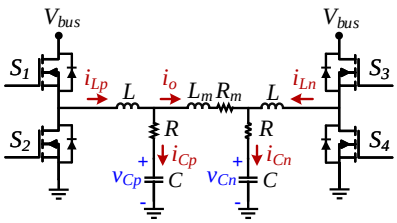

Figure 1: Schematic of the industrial power amplifier.

Fig. 1 demonstrates the topology of the industrial power amplifier, which has a symmetrical structure on the positive and negative sides [2]. The average power amplifier model can be represented by a SISO transfer function described by

$$\frac{i_o(s)}{d_{com}(s)} = \frac{V_{bus}}{L_m s + R_m} \frac{RCs+1}{LCs^2 + \sqrt{2/LC}s + 1}, \qquad (1)$$

where i_o is the output current and d_{com} is the common duty cycle.

3 Approach

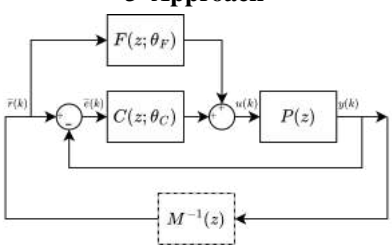

Figure 2: Closed-loop block diagram.

Fig. 2 depicts the closed-loop block diagram and the desired reference model $M(z)$. The proposed VRFT framework simultaneously synthesizes the feedback and feedforward controllers without the information about the plant model $P(z)$. Given the measured plant output $y(k)$, the virtual reference $\bar{r}(k)$ is computed by $\bar{r}(k) = M(z)^{-1}y(k)$, which generates the virtual error as $\bar{e}(k) = \bar{r}(k) - y(k)$. When the collected data is noiseless, the optimal controllers can be derived by minimizing the cost function

$$J_{VR}(\theta) = \|u(k) - C(z;\theta_C)\bar{e}(k) - F(z;\theta_F)\bar{r}(k)\|_2^2, \qquad (2)$$

where $C(z;\theta_C) = \theta_C^\top \beta_C(z)$, $F(z;\theta_F) = \theta_F^\top \beta_F(z)$. $\beta_C(z)$ and $\beta_F(z)$ represents the controller types, θ_C and θ_F are the parameters to be optimized. The optimal solution $\hat{\theta}^\top = [\hat{\theta}_C^\top, \hat{\theta}_F^\top]$ is computed by

$$\hat{\theta} = [\sum_{k=1}^{N} \Phi(k)\Phi(k)^\top]^{-1} \sum_{k=1}^{N} \Phi(k)u(k), \qquad (3)$$

where $\Phi(k)\top = [\phi_C(k)\top, \phi_F(k)\top]$, $\phi_C(k) = \beta_C(z)\bar{e}(k)$, $\phi_F(k) = \beta_F(z)\bar{r}(k)$. The step response of the reference model, together with the closed-loop performance, which is controlled by the optimal solution $C(z;\hat{\theta}_C)$ and $F(z;\hat{\theta}_F)$, are compared in Fig. 3. The output trajectories are close, which satisfies the objective. Fig. 4 reveals the induced position tracking performance.

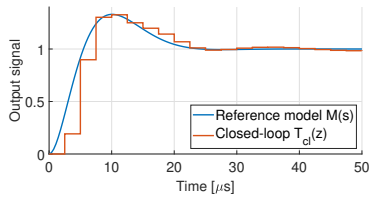

Figure 3: Step response comparison.

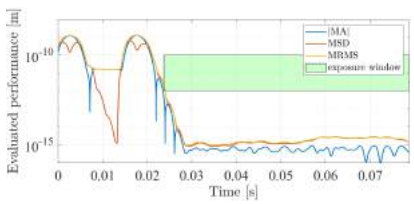

Figure 4: Position error evaluation.

References

[1] M. C. Campi, A. Lecchini, and S. M. Savaresi, "Virtual reference feedback tuning: A direct method for the design of feedback controllers," Automatica, vol. 38, 2002.

[2] M. Hajiheidari, D. Xu, J. van Duivenbode, B. Vermulst, and M. Lazar, "Analysis of power amplifier contribution to the precision of motion systems," 2022 IEEE 17th International Conference on Advanced Motion Control.

Augmented model identification for forward simulation of a robot arm

András Retzler[1,2,6], Roland Tóth[3,5], Jan Swevers[1,2], Jean-Philippe Noël[1,2], Zsolt Kollár[6], Gerben Izaak Beintema[3], Jonas Weigand[4], and Maarten Schoukens[3]

[1]MECO Research Team, Dept. of Mechanical Engineering, KU Leuven, Heverlee, Belgium
[2]Flanders Make@KU Leuven, Heverlee, Belgium
[3]Dept. of Electrical Engineering, Eindhoven University of Technology, Eindhoven, The Netherlands
[4]Siemens AG, Karlsruhe, Germany
[5]Systems and Control Laboratory, Institute for Computer Science and Control, Budapest, Hungary
[6]Dept. of Measurement and Inf. Systems, Budapest Univ. of Technology and Economics, Budapest, Hungary
Email address: andras.retzler@kuleuven.be

1 Problem statement

Our goal is to retrieve an accurate simulation model of a robot arm for model predictive control (MPC). In an MPC setting we often need to make an accurate prediction of how the arm behaves, for a given finite time window ahead. In robotic applications this window is typically 150-300 ms. A more accurate model leads to better tracking performance and faster solution time.

We study the robot arm [1] depicted in Figure 1, for which a detailed motion model is given. This model is based on physical knowledge such as the Denavit-Hartenberg parameters and known inertial parameters of the links, and it is formulated by the help of the recursive Newton-Euler method. The arm has 6 joints, and their positions are measured. A $150\,kg$ load is attached to the end effector. The nonlinearities in the dynamics include: backlash in all joints, pose-dependent inertia, pose-dependent gravitational loads, pose-dependent hydraulic forces, pose- and velocity-dependent centripetal and Coriolis forces as well as nonlinear friction.

The challenge is that the forward model diverges quickly from the measurements of the actual arm. Identifying a better model by the tuning of the friction parameters have failed to improve the simulation significantly. In this work we aim to exploit the already known dynamic aspects of the system, while we learn the unknown nonlinear effects of the system from data.

2 Proposed solution

In order to increase the accuracy, we augment the purely physics-based model with a neural network (NN) in parallel, with regularization added on the parameters of the physics-based model. The implementation is based on the deepSI framework [2].

Part of our approach is a formulation of the objective that applies a one-step-ahead prediction at the acceleration level, in order to increase the robustness of the estimation with respect to local minima, and also against the simulation becoming numerically unstable, and to decrease the computational complexity, all of which are often a problem in simulation-based formulations.

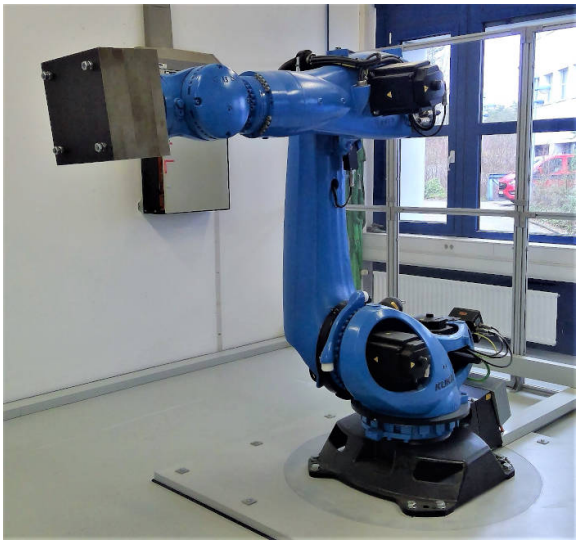

Figure 1: Industrial robot arm KUKA KR300 R2500 ultra SE [1]

We are comparing the average error of the simulation in a 150 ms window with that of the NN only, physics-only and augmented model.

References

[1] Jonas Weigand and Julian Götz and Jonas Ulmen and Martin Ruskowski, "Dataset and Baseline for an Industrial Robot Identification Benchmark", 2022.

[2] Gerben Beintema, Roland Tóth, Maarten Schoukens. Nonlinear State-Space Identification using Deep Encoder Networks; Proceedings of the 3rd Conference on Learning for Dynamics and Control, PMLR 144:241-250, 2021.

An experimental result on direct data-driven control of nonlinear systems using the LPV framework

Chris Verhoek[1], Sofie Haesaert[1], and Roland Tóth[1,2]
[1] Control Systems Group, Eindhoven University of Technology, The Netherlands.
[2] Systems and Control Laboratory, Institute for Computer Science and Control, Budapest, Hungary.
{c.verhoek, s.haesaert, r.toth}@tue.nl

1 Introduction

Behavioral data-driven analysis and control methods for *Linear Time-Invariant* (LTI) systems, which are based on Willems' *Fundamental Lemma* [1], have gained popularity in recent years. This is because these methods can provide *guarantees* in terms of closed-loop stability and performance, while the controller is synthesized using *only* measured data from the LTI system. While these methods have proved to be very powerful, they are mainly focussed on the class of LTI systems, and extensions to the *nonlinear* (NL) domain are rather immature. In this work, we take an 'intermediate' step to get to a NL data-driven framework, by using a linear surrogate model of a NL system by means of an *Linear Parameter-Varying* (LPV) *embedding*, see Fig. 1. LPV

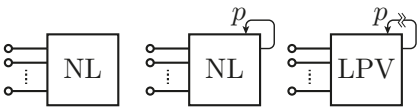

Fig. 1: LPV embedding of a NL system.

systems have a linear input-(state)-output relationship that varies along a *measurable* time-varying signal, the *scheduling variable*, which is used to express, e.g., nonlinearities. This allows to embed the NL system behavior into the solution set of the LPV system. Hence, the recently developed extension of the data-driven methods for the LPV framework [2] is a promising direction towards a behavioral data-driven analysis and control framework for NL systems.

In this work, we demonstrate that the direct data-driven LPV state-feedback control approaches in [2] can achieve reference tracking on a real-world NL unbalanced disc system, depicted in Fig. 2, see also [3], and hence that direct data-driven control of NL systems can be successfully accomplished through the LPV data-driven behavioral approach.

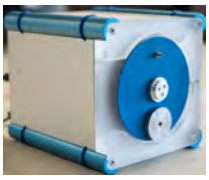

Fig. 2: Setup.

2 Approach

We apply the approaches in [2] on an experimental setup of the unbalanced disc that is depicted in Fig. 2. From this system we obtain a *data-dictionary* of 7 time-measurements of the input, scheduling and state, depicted in Fig. 3. With

This work has received funding from the European Research Council (ERC) under the European Union's Horizon 2020 research and innovation programme (grant agreement nr. 714663), and financial support in the scope of the AI4GNC project with SENER Aeroespacial S.A., contract nr. 4000133595/20/NL/CRS

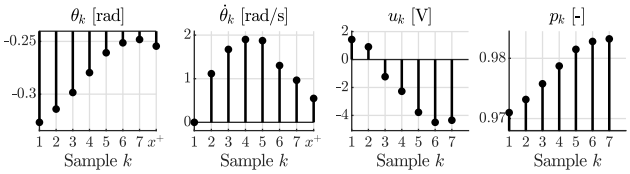

Fig. 3: Seven-step long data-dictionary used for controller synthesis.

this data-dictionary, we construct a data-driven representation of the LPV system, which embeds the NL unbalanced disc system. This data-driven representation is then incorporated in the state-feedback synthesis algorithms that are developed in [2]. Using *only* the data-dictionary in Fig. 3, we synthesize two stabilizing LPV state-feedback controllers, which we implement on the setup; one guaranteeing optimal quadratic performance, and one guaranteeing a minimal $\mathscr{L}_2$-gain of the closed-loop system.

3 Results

We applied the synthesized LPV state-feedback controllers on the experimental setup in a reference tracking scenario[1]. The tracking results are shown in Fig. 4, where the reference is depicted in gray. The results show that the closed-

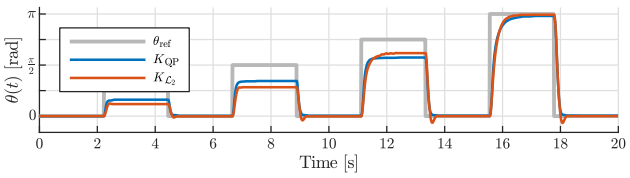

Fig. 4: Experimental results with changing origin

loop system achieves reference tracking along the full operating range of the NL system, with an LPV controller that is designed using only the 7 recorded data-points depicted in Fig. 3. The present steady-state error is expected and due the lack of integral action or a feed-forward term. These results show the potential of using the LPV framework to formulate data-driven methods for NL systems.

References

[1] Willems, J. C., Rapisarda, P., Markovsky, I., and De Moor, B. L. M. (2005). "A note on persistency of excitation," *Systems & Control Letters*, 54(4), 325–329.

[2] Verhoek, C., Tóth, R., and Abbas, H. S. (2022). Direct Data-Driven State-Feedback Control of Linear Parameter-Varying Systems. *Submitted to IEEE-TAC*. (Preprint arXiv:2211.17182).

[3] Verhoek, C., Abbas, H. S. and Tóth, R. (2022). "Direct data-driven LPV control of nonlinear systems: An experimental result." *Submitted to IFAC2023*. (Preprint arXiv:2211.17191).

[1] See https://youtu.be/SyyUVy1sPsc for a video.

Physics-Informed Online Learning of Gray-box Models by Moving Horizon Estimation

Kristoffer Fink Løwenstein[1,2,*], Lorenzo Fagiano[1], Daniele Bernardini[2], and Alberto Bemporad[3]
[1]DEIB, Politecnico di Milano, Via Ponzio 34/5, 20133, Milano, Italy
[2]ODYS s.r.l, Via Pastrengo 14, 20159, Milano, Italy
[3]IMT School for Advanced Studies, Piazza San Francesco 19, 55100, Lucca, Italy
*Email: kristofferfink.loewenstein@polimi.it

1 Introduction

A simple yet expressive prediction model is an essential ingredient in model-based control and estimation. Models derived from fundamental physical principles may fail to capture the complexity of the actual system dynamics. A potential solution is the use of a physics-informed, or gray-box model that extends a physics-based model with a data-driven part. Learning the latter might be challenging, due to noisy measurements and lack of full state information. This work presents a method based on Moving Horizon Estimation (MHE) for simultaneous state estimation and training of a neural network submodel.

2 Moving Horizon Estimation for Neural Network Learning

We consider a dynamical system governed by the (unknown) discrete-time dynamics

$$x_{k+1} = f(x_k, u_k, p_k) + v_{x,k} \tag{1a}$$

$$y_k = g(x_k, p_k) + v_{y,k} \tag{1b}$$

We assume that the model mismatch is governed by some unknown equation, i.e., $p_k = p(z_k)$, where z_k may collect states, inputs, and other exogenous signals to model degradation and environmental effects that can change over time. Accordingly, the prediction model used in this work is defined as

$$\hat{x}_{k+1} = \hat{f}(\hat{x}_k, u_k, f_{NN}(\mathbf{w}, z_k)) \tag{2a}$$

$$\hat{y}_k = \hat{g}(\hat{x}_k, f_{NN}(\mathbf{w}, z_k)) \tag{2b}$$

where $f_{NN}(\mathbf{w}, z_k)$ is a feedforward neural network (NN) trying to model $= p(z_k)$. Adapting the MHE scheme from [1] we develop a MHE algorithm for combined state-estimation and network parameter learning aiming to make the model in (2) match the true system in (1). The key features of the algorithm is the ability to preserve existing knowledge through the *arrival cost* and the possibility to impose constraints to make the learning meaningful from a physical point of view. Further, Preserving the physical knowledge allows one to use function approximations of rather limited size, thereby enhancing the potentials for real-time use. The algorithm presented consist of an offline learning phase used if a training dataset is available and an online phase to continuously adapt the model to time-varying changes of the system dynamics.

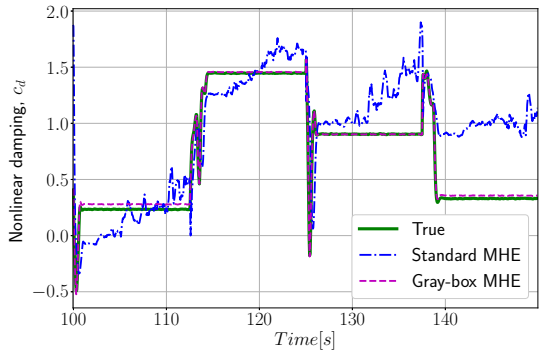

Figure 1: Comparison with standard MHE for estimation of unknown damping

.

3 Numerical Example: Two Degree of Freedom Robotic Manipulator

The proposed method is illustrated on two degree of freedom robotic manipulator to learn an unknown nonlinear state dependent damping term from noisy measurements. The NN estimating the unknown damping achieves a Mean Square Error(MSE) of $\text{MSE}_{c_d} = 1.67 \cdot 10^{-3}$ which compares favorably to estimating the unknown damping by standard MHE [1] where $\text{MSE}_{c_d} = 0.26$ is achieved. Further, it is illustrated how the algorithm is capable of online adaptation as the unknown damping is evolves time.

ACKNOWLEDGMENT

This project has received funding from the European Union's Horizon 2020 research and innovation programme under the Marie Skłodowska-Curie grant agreement No. 953348 (ELO-X).

References

[1] P. Kühl, M. Diehl, T. Kraus, J. P. Schlöder, and H. G. Bock, "A real-time algorithm for moving horizon state and parameter estimation," *Comput. Chem. Eng.*, vol. 35, pp. 71–83, 2011.

Removal of a disturbance using Gaussian process regression for improved impedance estimation applied to respiratory oscillometry

Antoine Marchal, Andy Keymolen, Gerd Vandersteen, John Lataire
Antoine.Marchal@vub.be,
dept. ELEC, Vrije Universiteit Brussels, Pleinlaan 2, 1050 Elsene Brussels, Belgium

1 Motivation and Context

Respiratory oscillometry consists of the identification of the human respiratory system pneumatic impedance. This can be achieved by exciting the respiratory system with a pressure excitation, coming from a medical ventilation device, and identify the relationship with the resulting flow as a transfer function.
This technique has the potential to provide information to medical practitioners non-invasively. However, for conscious, breathing patients, their breathing disturbs the identification procedure, resulting in a higher variance on the identified parameters.

2 Problem formulation

The problem to solve is to estimate and remove the breathing contribution of the patient on both the input pressure and the output flow in order to reduce the variance on the identified parameters. The input is chosen as a random phase multisine excitation, where the excited frequencies are placed as far as possible from the breathing frequency and its harmonics as done in [1] and illustrated in Figure 1, top.

3 Proposed approach

We propose here a Gaussian Process Regression scheme [2, chap. 2] in the frequency domain, carried out on both the measured pressure and flow, to estimate the breathing contribution in the frequency band of interest, including at the excited frequency bins k_{exc}. To achieve this, the non excited bins are provided as data points k_{data} in the frequency domain and the regression is done at $k_{\text{data}} \cup k_{\text{exc}}$. The identified disturbance is then removed before identifying the desired parameters.
We show the performance on a Monte Carlo simulation and show that the estimated parameters are unbiased and with a decreased variance, assuming that no model errors are present. In addition, on real patient data, we observe that the estimated variance on the parameters decreases as shown in the bottom of Figure 1.
The proposed technique relies a first measurement containing only breathing to quantify its statistical properties as hyperparameters of a locally periodic gaussian process kernel function. This first measurement is also used to design the multisine excitation and ensure spectral separation.

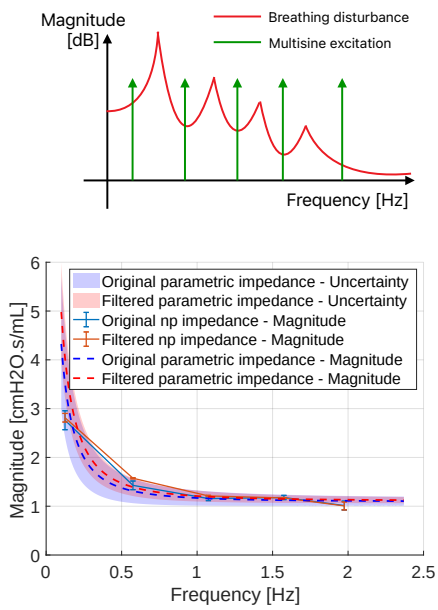

Figure 1: Top: Spectral separation of the breathing disturbance and the designed multisine excitation.
Bottom: result of the approach on a volunteer. A decrease of the variance can be observed on both the non-parametric and the parametric estimation of the transfer function.

This research was supported by the InVentiVe project, funded by the Interreg VA Flanders – The Netherlands program, CCI grant no. 2014TC16RFCB046, and by the Flemish Government (Methusalem Grant METH1).
The authors thank Demcon Macawi for the fruitful collaboration and the use of their device for the experiments.
The measurements on a volunteer was carried out according to the Helsinki protocol.

References

[1] C. Busschots, A. Keymolen, S. Verbanck, D. Schuermans, H. Maes, D. Peumans, J. Pattyn, Y. Rolain, G. Vandersteen, and J. Lataire. Adaptive excitation signals for low-frequency forced oscillation technique measurements in patients. *IEEE Transactions on Instrumentation and Measurement*, 70:1–9, 2021.

[2] C. E. Rasmussen and C. K. I. Williams. *Gaussian Processes for Machine Learning*. 2006.

Local identification in dynamic networks using the Multi-Step Least Squares method[1]

Stefanie Fonken, Karthik Ramaswamy, Paul Van den Hof
Control Systems Group, Department of Electrical Engineering,
Eindhoven University of Technology, The Netherlands
Email: {s.j.m.fonken, k.r.ramaswamy, p.m.j.vandenhof}@tue.nl

1 Introduction

The increasing scale and interconnectivity of engineering systems drives the need for data-driven modeling methods of these systems. Interconnected systems can be represented by dynamic networks, where signals are interconnected through dynamics (modules). Using the dynamic network framework the interconnecting modules of the full network or only a single module (local identification) is identified. For consistent identification we can use direct or indirect methods that do or do not rely on accurate noise modeling respectively. Due to the accurate noise modeling, direct methods obtain estimates with maximum likelihood properties, and can exploit unmeasured excitation signals in addition to known excitation signals to satisfy data-informativity conditions required for consistency. Therefore direct methods have the potential to require less known excitation signals which leads to less costly experiments compared to indirect methods. However, in local identification direct methods need to appropriately deal with confounding variables, that are unmeasured signals that can affect both the predictor inputs and outputs [2], which can lead to conservative data-informativity requirements.

The objective is to find a local identification method that has relaxed data-informativity conditions compared to current available methods.

2 Identification in dynamic networks

In the dynamic networks internal signals are represented by node signals $\left[w_1, \cdots, w_L\right]^\top$ represented by

$$w = G^0 w + H^0 e + r, \tag{1}$$

where G^0 is a hollow matrix, with modules G^0_{ji} as elements, the disturbances due to process noise are represented by filtered white noise innovation signals $v = H^0 e$. Both r and e are external excitation signals that are uncorrelated to each other, with signals r known and e unmeasured.
In local identification, dealing with confounding variables might lead to conservative data-informativity requirements in direct methods. To illustrate, consider the example shown in Figure 1, with target module G_{12}. In this example both e_1 and e_2 are confounding variables, where the local direct method [2] requires both excitation signals r_1 and r_2 to satisfy the data-informativity requirements. However, indirect methods require only one r signal to be present. The latter result also holds for the Multi-Step Least Squares method [1], while this methods relies on accurate modeling of the noise. This method, was originally developed for full network identification, but could be applied as a local identification method in this example. This example serves as a motivation to convert the Multi-Step Least Squares method for local identification since the relaxed data-informativity conditions might hold in other larger scale examples as well.

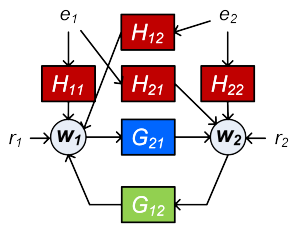

Figure 1: Example of a 2 node network with a full noise model and target module G_{12}.

3 Local identification using Multi-Step Least Squares method

The Multi-Step Least Squares method [1] relies on first reconstructing the innovation signal using high order ARX modeling, such that the reconstructed innovation can be used as a measured input in parametric identification steps. In order to convert the Multi-Step Least Squares method to a local identification method, we need to determine which signals need to be included in the identification procedure, such that the innovations reconstructed in the first step remain invariant in the second step. Furthermore, we show that this local identification method indeed obtains relaxed data-informativity conditions.

References

[1] S.J.M. Fonken, K.R. Ramaswamy, and P.M.J. Van den Hof. A scalable multi-step least squares method for network identification with unknown disturbance topology. *Automatica*, 141:110295, 2022.

[2] P.M.J. Van den Hof and K.R. Ramaswamy. Path-based data-informativity conditions for single module identification in dynamic networks. In *2020 59th IEEE CDC*, pages 4354–4359, 2020.

[1] This project has received funding from the European Research Council (ERC), Advanced Research Grant SYSDYNET, under the European Union's Horizon 2020 research and innovation programme (Grant Agreement No. 694504)

Identification of nonlinear systems using kernel-based nonlinear observer canonical models: method and convergence analysis

Jimei Li[1,2], Jan Swevers[1,3], Feng Ding[2]
[1]MECO Research Team, Dept. Mechanical Engineering, KU Leuven, 3001 leuven, Belgium.
[2]School of Internet of Things Engineering, Jiangnan University, Wuxi 214122, PR China.
[3]Flanders Make@KU Leuven, Belgium.
Email: jimeili0625@163.com

1 Introduction

It is essential for the structural design and safe operation of the systems under control to have models that can accurately capture and predict their dynamic behavior. Linear model identification techniques have reached a high level of maturity. However, when applied to nonlinear systems, they often yield models that fail to predict the dynamic behavior within an acceptable level of accuracy. As a result of that and because of the emergence of ever more intricate nonlinear designs, novel data driven modeling and optimization approaches capable of accounting for the nonlinear phenomena are required.

2 Methodology

Inspired by the multi-model control strategy [1], this work uses following kernel-based nonlinear observer canonical model form (K-NOCF) for dynamic systems

$$\begin{aligned} \boldsymbol{x}_{t+1} &= \boldsymbol{A}\boldsymbol{x}_t + \boldsymbol{b}u_t + \boldsymbol{D}\boldsymbol{k}(\boldsymbol{x}_t, u_t) + \boldsymbol{w}_t, \\ y_t &= \boldsymbol{c}\boldsymbol{x}_t + v_t, \end{aligned}$$

where $\boldsymbol{k}(\boldsymbol{x}_t, u_t) \in \mathbb{R}^n$ is the nonlinear term composed of the kernel functions depending on the states $\boldsymbol{x}_t \in \mathbb{R}^n$, the input $u_t \in \mathbb{R}$ and characteristic parameters, $\boldsymbol{w}_t \in \mathbb{R}^n$ is the process noise vector, $y_t \in \mathbb{R}$ is the output measurement which is corrupted with uncorrelated noise $v_t \in \mathbb{R}$. The unknown parameters are the elements of $\boldsymbol{A} \in \mathbb{R}^{n\times n}$, $\boldsymbol{b} \in \mathbb{R}^n$, $\boldsymbol{D} \in \mathbb{R}^{n\times n}$ and the characteristic parameters of the kernel functions. $\boldsymbol{A}$, $\boldsymbol{b}$ and $\boldsymbol{c} \in \mathbb{R}^{1\times n}$ have the observer canonical model structure, and hence $\boldsymbol{c}$ is known. The K-NOCF has a generic structure to model a large class of nonlinear dynamic systems and encompasses linear and bilinear systems as specific cases. The determination of the kernel functions in the K-NOCF needs to address the trade-off existing between the flexibility of the fitted model and its parsimony. So we consider polynomial kernel functions since they possess universal approximation properties.

The concurrent estimation of the system states and parameters for the given nonlinear model structure is challenging. In order to cope with this difficulty, the estimation of the states and parameters is performed alternately. The parameters are updated using the previous estimates of the states and process noise

$$\hat{\boldsymbol{\vartheta}}_{t-i} = [\boldsymbol{\vartheta}_{t-i}]\,|_{\hat{\boldsymbol{x}}_{t-i-1},\, \sum_{j=i+1}^{n} \hat{w}_{j,t-j}} \,.$$

A particle filter is used to estimate the states:

$$\hat{\boldsymbol{x}}_{t-i} = [\boldsymbol{x}_{t-i}]\,|_{\hat{\boldsymbol{\vartheta}}_{t-i},\, \hat{\boldsymbol{w}}_{t-i-1}} \,.$$

Since the distribution of the measurement noise is unknown in most cases, we use the Epanechnikov function to update the weight of each particle. The final step in each iteration is to update the process noise estimate:

$$\hat{\boldsymbol{w}}_{t-i} = [\boldsymbol{w}_{t-i}]\,|_{\hat{\boldsymbol{\vartheta}}_{t-i},\, \hat{\boldsymbol{x}}_{t-i}} \,.$$

To further reduce the computational burden, we introduce the hierarchical identification principle for the parameter estimation. The convergence of the proposed optimization algorithm is analyzed using the martingale convergence theorem.

3 Results

Numerical examples with known and unknown measurement noise distribution are given to demonstrate the effectiveness of the proposed method with respect to the parameter and state estimation accuracy, and with respect to the output prediction accuracy for both the identification data and different validation data. Furthermore, for validating the effectiveness of the devised model and the synchronous optimization scheme from a practical perspective, a third-order polynomial K-NOCF is employed to approximate the dynamic characteristics of the Silverbox system [2].

Acknowledgement: This work was supported by the China Scholarship Council (No. 202206790087).

References

[1] G.M. Prasad, A.S. Rao, "Evaluation of gap-metric based multi-model control schemes for nonlinear systems: An experimental study." ISA Transactions, 94: 246-254, 2019.

[2] T. Wigren, J. Schoukens, "Three free data sets for development and benchmarking in nonlinear system identification." 2013 European Control Conference (ECC), 2933-2938, July 17-19, 2013.

Stochastic $\mathscr{H}_2$ Optimization of Large-Scale Dynamic Systems

Pascal Den Boef
TU/e
p.d.boef@tue.nl

Jos Maubach
TU/e
j.m.l.maubach@tue.nl

Nathan van de Wouw
TU/e
n.v.d.wouw@tue.nl

Wil Schilders
TU/e
w.h.a.schilders@tue.nl

1 Abstract

Problems involving optimization of dynamic systems are encountered in areas such as model reduction, control design and design optimization. Often, these optimization problems involve input-to-output transfer of a parametrized dynamic system $G(\mu)$, with μ a parameter vector denoting application-dependent degrees-of-freedom. In applications where average performance over frequencies is of interest, the $\mathscr{H}_2$ norm is a natural candidate for measuring the quality of a solution. Figure 1 demonstrates how $\|G(\mu)\|_{\mathscr{H}_2}$ appears in several of the mentioned applications.

Often, the considered dynamics are large-scale (e.g., high-dimensional Finite Element Method (FEM) models), while the dimension of μ stays relatively small (e.g., compact controllers are required to achieve real-time performance). To render the large-scale problem numerically tractable, model reduction is applied and then the optimization is performed in a reduced space. However, the solution to the reduced problem does not generally match the solution to the original problem. Although $\mathscr{H}_2$ model reduction techniques have been extended for, e.g., frequency-weighted problems [2], these suffer from 2 drawbacks: 1) they do not allow optimization of arbitrary cost functions $\|G(\mu)\|_{\mathscr{H}_2}$; and 2) convergence guarantees are not known. To avoid these issues, inspiration can be drawn from work on optimization of large-scale *static* problems.

Large-scale static optimization problems are intensively studied in the field of deep learning. The vast amount of data renders exact computation of gradients intractable. A successful solution to this issue is to use Stochastic Gradient Descent (SGD), which substitutes exact gradients by stochastic estimates obtained by evaluating the cost function on randomly sampled subsets of the data. The practical success of SGD is supported by theoretical convergence guarantees [1].

In this work, an extension of SGD for large-scale *dynamic* optimization problems is proposed. Its main features are:

1. A novel stochastic algorithm is proposed to minimize $\|G(\mu)\|_{\mathscr{H}_2}$ for a large-scale dynamic system $G(\mu)$ with general (differentiable) dependence on μ.
2. Probabilistic convergence to the solution of the large-scale optimization problem is guaranteed, without ever evaluating the exact gradient.

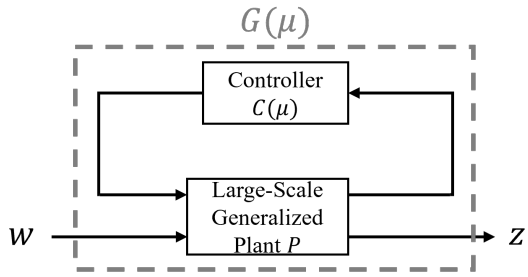

(a) **Reduced-order controller synthesis**: μ represents degrees-of-freedom of the controller

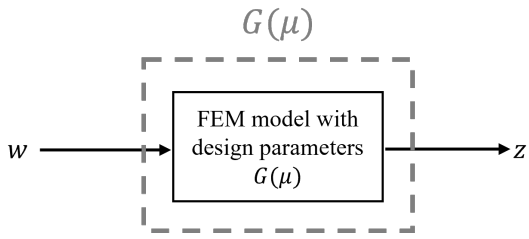

(b) **Design optimization**: μ represents shape or material parameters

Figure 1: Example applications in which minimizing $\|G(\mu)\|_{\mathscr{H}_2}$ is important. w and z are disturbance and performance channels, respectively.

3. Importance sampling is applied to speed up convergence through variance reduction of the estimated gradients.

The method is demonstrated on an $\mathscr{H}_2$ optimal PID tuning problem for a large-scale thermal FEM model of a circular rod.

Acknowledgment · This work has been funded in part by ITEA under the COMPAS project (ITEA project 19037).

References

[1] Panayotis Mertikopoulos, Nadav Hallak, Ali Kavis, and Volkan Cevher. On the almost sure convergence of stochastic gradient descent in non-convex problems. *Advances in Neural Information Processing Systems*, 2020.

[2] Umair Zulfiqar, Victor Sreeram, Mian Ilyas Ahmad, and Xin Du. Frequency-weighted $\mathscr{H}_2$-pseudo-optimal model order reduction. *IMA Journal of Mathematical Control and Information*, 38:622–653, 6 2021.

A new algorithm for EIV Nonlinear Continuous-time System Estimation Through Linearization

Mehrad Sharabiany, John Lataire
ELEC dept., Vrije Universiteit Brussel, Pleinlaan 2, Brussels, Belgium.
Email: mehrad.ghasem.sharabiany@vub.be

1 Introduction

Continuous time system modeling is important in analysis and simulation of many natural phenomena. As modeling by first principles is difficult and sometimes impossible, data-driven algorithms are preferable. Many algorithms have been proposed for this issue as can be seen in [3]. In this abstract, We propose a continuous-time nonlinear system identification from noisy input and output data along a specific trajectory. Generally speaking, one is usually interested in the system behavior just in a small operation region or number of trajectories without extensive prior knowledge. This is something that we address in our issue.

2 Problem formulation

Consider the continuous-time nonlinear system as below :

$$f\left(y(t),\ldots,y^{(n_a)}(t),u(t),\ldots,u^{(n_b)}(t)\right)=0 \qquad (1)$$

Where $u(t)$ denotes the input and $y(t)$ denotes the output and $\bullet^{(n)}$ shows derivative. We are interested to estimate f along the specific known trajectory $R_L(t)$ as below :

$$R_L(t)=[y_L(t),\ldots,y_L^{(n_a)}(t),u_L(t),\ldots,u_L^{(n_b)}(t)] \qquad (2)$$

In order to estimate the system, we need to add a small signal which is obtained by deviating the $R_L(t)$ a little bit. This signal is called $R(t)$ and we assume that this $R(t)$ is distorted by filtered white noise. The problem is to estimate the system f from noisy $R(t)$. As there is noise on the input and the output, we have an error-in-variables problem. We assume that there is no other source of noise (like generator noise or process noise.)

3 Proposed algorithm

Inspired by [2], the maximum likelihood estimator for error-in-variables problem is converted to an output- error problem with modified covariance vector which depends on the output and input noise covariance matrices. So, We need to somehow estimate the output and input noise characteristics. This estimation is done by a nonparametric sliding window algorithm which is proposed in [1] .
Nonlinear least square algorithms can be used to optimize the resulting cost function. In order to exploit these algorithms, we need to have initial values of the parameters, some kind of a structure for the cost function and also derivative of the cost function w.r.t the parametrs. In [4], an algorithm is developed to obtain a good initial value and appropriate structure for the nonlinear model. This algorithm works based on the linearization of the system (1) along the known trajectory and the linearization in the title comes from this. Finally, the derivatives of the cost function w.r.t parameters are calculated through implicitely (or explicitely) differentiating the cost function and numerically solving a bunch of ODEs (ordinary differential equations).
The covariance of the estmate is calculated based on the known characteristics of the nonlinear least squares optimizers. As the initial value is calculated asproposed in [4] and the data belong to the vicinity of the known trajectory, the estimated model is just valid around the known trajectory and not anywhere else.

This research was supported by the Fund for Scientific Research (FWO Vlaanderen, grant G005218N) and by the Flemish Government (Methusalem Grant METH1).

References

[1] N. Hallemans, R. Pintelon, E. Van Gheem, T. Collet, R. Claessens, B. Wouters, K. Ramharter, A. Hubin, Annick and J. Lataire, “Best linear time-varying approximation of a general class of nonlinear time-varying systems“ IEEE Transactions on Instrumentation and Measurement, IEEE, vol.70, pp. 1-14, 2021.

[2] M. Clutton-Brock,“ Likelihood distributions for estimating functions when both variables are subject to error“ Technometrics,Taylor & Francis, vol. 9(2), pp. 261 - 269, 1967

[3] Z. Kowalczuk, J. Kozłowski,“Continuous-time approaches to identification of continuous-time systems“ Automatica, Elsevier, vol. 36(8), pp. 1229 - 1236, 2000

[4] M. Ghasem Sharabiany, J. Lataire, and R. Pintelon, “Nonlinear Model Estimation Via Linearization Around Large Signals“ Abstract from 2021 workshop of the European Research Network on System Identification (ERNSI), Rennes, France.

Extended Kalman Filter with Intermittent Observations for Visual Servoing Application

M. Ambrosino [1], M. Mahmalji[1], N. Bono Rosselló[1], and E. Garone[1]

[1]Service d'Automatique et d'Analyse des Systèmes, Université Libre de Bruxelles, Brussels, Belgium.
[1]Email corresponding author: Michele.ambrosino@ulb.be

1 Problem Statement

Vision plays an important role in a robotic system, as it can be used to obtain information about the target with which the robot must interact. In this work, we propose to use an Extended Kalman Filter (EKF) with Intermittent Observations [1] to achieve correct tracking of a moving object by a robotic arm. This estimator makes use of the dynamic model of the moving object with which the robot has to interact and the evaluated pose of the object by a camera device to estimate the pose of the target at a higher rate than that of the camera and to feed the controller of the robot with a smooth and noise-free signal.

2 Extended Kalman Filter

The dynamics of the suspended object can be treated as that of a 5-DoF non-actuated pendulum. In particular, its configuration can be described by five variables, $q_p \in \mathbb{R}^5$, with $q_p = \left[q_{p1}, q_{p2}, q_{p3}, q_{p4}, q_{p5}\right]^T$. Where q_{p1} and q_{p2} are the radial sway and the tangential pendulation respectively, and q_{p3}, q_{p4}, q_{p5} are the orientations of the object *w.r.t.* the cable. Defining the state vector as $x = [x_1^{\mathrm{T}}\ x_2^{\mathrm{T}}]^{\mathrm{T}} \in \mathbb{R}^{10}$, where $x_1 = q_p$ and $x_2 = \dot{q}_p$, we can write the pendulum dynamic equation in the state-space representation as

$$\dot{x} = f(x) = \begin{bmatrix} x_2 \\ -B_P^{-1}(x_1)[C_p(x_1,x_2)x_2 + g_p(x_1)] \end{bmatrix}, \tag{1}$$

where $B_p(q_p) \in \mathbb{R}^{5\times5}$, $C_p(q_p,\dot{q}_p) \in \mathbb{R}^{5\times5}$, and $g_p(q_p) \in \mathbb{R}^5$. Discretizing the previous equations with a sampling time Ts and considering the output equation with intermittent camera observations, one can obtain

$$\begin{aligned} x_{k+1} &= f^d(x_k) + w_k \\ y_k &= \Gamma_k(h^d(x_k) + v_k). \end{aligned} \tag{2}$$

where $w_k \in \mathbb{R}^{10}$ and $v_k \in \mathbb{R}^{12}$ are white Gaussian noise processes, uncorrelated with zero mean and covariances $Q \in \mathbb{R}^{10\times10}$ and $R \in \mathbb{R}^{12\times12}$. Γ is equal to an identity matrix I_{12} if the measurements from the camera are available at the time instant k, otherwise is equal to a null matrix 0_{12}. Then, the implementation of an EKF with intermittent observations can be achieved by iteratively evaluating the following two steps.

Prediction step.

$$\begin{aligned} \hat{x}_{k+1|k} &= f^d(\hat{x}_{k|k}), \\ P_{k+1|k} &= A_k P_{k|k} A_k^T + Q, \end{aligned} \tag{3}$$

where $A_k = \left.\frac{\partial f^d}{\partial x}\right|_{x=\hat{x}_{k|k}}$ is the Jacobian matrix of the state equation evaluated around the state prediction $\hat{x}_{k|k}$.

Correction step.

$$\begin{aligned} \hat{x}_{k+1|k+1} &= \hat{x}_{k+1|k} + K_{k+1|k+1}(y_{k+1} - h^d(\hat{x}_{k+1|k})) \\ P_{k+1|k+1} &= P_{k+1|k} - K_{k+1|k+1} C_k P_{k+1|k}, \end{aligned} \tag{4}$$

where

$$K_{k+1|k+1} = P_{k+1|k} C_k^T \Gamma_{k+1}^T (\Gamma_{k+1}(C_k P_{k+1|k} C_k^T + R)\Gamma_{k+1}^T)^{-1} \tag{5}$$

is the corresponding equation of the EKF gain, and $C_k = \left.\frac{\partial h^d}{\partial x}\right|_{x=\hat{x}_{k+1|k}}$, is the Jacobian matrix of the output equation.

3 Experimental Results

As one can see in Fig. 1, the implemented EKF is able to estimate the oscillations of the block based on its dynamic model and the camera data. In addition, it reduces the noise of the measurements obtained in order to feed the robot controller with smooth signals so that the end-effector properly follows the oscillations of the block.

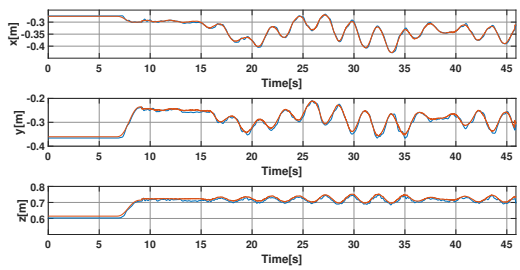

Figure 1: Blue line. Current Robot end-effector position. Red line. Desired Robot end-effector position.

References

[1] B. Sinopoli, L. Schenato, M. Franceschetti, K. Poolla, M. I. Jordan and S. S. Sastry, "Kalman filtering with intermittent observations."

Data-based electromagnetic calibration approaches for moving-magnet planar actuator systems

Yorick Broens[1], Hans Butler[1,2] and Roland Tóth[1,3]
[1] Control Systems Group, Eindhoven University of Technology, Eindhoven, The Netherlands
[2] ASML, Veldhoven, The Netherlands
[3] Systems and Control Laboratory, Institute for Computer Science and Control, Budapest, Hungary
Email: Y.L.C.Broens@tue.nl

1 Introduction

Moving-magnet planar actuator (MMPA) systems are becoming an increasingly attractive configuration for many high-precision positioning systems due to several advantageous properties, such as complete environmental decoupling of the moving-body and reduction of the stage mass, see [1]. Nonetheless, these advantages come at the cost of introducing additional complexity from a motion control perspective, originating from highly complex nonlinear electromagnetic relationships relating the currents in the coil arrays of the stator to the forces acting on the point of control on the magnetically levitated mover. Motion control design of MMPA systems is further complicated by position dependent effects which are introduced by relative actuation and sensing of the mover. To achieve desirable motion control objectives for MMPA systems, it is essential that the magnetic mover is accurately aligned to the coil arrays of the stator, thus minimizing mismatch between the control commutation algorithm and the physical relationship between the currents in the coil arrays and the forces that are exerted on the mover. This paper aims at presenting various approaches to be explored for accurate data-based electromagnetic calibration of the magnetic mover, such that commutation mismatch, upon initialization of the system, is minimized.

2 Problem description

A MMPA system is a MIMO system which exhibits position dependency in both sensing and actuation of the moving-body, see [1]. To efficiently capture the position dependent effects, these type of systems are typically expressed in *linear-parameter-varying* (LPV) form, where the position dependency is expressed by a scheduling vector $q(t) : \mathbb{R} \to \mathbb{Q} \subseteq \mathbb{R}^{n_q}$. Employment of the LPV paradigm allows for simplified motion control design by means of application of rigid-body coordinate transformations which relate the actuation and measurement frame to the point of control of the magnetically levitated mover, see [2]. Therefore motion control design for MMPA systems is achieved through well-understood LTI/LPV control design approaches. Consider the control interconnection illustrated by Figure 1, where K_{RB} corresponds to the feedback controller, K_{FF} denotes the feedforward controller, $\Omega^{\dagger}(\cdot)$ is the control commutation algorithm, $\Omega(\cdot)$ is the physical relationship between the currents in the coil arrays and the forces that are exerted on

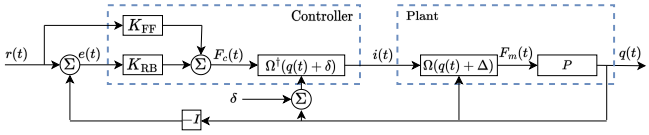

Figure 1: Schematic representation of the control interconnection of a MMPA system, where Δ represents the physical misalignment between the moving-body and the coil arrays.

the mover, while P corresponds to the motion dynamics of the mover. In case of misalignment of the magnetically levitated mover, introduced upon initialization of the system, i.e. $\Delta \neq \delta$, the control commutation algorithm does not perfectly cancel out the non-linearity represented by $\Omega(\cdot)$, resulting in a mismatch between the requested control forces $F_c(t)$ and the real forces acting on the motor $F_m(t)$, which are not measurable. Moreover, positioning accuracy of the mover is limited by misalignment of the mover with respect to the coil arrays, thus necessitating for the development of accurate data-based calibration approaches.

3 Proposed approaches

For calibration of the magnetically levitated mover, an additional control parameter δ is introduced to the control commutation algorithm $\Omega^{\dagger}(\cdot)$, see Figure 1. To tune the parameter δ, several research directions are to be explored while the system is in closed-loop position control, such as *gradient descent* optimization approaches, *extremum seeking control* approaches and *dynamic regulation approaches*. For the latter, we aim at reformulation of the electromagnetic calibration into a feedback control design problem. Consequently, this would allow for employment of classical (non)-parametric control design approaches that allow for quick and efficient calibration of the mover, while providing stability and performance guarantees on the closed-loop behaviour of the MMPA system.

References

[1] I. Proimadis, *Nanometer-accurate motion control of moving-magnet planar motors*. PhD thesis, Department of Electrical Engineering, 2020.

[2] H. Butler, "Position control in lithographic equipment," *IEEE Control Systems Magazine*, vol. 31, no. 5, pp. 28–47, 2011.

Integrating estimation into sensor-based servo loop control

Ruan Viljoen, Erwin Aertbeliën, Wilm Decré Joris De Schutter
Department of Mechanical Engineering, KU Leuven, Belgium
Flanders Make@KU Leuven, Belgium
Email: ruan.viljoen@kuleuven.be

1 Introduction

As the move toward industry 4.0 continues, there is an increasing interest in equipping robots with the ability to execute tasks in uncertain and unstructured environments. One way to deal with the uncertainty in the environment is through the use of sensor-based servo control loops.

This approach works well, but is limited by the fact that the task error has to be directly measured. Consider the scenario in Fig. 1, where a robot is equipped with a laser distance sensor, and is tasked to move along an unknown surface, while remaining perpendicular to the surface and maintaining a desired distance. Maintaining a desired distance can be accomplished using a standard servo control loop, as the distance is directly measured using the laser distance sensor. However, maintaining a desired orientation with regards to the surface poses a challenge, as the laser distance sensor does not directly measure the orientation of the surface.

This problem can be solved by making use of an estimator, which is able to estimate the orientation of the surface using consecutive laser distance measurements. It is shown that by integrating an estimator in the servo control loop, it is possible to move along the surface while maintaining both a desired distance and orientation with regards to the surface.

2 Methodology

The robot was programmed using the constraint-based task specification framework eTaSL [1], which implements a controller that enforce a first-order decay on the task errors, according to the task function approach of [2]. The elements K_i of the diagonal control gain matrix used by this approach determine the time constant of this first-order decay in task error as $\frac{1}{K_i}$ s, and are chosen so as to remain sufficiently below the bandwidth of the robot's internal motion controllers.

The estimator design was inspired by this control approach, and also enforces a first-order decay on the estimator innovations $\widetilde{\mathbf{z}} = \mathbf{e_z}(\hat{\mathbf{x}}, t)$. This results in the following estimator:

$$\mathbf{J}\dot{\hat{\mathbf{x}}} = -\mathbf{L}\widetilde{\mathbf{z}} - \frac{\partial \mathbf{e_z}}{\partial t}, \tag{1}$$

where $\mathbf{J}$ is the Jacobian of $\mathbf{e_z}$, and the gain $\mathbf{L}$ is a diagonal matrix with elements L_i which determine the time constant of the first-order decay in innovations as $\frac{1}{L_i}$ s. The values of L_i are chosen according to the bandwidth of the sensor noise. By formulating the estimator in this way, it is possible to exploit the similarity between the controller and estimator, such that the existing eTaSL framework can be used **as is** to perform both the control and estimation for sensor-based robot tasks, which forms the main contribution of this research. Moreover, the clear interpretation of K_i and L_i leads to an intuitive design procedure.

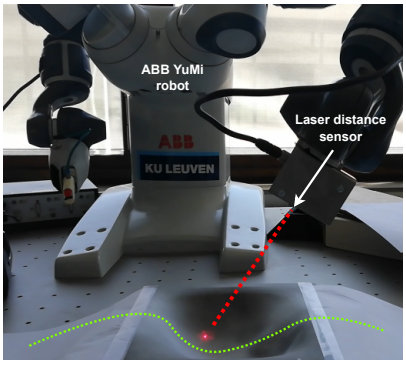

Figure 1: The surface following task.

3 Future work

The current approach is limited to the laser moving in a single plane, so only the orientation of the surface along one direction is taken into account. An extension to this work would be to find a general approach for surface following in full 3D. This would require the integration of several sensors, for example an array of laser sensors, or a combination of sensors with different sensing modalities, for example a laser distance sensor and a depth camera. This would further motivate the use of an estimator which can be used to fuse the measurements from the different sensing modalities.

References

[1] E. Aertbeliën, and J. De Schutter, "eTaSL/eTC: A constraint-based task specification language and robot controller using expression graphs" IEEE IROS, 2014.

[2] C. Samson, M. Le Borgne, and B. Espiau, "Robot Control, the Task Function Approach," Clarendon Press, 1991.

This research was supported by project G0D1119N of the Research Foundation - Flanders (FWO - Flanders).

Range-Only Bearing Estimator for Localization and Mapping

Matteo Marcantoni
Bernoulli Institute, Faculty of Science and Engineering, University of Groningen,
9747AG Groningen, The Netherlands, (email: m.marcantoni@rug.nl)

Bayu Jayawardhana
ENTEG Institute, Faculty of Science and Engineering, University of Groningen,
9747AG Groningen, The Netherlands, (email: b.jayawardhana@rug.nl)

1 Introduction

Range-only simultaneous localization and mapping (RO-SLAM) describes the problem of estimating the positions of a moving agent and of various landmarks using sensors capable of giving only relative distance information. Navigation in unknown environments (e.g. underwater or indoor) is a typical application where the SLAM problem arise [1]. The main challenge of RO-SLAM is due to the fact that we have to solve the estimation problem without having relative bearing information [2].

In this work, we propose a novel estimator able to localize the position of a static landmark starting from a random initialization without relying on multi-hypothesis nor on delayed approaches. In particular, the estimate of the position of the landmark is produced and updated by taking advantage of a change of coordinate so that the estimated relative bearing is update directly. The estimator convergence is proved analytically by employing results from contracting system theory [3], and the efficacy of the proposed method is shown via results from numerical simulations. Our contribution is three-fold: we describe the design of our estimator, we analyze its convergence, and we present results from numerical simulations.

2 Main Results

Let us consider a discrete-time system, with a constant sampling time T, defined as

$$\begin{cases} p(k+1) &= p(k)+Tu(k), \\ l(k+1) &= l^*, \\ y(k) &= \|l^*-p(k)\|, \end{cases} \tag{1}$$

where $p(k) \in \mathbb{R}^2$ is the position of the agent, $y(k) \in \mathbb{R}$ is the output of the system (i.e. the distance measurement), and $l^* \in \mathbb{R}^2$ is the position of the static landmark. The proposed observer is

$$\begin{cases} \hat{\theta}(k+1) &= \hat{\theta}(k)+T\left\langle u(k), \begin{bmatrix} \sin(\hat{\theta}(k)) \\ -\cos(\hat{\theta}(k)) \end{bmatrix} \right\rangle + \gamma\beta(k), \\ \hat{l}(k) &= y(k)\begin{bmatrix} \cos(\hat{\theta}(k)) \\ \sin(\hat{\theta}(k)) \end{bmatrix} + p(k), \end{cases} \tag{2}$$

in which $\langle \cdot,\cdot \rangle$ represents the inner product, $\text{sign}(\cdot)$ the sign function, γ the gain of the observer, and $\beta(k)$ a correction term defined as

$$\beta(k) = \text{sign}\left(\left\langle u(k), \begin{bmatrix} \sin(\hat{\theta}(k)) \\ -\cos(\hat{\theta}(k)) \end{bmatrix} \right\rangle\right) \left(\|l^*-p(k)-Tu(k)\|^2 - \|\hat{l}(k)-p(k)-Tu(k)\|^2\right). \tag{3}$$

We analytically analyze the convergence behaviour of the proposed observer used to estimate the true relative bearing $\theta(k)$ between the agent and the static landmark. In particular, we discuss its performance in the special case of straight trajectories showing that the position estimate can converge to two different positions depending on the initialization of $\theta(k)$, as shown in figure 1.

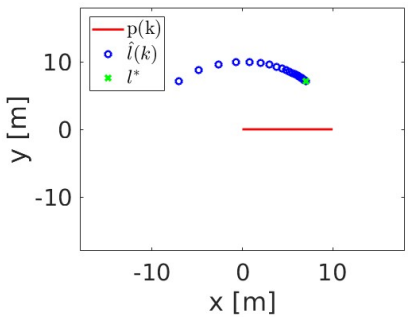

Figure 1: Evolution of the position estimate of a static landmark. The red line represents the trajectory of the moving agent (starting from the origin), the green cross the true position of the static landmark, and the blue circles the position estimates.

References

[1] Guo, M. et al. (2020). Simultaneous distributed localization, mapping and formation control of mobile robots based on local relative measurements. *IFAC-PapersOnLine*, 53(2), 9614-9620.

[2] Martinelli, F. et al. (2023). A resilient solution to Range-Only SLAM based on a decoupled landmark range and bearing reconstruction. *Robotics and Autonomous Systems*, 160, 104324.

[3] Lohmiller, W., & Slotine, J. J. E. (1998). On contraction analysis for non-linear systems. *Automatica*, 34(6), 683-696.

H_∞ optimal positive position feedback for vibration control

Bram Seinhorst, Marijn Nijenhuis, Wouter Hakvoort
chair of Precision Engineering, University of Twente
P.O. Box 217, 7500 AE Enschede, The Netherlands
Email: {b.seinhorst/m.nijenhuis/w.b.j.hakvoort}@utwente.nl

1 Introduction

Positive position feedback control (PPF) is a control strategy used for vibration suppression. The simple control structure and high frequency roll-off are some of the main benefits of the controller. Tuning a PPF controller is typically a manual process done using some rough guidelines. In this work we consider a simple cantilever beam vibration suppression problem. By requiring the open loop to have a certain gain margin, we show that the problem is analogous to designing an optimal shunt circuit as outlined in [1]. By following a procedure similar to [1], analytical expressions for the H_∞ optimal PPF controller are found.

2 Cantilevered beam case

Consider a cantilevered beam with a vibrating base and piezoelectric patches at the base used for sensing and actuation. The system P can be approximated close to the first resonance as $\tilde{P}$, with the equations of motion:

$$\ddot{x} = -\omega_n^2 x + \begin{bmatrix} b_1 & b_2 \end{bmatrix} \begin{bmatrix} x_{in} \\ V_{in} \end{bmatrix} \tag{1}$$

$$\begin{bmatrix} x_{out} \\ V_{out} \end{bmatrix} = \begin{bmatrix} c_1 \\ c_2 \end{bmatrix} x + \begin{bmatrix} 0 & 0 \\ 0 & d_{22} \end{bmatrix} \begin{bmatrix} x_{in} \\ V_{in} \end{bmatrix} \tag{2}$$

The effect of higher resonances are modelled by a direct feedthrough term, of which d_{22} is the most important. The frequency response functions of the P and $\tilde{P}$ are shown in figure 2.

The PPF controller is given by:

$$C = \frac{V_{in}}{V_{out}} = K \frac{\omega_c^2}{s^2 + 2\zeta_c \omega_c s + \omega_c^2} \tag{3}$$

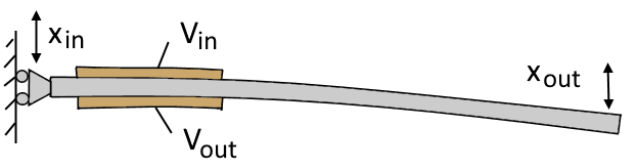

Figure 1: A cantilever beam. An input vibration is applied at the base x_{in}. The output is the tip vibration x_{out}. The controller only has access to the piezo input voltage V_{in} and piezo sensing voltage V_{out}.

Through several substitutions and by requiring the open loop to have a specified gain margin G, which is related to the DC gain, the closed loop equations can be rewritten as:

$$\begin{bmatrix} \ddot{x} \\ \ddot{q} \end{bmatrix} + \begin{bmatrix} 0 \\ r\omega_n \delta \dot{q} \end{bmatrix} + \omega_n^2 \begin{bmatrix} 1 & -\delta\alpha \\ -\delta\alpha & \delta^2 \end{bmatrix} \begin{bmatrix} x \\ q \end{bmatrix} = \begin{bmatrix} b_1 \\ 0 \end{bmatrix} x_{in} \tag{4}$$

$$x_{out} = \begin{bmatrix} c_1 & 0 \end{bmatrix} \begin{bmatrix} x \\ q \end{bmatrix} \tag{5}$$

Here α is a composition of coefficients from (1), (2) and the gain margin G. The objective is to find optimal δ and r, which are related to the controller resonance and damping.

The structure is similar to the equations given in [1], which represent the closed loop state space equations of a system with shunt circuits, where the aim is to find optimal resistance R and inductance L. Following the procedure outlined in [1], analytical expressions for the H_∞ optimal choice of δ and r can be obtained.

The resulting closed loop is given in Figure 2. The controller is optimal in the H_∞ sense only for the approximate plant $\tilde{P}$. The closed loop shows near optimal suppression of the first resonance if the actual plant P is used.

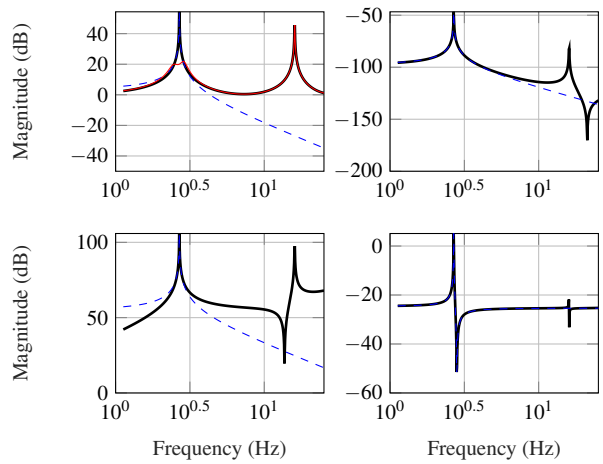

Figure 2: Bode plots of the Plant P (——), approximate plant $\tilde{P}$ (- - -) and closed loop (——)

References

[1] P Soltani et al 2014 Smart Mater. Struct. 23 125014

Sontag's Universal Formula for Safe Stabilization

Ming Li and Zhiyong Sun
Department of Electrical Engineering, Eindhoven University of Technology, Eindhoven, The Netherlands
Email: {m.li3; z.sun}@tue.nl

I. Introduction

Control Lyapunov functions (CLFs) and control barrier functions (CBFs) are powerful tools for designing feedback control laws to achieve asymptotic stability and safety of dynamical systems. If CLFs or CBFs are known, one can use Sontag's "universal" formulas [1] to compute stabilizing or safety control laws. However, generalizing Sontag's idea to obtain a universal formula which guarantees both properties is challenging. This is because it's hard to find a unified (analytical) formula that satisfies two inequalities by the respective conditions of CLF and CBF. In this paper, we address this challenge and construct a universal formula by recognizing that Sontag's formula is a special solution for the point-wise minimal norm (PMN) controller.

II. Preliminaries

Consider a control-affine system

$$\dot{\mathbf{x}} = \mathbf{f}(\mathbf{x}) + \mathbf{g}(\mathbf{x})\mathbf{u}, \tag{1}$$

where $\mathbf{x} \in \mathcal{X}$, $\mathbf{u} \in \mathbb{R}^m$, and $\mathbf{f} : \mathbb{R}^n \to \mathbb{R}^n$ and $\mathbf{g} : \mathbb{R}^n \to \mathbb{R}^{n\times m}$ are locally Lipschitz continuous.

Definition 1. *(CLF) A continuously differentiable and positive definite function $V : \mathcal{X} \to \mathbb{R}_{\geq 0}$ is a CLF for the system* (1) *on $\mathcal{X}$ if there exists a control $\mathbf{u} \in \mathbb{R}^m$ satisfying*

$$a(\mathbf{x}) + \mathbf{b}(\mathbf{x})\mathbf{u} \leq 0 \tag{2}$$

for all $\mathbf{x} \in \mathcal{X}\backslash\{\mathbf{0}\}$, where $a(\mathbf{x}) = L_{\mathbf{f}}V(\mathbf{x}) + \alpha(V(\mathbf{x}))$ and $\mathbf{b}(\mathbf{x}) = L_{\mathbf{g}}V(\mathbf{x})$. $L_{\mathbf{f}}$ and $L_{\mathbf{g}}$ denote the Lie derivatives along $\mathbf{f}$ and $\mathbf{g}$, respectively.

To find a specific feedback control law for (1) that satisfies (2), the following PMN approach can be used.

$$\underset{\mathbf{u}\in\mathbb{R}^m}{\operatorname{argmin}} \frac{1}{2}\|\mathbf{u}\|^2, \qquad \text{s.t. } a(\mathbf{x}) + \mathbf{b}(\mathbf{x})\mathbf{u} \leq -\sigma(\mathbf{x}), \tag{3}$$

where $\sigma(\mathbf{x})$ is a continuous, positive semi-definite function, and $a(\mathbf{x}) + \sigma(\mathbf{x}) \leq 0$ whenever $\mathbf{b}(\mathbf{x}) = \mathbf{0}$. The solution of (3) can be explicitly expressed as

$$\mathbf{u}^\star_{\mathrm{QP-CLF}}(\mathbf{x}) = \begin{cases} \mathbf{m}^\star_{\mathrm{QP-CLF}}(\mathbf{x}) & \mathbf{b}(\mathbf{x}) \neq \mathbf{0} \text{ and } a(\mathbf{x}) + \sigma(\mathbf{x}) > \mathbf{0} \\ \mathbf{0} & \text{otherwise,} \end{cases}$$

where the superscript "$\star$" indicates that $\mathbf{u}^\star_{\mathrm{QP-CLF}}(\mathbf{x})$ is the optimal solution of (3), and $\mathbf{m}^\star_{\mathrm{QP-CLF}}(\mathbf{x}) = -\frac{a(\mathbf{x})+\sigma(\mathbf{x})}{\mathbf{b}(\mathbf{x})\mathbf{b}(\mathbf{x})^\top}\mathbf{b}(\mathbf{x})^\top$. Sontag's universal formula can be obtained by choosing $\sigma(\mathbf{x}) = \sqrt{a^2(\mathbf{x}) + \phi(\mathbf{x})\|\mathbf{b}(\mathbf{x})\|^4}$, which gives

$$\mathbf{u}^\star_{\mathrm{Stg-CLF}}(\mathbf{x}) = \begin{cases} \mathbf{m}^\star_{\mathrm{Stg-CLF}}(\mathbf{x}), & \mathbf{b}(\mathbf{x}) \neq \mathbf{0} \\ \mathbf{0}, & \mathbf{b}(\mathbf{x}) = \mathbf{0} \end{cases} \tag{4}$$

where $\mathbf{m}^\star_{\mathrm{Stg-CLF}}(\mathbf{x}) = -\frac{a(\mathbf{x})+\sqrt{a^2(\mathbf{x})+\phi(\mathbf{x})\|\mathbf{b}(\mathbf{x})\|^4}}{\mathbf{b}(\mathbf{x})\mathbf{b}(\mathbf{x})^\top}\mathbf{b}(\mathbf{x})^\top$, and $\phi(\mathbf{x})$ is a positive definite function.

Consider a closed convex set $\mathcal{C} \subset \mathbb{R}^n$ as the 0-superlevel set of a continuously differentiable function $h : \mathbb{R}^n \to \mathbb{R}$, which is defined as $\mathcal{C} \triangleq \{\mathbf{x} \in \mathcal{X} \subseteq \mathbb{R}^n : h(\mathbf{x}) \geq 0\}$.

Definition 2. *(CBF). Let $\mathcal{C} \subseteq \mathcal{X} \subset \mathbb{R}^n$ be the 0-superlevel set of a continuously differentiable function $h : \mathcal{X} \to \mathbb{R}$. Then h is a CBF for* (1) *if there exists $\beta \in \mathcal{K}_e$ ($\mathcal{K}_e$ is the notation for an extended class $\mathcal{K}$ function) such that, for all $\mathbf{x} \in \mathcal{X}$, there exists a control $\mathbf{u} \in \mathbb{R}^m$ satisfying*

$$c(\mathbf{x}) + \mathbf{d}(\mathbf{x})\mathbf{u} \geq 0 \tag{5}$$

where $c(\mathbf{x}) = L_{\mathbf{f}}h(\mathbf{x}) + \beta(h(\mathbf{x}))$ and $\mathbf{d}(\mathbf{x}) = L_{\mathbf{g}}h(\mathbf{x})$.

Similar to the stabilizing problem, we modify (5) to $c(\mathbf{x}) + \mathbf{d}(\mathbf{x})\mathbf{u} \geq \Gamma(\mathbf{x})$, where $\Gamma(\mathbf{x}) = \sqrt{c^2(\mathbf{x}) + \varphi(\mathbf{x})\|\mathbf{d}(\mathbf{x})\|^4}$ and $\varphi(\mathbf{x})$ is a positive semi-definite function. Then the universal control law for CBF is given as

$$\mathbf{u}^\star_{\mathrm{Stg-CBF}}(\mathbf{x}) = \begin{cases} \mathbf{n}^\star_{\mathrm{Stg-CBF}}(\mathbf{x}), & \mathbf{d}(\mathbf{x}) \neq \mathbf{0}, \\ \mathbf{0}, & \mathbf{d}(\mathbf{x}) = \mathbf{0}, \end{cases}$$

where $\mathbf{n}^\star_{\mathrm{Stg-CBF}}(\mathbf{x}) = \frac{\sqrt{(L_{\mathbf{f}}h(\mathbf{x}))^2(\mathbf{x})+\varphi(\mathbf{x})\|\mathbf{d}(\mathbf{x})\|^4-c(\mathbf{x})}}{\mathbf{d}(\mathbf{x})\mathbf{d}(\mathbf{x})^\top}\mathbf{d}(\mathbf{x})^\top$.

III. Universal Formula for Safe stabilization

We construct a generalized Sontag's formula for safe stabilization by recognizing that it is a special solution for PMN controller [2]. Consider the following optimization problem:

$$\underset{\mathbf{u}\in\mathbb{R}^m}{\operatorname{argmin}} \frac{1}{2}\|\mathbf{u}\|^2 \quad \text{s.t. Constraints in (2) and (5).} \tag{6}$$

Firstly, analytical solutions of (6) can be obtained since both of the constraints in (6) have control-affine structure. Next, we extend the solution (6) to a more general case by introduce $\sigma(\mathbf{x})$ and $\Gamma(\mathbf{x})$ into the conditions of CLFs and CBFs. Finally, by specifying $\sigma(\mathbf{x}) = \sqrt{a^2(\mathbf{x}) + \phi(\mathbf{x})\|\mathbf{b}(\mathbf{x})\|^4}$ and $\Gamma(\mathbf{x}) = \sqrt{c^2(\mathbf{x}) + \varphi(\mathbf{x})\|\mathbf{d}(\mathbf{x})\|^4}$ and solving a modified (6), the following generalized universal feedback control law is obtained.

$$\mathbf{u}^*_{\mathrm{Uni}}(\mathbf{x}) = \begin{cases} \mathbf{p}^*_{\mathrm{Uni}}(\mathbf{x}), & \mathbf{b}(\mathbf{x}) \neq \mathbf{0} \text{ and } \mathbf{d}(\mathbf{x}) \neq \mathbf{0} \\ \mathbf{m}^\star_{\mathrm{Stg-CLF}}(\mathbf{x}), & \mathbf{b}(\mathbf{x}) \neq \mathbf{0} \text{ and } \mathbf{d}(\mathbf{x}) = \mathbf{0} \\ \mathbf{n}^\star_{\mathrm{Stg-CBF}}(\mathbf{x}), & \mathbf{b}(\mathbf{x}) = \mathbf{0} \text{ and } \mathbf{d}(\mathbf{x}) \neq \mathbf{0} \\ \mathbf{0}, & \text{Otherwise.} \end{cases},$$

where $\mathbf{p}^*_{\mathrm{Uni}}(\mathbf{x}) = \widetilde{\gamma}_1\mathbf{m}^\star_{\mathrm{Stg-CLF}}(\mathbf{x}) + \widetilde{\gamma}_2\mathbf{n}^\star_{\mathrm{Stg-CBF}}(\mathbf{x})$, $\widetilde{\gamma}_1$ and $\widetilde{\gamma}_2$ are weighting parameters. They can be obtained by substituting $\sigma(\mathbf{x})$ and $\Gamma(\mathbf{x})$ into the weighting parameters γ_1 and γ_2 given in the solution of (6).

References

[1] Eduardo D Sontag. A 'universal'construction of Artstein's theorem on nonlinear stabilization. *Systems & control letters*, 13(2):117–123, 1989.
[2] Xiao Tan and Dimos V Dimarogonas. On the undesired equilibria induced by control barrier function based quadratic programs. *arXiv preprint arXiv:2104.14895*, 2021.

Distributed Current Control of Battery Energy System in DC Microgrids

Lihua Zhou, Saeed Ahmed and Jacquelien M. A. Scherpen [1]

1 Introduction

DC microgrids have shown great potential for combining distribution systems with renewable energy sources. We explore distributed current control in a passivity setting combined with battery energy storage systems (BESS), and briefly summarize optimization problems pertaining to them.

2 DC Microgrids Model based on BESS with ZI Load

We consider a typical DC microgrid combined with a BESS, distributed generation unit (DGU), and constant ZI load. We also consider the monitoring of the storage state of charge (SoC), which can prevent overcharging and discharging of battery and prolong the life cycle. All these DGUs are linked together through m resistive-inductive lines in Fig 1. The

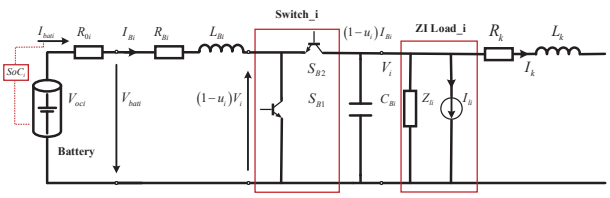

Figure 1: Electrical scheme of DGU$_i$ and line k of BESS

battery bank is characterized by an equivalent circuit model as

$$V_{bat} = V_{oc} - R_0 I_{bat}, \tag{1}$$

where V_{oc}, R_0, I_{bat} is the internal voltage source, equivalent impedance, and electrical current of the battery, respectively. The energy SoC in the battery bank can be computed by the Coulomb counting (ampere-hour balance) method [1]:

$$SoC(t) = SoC_0 - \frac{\int I_{bat} dt}{C_e}, \tag{2}$$

where SoC_0 is the initial value, and ignoring the operating conditions and aging status, C_e is defined as the maximum available capacity. The overall dynamical DC network characterized with $\mathscr{B}$ the incidence matrix, is given by

$$\begin{aligned} L_B \dot{I}_B &= -R_B I_B - (1-u)V + V_{bat} \\ C_B \dot{V} &= (1-u)I_B + \mathscr{B} I_k - Z_l^{-1} V - I_l \\ L_k \dot{I}_k &= -R_k I_k - \mathscr{B}^T V \\ V_{bat} &= V_{oc} + R_0 C_e \dot{SoC}, \end{aligned} \tag{3}$$

where R_B, L_B, C_B, $Z_l :\in \mathbb{R}^{n\times n}$, $I_l \in \mathbb{R}^n$ and R_k, $L_k \in \mathbb{R}^{m\times m}$ are positive definite diagonal matrices, I_B, $V : \mathbb{R} \to \mathbb{R}^n$, $u : \mathbb{R}_{\geq 0} \to [0,1)$, and $I_k :\in \mathbb{R} \to \mathbb{R}^m$.

Let $x = [I_B, I_k, V, V_{oc}]^T$ denote the state of system (3). Given a constant input u, the steady state solution $(\bar{I}_B, \bar{I}_k, \bar{V}, \bar{V}_{oc})$ to system (3) satisfies

$$\begin{aligned} \bar{V} &= (1-\bar{u})^{-1}(-R_B \bar{I}_B + \bar{V}_{bat}) \\ (1-\bar{u})\bar{I}_B &= -\mathscr{B}\bar{I}_k + Z_l^{-1}\bar{V} + I_l \\ \bar{I}_k &= -R_k{}^{-1}\mathscr{B}^T \bar{V} \\ \bar{V}_{oc} &= -R_0 C_e \dot{SoC}. \end{aligned} \tag{4}$$

The passivity property of (3) will be explored. The control objectives are

Objective 1: **Feasible current sharing**

$$\underset{(\hat{u},\hat{I}_B,\hat{V},\hat{V}_{\text{int}})\in\bar{\varepsilon}_p}{\textit{minimize}} \quad \mathscr{F}\left(\hat{u},\hat{I}_B,\hat{V},\hat{V}_{\text{oc}}\right) \tag{5}$$

Objective 2: **SoC requirement**

$$SoC_{\min} \leq \lim_{t\to\infty} SoC_i(t) \leq SoC_{\max} \tag{6}$$

We aim to explore passivity property of microgrid and desired controller [2]. If the overall dynamical model and a distributed controller under the primal-dual dynamics of optimization are both passive [3], we can get an optimal solution of the above system within the constraints of the SoC, which will ensure the BESS system in a stable operation and prolong the life cycle.

References

[1] P. J. dos Santos Neto, T. A. Barros, J. P. Silveira, E. Ruppert Filho, J. C. Vasquez and J. M. Guerrero, "Power management techniques for grid-connected DC microgrids: A comparative evaluation," *Applied Energy*, vol. 269, 115057, 2020.

[2] Y. Kawano, K. C. Kosaraju and J. M. A. Scherpen, "Krasovskii and Shifted Passivity-Based Control," *IEEE Transactions on Automatic Control*, vol. 66, no. 10, pp. 4926-4932, 2021.

[3] K. C. Kosaraju, M. Cucuzzella and J. M. A. Scherpen, "Distributed control of DC microgrids using primal-dual dynamics," *in 58th Conference on Decision and Control (CDC)*, France, pp. 6215-6220, 2019.

[1]The authors are with Jan C. Willems Center for Systems and Control, Engineering and Technology Institute Groningen, Faculty of Science and Engineering, University of Groningen, The Netherlands.{lihua.zhou, s.ahmed, j.m.a.scherpen}@rug.nl

Smart abstraction based on iterative ellipsoidal covering

Julien Calbert
UCLouvain, ICTEAM
julien.calbert@uclouvain.be

Lucas N. Egidio
UCLouvain, ICTEAM
lucas.egidio@uclouvain.be

Raphaël M. Jungers
UCLouvain, ICTEAM
raphael.jungers@uclouvain.be

1 Abstract

Classic abstraction-based techniques consist of discretizing both the input space and the state space and in general, this discretization is done with hyperrectangles [1]. One problem with discretizing the input space is that one needs a growth-bound on the error between the actual state and the quantized state which is used to take into account the discretization error. This yields an over-approximation of the image set of a cell, which increases the level of non-determinism in the symbolic system. Instead, we propose to build an abstraction based on an ellipsoidal covering of the state space, a finite set of local affine controllers, and a lazy/iterative construction of the abstraction. One benefit of this approach is the fact that the state and input spaces need not be discretized and the symbolic-input space is reduced to a finite set of controllers. Moreover, when ellipsoidal cells and affine controllers are considered, it is possible to compute an optimal controller via the solution of a semi-definite program (SDP). Another advantage is that the covering is computed smartly and even designed with the help of classic controller design techniques, unlike classical ones, which use an *a priori* defined, suboptimal, and prone to the curse of dimensionality, grinding approach. To achieve this goal we combine and extend the ideas of the following three papers: [2], [3] and [4].

In the paper [2], the authors provide a strategy to lazily (i.e., postponing heavier numerical operations) build a smart abstraction for a discrete input space. However, in [2], this strategy was based on the use of a growth-bound function on the error between the state and the quantized state. A major drawback is that in the absence of incremental stability, it gives an over-approximation which increases the level of non-determinism in the symbolic system, eventually making the abstract-control synthesis impossible.

More recently, in paper [3], pre-defined ellipsoids covering the state space were used to build a deterministic abstraction and local affine feedback controllers between nearby cells are calculated to define the abstract transitions. This method of calculating transitions requires more computational effort than other methods (such as those based on growth-bound functions used with a discretized input space), but the advantage is that the abstraction is a weighted digraph, instead of a hypergraph. In addition, the state-dependent nature of the controllers allows the use of larger discretization cells, reducing the complexity of the abstraction. To leverage the optimal control solution proposed in [3] while building a smart abstraction, we must design not only the transitions but also the positioning and shape of the ellipsoids along the optimal path, similarly to [2].

To achieve this goal, we propose a strategy using Rapidly-exploring Random Trees (RRT). Building a smart abstraction based on the ellipsoidal cells requires solving ellipsoidal inclusion subproblems, which can be done efficiently by leveraging the results from [4]. An example of the execution of the algorithm is shown in Figure 1: a random tree of cells and the values of a Lyapunov-like function valid inside each of them. This value is also an upper-bound on the worst-case cost for taking any state in a given ellipsoid towards a given goal set.

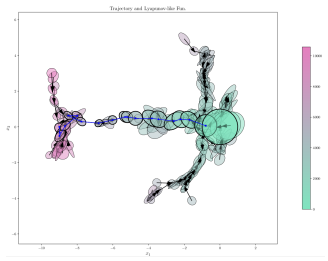

Figure 1: Result of our main algorithm. Ellipsoidal cells and controllers performing transitions among them are simultaneously designed by an RRT-based algorithm. The color-map represents the value of the Lyapunov-like function (i.e., an upper bound on the cost to reach the target from a given state).

References

[1] M. Rungger and M. Zamani, "Scots: A tool for the synthesis of symbolic controllers," in *Proceedings of the 19th international conference on hybrid systems: Computation and control*, pp. 99–104, 2016.

[2] J. Calbert, B. Legat, L. N. Egidio, and R. Jungers, "Alternating simulation on hierarchical abstractions," in *IEEE Conference on Decision and Control (CDC)*, pp. 593–598, 2021.

[3] L. N. Egidio, T. A. Lima, and R. M. Jungers, "State-feedback abstractions for optimal control of piecewise-affine systems," in *IEEE Conference on Decision and Control (CDC)*, pp. 7455–7460, 2022.

[4] J. Calbert, L. N. Egidio, and R. M. Jungers, "An efficient method to verify the inclusion of ellipsoids," *arXiv preprint arXiv:2211.06237*, 2022.

Part 3

Plenary Lectures

Part 4

List of Participants

Flavia Sofia Acerbo
KU Leuven
Belgium
flavia.acerbo@siemens.com

Saeed Ahmed
University of Groningen
The Netherlands
s.ahmed@rug.nl

Sanaz Akbarisisi
KU Leuven
Belgium
sanaz.akbarisisi@kuleuven.be

Javier Alonso Mora
Delft University of Technology
The Netherlands
j.alonsomora@tudelft.nl

Michele Ambrosino
Université Libre de Bruxelles
Belgium
michele.ambrosino@ulb.be

Oscar Fabian Archila Cruz
Brandenburg University of Technology
Germany
archilac@b-tu.de

Zemerart Asani
Vrije Universiteit Brussel
Belgium
zemerart.asani@vub.be

Alejandro Astudillo
KU Leuven
Belgium
alejandro.astudillovigoya@kuleuven.be

Mirko Baglioni
Delft University of Technology
The Netherlands
m.baglioni@tudelft.nl

Muhammed Bahadir Saltik
University of Groningen
The Netherlands
m.b.saltik@rug.nl

Gianpietro Battocletti
Delft University of Technology
The Netherlands
g.battocletti@tudelft.nl

Frederik Baymler Mathiesen
Delft University of Technology
The Netherlands
f.b.mathiesen@tudelft.nl

Gerben Beintema
Eindhoven University of Technology
The Netherlands
g.i.beintema@tue.nl

Ouassim Benhamouche
Université Libre de Bruxelles
Belgium
ouassim.benhamouche@ulb.be

Joris Bergman
Wageningen University & Research
The Netherlands
joris.bergman@wetsus.nl

Riccardo Bertollo
Eindhoven University of Technology
The Netherlands
r.b.bertollo@tue.nl

Bart Besselink
University of Groningen
The Netherlands
b.besselink@rug.nl

Ruben Beumer
Eindhoven University of Technology
The Netherlands
r.m.beumer@tue.nl

Gianluca Bianchin
Université Catholique de Louvain
Belgium
gianluca.bianchin@uclouvain.be

Francois-Gregoire Bierwart
University of Namur
The Netherlands
francois-gregoire.bierwart@unamur.be

Christian Birkner
DIFFER
Germany
christian.birkner@thi.de

Pascal den Boef
Eindhoven University of Technology
The Netherlands
p.d.boef@tue.nl

Max Bolderman
Eindhoven University of Technology
The Netherlands
m.bolderman@tue.nl

Bart van den Boorn
DIFFER
The Netherlands
b.f.h.vandenboorn@differ.nl

Mathias Bos
KU Leuven
Belgium
mathias.bos@kuleuven.be

Martijn Boussé
Maastricht University
The Netherlands
m.bousse@maastrichtuniversity.nl

Yorick Broens
Eindhoven University of Technology
The Netherlands
y.l.c.broens@tue.nl

Kamil Bujnarowski
Maastricht University
The Netherlands
k.bujnarowski@maastrichtuniversity.nl

Michiel Busschaert
KU Leuven
Belgium
michiel.busschaert@kuleuven.be

Maxime Bussios
Université Libre de Bruxelles
Belgium
maxime.bussios@ulb.be

Julien Calbert
Université Catholique de Louvain
Belgium
julien.calbert@uclouvain.be

Louis Callens
KU Leuven
Belgium
louis.callens@kuleuven.be

Raffaella Carloni
University of Groningen
The Netherlands
r.carloni@rug.nl

Lennard Ceelen
DIFFER
The Netherlands
l.ceelen@differ.nl

Paula Chanfreut
Eindhoven University of Technology
The Netherlands
paula.chanfreut@gmail.com

Hamin Chang
University of Groningen
The Netherlands
h.chang@rug.nl

Jin Chen
University of Groningen
The Netherlands
jin.chen@rug.nl

Xiupeng Chen
University of Groningen
The Netherlands
xiupeng.chen@rug.nl

Xiaodong Cheng
Wageningen University & Research
The Netherlands
xiaodong.cheng@wur.nl

Askish Cherukuri
University of Groningen
The Netherlands
a.k.cherukuri@rug.nl

Ramachandran Chittur Anantharaman
University of Namur
Belgium
ramachandran.chittur@unamur.be

Margarita Chli
ETH Zurich & University of Cyprus
Switzerland
chlim@ethz.ch

Michelle Chong
Eindhoven University of Technology
The Netherlands
m.s.t.chong@tue.nl

Lucian Christian Iacob
Eindhoven University of Technology
The Netherlands
l.c.iacob@tue.nl

Radu Cimpean
University of Groningen
The Netherlands
r.cimpean@rug.nl

Koen Classens
Eindhoven University of Technology
The Netherlands
k.h.j.classens@tue.nl

Maurizio Clemente
Eindhoven University of Technology
The Netherlands
m.clemente@tue.nl

Sribalaji Coimbatore Anand
Uppsala University
Sweden
sribalaji.anand@angstrom.uu.se

Sébastien Colla
Université Catholique de Louvain
Belgium
sebastien.colla@uclouvain.be

Francesco Cordiano
Delft University of Technology
The Netherlands
f.cordiano@tudelft.nl

Andres Cotoruello Jimenez
Université Libre de Bruxelles
Belgium
andres.cotorruelo.jimenez@ulb.be

Mathyn van Dael
Eindhoven University of Technology
The Netherlands
m.r.v.dael@tue.nl

Amritam Das
Eindhoven University of Technology
The Netherlands
am.das@tue.nl

Janset Dasdemir
University of Twente
The Netherlands
j.dasdemir@utwente.nl

Sarthak De
KU Leuven
Belgium
sarthak.de235@gmail.com

Sonia De Santis
KU Leuven
Belgium
sonia.desantis@kuleuven.be

Virginie Debauche
Université Catholique de Louvain
Belgium
virginie.debauche@uclouvain.be

Wilm Decré
KU Leuven
Belgium
wilm.decre@kuleuven.be

Gilles Delansnay
Université de Mons
Belgium
gilles.delansnay@umons.ac.be

Cosimo Della Santina
Delft University of Technology
The Netherlands
c.dellasantina@tudelft.nl

Jean-Charles Delvenne
Université Catholique de Louvain
Belgium
jean-charles.delvenne@uclouvain.be

Gijs Derks
DIFFER
The Netherlands
g.l.derks@differ.nl

Abhished Dhyani
Delft University of Technology
The Netherlands
a.dhyani-1@tudelft.nl

Ousmane Diao
Université Catholique de Louvain
Belgium
ousmane.diao@uclouvain.be

Stefan van Dijk
Eindhoven University of Technology
The Netherlands
stefan.van.dijk.96@gmail.com

Dries Dirckx
KU Leuven
Belgium
dries.dirckx@kuleuven.be

Peter van Dooren
Eindhoven University of Technology
The Netherlands
p.v.dooren@tue.nl

Yangming Dou
University of Groningen
The Netherlands
y.dou@rug.nl

Philippe Dreesen
Maastricht University
The Netherlands
philippe.dreesen@maastrichtuniversity.nl

Sadegh Ebrahimkhani
Vrije Universiteit Brussel
Belgium
sadegh.ebrahimkhani@vub.be

Thomas Edridge
Delft University of Technology
The Netherlands
thomasedridge@gmail.com

Luke van Eijk
Delft University of Technology
The Netherlands
l.f.vaneijk@tudelft.nl

Merijn Floren
KU Leuven
Belgium
merijn.floren@kuleuven.be

Alvaro Florez
KU Leuven
Belgium
alvaro.florez@kuleuven.be

Stefanie Fonken
Eindhoven University of Technology
The Netherlands
s.j.m.fonken@tue.nl

Karlijn Fransen
Vanderlande Industries B.V.
The Netherlands
karlijn.fransen@vanderlande.com

Kathinka Frieswijk
University of Groningen
The Netherlands
k.frieswijk@rug.nl

Prasoon Garg
Eindhoven University of Technology
The Netherlands
p.garg.1@tue.nl

Kurt Geebelen
Flanders Make
Belgium
kurt.geebelen@flandersmake.be

Merlijne Geurts
Eindhoven University of Technology
The Netherlands
m.e.geurts@tue.nl

Mehrad Ghasem Sharabiany
Vrije Universiteit Brussel
Belgium
mehrad.ghasem.sharabiany@vub.be

Raphaël Goetz
Eindhoven University of Technology
The Netherlands
r.p.p.f.goetz@tue.nl

Alejandro Goldar Davila
Université Libre de Bruxelles
Belgium
alejandro.goldar.davila@ulb.be

Rodrigo González
Eindhoven University of Technology
The Netherlands
r.a.gonzalez@tue.nl

Alejandro Gonzalez Garcia
KU Leuven
Belgium
alex.gonzalezgarcia@kuleuven.be

Viral Gosar
Eindhoven University of Technology
The Netherlands
v.v.gosar@tue.nl

Stefanny Guadalupe Ramirez Juarez
University of Groningen
The Netherlands
s.g.ramirez.juarez@rug.nl

Marvyn Gulina
University of Namur
Belgium
marvyn.gulina@unamur.be

Redmer de Haan
Eindhoven University of Technology
The Netherlands
r.d.haan@tue.nl

Rick Haasjes
University of Twente
The Netherlands
r.haasjes@utwente.nl

Sofie Haesaert
Eindhoven University of Technology
The Netherlands
s.haesaert@tue.nl

Wouter Hakvoort
University of Twente
The Netherlands
wouter.hakvoort@utwente.nl

Caspar Hanselaar
Eindhoven University of Technology
The Netherlands
c.a.j.hanselaar@tue.nl

Max van Haren
Eindhoven University of Technology
The Netherlands
m.j.v.haren@tue.nl

Anthony Hastir
University of Namur
Belgium
anthony.hastir@unamur.be

Mohaddese Hazini
University of Twente
The Netherlands
m.hazini@utwente.nl

Maurice Heemels
Eindhoven University of Technology
The Netherlands
m.heemels@tue.nl

Marieke Heidema
University of Groningen
The Netherlands
h.m.heidema@rug.nl

Peter van Heijster
Wageningen University & Research
The Netherlands
peter.vanheijster@wur.nl

Julien Hendrickx
Université Catholique de Louvain
Belgium
julien.hendrickx@uclouvain.be

Yannick Heuts
Eindhoven University of Technology
The Netherlands
y.j.j.heuts@tue.nl

Teimour Hosseinalizadeh
University of Groningen
The Netherlands
t.hosseinalizadeh@rug.nl

Anne-Men Huijzer
University of Groningen
The Netherlands
m.a.huijzer@rug.nl

Jilles van Hulst
Eindhoven University of Technology
The Netherlands
j.s.v.hulst@tue.nl

Ibrahim Ibrahim
KU Leuven
Belgium
ibrahim.ibrahim@kuleuven.be

Santiago Iregui
KU Leuven
Belgium
santiago.iregui@kuleuven.be

Aykut Isleyen
Eindhoven University of Technology
The Netherlands
a.isleyen@tue.nl

Laurens Jacobs
KU Leuven
Belgium
laurens.jacobs@kuleuven.be

Lars Janssen
Eindhoven University of Technology
The Netherlands
l.a.l.janssen@tue.nl

Najmeh Javanmardi
University of Groningen
The Netherlands
n.javanmardi@rug.nl

Bayu Jayawardhana
University of Groningen
The Netherlands
b.jayawardhana@rug.nl

Joppe de Jonghe
KU Leuven
The Netherlands
joppe.dejonghe@student.kuleuven.be

Dominique Joubert
Wageningen University & Research
The Netherlands
dominique.joubert@wur.nl

Marcin Kaczmarek
Delft University of Technology
The Netherlands
m.b.kaczmarek@tudelft.nl

Jacques Kadima Kazaku
Université Catholique de Louvain
The Netherlands
jacques.kadima@uclouvain.be

Lars van de Kamp
Eindhoven University of Technology
The Netherlands
l.g.j.v.d.kamp@tue.nl

Jorn van Kampen
Eindhoven University of Technology
The Netherlands
j.h.e.v.kampen@tue.nl

Karel Keesman
Wageningen University & Research
The Netherlands
karel.keesman@wur.nl

Bas Kessels
Eindhoven University of Technology
The Netherlands
b.m.kessels@tue.nl

Mahboubeh Keyvanara
Eindhoven University of Technology
The Netherlands
m.keyvanara@tue.nl

Azin Khaleghi
University of Groningen
The Netherlands
a.khaleghi@rug.nl

Mustafa Khammash
ETH ZÃijrich
Switzerland
mustafa.khammash@bsse.ethz.ch

David Kiessling
KU Leuven
Belgium
david.kiessling@kuleuven.be

Lizan Kivits
Eindhoven University of Technology
The Netherlands
e.m.m.kivits@tue.nl

Jesse Koenders
DIFFER
The Netherlands
j.t.w.koenders@differ.nl

Johan Kon
Eindhoven University of Technology
The Netherlands
j.j.kon@tue.nl

Bob Kool
DIFFER
The Netherlands
bob.kool97@gmail.com

Hakan Köroğlu
University of Twente
The Netherlands
h.koroglu@utwente.nl

Robbert van der Kruk
Eindhoven University of Technology
The Netherlands
r.j.v.d.kruk@tue.nl

Sibren Lagauw
KU Leuven
Belgium
sibren.lagauw@esat.kuleuven.be

Esteban Lage Cano
Eindhoven University of Technology
The Netherlands
e.c.lage.cano@tue.nl

Francis le Roux
Eindhoven University of Technology
The Netherlands
f.a.l.le.roux@tue.nl

Erjen Lefeber
Eindhoven University of Technology
The Netherlands
a.a.j.lefeber@tue.nl

Antoine Legat
Université Catholique de Louvain
Belgium
antoine.legat@uclouvain.be

Jimei Li
KU Leuven
Belgium
jimei.li@student.kuleuven.be

Ming Li
Eindhoven University of Technology
The Netherlands
mingliuestc@outlook.com

Tinghua Li
University of Groningen
The Netherlands
t.li@rug.nl

Yifei Li
Delft University of Technology
The Netherlands
y.li-34@tudelft.nl

Yongzhang Li
University of Groningen
The Netherlands
yongzhang.li@rug.nl

Yun Li
Delft University of Technology
The Netherlands
yunli.tudelft@gmail.com

Zirui Liao
Eindhoven University of Technology
The Netherlands
z.liao@tue.nl

Yankai Lin
Eindhoven University of Technology
The Netherlands
y.lin2@tue.nl

Changrui Liu
Delft University of Technology
The Netherlands
c.liu-14@tudelft.nl

Xinghua Liu
University of Groningen
The Netherlands
xinghua.liu@rug.nl

Zhiyuan Liu
University of Groningen
The Netherlands
z.liu@rug.nl

Le Liu
University of Groningen
The Netherlands
le.liu@rug.nl

Kristoffer Lowenstein
KU Leuven
Belgium
kristofferfink.loewenstein@polimi.it

Samuel Mallick
Delft University of Technology
The Netherlands
s.h.mallick@tudelft.nl

Shamil Mamedov
KU Leuven
Belgium
shamil.mamedov@kuleuven.be

Matteo Marcantoni
University of Groningen
The Netherlands
m.marcantoni@rug.nl

Antoine Marchal
Vrije Universiteit Brussel
Belgium
antoine.marchal@vub.be

Max van Meer
Eindhoven University of Technology
The Netherlands
m.v.meer@tue.nl

Siamak Mehrkanoon
Utrecht University
The Netherlands
s.mehrkanoon@uu.nl

La Mi
University of Luxembourg
Luxembourg
la.mi@uni.lu

Wim Michiels
KU Leuven
Belgium

Philipp Mitterbach
Eindhoven University of Technology
The Netherlands
p.mitterbach@tue.nl

Judicaël Mohet
University of Namur
Belgium
judicael.mohet@unamur.be

Nima Monshizadeh
University of Groningen
The Netherlands
n.monshizadeh@rug.nl

Sarvin Moradi
Eindhoven University of Technology
The Netherlands
s.moradi@tue.nl

Maria Morao Patricio
Delft University of Technology
The Netherlands
m.l.moraopatricio@tudelft.nl

Simon van Mourik
Wageningen University & Research
The Netherlands
simon.vanmourik@wur.nl

Christian Mugisho Zagabe
University of Namur
Belgium
christian.mugisho@unamur.be

Abdul Muiz Ahmad Sheikh
Eindhoven University of Technology
The Netherlands
muizabdul29@gmail.com

Frank Mukwege
Université Libre de Bruxelles
Belgium
frank.mukwege@ulb.be

Manuel Munñoz Sánchez
Eindhoven University of Technology
The Netherlands
manuel.munoz.sanchez@gmail.com

Lotfi Mustapha Chaouach
Delft University of Technology
The Netherlands
l.chaouach@tudelft.nl

Marijn Nijenhuis
University of Twente
The Netherlands
m.nijenhuis@utwente.nl

Henk Nijmeijer
Eindhoven University of Technology
The Netherlands
h.nijmeijer@tue.nl

Jean-Philippe Noël
KU Leuven
Belgium
jp.noel@kuleuven.be

Sven Nouwens
Eindhoven University of Technology
The Netherlands
s.a.n.nouwens@tue.nl

Tom Oomen
Eindhoven University of Technology
The Netherlands
t.a.e.oomen@tue.nl

Christopher Orrico
Eindhoven University of Technology
The Netherlands
c.a.orrico@student.tue.nl

Younes Oudich
Université Libre de Bruxelles
Belgium
younes.oudich@ulb.be

Esma ÖŰzdemir
Delft University of Technology
The Netherlands
e.ozdemir-1@tudelft.nl

Nick Paape
Eindhoven University of Technology
The Netherlands
n.paape@tue.nl

Juan Pablo Bertucci
Eindhoven University of Technology
The Netherlands
j.p.bertucci@tue.nl

Jiahao Pan
University of Groningen
The Netherlands
j.pan@rug.nl

Fabio Paparella
Eindhoven University of Technology
The Netherlands
f.paparella@tue.nl

Leonardo Pedroso
Eindhoven University of Technology
The Netherlands
l.pedroso@tue.nl

Ralph Peeters
Maastricht University
The Netherlands
ralf.peeters@maastrichtuniversity.nl

Matthias Pezzuto
Université Libre de Bruxelles
Belgium
matthias.pezzutto@ulb.be

Jean Pierre Allamaa
Siemens Industry Software
Belgium
jean.pierre.allamaa@siemens.com

Armin Pirastehzad
University of Groningen
The Netherlands
a.pirastehzad@rug.nl

Chris van der Ploeg
Eindhoven University of Technology
The Netherlands
vanderploeg.cj@gmail.com

Luuk Poort
Eindhoven University of Technology
The Netherlands
l.poort@tue.nl

Maurice Poot
Eindhoven University of Technology
The Netherlands
m.m.poot@tue.nl

Christian Portilla
Eindhoven University of Technology
The Netherlands
c.r.portilla@tue.nl

Benn Proper
Eindhoven University of Technology
The Netherlands
b.w.b.proper@tue.nl

Evert Provoost
KU Leuven
Belgium
evert.provoost@kuleuven.be

Ruixuan Qi
University of Groningen
The Netherlands
r.qi@rug.nl

Shuhao Qi
Eindhoven University of Technology
The Netherlands
s.qi@tue.nl

Nishant Rajesh
Eindhoven University of Technology
The Netherlands
n.rajesh@tue.nl

Fatemeh Rastgar
KU Leuven
Belgium
fatemeh.rastgar2@gmail.com

András Retzler
KU Leuven
Belgium
andras.retzler@kuleuven.be

Victor Reyes Dreke
Eindhoven University of Technology
The Netherlands
v.d.reyes.dreke@tue.nl

Knut Roar Lende
Delft University of Technology
The Netherlands
k.r.lende@student.tudelft.nl

Daniele Ronzani
KU Leuven
Belgium
daniele.ronzani@kuleuven.be

Edwin Ross
Wageningen University & Research
The Netherlands
edwin.ross@wur.nl

Anne Rubbens
Université Catholique de Louvain
Belgium
anne.rubbens@outlook.be

Mauro Salazar
Eindhoven University of Technology
The Netherlands
m.r.u.salazar@tue.nl

Adrian Saldanha
KU Leuven
Belgium
adrian.saldanha@kuleuven.be

Santiago Sanchez-Escalonilla Plaza
University of Groningen
The Netherlands
santiago.sanchez@rug.nl

Arijit Sarkar
University of Groningen
The Netherlands
a.sarkar@rug.nl

Jacquelien Scherpen
University of Groningen
The Netherlands
f.g.fokkens@rug.nl

Johan Schoukens
Vrije Universiteit Brussel
Belgium
johan.schoukens@vub.be>

Maarten Schoukens
Eindhoven University of Technology
The Netherlands
m.schoukens@tue.nl

Bram Seinhorst
University of Twente
The Netherlands
b.seinhorst@utwente.nl

Seyed Shahriar Sheikh Aboumasoudi
University of Twente
The Netherlands
s.s.sheikhaboumasoudi@utwente.nl

Amir Shakouri
University of Groningen
The Netherlands
a.shakouri@rug.nl

Brayan Shali
University of Groningen
The Netherlands
b.m.shali@rug.nl

Max Sibeijn
Delft University of Technology
The Netherlands
m.w.sibeijn@tudelft.nl

Taranjitsingh Singh
Flanders Make
Belgium
taranjitsingh.singh@flandersmake.be

Sil Spanjer
University of Twente
The Netherlands
s.t.spanjer@utwente.nl

Luuk Spin
Eindhoven University of Technology
The Netherlands
l.m.spin@tue.nl

Jari van Steen
Eindhoven University of Technology
The Netherlands
j.j.v.steen@tue.nl

Hans Stigter
Wageningen University & Research
The Netherlands
hans.stigter@wur.nl

Zhiyong Sun
Eindhoven University of Technology
The Netherlands
z.sun@tue.nl

Ajay Suresha Sathya
KU Leuven
Belgium
ajay.sathya@kuleuven.be

Filip Surma
Delft University of Technology
The Netherlands
f.surma@tudelft.nl

Venkata Surya Prakash Malladi
University of Groningen
The Netherlands
v.s.p.malladi@rug.nl

Sutrisno Sutrisno
University of Groningen
The Netherlands
s.sutrisno@rug.nl

Jan Swevers
KU Leuven
Belgium
jan.swevers@kuleuven.be

Paul Tacx
Eindhoven University of Technology
The Netherlands
p.j.m.m.tacx@tue.nl

Laurane Thielemans
KU Leuven
Belgium
laurane.thielemans@siemens.com

Leon Tolksdorf
Eindhoven University of Technology
The Netherlands
l.t.tolksdorf@tue.nl

Kevin Tom Kurian
Eindhoven University of Technology
The Netherlands
k.tom.kurian@tue.nl

Stephan Trenn
University of Groningen
The Netherlands
s.trenn@rug.nl

Kentaro Tsurumoto
Eindhoven University of Technology
The Netherlands
tsurumoto-kentaro959@g.ecc.u-tokyo.ac.jp

Johan Ubbink
KU Leuven
Belgium
johan.ubbink@kuleuven.be

Léopold Van Brandt
Université Catholique de Louvain
Belgium
leopold.vanbrandt@uclouvain.be

Paul Van den Hof
Eindhoven University of Technology
The Netherlands
p.m.j.vandenhof@tue.nl

Guillaume Van Dessel
Université Catholique de Louvain
Belgium
guillaume.vandessel@uclouvain.be

Wim Van Roy
KU Leuven
Belgium
wim.vanroy@kuleuven.be

Freja Vandeputte
Vrije Universiteit Brussel
Belgium
freja.vandeputte@vub.be

Bastiaan Vandewal
KU Leuven
Belgium
bastiaan.vandewal@kuleuven.be

Finn Vehlhaber
Eindhoven University of Technology
The Netherlands
f.n.vehlhaber@tue.nl

Michel Verhaegen
Delft University of Technology
The Netherlands
m.verhaegen@tudelft.nl

Peter Verheijen
Eindhoven University of Technology
The Netherlands
p.c.n.verheijen@tue.nl

Chris Verhoek
Eindhoven University of Technology
The Netherlands
c.verhoek@tue.nl

Christof Vermeersch
KU Leuven
Belgium
christof.vermeersch@esat.kuleuven.be

Ruan Viljoen
KU Leuven
Belgium
ruan.viljoen@kuleuven.be

Sem Viroux
KU Leuven
Belgium
sem.viroux@esat.kuleuven.be

Renato Vizuete
Université Catholique de Louvain
Belgium
renato.vizueteharo@uclouvain.be

Maarten Vlaswinkel
Eindhoven University of Technology
The Netherlands
m.g.vlaswinkel@tue.nl

Koen de Vos
Eindhoven University of Technology
The Netherlands
k.d.vos@tue.nl

Renzi Wang
KU Leuven
The Netherlands
renzi.wang@kuleuven.be

Zhen Wang
Delft University of Technology
The Netherlands
z.wang-21@tudelft.nl

Benjamin Wauthion
Université Libre de Bruxelles
Belgium
benjamin.wauthion@ulb.be

Wouter Weekers
Eindhoven University of Technology
The Netherlands
w.weekers@tue.nl

Roeland Wildemans
Eindhoven University of Technology
The Netherlands
r.wildemans@tue.nl

Nathan van de Wouw
Eindhoven University of Technology
The Netherlands
n.v.d.wouw@tue.nl

Duo Xu
Eindhoven University of Technology
The Netherlands
d.xu@tue.nl

Rishikesh Yadav
University of Namur
Belgium
rishikesh.yadav@unamur.be

Hao Yin
University of Groningen
The Netherlands
hao.yin@rug.nl

Bangguo Yu
University of Groningen
The Netherlands
b.yu@rug.nl

Luca Zaccarian
LAAS-CNRS & University of Trento
Italy
luca.zaccarian@unitn.it

Henkai Zhang
Delft University of Technology
The Netherlands
h.zhang-39@student.tudelft.nl

Shuhao Zhang
KU Leuven
Belgium
shuhao.zhang@kuleuven.be

Xinxin Zhang
Delft University of Technology
The Netherlands
x.zhang-15@tudelft.nl

Zengjie Zhang
Eindhoven University of Technology
The Netherlands
z.zhang3@tue.nl

Lihua Zhou
University of Groningen
The Netherlands
lihua.zhou@rug.nl

Zhihe Zhuang
Eindhoven University of Technology
The Netherlands
z.h.z.zhuang@tue.nl

Menno van Zutphen
Eindhoven University of Technology
The Netherlands
m.j.t.c.v.zutphen@tue.nl

Hans Zwart
University of Twente
The Netherlands
h.j.zwart@utwente.nl

Part 5

Organizational Comments

Welcome

The Organizing Committee has the pleasure of welcoming you to the *42nd Benelux Meeting on Systems and Control*, at the Hotel Mennorode in Elspeet, The Netherlands.

Aim

The aim of the Benelux Meeting is to promote research activities and to enhance cooperation between researchers in Systems and Control. This is the forty-second in a series of annual conferences that are held alternately in Belgium and The Netherlands.

Scientific Program Overview

1. Two plenary lectures by *Mustafa Khammash* (ETH Zürich, Switzerland) on **Cybergenetics: Theory and implementation of biomolecular control systems**.
2. Two plenary lectures by *Luca Zaccarian* (LAAS-CNRS, France & University of Trento, Italy) on:
   - **Two decades of saturated linear feedback design via global and generalized sector conditions.**
   - **Optimizing shifted equilibria for enlarged basins of attraction in quadratically stabilizing saturated feedback.**
3. One plenary lecture by *Jacquelien Scherpen* (University of Groningen, The Netherlands) on **Krasovskii passivity based control and output consensus**.
4. One plenary lecture by *Margarita Chli* (ETH Zurich, Switzerland & University of Cyprus, Cyprus) on **Vision-based robotic perception: Are we there yet?**.
5. Contributed short lectures. See the list of sessions for the titles and authors of these lectures.

Directions for speakers

For a contributed lecture, the available time is 20 minutes. Please leave a few minutes for discussion and room changes, and adhere to the indicated schedule. In each room LCD projectors are available, as well as HDMI cables. *When using a projector, you have to provide a notebook yourself.*

Registration

The Benelux Meeting registration desk, located in the foyer, will be open on Tuesday, March 21, from 10:15 to 14:00. Late registrations can be made at the Benelux Meeting registration desk, when space is still available. The on-site fee schedule is:

Arrangement	Price
single room	€675
shared room	€575
only meals (no dinners)	€375
one day (no dinner)	€275

The registration fee includes:

- Admission to all sessions.
- Coffee and tea during the breaks.
- In the case of *accommodation* arrangement: lunch and dinner on Tuesday; breakfast, lunch, dinner on Wednesday; breakfast and lunch on Thursday.
- In the case of *only meals (no dinner)* arrangement: lunch on Tuesday, Wednesday, Thursday.
- In the case of *one day (no dinner)* arrangement: lunch on Tuesday, or Wednesday, or Thursday.
- Free use of a wireless Internet connection (no password required).

Organization

The meeting has been organized by Javier Alonso-Mora (Delft University of Technology), Raffaella Carloni (University of Groningen), Bayu Jayawardhana (University of Groningen), and Erjen Lefeber (Eindhoven University of Technology).

The Organizing Committee of the 42nd Benelux Meeting consists of

```
Javier Alonso-Mora
Delft University of Technology

Robert Babuska
Delft University of Technology

Raffaella Carloni
University of Groningen

Ming Cao
University of Groningen

Bart De Moor
Katholieke Universiteit Leuven
```

Bart De Schutter
Delft University of Technology

Laurent Dewasme
University of Mons

Dennis Dochain
Universite Catholique de Louvain

Jorge Goncalves
University of Luxemburg

Maurice Heemels
Eindhoven University of Technology

Julien Hendrickx
Universite Catholique de Louvain

Clara-Mihaela Ionescu
Ghent University

Bayu Jayawardhana
University of Groningen

Raphaël Jungers
Universite Catholique de Louvain

Karel Keesman
Wageningen University

Michel Kinnaert
Universite Libre de Bruxelles

Erjen Lefeber
Eindhoven University of Technology

Henk Nijmeijer
Eindhoven University of Technology

Tom Oomen
Eindhoven University of Technology

Panos Patrinos
Katholieke Universiteit Leuven

Arjan J. van der Schaft
University of Groningen

Hans Stigter
Wageningen University

Paul M.J. Van den Hof
Eindhoven University of Technology

Joseph Winkin
Universite de Namur

Nathan van de Wouw
Eindhoven University of Technology

Hans J. Zwart
University of Twente

Sponsor

The meeting is supported by the Dutch Institute for Systems and Control (DISC).

Conference location

The lecture rooms of the Hotel Mennorode are situated on the ground and first floors. Consult the map at the end of this booklet to locate rooms. Breakfast will be served between 7:30 and 10:00 AM. Room keys can be picked up at the reception from Tuesday at 15:00, and need to be returned before 10:00 on the day of departure. Parking is free of charge.

The address of the Hotel Mennorode is

Apeldoornseweg 185
8075 RJ Elspeet
The Netherlands

Best junior presentation award

Continuing a tradition that started in 1996, the 42nd Benelux Meeting will close with the announcement of the winner of the Best Junior Presentation Award. This award is given for the best presentation, given by a junior researcher, and it consists of a trophy that may be kept for one year and a certificate. The award is specifically given for quality of presentation rather than quality of research, which is judged in a different way. At the meeting, the chairs of sessions will ask three volunteers in the audience to fill out an evaluation form. After the session, the evaluation forms will be collected by the Prize Commissioners who will then compute a ranking. The winner will be announced on Thursday, March 23, in room **De Grote Zaal**, 12:15–12:45. The evaluation forms of each presentation will be returned to the junior researcher who gave the presentation. The Prize Commissioners are Michelle Chong (Eindhoven University of Technology), Wilm Decré (Katholieke Universiteit Leuven), and Wouter Hakvoort (University of Twente). The organizing committee counts on the cooperation of the participants to make this contest a success.

Website

An *electronic version* of the Book of Abstracts can be downloaded from the Benelux Meeting web site.

Meeting

The following meeting is scheduled: Management Team DISC on Tuesday, March 21, room De Grote Zaal, 20:00 – 22:00.

DISC certificates and best thesis award

The ceremony for the distribution of the DISC certificates and for the Best Thesis Award will be held on Thursday, March 23, room **De Grote Zaal**, 12:15–12:45. The jury of the Best Thesis Award is formed by Bart De Moor (Katholieke Universiteit Leuven), Ralf Peeters (Maastricht University), and Hans Zwart (University of Twente).

Tuesday March 21, 2023

11:25 – 11:30	P0 – De Grote Zaal *Welcome and Opening*							
11:30 – 12:30	P1 – De Grote Zaal Luca Zaccarian – *Two decades of saturated linear feedback design via global and generalized sector conditions*							
12:30 – 13:40	Lunch							
13:40 – 14:40	P2 – De Grote Zaal Luca Zaccarian – *Optimizing shifted equilibria for enlarged basins of attraction in quadratically stabilizing saturated feedback*							
14:40 – 15:00	Coffee Break							
Room TuA	Groenendaal TuA01 *Games and Agent-Based Models*	Solse Gat TuA02 *Distributed Control and Estimation 1*	Hooge Duvel TuA03 *System Identification 1*	Lucasgat A TuA04 *Optimal Control 1*	Lucasgat B TuA05 *Automated Vehicles 1*	Lucasgat C TuA06 *Robotics 1*	Lucasgat D TuA07 *Model-Based Control 1*	Lucasgat E TuA08 *Optimization 1*
15:00 – 15:20	Vizuete	Heidema	Gulina	De Santis	Muñoz Sánchez	Liu C.	Thielemans	Baymler Mathiesen
15:20 – 15:40	Bertucci	Javanmardi	Vandeputte	Haasjes	Yu	van Steen	Zhuang	Lage Cano
15:40 – 16:00	Pedroso	Yin	Moradi	Nouwens	Gosar	Iregui	Archila	Ibrahim
16:00 – 16:20	Frieswijk	Liu Z.	Viroux	Li Y.	Zhang S.	Proper	Orrico	Surma
16:20 – 16:40	Ramirez	Reyes Dreke	Legat	Cordiano	Qi	Chen	Verheijen	Suresha Sathya
16:40 – 17:00	Mi	Edridge	Kivits	Ahmed	Mukwege	Pan	Koenders	Astudillo
17:00 – 17:20	Chenn	Bianchin	Vizuete	Beumer	Hanselaar	Hazini	Özdemir	Rastgar
18:00 – 20:00	Dinner							
20:00 – 22:00	Management Team DISC (room De Grote Zaal)							

Wednesday March 22, 2023

8:30 – 9:30	P3 – De Grote Zaal Jacquelien Scherpen – *Krasovskii passivity based control and output consensus*							
9:30 – 9:45	Coffee break							
Room WeM	Groenendal WeM01 *Distributed Parameter Systems*	Solse Gat WeM02 *Optimal Model Based Control*	Hooge Duvel WeM03 *Optimal Control 2*	Lucasgat A WeM04 *System Identification 2*	Lucasgat B WeM05 *Optimization 2*	Lucasgat C WeM06 *Robotics 2*	Lucasgat D WeM07 *Non-Linear Control 1*	Lucasgat E WeM08 *Systems Theory*
9:45 – 10:05	Kaczmarek	Baglioni	Heuts	Beintema	Rajesh	Ubbink	Gonzalez-Garcia	Huijzer
10:05 – 10:25	Provoost	Dirckx	Sibeijn	Vermeersch	Van Roy	İşleyen	van Eijk	Pirastehzad
10:25 – 10:45	Liao	Spanjer	Akbarisisi	De	Paparella	van Dooren	Chang	Shali
10:45 – 11:05	Saldanha	van Zutphen	van Hulst	Floren	Ahmad	Asani	Poot	Li Y.
11:05 – 11:25	Mohet	Wang R.	Van Dessel	De Jonghe	Vehlhaber	Geebelen	Zhang X.	Spin
11:25 – 11:45	van den Boorn	Bos	Florez	González	Weekers	Van der Wilt	Sheikh Aboumasoudi	Cotorruelo
11:45 – 12:05	Fatemeh Sharifi	Singh	Rubbens	Ebrahimkhani	Portilla	Keyvanara	Wang Z.	Boussé
12:15 – 13:30	Lunch							
13:30 – 14:30	P4 – De Grote Zaal Margarita Chli – *Vision-based robotic perception: Are we there yet?*							
14:30 – 14:45	Break							
Room WeA	Groenendal WeA01 *Optimization 3*	Solse Gat WeA02 *Optimal Control 3*	Hooge Duvel WeA03 *Non-Linear Control 2*	Lucasgat A WeA04 *Vehicles & Aerospace*	Lucasgat B WeA05 *Mechanical Engineering*	Lucasgat C WeA06 *System Identification 3*	Lucasgat D WeA07 *Robotics 3*	Lucasgat E WeA08 *Model-Based Control 2*
14:45 – 15:05	Bergman	Geurts	Mugisho Zagabe	van Kampen	van Meer	van Haren	Shakouri	Tsurumoto
15:05 – 15:25	Colla	Li Y.	Sutrisno	de Haan	Dhyani	Kessels	Mamedov	Liu L.
15:25 – 15:45	Kiessling	Garg	Iacob	Kurian	Kon	Hosseinalizadeh	de Vos	Bolderman
15:45 – 16:05	Anand	Vlaswinkel	Bierwart	Tolksdorf	Classens	Wildemans	Mitterbach	Patrício
16:05 – 16:25	Chaouach	van der Ploeg	Debauche	Clemente	Schoukens	Ceelen	Bujnarowski	van Dael
16:25 – 16:45	Diao	Acerbo	Bertollo	Delansnay	Tacx	Dreesen	Ronzani	Lin
16:45 – 17:05	Khaleghi	Allamaa	Van Brandt	Vandewal	Paape	Mehrkanoon	Pezzutto	Bahadir Saltik
18:30 – 20:30	Dinner							

Thursday March 23, 2023

8:30 – 9:30	P6 – De Grote Zaal Mustafa Khammash – *Cybergenetics: Theory and implementation of biomolecular control systems - Part 1*									
9:30 – 9:45	Coffee break									
9:45 – 10:45	P7 – De Grote Zaal Mustafa Khammash – *Cybergenetics: Theory and implementation of biomolecular control systems - Part 2*									
Room ThM	Groenendal ThM01 *Observers*	Solse Gat ThM02 *Optimal Control 4*	Hooge Duvel ThM03 *Robotics 4*	't Leesten A ThM04 *Model Reduction*	't Leesten C ThM05 *Systems Biology & Medical Applications*	't Leesten D ThM06 *Electro-Mechanical Engineering*	't Leesten E+F ThM07 *System Identification 4*	Grote Zaal ThM08 *Optimization 4*	Kleine Zaal ThM09 *Robotics 5*	Broodberg ThM10 *Optimal Control 5*
10:45 – 11:05	le Roux	Mallick	Battocletti	Poort	Busschaert	Oudich	Retzler	Fonken	Ambrosino	Seinhorst
11:05 – 11:25	Wauthion	Callens	Liu X.	Janssen	van de Kamp	Qi	Verhoek	Li J.	Broens	Li M.
11:25 – 11:45	Ross	Joubert	Li T.	Sarkar	Cimpean	Jacobs	Fink Lowenstein	Den Boef	Viljoen	Zhou
11:45 – 12:05	van der Kruk	Goldar	Zhang Z.	Lagauw	Benhamouche	Xu	Marchal	Sharabiany	Marcantoni	Calbert
12:15 – 12:45	Award Ceremony – De Grote Zaal *Best Thesis Award, DISC Certificates & Best Junior Presentation Award*									
12:45 – 13:00	P8 – De Grote Zaal *Closure of the 42nd Benelux Meeting*									
13:00 – 14:00	*Lunch*									

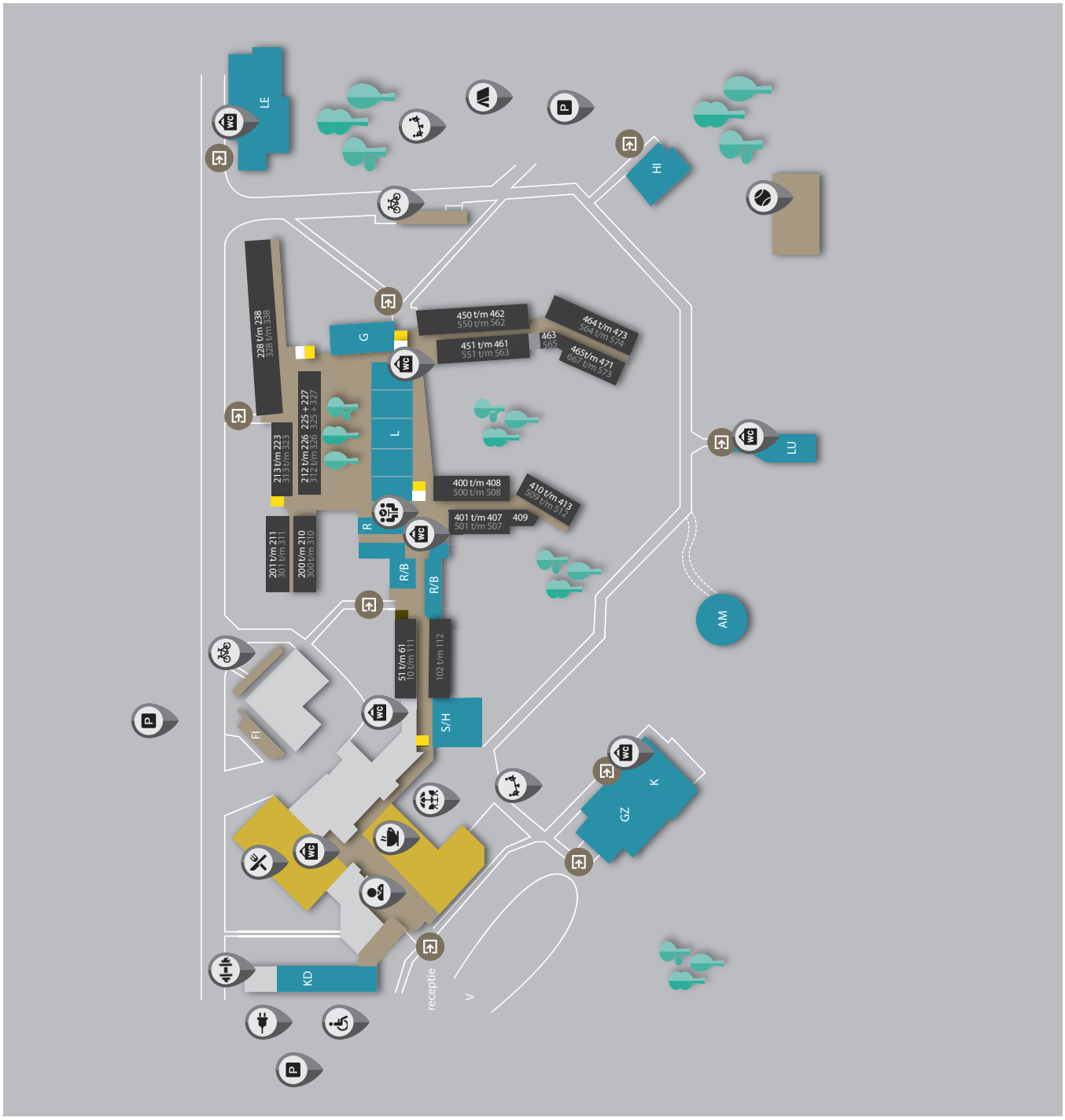

HOTEL MENNORODE

Vergaderzalen b.g. / Meeting rooms
Openbare ruimten / Public areas
Hotelkamers / Hotel rooms
Bars & restaurants
Lift / Elevator
Ingang / Entrance
Trap / Stairs

Hotel

51 - 61 begane grond / ground floor
100, 300, 500 - serie 1e verdieping / 1st floor
200, 400 - serie begane grond / ground floor

Zalen / Meeting rooms

K Kleine Zaal
S Solse Gat
H Hooge Duvel *
R Roode Heggen
B Broodberg *
L Lucasgat
G Groenendaal
V Voorplein
GZ Grote Zaal
LE 't Leesten
HI Hindeloopen
LU De Luwte
AM Amfitheater
KD Kroondomein
FI Fietsverhuur & E-bikes
* 1e verdieping / 1st floor

Algemene ruimten / Public areas

Receptie / Front desk
Ontbijt restaurant
Grand Café De Schaapskooi
Terras / Terrace
Vergaderfoyer
Tennis
Fietsenstalling / Bicycle storage
Fitness & Recreatie
Minder valide parkeerplaats
Oplaadpaal